Type IIA string theory on $T^6/(\mathbb{Z}_2 \times \mathbb{Z}_6 \times \Omega\mathcal{R})$: Model building and string phenomenology with intersecting D6-branes

Dissertation
zur Erlangung des Grades
"Doktor
der Naturwissenschaften"
am Fachbereich Physik, Mathematik und Informatik
der Johannes Gutenberg-Universität
in Mainz

Jill Ecker

geboren in Luxemburg
Mainz, March 2016

Datum der mündlichen Prüfung: 27. Juli 2016

Abstract

In this doctoral thesis, various aspects of string model building and phenomenology are investigated within the framework of Type IIA string theory on the $T^6/(\mathbb{Z}_2 \times \mathbb{Z}_6 \times \Omega\mathcal{R})$ orbifold with discrete torsion. The aim is the reproduction of supersymmetric versions of well-known particle physics models using intersecting rigid D6-branes wrapped on fractional three-cycles. The models analyzed include the minimal supersymmetric Standard Model as well as supersymmetric Pati-Salam models, left-right symmetric models and $SU(5)$ models. The analysis starts with the detection of symmetries among the various lattice configurations of the underlying six-torus T^6. It will be shown that the six a priori independent torus lattices can be reduced to two independent lattice configurations. The next step consists in determining all possible bulk three-cycles apt to support supersymmetric D6-branes. The foreseen search will be exhaustive, allowing subsequently a complete classification of the D6-branes for all values of the complex structure modulus ϱ. The classification of D6-branes uses several criteria, including the type of gauge group supported by the D6-branes, the rigidity of the D6-branes and the multiplicity of matter states transforming in the (anti)symmetric representation of the gauge group. Once the classification of D6-branes is complete, systematic computer scans test numerous combinations of intersecting D6-branes in order to detect those that give rise to the correct chiral particle content of the considered models. For each type of the aforementioned models, concrete examples will be found which satisfy the constraints on the particle spectrum and fulfill all consistency conditions. Finally, the thesis will focus on phenomenological aspects of the particle physics models found, including the detection of massless $U(1)$ combinations, discrete $\mathbb{Z}_n$-symmetries and cubic couplings such as the Yukawa couplings.

Zusammenfassung

In dieser Doktorarbeit erforsche ich verschiedene Aspekte von Stringtheorie-Modellbildung und -Phänomenologie auf der Orbifaltigkeit $T^6/(\mathbb{Z}_2 \times \mathbb{Z}_6 \times \Omega\mathcal{R})$ im Rahmen der Typ IIA Stringtheorie. Das Ziel besteht darin, mit Hilfe von starren, sich schneidenden D6-Branen, supersymmetrische Varianten von bekannten Modellen der Teilchenphysik zu konstruieren. Die in dieser Doktorarbeit in Betracht gezogenen Modelle umfassen das minimal supersymmetrische Standardmodell, Pati-Salam Modelle und links-rechts symmetrische Modelle, sowie $SU(5)$ Modelle. Wir starten mit dem Aufspüren von Symmetrien zwischen den verschiedenen Gitter-Konfigurationen vom Sechs-Torus T^6. Wir werden sehen, dass die a priori sechs unabhängigen Gitter zu zwei unabhängigen Gittern reduziert werden können. Im nächsten Schritt bestimmen wir alle "bulk" Drei-Zykel, die von supersymmetrischen D6-Branen umwunden werden können. Dies erlaubt uns, die gefundenen D6-Branen zu klassifizieren nach verschiedenen Kriterien, welche folgende Aspekte umfassen: Der Typ der resultierenden Eichgruppe der D6-Branen, die Starrheit der D6-Branen sowie die Multiplizität der Zustände, die sich in der (Anti)symmetrischen Darstellung der Eichgruppe transformieren. Nachdem die Klassifizierung abgeschlossen ist, wenden wir systematische Rechner Suchen an, um verschiedene Konfigurationen von sich schneidenden D6-Branen zu testen auf ihre Tauglichkeit, realistische Teilchenspektra zu reproduzieren. Mehrere realistische und konsistente Teilchenmodelle werden explizit angegeben. Zum Abschluss befassen wir uns mit zusätzlichen Eigenschaften der Modelle, wie die Existenz von masselosen $U(1)$ Kombinationen, diskrete $\mathbb{Z}_n$-Symmetrien und Dreipunktkopplungen wie beispielsweise den Yukawa-Kopplungen.

Contents

1 Introduction **1**
- 1.1 Basics of string theory . . . 1
- 1.2 General features of string phenomenology . . . 2
- 1.3 Layout of the thesis . . . 5

2 Type IIA string theory on the $T^6/(\mathbb{Z}_2 \times \mathbb{Z}_6 \times \Omega\mathcal{R})$ orientifold **9**
- 2.1 General aspects of toroidal orbifolds . . . 9
- 2.2 Geometry of $T^6/(\mathbb{Z}_2 \times \mathbb{Z}_6 \times \Omega\mathcal{R})$ . . . 12
  - 2.2.1 The orbifold action and the orientifold projection on T^6 . . . 12
  - 2.2.2 Hodge numbers . . . 13
  - 2.2.3 Bulk three-cycles . . . 16
  - 2.2.4 Exceptional three-cycles . . . 21
- 2.3 Strings and D6-branes on $T^6/(\mathbb{Z}_2 \times \mathbb{Z}_6 \times \Omega\mathcal{R})$ . . . 25
  - 2.3.1 Closed string spectrum . . . 25
  - 2.3.2 D6-branes and open strings . . . 28
- 2.4 Consistency conditions . . . 32
  - 2.4.1 Supersymmetry and Special Lagrangian Cycles . . . 32
  - 2.4.2 RR-tadpole cancellation conditions . . . 36
  - 2.4.3 K-theory constraints . . . 37

3 Introduction to model building with intersecting D6-branes **39**
- 3.1 Overview of basic aspects in D6-brane model building . . . 39
- 3.2 Particle physics models considered in this work . . . 42
  - 3.2.1 MSSM-like models . . . 43
  - 3.2.2 The left-right symmetric model . . . 50
  - 3.2.3 The Pati-Salam model . . . 52
  - 3.2.4 The $SU(5)$ model . . . 52
- 3.3 Collection of formulas for the massless open string spectrum . . . 53
  - 3.3.1 Orbifold invariant intersection numbers . . . 53
  - 3.3.2 The sector-per-sector intersection numbers . . . 54
  - 3.3.3 The beta-function coefficients . . . 56

4 Preliminary steps to string model building **59**
- 4.1 Equivalences between the torus lattices . . . 59
  - 4.1.1 Number of shortest supersymmetric three-cycles . . . 60
  - 4.1.2 The Hodge numbers and the massless closed string spectrum . . . 61
  - 4.1.3 Consistency conditions of different lattices . . . 62

4.2 Supersymmetric three-cycles . . . 67
4.2.1 Upper bounds on the bulk wrapping numbers . . . 67
4.2.2 Full classification of bulk three-cycles . . . 69

5 Classification of D6-branes 73
5.1 Gauge symmetry enhancement to USp and SO groups . . . 73
5.2 Criteria for rigid D6-branes . . . 75
5.2.1 Rigidity criteria for MSSM-type models . . . 75
5.2.2 Non-rigidity criteria for SU(5) models . . . 77
5.3 Matter states in (anti)symmetric representations . . . 79
5.3.1 Chiral spectrum . . . 80
5.3.2 Non-chiral spectrum . . . 85
5.4 Towards a three-generation particle spectrum . . . 88
5.4.1 ϱ-independent configurations . . . 88
5.4.2 ϱ-dependent configurations . . . 90

6 The construction of $SU(5)$ and Pati-Salam models 99
6.1 Construction of local $SU(5)$ models . . . 99
6.2 Archetypes of local and global Pati-Salam models . . . 102
6.2.1 Local Pati-Salam models on the **bAA** lattice . . . 103
6.2.2 Global ϱ-independent Pati-Salam models on the **aAA** lattice . . . 107
6.2.3 The situation of ϱ-dependent Pati-Salam models on the **aAA** lattice . 110

7 The construction of left-right symmetric and MSSM-like models 115
7.1 Five-stack and six-stack left-right symmetric models . . . 115
7.1.1 Search for the visible sector of left-right symmetric models . . . 116
7.1.2 Semi-global five-stack left-right symmetric models . . . 119
7.1.3 Global six-stack left-right symmetric models . . . 121
7.2 Searching for global MSSM-like D6-brane models . . . 131
7.2.1 Global five-stack ϱ-independent MSSM-like models . . . 132
7.2.2 Some results for ϱ-dependent models . . . 138

8 Discrete Symmetries 143
8.1 Massless $U(1)$ and discrete $\mathbb{Z}_n$-symmetries . . . 143
8.2 Explicit expression for the conditions on $\mathbb{Z}_n$-symmetries . . . 145
8.3 $\mathbb{Z}_n$-symmetries in the global five-stack MSSM . . . 152
8.4 $\mathbb{Z}_n$-symmetries in the global six-stack left-right symmetric models . . . 161
8.4.1 Prototype I left-right symmetric model . . . 161
8.4.2 Prototype II left-right symmetric model . . . 164
8.4.3 Brief overview of the results for the other prototypes . . . 166

9 Three- and four-point couplings at leading order 173
9.1 Yukawa and other cubic couplings . . . 173
9.2 Cubic couplings in the global MSSM-like model . . . 175
9.2.1 Quarkonic cubic couplings . . . 179
9.2.2 Leptonic cubic couplings . . . 187
9.2.3 Alternative couplings for the neutrinos . . . 195

9.2.4 Hidden sector cubic couplings 200
9.3 Yukawa couplings for the global left-right symmetric models 206
9.3.1 Cubic couplings 206
9.3.2 Quartic couplings 208

10 Conclusion **213**
10.1 Summary and discussion 213
10.2 Outlook 216

A Explicit examples of constructions and computations **219**
A.1 Explicit construction of a fractional cycle 219
A.2 Example of the calculation of beta-function coefficients 224
A.2.1 Preliminary considerations 224
A.2.2 Example of computation 225

B Additional information **233**
B.1 Other definitions of the hypercharge 233
B.2 Addendum to chapter 8 234
B.2.1 Linearly independent fractional three-cycles 235
B.2.2 Details about the $\mathbb{Z}_n$-symmetries for the global MSSM 236
B.3 Classification of SUSY two-cycles on $T^2_{(2)} \times T^2_{(3)}$ with lattice **AA** 239
References 239

Chapter 1

Introduction

1.1 Basics of string theory

Currently, our universe is described by two theories: the Standard Model of particle physics and general relativity. The Standard Model is a description of three out of the four fundamental interactions, namely the strong interaction, electromagnetism, and the weak interaction. General relativity on the other hand is a theory describing gravitational interactions.
Both theories have been tested experimentally up to very precise measurements. Nonetheless, the present situation is unsatisfying: the Standard Model has 28 free parameters [1], the numerical values of which have to be determined entirely by experimental data. Also, it fails to account for cosmological phenomena such as dark matter [2–4]. Finally, it would be more elegant to have just one theory instead of two to describe the universe.
Theories based on quantum gravity, such as supergravity [5], loop quantum gravity [6–9] or asymptotic safe gravity [10, 11] aim to provide a quantum description of gravity. These theories only describe the gravitational interaction, but they do not comprise a theory of the other three fundamental gauge interactions. On the other hand, Grand Unified Theories (GUTs) (see [12–15] and also [16–18]) aim to provide a unified description of the strong, weak and electromagnetic interaction, but they do not include gravity. For a recent review about these models, see for example [19]. String theory is special in the sense that its goal is not only to provide a quantum theory of gravity, but also to reproduce the Standard Model or Grand Unified Theories. Therefore, it is one of the best candidate theories to truly provide a Theory of Everything. Moreover, it has found applications in many areas of physics beyond particle physics, such as cosmology [20, 21] or condensed matter physics via the AdS/CFT correspondence [22–24]. Also, string theory has found applications in mathematics, providing for example a proof of the Monstrous Moonshine conjecture [25, 26] or introducing mirror symmetry [27, 28], which allows to solve problems in enumerative algebraic geometry [29].

The fundamental idea behind string theory is to replace the point-like particle by a one-dimensional oscillating string of finite length $l_s \geq l_P = 1.6 \cdot 10^{-35} m$, where l_P is called the Planck length. The advantage of this replacement is that some divergences related to zero-size point-like particles occurring in quantum field theory are no longer present in string theory. Furthermore, the different oscillation modes of the string give rise to different types of particles. When moving through space-time, a point-like particle sweeps out a line, called worldline. A one-dimensional string sweeps out a two-dimensional surface when

moving in space-time, which is called worldsheet. The worldsheet can be parametrized by two coordinates τ and σ, where the first one is associated to a time-like coordinate and the second one corresponds to a space-like coordinate along the extent of the string. A string is represented by maps $X^\mu(\tau,\sigma)$, $\mu = 1 \dots d$ which map the worldsheet to the ambient space-time of dimension d. One can distinguish two types of strings depending on their boundary conditions:

- The closed string, which has periodic boundary conditions:

$$X^\mu(\tau, \sigma + 2\pi) = X^\mu(\tau, \sigma)\,. \tag{1.1}$$

  Closed strings are associated to the space-time metric and thus give rise to gravity.

- The open strings, which can have either Neumann boundary conditions, i.e. free endpoints:

$$\partial_\sigma X^\mu(\tau,\sigma)|_{\text{endpoints}} = 0\,, \tag{1.2}$$

  or Dirichlet boundary conditions, i.e. the endpoints are fixed to a subspace:

$$X^\mu(\tau,\sigma)|_{\text{endpoints}} = 0\,. \tag{1.3}$$

  The subspaces these open strings are attached to are called D_p -branes[1], which have p spatial dimensions and one dimension in time, so that they are p+1 dimensional objects. D-branes are generalizations of strings to higher dimensions; they are dynamical objects which have a tension and thus energy.
  Open strings with Neumann boundary conditions give rise to gauge bosons whereas open strings with Dirichlet boundary conditions lead amongst other to the fermionic matter states of the Standard Model, which are localized at the intersections of D-branes. We will come back to this in section 3.1.

The original so-called bosonic string theory includes only bosonic degrees of freedom. In order to include fermionic degrees of freedom, supersymmetry (SUSY) has to be introduced on the worldsheet [30], which in turn can lead to SUSY in space-time. The resulting theories are called superstring theories. The gauge bosons and their fermionic superpartners, the gauginos, form together a so-called vector multiplet. The fermionic matter states of the Standard Model and their bosonic partners form so-called chiral multiplets.

An introductory textbook to string theory and applications of string theory to cosmology and condensed matter is given by [31]. Other standard textbooks are given by [32–35] and [36, 37]. For an introductory textbook to branes, we refer the reader to [38].
This doctoral work focuses on string phenomenology, which is a subbranch of string theory. In the next section, we will sketch some important ideas and concepts used in string phenomenology.

1.2 General features of string phenomenology

Nowadays, there are in total five superstring theories: Type I string theory, Type IIA and Type IIB string theories, as well as two types of heterotic string theory. SUSY can be included consistently in string theory if the number of space-time dimensions is ten, meaning

[1] Note that the "D" in "D-brane" stands for Dirichlet, while "brane" is derived from "membrane".

that there are nine spatial dimensions and one time dimension. To allow for an effective four-dimensional Minkowski space, six of the spatial dimensions have to be "curled up", or in mathematical language, compactified. In other words, the space spanned by these six dimensions has to be small enough to avoid detection by modern particle accelerators. The way these extra dimensions are compactified has an impact on SUSY in the effective four-dimensional Minkowski space-time.

Type I string theory and the heterotic string theories preserve so-called minimal $\mathcal{N} = 1$ SUSY in ten dimensions, whereas the Type II string theories have $\mathcal{N} = 2$ SUSY. This means that in ten dimensions, two sets of supercharges are used, with each set containing sixteen supercharges. Each supercharge acts on one component of a Majorana-Weyl spinor, which has sixteen real components in ten dimensions.
The simplest choice of a compact space would be a six-dimensional torus, but this is not viable from a phenomenological point of view. Indeed, such a compactification does not break any symmetries associated to the supercharges, so all of them remain intact in four-dimensional Minkowski space-time. In four dimensions, a Weyl spinor has two complex components, so in total the 32 supercharges would be arranged in eight sets, giving $\mathcal{N} = 8$ SUSY when starting from Type II string theory. However, in order to have chiral fermions as observed in nature, $\mathcal{N}$ has to be equal to one or less in four dimensions. This means that in four dimensions, each boson of the Standard Model should have at most one fermionic superpartner, and each fermion comes with at most one bosonic superpartner.
Thus, instead of compactifying the extra dimensions on a six-torus, one has to turn to an internal space equipped with $SU(3)$ holonomy, which allows for $\mathcal{N} = 2$ SUSY in four dimensions after compactification. $SU(3)$ holonomy on a manifold means that if we parallel transport a vector along a closed loop on the manifold, the resulting vector is related to the initial vector by an element of the group $SU(3)$. A n-dimensional sphere for example has holonomy group $SO(n)$, and the holonomy group of the torus is equal to the identity. Compactification on a manifold with holonomy group bigger than $SU(3)$ would break SUSY completely. This is also undesirable as SUSY has many advantages, e.g. the cancellation of quadratically divergent contributions to the Higgs mass squared [39].
The link between holonomy and SUSY breaking is given by spinors. Indeed, the supercharges are related to spinors and are only well-defined globally if they are invariant under the holonomy group. In other words, the decomposition of the ten-dimensional spinors upon compactification should lead to covariantly constant spinors on the six-dimensional internal space, called Killing spinors. Consequently, the number of Killing vectors is related to the number of supersymmetries preserved in four dimensions. Original work on this topic is given by [40]. For a recent overview, see for instance [41].

On a complex manifold, one can locally introduce a metric whose only non-zero components are mixed, i.e. of the form $g_{i\bar{k}}$. Using this metric, we can introduce the following two-form written in local complex coordinates z^i and $\bar{z}^i$:

$$J_{1,1}^{\text{Kähler}} = \sum_{i,k=1}^{3} g_{i\bar{k}} dz^i \wedge d\bar{z}^k \,. \tag{1.4}$$

A manifold is Kähler if this two-form is closed,

$$dJ_{1,1}^{\text{Kähler}} = 0\,, \tag{1.5}$$

which is called Kähler two-form in that case. Subsequently, we can introduce the notion of Calabi-Yau threefolds, which satisfy the condition of $SU(3)$ holonomy. A Calabi-Yau threefold CY_3 of three complex dimensions or equivalently of six real dimensions is a compact Kähler manifold satisfying one of the following equivalent conditions:

- CY_3 is Ricci-flat, i.e. the Ricci-tensor is zero: $R_{ij}^{\text{Ricci}} = 0$.
- CY_3 has a Levi-Civita connection with $SU(3)$ holonomy.
- There exists a nowhere vanishing globally defined holomorphic three-form Ω_3.

Note that the three-form Ω_3 will be associated to the holomorphic volume form, which will be relevant in section 2.4.1. For more details on Calabi-Yau manifolds, see e.g. [42–44].

After compactification on the Calabi-Yau manifold, some of the SUSY is broken since Calabi-Yau spaces have $SU(3)$ holonomy, and one ends up with $\mathcal{N} = 2$ SUSY in four dimensions. This is still too much SUSY, so until the mid nineties, Type II string theories remained unpopular for model building as they seemed unable to give rise to a chiral matter content.

A breakthrough in Type II string theory model building was achieved by introducing the concept of orientifolding [45–49] and D-branes [50]. In Type IIA string theory, orientifolding consists in replacing a compactified space CY_3 by the quotient space $CY_3/\Omega\mathcal{R}$, where the orientifold projection $\Omega\mathcal{R}$ corresponds to parity on the string worldsheet (Ω) combined with an anti-holomorphic involution ($\mathcal{R}$) on the Calabi-Yau space. In our case, the action of $\mathcal{R}$ corresponds to complex conjugation $\mathcal{R} : X^i(\tau,\sigma) \to \overline{X^i(\tau,\sigma,)}$, $i = 1,2,3$ on the compact space, while worldsheet parity Ω reverses the orientation of a string: $\Omega : X^\mu(\tau,\sigma,) \to X^\mu(\tau,-\sigma,)$, $\mu = 1\ldots10$. By introducing this extra symmetry, SUSY is further broken from $\mathcal{N} = 2$ to $\mathcal{N} = 1$ after compactification. Indeed, it is a general property in physics that states which are not invariant under a given symmetry are projected out, meaning they disappear from the theory. Orientifolding projects half of the SUSY charges out.
The addition of this new symmetry leads to the appearance of new mathematical objects called orientifold planes (O-planes), which correspond to the fixed loci of the orientifold projection $\Omega\mathcal{R}$. These O-planes are charged under the so-called Ramond-Ramond fields, which will be introduced in section 2.3.1. The Ramond-Ramond fields arise from closed string oscillations, and the RR-charges of the O-planes can be considered as generalizations of the electromagnetic charge.

The space used for compactifying is a compact space without a boundary. Since Gauss' theorem states that the total charge on a compact space without boundary must be zero, the charges of the O-planes must be canceled by introducing D-branes, which have charges opposite to the O-planes. Charge neutrality is ensured by consistency equations named the "RR-tadpole cancellation conditions".
Other than orientifolding, the introduction of D-branes also breaks SUSY. A heuristic argument for this statement can be given as follows: In general, D-branes do not fill out the

entire ten-dimensional space, but only a subspace, which breaks translation invariance in ten dimensions. Since the translation generators are related to the supercharges via the relation $\left\{Q_\alpha, Q_\beta^\dagger\right\} = 2(\sigma^\mu)_{\alpha\beta}P_\mu$, the introduction of one D-brane breaks half of the SUSY, preserving the other half. The addition of a second D-brane can either preserve the same half of SUSY, or it can lead to further SUSY breaking. Model building requires the introduction of several D-branes, so the D-branes have to be chosen carefully in order to break the same half of SUSY. This is guaranteed by calibrating the submanifolds on which the D-branes are wrapped with respect to an appropriate p-form such that they are volume-minimizing. Indeed, just as the strings, the D-branes have a tension related to the energy. Thus, minimal volume corresponds to minimal tension and consequently to minimal energy. The conditions the D6-branes have to satisfy are called "special Lagrangian conditions". We will come back to this in more detail in section 2.4.1.

A major difference between Type IIA and Type IIB string theory consists in the fact that in the former theory, D_p-branes ($p = 1, \ldots 10$) with p even are present, whereas p is odd in the latter. In the present set-up, we are working with D6-branes, which fill out the four-dimensional Minkowski space-time and wrap three dimensions of the compact space, which will be referred to as "three-cycles".

An introductory textbook to string phenomenology is given by [51]. Previews on string phenomenology and model building on topics closely related to this work can be found in [52, 53]. Other publications focusing on various aspects of D-brane model building are given by [54–60]. The textbooks [61, 62] are excellent references for almost all mathematical aspects discussed in this section. The same holds true for the textbook [44] with focus on Calabi-Yau manifolds.

1.3 Layout of the thesis

In this section, I will briefly comment on the organization of my thesis and point out my personal contribution to this project. All notions mentioned in this section will be introduced properly in the respective chapters. This doctoral work is based on the two publications [63] and [64] and organized as follows:

Chapter 2 is an introductory chapter, where I introduce those results derived in [65] that are relevant for my doctoral thesis. These results will be used in the rest of my doctoral work, which focuses on string model building with intersecting D6-branes on the toroidal orbifold $T^6/(\mathbb{Z}_2 \times \mathbb{Z}_6 \times \Omega\mathcal{R})$. The expectation is that the orbifold $T^6/(\mathbb{Z}_2 \times \mathbb{Z}_6 \times \Omega\mathcal{R})$ with discrete torsion will provide ample possibilities for model building, since it includes the $\mathbb{Z}_6'$ group as a subgroup. The orbifold $T^6/(\mathbb{Z}_6' \times \Omega\mathcal{R})$ proved to be a particular fertile background for model building, see [66–75]. My personal contribution to this chapter consisted in checking some of the results presented in [65] and in defining the discrete shift of D6-branes on the first two-torus in accordance with the orientifold action as described in [76].

Chapter 3 is an introductory chapter to model building in Type IIA string theory with intersecting D6-branes. Also, I present the particle physics models relevant for this work

and their realization in the string theoretical context. This chapter is based on textbook knowledge. Moreover, it contains a collection of formulas used in my work. These have been derived in [77] and [72].

Chapter 4 is a preparatory chapter to chapter 5, which is about string model building. String model building on toroidal orbifolds involves important computational power, as it consists in testing all possible D6-branes configurations in order to find combinations which reproduce a realistic particle content. Hence, it is sensible to reduce the number of configurations to test as much as possible right from the start.
In the first section of chapter 4, I render evident symmetries between torus lattices in order to reduce the number of D6-brane configurations to test. I found that a symmetry pointed out in [66] for the background $\mathbb{Z}_6'$ is also valid in the background used in my doctoral work, at least for the so-called **a**-type lattices. I generalized this symmetry to include the **b**-type lattices. I performed this analysis analytically, following the procedure presented in [76].
In the second section of chapter 4, I present the results of a computer code I wrote on Mathematica to find all three-cycles apt to support SUSY D6-branes. Although I wrote the code on my own, I followed the instructions of my supervisor Jun.- Prof. Dr. Gabriele Honecker to approach the detection of D6-branes which preserve SUSY. The D6-branes found can be distinguished into two types of D6-branes: Those that are SUSY for every value of the complex structure parameter ϱ and those that are SUSY only for fixed values of ϱ.

Chapter 5 introduces the first steps in string model building on $T^6/(\mathbb{Z}_2 \times \mathbb{Z}_6 \times \Omega\mathcal{R})$ and follows our publication [63]. The focus of this chapter lies on the classification of D6-branes according to several criteria, including the type of gauge group supported by the D6-branes, the rigidity of the D6-branes and the absence/presence of phenomenologically unwanted matter states transforming in (anti)symmetric representations.
In the first section, I analyzed the type of supported gauge group and found that the results for the **b**-type lattices are equivalent to the ones computed in [76, 78], while the results for the **a**-type lattices were presented for the first time in the context of this doctoral work. This part of the analysis was done analytically.
The next two sections focus on the remaining two classification criteria. The analysis in these sections was prepared analytically, but needed to be completed and cross-checked with computer scans. The last section contains the first steps in model building and concentrates on finding pairs of D6-branes intersecting in the correct way to produce three generations of a first set of matter states. This analysis cannot be done analytically, but needs large computer scans. Our approach was as follows: Dr. Wieland Staessens and I both wrote computer codes independently from each other. Subsequently, we used both codes on the first scans in order to cross-check the results. In the following, I used my own codes to derive the remaining results, while Dr. Staessens and my supervisor guided the analysis. Since there are two different methods to compute the intersection numbers of D6-branes, the first one given by the orbifold-invariant approach and the second one proceeding orbifold-sector per orbifold-sector, I encoded both methods in Mathematica in order to cross-check my results, for part of the computer scans.

Chapter 6 and chapter 7 are based on both publications [63] and [64] and focus on the search for particle physics models presenting a full three-generation spectrum and satisfying

all consistency conditions such as the RR-tadpole cancellation conditions. We separated the models into two types: the so-called ϱ-dependent models and the ϱ-independent models.
The ϱ-dependent models producing a correct particle spectrum come in vast numbers, which makes the detection of models satisfying all the consistency conditions difficult. The computer scans involved in this part of the work were the most time- and processing power-consuming ones. In order to speed up the analysis, I acquired a custom-built PC with twelve processors and parallelized my codes. The longest computer scan took six days. Unfortunately, the analysis did not yield any globally consistent models although I had it running for months in total. I finally decided to suspend the examination and leave it for future work. In this thesis, I provide some results concerning the fruitless search for globally consistent ϱ-dependent models in sections 6.2.3 and 7.2.2, which have not been included in our publications.
The quite reduced number of possibilities for ϱ-independent models at first seemed not to yield three generations of particles. However, I managed to dig out configurations of D6-branes we had at first not considered, and which can be used for model building purposes only with a very restricted set of parameters. Surprisingly, these restricted ϱ-independent models did not only provide a realistic three-generation particle content, but they also gave rise to globally consistent models. Even more astonishing, they gave rise to hundred-thousands of consistent models, ranging from Pati-Salam models over left-right symmetric models to the Standard Model.
As a final remark, note that the data of all models presented explicitly have been checked numerically and analytically by both Dr. Staessens and me.

Chapter 8 is based on our second publication [64] and concentrates on the phenomenological aspects of the globally consistent models found in the previous chapters. More concretely, it focuses on the search for discrete $\mathbb{Z}_n$-symmetries, following the procedure presented in [78]. My supervisor derived analytically explicit expressions for the equations determining the existence of massless $U(1)$ combinations and discrete $\mathbb{Z}_n$-symmetries. I cross-checked these by hand. The establishing of these equations needs the reduction of linearly dependent three-cycles (about $\mathcal{O}(10^2)$) to linearly independent three-cycles, which number 16. I performed the reduction numerically in order to provide a cross-check for the analytical methods used by Dr. Staessens and my supervisor. In our publication [64], the analytical method was illustrated, but in this thesis, I will rather briefly comment on the numerical procedure.

Chapter 9 concentrates on further phenomenological properties of the globally consistent models, namely the existence of cubic couplings such as Yukawa couplings. This chapter is based on our second publication [64], though I provide more details about the computation here.
This analysis can be done completely analytically, though I used the software *GeoGebra* to facilitate the computation. The cubic couplings were derived by both Dr. Staessens and me in order to cross-check the results. The development of the techniques allowing to locate the matter states exactly at $\mathbb{Z}_2$-fixed points was done by my supervisor and Dr. Staessens, as given in [64]. Since the procedure is quite technical, I will not present it in this doctoral work but only use the results.
The Yukawa couplings given in section 9.2.4 correspond to unpublished results.

Chapter 10 corresponds to the conclusion and contains two sections. In the first section, I give a summary of the doctoral thesis and complement it with discussions. The second section provides an outlook indicating several directions along which the work of this thesis could be expanded and deepened.

Appendix The appendix is split into two parts: the first part contains details about the tools used in this work and illustrates their use by providing explicit examples of computations and constructions, in order to render these more transparent. The examples include the explicit construction of fractional three-cycles and the computation of beta-function coefficients.
The second part of the appendix contains additional results compared to those given in the main text and details about their derivation. I put these into the appendix in order to avoid overloading the main part. More precisely, it provides an example of an alternative definition for the hypercharge, an addendum to chapter 8 and additional results concerning SUSY two-cycles living on the second and third two-torus, which are related to section 4.2.

Finally, I want to point out that most of the tables given in this work are taken and adapted from our publications [63] and [64]. The same holds true for figures 4.1 and 5.1. All other figures appearing in this work were produced by myself in the context of this doctoral thesis.

Chapter 2

Type IIA string theory on the $T^6/(\mathbb{Z}_2 \times \mathbb{Z}_6 \times \Omega\mathcal{R})$ orientifold

We will start this chapter with an introductory section about orbifolds and toroidal orbifolds in particular. In the second section, we will describe the purely geometrical aspects of the toroidal orbifold used in this work. The string theoretical aspects are considered in the third section of this chapter, where we introduce Type IIA string theory on the particular background used in the present set-up. The chapter ends with a fourth section discussing consistency conditions any particle physics model has to satisfy in our set-up. Discussions of derivations not performed in the context of this doctoral work will be kept at a minimum. Instead, we provide the final results and indicate the literature where the details of the computations can be found.

2.1 General aspects of toroidal orbifolds

Manifolds such as smooth Calabi-Yau spaces CY_3 are difficult to use for model building purposes because the global metric is unknown in general. This leads to the fact that the string equations of motions cannot be solved explicitly. Hence, instead of using Calabi-Yau spaces, we will use orbifolds in this work. If $\mathcal{M}$ is a manifold and if Γ is a discrete group acting on $\mathcal{M}$, then the coset or quotient space $\mathcal{M}/\Gamma$ is called an orbifold. Two points on $\mathcal{M}$ linked by the action of Γ are identified. Orbifolds are well-suited for model building purposes, for if the initial space $\mathcal{M}$ is flat, they correspond to flat spaces except at isolated singular points corresponding to the fixed points of Γ, where the curvature becomes infinite. These singular points can in general be resolved by blowing them up or by deforming them, which leads to a class of smooth Calabi-Yau spaces.
An example of an orbifold is given by the coset space $\mathbb{C}/\mathbb{Z}_3$, where the action of $\mathbb{Z}_3$ on $\mathbb{C}$ corresponds to a rotation by $2\pi/3$ on the complex coordinate z, i.e. $z \to e^{\frac{2i\pi}{3}} z$. The coset space corresponds to a cone with the singular point situated at the origin. The opening angle at the base of the cone equals $60°$, as illustrated in figure 2.1.

Toroidal orbifolds are of particular interest to string theorists. On toroidal orbifolds, the string equations of motion can be solved explicitly in order to obtain the massless spectrum, and the toolkit of conformal field theory (CFT) methods is well developed. These features render toroidal orbifolds one of the best understood backgrounds for string theory and its

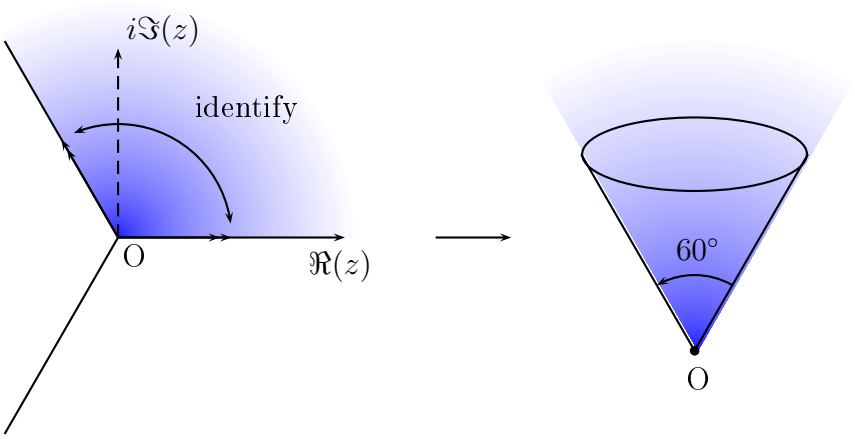

Figure 2.1: Construction of the cone $\mathbb{C}/\mathbb{Z}_3$ out of the complex plane $\mathbb{C}$. On the left, a fundamental domain in $\mathbb{C}$ is defined corresponding to one third of the complex plane as illustrated in blue. The identification of the borders of the fundamental domain results in the cone on the right.

compactifications.

Original work on orbifold compactifications is given by [79–81]. For a review on string theory on orbifolds see for instance [82]. Some general references on CFT are, e.g. [83–85].

The compact internal space for four-dimensional models of string theory is six-dimensional, thus a six-dimensional torus seems to be the perfect candidate for the initial space $\mathcal{M}$. In order to simplify the analysis, it is generally assumed that the six-torus is factorisable[1] and can be written as a product of three two-dimensional tori: $T^6 = T^2_{(1)} \times T^2_{(2)} \times T^2_{(3)}$. A two-dimensional torus can easily be described by the complex plane $\mathbb{C}$ divided by a lattice $\Lambda = \{n\lambda_1 + m\lambda_2 | n, m \in \mathbb{Z},\ \lambda_1, \lambda_2 \in \mathbb{C}\}$ such that $T^2 = \mathbb{C}/\Lambda$. In the case of a two-dimensional torus T^2, we have two generators $\lambda_1, \lambda_2 \in \mathbb{C}$ in the lattice Λ, so we have two identifications $z \sim z + \lambda_1$ and $z \sim z + \lambda_2$. These identifications can be rescaled by a factor $1/\lambda_1$, leading to the identifications $z \sim z + 1$ and $z \sim z + \rho$, with $\rho = \lambda_2/\lambda_1$. The complex parameter ρ is called the complex structure of the lattice Λ. The fundamental domain consists of all nonequivalent points. By gluing together opposite sides of the fundamental domain, a cylinder is obtained, which is closed into a torus once the two remaining sides are identified, see figure 2.2.

A simple example of a toroidal orbifold is given by the quotient space $T^2/\mathbb{Z}_2$, where the action of $\mathbb{Z}_2$ on T^2 corresponds to a rotation by an angle π in the complex plane $z \to e^{i\pi}z$, with $z \in \mathbb{C}$. Two points on T^2 related by the $\mathbb{Z}_2$-action are identified, and the resulting space is the so-called "four-pillow" [90]. The four singular points located at the four corners of this "four-pillow" appear as the fixed points under the action of $\mathbb{Z}_2$ on T^2. They are indicated in the fundamental domain of T^2, see figure 2.3.

Since the six-dimensional torus T^6 is a flat space, the holonomy group of a toroidal orbifold of the form T^6/Γ is precisely Γ. Restricting ourselves to Abelian point groups, the group Γ is of the form $\mathbb{Z}_N$ or $\mathbb{Z}_N \times \mathbb{Z}_M$, with fixed values for N, M as given for example in [42, 91], in order to obtain the correct amount of SUSY in four dimensions. Products of more than two $\mathbb{Z}_N$'s are not contained in $SU(3)$ anymore and thus do not lead to the right amount of

[1]Note that also non-factorisable six-tori have been used for string model building. Certain toroidal orbifolds with for example $\Gamma = \mathbb{Z}_7, \mathbb{Z}_8, \mathbb{Z}_{12}$ come with a complex structure ρ which does not allow a complete factorization. For more details, see for example [86, 87] and [88, 89]

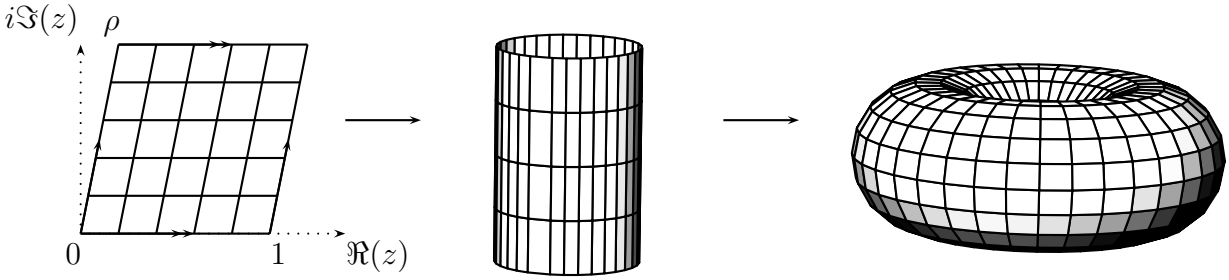

Figure 2.2: Construction of a two-dimensional torus out of the complex plane. The first step consists in gluing together two opposite sides of the fundamental domain along the arrows. The resulting space is a two-dimensional hollow cylinder. In a second step, the two ends of the cylinder are glued together, which yields a two-torus.

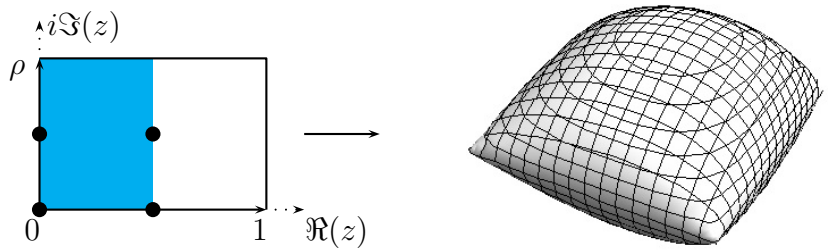

Figure 2.3: The figure on the left depicts the fundamental domain of a rectangular two-torus T^2 and the four singular points which arise after dividing out $\mathbb{Z}_2$. The area in blue corresponds to the fundamental domain of the orbifold $T^2/\mathbb{Z}_2$. The resulting space is the four-pillow indicated in the figure on the right side.

SUSY. In the present doctoral work I will focus on the orbifold $T^6/(\mathbb{Z}_2 \times \mathbb{Z}_6)$, where each of the discrete group factors acts on two of the three two-dimensional tori $T^2_{(i)}$. For instance, $\mathbb{Z}_2$ can be taken to act on the first and the second torus, while $\mathbb{Z}_6$ acts on the second and the third torus. Details about the geometry are given in the next section.
The advantage of model building on toroidal orbifolds of the form $T^6/(\mathbb{Z}_2 \times \mathbb{Z}_{2M})$ compared to orbifolds of the form $T^6/\mathbb{Z}_N$ is that the former allow for rigidity of the D6-branes, which implies the absence of position moduli. This is an advantage, as these position moduli correspond to scalar fields, which together with their fermionic superpartners form chiral multiplets transforming in the adjoint representation of the gauge group supported by the D6-brane. In the particle physics models considered in this work, chiral multiplets transforming in the adjoint representation of non-Abelian gauge groups generally do not appear, see section 3.2. Thus, the scalar degrees of freedom associated to the position moduli are unwanted from a phenomenological point of view. We will come back to this later in sections 2.3.2 and 3.1. Moreover, toroidal orbifolds of the form $T^6/(\mathbb{Z}_2 \times \mathbb{Z}_{2M})$ allow for a phenomenon called discrete torsion, which enhances the possibilities for model building. We will come back to the issue of discrete torsion in section 2.2.4. Similar work was already done on the following backgrounds:

- $T^6/(\mathbb{Z}_2 \times \mathbb{Z}_2)$ with discrete torsion: On this background, Pati-Salam models with a four-generation particle spectrum have been found [92]. These have been given as

examples, as the focus of [92] did not include a systematic and exhaustive search for realistic particle physics models. Still, to our best knowledge, no global[2] three-generation Minimal Supersymmetric Standard Model (MSSM) has been found on this background with discrete torsion so far.

- $T^6/(\mathbb{Z}_2 \times \mathbb{Z}_{2M})$ with discrete torsion: An analysis of mathematical aspects of these backgrounds, such as the SUSY conditions, the RR-tadpole cancellation conditions or the lattice of three-cycles, has been given in [65, 72].

- $T^6/(\mathbb{Z}_2 \times \mathbb{Z}_6')$ with discrete torsion[3]: This background allows for classes of three-generation global Pati-Salam models, as was found in [76, 93]. Concerning three-generation MSSM-like models, only local ones were found.

One of the reasons to choose precisely $M = 3$ in $T^6/(\mathbb{Z}_2 \times \mathbb{Z}_{2M})$ is that previous work showed that orbifolds containing a $\mathbb{Z}_3$ subgroup seemed to be particularly apt to produce three generations of particles, which corresponds to the number of generations wanted in the particle models we are considering, see section 3.2. However, this is an empirical observation and not a strict no-go theorem derived from fundamental principles. For example, the works on the orbifolds $T^6/(\mathbb{Z}_6 \times \Omega\mathcal{R})$ in [94–96, 67] and $T^6/(\mathbb{Z}_6' \times \Omega\mathcal{R})$ in [66–71] yielded three-generation models, whereas the orbifolds $T^6/(\mathbb{Z}_4 \times \Omega\mathcal{R})$ in [97] and $T^6/(\mathbb{Z}_2 \times \mathbb{Z}_4 \times \Omega\mathcal{R})$ in [98, 99, 95, 65] did not allow such constructions.
The orbifold $T^6/(\mathbb{Z}_6' \times \Omega\mathcal{R})$ proved to be a particular fertile background for model building, so that its study has been extended to the associated low-energy field theory, see [67, 72–75]. Based on the pioneering work given in [100], the detection of discrete gauge symmetries in orbifold models was investigated for the first time in [78], and the search for Peccei-Quinn symmetries and axionic dark matter was launched in [101, 102].
For a summary of the work performed on these orbifolds within our working group, see [103].

2.2 Geometry of $T^6/(\mathbb{Z}_2 \times \mathbb{Z}_6 \times \Omega\mathcal{R})$

2.2.1 The orbifold action and the orientifold projection on T^6

The action of $\mathbb{Z}_2 \times \mathbb{Z}_6$

The group $\mathbb{Z}_2 \times \mathbb{Z}_6$ has two generators[4] whose action is given by:

$$\theta : z_i \to e^{2\pi i v_i} z_i \text{ with } \vec{v} = \frac{1}{2}(1, -1, 0)\,, \tag{2.1}$$

[2] A model is called global if it satisfies all the consistency conditions. We will come back to this in section 2.4.3.

[3] We have different $\mathbb{Z}_6$-generators for the different orbifolds:

$$\begin{aligned}
&\mathbb{Z}_6 : && \vec{w} = \tfrac{1}{6}(-2, 1, 1)\,,\\
&\mathbb{Z}_6' : && \vec{w} = \tfrac{1}{6}(1, 2, -3)\,,\\
&\mathbb{Z}_2 \times \mathbb{Z}_6' : && \vec{v} = \tfrac{1}{2}(1, -1, 0) \text{ and } \vec{w} = \tfrac{1}{6}(-2, 1, 1)\,,\\
&\mathbb{Z}_2 \times \mathbb{Z}_6 : && \vec{v} = \tfrac{1}{2}(1, -1, 0) \text{ and } \vec{w} = \tfrac{1}{6}(0, 1, -1)\,.
\end{aligned}$$

[4] The orbifold actions need to preserve four-dimensional $\mathcal{N} = 1$ SUSY, which puts constraints on them. The allowed actions were derived in [79, 80].

$$\omega : z_i \to e^{2\pi i w_i} z_i \text{ with } \vec{w} = \frac{1}{6}(0, 1, -1)\,, \tag{2.2}$$

where z^i with $i = 1, 2, 3$ are the complex coordinates on the three complex directions of the three two-tori $T^2_{(i)}$. Since we mod out the action $\mathbb{Z}_2 \times \mathbb{Z}_6$, the lattice Λ has to be invariant under the action of these group factors, i.e. $\mathbb{Z}_2 \times \mathbb{Z}_6$ has to act cristallographically[5] on the lattice: $\lambda \in \Lambda \Rightarrow \theta^n \omega^m \lambda \in \Lambda,\ n = 0, 1,\ m = 0, \ldots 5$.
Invariance under the action of $\mathbb{Z}_3 \subset \mathbb{Z}_6$ forces the basis lattice vectors of the second and third torus to be of equal length and fixes the angle between them to 60° or 120°, which is equivalent. However, on the first torus, only a $\mathbb{Z}_2$-action is present, leaving the shape of the lattice of the first torus unfixed. This is illustrated in figure 2.4.

The action of $\Omega\mathcal{R}$

On top of the action of $\mathbb{Z}_2 \times \mathbb{Z}_6$, there is also the action of the so-called orientifold projection $\Omega\mathcal{R}$ with $\mathcal{R}$ acting as complex conjugation $z_i \to \bar{z}_i$ in our case. Worldsheet parity Ω only acts on the orientation of the strings and has no influence on the geometry. Still, we will refer to the orientifold action by the symbol $\Omega\mathcal{R}$ although only the $\mathcal{R}$ is relevant for the geometrical considerations.
Invariance of the lattice under $\Omega\mathcal{R}$ implies that the $\Omega\mathcal{R}$-invariant direction, i.e. here the real axis, must be chosen to lie either along one of the basis lattice vectors or along the diagonal of the lattice on the second and third torus. We refer to the first case as the **A**-type lattice and to the second case as the **B**-type lattice.
On the first two-torus $T^2_{(1)}$, the orientifold action forces the fundamental domain to be either rectangular, called **a**-type lattice, or tilted, called **b**-type lattice. The real axis has to lie along a basis lattice vector in case of the **a**-type lattice and along $\pi_1 - \frac{1}{2}\pi_2$ in case of the **b**-type lattice, where π_1 and π_2 are the basis lattice vectors of $T^2_{(1)}$. This is parametrized by $\pi_1 - b\pi_2$ with $b = 0$ for the **a**-type lattice and $b = \frac{1}{2}$ for the **b**-type lattice. The orientifold action thus constrains the shape of the first two-torus, truncating its complex structure ρ down to a real parameter. This real parameter corresponds to the ratio of the length of the two basis lattice vectors: $\varrho \equiv \sqrt{3}\frac{R_2}{R_1}$, where R_1 and R_2 are the two circumferences of the two-torus as depicted in figure 2.4. The factor $\sqrt{3}$ is introduced in the definition of ϱ for later convenience. Note that the real parameter ϱ introduced here differs from the complex parameter ρ introduced in the previous section. In the case of the rectangular lattice for example, they are related by $\rho = i\varrho/\sqrt{3}$. Still, we will refer to the real parameter ϱ as complex structure modulus.
There are thus a priori six different lattice combinations given by **aAA, bAA, aAB, bAB, aBB** and **bBB**. Note that the lattice **a**/**bBA** would be equivalent to the lattice **a**/**bAB**.

2.2.2 Hodge numbers

In general, the metric of a Calabi-Yau space or toroidal orbifold can be deformed. The parameters describing the deformations are called moduli in string compactifications. In case of Calabi-Yau threefolds or six-dimensional toroidal orbifolds, the metric can be deformed in two ways: either by varying its complex structure, related to the shape of the space, or its

[5]The various lattices permitted by the orbifold actions have been derived in [104]. The actions of all allowed $\mathbb{Z}_N$ and $\mathbb{Z}_N \times \mathbb{Z}_M$ generators and the corresponding lattices can be found e.g. in [42, 91, 82].

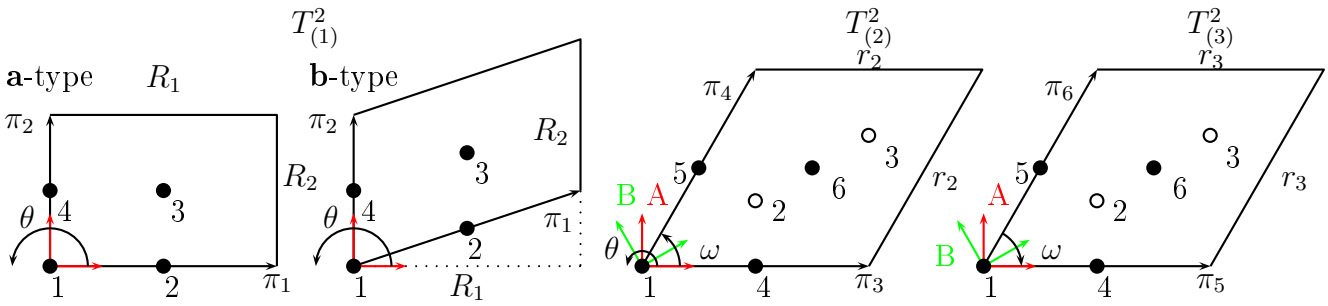

Figure 2.4: The action of $\mathbb{Z}_2 \times \mathbb{Z}_6 \times \Omega\mathcal{R}$ fixes the shape of the six-torus to the root lattices of $SU(2)^2 \times SU(3) \times SU(3)$, with one real complex structure modulus $\varrho \equiv \sqrt{3}R_2/R_1$ inherited from the first two-torus $T^2_{(1)}$, and two possible choices for the $\Omega\mathcal{R}$-invariant direction per two-torus. The black points labeled by 1,2,3,4 on the first torus and by 1,4,5,6 on the second and third torus are fixed points of the $\mathbb{Z}_2$-action. The points denoted by 2,3 on the second and third torus are fixed points under $\mathbb{Z}_3$. In the present context, only $\mathbb{Z}_2$-fixed points are relevant for D6-brane model building. We will comment on this issue briefly in section 2.3.2. The $\mathbb{Z}_6$-action is trivial on the first torus and cyclically permutes three $\mathbb{Z}_2$-fixed points on the second and third torus: $1 \overset{e^{\pi i/3}}{\circlearrowleft}, 4 \overset{e^{\pi i/3}}{\to} 5 \overset{e^{\pi i/3}}{\to} 6 \overset{e^{\pi i/3}}{\to} 4$. The $\mathbb{Z}_3$-fixed points are permuted under the $\mathbb{Z}_6$ action $2 \overset{e^{\pi i/3}}{\leftrightarrow} 3$. The orientifold projection $\Omega\mathcal{R}$ acts on the fixed points on the first two-torus as follows: $2 \overset{\mathcal{R}}{\circlearrowleft}, 3 \overset{\mathcal{R}}{\circlearrowleft}, 4 \overset{\mathcal{R}}{\circlearrowleft}$ in case of the **a**-type lattice and on the **b**-type lattice as: $4 \overset{\mathcal{R}}{\circlearrowleft}, 2 \overset{\mathcal{R}}{\leftrightarrow} 3$. On the second and third two-torus, $\Omega\mathcal{R}$ permutes the fixed points as follows: $4 \overset{\mathcal{R}}{\circlearrowleft}, 5 \overset{\mathcal{R}}{\leftrightarrow} 6$ in case of the **A**-type lattice and $4 \overset{\mathcal{R}}{\leftrightarrow} 5, 6 \overset{\mathcal{R}}{\circlearrowleft}$ in case of the **B**-type lattice. The basis lattice vectors on $T^2_{(i)}$ $(i = 1, 2, 3)$ are denoted by π_{2i-1} and π_{2i}.

Kähler structure, related to the size of the space. The former corresponds to a three-form, the latter to a two-form.

Two-forms can be holomorphic $\omega^{2,0} = dz^i \wedge dz^j$, antiholomorphic $\omega^{0,2} = d\bar{z}^i \wedge d\bar{z}^j$ or of mixed type, e.g. $\omega^{1,1} = dz^i \wedge d\bar{z}^j$, with $i, j = 1, 2, 3$ corresponding to the three complex directions. The upper index on the forms indicates the number of holomorphic and antiholomorphic components, respectively. The same holds true for the three-forms. The so-called Hodge numbers count the number of complex (r, s)-forms, and they can be arranged into the Hodge diagram below :

$$\begin{array}{ccccccc} & & h^{0,0} & & & & \\ & h^{1,0} & & h^{0,1} & & & \\ h^{2,0} & & h^{1,1} & & h^{0,2} & & \\ h^{3,0} & & h^{2,1} & & h^{1,2} & & h^{0,3} \\ & h^{3,1} & & h^{2,2} & & h^{1,3} & \\ & & h^{3,2} & & h^{2,3} & & \\ & & & h^{3,3} & & & \end{array} \overset{CY_3}{=} \begin{array}{ccccccc} & & 1 & & & & \\ & 0 & & 0 & & & \\ 0 & & h^{1,1} & & 0 & & \\ 1 & & h^{2,1} & & h^{2,1} & & 1 \\ & 0 & & h^{1,1} & & 0 & \\ & & 0 & & 0 & & \\ & & & 1 & & & \end{array} \tag{2.3}$$

where we have, in case of a Kähler manifold, the symmetries of complex conjugation $h^{p,q} = h^{q,p}$ and Poincaré duality $h^{p,q} = h^{m-q,m-p}$ with $m = 3$ corresponding to three complex dimensions. In case of Calabi-Yau threefolds or toroidal orbifolds, only two Hodge numbers are independent, namely $h^{2,1}$ and $h^{1,1}$. The three form given by $h^{3,0}$ corresponds to the

holomorphic volume three-form Ω_3.
In general, a p-form ω can couple to a p-dimensional subspace c via the duality relation given by:

$$(c, \omega) \to \int_c \omega \,. \tag{2.4}$$

In our case, the two-forms couple to two-cycles and the three-forms couple to three-cycles. The number of independent two-dimensional and three-dimensional submanifolds (i.e. two- and three-cycles, respectively) is given by the Betti numbers

$$\begin{aligned} b^2 &= h^{2,0} + h^{1,1} + h^{0,2} \quad \overset{CY_3}{=} \quad h^{1,1} \,, \\ b^3 &= h^{3,0} + h^{2,1} + h^{1,2} + h^{0,3} \quad \overset{CY_3}{=} \quad 2 + 2h^{2,1} \,. \end{aligned} \tag{2.5}$$

The Hodge numbers $h^{p,q}$ correspond to the dimensions of the Dolbeault cohomology groups $H^{p,q}(M, \mathbb{C})$ and the Betti numbers b^r correspond to the dimensions of the homology groups $H_r(M, \mathbb{R})$. For a more detailed discussion on Hodge numbers, see for example [61].

In case of orbifolds, the Hodge numbers count orbifold-invariant two- and three-forms. We have a so-called untwisted sector, which contains the differential forms and cycles inherited from the underlying six-torus T^6, and the so-called twisted sectors. The twisted sectors refer to cycles containing exceptional divisors. This will become clearer in section 2.2.4 when we provide explicit expressions for the twisted three-cycles. The Hodge numbers contain information about both untwisted and twisted sectors. In case of the untwisted sector, the Hodge numbers can be easily derived. Indeed, we have three two-forms $dz^i \wedge d\bar{z}^i$, $i = 1, 2, 3$ invariant under all orbifold actions. These are associated to the volumes of the three two-tori $T^2_{(i)}$, $i = 1, 2, 3$. On the other hand, apart from the holomorphic volume three-form, we only have one three-form (and its complex conjugate) invariant under the orbifold actions, namely $d\bar{z}^1 \wedge dz^2 \wedge dz^3$. The complex structure modulus encountered in the previous section is related to this three-form.
The calculation of the Hodge numbers in the twisted sectors is more involved. We will illustrate the computation by counting orbifold-invariant combinations of exceptional cycles in section 2.2.4, but we refer the interested reader to [91, 42, 105] for more details. The final results with and without discrete torsion can be found e.g. in [65] and are reproduced here in table 2.1. The parameter η appearing in table 2.1 characterizes whether discrete torsion is switched on ($\eta = -1$) or not ($\eta = 1$). We will come back to this in section 2.2.4.

Hodge numbers per twist sector on $T^6/(\mathbb{Z}_2 \times \mathbb{Z}_6)$, with and without discrete torsion										
torsion	Hodge numbers	1	ω	ω^2	ω^3	θ	$\theta\omega$	$\theta\omega^2$	$\theta\omega^3$	total
			$(0, \frac{1}{6}, -\frac{1}{6})$	$(0, \frac{1}{3}, -\frac{1}{3})$	$(0, \frac{1}{2}, -\frac{1}{2})$	$(\frac{1}{2}, -\frac{1}{2}, 0)$	$(\frac{1}{2}, -\frac{1}{3}, -\frac{1}{6})$	$(\frac{1}{2}, -\frac{1}{6}, -\frac{1}{3})$	$(\frac{1}{2}, 0, -\frac{1}{2})$	
$\eta = 1$	$h^{1,1}$	3	2	8	6	8	8	8	8	51
	$h^{2,1}$	1	0	2	0	0	0	0	0	3
$\eta = -1$	$h^{1,1}$	3	0	8	0	0	4	4	0	19
	$h^{2,1}$	1	2	2	6	4	0	0	4	19

Table 2.1: Hodge numbers of the $T^6/(\mathbb{Z}_2 \times \mathbb{Z}_6)$ orbifold for each twisted sector, with and without discrete torsion. The parameter η characterizes whether discrete torsion is switched on ($\eta = -1$) or not ($\eta = 1$).

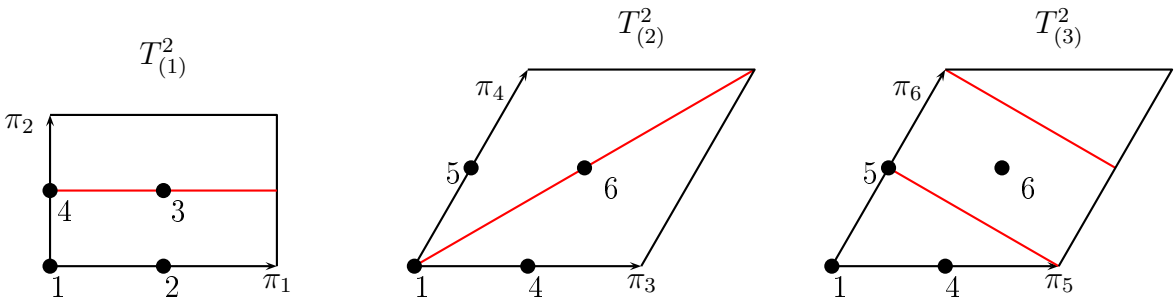

Figure 2.5: Torus three-cycle wrapping on the $T^2/(\mathbb{Z}_2 \times \mathbb{Z}_6)$ orbifold with wrapping numbers $(n^1, m^1; n^2, m^2; n^3, m^3) = (1, 0; 1, 1; 2, -1)$.

In sections 2.2.3 and 2.2.4, we will provide explicit expressions for the three-cycles arising in the untwisted sector and each $\mathbb{Z}_2$-twisted sector, as they have been established for the first time in [65]. Also, we will examine the orientifold action on the cycles. The two-forms can be classified as $\Omega\mathcal{R}$-odd and $\Omega\mathcal{R}$-even two-forms, which needs to be taken into account. The results are given and discussed in section 2.3.1.

2.2.3 Bulk three-cycles

We will first focus on the three-cycles arising from the untwisted sector, i.e. the three-cycles inherited from the underlying six-torus, which we call bulk three-cycles. Since the six-torus is factorisable, a three-cycle can be written as a product of three one-cycles π_{2i-1}, π_{2i}, $i = 1, 2, 3$ with coefficients (n^j, m^j), $j = 1, 2, 3$

$$\Pi^{\text{torus}} = \bigotimes_{i=1}^{3} (n^i \pi_{2i-1} + m^i \pi_{2i}) \,. \tag{2.6}$$

The coefficients (n^j, m^j) are referred to as torus wrapping numbers. They indicate the number of times the cycle winds around the torus before it closes on itself, see figure 2.5.

On the first torus in figure 2.5, the cycle is shifted, i.e. it does not pass through the origin.[6]

The expression given in (2.6) is not invariant under the orbifold action. In order to obtain orbifold-invariant three-cycles, the sum over all orbifold images has to be taken:

$$\Pi^{\text{bulk}} = 4 \sum_{m=0}^{2} \omega^m \left[\bigotimes_{i=1}^{3} (n^i \pi_{2i-1} + m^i \pi_{2i}) \right] . \tag{2.7}$$

The θ-action maps the cycle to itself and gives an overall factor of two. The ω^k-action with $k = 3, 4, 5$ maps the sum above onto itself and gives another overall factor of two, leading to a total factor of four in front of the sum. The Betti numbers indicate the number of independent three-cycles: $b^3_{\text{Untwisted}} = h^{3,0}_U + h^{2,1}_U + h^{1,2}_U + h^{0,3}_U = 1 + 1 + 1 + 1 = 4$. We have thus four independent three-cycles. A basis of orbifold-invariant three-cycles is for example

[6] Note that we consider only discrete shifts by half a lattice vector, such that the three-cycle always passes through $\mathbb{Z}_2$-fixed points. We will come back to this point in section 3.1.

given by:

$$\begin{aligned}
\rho_1 \equiv 4(1+\omega+\omega^2)\pi_{135} &= 4(\pi_{135}+\pi_{1,4,5-6}+\pi_{1,4-3,-6}) \\
&= 4(\pi_{135}+\pi_{145}-\pi_{146}-\pi_{146}+\pi_{136}) \\
&= 4(\pi_{135}+\pi_{145}-2\pi_{146}+\pi_{136}), \\
\rho_2 \equiv 4(1+\omega+\omega^2)\pi_{136} &= 4(2\pi_{136}+2\pi_{145}-\pi_{146}-\pi_{135}), \\
\rho_3 \equiv 4(1+\omega+\omega^2)\pi_{235} &= 4(\pi_{235}+\pi_{245}-2\pi_{246}+\pi_{236}), \\
\rho_4 \equiv 4(1+\omega+\omega^2)\pi_{236} &= 4(2\pi_{236}+2\pi_{245}-\pi_{246}-\pi_{235}),
\end{aligned} \tag{2.8}$$

where π_{ijk} or $\pi_{i,j,k}$ corresponds to the tensor product $\pi_i \otimes \pi_j \otimes \pi_k$. The next step consists in determining the intersection numbers between these bulk cycles. The intersection numbers are important for model building purposes since they are associated to the number of generations of particles. This will be discussed in more detail in sections 3.1 and 3.2.1. Using the generic torus intersection number between two torus three-cycles Π_a^{torus} and Π_b^{torus} on T^6 defined by

$$\Pi_a^{\text{torus}} \circ \Pi_b^{\text{torus}} \equiv -\prod_{i=1}^{3}(n_a^i m_b^i - m_a^i n_b^i)\,, \tag{2.9}$$

the intersection numbers of the bulk cycles can be calculated as follows:

$$\begin{aligned}
\rho_1 \cdot \rho_3 =& \frac{1}{12}4(\pi_{135}+\pi_{145}-2\pi_{146}+\pi_{136})\cdot 4(\pi_{235}+\pi_{245}-2\pi_{246}+\pi_{236}) \\
=& \frac{16}{12}(\underbrace{\pi_{135}\cdot\pi_{235}}_{=0}+\underbrace{\pi_{135}\cdot\pi_{245}}_{=0}-\underbrace{\pi_{135}\cdot 2\pi_{246}}_{=-2}+\underbrace{\pi_{135}\cdot\pi_{236}}_{=0}) \\
&+\frac{16}{12}(\underbrace{\pi_{145}\cdot\pi_{235}}_{=0}+\underbrace{\pi_{145}\cdot\pi_{245}}_{=0}-\underbrace{\pi_{145}\cdot 2\pi_{246}}_{=0}+\underbrace{\pi_{145}\cdot\pi_{236}}_{=1}) \\
&-\frac{32}{12}(\underbrace{\pi_{146}\cdot\pi_{235}}_{=-1}+\underbrace{\pi_{146}\cdot\pi_{245}}_{=0}-\underbrace{\pi_{146}\cdot 2\pi_{246}}_{=0}+\underbrace{\pi_{146}\cdot\pi_{236}}_{=0}) \\
&+\frac{16}{12}(\underbrace{\pi_{136}\cdot\pi_{235}}_{=0}+\underbrace{\pi_{136}\cdot\pi_{245}}_{=1}-\underbrace{\pi_{136}\cdot 2\pi_{246}}_{=0}+\underbrace{\pi_{136}\cdot\pi_{236}}_{=0}) = 8\,.
\end{aligned}$$

The intersection number includes the orbifold images. Since a cycle and its orbifold image are considered to be equivalent, the orbifold images should not be included in the intersection numbers. On the $\mathbb{Z}_2 \times \mathbb{Z}_6$ orbifold, we have in total twelve orbifold images, which implies that we have to add an overall factor of $\frac{1}{12}$ in front.
Proceeding similarly for the other intersection numbers, one obtains [65]:

$$\begin{aligned}
\rho_1 \cdot \rho_3 = \rho_2 \cdot \rho_4 = 8\,, \\
\rho_1 \cdot \rho_4 = \rho_2 \cdot \rho_3 = 4\,.
\end{aligned} \tag{2.10}$$

The determinant of the intersection matrix is different from ± 1. This means that the lattice formed by these three-cycles is not unimodular, which implies that the bulk three-cycles given above only span a sublattice. We will come back to this issue in section 2.3.2.
A general bulk three-cycle can be expressed in terms of the basis bulk three-cycles as follows:

$$\Pi^{\text{bulk}} = P\,\rho_1 + Q\,\rho_2 + U\,\rho_3 + V\,\rho_4, \tag{2.11}$$

where we introduced the orbifold-invariant bulk wrapping numbers:

$$\begin{aligned} &P \equiv n^1 X, \qquad Q \equiv n^1 Y, \qquad U \equiv m^1 X, \qquad V \equiv m^1 Y, \\ &\text{with} \quad X \equiv n^2 n^3 - m^2 m^3, \qquad Y \equiv n^2 m^3 + m^2 n^3 + m^2 m^3. \end{aligned} \tag{2.12}$$

These bulk wrapping numbers can be deduced by writing a general three-cycle in terms of the torus three-cycles, applying the orbifold generators and expressing the result in terms of the bulk three-cycles:

$$\begin{aligned} &(n^1\pi_1 + m^1\pi_2) \otimes (n^2\pi_3 + m^2\pi_4) \otimes (n^3\pi_5 + m^3\pi_6) \\ &= n^1n^2n^3\pi_{135} + n^1n^2m^3\pi_{136} + n^1m^2n^3\pi_{145} + n^1m^2m^3\pi_{146} + m^1n^2n^3\pi_{235} + m^1n^2m^3\pi_{236} \\ &+ m^1m^2n^3\pi_{245} + m^1m^2m^3\pi_{246}\,. \end{aligned}$$

Applying $(1+\omega+\omega^2)$ to this whole expression gives us

$$\begin{aligned} &(1+\omega+\omega^2)n^1n^2n^3\pi_{135} = n^1n^2n^3\rho_1\,, \\ &(1+\omega+\omega^2)n^1n^2m^3\pi_{136} = n^1n^2m^3\rho_2\,, \\ &(1+\omega+\omega^2)n^1m^2n^3\pi_{145} = n^1m^2n^3(\pi_{145} + \pi_{1,-3+4,5-6} + \pi_{1,-3,-6}) = n^1m^2n^3\rho_2\,, \\ &(1+\omega+\omega^2)n^1m^2m^3\pi_{146} = n^1m^2m^3(\pi_{146} + \pi_{1,-3+4,5} + \pi_{1,-3,5-6}) = n^1m^2m^3(\rho_2 - \rho_1)\,, \\ &(1+\omega+\omega^2)m^1n^2n^3\pi_{235} = m^1n^2n^3\rho_3\,, \\ &(1+\omega+\omega^2)m^1n^2m^3\pi_{236} = m^1n^2m^3\rho_4\,, \\ &(1+\omega+\omega^2)m^1m^2n^3\pi_{245} = m^1m^2n^3(\pi_{245} + \pi_{2,-3+4,5-6} + \pi_{2,-3,-6}) = m^1m^2n^3\rho_4\,, \\ &(1+\omega+\omega^2)m^1m^2m^3\pi_{246} = m^1m^2m^3(\pi_{246} + \pi_{2,-3+4,5} + \pi_{2,-3,5-6}) = m^1m^2m^3(\rho_4 - \rho_3)\,. \end{aligned}$$

Summing up all of these, we obtain

$$\begin{aligned} &(n^1n^2n^3 - n^1m^2m^3)\rho_1 = P\rho_1\,, \\ &(n^1n^2m^3 + n^1m^2n^3 + n^1m^2m^3)\rho_2 = Q\rho_2\,, \\ &(m^1n^2n^3 - m^1m^2m^3)\rho_3 = U\rho_3\,, \\ &(m^1n^2m^3 + m^1m^2n^3 + m^1m^2m^3)\rho_4 = V\rho_4\,. \end{aligned}$$

The orbifold-invariance of the bulk wrapping numbers can be checked by using the orbifold transformations of the torus wrapping numbers given by:

$$\begin{pmatrix} n^1 & m^1 \\ n^2 & m^2 \\ n^3 & m^3 \end{pmatrix} \xrightarrow{\omega} \begin{pmatrix} n^1 & m^1 \\ m^2 & -(n^2+m^2) \\ -(n^3+m^3) & n^3 \end{pmatrix} \xrightarrow{\omega} \begin{pmatrix} n^1 & m^1 \\ -(n^2+m^2) & n^2 \\ m^3 & -(n^3+m^3) \end{pmatrix}. \tag{2.13}$$

Note that here the first ω-action on the second and third torus includes an additional overall sign flip with respect to the ω-action defined in [65].
Using (2.10) and (2.11), it is straightforward to produce an expression for the intersection number of two generic bulk three-cycles, as it was first given in [65]:

$$\Pi_a^{\text{bulk}} \circ \Pi_b^{\text{bulk}} = 8\,(P_aU_b - P_bU_a + Q_aV_b - Q_bV_a) + 4\,(P_aV_b - P_bV_a + Q_aU_b - Q_bU_a)\,, \tag{2.14}$$

where a and b label the two three-cycles. This completes the introduction of orbifold-invariant bulk three-cycles on $T^6/(\mathbb{Z}_2 \times \mathbb{Z}_6)$.

The orientifold action $\Omega\mathcal{R}$ on the bulk three-cycles

It remains to be determined how the orientifold action $\Omega\mathcal{R}$ acts on these bulk cycles, the $\mathcal{R}$-part of which corresponds to complex conjugation on all three tori and has to be applied on each lattice basis vector π_i, $i = 1, ..., 6$. As an example, let us consider the action of $\mathcal{R}$ on π_1 and π_2 in case of a tilted lattice, i.e. $b = 1/2$. In this lattice, the real axis lies along $\pi_1 - b\pi_2$. Complex conjugation with respect to the real axis leads to

$$\pi_2 \overset{\Omega\mathcal{R}}{\to} -\pi_2 \,, \tag{2.15}$$

$$\pi_1 \overset{\Omega\mathcal{R}}{\to} \pi_1 - \pi_2 \,. \tag{2.16}$$

From these, the transformation of the torus wrapping numbers can be read off as follows:

$$n^1\pi_1 + m^1\pi_2 \overset{\Omega\mathcal{R}}{\to} n^1(\pi_1 - \pi_2) - m^1\pi_2 = n^1\pi_1 - (n^1 + m^1)\pi_2 \,. \tag{2.17}$$

Applying the same procedure on the other cycles and lattices, we find the results given in [65]:

$$(n^1_{a'}, m^1_{a'}) = \begin{cases} (n^1_a,\, -m^1_a) & (\mathbf{a}) \\ (n^1_a, -n^1_a - m^1_a) & (\mathbf{b}) \end{cases} , \qquad (n^i_{a'}, m^i_{a'})_{i=2,3} = \begin{cases} (n^i_a + m^i_a\,,\, -m^i_a) & (\mathbf{A}) \\ (m^i_a, n^i_a) & (\mathbf{B}) \end{cases} , \tag{2.18}$$

where a refers to a three-cycle Π_a and a' denotes the orientifold image of a: $\mathcal{R}\Pi_a = \Pi_{a'}$. The transformation laws under $\Omega\mathcal{R}$ of the bulk three-cycles in (2.8) were derived in [65] and are reproduced in table 2.2.

Orientifold images of bulk 3-cycles on $T^6/(\mathbb{Z}_2 \times \mathbb{Z}_6 \times \Omega\mathcal{R})$				
$3-$cycle	ρ_1	ρ_2	ρ_3	ρ_4
a/bAA	$\rho_1 - (2b)\rho_3$	$\rho_1 - \rho_2 - (2b)[\rho_3 - \rho_4]$	$-\rho_3$	$\rho_4 - \rho_3$
a/bAB	$\rho_2 - (2b)\rho_4$	$\rho_1 - (2b)\rho_3$	$-\rho_4$	$-\rho_3$
a/bBB	$\rho_2 - \rho_1 - (2b)[\rho_4 - \rho_3]$	$\rho_2 - (2b)\rho_4$	$\rho_3 - \rho_4$	$-\rho_4$

Table 2.2: Action of $\mathcal{R}$ on the bulk three-cycles defined in (2.8) on the orbifold $T^6/(\mathbb{Z}_2 \times \mathbb{Z}_6)$, with and without discrete torsion, for all six lattice configurations. The **a**-type lattices correspond to $b = 0$ and the **b**-type lattices are associated to $b = 1/2$.

Since the action of $\Omega\mathcal{R}$ on the cycles is now determined, we can proceed to find the O6-planes, which correspond by definition to the fixed points of $\Omega\mathcal{R}$. In order to be invariant under the orientifold projection, the O6-planes have to be either parallel or orthogonal to the real axis. The different possibilities are depicted in figure 2.6 for the lattice **aAA**. Note that in the case of the **a**-type lattice, the O6-plane can be displaced by half a lattice vector, so two parallel O6-planes are present, indicated by the solid line and the dotted line. This is not the case for the **b**-type lattice. In fact, albeit displacing the O6-plane by half a lattice vector would give here an $\Omega\mathcal{R}$-invariant cycle, it would not be point-wise invariant. Hence, it would not correspond to the set of fixed loci of the orientifold projection. Note that in the case of cycles orthogonal to the real axis, these are point-wise invariant due to the $\mathbb{Z}_2$ identification in the coset space $T^6/(\mathbb{Z}_2 \times \mathbb{Z}_6)$. In total, we have eight orientifold planes for

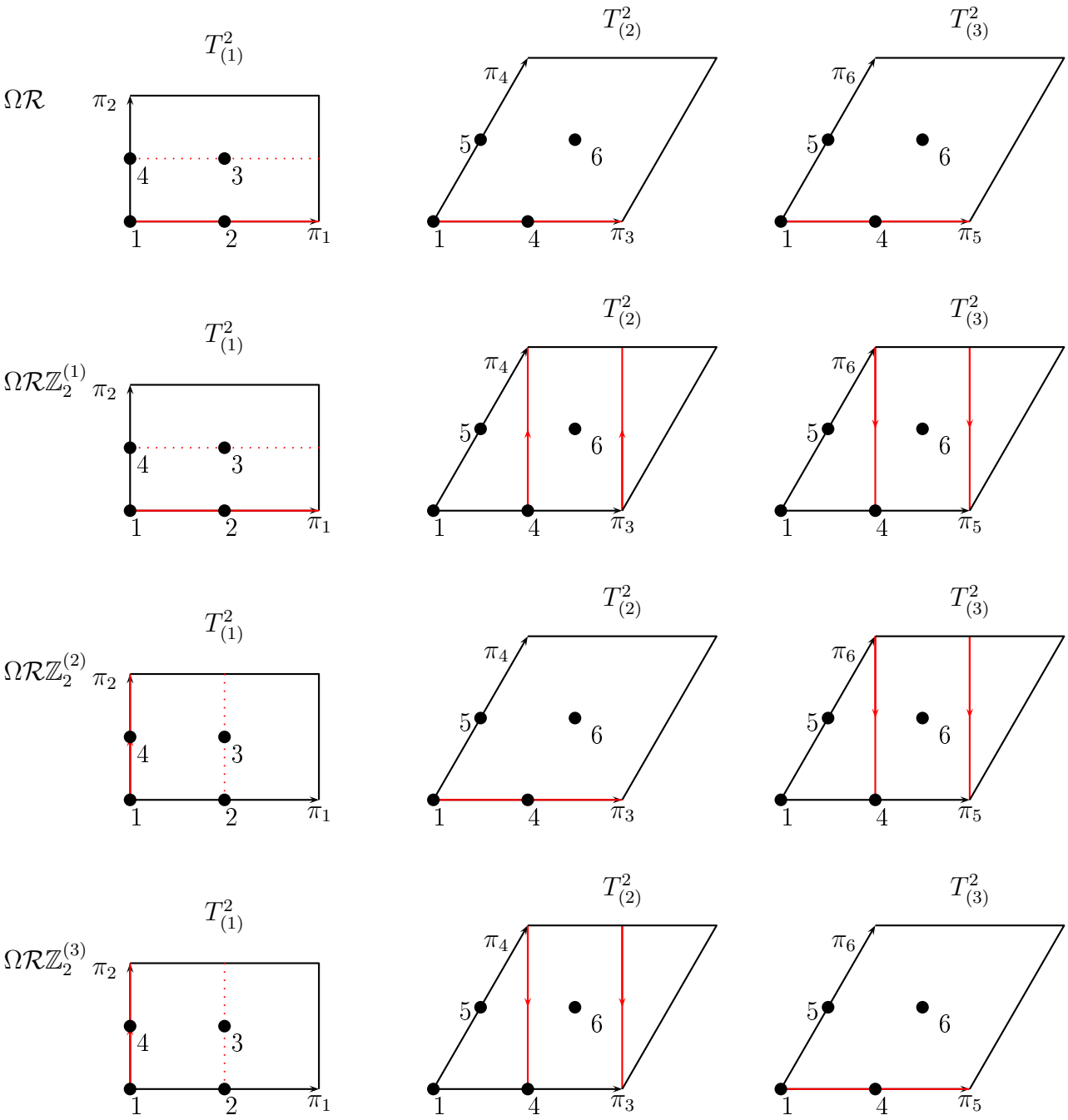

Figure 2.6: Depiction of orbifold representatives of the four O6-planes on the $T^2/(\mathbb{Z}_2 \times \mathbb{Z}_6 \times \Omega\mathcal{R})$ orientifold. The lattice under consideration is the **aAA** configuration. On the first two-torus $T^2_{(1)}$, the O6-plane can be deplaced by half a lattice vector, leading to a total of eight O6-planes.

the **a**-type lattices and four for the **b**-type lattices. The orientifold planes are denoted by $\Omega\mathcal{R}$, $\Omega\mathcal{R}\mathbb{Z}_2^{(i)}$ with $i = 1, 2, 3$, as indicated in figure 2.6. In order to obtain O6-planes invariant under the orbifold action, all the orbifold images of the cycles depicted in figure 2.6 have to be summed up.
The geometric data of the four O6-planes are collected in table 2.3.

In order to avoid double counting of equivalent models, it is sensible to define rules to select a representative of the orbifold and orientifold equivalence classes. The rules for selecting an

Torus and bulk wrapping numbers for the four O6-plane orbits on $T^6/(\mathbb{Z}_2 \times \mathbb{Z}_6 \times \Omega\mathcal{R})$							
O6-plane	$\frac{\text{angle}}{\pi}$	**a/bAA**		**a/bAB**		**a/bBB**	
		(n^i, m^i)	(P, Q, U, V)	(n^i, m^i)	(P, Q, U, V)	(n^i, m^i)	(P, Q, U, V)
$\Omega\mathcal{R}$	$(0, 0, 0)$	$(\frac{1}{1-b}, \frac{-b}{1-b}; 1, 0; 1, 0)$	$\frac{1}{1-b}(1, 0, -b, 0)$	$(\frac{1}{1-b}, \frac{-b}{1-b}; 1, 0; 1, 1)$	$\frac{1}{1-b}(1, 1, -b, -b)$	$(\frac{1}{1-b}, \frac{-b}{1-b}; 1, 1; 1, 1)$	$\frac{3}{1-b}(0, 1, 0, -b)$
$\Omega\mathcal{R}\mathbb{Z}_2^{(1)}$	$(0, \frac{1}{2}, \frac{-1}{2})$	$(\frac{1}{1-b}, \frac{-b}{1-b}; -1, 2; 1, -2)$	$\frac{3}{1-b}(1, 0, -b, 0)$	$(\frac{1}{1-b}, \frac{-b}{1-b}; -1, 2; 1, -1)$	$\frac{1}{1-b}(1, 1, -b, -b)$	$(\frac{1}{1-b}, \frac{-b}{1-b}; -1, 1; 1, -1)$	$\frac{1}{1-b}(0, 1, 0, -b)$
$\Omega\mathcal{R}\mathbb{Z}_2^{(3)}$	$(\frac{1}{2}, \frac{-1}{2}, 0)$	$(0, 1; 1, -2; 1, 0)$	$(0, 0, 1, -2)$	$(0, 1; 1, -2; 1, 1)$	$(0, 0, 3, -3)$	$(0, 1; 1, -1; 1, 1)$	$(0, 0, 2, -1)$
$\Omega\mathcal{R}\mathbb{Z}_2^{(2)}$	$(\frac{1}{2}, 0, \frac{-1}{2})$	$(0, 1; 1, 0; 1, -2)$	$(0, 0, 1, -2)$	$(0, 1; 1, 0; 1, -1)$	$(0, 0, 1, -1)$	$(0, 1; 1, 1; 1, -1)$	$(0, 0, 2, -1)$

Table 2.3: The first column gives the labels of each O6-plane and the second column gives the angles of a chosen orbifold representative of the O6-planes with respect to the real axis, on each two-torus $T^2_{(i)}$, $i = 1, 2, 3$. The third column lists the torus wrapping numbers $(n^i, m^i)_{i\in\{1,2,3\}}$ for the chosen orbifold representative, and the fourth column gives the orbifold-invariant bulk wrapping numbers (P, Q, U, V). The data are given for each lattice configuration.

orbifold and orientifold representative have first been derived in [65]:

- (n^3, m^3) = (odd,odd) selects an orbifold image of the $\mathbb{Z}_6$-orbit generated by ω. The additional constraint $n^3 > 0$ fixes the orientation of the one-cycle on the third two-torus $T^2_{(3)}$.

- The condition on the wrapping numbers of the first two-torus $T^2_{(1)}$ are as follows: $(n^1, m^1 + bn^1) \in \{(\frac{1}{1-b}, 0), (0, 1), (n^1 > 0, m^1 + bn^1 > 0)\}$, which permits to choose an orientifold representative.

This completes the discussion of three-cycles arising in the untwisted sector. The next step consists in turning our attention to the three-cycles present in the $\mathbb{Z}_2$-twisted sectors, which are commonly referred to as exceptional cycles.

2.2.4 Exceptional three-cycles

The discussion in this section concentrates solely on the $\mathbb{Z}_2$-twisted sectors, as only the three-cycles arising from these sectors together with the three-cycles from the untwisted sector will be used for model building in this work.
The $\mathbb{Z}_2$-twisted sectors will be denoted by $\mathbb{Z}_2^{(i)}$, $i = 1, 2, 3$. A $\mathbb{Z}_2^{(i)}$-action leaves the ith two-torus invariant and acts on the other two two-tori. More precisely, the $\mathbb{Z}_2^{(1)}$-sector is generated by ω^3, $\mathbb{Z}_2^{(2)}$ will be associated to $\theta\omega^3$ and $\mathbb{Z}_2^{(3)}$ is generated by θ. The $\mathbb{Z}_2^{(i)}$-fixed points on the two-tori correspond to curvature singularities and can be resolved by blowing them up, i.e. replacing the singular point by the smooth projective space $\mathbb{CP}^1 \simeq S^2$ [105]. The resulting exceptional divisor, called exceptional two-cycle, will be denoted by $e^{(i)}_{\alpha\beta}$ in the following, with α, β referring to the labels of the $\mathbb{Z}_2^{(i)}$-fixed points on a four-torus $T^2_{(j)} \times T^2_{(k)}$, $j, k = 1, 2, 3$, $j \neq k \neq i \neq j$.

Before deriving an explicit basis of exceptional cycles, we will discuss discrete torsion, which has an impact on the type of orbifold-invariant exceptional cycles. Discrete torsion arises in the case of orbifolds containing a subgroup of the form $\mathbb{Z}_N \times \mathbb{Z}_N$. The introduction of discrete torsion is motivated from the string theoretical side, where discrete torsion is manifest as a phase factor in the computation of partition functions, see [106, 105] for details. Geometrically, discrete torsion implies the action of one $\mathbb{Z}_2^{(i)}$, $i = 1, 2, 3$ generator on

another $\mathbb{Z}_2^{(j)}$-exceptional cycle, $j = 1, 2, 3$, $j \neq i$ as follows:

$$e_{\alpha\beta}^{(i)} \overset{\mathbb{Z}_2^{(j)}}{\to} \eta e_{\alpha\beta}^{(i)}\,, \tag{2.19}$$

where we set $\eta = 1$ if we do not consider discrete torsion and $\eta = -1$ if we do work with discrete torsion. Clearly, this has consequences on the orbifold-invariance of the two-cycles $e_{\alpha\beta}^{(i)} \simeq S^2$ and thus also on the Hodge numbers for the twisted sectors. For a general orbifold of the form $\mathbb{Z}_N \times \mathbb{Z}_M$, the phase factor η associated to discrete torsion is given by the following formula [106, 107]:

$$\eta = e^{2\pi n i/gcd(N,M)},\ n \in \mathbb{Z}\,. \tag{2.20}$$

Let us illustrate this point on a concrete example from table 2.1. Consider the θ-twisted sector, i.e. the $\mathbb{Z}_2^{(3)}$-twisted sector, acting as rotations by angles $(\frac{1}{2}, -\frac{1}{2}, 0)$ on $T^2_{(1)} \times T^2_{(2)} \times T^2_{(3)}$. The two-cycles associated to this twisted sector are of the form $e_{\alpha\beta}^{(3)}$ with $\alpha \in \{1, 2, 3, 4\}$ and $\beta \in \{1, 4, 5, 6\}$ and are 16 in number, since we have four $\mathbb{Z}_2^{(3)}$-fixed points on the first two-torus $T^2_{(1)}$ combined with four $\mathbb{Z}_2^{(3)}$-fixed points on the second two-torus $T^2_{(2)}$. Only those combinations of two-cycles that are orbifold-invariant are kept.
First, consider the case without discrete torsion. The $\mathbb{Z}_6$-generators act as follows on the labels $1 \overset{e^{\pi i/3}}{\circlearrowleft}, 4 \overset{e^{\pi i/3}}{\to} 5 \overset{e^{\pi i/3}}{\to} 6 \overset{e^{\pi i/3}}{\to} 4$ on the second two-torus $T^2_{(2)}$, whereas they act trivially on the first two-torus $T^2_{(1)}$. In order to find all orbifold-invariant combinations of two-cycles $e_{\alpha\beta}^{(3)}$, it suffices to take all 16 two-cycles and apply the orbifold actions on each one. Some of the resulting combinations are equal, so that in the end only eight different orbifold-invariant combinations remain, which can be summarized as follows:

$$\begin{aligned} &e_{\alpha 1}^{(3)} && \alpha = 1, 2, 3, 4\,, \\ &e_{\alpha 4}^{(3)} + e_{\alpha 5}^{(3)} + e_{\alpha 6}^{(3)} && \alpha = 1, 2, 3, 4\,. \end{aligned}$$

In the presence of discrete torsion, we have $\eta = -1$, and the exceptional two-cycles are no longer invariant under every $\mathbb{Z}_2$-action, as indicated in (2.19). In order to obtain $\mathbb{Z}_2$-invariant cycles, the exceptional two-cycle needs to be tensored with a torus one-cycle on the left-over two-torus, resulting in a three-cycle:

$$\begin{aligned} &e_{\alpha\beta}^{(i)} \otimes \left(n^i \pi_{2i-1} + m^i \pi_{2i}\right) \overset{\mathbb{Z}_2^{(j)}}{\to} -e_{\alpha\beta}^{(i)} \otimes \left(-n^i \pi_{2i-1} - m^i \pi_{2i}\right) = e_{\alpha\beta}^{(i)} \otimes \left(n^i \pi_{2i-1} + m^i \pi_{2i}\right)\,, \\ &\text{with}\ \ i, j = 1, 2, 3 \text{ and } \ i \neq j\,. \end{aligned}$$

Under a $\mathbb{Z}_2^{(j)}$-rotation, the one-cycle $n^i \pi_{2i-1} + m^i \pi_{2i}$ transforms with a minus sign, which cancels the minus sign coming from the exceptional two-cycle $e_{\alpha\beta}^{(i)}$ due to the $\mathbb{Z}_2^{(j)}$-action combined with discrete torsion. This combination of the exceptional two-cycle with a one-cycle is called an exceptional three-cycle. In order to obtain three-cycles invariant under the generators of $\mathbb{Z}_2 \times \mathbb{Z}_6$, we have to sum once again over orbifold images.
Let us come back to the example of the $\mathbb{Z}_2^{(3)}$-twisted sector generated by θ. If discrete torsion is present, no combination of exceptional two-cycles $e_{\alpha\beta}^{(3)}$ can be found which is invariant under the $\mathbb{Z}_2^{(1)}$- and $\mathbb{Z}_2^{(2)}$-actions implying that the related Hodge number $h^{1,1}$ is zero, as indicated in table 2.1. On the other hand, we can find eight orbifold-invariant combinations of three-cycles if discrete torsion is switched on, the explicit expression of which will be given

below.
In summary, we can conclude that, in the absence of discrete torsion, the resolution of the singularities leads to two-cycles, whereas in the presence of discrete torsion, the resolution gives rise to three-cycles. This is linked to the fact that a singularity can be resolved either by deforming it or by blowing it up, see [105] for details. In general, the resolution of a singularity arising by degeneration of the Kähler structure is referred to as blow-up, while the resolution of a singularity arising by complex structure degeneration is rather called deformation. Thus, without discrete torsion, we encounter blow-up rather than deformation, whereas discrete torsion rather leads to deformation [105].

In the following, we will provide the explicit expressions of orbifold-invariant exceptional three-cycles for all $\mathbb{Z}_2$-twisted sectors $\mathbb{Z}_2^{(i)}$, $i = 1, 2, 3$, as they have been derived for the first time in [65].
As in the case of the bulk three-cycles, a basis has to be chosen for the exceptional cycles. In the $\mathbb{Z}_2^{(1)}$ sector, the Betti numbers are: $b^3 = h^{3,0} + h^{0,3} + h^{2,1} + h^{1,2} = 0 + 0 + 6 + 6 = 12$ and thus, we can choose a basis of twelve independent three-cycles as follows:

$$\begin{aligned}
\varepsilon_0^{(1)} &= 6e_{11}^{(1)} \otimes \pi_1 \,, & \tilde{\varepsilon}_0^{(1)} &= 6e_{11}^{(1)} \otimes \pi_2 \,, \\
\varepsilon_1^{(1)} &= 2(e_{41}^{(1)} + e_{51}^{(1)} + e_{61}^{(1)}) \otimes \pi_1 \,, & \tilde{\varepsilon}_1^{(1)} &= 2(e_{41}^{(1)} + e_{51}^{(1)} + e_{61}^{(1)}) \otimes \pi_2 \,, \\
\varepsilon_2^{(1)} &= 2(e_{14}^{(1)} + e_{15}^{(1)} + e_{16}^{(1)}) \otimes \pi_1 \,, & \tilde{\varepsilon}_2^{(1)} &= 2(e_{14}^{(1)} + e_{15}^{(1)} + e_{16}^{(1)}) \otimes \pi_2 \,, \\
\varepsilon_3^{(1)} &= 2(e_{44}^{(1)} + e_{56}^{(1)} + e_{65}^{(1)}) \otimes \pi_1 \,, & \tilde{\varepsilon}_3^{(1)} &= 2(e_{44}^{(1)} + e_{56}^{(1)} + e_{65}^{(1)}) \otimes \pi_2 \,, \\
\varepsilon_4^{(1)} &= 2(e_{45}^{(1)} + e_{54}^{(1)} + e_{66}^{(1)}) \otimes \pi_1 \,, & \tilde{\varepsilon}_4^{(1)} &= 2(e_{45}^{(1)} + e_{54}^{(1)} + e_{66}^{(1)}) \otimes \pi_2 \,, \\
\varepsilon_5^{(1)} &= 2(e_{46}^{(1)} + e_{55}^{(1)} + e_{64}^{(1)}) \otimes \pi_1 \,, & \tilde{\varepsilon}_5^{(1)} &= 2(e_{46}^{(1)} + e_{55}^{(1)} + e_{64}^{(1)}) \otimes \pi_2 \,,
\end{aligned} \tag{2.21}$$

where once again the orbifold images have been summed up in order to obtain orbifold-invariant three-cycles. Note that we obtain an overall factor of 2 and not 4 because we only sum over $\mathbb{Z}_6$-images. Indeed, there is no need to sum over $\mathbb{Z}_2$-images as the exceptional three-cycles are already invariant under $\mathbb{Z}_2$ per construction. The same can be done for the second and third twisted sectors $\mathbb{Z}_2^{(2)}$ and $\mathbb{Z}_2^{(3)}$. For each of these sectors, we have the following Betti numbers: $b^3 = h^{3,0} + h^{0,3} + h^{2,1} + h^{1,2} = 0 + 0 + 4 + 4 = 8$. A basis of eight orbifold-invariant exceptional three-cycles per sector is given in [65]:

$$\begin{aligned}
\varepsilon_\kappa^{(l)} &= 2\left(e_{\kappa 4}^{(l)} \otimes \pi_{(2l-1)} + e_{\kappa 6}^{(l)} \otimes \pi_{-(2l)} + e_{\kappa 5}^{(l)} \otimes \pi_{(2l)-(2l-1)}\right) \,, \\
\tilde{\varepsilon}_\kappa^{(l)} &= 2\left(e_{\kappa 4}^{(l)} \otimes \pi_{(2l)} + e_{\kappa 6}^{(l)} \otimes \pi_{(2l-1)-(2l)} + e_{\kappa 5}^{(l)} \otimes \pi_{-(2l-1)}\right) \,,
\end{aligned} \tag{2.22}$$

where $l = 2, 3$ denotes the torus where $\mathbb{Z}_2$ acts trivially. The label κ refers to the $\mathbb{Z}_2$-fixed points on the first torus, i.e. $\kappa = 1, 2, 3, 4$. Due to the introduction of the overall sign-flip in the transformations (2.13) of the torus-wrapping numbers, a subtlety arises in the definition (2.22). Consider for example the second twisted sector with $l = 2$. The generator ω acts as a rotation of $+60°$ on the second torus, so $\pi_3 \xrightarrow{\omega} +\pi_4$. However, due to the additional sign-flip, the fourth lattice vector in the expression of ε above has to appear with a minus sign $-\pi_4$. The same is true for $\tilde{\varepsilon}$, where we have $\pi_4 \xrightarrow{\omega} \pi_{3-4}$ instead of $\pi_4 \xrightarrow{\omega} \pi_{4-3}$. The same holds for the action of ω in the third sector, where ω acts as a rotation of $-60°$ on the third torus. Thus, the definition of the exceptional three-cycles in (2.22) is consistent with the sign-flip in (2.13).

Just as the bulk three-cycles, the exceptional three-cycles give also rise to intersection numbers. The intersection between two exceptional two-cycles is minus two or zero, as explained in [77]:

$$e^{(l)}_{\kappa\lambda} \circ e^{(k)}_{\alpha\beta} = -2\delta^{lk}\delta_{\kappa\alpha}\delta_{\lambda\beta}\,. \tag{2.23}$$

Using equation (2.23), the intersection numbers for the basis of orbifold-invariant exceptional three-cycles (2.21) and (2.22) can be found as was done in [65]:

$$\begin{aligned} &\varepsilon^{(1)}_0 \circ \tilde{\varepsilon}^{(1)}_0 = -12, \quad \varepsilon^{(1)}_\alpha \circ \tilde{\varepsilon}^{(1)}_\beta = -4\,\delta_{\alpha\beta}, \quad \alpha,\beta \in \{1,2,3,4,5\}\,, \\ &\varepsilon^{(l)}_\alpha \circ \tilde{\varepsilon}^{(l)}_\beta = -4\,\delta_{\alpha\beta} \quad \text{with } l=2,3 \qquad\qquad \alpha,\beta \in \{1,2,3,4\}\,. \end{aligned} \tag{2.24}$$

Note that an overall factor of $1/6$ has to be included in the computation of the intersection numbers instead of a factor $1/12$, as we had done before for the bulk cycles. This is due to the fact that we do not sum over all the orbifold images in (2.21) and (2.22).

The $\mathbb{Z}_6$-orbit of an exceptional three-cycle $e^{(i)}_{\alpha\beta} \otimes (n^i\pi_{2i-1} + m^i\pi_{2i})$ can be expressed in terms of the basis three-cycles (2.21) and (2.22). The correspondence is given in table 2.4. An extended version of table 2.4 is given by table A.1 in appendix A.1. These tables are used to construct fractional three-cycles, which we introduce in section 2.3.2.

$\mathbb{Z}_2^{(k)}$ **fixed points and exceptional 3-cycles on** $T^6/(\mathbb{Z}_2\times\mathbb{Z}_6)$ **with discrete torsion** $(\eta=-1)$			
$\mathbb{Z}_2^{(1)}$ **twisted sector**		$\mathbb{Z}_2^{(l)}$ **twisted sector with** $l=2,3$	
f.p.$^{(1)} \otimes (n^1\pi_1 + m^1\pi_2)$	orbit	f.p.$^{(l)} \otimes (n^l\pi_{2l-1} + m^l\pi_{2l})$	orbit
11	$n^1\varepsilon^{(1)}_0 + m^1\tilde{\varepsilon}^{(1)}_0$	$\kappa 1$	–
41, 51, 61	$n^1\varepsilon^{(1)}_1 + m^1\tilde{\varepsilon}^{(1)}_1$	$\kappa 4$	$n^l\varepsilon^{(l)}_\kappa + m^l\tilde{\varepsilon}^{(l)}_\kappa$
14, 15, 16	$n^1\varepsilon^{(1)}_2 + m^1\tilde{\varepsilon}^{(1)}_2$	$\kappa 5$	$m^l\varepsilon^{(l)}_\kappa - (n^l+m^l)\tilde{\varepsilon}^{(l)}_\kappa$
44, 56, 65	$n^1\varepsilon^{(1)}_3 + m^1\tilde{\varepsilon}^{(1)}_3$	$\kappa 6$	$-(n^l+m^l)\varepsilon^{(l)}_\kappa + n^l\tilde{\varepsilon}^{(l)}_\kappa$
45, 54, 66	$n^1\varepsilon^{(1)}_4 + m^1\tilde{\varepsilon}^{(1)}_4$		
46, 55, 64	$n^1\varepsilon^{(1)}_5 + m^1\tilde{\varepsilon}^{(1)}_5$		

Table 2.4: Correspondence between an exceptional three-cycle $e^{(k)}_{\kappa\lambda} \otimes (n^k\pi_{2k-1} + m^k\pi_{2k})$ and its $\mathbb{Z}_6$-orbit expressed in terms of the exceptional basis three-cycles $\varepsilon^{(k)}_\alpha$ and $\tilde{\varepsilon}^{(k)}_\alpha$, as first computed in [65].

The orientifold action $\Omega\mathcal{R}$ on the exceptional three-cycles

Just as in the case of the bulk three-cycles, the last step consists in verifying how the $\Omega\mathcal{R}$ projection acts on the exceptional three-cycles. Let us introduce the following sign factors $\eta_{\Omega\mathcal{R}}, \eta_{\Omega\mathcal{R}\mathbb{Z}_2^{(i)}} \in \{-1,1\}$, $i=1,2,3$, satisfying the following relation:

$$\eta = \eta_{\Omega\mathcal{R}} \prod_{i=1}^{3} \eta_{\Omega\mathcal{R}\mathbb{Z}_2^{(i)}}\,. \tag{2.25}$$

The motivation for these sign factors comes from the stringy approach. In fact, the sign factors are related to the signs of the RR-charges of the O6-planes. Discrete torsion affects

the RR-charges of the O6-planes. Without discrete torsion, the RR-charges of all the O6-planes are negative. In the presence of discrete torsion, one must have an odd number of exotic O6-planes with positive RR-charge, i.e. $\eta_{\Omega\mathcal{R}(\mathbb{Z}_2^{(i)})} = -1$ occurs. The relation above has to be fulfilled in order to have worldsheet consistency of the Klein bottle amplitude, see [92, 65] for details.
The transformation law of the exceptional three-cycles under the orientifold action $\Omega\mathcal{R}$ is given by

$$\Omega\mathcal{R} : e^{(l)}_{\alpha\beta} \to -\eta_{(l)} e^{(l)}_{\alpha'\beta'} \qquad \text{with } \eta_{(l)} \equiv \eta_{\Omega\mathcal{R}}\eta_{\Omega\mathcal{R}\mathbb{Z}_2^{(l)}}, \qquad l = 1,2,3\,, \tag{2.26}$$

This transformation law was first introduced in [92]. The $\mathbb{Z}_2$-fixed point labels α and β of the exceptional divisor $e^{(i)}_{\alpha\beta}$ in $e^{(i)}_{\alpha\beta} \otimes (n^i\pi_{2i-1} + m^i\pi_{2i})$ are permuted under the $\Omega\mathcal{R}$-projection as described in section 2.2.1. The $\Omega\mathcal{R}$-projection acts on the one-cycles $n^i\pi_{2i-1} + m^i\pi_{2i}$ in the expression of the exceptional cycles $e^{(i)}_{\alpha\beta} \otimes (n^i\pi_{2i-1} + m^i\pi_{2i})$ as complex conjugation, see eq. (2.18). Taking these three actions of $\Omega\mathcal{R}$ on the exceptional three-cycle into account, one obtains the transformations laws as given in table 2.5.

Orientifold images of exceptional three-cycles on $T^6/(\mathbb{Z}_2 \times \mathbb{Z}_6 \times \Omega\mathcal{R})$ with discrete torsion $(\eta = -1)$								
	$\mathbb{Z}_2^{(1)}$ twisted sector				**$\mathbb{Z}_2^{(l)}$ twisted sector with $l = 2,3$**			
lattice	$\Omega\mathcal{R}(\varepsilon^{(1)}_\alpha)$	$\Omega\mathcal{R}(\tilde{\varepsilon}^{(1)}_\alpha)$	$\alpha = \alpha'$	$\alpha \leftrightarrow \alpha'$	$\Omega\mathcal{R}(\varepsilon^{(l)}_\alpha)$	$\Omega\mathcal{R}(\tilde{\varepsilon}^{(l)}_\alpha)$	$\alpha = \alpha'$	$\alpha \leftrightarrow \alpha'$
a/bAA	$\eta_{(1)}\left(-\varepsilon^{(1)}_{\alpha'} + (2b)\tilde{\varepsilon}^{(1)}_{\alpha'}\right)$	$\eta_{(1)}\,\tilde{\varepsilon}^{(1)}_{\alpha'}$	$0,1,2,3$	$4,5$	$-\eta_{(l)}\,\varepsilon^{(l)}_{\alpha'}$	$\eta_{(l)}\left(\tilde{\varepsilon}^{(l)}_{\alpha'} - \varepsilon^{(l)}_{\alpha'}\right)$	$1,4$	$2+2b, 2$
a/bAB			$0,1,2,5$	$3,4$	$(-)^l\,\eta_{(l)}\,\tilde{\varepsilon}^{(l)}_{\alpha'}$	$(-)^l\,\eta_{(l)}\,\varepsilon^{(l)}_{\alpha'}$		$3-2b, 3$
a/bBB			$0,1,2,4$	$3,5$	$\eta_{(l)}\left(\tilde{\varepsilon}^{(l)}_{\alpha'} - \varepsilon^{(l)}_{\alpha'}\right)$	$\eta_{(l)}\,\tilde{\varepsilon}^{(l)}_{\alpha'}$		

Table 2.5: Action of the orientifold projection on the $\mathbb{Z}_2^{(k)}$ ($k = 1,2,3$) exceptional three-cycles. The action depends on the lattice type and the choice of the exotic O6-plane, the latter manifesting via the sign factor $\eta_{(k)} \equiv \eta_{\Omega\mathcal{R}}\eta_{\Omega\mathcal{R}\mathbb{Z}_2^{(k)}}$. The label α is switched to the label α' under the orientifold action.

So far, we concentrated entirely on the geometry of our orbifold, and the results were introduced by purely geometrical means. In the next section, we will introduce string theory, namely closed strings and D6-branes, which come with open strings.

2.3 Strings and D6-branes on $T^6/(\mathbb{Z}_2 \times \mathbb{Z}_6 \times \Omega\mathcal{R})$

2.3.1 Closed string spectrum

In the ten-dimensional space-time, the following massless closed string states are present:

- The graviton, given by a symmetric and traceless metric.
- The dilaton, a scalar field given by the trace of the metric.
- The Kalb-Ramond field B_2, corresponding to an antisymmetric tensor of second order.
- The Ramond-Ramond fields C_p, which are p-forms with $p = 0, \ldots 10$. In Type IIA string theory, p is odd, whereas in Type IIB string theory, it is even. However, not all the Ramond-Ramond fields are independent degrees of freedom due to the so-called Hodge duality in ten dimensions given by: $F_p = \star F_{10-p}$, where $\star$ is the Hodge star and the F_p are the fluxes associated to the Ramond-Ramond fields, i.e. $F_p = dC_{p-1}$. Hence, in Type IIA, C_1 and C_3 are the independent degrees of freedom.

The fields listed above correspond to the bosonic degrees of freedom, which come with fermionic SUSY partners. We will only discuss the bosonic part in this section.
The Ramond-Ramond fields C_p couple to p-dimensional subspaces, the D_{p-1}-branes, via the following relation:

$$S_{p-1} = Q_{p-1} \int_{D_{p-1}\text{-brane}} C_p \,, \tag{2.27}$$

where Q_{p-1} is the RR-charge of the D_{p-1}-brane. The Chern-Simons coupling (2.27) is the generalization of the coupling of the electromagnetic gauge potential to a charged particle in electromagnetism. Due to the coupling (2.27), the D_{p-1}-branes acquire RR-charges under the Ramond-Ramond fields C_p. The same holds true for the O-planes.
The dimensional reduction of the ten-dimensional fields is obtained by integration over the two-cycles and three-cycles present on the internal space, resulting into four-dimensional scalar fields and one-forms. For example, the reduction of C_3 and B_2 is given by:

$$\begin{aligned} A^i &= \textstyle\int_{i^{th}(1,1)\text{-cycle}} C_3 \qquad & i &= 1 \dots h^{1,1} \\ b^i &= \textstyle\int_{i^{th}(1,1)\text{-cycle}} B_2 \qquad & i &= 1 \dots h^{1,1} \\ \zeta^k &= \textstyle\int_{k^{th}3\text{-cycle}} C_3 \qquad & k &= 1 \dots 2(h^{2,1}+1) \end{aligned} \tag{2.28}$$

The one-forms A^i are $U(1)$ gauge bosons called closed or RR-gauge bosons. Without the orientifold projection, the fields obtained after dimensional reduction arrange into $\mathcal{N} = 2$ SUSY multiplets.
By introducing the orientifold projection, these $\mathcal{N} = 2$ SUSY multiplets are reduced to $\mathcal{N} = 1$ SUSY multiplets, since some states are projected out. Indeed, under the worldsheet parity Ω, C_3 is even (i.e. invariant), whereas B_2 is odd (i.e. $\Omega(B_2) = -B_2$). Consequently, the dimensional reduction is done by integration over two- and three-cycles which are odd or even under $\mathcal{R}$:

$$\begin{aligned} A^i &= \textstyle\int_{i^{th}\mathcal{R}\text{-even }(1,1)\text{-cycle}} C_3 \qquad & i &= 1 \dots h^{1,1}_+ \\ b^i &= \textstyle\int_{i^{th}\mathcal{R}\text{-odd }(1,1)\text{-cycle}} B_2 \qquad & i &= 1 \dots h^{1,1}_- \\ \xi^k &= \textstyle\int_{k^{th}\mathcal{R}\text{-even }3\text{-cycle}} C_3 \qquad & k &= 0 \dots h^{2,1} \end{aligned} \tag{2.29}$$

We see that the numbers of fields obtained in (2.29) is reduced compared to the ones obtained in (2.28), which leads to the truncation of the $\mathcal{N} = 2$ SUSY multiplets to $\mathcal{N} = 1$ SUSY multiplets. However, note that the total number of multiplets per se is conserved, only the field content of the multiplets is reduced.
The various obtained $\mathcal{N} = 1$ SUSY multiplets in four dimensions are listed in table 2.6. The gravity multiplet contains the graviton given by the four-dimensional metric, while the dilaton-axion multiplet contains the dilaton and one of the fields ξ^k.
The $\mathcal{N} = 1$ SUSY multiplets called Kähler, whose number is given by $h^{1,1}_-$, contain the fields b^i and also real scalar components corresponding to Kähler moduli, i.e. deformations of the type $\delta g_{i\bar{j}}$ of the metric. These scalar fields arise from the dimensional reduction of the Kähler two-form, and roughly speaking correspond to deformations of the "size" of the internal space.
The $h^{1,1}_+$ $\mathcal{N} = 1$ SUSY multiplets associated to vector multiplets contain the RR-gauge bosons A^i, hence the name.
The $\mathcal{N} = 1$ SUSY multiplets called complex structure, the number of which is given by $h^{2,1}$,

contain aside from the remaining fields ξ^k also complex structure moduli, i.e. deformations of the type δg_{ij} and $\delta g_{\bar{i}\bar{j}}$ of the metric. These moduli arise from the complex structure (2,1)-form, whose explicit expression can be found for example in [91, 42], and correspond to deformations of the "shape" of the internal space.
For more details and the exact form and field content of the multiplets, see for example appendix A in [65], or [108].
Since we are working with the orbifold $T^6/(\mathbb{Z}_2\times\mathbb{Z}_6)$, the analysis separates into the untwisted and the twisted sectors. Indeed, massless closed strings on the orbifold $T^6/(\mathbb{Z}_2 \times \mathbb{Z}_6)$ are characterized by the following boundary condition:

$$X^i(\tau, \sigma + 2\pi) = \theta^n \omega^m X^i(\tau, \sigma) + \lambda \text{ with } i = 1, 2, 3\,, \tag{2.30}$$

where θ and ω correspond to the generators of $\mathbb{Z}_2 \times \mathbb{Z}_6$, and $\lambda \in \Lambda$ is a lattice vector of the torus lattice. The coordinates τ and σ correspond to the worldsheet coordinates as usual. The closed string sector thus comprises:

- The untwisted sector with $n = 0$ and $m = 0$: these are states freely propagating on the six-dimensional torus T^6. This sector includes the gravity multiplet and the dilaton-axion multiplet. Also, it gives rise to three Kähler multiplets. The three Kähler moduli arising from the untwisted sector are associated to the volumes of the three two-tori. Moreover, the untwisted sector also gives rise to a single complex structure multiplet. The associated complex structure modulus corresponds to the complex structure parameter ϱ introduced in section 2.2.1.

- The twisted sectors with $n \neq 0$ or $m \neq 0$: these are states localized at singularities. On T^6, these would correspond to open strings, which become closed only on the orbifold $T^6/(\mathbb{Z}_2 \times \mathbb{Z}_6)$ and are stuck at fixed points of $\mathbb{Z}_2 \times \mathbb{Z}_6$. These sectors give rise to the remaining $\mathcal{N} = 1$ SUSY multiplets in table 2.6. The associated moduli correspond to the moduli of the fixed points. In this thesis, we work at the orbifold point, i.e. we do not deform explicitly the fixed points. The phenomenology of Type IIA string theory arising away from the orbifold point has been investigated e.g. in [109–111] on orbifolds $\mathbb{Z}_N \times \mathbb{Z}_M$ with discrete torsion in the context of intersecting D6-branes.

The total contributions are obtained by summing over the contributions per sector. In table 2.6, the various contributions per sector have already been summed up. The contributions per sector, also with the separation $h^{1,1} = h^{1,1}_+ + h^{1,1}_-$, can be found in appendix D of [65].

Closed string spectrum on $T^6/(\mathbb{Z}_2 \times \mathbb{Z}_6 \times \Omega\mathcal{R})$ with discrete torsion $\eta = -1$				
$\mathcal{N} = 1$ multiplet	#	**a/bAA**	**a/bAB**	**a/bBB**
gravity	1			
dilaton - axion	1			
vector	$h^{1,1}_+$	$4 + 2(1-b)(\eta_{(2)} + \eta_{(3)})$	$4 + 2(1-b)(\eta_{(2)} - \eta_{(3)})$	$4 - 2(1-b)(\eta_{(2)} + \eta_{(3)})$
Kähler	$h^{1,1}_-$	$15 - 2(1-b)(\eta_{(2)} + \eta_{(3)})$	$15 - 2(1-b)(\eta_{(2)} - \eta_{(3)})$	$15 + 2(1-b)(\eta_{(2)} + \eta_{(3)})$
complex structure	$h^{2,1}$	19		

Table 2.6: Overview of the $\mathcal{N} = 1$ SUSY closed string spectrum of Type IIA string theory on the $T^6/(\mathbb{Z}_2 \times \mathbb{Z}_6 \times \Omega\mathcal{R})$ orientifold with discrete torsion, as computed in [65].

2.3.2 D6-branes and open strings

In Type IIA string theory, model building is performed with D6-branes having six dimensions in space and one dimension in time and lying on $\mathcal{M}^{1,3} \times \Pi^{3\text{-cycle}}$. They fill the whole effective four-dimensional Minkowski space-time $\mathcal{M}^{1,3}$ and wrap three-cycles $\Pi^{3\text{-cycle}}$, which are three-dimensional submanifolds of the compactified space. These three-cycles have to satisfy certain geometric conditions, as will be explained in section 2.4.1.

Rigid D6-branes

Although there are three-cycles in the $\mathbb{Z}_3$-twisted sectors as indicated in table 2.1, these will not be used to support D6-branes. Indeed, the massless open string spectrum can been computed via CFT techniques (e.g. [112–114]), see for example [115] for an overview. Alternatively, it can be related to topological intersection numbers of three-cycles in the set-up of intersecting branes, so that it is not necessary to write down explicit string partition functions. However, only the three-cycles arising in the untwisted and the $\mathbb{Z}_2$-twisted sectors have an equivalent on the CFT side. Three-cycles from $\mathbb{Z}_3$-twisted sectors found no interpretation in terms of string partition functions [77]. Thus, D6-branes are taken to wrap only three-cycles from the untwisted sectors and the $\mathbb{Z}_2$-twisted sectors. Clearly, table 2.1 reveals that such $\mathbb{Z}_2$-twisted exceptional three-cycles only exist if discrete torsion is switched on, i.e $\eta = -1$. Hence, in the following we always assume that discrete torsion is present.

The open strings give rise to various moduli, including position moduli corresponding to displacements of the D6-branes, and recombination moduli leading to a recombination of D6-branes. These degrees of freedom are internal degrees of freedom of the D6-branes, i.e. they can be related to properties of the three-cycles on the internal space. The displacement moduli can be stabilized by considering D6-branes wrapping three-cycles passing through $\mathbb{Z}_2$-fixed points, see [92] for details. Remnants of these displacement moduli are given by the so-called shift parameters and discrete Wilson lines. Thus, choosing D6-branes passing through $\mathbb{Z}_2$-fixed points eliminates the displacement moduli. Since we have three $\mathbb{Z}_2$-generators, there are $\mathbb{Z}_2$-fixed points on all three two-tori $T^2_{(i)}$, $i = 1, 2, 3$, rendering the D6-brane completely rigid insofar that all displacement moduli are projected out. There remains the issue of recombination addressed in section 5.2, which we also refer to as "rigidity".

Hence, in order to stabilize the displacement moduli, the D6-branes have to wrap orbifold invariant exceptional three-cycles from the $\mathbb{Z}_2$-twisted sectors and come with a set of discrete parameters manifesting as sign factors:

$$\Pi^{\mathbb{Z}_2^{(i)}} = 2(-1)^{\tau^{\mathbb{Z}_2^{(i)}}} \sum_{m=0}^{2} \omega^m \left[\sum_{(\alpha,\beta)\in T^2_{(j)}\times T^2_{(k)}} (-1)^{\tau_j^\alpha + \tau_k^\beta} e^{(i)}_{\alpha\beta} \otimes (n^i \pi_{2i-1} + m^i \pi_{2i}) \right] , \tag{2.31}$$

where i corresponds to the two-torus left invariant under $\mathbb{Z}_2^{(i)}$, and (i, j, k) are cyclic permutations of $(1, 2, 3)$. The indices α, β label the four $\mathbb{Z}_2$-fixed points on each torus. In the expression above, the following discrete parameters appear:

- The $\mathbb{Z}_2$-eigenvalues $(-1)^{\tau^{\mathbb{Z}_2^{(i)}}} \in \{-1, 1\}$: This parameter is interpreted geometrically as the orientation of the exceptional two-cycle $e^{(i)}_{\alpha\beta}$ arising after the blow-up of a $\mathbb{Z}_2^{(i)}$-fixed

point on a four-torus $T^2_{(j)} \times T^2_{(k)}$. The exceptional two-cycle $e^{(i)}_{\alpha\beta}$ can encircle either "clockwise" $\tau^{\mathbb{Z}_2^{(i)}} = 0$ or "counter-clockwise" $\tau^{\mathbb{Z}_2^{(i)}} = 1$ the $\mathbb{Z}_2^{(i)}$-fixed point. The three $\mathbb{Z}_2$-eigenvalues are not independent but related in the following way: $\tau^{\mathbb{Z}_2^{(1)}} = \tau^{\mathbb{Z}_2^{(2)}} + \tau^{\mathbb{Z}_2^{(3)}}$. This is due to the fact that a $\mathbb{Z}_2^{(1)}$-action followed by a $\mathbb{Z}_2^{(2)}$-action boils down to a $\mathbb{Z}_2^{(3)}$-action.

- The discrete Wilson lines $\tau^\alpha_j \in \{0, 1\}$: Whereas the $\mathbb{Z}_2$-eigenvalues correspond to the absolute orientation of an exceptional two-cycle, the Wilson lines correspond to the relative orientation of different exceptional two-cycles located at two different $\mathbb{Z}_2$-fixed points. In general, the $\mathbb{Z}_2$-fixed point labeled by 1 is chosen as a reference fixed point, and the Wilson lines of exceptional two-cycles wrapped around other $\mathbb{Z}_2$-fixed points are given with respect to this point. The convention is that $\tau^\alpha_j = 0$ means the same orientation as the reference exceptional two-cycle, while $\tau^\alpha_j = 1$ refers to the opposite orientation. If the bulk cycle is shifted by half a lattice vector, a new reference point is chosen. As we will see later in 2.8, this choice is not completely arbitrary. Note that the superscript α in τ^α_j can be omitted after introducing reference points and fractional three-cycles in the next section.

- The discrete shifts $\sigma^j \in \{0, 1\}, j = 1, 2, 3$: They parametrize whether a torus one-cycle on the two-torus $T^2_{(j)}$ passes through the origin ($\sigma^j = 0$) or whether it is shifted by half a lattice vector ($\sigma^j = 1$). The shifts do not appear explicitly in the expression above, but are rather hidden in the labels α, β of the $\mathbb{Z}_2$-fixed points. For reasons of convenience, it is useful to introduce them explicitly when calculating intersection numbers in the framework of model building, c.f. appendix A.2.

In total, there are $2^2 \cdot 2^3 \cdot 2^3 = 256$ possible choices for the set of discrete parameters. For details about the derivation of the sign factors, see e.g. [92].
An example of an exceptional three-cycle of the second twisted sector is depicted in figure 2.7.

Fractional three-cycle

There are two sorts of three-cycles the D6-branes can wrap: the bulk three-cycles arising from the untwisted sector, and the exceptional three-cycles arising in the $\mathbb{Z}_2$ -twisted sectors. Combining both gives rise to so-called fractional cycles, given as a superposition of a bulk three-cycle and the sum over the three $\mathbb{Z}_2$-twisted sectors containing the exceptional three-cycles

$$\Pi^{\text{frac}} = \frac{1}{4}\left(\Pi^{\text{bulk}} + \sum_{i=1}^{3} \Pi^{\mathbb{Z}_2^{(i)}}\right) . \tag{2.32}$$

The advantage of fractional three-cycles in model building is that they are pinned down at the $\mathbb{Z}_2$-fixed points such that none of the continuous displacement moduli survives. Also, since both the bulk part and the exceptional part of the fractional three-cycle can contribute to the intersection numbers, the possibilities for model building are enriched. In order for the basis of the four bulk cycles and all 28 exceptional cycles to form an unimodular lattice, the overall factor in front has to be 1/4. The overall factor 1/4 is related to the fact that three-cycles passing through $\mathbb{Z}_2$-fixed points are mapped to themselves under a $\mathbb{Z}_2$-rotation.

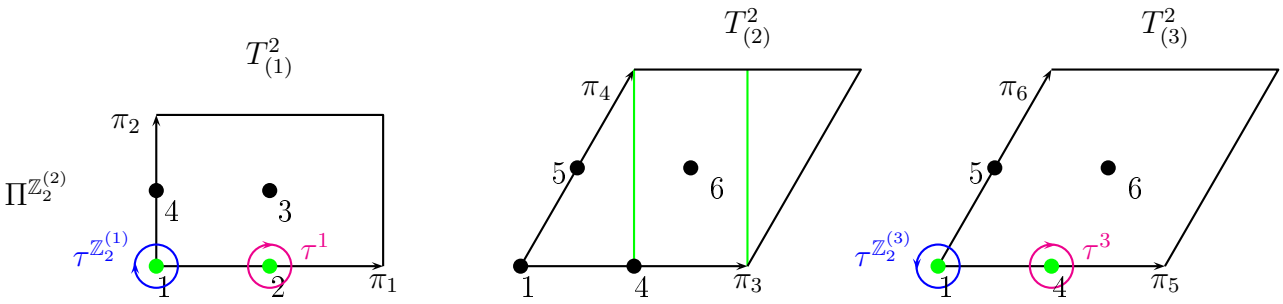

Figure 2.7: Pictorial representation of an orbifold representative of an exceptional three-cycle arising in the $\mathbb{Z}_2^{(2)}$-twisted sector. The action of $\mathbb{Z}_2^{(2)}$ is non-trivial on the first and third two-torus $T^2_{(1)} \times T^2_{(3)}$ and trivial on the second two-torus $T^2_{(2)}$. The exceptional three-cycle appears as a tensor product of a one-cycle on $T^2_{(2)}$ with two-cycles arising from blowing up $\mathbb{Z}_2^{(2)}$-fixed points on $T^2_{(1)} \times T^2_{(3)}$. The circles indicate the $\mathbb{Z}_2$-fixed points contributing to the exceptional three-cycle. The points encircled in blue correspond to the reference points and contribute with a factor $(-1)^{\tau^{\mathbb{Z}_2^{(i)}}}$, $i = 1, 3$, to the exceptional three-cycle $\Pi^{\mathbb{Z}_2^{(2)}}$. The points encircled in magenta contribute to $\Pi^{\mathbb{Z}_2^{(2)}}$ with a factor $(-1)^{\tau^{\mathbb{Z}_2^{(i)}}+\tau^i}$. Concretely, the three-cycle depicted above can be written as $(-1)^{\tau^{\mathbb{Z}_2^{(2)}}} \left(e^{(2)}_{11} + e^{(2)}_{14}(-1)^{\tau^3} + e^{(2)}_{21}(-1)^{\tau^1} + e^{(2)}_{24}(-1)^{\tau^1+\tau^3}\right) \otimes (\pi_3 - 2\pi_4)$. The factor $(-1)^{\tau^{\mathbb{Z}_2^{(2)}}}$ in front is obtained by using the relation $\tau^{\mathbb{Z}_2^{(1)}} = \tau^{\mathbb{Z}_2^{(2)}} + \tau^{\mathbb{Z}_2^{(3)}}$. In order to get the orbifold-invariant three-cycle, the orbifold images have to be added.

Only the exceptional cycles associated to the fixed points traversed by the bulk three-cycle contribute to the fractional cycle.
A generic fractional cycle can thus be expressed in terms of the basis cycles as follows:

$$\begin{aligned}\Pi_a^{\text{frac}} =& \frac{1}{4}\Pi_a^{\text{bulk}} + \frac{1}{4}\sum_{i=1}^{3}\Pi_a^{\mathbb{Z}_2^{(i)}} \\ =& \frac{1}{4}\left(P_a\rho_1 + Q_a\rho_2 + U_a\rho_3 + V_a\rho_4\right) + \frac{1}{4}\sum_{\alpha=0}^{5}\left(x^{(1)}_{\alpha,a}\,\varepsilon^{(1)}_\alpha + y^{(1)}_{\alpha,a}\,\tilde{\varepsilon}^{(1)}_\alpha\right) + \frac{1}{4}\sum_{l=2,3}\sum_{\alpha=1}^{4}\left(x^{(l)}_{\alpha,a}\,\varepsilon^{(l)}_\alpha + y^{(l)}_{\alpha,a}\,\tilde{\varepsilon}^{(l)}_\alpha\right),\end{aligned} \tag{2.33}$$

with the bulk wrapping numbers as defined in (2.12), and a is the D6-brane label. The exceptional wrapping numbers $(x^{(k)}_{\alpha,a}, y^{(k)}_{\alpha,a})$, $k = 1, 2, 3$ are fixed by the torus wrapping numbers (n^k_a, m^k_a) and the discrete parameters. This is due to the fact that the bulk cycle needs to pass through the $\mathbb{Z}_2$-fixed points at which the exceptional cycles are stuck. The exceptional wrapping numbers are linear combinations of the torus wrapping numbers (n^k_a, m^k_a) of the $\mathbb{Z}_2^{(k)}$-invariant torus, with the pre-factor determined by the discrete parameters.
The general form of the exceptional wrapping numbers can be divided into two classes (I) and (II), where the first (second) class corresponds to coefficients receiving contributions from one (two) fixed points. Not all of the exceptional wrapping numbers $(x^{(k)}_{\alpha,a}, y^{(k)}_{\alpha,a})$ in table 2.7 are non-zero. The following rules are valid:

- In the first twisted sector $k = 1$, exactly three of the six pairs $(x^{(1)}_{\alpha,a}, y^{(1)}_{\alpha,a})$ are different from zero if the bulk cycle is shifted on the second or third torus, i.e. $(\sigma^2, \sigma^3) \neq (0, 0)$. Two of them belong to class (I), and one belongs to class (II). In the absence of shifts on both the second and third torus, i.e. $(\sigma^2, \sigma^3) = (0, 0)$, four pairs $(x^{(1)}_{\alpha,a}, y^{(1)}_{\alpha,a})$ are non-zero, each pair belonging to class (I). The remaining exceptional wrapping numbers are zero.

Exceptional wrapping numbers $(x^{(k)}_{\alpha,a}, y^{(k)}_{\alpha,a})$ **on** $T^6/(\mathbb{Z}_2 \times \mathbb{Z}_6 \times \Omega\mathcal{R})$ **in terms of torus wrapping numbers** (n^k_a, m^k_a)			
$\mathbb{Z}_2^{(1)}$**twisted sector**		$\mathbb{Z}_2^{(l)}$**twisted sector with** $l = 2, 3$	
I.	II.	I.	II.
$(z^{(1)}_{\alpha,a}\, n^1_a, z^{(1)}_{\alpha,a}\, m^1_a)$	$(\hat{z}^{(1)}_{\alpha,a}\, n^1_a, \hat{z}^{(1)}_{\alpha,a}\, m^1_a)$	$(\zeta^{(l)}_{\alpha,a}\, n^l_a\ ,\ \zeta^{(l)}_{\alpha,a}\, m^l_a)$ $(\zeta^{(l)}_{\alpha,a}\, m^l_a\ ,\ -\zeta^{(l)}_{\alpha,a}\, (n^l_a + m^l_a))$ $(-\zeta^{(l)}_{\alpha,a}\, (n^l_a + m^l_a)\ ,\ \zeta^{(l)}_{\alpha,a}\, n^l_a)$	$\left(-\zeta^{(l)}_{\alpha,a}\, n^l_a + (\hat{\zeta}^{(l)}_{\alpha,a} - \zeta^{(l)}_{\alpha,a})\, m^l_a\ ,\ (\zeta^{(l)}_{\alpha,a} - \hat{\zeta}^{(l)}_{\alpha,a})\, n^l_a - \hat{\zeta}^{(l)}_{\alpha,a}\, m^l_a\right)$ $\left((\zeta^{(l)}_{\alpha,a} - \hat{\zeta}^{(l)}_{\alpha,a})\, n^l_a - \hat{\zeta}^{(l)}_{\alpha,a}\, m^l\ ,\ \zeta^{(l)}_{\alpha,a}\, m^l_a + \hat{\zeta}^{(l)}_{\alpha,a}\, n^l_a\right)$ $\left(\hat{\zeta}^{(l)}_{\alpha,a}\, n^l_a + \zeta^{(l)}_{\alpha,a}\, m^l_a\ ,\ -\zeta^{(l)}_{\alpha,a}\, n^l_a + (\hat{\zeta}^{(l)}_{\alpha,a} - \zeta^{(l)}_{\alpha,a})\, m^l_a\right)$

Table 2.7: The denomination type I refers to exceptional wrapping numbers receiving a single contribution from an orbit of an exceptional three-cycle given in table 2.4. Type II exceptional wrapping numbers stem from an orbit contributing twice, which is due to two different $\mathbb{Z}_2$ fixed points on $T^2_{(j)} \times T^2_{(k)}$. The exact form of the pre-factors $z^{(1)}_{\alpha,a}, \zeta^{(l)}_{\alpha,a}, \hat{\zeta}^{(l)}_{\alpha,a} \in \{\pm 1\}$ and $\hat{z}^{(1)}_{\alpha,a} \in \{0, \pm 2\}$, is given in appendix A.1.

- For each twisted sector $k = 2, 3$, exactly two of the four pairs $(x^{(k)}_{\alpha,a}, y^{(k)}_{\alpha,a})$ have non-zero entries, independently of shifts.

The exact form of the pre-factors $z^{(1)}_{\alpha,a}, \zeta^{(l)}_{\alpha,a}, \hat{\zeta}^{(l)}_{\alpha,a} \in \{\pm 1\}$ and $\hat{z}^{(1)}_{\alpha,a} \in \{0, \pm 2\}$ can be read off case-by-case from table A.1, which is illustrated on examples in appendix A.1.
Note that the Wilson lines τ^i appearing in table A.1 only support one index i corresponding to the label of the three two-tori, in contrast to the Wilson lines τ^α_j appearing in (2.31) supporting two indexes j, corresponding to the torus label, and α, corresponding to one of the four fixed points on a given two-torus. The index α has become superfluous upon introducing fractional cycles and reference points. Indeed, a torus three-cycle traverses exactly two $\mathbb{Z}_2$-fixed points on each two-torus. In the fractional three-cycles, only those exceptional three-cycles whose $\mathbb{Z}_2$-fixed points are traversed by the torus three-cycles contribute. Thus, we only obtain one Wilson line per two-torus, corresponding to the relative orientation between the reference point and the second fixed point the torus three-cycles traverses. The statement remains true when summing over orbifold images, as the orbifold action does not change the discrete Wilson lines.
To clarify the meaning of tables 2.7 and A.1, concrete examples of the construction of fractional cycles are given in appendix A.1.
Note that table A.1 contains only the possibilities for (n^3_a, m^3_a)=(odd,odd). This is due to our choice of the orbifold representative, see page 21.

The chiral massless open string sector can be computed through the intersection numbers of fractional three-cycles [77], which are topological quantities. The formulas to compute these intersection numbers are given in section 3.3.

Finally, note that there is a subtlety in the way a torus one-cycle is shifted. Indeed, the shift cannot be defined arbitrarily, otherwise contradictions arise. Let us write the labels of the $\mathbb{Z}_2$-fixed points a one-cycle traverses on a two-torus as an array of the form $\begin{pmatrix} \alpha \\ \beta \end{pmatrix}$, where the upper entry α is the reference point.
Consider as a concrete example a one-cycle on the second two-torus $T^2_{(2)}$ with wrapping numbers (n^2_a, m^2_a) =(even,odd), passing through the fixed points $\begin{pmatrix} 1 \\ 5 \end{pmatrix}$. There are two possibilities to shift this one-cycle: it can either be shifted along $\frac{1}{2}\pi_3$, so that the shifted cycle

passes through the fixed points $\begin{pmatrix} 4 \\ 6 \end{pmatrix}$, or it can be shifted by $\frac{1}{2}(\pi_3 + \pi_4)$, so that the shifted cycle passes through $\begin{pmatrix} 6 \\ 4 \end{pmatrix}$. We obtain different reference points for different definitions of the shift. Let us keep the first definition for the shift.
Next, consider the one-cycle with wrapping numbers (n_a^2, m_a^2) =(odd,odd) traversing the fixed points $\begin{pmatrix} 1 \\ 6 \end{pmatrix}$. Let us define the shift along $\frac{1}{2}\pi_3$ with the shifted cycle passing through $\begin{pmatrix} 4 \\ 5 \end{pmatrix}$. However, the two definitions of the shifts we chose in this example are incompatible, because they do not commute with the orbifold action ω on $T^2_{(2)}$:

$$\begin{pmatrix} 1 \\ 5 \end{pmatrix} \overset{\sigma_a^2}{\to} \begin{pmatrix} 4 \\ 6 \end{pmatrix} \overset{\omega}{\to} \begin{pmatrix} 5 \\ 4 \end{pmatrix}$$
$$\begin{pmatrix} 1 \\ 5 \end{pmatrix} \overset{\omega}{\to} \begin{pmatrix} 1 \\ 6 \end{pmatrix} \overset{\sigma_a^2}{\to} \begin{pmatrix} 4 \\ 5 \end{pmatrix} \lightning$$

This leads to inconsistencies in the computation of intersection numbers. The problem can be solved by defining the shifts in accordance with the orbifold action. In our example given here, the situation can be salvaged by using for example the second definition of the shift for one-cycles with (n_a^2, m_a^2) =(even,odd):

$$\begin{pmatrix} 1 \\ 5 \end{pmatrix} \overset{\sigma_a^2}{\to} \begin{pmatrix} 6 \\ 4 \end{pmatrix} \overset{\omega}{\to} \begin{pmatrix} 4 \\ 5 \end{pmatrix}$$
$$\begin{pmatrix} 1 \\ 5 \end{pmatrix} \overset{\omega}{\to} \begin{pmatrix} 1 \\ 6 \end{pmatrix} \overset{\sigma_a^2}{\to} \begin{pmatrix} 4 \\ 5 \end{pmatrix} \checkmark$$

This subtlety was taken into account for the first time in [76]. In table 2.8, we give the definitions of the shifts we use in the present work, which are compatible with the orbifold action.
Since there is no $\mathbb{Z}_6$-action on the first two-torus $T^2_{(1)}$, the shifts can be defined arbitrarily in case of the **a**-type lattice. For the **b**-type lattice, fixed points 2 and 3 are permuted under the orientifold projection $\Omega\mathcal{R}$, so that the shifts must be defined in accordance with the $\Omega\mathcal{R}$-action.

Figure 2.8 provides an explicit example of a fractional three-cycle in the presence of a shift on the first two-torus.

Note that in figure 2.8, due to the choice of the reference points in table 2.8, the point 3 becomes the new reference point after a shift on the first torus.

2.4 Consistency conditions

2.4.1 Supersymmetry and Special Lagrangian Cycles

In order to end up with $\mathcal{N} = 1$ SUSY in four dimensions, the D6-branes need to preserve SUSY by satisfying the SUSY conditions. In Type IIA string theory, it turned out that the

Assignment of prefactors $(-1)^{\mathbb{Z}_2^{(i)}\tau_a}$ or $(-1)^{\mathbb{Z}_2^{(i)}\tau_a+\tau_a^i}$			
	Assignment on $T^2_{(1)}$	Assignment on $T^2_{(2)}$	Assignment on $T^2_{(3)}$
(n_a^i, m_a^i)	(odd,odd) (odd,even) (even,odd)	(odd,odd) $\xrightarrow{\omega}$ (odd,even) $\xrightarrow{\omega}$ (even,odd)	(odd,odd) $\xrightarrow{\omega}$ (even,odd) $\xrightarrow{\omega}$ (odd,even)
$\sigma_a^i = 0$	$\begin{pmatrix}1\\3\end{pmatrix} \overset{\Omega\mathcal{R}_\mathbf{b}}{\to} \begin{pmatrix}1\\2\end{pmatrix} \quad \begin{pmatrix}1\\4\end{pmatrix} \overset{\Omega\mathcal{R}_\mathbf{b}}{\circlearrowleft}$	$\begin{pmatrix}1\\6\end{pmatrix} \to \begin{pmatrix}1\\4\end{pmatrix} \to \begin{pmatrix}1\\5\end{pmatrix}$	$\begin{pmatrix}1\\6\end{pmatrix} \to \begin{pmatrix}1\\5\end{pmatrix} \to \begin{pmatrix}1\\4\end{pmatrix}$
$\sigma_a^i = 1$	$\begin{pmatrix}2\\4\end{pmatrix} \overset{\Omega\mathcal{R}_\mathbf{b}}{\to} \begin{pmatrix}3\\4\end{pmatrix} \quad \begin{pmatrix}2\\3\end{pmatrix} \updownarrow \Omega\mathcal{R}_\mathbf{b}$	$\begin{pmatrix}4\\5\end{pmatrix} \to \begin{pmatrix}5\\6\end{pmatrix} \to \begin{pmatrix}6\\4\end{pmatrix}$	$\begin{pmatrix}4\\5\end{pmatrix} \to \begin{pmatrix}6\\4\end{pmatrix} \to \begin{pmatrix}5\\6\end{pmatrix}$

Table 2.8: Consistent definition of the shift of one-cycles on each two-torus $T^2_{(i)}$, $i = 1, 2, 3$. The shift on the second and third two-torus is defined in accordance with the orbifold action, as has been established in [76]. The definition of the shift on the first two-torus $T^2_{(1)}$ is consistent with the $\Omega\mathcal{R}$-projection on the **b**-type lattice. The upper entry corresponds to the reference point and contributes with sign factor $(-1)^{\mathbb{Z}_2^{(i)}\tau_a}$ to the exceptional three-cycle $\Pi_a^{\mathbb{Z}_2^{(j),j\neq i}}$. The contribution of the lower entry is given by the sign factor $(-1)^{\mathbb{Z}_2^{(i)}\tau_a+\tau_a^i}$.

SUSY equations boil down to a set of geometrical conditions on the D6-branes, namely the Lagrangian condition and the special Lagrangian condition, see [53] for details. Since we are working at the orbifold point, only the bulk part of the fractional three-cycles is relevant. Away from the orbifold point, also the exceptional three-cycles become important, see e.g. [110, 109, 111].

The Lagrangian conditions involve the Kähler two-form, which can locally be written as follows:

$$J_{1,1}^{\text{Kähler}} = \sum_{i,k=1}^{3} g_{i\bar{k}} dz_i \wedge d\bar{z}_k = \sum_{i=1}^{3} g_{i\bar{i}} dz_i \wedge d\bar{z}_i \,, \tag{2.34}$$

where i, k label the three complex directions, namely the three two-tori $T^2_{(i)}$, $i = 1, 2, 3$, and $g_{i\bar{k}}$ corresponds to the torus metric. Mixing terms $dz_i \wedge d\bar{z}_k$, $i \neq k$ are not invariant under the action of $\mathbb{Z}_2 \times \mathbb{Z}_6$ and are thus forbidden. A cycle Π_a is called Lagrangian if it satisfies the Lagrangian condition

$$J_{1,1}^{\text{Kähler}}|_{\Pi_a} = 0 \,. \tag{2.35}$$

This condition means that the Kähler form must vanish on the three-cycle Π_a.
The special Lagrangian conditions are introduced via the holomorphic volume three-form Ω_3, which is defined up to a global phase factor $e^{i\varphi_a}$. The volume of a three-cycle is given by

$$\text{Vol}(\Pi_a) = \int_{\Pi_a} |\Omega_3| \quad \text{with} \quad \Omega_3 = e^{i\varphi_a}\sqrt{|g|}(dz_1 \wedge dz_2 \wedge dz_3) \,, \tag{2.36}$$

where g is the determinant of the metric. A three-cycle Π_a is called special Lagrangian if it satisfies the special Lagrangian conditions given by

$$\Re(\Omega_3)|_{\Pi_a} > 0 \,, \qquad \Im(\Omega_3)|_{\Pi_a} = 0 \,. \tag{2.37}$$

The three-form Ω_3 is a so-called calibration form, and we say that the three-cycle Π_a is calibrated with respect to the three-form $\Re(\Omega_3)$. A cycle which is calibrated is automatically volume minimizing in its own homology class. In the picture of the three two-tori, a calibrated cycle appears as straight lines and not as random curves.
Since the $\mathcal{R}$ part of the orientifold action acts on the Kähler two-form and the holomorphic volume three-form as $\mathcal{R}(J_{1,1}^{\text{Kähler}}) = -J_{1,1}^{\text{Kähler}}$ and $\mathcal{R}(\Omega_3) = \overline{\Omega}_3$, and since the O6-planes

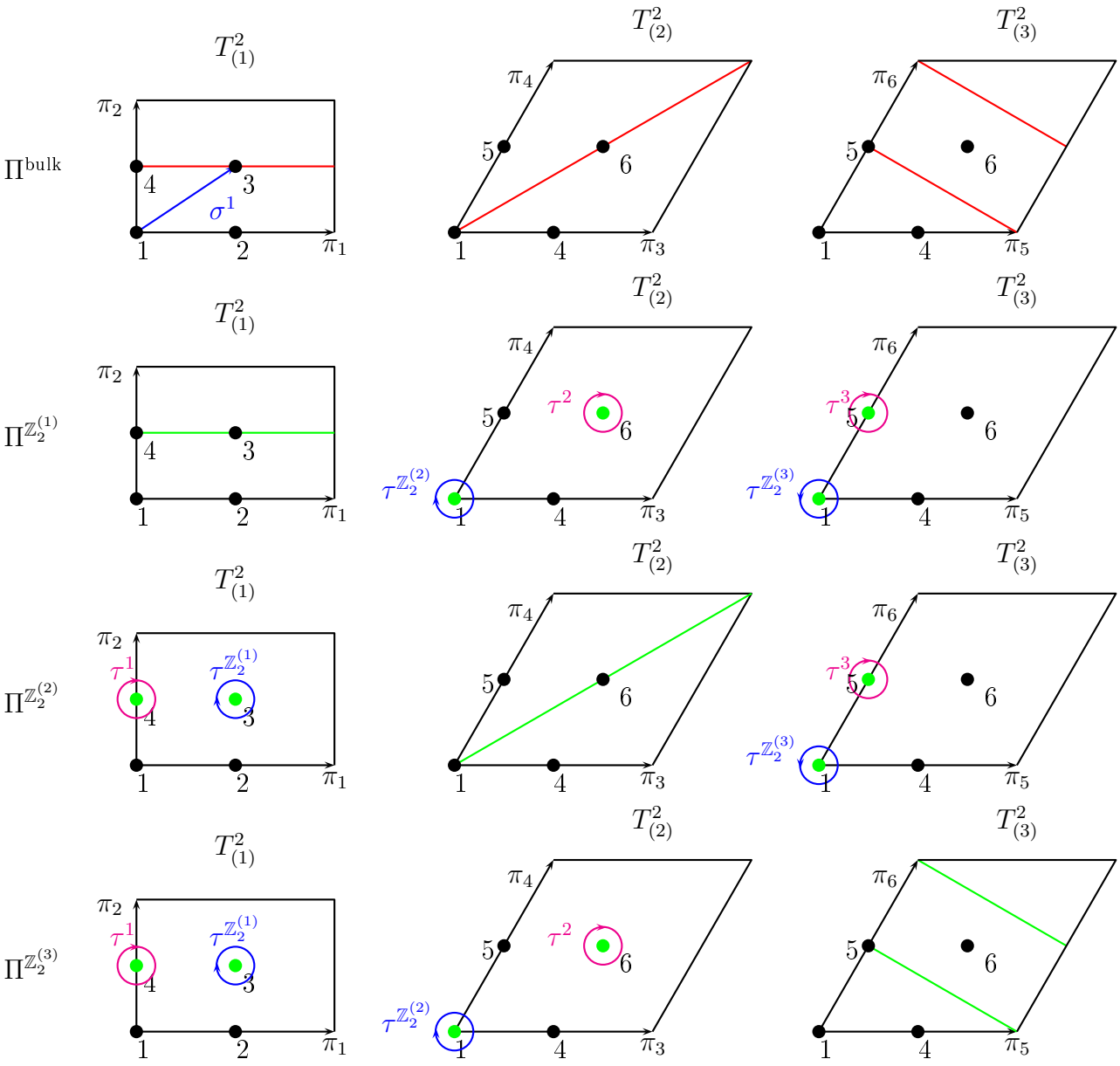

Figure 2.8: Example of an orbifold representative of a fractional three-cycle. The bulk three-cycle Π^{bulk} is indicated in red, and the three associated exceptional three-cycles $\Pi^{\mathbb{Z}_2^{(1)}}$, $\Pi^{\mathbb{Z}_2^{(2)}}$ and $\Pi^{\mathbb{Z}_2^{(3)}}$ are depicted in green. The points encircled in blue correspond to the reference points and contribute with a factor $(-1)^{\tau^{\mathbb{Z}_2^{(j)}}}$ to the exceptional three-cycles $\Pi^{\mathbb{Z}_2^{(i)}}$ with $i, j = 1, 2, 3$ and $i \neq j$. The points encircled in magenta contribute to $\Pi^{\mathbb{Z}_2^{(i)}}$ with a factor $(-1)^{\tau^{\mathbb{Z}_2^{(j)}}+\tau^j}$.

correspond to the fixed loci under $\mathcal{R}$, it follows that the O6-planes satisfy both the Lagrangian and special Lagrangian conditions with $\varphi_{O6} = 0$:

$$J_{1,1}^{\text{Kähler}}|_{\Pi_{O6}} = 0\,, \tag{2.38}$$

$$\Re(\Omega_3)|_{\Pi_{O6}} > 0\,, \qquad \Im(\Omega_3)|_{\Pi_{O6}} = 0\,. \tag{2.39}$$

In the language of SUSY, the phase factor $e^{i\varphi_a}$ in the definition of the holomorphic volume form Ω_3 actually parametrizes which $\mathcal{N} = 1$ SUSY is preserved by the D6-brane wrapping the three-cycle Π_a. For factorisable six-tori this phase factor φ_a can be a given geometric meaning in terms of the (sum of the) angle(s) between the real axis and the three-cycle, as we will see below.

In order to preserve $\mathcal{N}=1$ SUSY, all the D6-branes present in a model have to be calibrated with respect to the same holomorphic volume three-form as the O6-planes, i.e. $\varphi_a = \varphi_{O6} = 0 \; \forall \; a$. For more details, see [77, 116, 117].

The equations (2.37) are of a local differential form. As usual in physics, one can work with the differential or the integral form of equations. Commonly, in the present context one works with the integral form of equations. In order to write these down, we introduce the complex number $\mathcal{Z}_a$ corresponding to the following integral:

$$\mathcal{Z}_a \equiv \int_{\Pi_a} \Omega_3 \, . \tag{2.40}$$

If the cycle Π_a is special Lagrangian, the quantity $\mathcal{Z}_a$ is a real number and corresponds to the volume of the three-cycle Π_a. In order to find explicit expressions for special Lagrangian cycles, the integrated and normalized forms of equations (2.37) are used [65]:

$$\Im(\mathcal{Z}_a) = 0 \; , \qquad \Re(\mathcal{Z}_a) > 0 \, . \tag{2.41}$$

In the geometrical set-up of the present work, the number $\mathcal{Z}_a$ has been given in [65]:

$$\mathcal{Z}_a = \prod_{k=1}^{3} \left(e^{-i\pi\tilde{\phi}_k} x_a^k \right) \, , \tag{2.42}$$

where $\tilde{\phi}_k$ encodes the information about the choice of the orientifold-invariant direction, i.e. whether the lattice is of **a**-, **b**-, **A**- or **B**-type, and x_a^k involves the torus wrapping numbers of the one-cycle a wrapped on the two-torus $T^2_{(k)}$. We have

$$\tilde{\phi}_k = \begin{cases} 0 & \text{for } \mathbf{a}, \mathbf{b}, \mathbf{A} \\ \frac{1}{6} & \text{for } \mathbf{B} \end{cases} \, , \tag{2.43}$$

$$x_a^k = \begin{cases} n_a^1 + i\frac{R_2}{R_1}(m_a^1 + b n_a^1) & \text{for } T^2_{(1)} \\ n_a^l + e^{i\frac{\pi}{3}} m_a^l & \text{for } T^2_{(l)}, l = 2,3 \end{cases} \, . \tag{2.44}$$

The SUSY conditions boil down to requiring that the sum of the angles between Π_a and the real axis on the three two-tori must be zero. So it is useful to express the angle $\pi\phi_a$ of the one-cycle a with respect to the real axis on the two-torus $T^2_{(k)}$ in terms of torus wrapping numbers:

$$\tan\left(\pi\phi_a\right)_k = \begin{cases} \frac{m_a + b n_a}{n_a} \frac{R_2}{R_1} & \text{for } \mathbf{a}, \mathbf{b} \\ \sqrt{3}\frac{m_a}{2n_a + m_a} & \text{for } \mathbf{A} \\ \frac{1}{\sqrt{3}} \frac{m_a - n_a}{n_a + m_a} & \text{for } \mathbf{B} \end{cases} \, . \tag{2.45}$$

The conditions (2.41) can be calculated in terms of the torus wrapping numbers, which in turn can be expressed in terms of the bulk wrapping numbers (2.12), giving:

a/bAA	$3Q_a + \varrho\,[2U_a + V_a + b(2P_a + Q_a)] = 0$ $2P_a + Q_a - \varrho\,[V_a + bQ_a] > 0$
a/bAB	$Q_a - P_a + \varrho\,[U_a + V_a + b(P_a + Q_a)] = 0$ $3(P_a + Q_a) + \varrho\,[U_a - V_a + b(P_a - Q_a)] > 0$
a/bBB	$-3P_a + \varrho\,[U_a + 2V_a + b(P_a + 2Q_a)] = 0$ $P_a + 2Q_a + \varrho\,[U_a + bP_a] > 0$

(2.46)

The SUSY conditions correspond to the first set of consistency conditions a stable particle physics model has to fulfill.

2.4.2 RR-tadpole cancellation conditions

The D6-branes and O6-planes couple via the Chern-Simons coupling (2.27) to the Ramond-Ramond field C_7 and are thus charged under this field. The RR-charges of the O6-planes are related to the RR-charges of the D6-branes as $Q_{D6} = -4Q_{O6}$ [50]. This results from imposing the cancellation of the so-called RR-tadpole diagram, which can be computed via CFT methods. For details about the derivation of RR-tadpoles, see for example [118, 87, 119]. Other than by cancellation of RR-tadpole diagrams, the RR-tadpole cancellation conditions can be derived by computing the equations of motion of the C_7 field, starting from the ten-dimensional action of Type IIA string theory, see for example [77, 120, 53] and references therein.
In the present set-up, the RR-charges are encoded in terms of cohomology classes. By virtue of Poincaré duality, the encoding can be translated into the language of three-cycle homology for D6-branes, so that charge neutrality leads to a set of homology conditions called RR-tadpole cancellation conditions [53, 121]:

$$\sum_a N_a \left(\Pi_a + \Pi_{a'}\right) = 4\Pi_{O6}\,. \tag{2.47}$$

The sum goes over all the cycles Π_a present in the model, and N_a is the number of cycles in the homology class of the fractional three-cycle Π_a. The D6-branes wrapping the orientifold images $\Pi_{a'}$ of three-cycles Π_a also carry RR-charges.
As a side-remark, note that the RR-tadpole cancellation conditions also imply the cancellation of non-Abelian gauge anomalies. The other anomalies of type Abelian, mixed Abelian-non-Abelian and mixed Abelian-Gravitational are canceled by the Green-Schwarz mechanism [122] which can be generalized to the set-up of intersecting D6-branes [123].

In general, models which do not satisfy the RR-tadpole cancellation conditions are called **local** models. On the other hand, models which satisfy the RR-tadpole cancellation conditions will be called **semi-global** models in this thesis.
In the present set-up, the RR-tadpole cancellation conditions can be divided into a bulk and an exceptional part:

$$\frac{1}{4}\sum_a N_a \left(\Pi_a^{\text{bulk}} + \Pi_{a'}^{\text{bulk}}\right) = 4N_{O6}\sum_{i=0}^{4}(\eta_{\Omega\mathcal{R}\mathbb{Z}_2^{(i)}}\frac{1}{4}\Pi_{\Omega\mathcal{R}\mathbb{Z}_2^{(i)}})\,, \tag{2.48}$$

$$\sum_a N_a \left(\Pi_a^{\mathbb{Z}_2^{(i)}} + \Pi_{a'}^{\mathbb{Z}_2^{(i)}}\right) = 0 \quad \text{for} \quad i = 1,2,3\,, \tag{2.49}$$

where $\Omega\mathcal{R}\mathbb{Z}_2^{(0)} \equiv \Omega\mathcal{R}$ and $N_{O6} = 2(1-b)$ is the number of identical O6-planes. The right-hand side of the second equation is zero since the O6-planes have no exceptional part [113]. This is due to the fact that there are no twisted sector contributions to the so-called Klein-Bottle amplitude, which is a result from CFT. Using formulas (2.11), (2.48) and table 2.2, the bulk part of the equations can be expressed in terms of the bulk wrapping numbers

P, Q, U, V:

$$\begin{array}{c|c} \textbf{a/bAA} & \begin{array}{l} \sum_a N_a\,(2\,P_a + Q_a) = 8\,\left(\eta_{\Omega\mathcal{R}} + 3\,\eta_{\Omega\mathcal{R}\mathbb{Z}_2^{(1)}}\right) \\ -\sum_a N_a \frac{V_a + b\,Q_a}{1-b} = 8\,\left(\eta_{\Omega\mathcal{R}\mathbb{Z}_2^{(2)}} + \eta_{\Omega\mathcal{R}\mathbb{Z}_2^{(3)}}\right) \end{array} \\ \hline \textbf{a/bAB} & \begin{array}{l} \sum_a N_a\,(P_a + Q_a) = 8\,\left(\eta_{\Omega\mathcal{R}} + \eta_{\Omega\mathcal{R}\mathbb{Z}_2^{(1)}}\right) \\ \sum_a N_a \frac{U_a - V_a + b\,(P_a - Q_a)}{1-b} = 8\,\left(\eta_{\Omega\mathcal{R}\mathbb{Z}_2^{(2)}} + 3\,\eta_{\Omega\mathcal{R}\mathbb{Z}_2^{(3)}}\right) \end{array} \\ \hline \textbf{a/bBB} & \begin{array}{l} \sum_a N_a\,(P_a + 2\,Q_a) = 8\,\left(3\,\eta_{\Omega\mathcal{R}} + \eta_{\Omega\mathcal{R}\mathbb{Z}_2^{(1)}}\right) \\ \sum_a N_a \frac{U_a + b\,P_a}{1-b} = 8\,\left(\eta_{\Omega\mathcal{R}\mathbb{Z}_2^{(2)}} + \eta_{\Omega\mathcal{R}\mathbb{Z}_2^{(3)}}\right) \end{array} \end{array} \tag{2.50}$$

The same can be done for the exceptional wrapping numbers, using equations (2.33), (2.48) and table 2.5. The results are given in table 2.9.

Twisted RR-tadpole cancellation conditions on $T^6/(\mathbb{Z}_2 \times \mathbb{Z}_6 \times \Omega\mathcal{R})$ with discrete torsion ($\eta = -1$)		
lattice	$\mathbb{Z}_2^{(1)}$ **twisted sector**	$\mathbb{Z}_2^{(l)}$ **twisted sector with** $l = 2, 3$
a/bAA	$\sum_a N_a(1-\eta_{(1)})x^{(1)}_{\alpha,a} = 0, \quad \alpha = 0,1,2,3$ $\sum_a N_a[(1+\eta_{(1)})y^{(1)}_{\alpha,a} + \eta_{(1)}2b\,x^{(1)}_{\alpha,a}] = 0, \quad \alpha = 0,1,2,3$ $\sum_a N_a(x^{(1)}_{4,a} - \eta_{(1)}x^{(1)}_{5,a}) = 0,$ $\sum_a N_a[y^{(1)}_{4,a} + \eta_{(1)}y^{(1)}_{5,a} + b\,(x^{(1)}_{4,a} + \eta_{(1)}x^{(1)}_{5,a})] = 0,$	$\sum_a N_a[(1-\eta_{(l)})x^{(l)}_{\alpha,a} - \eta_{(l)}y^{(l)}_{\alpha,a}] = 0, \quad \alpha = 1,4$ $\sum_a N_a(1+\eta_{(l)})y^{(l)}_{\alpha,a} = 0, \quad \alpha = 1,4$ $\sum_a N_a[x^{(l)}_{2,a} - \eta_{(l)}x^{(l)}_{2+2b,a} - \eta_{(l)}y^{(l)}_{2+2b,a}] = 0,$ $\sum_a N_a[x^{(l)}_{3,a} - \eta_{(l)}x^{(l)}_{3-2b,a} - \eta_{(l)}y^{(l)}_{3-2b,a}] = 0,$ $\sum_a N_a(y^{(l)}_{3,a} + \eta_{(l)}y^{(l)}_{3-2b,a}) = 0,$ $\sum_a N_a(y^{(l)}_{2,a} + \eta_{(l)}y^{(l)}_{2+2b,a}) = 0,$
a/bAB	$\sum_a N_a(1-\eta_{(1)})x^{(1)}_{\alpha,a} = 0, \quad \alpha = 0,1,2,5$ $\sum_a N_a[(1+\eta_{(1)})y^{(1)}_{\alpha,a} + \eta_{(1)}2b\,x^{(1)}_{\alpha,a}] = 0, \quad \alpha = 0,1,2,5$ $\sum_a N_a(x^{(1)}_{3,a} - \eta_{(1)}x^{(1)}_{4,a}) = 0,$ $\sum_a N_a[y^{(1)}_{3,a} + \eta_{(1)}y^{(1)}_{4,a} + b\,(x^{(1)}_{3,a} + \eta_{(1)}x^{(1)}_{4,a})] = 0,$	$\sum_a N_a(x^{(l)}_{\alpha,a} + (-1)^l\,\eta_{(l)}\,y^{(l)}_{\alpha,a}) = 0, \quad \alpha = 1,4$ $\sum_a N_a(x^{(l)}_{2,a} + (-1)^l\,\eta_{(l)}y^{(l)}_{2+2b,a}) = 0,$ $\sum_a N_a(x^{(l)}_{3,a} + (-1)^l\,\eta_{(l)}y^{(l)}_{3-2b,a}) = 0,$
a/bBB	$\sum_a N_a(1-\eta_{(1)})x^{(1)}_{\alpha,a} = 0, \quad \alpha = 0,1,2,4$ $\sum_a N_a[(1+\eta_{(1)})y^{(1)}_{\alpha,a} + \eta_{(1)}2b\,x^{(1)}_{\alpha,a}] = 0, \quad \alpha = 0,1,2,4$ $\sum_a N_a(x^{(1)}_{3,a} - \eta_{(1)}x^{(1)}_{5,a}) = 0,$ $\sum_a N_a[y^{(1)}_{3,a} + \eta_{(1)}y^{(1)}_{5,a} + b\,(x^{(1)}_{3,a} + \eta_{(1)}x^{(1)}_{5,a})] = 0,$	$\sum_a N_a(1-\eta_{(l)})x^{(l)}_{\alpha,a} = 0, \quad \alpha = 1,4$ $\sum_a N_a[(1+\eta_{(l)})y^{(l)}_{\alpha,a} + \eta_{(l)}x^{(l)}_{\alpha,a}] = 0, \quad \alpha = 1,4$ $\sum_a N_a(y^{(l)}_{2,a} - \eta_{(l)}y^{(l)}_{2+2b,a}) = 0,$ $\sum_a N_a(y^{(l)}_{3b,a} - \eta_{(l)}y^{(l)}_{3-2b,a}) = 0,$ $\sum_a N_a[x^{(l)}_{2,a} + \eta_{(l)}x^{(l)}_{2+2b,a} + \eta_{(l)}y^{(l)}_{2+2b,a}] = 0,$ $\sum_a N_a[x^{(l)}_{3,a} + \eta_{(l)}x^{(l)}_{3-2b,a} + \eta_{(l)}y^{(l)}_{3-2b,a}] = 0.$

Table 2.9: Twisted RR-tadpole cancellation conditions for all lattice configurations and $\mathbb{Z}_2^{(i)}$-twisted sectors ($i = 1, 2, 3$) on $T^6/(\mathbb{Z}_2 \times \mathbb{Z}_6 \times \Omega\mathcal{R})$ with discrete torsion.

2.4.3 K-theory constraints

In general, (co-)homology classes are used to classify the three-cycles and thus the D6-branes. In chapter 5 about model building though, we will see that the D6-branes have an additional structure due to gauge fields living on them. A better description of the D6-branes would be given by K-theory, which arises in a side-branch of algebraic geometry. To get an overview of K-theory, see [124] and references therein. K-theory is able to detect D6-brane charges missed by ordinary cohomology [125, 126]. In particular, imposing the so-called K-theory constraints on the D6-branes cancels the K-theory charges not captured by the RR-tadpole cancellation conditions. The K-theory constraints are quite involved and deriving an explicit expression for them goes beyond the scope of this thesis. Traditionally, instead of using the

K-theory constraints, one uses the so-called probe-brane constraints [127]. Both constraints coincide for compactifications on smooth manifolds. The probe-brane argument states that the number of particles charged under the $USp(2N)$ gauge group must be even, lest the corresponding gauge theory becomes inconsistent [128]. The probe-brane argument can be considered as necessary conditions, but it is unknown whether these conditions are also sufficient. The probe-brane constraints can be given in terms of intersection numbers:

$$\sum_a N_a \Pi_a \circ \Pi_{\text{probe}} = 0 \text{ mod } 2\,. \tag{2.51}$$

Once again, the sum goes over all the cycles present in the model. The probe-brane Π_{probe} corresponds to any D6-brane carrying a symplectic gauge group $USp(2N)$. The D6-branes supporting such a gauge group will be classified in section 5.1.
Consistent models satisfy all the conditions, i.e. both the RR-tadpole cancellation conditions and the K-theory constraints. Semi-global models (i.e. models satisfying the RR-tadpole cancellation conditions) which fulfill the K-theory constraints are called **global** models[7].

[7]Note that the terminology used here is slightly different from the one used in our publication [64].

Chapter 3

Introduction to model building with intersecting D6-branes

We will start this chapter with a basic overview of features and assumptions used in model building with intersecting D6-branes. We will continue with a review of the particle physics models considered in this work and provide a collection of formulas used in the context of this doctoral work.

3.1 Overview of basic aspects in D6-brane model building

A fundamental result in Type IIA string theory is the association of an Abelian $U(1)$ gauge factor to each D6-brane. Indeed, along the Neumann boundary conditions, the massless open string excitations give rise to a gauge theory living on the D6-brane worldvolume. Note that this is a general result, valid for generic D-branes.
Coincident D6-branes form a so-called "stack" of D6-branes. A stack of N coincident D6-branes carries a non-Abelian unitary $U(N)$ gauge group. In case the stack of D6-brane wraps a three-cycle invariant under the $\mathcal{R}$-part of the orientifold projection $\Omega\mathcal{R}$, it can also give rise to symplectic $USp(2N)$ or orthogonal $SO(2N)$ groups. Most particle physics models possess a gauge group consisting of several gauge factors, so that several stacks are present in the model. Besides, in order to fulfill the RR-tadpole cancellation conditions, additional stacks have to be introduced generally, which are called "hidden stacks".

The massless open string excitations give rise to states transforming in the following representations of the gauge groups supported by the D6-branes:

The bifundamental representation: This representation arises when the string has the two endpoints attached to two different intersecting stacks of D6-branes a and b. The string is localized at the intersection point, where its length is zero. In general, open strings are oriented. Thus, depending on the orientation of the string, the resulting state transforms either in the bifundamental representation $(\mathbf{N_a}, \overline{\mathbf{N}}_\mathbf{b})$ or its complex conjugate $(\overline{\mathbf{N}}_\mathbf{a}, \mathbf{N_b})$. This is reflected in the sign of the intersection numbers, as we will see in the next section in more detail. The orientifold projection reverses the orientation of a string and effectively leads to taking the complex conjugate of a representation. More precisely, a string spanned between a and the orientifold image b' of b supports states transforming either in $(\mathbf{N_a}, \mathbf{N_b})$

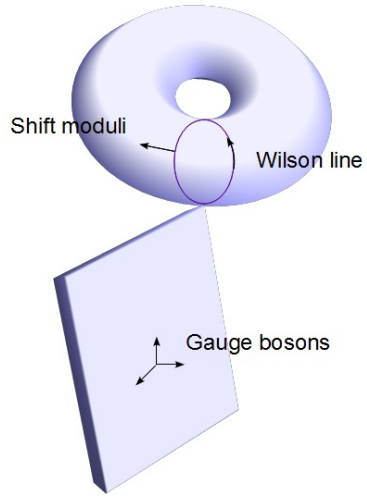

Figure 3.1: The degrees of freedom (d.o.f.) of D6-branes in Minkowski space correspond to vector multiplets containing the gauge bosons and their SUSY partners. The longitudinal d.o.f. of the D6-branes in the internal space are called Wilson lines. The transverse d.o.f. of the D6-branes in the internal space correspond to position moduli. The Wilson lines and shift moduli combine into $\mathbb{C}$-scalars in the $\mathcal{N} = 1$ chiral multiplets transforming in the adjoint representation.

or $(\overline{\mathbf{N}}_\mathbf{a}, \overline{\mathbf{N}}_\mathbf{b})$.
The particles transforming in the bifundamental representations form candidates for matter particles, i.e. quarks and leptons. Details are given in the next section.

The adjoint representation: A string having both endpoints attached to the same stack a of D6-branes gives rise to the adjoint representation $\mathbf{N}_\mathbf{a} \otimes \overline{\mathbf{N}}_\mathbf{a} = \mathbf{Adj}_a$ for a unitary group $U(N_a)$. Two cases can be distinguished:

- The string has both endpoints attached to the same stack of D6-branes on the underlying torus, in which case it gives rise to states transforming in the adjoint representation. These can be either associated to vector multiplets or to chiral multiplets transforming in the adjoint representation.
  The seven-dimensional gauge field A_M, $M = 0 \ldots 6$ of a D6-brane can be written as $A_M = (A_\mu, A_i^{\text{internal}})$ where $\mu = 0, \ldots 3$ labels the directions of the Minkowski space and $i = 4, 5, 6$ labels the three directions of the D6-brane in the compact space. After dimensional reduction, the gauge field decomposes as follows:

  1. The vector field A_μ, $\mu = 0, \ldots 3$ living in four-dimensional Minkowski space-time $\mathcal{M}^{1,3}$. This field corresponds to the usual gauge boson.
  2. The one-form $A^{\text{internal}} = \sum_i a_i(x)\eta^i$, where the η^i $(i = 4, 5, 6)$ correspond to a basis of one-forms[1] associated to the three-cycle wrapped by the D6-brane in the compact space. The coefficients a_i are called continuous Wilson lines.

  Furthermore, we have three scalars ϕ_i $(i = 7, 8, 9)$ associated to the three transverse degrees of freedom of the seven-dimensional D6-brane in the ten-dimensional space-time. These are called position moduli or shift moduli, as they cause a continuous displacement of the D6-brane along the compact space.
  The situation described above is summarized schematically in figure 3.1.

  For a stack of N_a D6-branes, we obtain multiplets transforming in the adjoint representation of the non-Abelian group $U(N_a)$. The Wilson lines a_i and shift moduli ϕ_i

[1] Although a Calabi-Yau threefold does not have (non-trivial) one-forms, a special Lagrangian submanifold can still support one-forms. This goes back to the theorem of McLean [129].

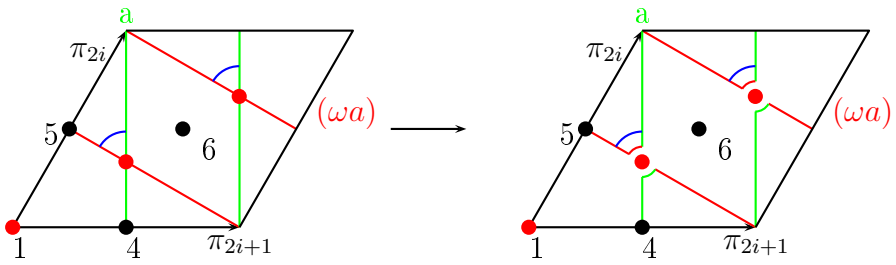

Figure 3.2: The strings depicted in blue correspond to chiral multiplets transforming in the adjoint representation of the gauge group supported by the D6-brane. These strings lead to a recombination of the D6-brane with one of its orbifold images, resulting in a breaking of the gauge group.

combine into complex scalars $\phi_i + ia_i$, forming the scalar components of three $\mathcal{N} = 1$ chiral multiplets transforming in the adjoint representation of the gauge group $U(N_a)$. The fermionic components of the chiral multiplets arise from the decomposition of the seven-dimensional gaugino. Such chiral multiplets are phenomenologically unwanted for non-Abelian gauge groups, as they do not appear in any model of particle physics. Moreover, they cause a breaking of the gauge group, which is in general also not desirable from a phenomenological point of view. However, in the case of toroidal orbifolds of the form $\mathbb{Z}_2 \times \mathbb{Z}_M$, the D6-branes wrap around fractional three-cycles passing through $\mathbb{Z}_2$-fixed points, which fixes the D6-branes. Indeed, these chiral multiplets transforming in the adjoint representation are not invariant under the $\mathbb{Z}_2$-actions and are thus projected out of the theory [65, 76, 77, 66, 92–96, 67–71, 97, 130–134]. Only toroidal orbifolds of the form $\mathbb{Z}_2 \times \mathbb{Z}_{2M}$ have a $\mathbb{Z}_2$-action on all three two-tori [92, 131, 76, 93, 65], which suppresses the continuous displacement moduli completely. The Wilson lines and shifts appearing as discrete parameters in the present work are remnants of these chiral multiplets in the adjoint representation.

- The string has its endpoints attached to different intersecting orbifold images of the same stack of D6-branes. This also gives rise to a chiral multiplet transforming in the adjoint representation, associated to a recombination modulus [135–138, 92, 139, 97]. If this modulus develops a non-vanishing VEV, it causes a deformation of the intersection point and a recombination of the D6-branes, as schematically illustrated in figure 3.2.

  This recombination triggers the breaking of the gauge group supported by the D6-brane. Special topological conditions have to be imposed on the D6-branes in order to ensure complete rigidity of the latter, see section 5.2.

The symmetric and antisymmetric representations: The (anti)symmetric representation arises from unoriented strings attached to the intersection point of a D6-brane a and its orientifold image a' as follows: $\mathbf{N_a} \otimes \mathbf{N_a} = \mathbf{Anti}_a \oplus \mathbf{Sym}_a$. The antisymmetric and symmetric representations are selected by adding and subtracting respectively the intersection number of the D6-brane a and the orientifold planes. We will give the explicit formulas in sections 3.2 and 3.3. Matter states transforming in the (anti)symmetric representation are only of limited use in particle physics models, as we will see in the next section.

Non-chiral representations: Non-chiral representations refer to particle states which come in pairs, one state transforming in a representation $\mathbf{R}$ under a certain gauge group, the

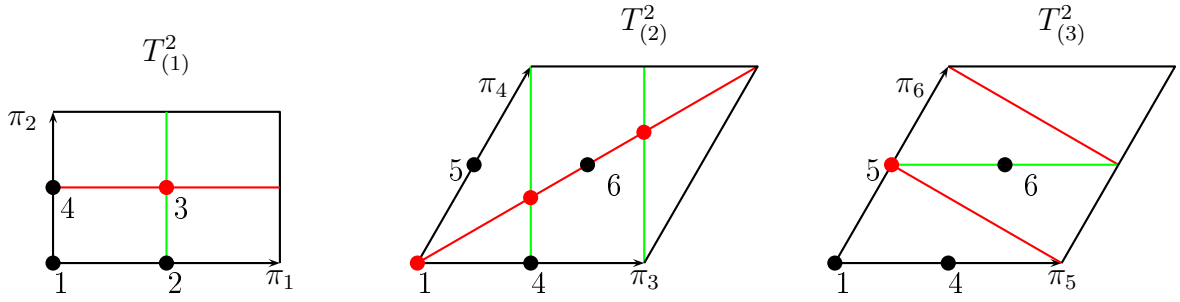

Figure 3.3: Example of orbifold representatives of intersecting bulk three-cycles. The two three-cycles depicted in green and red intersect once on the first two-torus $T^2_{(1)}$, thrice on the second two-torus $T^2_{(2)}$ and again once on the third two-torus $T^2_{(3)}$. In this example, the three-cycles thus seem to produce three matter states a priori. However, also the exceptional part and the orbifold images have to be taken into account, which may alter the results.

second state transforming in the complex conjugate representation $\overline{\mathbf{R}}$ of the gauge group. The multiplicity of non-chiral particles cannot be computed via the usual topological intersection numbers, for these take chirality into account via a sign factor and thus always give zero for non-chiral particles. Instead, they have to be counted via the so-called beta-function coefficients, which we introduce in section 3.3. These coefficients count the particle states independently of chirality. By comparing with results from CFT, these coefficients can also be related to intersection numbers. Thus, just as for the chiral spectrum, the non-chiral spectrum can also be determined via intersection numbers, although the formulas for the latter are more involved. Note that states transforming in the adjoint representation also have to be computed via the beta-function coefficients.

Up to this point, we have explained how the different representations associated to the different particles of a model can be realized in the stringy set-up with intersecting D6-branes. There remains one last ingredient for model building which consists in the determination of the multiplicity of the states in the various representations, i.e., the number of generations of the particles. This number is given by the numerical value of the topological intersection numbers. For example, in figure 3.3, the intersection number of the two three-cycles depicted in green and red is three. Indeed, the intersection points are colored in red: one intersection point on the first two-torus $T^2_{(1)}$, three intersection points on the second two-torus $T^2_{(2)}$ and again one intersection point on the third two-torus $T^2_{(3)}$. Taking the product of intersection points of each two-torus, we would a priori expect three generations.

However, in case of fractional three-cycles, the exceptional part can alter the result. Also the orbifold images have to be taken into account. The formulas allowing to compute the correct number of generations will be given in section 3.3.

3.2 Particle physics models considered in this work

In this section, we will briefly present the models considered in this work, namely the MSSM, the left-right symmetric model, the Pati-Salam model and the $SU(5)$ model.

3.2.1 MSSM-like models

We will start by indicating the particle content of the Standard Model (SM). Subsequently, mass terms and Yukawa couplings will be discussed.
The MSSM is the simplest SUSY extension of the SM. Pioneering SUSY versions of the Standard Model were constructed in [140–144] and also [145–147].
In a first step, we will discuss the (MS)SM in a purely field theoretical context. In a second step, we will show how the (MS)SM is realized in the context of intersecting D6-branes in Type IIA string theory.

The SM and MSSM in the field theoretical context

The gauge group of the SM is the following:

$$SU(3)_{QCD} \times SU(2)_L \times U(1)_Y \,,$$

where the first gauge factor corresponds to the strong interactions, described by *quantum chromodynamics* , and the second and third gauge factors describe the electroweak interactions. The "L" in $SU(2)_L$ stands for "left", as the gauge bosons of the weak interactions couple to left-handed particles only. The symbol "Y" in $U(1)_Y$ stands, for the so-called hypercharge Q_Y.
The particle content of the SM is given in table 3.1. In table 3.1, we only wrote down one

Particle content of the SM		
Denomination	Symbol	Hypercharge
Left-handed leptons	$L \equiv \begin{pmatrix} \nu_L \\ e_L \end{pmatrix}$	$-\frac{1}{2}$
Right-handed electron	e_R	1
Right-handed neutrino	ν_R	0
Left-handed quarks	$Q_L \equiv \begin{pmatrix} u_L \\ d_L \end{pmatrix}$	$\frac{1}{6}$
Right-handed up-quark	u_R	$-\frac{2}{3}$
Right-handed down-quark	d_R	$\frac{1}{3}$

Table 3.1: List of the left-handed and right-handed quarks and leptons appearing in the SM. The first column provides the names of the particles, the second column gives the symbols used in this thesis to refer to the particles, and the third column contains the associated hypercharges.

generation of particles. The SM comes with three copies of this spectrum, called generations, which we will label with $i = 1, 2, 3$. These generations present a mass hierarchy, i.e. the members of a given generation have higher masses than the corresponding particles in the previous generation. This feature of the SM has been discovered experimentally.

In quantum field theory, particles can be given a mass by adding explicit mass terms in the Lagrangian, which have to be singlets under the gauge group. The simplest way is to pair off

particles transforming in a representation $\mathbf{R}$ of the gauge group with particles transforming in the complex conjugate representation $\overline{\mathbf{R}}$ of the gauge group. Indeed, mass terms of the form $\mathbf{R} \otimes \overline{\mathbf{R}}$ contain amongst others the singlet representation of the gauge group $SU(N)$. However, a look at table 3.1 reveals that this prescription does not work for the SM. Indeed, the fermions of the SM are chiral under the gauge group $SU(2)_L$. The left-handed leptons transform as doublets under $SU(2)_L$ while the right-handed leptons transform as singlets under $SU(2)_L$, so they cannot be paired off directly to provide gauge invariant mass terms. In order to provide gauge invariant mass terms nonetheless, a so-called Higgs doublet has to be inserted, which leads to gauge-singlet cubic couplings

$$\mathcal{L}_{\mathcal{Y}} = y_u Q_L \cdot H_u u_R + y_d Q_L \cdot H_d d_R + y_e L \cdot H_u e_R + y_\nu L \cdot H_d \nu_R \,. \tag{3.1}$$

These are called Yukawa couplings. After electroweak symmetry breaking (EWSB)[2] and the Brout-Englert-Higgs mechanism[3] [152–155], these give rise to mass terms. EWSB corresponds to the breaking of the electroweak gauge group $SU(2)_L \times U(1)_Y$ to the Abelian gauge group $U(1)_{\mathrm{EM}}$, describing electromagnetism. We will not describe the process of EWSB here, but refer the reader for example to the textbook [156] for details.

The features described here for the SM are also mostly valid for the MSSM. The MSSM comes with the same particle content as the SM, except that each fermion of the SM is put into a multiplet with a bosonic superpartner, and each boson acquires a fermionic partner, forming together a $\mathcal{N} = 1$ SUSY multiplet.
Moreover, note that for the SM, only one electroweak Higgs doublet is necessary as the second one can be obtained from the first by complex conjugation. In the MSSM though, two different Higgs doublets H_u and H_d are needed. This is due to the fact that in order for the superpotential to be invariant under SUSY, it must be a holomorphic function, so that the second Higgs doublet cannot be obtained from the first by complex conjugation, see for example [39] for details. An additional argument for the existence of a second Higgs doublet arises from gauge anomaly cancellation considerations. The presence of the Higgsino, superpartner of the Higgs doublet, leads to a gauge anomaly. In order to cancel that anomaly, a second Higgs doublet has to be introduced [39].
Finally, the MSSM allows for couplings which can give rise to undesired effects such as a high decay rate for the proton. Such couplings can be suppressed by adding extra discrete $\mathbb{Z}_n$-symmetries by hand, see for example [157] for details.

The MSSM in the string theoretical context

In Type IIA string model building, the aim is in the first place to reproduce the particle content of the SM. Since SUSY is naturally integrated in superstring theory, the superpartners are obtained automatically by the associated bosonic and fermionic excitations of the open and closed strings.
In Type IIA string theory, the standard realization of the particle content in table 3.1 involves four stacks of D6-branes, two of them carrying non-Abelian gauge factors and the other two carrying Abelian gauge factors:

$$U(3)_a \times U(2)_b \times U(1)_c \times U(1)_d$$

[2] Original work on spontaneous symmetry breaking was done in [148].
[3] See also [149], [150] and [151].

$$\begin{aligned}\simeq & SU(3)_a \times SU(2)_b \times U(1)_c \times U(1)_d \times U(1)_a \times U(1)_b \\ = & SU(3)_a \times SU(2)_b \times U(1)_Y \times U(1)_b \times U(1)_{B-L} \times U(1)_{PQ}\,,\end{aligned}$$

with the definitions of the hypercharge $U(1)_Y$, Peccei-Quinn $U(1)_{PQ}$, $U(1)_b$ and baryon-lepton number $U(1)_{B-L}$ symmetries given in terms of the $U(1)$-charges Q_x by:

$$\begin{aligned}Q_Y &= \tfrac{1}{6}Q_a + \tfrac{1}{2}Q_c + \tfrac{1}{2}Q_d\,, \\ Q_{PQ} &= Q_c - Q_d\,, \\ Q_{B-L} &= \tfrac{1}{3}Q_a + Q_d\,,\end{aligned} \qquad . \tag{3.2}$$

The Peccei-Quinn symmetry is often introduced in extensions of the SM in order to explain the strong CP problem, where C stands for the operation of charge conjugation and P for parity symmetry. The strong CP problem consists in the fact that the strong sector of the SM, i.e. QCD, preserves the so-called CP symmetry, although it is no symmetry of the SM, as the electroweak sector violates it via the CKM[4] matrix [158]. The preservation of the CP symmetry by QCD is reflected in the smallness of the electric dipole moment of the neutron [159, 160], which can be measured experimentally [161]. We will not give further details here, but refer the reader to [162–165] for details.

The baryon-lepton number symmetry involves two quantum numbers. The baryon number B is zero for leptons and $\pm 1/3$ for quarks. The lepton number L is zero for quarks and ± 1 for leptons. The baryon/lepton numbers give the difference between particles and antiparticles. In general, B/L is taken to be positive for particles and negative for antiparticles. These quantum numbers are additive, i.e. the total baryon/lepton number of a particle interaction is given by the sum of the baryon/lepton numbers of each quark/lepton appearing in the interaction. The interactions in the SM generally preserve the baryon number and lepton number separately, i.e. the total baryon/lepton number of the initial particles equals the total baryon/lepton number of the final particles. However, in extensions of the SM, they may not be conserved separately anymore. Instead, one uses the difference $B-L$ as quantum number, which is conserved during elementary particle interactions even in extensions of the SM. Proton decay is an example of a reaction violating B and L but conserving $B-L$.

These originally local $U(1)$ symmetries are broken spontaneously by the Stückelberg mechanism. The Stückelberg mechanism is similar to the Higgs mechanism, see for example [166] for details. In the Stückelberg mechanism of our stringy set-up, the gauge boson associated to a $U(1)$ symmetry will become massive after absorption of a closed string axion. Therefore, spontaneously broken $U(1)$ symmetries are also called "massive" $U(1)$'s. Note that the coupling of the gauge boson to the axion is given by a Chern-Simon coupling resulting directly from the generalized Green-Schwarz-mechanism. Thus, in our stringy set-up, the Stückelberg mechanism arises explicitly as a consequence of the generalized Green-Schwarz-mechanism.

The associated remnant global $U(1)$ symmetries are exact at the perturbative level, but they are broken down to discrete $\mathbb{Z}_n$-symmetries by non-perturbative effects like instantons, see [100, 78, 93, 102] and also [167, 168]. Thus, in string theory, $\mathbb{Z}_n$-symmetries are naturally integrated and need not be introduced by hand as is the case for the MSSM. However, the existence of these discrete $\mathbb{Z}_n$-symmetries is model-dependent and has to be checked for each model individually. We will do this in chapter 8.

[4] CKM stands for Cabibbo-Kobayashi-Maskawa.

Remember that Type IIA string models generally come with additional hidden stacks in order to fulfill the RR-tadpole cancellation conditions given in (2.50) and table 2.9. The hidden stacks are generally accompanied by additional $U(1)$ factors, which can be local, giving rise to dark photons, or global, giving rise to massive gauge bosons just as the mediators of the weak force after electroweak symmetry breaking. Dark photons are interesting in cosmology, since they can act as a force carrier of dark matter [169]. In fact, they would correspond to a fifth fundamental force behaving similarly as electromagnetism. Dark photons were considered to possibly provide a solution for the so-called "g-2" anomaly, which refers to a deviation of the measured muon anomalous magnetic moment [170] from the predictions of the Standard Model [171, 172].

The charges Q_x, $x \in \{a, c, d\}$ appearing in (3.2) are either -2, -1, 0, 1 or 2. An open oriented string spanned between a stack x and a stack y carries charges with opposite signs $Q_x = \pm 1$ and $Q_y = \mp 1$ at its endpoints. An open string with both endpoints attached to the same stack x has charge zero. An open string spanned between a stack x and its orientifold image x' has charge ± 2.
The multiplicity of the states in a representation is given by the numerical value of the intersection numbers $\Pi_x \circ \Pi_y$[5], the charges Q_x are related to the sign of the intersection numbers. The explicit formulas to compute $\Pi_x \circ \Pi_y$ will be provided in the next section. There are two possibilities to associate the intersection numbers to representations. One possibility is:

$$\begin{aligned} \Pi_x \circ \Pi_y \geq 0 &\Longrightarrow (\mathbf{N_x}, \overline{\mathbf{N}}_\mathbf{y}) \Longleftrightarrow Q_x = 1 \text{ and } Q_y = -1 \\ \Pi_x \circ \Pi_y \leq 0 &\Longrightarrow (\overline{\mathbf{N}}_\mathbf{x}, \mathbf{N_y}) \Longleftrightarrow Q_x = -1 \text{ and } Q_y = 1 \end{aligned} \quad , \tag{3.3}$$

while the other possibility is given by:

$$\begin{aligned} \Pi_x \circ \Pi_y \leq 0 &\Longrightarrow (\mathbf{N_x}, \overline{\mathbf{N}}_\mathbf{y}) \Longleftrightarrow Q_x = 1 \text{ and } Q_y = -1 \\ \Pi_x \circ \Pi_y \geq 0 &\Longrightarrow (\overline{\mathbf{N}}_\mathbf{x}, \mathbf{N_y}) \Longleftrightarrow Q_x = -1 \text{ and } Q_y = 1 \end{aligned} \quad . \tag{3.4}$$

Note that the following relation is always valid for three-cycles within Calabi-Yau threefolds: $\Pi_x \circ \Pi_y = -\Pi_y \circ \Pi_x$. Let us introduce the following definitions:

$$\begin{aligned} \chi^{xy} &\equiv \Pi_x \circ \Pi_y \,, \\ \chi^{\mathbf{Anti}_x} &\equiv \frac{1}{2}(\Pi_x \circ \Pi_{x'} + \Pi_x \circ \Pi_{\mathrm{O6}}) \,, \\ \chi^{\mathbf{Sym}_x} &\equiv \frac{1}{2}(\Pi_x \circ \Pi_{x'} - \Pi_x \circ \Pi_{\mathrm{O6}}) \,. \end{aligned}$$

In order to illustrate how the particle content of the MSSM in table 3.1 can be reproduced using the intersection numbers, we will choose the first convention. Using the other convention (3.4), the signs are simply flipped everywhere.
Remember that a string spanned between a cycle x and the orientifold image of a cycle y corresponds to an unoriented string. With convention (3.3), we have the following representations in case orientifold images are involved:

$$\Pi_x \circ \Pi_{y'} \leq 0 \Longrightarrow (\overline{\mathbf{N}}_\mathbf{x}, \overline{\mathbf{N}}_\mathbf{y}) \Longleftrightarrow Q_x = -1 \text{ and } Q_y = -1 \,, \tag{3.5}$$

[5]Note that we denote the fractional three-cycles Π_x^{frac} introduced in (2.33) in the following by Π_x, omitting the superscript.

$$\Pi_x \circ \Pi_{y'} \geq 0 \Longrightarrow (\mathbf{N_x}, \mathbf{N_y}) \Longleftrightarrow Q_x = 1 \text{ and } Q_y = 1\,. \tag{3.6}$$

In general, the first step consists in aiming to reproduce three generations of left-handed quarks, which arise in the chiral ab and ab' sectors[6]. The conditions to impose on the intersection numbers of the a and b stacks are reproduced in the table below:

Intersection	Chirality	Representation under $(SU(3), SU(2))_{(Q_a,Q_b,Q_c,Q_d)}$	Q_Y
χ^{ab}	≥ 0	$(\mathbf{3}, \overline{\mathbf{2}})_{(1,-1,0,0)}$	1/6
$\chi^{ab'}$	≥ 0	$(\mathbf{3}, \mathbf{2})_{(1,1,0,0)}$	1/6
	Multiplicity	Particle	
$\chi^{ab} + \chi^{ab'}$	3	Q_L	1/6

(3.7)

Thus, in order to reproduce the left-handed quarks with correct multiplicity and chirality, three conditions are imposed on the intersection numbers of the a stack with the b stack, namely $\chi^{ab} \geq 0$, $\chi^{ab'} \geq 0$ and $\chi^{ab} + \chi^{ab'} = 3$. The conditions on the intersection numbers given above (3.7) are rather stringent. Indeed, if three generations cannot be achieved with the conditions on the intersection numbers in (3.7), the first two conditions $\chi^{ab} \geq 0$ and $\chi^{ab'} \geq 0$ can be omitted, leaving only the condition on the sum of the intersection numbers $\chi^{ab} + \chi^{ab'} = 3$. This leads effectively to three chiral generations of left-handed quarks, although it allows for the presence of non-chiral pairs of left handed quarks of the form $(\mathbf{3}, \mathbf{2})_{(1/6)} + (\overline{\mathbf{3}}, \mathbf{2})_{(-1/6)}$, where the lower index refers to the hypercharge. However, even by imposing all three conditions, non-chiral pairs of left-handed quarks may still arise within a same sector ab or ab'. These can only be detected via the beta-function coefficients given in section 3.3.

In case of an enhancement of the gauge group from $U(1)_b$ to $USp(2)_b$ on the b stack, the sectors ab and ab' are equivalent and count only once, i.e. $\chi^{ab} = \chi^{ab'} = 3$.

As a side-remark, note that under the $SU(2)$ group, the fundamental representation is equivalent to its complex conjugate, i.e. $\mathbf{2}$=$\overline{\mathbf{2}}$. The bar over the representation is thus sometimes omitted.

The next step in model building is generally dedicated to the reproduction of three generations of right-handed quarks. These arise in the ac, ac', ad and ad' sectors, and the conditions

[6] Instead of referring to the intersection number between a stack x and a stack y by the symbol $\Pi_x \circ \Pi_{y'}$, we simply refer to it by the brane labels x and y and call it "the xy sector".

to impose on the intersection numbers are the following:

Intersection	Chirality	Representation under $(SU(3), SU(2))_{(Q_a,Q_b,Q_c,Q_d)}$	Q_Y
χ^{ac}	≤ 0	$(\overline{\mathbf{3}}, \mathbf{1})_{(-1,0,1,0)}$	$1/3$
$\chi^{ac'}$	≤ 0	$(\overline{\mathbf{3}}, \mathbf{1})_{(-1,0,-1,0)}$	$-2/3$
χ^{ad}	≤ 0	$(\overline{\mathbf{3}}, \mathbf{1})_{(-1,0,0,1)}$	$1/3$
$\chi^{ad'}$	≤ 0	$(\overline{\mathbf{3}}, \mathbf{1})_{(-1,0,0,-1)}$	$-2/3$
$\chi^{\mathbf{Anti}_a}$	≥ 0	$(\overline{\mathbf{3}}, \mathbf{1})_{(2,0,0,0)}$	$1/3$
	Multiplicity	Particle	
$\chi^{ac} + \chi^{ad} - \chi^{\mathbf{Anti}_a}$	-3	d_R	$1/3$
$\chi^{ac'} + \chi^{ad'}$	-3	u_R	$-2/3$

(3.8)

Once again, the conditions can be loosened by imposing only the last two equations. Here, we have two separate conditions for the up-type and down-type right-handed quarks, since these form singlets under the group $SU(2)_L$, and have different hypercharges.
The third step consists in reproducing three chiral generations of left-handed leptons, which can arise in the bc, bc', bd and bd' sectors. The conditions on the intersection numbers are as follows:

Intersection	Chirality	Representation under $(SU(3), SU(2))_{(Q_a,Q_b,Q_c,Q_d)}$	Q_Y
χ^{bc}	≥ 0	$(\mathbf{1}, \mathbf{2})_{(0,1,-1,0)}$	$-1/2$
$\chi^{bc'}$	≤ 0	$(\mathbf{1}, \overline{\mathbf{2}})_{(0,-1,-1,0)}$	$-1/2$
χ^{bd}	≥ 0	$(\mathbf{1}, \mathbf{2})_{(0,1,0,-1)}$	$-1/2$
$\chi^{bd'}$	≤ 0	$(\mathbf{1}, \overline{\mathbf{2}})_{(0,-1,0,-1)}$	$-1/2$
	Multiplicity	Particle	
$\chi^{bc} + \chi^{bd} - \chi^{bc'} - \chi^{bd'}$	3	L	$-1/2$

(3.9)

As usual, the conditions can be loosened by keeping only the last constraint. Note that the conditions change if enhancement on b is present. Indeed, we have the following relation between the intersection numbers: $\Pi_x \circ \Pi_y = -\Pi_{x'} \circ \Pi_{y'}$ and $\Pi_x \circ \Pi_{y'} = -\Pi_{x'} \circ \Pi_y$. Hence, enhancement on b implies $|\chi^{bx}| = |\chi^{bx'}|$ so that the sectors bx and bx' are considered as being equivalent and are counted only once. Consequently, the second and the fourth conditions are superfluous in case of $USp(2)_b$, and the last condition reduces to $\chi^{bc} + \chi^{bd} = 3$.
The second-to-last step consists in obtaining three generations of chiral right-handed electrons, which arise in the cd' and the symmetric sectors of cc' and dd'. The conditions on the

intersection numbers are the following:

Intersection	Chirality	Representation under $(SU(3), SU(2))_{(Q_a,Q_b,Q_c,Q_d)}$	Q_Y
$\chi^{cd'}$	≥ 0	$(\mathbf{1},\mathbf{1})_{(0,0,1,1)}$	1
$\chi^{\mathbf{Sym}_c}$	≥ 0	$(\mathbf{1},\mathbf{1})_{(0,0,2,0)}$	1
$\chi^{\mathbf{Sym}_d}$	≥ 0	$(\mathbf{1},\mathbf{1})_{(0,0,0,2)}$	1
	Multiplicity	Particle	
$\chi^{cd'} + \chi^{\mathbf{Sym}_c} + \chi^{\mathbf{Sym}_d}$	3	e_R	1

(3.10)

Once more, the conditions can be relaxed to only the last equation.
Finally, the particle physics model should also come with three generations of right-handed neutrinos. Although the right-handed neutrinos are commonly associated to the cd sectors, they can in principle arise from any singlet gauge representation. In particular, the following sectors can give rise to singlet representations under the full gauge group:

Intersection	Chirality/ Multiplicity	Representation under $(SU(3), SU(2))_{(Q_a,Q_b,Q_c,Q_d)}$	Q_Y
χ^{cd}	≥ 0 or ≤ 0	$(\mathbf{1},\mathbf{1})_{(0,0,\pm1,\mp1)}$	0
$\chi^{\mathbf{Anti}_b}$	≥ 0 or ≤ 0	$(\mathbf{1},\mathbf{1})_{(0,\pm2,0,0)}$	0
$\varphi^{\mathbf{Adj}_c}$	≥ 0 or ≤ 0	$(\mathbf{1},\mathbf{1})_{(0,0,0,0)}$	0
$\varphi^{\mathbf{Adj}_d}$	≥ 0 or ≤ 0	$(\mathbf{1},\mathbf{1})_{(0,0,0,0)}$	0

(3.11)

The number of states in the adjoint representation $\varphi^{\mathbf{Adj}_x}$ has to be computed via the beta-function coefficients, as we will do in section 5.2. Ideally, the intersection numbers above should sum up to ± 3 with the correct sign factors. However, since these are total gauge singlets, they have escaped direct detection techniques so far. Thus, in string model building no conditions are put on the number of these gauge singlet states.

The conditions on the intersection numbers we have derived in this section are only valid for the standard hypercharge defined with plus signs. Other definitions of the hypercharge involving different signs need a modification of the conditions on the intersection numbers. We give an example of another choice of the hypercharge in appendix B.1.

A relevant difference between the field theoretical and stringy approach to the MSSM consists in the fact that, on top of the chiral particle spectrum we have presented in this section, the stringy approach usually comes with exotic particles, i.e. particles charged under both the gauge group of the MSSM and some additional hidden gauge group factors which are necessary for global consistency. These exotic particles can provide candidates for dark matter.
Moreover, in Type IIA string theory we also encounter non-chiral particles coming in pairs of a certain representation $\mathbf{R}$ and its complex conjugate $\overline{\mathbf{R}}$. The electroweak Higgs doublets H_u and H_d of the MSSM form such a pair. All other non-chiral pairs of particles, however, have no equivalent on the field theoretical side of the MSSM, and are characteristic for

stringy realizations of particle physics models. Thus, these non-chiral pairs are somewhat an annoyance from a phenomenological point of view. However, since these states come in pairs $\mathbf{R}+\overline{\mathbf{R}}$, they can easily be paired off in gauge-invariant mass terms of the form $\mathbf{R}\otimes\overline{\mathbf{R}}$, although in Type IIA string theory, the couplings must also fulfill the stringy selection rule, which is more stringent than gauge invariance, see chapter 9. Therefore, they can in principle acquire a mass high enough to lift them out of today's particle detectors' reach. Due to this possibility to effectively remove these states from the low-energy effective theory, no conditions are put on the number of non-chiral particle states.
Because of the presence of additional chiral and non-chiral particles as well as potential extra $U(1)$ or $\mathbb{Z}_n$-symmetries, the models are referred to as MSSM-like models rather than MSSMs.
In Type IIA string theory, the Yukawa couplings (3.1) and n-point couplings in general (involving n interacting fields) can be realized in a geometrical manner. Indeed, the Yukawa couplings can be related to the triangular areas defined by three intersecting three-cycles on the six-torus $T^2_{(1)}\times T^2_{(2)}\times T^2_{(3)}$. We will come back to this in some more detail in chapter 9.
We explained how the chiral particle content of the SM or MSSM is reproduced via the intersection numbers. However, there are also conditions on the absence of certain matter states given by $\chi^{\mathbf{Sym}_a}=0$ and $\chi^{\mathbf{Sym}_b}=0$. Also the stacks need to satisfy conditions of rigidity. This is described in chapter 5 in more detail. In the following, we will briefly present the GUT models appearing in this work.

The three gauge coupling "constants" associated to the three gauge factors of the MSSM are only constant over small intervals of the energy scale. The energy dependence is due to the self-interaction of particles. The coupling constants of the weak and electromagnetic interactions increase with increasing energy, while the coupling strength of the strong interaction decreases logarithmically with increasing energy. The running of coupling constants is determined by the one-loop beta-function.
At order of magnitudes $\mathcal{O}(10^{16})$ GeV, the three coupling constants almost come together in a point in the SM. This inspired physicists to speculate whether the beta-functions should not be adapted at high energies, so that the three coupling strengths exactly meet in one point and unify into a single coupling constant, meaning only one fundamental interaction exists at high energies [173, 174]. This is known as Grand Unification, schematically indicated in figure 3.4. However, to the present day, no fully satisfying unification theory has been derived.

3.2.2 The left-right symmetric model

The left-right symmetric model [175, 176] arises upon pondering whether the $U(1)_Y$ gauge group can be seen as a broken $SU(2)_R$ gauge group. In order to achieve this, the right-handed up-type and down-type quarks need to be unified in a $SU(2)_R$-doublet, just as the left-handed quarks come in electroweak $SU(2)_L$-doublets. The same holds true for the right-handed leptons. Therefore, the gauge group of the SM would change to

$$SU(3)\times SU(2)_L\times SU(2)_R\times U(1)_{B-L}\,,$$

which is the gauge group of the left-right symmetric model. $U(1)_{B-L}$ is the baryon-lepton number symmetry we encountered in the previous section. Under this gauge group, the

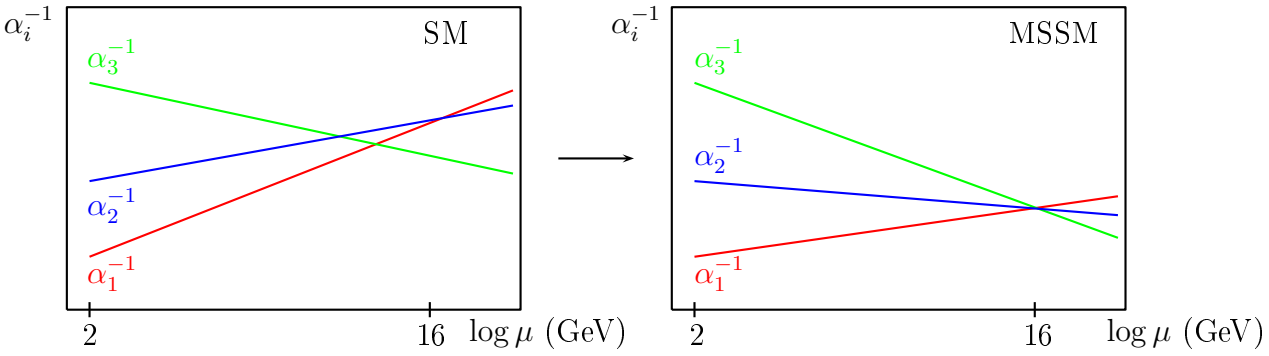

Figure 3.4: Schematic drawing of the running with energy of the gauge coupling constants. The quantities α_i are related to the gauge couplings g_i $(i = 1, 2, 3)$ of $U(1)_Y$, $SU(2)_L$ and $SU(3)_{QCD}$ respectively via the relation: $\alpha_i = \frac{g_i^2}{4\pi}$. The quantity μ corresponds to the energy scale. The left plot depicts the running of the gauge couplings for the SM, while the right plot does the same for the MSSM. We see that in the SM, the three couplings almost meet in a point, whereas they meet exactly at $\sim \mathcal{O}(10^{16})$ GeV in the case of the MSSM. This is a strong hint for Grand Unification at high energy scales.

right-handed quarks and leptons of the MSSM combine into doublets as follows:

Intersection	Chirality/ Multiplicity	Representation under $(SU(3), SU(2), SU(2))_{(Q_a,Q_b,Q_c,Q_d)}$	Q_{B-L}
χ^{ab}	≥ 0	$(\mathbf{3}, \overline{\mathbf{2}}, \mathbf{1})_{(1,-1,0,0)}$	$1/3$
$\chi^{ab'}$	≥ 0	$(\mathbf{3}, \mathbf{2}, \mathbf{1})_{(1,1,0,0)}$	$1/3$
$\chi^{ab} + \chi^{ab'}$	3	Q_L	$1/3$
χ^{ac}	≤ 0	$(\overline{\mathbf{3}}, \mathbf{1}, \mathbf{2})_{(-1,0,1,0)}$	$-1/3$
$\chi^{ac'}$	≤ 0	$(\overline{\mathbf{3}}, \mathbf{1}, \overline{\mathbf{2}})_{(-1,0,-1,0)}$	$-1/3$
$\chi^{ac} + \chi^{ac'}$	-3	Q_R	$-1/3$
χ^{bd}	≥ 0	$(\mathbf{1}, \mathbf{2}, \mathbf{1})_{(0,1,0,-1)}$	-1
$\chi^{bd'}$	≤ 0	$(\mathbf{1}, \overline{\mathbf{2}}, \mathbf{1})_{(0,-1,0,-1)}$	-1
$\chi^{bd} - \chi^{bd'}$	3	L	-1
χ^{cd}	≤ 0	$(\mathbf{1}, \mathbf{1}, \overline{\mathbf{2}})_{(0,-1,0,1)}$	1
$\chi^{cd'}$	≥ 0	$(\mathbf{1}, \mathbf{1}, \mathbf{2})_{(0,1,0,1)}$	1
$-\chi^{cd} + \chi^{cd'}$	3	R	1

(3.12)

As in the case of the SM or MSSM, the conditions on the intersection numbers above can be relaxed by keeping only the conditions on the sums. Also, in case of the left-right symmetric models, symmetry enhancement to symplectic groups can occur not only on the b stack but also on the c stack, i.e. $U(1)_x \to USp(2)_x$ $(x = b, c)$, in which case the conditions above have to be modified accordingly.

The Higgs fields (H_u, H_d) should arise in the sectors bc and bc'. In this thesis, we choose not to put conditions on the number of Higgs fields, although the presence of at least one Higgs field renders the model more appealing from a phenomenological point of view.

The sectors ad and ad' can give rise to additional particles not foreseen in the left-right symmetric models. We put a priori no conditions on these, although it is preferable if these sectors give rise to at most non-chiral pairs of particles.

3.2.3 The Pati-Salam model

The Pati-Salam model, first proposed in [12, 13], can be derived from the left-right symmetric model by taking the unification of the particle content one step further. Indeed, a sensible question to ask is whether the lepton number can be seen as a fourth flavor symmetry. Basically, this corresponds to identifying the groups $SU(3) \times U(1)_{B-L}$ as a subset of a $SU(4)$ group. The unification of these two groups to a $SU(4)$ group implies that the quarks and leptons are unified in fundamental representations under $SU(4)$. The new gauge group thus obtained is the group of the Pati-Salam model:

$$SU(4) \times SU(2)_L \times SU(2)_R \,.$$

Under this gauge group, quarks and leptons are no longer distinguishable, and the matter content separates into mere left-handed and right-handed particles:

Intersection	Chirality/ Multiplicity	Representation under $(SU(4), SU(2), SU(2))_{(Q_a,Q_b,Q_c)}$
χ^{ab}	≥ 0	$(\mathbf{4}, \overline{\mathbf{2}}, \mathbf{1})_{(1,-1,0,0)}$
$\chi^{ab'}$	≥ 0	$(\mathbf{4}, \mathbf{2}, \mathbf{1})_{(1,1,0,0)}$
$\chi^{ab} + \chi^{ab'}$	3	(Q_L, L)
χ^{ac}	≤ 0	$(\overline{\mathbf{4}}, \mathbf{1}, \mathbf{2})_{(-1,0,1,0)}$
$\chi^{ac'}$	≤ 0	$(\overline{\mathbf{4}}, \mathbf{1}, \overline{\mathbf{2}})_{(-1,0,-1,0)}$
$\chi^{ac} + \chi^{ac'}$	-3	(Q_R, R)

(3.13)

As usual, the conditions can be relaxed by retaining only the conditions on the sum, and in case of enhancement $U(1)_x \to USp(2)_x$ on the b and/or c stacks, the conditions have to be modified accordingly. Once again, the Higgs fields (H_u, H_d) arise from the bc and bc' sectors.

3.2.4 The $SU(5)$ model

Until now, the unified gauge group of the models with left-right symmetry included several gauge factors. The first model including only one gauge factor was the $SU(5)$ model, first proposed in [15]. Obviously, the gauge group of this model is $SU(5)$ as its name already indicates. Under this gauge group, the particles of the SM or MSSM regroup as follows:

$$aa' : \ \mathbf{10_{Anti_a}} = \begin{pmatrix} 0 & u_R^3 & u_R^2 & u_L^1 & d_L^1 \\ & 0 & u_R^1 & u_L^2 & d_L^2 \\ & & 0 & u_L^3 & d_L^3 \\ & & & 0 & e_R \\ & & & & 0 \end{pmatrix} \qquad ab : \ \overline{\mathbf{5}} = \begin{pmatrix} d_R^1 \\ d_R^2 \\ d_R^3 \\ e \\ \nu_L \end{pmatrix} ,$$

where the index i refers to the color-charge under $SU(3)_{QCD}$. In order to reproduce the representation $\overline{\mathbf{5}}$ under $SU(5)$ in Type IIA string model building, at least two stacks are needed: one to support a $U(5)$ group and one to support an artificial $U(1)$ group. In that set-up, the two representations are realized as follows by the intersection numbers:

Intersection	Chirality/ Multiplicity	Representation under $(SU(5))_{(Q_a,Q_b)}$
χ^{ab}	≤ 0	$(\overline{\mathbf{5}})_{(-1,1)}$
$\chi^{ab'}$	≤ 0	$(\overline{\mathbf{5}})_{(-1,-1)}$
$\chi^{ab}+\chi^{ab'}$	-3	$\overline{\mathbf{5}}$
$\chi^{\mathbf{Anti}_a}$	3	$(\mathbf{10})_{(1,0)}$

(3.14)

The first three conditions can once again be relaxed by keeping only the third one. Also, enhancement on the b stack is tolerated, meaning that the first three conditions have to be adapted if enhancement arises: $\chi^{ab}=\chi^{ab'}=-3$. On top of the chiral matter spectrum, we also have conditions on the rigidity of the a stack. Indeed, one chiral multiplet transforming in the adjoint representation of $SU(5)$ should be present in order to play the role of the GUT Higgs, breaking the $SU(5)$ group down to the gauge group of the SM or MSSM at low energies. Thus, the GUT models presented in this section are only valid at high energies.

An introductory textbook to the SM and extensions thereof is given by [177]. For the incorporation of particle physics models in Type II string theory with intersecting branes, see for example [121, 178, 52, 54, 179, 180, 53, 181–184]

3.3 Collection of formulas for the massless open string spectrum

At the intersection points of two D6-branes, matter states arise whose multiplicity is determined by the topological intersection number. There are two possibilities to calculate the intersection numbers, the first one is the "orbifold invariant" one and involves the bulk and exceptional wrapping numbers whereas the second method is based on the torus wrapping numbers weighted by sign factors.
Both methods only compute the net-chirality of a representation, i.e. they only count the number of chiral states transforming in the representation under consideration.
The formulas allowing to determine the chiral massless open string spectrum via intersection numbers can be found in [77]. The formulas permitting the computation of the non-chiral massless open string spectrum via intersection numbers on orbifolds of the form $T^6/(\mathbb{Z}_2\times\mathbb{Z}_{2M})$ with discrete torsion were provided for the first time in appendix B of [65].

3.3.1 Orbifold invariant intersection numbers

The "orbifold invariant" intersection number on $T^6/(\mathbb{Z}_2\times\mathbb{Z}_6)$ can be directly calculated using the expression of a generic fractional cycle (2.33) and formulas (2.10) and (2.24). Considering two fractional three-cycles Π_a and Π_b, the multiplicities of the chiral matter states in the

bifundamental representations of a model are given by:

$$\begin{aligned}\Pi_a \circ \Pi_b = &\frac{1}{4}\Big(2\left(P_aU_b - P_bU_a + Q_aV_b - Q_bV_a\right) + \left(P_aV_b - P_bV_a + Q_aU_b - Q_bU_a\right)\Big) \\ &- \frac{1}{4}\left(3\left[x^{(1)}_{0,a}y^{(1)}_{0,b} - x^{(1)}_{0,b}y^{(1)}_{0,a}\right] + \sum_{\alpha=1}^{5}\left[x^{(1)}_{\alpha,a}y^{(1)}_{\alpha,b} - x^{(1)}_{\alpha,b}y^{(1)}_{\alpha,a}\right]\right) \\ &- \frac{1}{4}\sum_{i=2}^{3}\sum_{\alpha=1}^{4}\left[x^{(i)}_{\alpha,a}y^{(i)}_{\alpha,b} - x^{(i)}_{\alpha,b}y^{(i)}_{\alpha,a}\right] .\end{aligned} \tag{3.15}$$

The multiplicities of the states in the (anti)symmetric representations are obtained by replacing the cycle b by the orientifold image of a in expression (3.15), and adding the intersection number between the cycle a and the O6-planes:

$$\chi^{\mathbf{Anti}_a/\mathbf{Sym}_a} = \frac{\Pi_a \circ \Pi_{a'} \pm \Pi_a \circ \Pi_{O6}}{2} , \tag{3.16}$$

where Π_{O6} is defined as follows:

$$\Pi_{O6} = \frac{N_{O6}}{4}\left(\eta_{\Omega\mathcal{R}}\Pi_{\Omega\mathcal{R}} + \sum_{k=1}^{3}\eta_{\Omega\mathcal{R}\mathbb{Z}_2^{(k)}}\Pi_{\Omega\mathcal{R}\mathbb{Z}_2^{(k)}}\right) , \tag{3.17}$$

with $N_{O6} = 2(1-b)$. Remember from section 2.4.2 that the O6-planes have no exceptional part. The intersection number $\Pi_a \circ \Pi_{O6}$ is thus given by:

$$\Pi_a \circ \Pi_{O6} = -\frac{\left(\eta_{\Omega\mathcal{R}} + 3\eta_{\Omega\mathcal{R}\mathbb{Z}_2^{(1)}}\right)}{2}\left[2\tilde{U}_a + \tilde{V}_a\right] - \frac{3(1-b)\left(\eta_{\Omega\mathcal{R}\mathbb{Z}_2^{(2)}} + \eta_{\Omega\mathcal{R}\mathbb{Z}_2^{(3)}}\right)}{2}Q_a , \tag{3.18}$$

where we introduced the short-hand notations $\tilde{U}_a = U_a + bP_a$ and $\tilde{V}_a = V_a + bQ_a$.

The orbifold invariant intersection numbers miss some information, as they cannot provide the intersection numbers between an orbifold representative of a fractional three-cycle and its orbifold images separately. This is due to the fact that the bulk and exceptional wrapping numbers are orbifold invariant by definition. On the bright side, formula (3.15) can be easily integrated into numerical codes. The determination of the exceptional wrapping numbers $x^{(1)}_\alpha y^{(1)}_\alpha$ ($\alpha = 0, \dots 5$), and $x^{(l)}_\alpha y^{(l)}_\alpha$ ($l = 2, 3$, $\alpha = 1, \dots 4$) is done via table A.1 and corresponds to the most tedious part to encode. Yet, the exceptional wrapping numbers need to be computed anyway since they enter in the twisted RR-tadpole cancellation conditions, see table 2.9.

3.3.2 The sector-per-sector intersection numbers

The information about the localization of matter states per intersection sector is contained in the "sector-per-sector" intersection numbers. The sector-per-sector approach gives the intersection numbers between an orbifold representative of a fractional three-cycle a and its orbifold images $(\omega^k a)$ $(k = 0, 1, 2)$ separately, i.e. it provides the number of chiral states per sector k in $a(\omega^k a)$, $k = 0, 1, 2$. This information is relevant in the context of the determination of the Yukawa couplings, as we will see in chapter 9.
The construction of these intersection numbers starts with the torus three-cycles:

$$\Pi_a^{\text{torus}} \circ \Pi_b^{\text{torus}} \equiv -I_{ab} \equiv -\prod_{i=1}^{3} I^{(i)}_{ab} \equiv -\prod_{i=1}^{3}(n^i_a m^i_b - m^i_a n^i_b) . \tag{3.19}$$

The bulk three-cycle intersection numbers are obtained by summing over the orbifold images of each cycle a and b. We obtain for the bulk and exceptional intersection numbers:

$$\Pi_a^{\text{bulk}} \circ \Pi_b^{\text{bulk}} = \frac{1}{12}\left(4\sum_{l=0}^{2}\Pi^{\text{torus}}_{(\omega^l a)}\right)\circ\left(4\sum_{m=0}^{2}\Pi^{\text{torus}}_{(\omega^m a)}\right) = -4\sum_{k=0}^{2} I_{a(\omega^k b)}\,, \tag{3.20}$$

$$\Pi_a^{\mathbb{Z}_2^{(i)}} \circ \Pi_b^{\mathbb{Z}_2^{(i)}} \equiv -4\sum_{k=0}^{2} I^{\mathbb{Z}_2^{(i)}}_{a(\omega^k b)} \equiv -4\sum_{k=0}^{2} I^{(i)}_{a(\omega^k b)} I^{\mathbb{Z}_2^{(i)},(j,l)}_{a(\omega^k b)}\,, \tag{3.21}$$

$$\text{with}\quad I^{\mathbb{Z}_2^{(i)},(j,l)}_{a(\omega^k b)} \equiv (-1)^{\tau_a^{\mathbb{Z}_2^{(i)}}+\tau_b^{\mathbb{Z}_2^{(i)}}} I^{\mathbb{Z}_2^{(i)},(j)}_{a(\omega^k b)} I^{\mathbb{Z}_2^{(i)},(l)}_{a(\omega^k b)}\,, \tag{3.22}$$

where i,j,l are cyclic permutations of $1,2,3$. In the first line, we used the following relation between intersection numbers: $I^{(i)}_{(\omega^l a)(\omega^m b)} = I^{(i)}_{a(\omega^{m-l} b)}$.
The intersection numbers $I^{\mathbb{Z}_2^{(i)},(j)}_{a(\omega^k b)}$ can be computed as described in appendix A of [67]. Concretely, for a torus three-cycle Π_a^{torus} passing on the two-torus $T^2_{(j)}$ through the $\mathbb{Z}_2^{(i)}$-fixed points α and β, and a torus three-cycle $\Pi^{\text{torus}}_{(\omega^k b)}$ traversing the $\mathbb{Z}_2^{(i)}$-fixed points λ and κ on $T^2_{(j)}$, then $I^{\mathbb{Z}_2^{(i)},(j)}_{a(\omega^k b)}$ is given by:

$$I^{\mathbb{Z}_2^{(i)},(j)}_{a(\omega^k b)} = \begin{pmatrix}\alpha\\ \beta\end{pmatrix}\cdot\begin{pmatrix}\lambda\\ \kappa\end{pmatrix} = \delta_{\alpha\lambda} + (-1)^{\tau_a^j}\delta_{\beta\lambda} + (-1)^{\tau_b^j}\delta_{\alpha\kappa} + (-1)^{\tau_a^j+\tau_b^j}\delta_{\beta\kappa},, \tag{3.23}$$

where the upper entries correspond to the reference points. Thus, equal indices in the upper positions contribute with a term equal to one, equal indices in the lower positions give a term $(-1)^{\tau_a^j+\tau_b^j}$, and equal indices in an upper and a lower position contribute with $(-1)^{\tau_a^j}$ or $(-1)^{\tau_b^j}$. Note that the orbifold action has no influence on the Wilson lines, i.e. $\tau_b^j = \tau^j_{(\omega b)}$. The same can be done for $I^{\mathbb{Z}_2^{(i)},(k)}_{a(\omega^k b)}$, which involves the $\mathbb{Z}_2^{(i)}$-fixed points on the two-torus $T^2_{(k)}$.

The net-chiralities $\chi^{a(\omega^k b)}$ per sector k ($k=0,1,2$) for bifundamental representations are defined as:

$$\chi^{a(\omega^k b)} \equiv -\frac{I_{a(\omega^k b)} + \sum_{i=0}^{3} I^{\mathbb{Z}_2^{(i)}}_{a(\omega^k b)}}{4} \tag{3.24}$$

The total multiplicity of the states in a bifundamental representation is obtained by summing over the net-chiralities per sector $-\Pi_a\circ\Pi_b \equiv \sum_{k=0}^{2}\chi^{a(\omega^k b)}$, as indicated in table 3.2.

Using table 3.2 and formula (3.16), we can also provide an explicit expression for the computation of the multiplicity of the states in the (anti)symmetric representation in terms of the sector-per-sector approach:

$$\begin{aligned}\chi^{\mathbf{Anti}_a/\mathbf{Sym}_a} &= -\sum_{k=0}^{2}\frac{\left(I_{(\omega^k a)(\omega^k a)'} + \sum_{i=1}^{3} I^{\mathbb{Z}_2^{(i)}}_{(\omega^k a)(\omega^k a)'}\right) \pm \left(\sum_{n=0}^{3}\eta_{\Omega\mathcal{R}\mathbb{Z}_2^{(n)}}\,\tilde{I}^{\Omega\mathcal{R}\mathbb{Z}_2^{(n)}}_{(\omega^k a)}\right)}{8}\\ &\equiv \sum_{k=0}^{2}\chi^{\mathbf{Anti}_a/\mathbf{Sym}_a}_{(\omega^k a)}\,.\end{aligned} \tag{3.25}$$

The sector-per-sector method is more difficult to integrate into numerical codes, at least for cycles with generic torus wrapping numbers. In this thesis, I wrote a code based on the

Three-cycle "sector-per-sector" intersection numbers	
$-\Pi_a \circ \Pi_b$	$-\Pi_a \circ \Pi_{O6}$
$\sum_{k=0}^{2} \frac{I_{a(\omega^k b)} + \sum_{i=0}^{3} I^{\mathbb{Z}_2^{(i)}}_{a(\omega^k b)}}{4}$	$\sum_{k=0}^{2} \frac{\eta_{\Omega\mathcal{R}} \tilde{I}^{\Omega\mathcal{R}}_{(\omega^k a)} + \sum_{i=1}^{3} \eta_{\Omega\mathcal{R}\mathbb{Z}_2^{(i)}} \tilde{I}^{\Omega\mathcal{R}\mathbb{Z}_2^{(i)}}_{(\omega^k a)}}{4}$

Table 3.2: Explicit expression for the fractional three-cycle intersection numbers, in terms of the "sector-per-sector" intersection numbers. The left column provides the intersection numbers giving the net-chirality χ^{ab} of the bifundamental representations. To obtain the net-chirality $\chi^{\mathbf{Anti}_a/\mathbf{Sym}_a}_{(\omega^k a)}$ of the (anti)symmetric representations, the intersection numbers of both columns must be combined as described in the main text. We have $\tilde{I}^{\Omega\mathcal{R}\mathbb{Z}_2^{(i)}}_{(\omega^k a)} \equiv 2(1-b) I^{\Omega\mathcal{R}\mathbb{Z}_2^{(i)}}_{(\omega^k a)}$, where $I^{\Omega\mathcal{R}\mathbb{Z}_2^{(i)}}_{(\omega^k a)}$ are the bulk intersection numbers (3.19) between $\Pi_{(\omega^k a)}$ and the O6-plane $\Omega\mathcal{R}\mathbb{Z}_2^{(i)}$. The quantity $2(1-b)$ counts the number of parallel O6-planes depending on the shape of the first two-torus.

sector-per-sector approach to determine the multiplicities of the states in the (anti)symmetric representations only, for generic fractional three-cycles. This served as a partial cross-check for the results obtained from the orbifold invariant intersection numbers. In chapter 9, I computed by hand the multiplicities per sector for all representations, but only for the specific models involved in that chapter.

3.3.3 The beta-function coefficients

In this section, we provide a brief introduction to the beta-function coefficients and the formulas to compute them. In appendix A.2, we will present more details of the beta-function coefficients and illustrate their use on concrete examples of computation.
The non-chiral spectrum can be deduced from the beta-function coefficients, which give the total amount of matter, i.e. the chiral and non-chiral spectrum. The beta-function coefficients need the sector-per-sector intersection numbers as input. A priori, one could think that the total spectrum is computed by summing the absolute value of the net-chiralities over the sectors: $\varphi^{ab} = \sum_{k=0}^{2} |\chi^{a(\omega^k b)}|$. However, non-chiral pairs of states can also arise within a same sector k, which are not counted when simply summing over the net-chiralites per sector. These states can only be determined via the beta-function coefficients as mentioned before. The generic form of the beta-function coefficient for a stack a supporting a unitary gauge group was found by field theoretical considerations in [66, 72] and is given by:

$$\begin{aligned} b_{SU(N_a)} = & \underbrace{N_a(-3+\varphi^{\mathbf{Adj}_a})}_{} + \underbrace{\frac{N_a}{2}(\varphi^{\mathbf{Sym}_a}+\varphi^{\mathbf{Anti}_a})}_{} + \underbrace{(\varphi^{\mathbf{Sym}_a}-\varphi^{\mathbf{Anti}_a})}_{} + \underbrace{\sum_{b\neq a}\frac{N_b}{2}(\varphi^{ab}+\varphi^{ab'})}_{} \\ \equiv & \quad b^A_{aa} + b^A_{aa'} + b^M_{aa'} + \textstyle\sum_{b\neq a}(b^A_{ab}+b^A_{ab'}) \end{aligned} \tag{3.26}$$

The computation of the beta-function coefficients can be done in String Theory using CFT methods to determine the so-called annulus part and Möbius part of the string amplitude. The annulus part corresponds to the exchange of a closed string between two D6-branes, so that the worldsheet of the string corresponds to a cylinder spanned between the D6-branes. Alternatively, the cylinder amplitude can be interpreted as arising from an open string spanned between two D6-branes and moving in a loop. The cylinder can be mapped to an annulus, hence the superscript A refers to the annulus or cylinder part of the string

amplitude.
Inserting a so-called crosscap at one end of the cylinder leads to the so-called Möbius part of the string amplitude. A crosscap is obtained by removing a disc from the worldsheet surface and identifying opposite points on the boundary. It corresponds to the exchange of a closed string between a D6-brane and an O6-plane, or equivalently, to an unoriented open string spanned between a D6-brane and an O6-plane and running in a loop. The superscript M thus refers to the Möbius part [72].

The results for the different contributions to the beta-function coefficient can be found in [65] or [72] and are listed in tables 3.3 and 3.4.
Table 3.3 provides the contributions from the bifundamental and adjoint representations. Concerning the bifundamental representations, the beta-function coefficients are obtained sector-per-sector, i.e. the label b in table 3.3 has to be replaced successively by (ωb) and $(\omega^2 b)$, so that the total contribution from a bifundamental representation is given by: $b^A = b^A_{ab} + b^A_{a(\omega b)} + b^A_{a(\omega^2 b)}$.
As for the adjoint representations, they can be obtained from table 3.3 by replacing the label b successively by a, (ωa) and $(\omega^2 a)$. In that case, the contribution b^A_{aa} gives rise to one vector multiplet containing the gauge boson of the D6-brane, and its SUSY partner the gaugino. Also, it would give rise to three chiral multiplets containing the position moduli of the D6-brane if we were not working with fixed D6-branes passing through $\mathbb{Z}_2$-fixed points. The sectors $b^A_{a(\omega a)}$ and $b^A_{a(\omega^2 a)}$ each provide one half of the degrees of freedom of the $\mathcal{N} = 1$ chiral multiplet. The states from these sectors give rise to recombination moduli, as explained in section 3.1. The total contribution of an adjoint representation is thus given by: $b^A = b^A_{aa} + b^A_{a(\omega a)} + b^A_{a(\omega^2 a)}$.
Similarly, using table 3.4, the total contribution of the (anti)symmetric representations is given sector-per-sector $b^A + b^M = b_{aa'} + b_{(\omega a)(\omega a)'} + b_{(\omega^2 a)(\omega^2 a)'}$.

Contributions to $b_{SU(N_a)}$ from adjoint and bifundamental matter	
$(\phi^{(1)}_{ab}, \phi^{(2)}_{ab}, \phi^{(3)}_{ab})$	$b^A_{ab} = \frac{N_b}{2}\varphi^{ab}$
$(0,0,0)$	$-N_b(\prod_{n=1}^3 \delta_{\sigma^n_{ab},0}\delta_{\tau^n_{ab},0}) \sum_{i=1}^3 (-1)^{\tau^{\mathbb{Z}_2^{(i)}}_{ab}}$
$(0^{(i)}, \phi^{(j)}, \phi^{(k)})$	$\frac{N_b}{4}\delta_{\sigma^i_{ab},0}\delta_{\tau^i_{ab},0}\left(\lvert I^{(j\cdot k)}_{ab}\rvert - I^{\mathbb{Z}_2^{(i)},(j\cdot k)}_{ab}\right)$
$\phi^{(n)}_{ab} \neq 0\ \forall n,\ \sum_{n=1}^3 \varphi^{(n)}_{ab} = 0$	$\frac{N_b}{8}\left(\lvert I_{ab}\rvert + \mathrm{sgn}(I_{ab}) \sum_{i=1}^3 I^{\mathbb{Z}_2^{(i)}}_{ab}\right)$

Table 3.3: Contributions to the $SU(N_a)$ beta function coefficients from matter states transforming in the bifundamental or adjoint representations, as explained in the main text. The results are given for different configurations of intersecting D6-branes, i.e. at three, one and zero vanishing angles. Wilson lines or shifts appearing with two indexes ab denote the relative Wilson lines respectively shifts between two D6-branes, i.e. $\tau^n_{ab} \equiv \tau^n_a - \tau^n_b$ and $\sigma^n_{ab} \equiv \sigma^n_a - \sigma^n_b$.

For a stack giving rise to gauge symmetry enhancement $U(N) \to USp(2N)/SO(2N)$, the adjoint representation is equivalent to the antisymmetric/symmetric representation, with the result that the states transforming in the adjoint and (anti)symmetric representations can no longer be distinguished. This causes the beta-function coefficient to be of a slightly different form. The precise form depends on the type of enhancement, i.e. USp or SO enhancement.

Contributions to $b_{SU(N_a)}$ from symmetric and antisymmetric matter	
$(\phi^{(1)}_{aa'}, \phi^{(2)}_{aa'}, \phi^{(3)}_{aa'})$	$b^A_{aa'} + b^M_{aa'} = \frac{N_a}{2}(\varphi^{\mathbf{Sym}_a} + \varphi^{\mathbf{Anti}_a}) + (\varphi^{\mathbf{Sym}_a} - \varphi^{\mathbf{Anti}_a})$
$(0,0,0)\ \uparrow\uparrow \Omega\mathcal{R}$	$-\frac{N_a}{4}\sum_{i=1}^3 I^{\mathbb{Z}_2^{(i)},(j\cdot k)}_{aa'} - \frac{1}{2}\sum_{i=1}^3 \eta_{\Omega\mathcal{R}\mathbb{Z}_2^{(i)}}(-1)^{2b^i\sigma^i_a\tau^i_a}\lvert\tilde{I}^{\Omega\mathcal{R}\mathbb{Z}_2^{(i)},(j\cdot k)}_a\rvert$
$(0,0,0)\ \uparrow\uparrow \Omega\mathcal{R}\mathbb{Z}_2^{(i)}$	$-\frac{N_a}{4}\sum_{l=1}^3 I^{\mathbb{Z}_2^{(l)},(m\cdot n)}_{aa'} - \frac{1}{2}\left(\eta_{\Omega\mathcal{R}}(-1)^{2b^i\sigma^i_a\tau^i_a}\lvert\tilde{I}^{\Omega\mathcal{R},(j\cdot k)}_a\rvert + \sum_{j\neq i}\eta_{\Omega\mathcal{R}\mathbb{Z}_2^{(j)}}(-1)^{2b^k\sigma^k_a\tau^k_a}\lvert\tilde{I}^{\Omega\mathcal{R}\mathbb{Z}_2^{(j)},(i\cdot j)}_a\rvert\right)$
$(0^{(i)}, \phi^{(j)}_{aa'}, \phi^{(k)}_{aa'}) \uparrow\uparrow \left(\Omega\mathcal{R} + \Omega\mathcal{R}\mathbb{Z}_2^{(i)}\right)$	$\frac{N_a}{4}\left(\lvert I^{(j\cdot k)}_{aa'}\rvert - I^{\mathbb{Z}_2^{(i)},(j\cdot k)}_{aa'}\right) - \frac{1}{2}\left(\eta_{\Omega\mathcal{R}}(-1)^{2b^i\sigma^i_a\tau^i_a}\lvert\tilde{I}^{\Omega\mathcal{R},(j\cdot k)}_a\rvert + \eta_{\Omega\mathcal{R}\mathbb{Z}_2^{(i)}}(-1)^{2b^i\sigma^i_a\tau^i_a}\lvert\tilde{I}^{\Omega\mathcal{R}\mathbb{Z}_2^{(i)},(j\cdot k)}_a\rvert\right)$
$(0^{(i)}, \phi^{(j)}_{aa'}, \phi^{(k)}_{aa'}) \uparrow\uparrow \left(\Omega\mathcal{R}\mathbb{Z}_2^{(j)} + \Omega\mathcal{R}\mathbb{Z}_2^{(k)}\right)$	$\frac{N_a}{4}\left(\lvert I^{(j\cdot k)}_{aa'}\rvert - I^{\mathbb{Z}_2^{(i)},(j\cdot k)}_{aa'}\right) - \frac{1}{2}\left(\eta_{\Omega\mathcal{R}\mathbb{Z}_2^{(j)}}(-1)^{2b^i\sigma^i_a\tau^i_a}\lvert\tilde{I}^{\Omega\mathcal{R},(j\cdot k)}_a\rvert + \eta_{\Omega\mathcal{R}\mathbb{Z}_2^{(k)}}(-1)^{2b^i\sigma^i_a\tau^i_a}\lvert\tilde{I}^{\Omega\mathcal{R}\mathbb{Z}_2^{(k)},(j\cdot k)}_a\rvert\right)$
$\phi^{(n)}_{aa'} \neq 0\ \forall n,\ \sum_{n=1}^3 \phi^{(n)}_{aa'} = 0$	$\frac{N_a}{8}\left(\lvert I_{aa'}\rvert + \mathrm{sgn}(I_{aa'})\sum_{i=1}^3 I^{\mathbb{Z}_2^{(i)}}_{aa'}\right) + \frac{1}{4}\left(c^{\Omega\mathcal{R}}_a\eta_{\Omega\mathcal{R}}\lvert\tilde{I}^{\Omega\mathcal{R}}_a\rvert + \sum_{i=1}^3 c^{\Omega\mathcal{R}\mathbb{Z}_2^{(i)}}_a\eta_{\Omega\mathcal{R}\mathbb{Z}_2^{(i)}}\lvert\tilde{I}^{\Omega\mathcal{R}\mathbb{Z}_2^{(i)}}_a\rvert\right)$

Table 3.4: Contributions to the $SU(N_a)$ beta function coefficients from matter states transforming in the symmetric or antisymmetric representations. The results are given for different configurations of D6-branes, i.e. D6-branes parallel to some O6-plane on one two-torus, all three two-tori or not parallel to an O6-plane at all. The factor $(-1)^{2b^i\sigma^i_a\tau^i_a}$ was introduced for the first time in the caption of table 49 in [65] for reasons of consistency. A concrete example to illustrate the necessity of this factor was given in appendix B.1 of [76]. Note that b^i refers to the shape of the lattice of the ith torus, i.e. in the present geometrical background we have $\vec{b} = (b, \frac{1}{2}, \frac{1}{2})$ with $b = 0$ for **a**-type lattices and $b = 1/2$ for **b**-type lattices. The coefficients $c_a^{\Omega\mathcal{R}\mathbb{Z}_2^{(i)}} \in \{\pm 1\}$ appearing in table 3.4 satisfy the following relation, as was found in appendix A of [72]: $c_a^{\Omega\mathcal{R}\mathbb{Z}_2^{(i)}} = -\mathrm{sgn}\left(I_a^{\Omega\mathcal{R}\mathbb{Z}_2^{(i)}}\right)\cdot\mathrm{sgn}(I_{aa'}),\ i = 0,1,2,3$.

We will discuss the special cases with gauge symmetry enhancement in appendix A.2 in more detail, along with concrete examples.

The formulas given in this section are sufficient to determine the total particle content of the models. In the following chapters, they are used to classify the D6-branes, the classification being based on the presence or absence of particles transforming in the adjoint or (anti)symmetric representation, and to compute the total particle content of the models. This last step is performed only after global models with correct chiral spectrum have been found.

As before in the case of the sector-per-sector intersection numbers, I did not write down a code computing the beta-function coefficients for generic fractional three-cycles. Instead, I wrote a code doing this for fractional three-cycles with a specific bulk part, in accordance with the global models we found. Thus, the torus wrapping numbers were fixed, and the only input of the code were the discrete parameters.

Chapter 4

Preliminary steps to string model building

The aim of model building consists in reproducing models describing particle physics. The models in this thesis arise from intersecting D6-branes, so the goal in model building is to test all possible combinations of intersecting D6-branes in order to find configurations giving rise to suitable models. However, the amount of combinations is tremendous, thus it is not possible to launch a direct computer scan. Instead, simplifications have to be made by hand, and the computer scan has to proceed step-by-step.
A first simplification can be made by detecting equivalences between the six lattices introduced in section 2.2.1. The existence of such equivalences was discovered for the first time in [66]. The procedures of detection of such equivalences has been systematized in [76]. In section 4.1, we follow the methods developed in [76].
The second simplification we consider in this chapter is to classify the D6-branes according to the consistency conditions. More precisely, the aim is to find D6-branes preserving $\mathcal{N} = 1$ SUSY, i.e. bulk three-cycles satisfying the SUSY conditions (2.46). Besides, the bulk part of the three-cycles should also be in agreement with the bulk RR-tadpole cancellation conditions (2.50).

4.1 Equivalences between the torus lattices

There are several hints indicating redundancies among the six lattices **aAA**, **aAB**, **aBB**, **bAA**, **bAB** and **bBB**. Following the methods of [76] and [66], hints can be searched among the following quantities:

- The number of shortest SUSY cycles for each lattice,
- The Hodge numbers associated to the massless closed string spectrum,
- The map between the consistency conditions of different lattices.

We start by comparing the numbers of shortest possible cycles on the six lattices. Symmetries among these point to relations among lattices. The second step consists in finding symmetries between the Hodge numbers of the closed string spectrum, which depend on the choice of the exotic O6-plane and the lattices. Finally, a map can be found transforming the consistency conditions of one lattice to the ones of another lattice. As we will see, this map corresponds

to a rotation on two of the three tori, thus it preserves the relative angles between D6-branes, meaning that the intersection numbers and Yukawa couplings remain unchanged under the map. It follows that all lattices related by this map will give rise to equivalent models.

4.1.1 Number of shortest supersymmetric three-cycles

The quantity needed in this section is the length or volume of the three-cycles. This just corresponds to the product of the lengths of the three one-cycles on each torus. In section 2.4.1, we gave $\tan(\pi\phi_a)$ in (2.45) in terms of the torus wrapping numbers (n^i, m^i), $i = 1, 2, 3$. The length squared is just the sum of the numerator squared and the denominator squared appearing in (2.45). Up to normalization factors, the length squared is given by:

$$\ell^2 = \left(n_1^2 + \left(\frac{\varrho}{\sqrt{3}} (m_1 + b n_1) \right)^2 \right) (n_2^2 + n_2 m_2 + m_2^2)(n_3^2 + n_3 m_3 + m_3^2) \,, \tag{4.1}$$

with $\varrho = \sqrt{3} R_2/R_1$ and $b = 0, 1/2$ for the **a**-type respectively **b**-type lattices. This expression can be rewritten as a function of the bulk wrapping numbers (2.12):

$$\ell^2 = \left(P^2 + PQ + Q^2 \right) + \frac{\varrho}{3} \left(\tilde{U}^2 + \tilde{U}\tilde{V} + \tilde{V}^2 \right) \,, \tag{4.2}$$

where we introduced the short-hand notation $\tilde{m}^1 \equiv m^1 + b n^1$, so that we have: $\tilde{U} = U + bP$ and $\tilde{V} = V + bQ$, which we already used in section 3.3.1.

The quantity ℓ^2 can be used to compare the lengths of the three-cycles. In table 4.1, we indicated the number of shortest cycles (S) for different values of the complex structure parameter ϱ, for the six lattices. Also, the next-to-shortest (NS), next-to-next-to-shortest (NNS) and so on, are indicated.

To find these numbers, certain combinations of torus wrapping numbers (n^i, m^i) are tested as to whether they give rise to three-cycles satisfying the SUSY conditions (2.46), subsequently they are classified according to ℓ^2. We only consider combinations of (n^i, m^i) which permit to single out an orbifold and orientifold representative as described on page 21, in order to avoid double-counting. Moreover, n^i and m^i for a given i have to be co-prime. Otherwise, the D6-branes would wrap several times around the same cycle and falsify the determination of the number N_a, which corresponds to the rank of the gauge groups supported by the D6-branes, via the RR-tadpole cancellation conditions given in (2.50) and table 2.9.

Obtaining an equal amount of shortest possible cycles for different lattices is a strong indication that these lattices are equivalent. In table 4.1, the first line provides different values of the complex structure parameter ϱ. The subsequent lines give the number of shortest cycles for each ϱ for the lattices **a/bAA**. The same is done for the other lattices. We see that the columns are pairwise switched when going from lattice **aAA** to **aAB** and then from **aAB** to **aBB**. The same observation holds true for the **b**-type lattices. It means that **a/bAA** lattices with a given complex structure parameter ϱ yield the same number of shortest possible cycles as **a/bAB** lattices with complex structure parameter

$$\varrho' = \frac{3}{(1-b)^2 \varrho} = \begin{cases} \frac{3}{\varrho} & \text{for } b = 0 \\ \frac{12}{\varrho} & \text{for } b = 1/2 \end{cases} \,. \tag{4.3}$$

This suggests the existence of a map between the lattices which is accompanied by a rescaling map of the complex structure parameter.

ϱ	1	3	2	$\frac{3}{2}$	4	$\frac{3}{4}$	6	$\frac{1}{2}$	12	$\frac{1}{4}$	1	12	2	6	3	4	8	$\frac{3}{2}$	9	$\frac{4}{3}$
	aAA										**bAA**									
S	3	1	1	1	1	2	1	2	1	2	2	1	6	2	1	1	1	2	1	2
NS	3	1	2	2	1	1	1	1	1	1	1	1	2	6	2	2	1	1	1	1
NNS	1	3	1	1	2	1	1	3	1	2	2	1	27	9	2	1	2	1	2	1
$NNNS$	1	3	3	1	1	1	2	1	1	3	3	2	27	9	1	4	1	2	2	4
	aAB										**bAB**									
S	1	3	1	1	2	1	2	1	2	1	1	2	2	6	1	1	2	1	2	1
NS	1	3	2	2	1	1	1	1	1	1	1	1	6	2	2	2	1	1	1	1
NNS	3	1	1	1	1	2	3	1	2	1	1	2	9	27	1	2	1	2	1	2
$NNNS$	3	1	1	3	1	1	1	2	3	1	2	3	9	27	4	1	2	1	4	2
	aBB										**bBB**									
S	3	1	1	1	1	2	1	2	1	2	2	1	6	2	1	1	1	2	1	2
NS	3	1	2	2	1	1	1	1	1	1	1	1	2	6	2	2	1	1	1	1
NNS	1	3	1	1	2	1	1	3	1	2	2	1	27	9	2	1	2	1	2	1
$NNNS$	1	3	3	1	1	1	2	1	1	3	3	2	27	9	1	4	1	2	2	4

Table 4.1: The number of shortest SUSY three-cycles is given for the different lattice types and arbitrary values of the complex structure parameter ϱ. The columns are pairwise switched when going from **A**-type lattices to **B**-type lattices. This is a hint for a symmetry between lattices which is accompanied by a rescaling of ϱ. The pairing of the specific ϱ-values was suggested by the SUSY conditions (2.46).

4.1.2 The Hodge numbers and the massless closed string spectrum

The Hodge numbers and the massless closed string spectrum can be found in table 2.6. The counting of the Hodge numbers $(h^{1,1}_+, h^{11}_-)$ is a first hint of equivalences between **A**-type and **B**-type lattices for fixed $b \in \left\{0, \frac{1}{2}\right\}$ and simultaneous permutations of the exotic O6-plane label $\eta_{(i)} \equiv \eta_{\Omega\mathcal{R}}\eta_{\Omega\mathcal{R}\mathbb{Z}_2^{(i)}}$, $i = 1, 2, 3$. The Hodge numbers in table 2.6 suggest the following transformation law for the choice of the exotic O6-plane when going from lattices **AA** to **AB**: $\eta_{(2)} \to \eta_{(2)}$ and $\eta_{(3)} \to -\eta_{(3)}$. Similarly, the lattices **AB** and **BB** are linked by the map: $\eta_{(2)} \to -\eta_{(2)}$ and $\eta_{(3)} \to \eta_{(3)}$. Consequently, $\eta_{(1)} \to -\eta_{(1)}$ in both cases due to the relation $\eta = \eta_{(1)}\eta_{(2)}\eta_{(3)} = -1$ with discrete torsion. This ensures that we still have the same number of exotic O6-planes on each lattice.
The permutation of the exotic O6-plane label can be translated into a permutation of the four O6-planes. The following permutations of O6-planes for example would be in agreement with the transformation laws of the exotic charges:

$$\text{From } \mathbf{AA} \text{ to } \mathbf{AB}\text{:} \quad \begin{matrix} \Omega\mathcal{R} \leftrightarrow \Omega\mathcal{R}\mathbb{Z}_2^{(2)} \\ \Omega\mathcal{R}\mathbb{Z}_2^{(1)} \leftrightarrow \Omega\mathcal{R}\mathbb{Z}_2^{(3)} \end{matrix} \qquad \text{From } \mathbf{AB} \text{ to } \mathbf{BB}\text{:} \quad \begin{matrix} \Omega\mathcal{R} \leftrightarrow \Omega\mathcal{R}\mathbb{Z}_2^{(3)} \\ \Omega\mathcal{R}\mathbb{Z}_2^{(1)} \leftrightarrow \Omega\mathcal{R}\mathbb{Z}_2^{(2)} \end{matrix} \tag{4.4}$$

4.1.3 Consistency conditions of different lattices

The analysis can be separated into two parts: one part focusing on the bulk three-cycles appearing in the fractional three-cycle, and the other part concentrating on the exceptional three-cycles appearing in the fractional three-cycle.

Bulk three-cycles

The form of the consistency conditions depends on the type of lattice under consideration. A reparametrization of the discrete variables P, Q, U and V of one lattice leads to the the variables $\overline{P}, \overline{Q}, \overline{U}$ and $\overline{V}$ of another lattice, meaning that the solutions of the consistency conditions of different lattices are in one-to-one correspondence. This is a strong hint for equivalences between the lattices in the sense that they will produce equivalent models. The consistency conditions we take into consideration correspond to the SUSY conditions (2.46) and the bulk as well as the twisted part of the RR-tadpole cancellation conditions, which can be found in (2.50) and table 2.9.
Let us consider the following reparametrization:

$$\phi : \begin{pmatrix} P \\ Q \\ U \\ V \end{pmatrix} \to \begin{pmatrix} \overline{P} \\ \overline{Q} \\ \overline{U} \\ \overline{V} \end{pmatrix} = \begin{pmatrix} -\frac{1}{1-b}(V + bQ) \\ \frac{1}{1-b}(U + V + b(P + Q)) \\ (1-b)Q + \frac{b}{1-b}(V + bQ) \\ -(1-b)(P+Q) - \frac{b}{1-b}(U + V + b(P+Q)) \end{pmatrix} . \tag{4.5}$$

By replacing the barred variables $\overline{P}, \overline{Q}, \overline{U}, \overline{V}$ appearing in the **AA** lattices by the variables appearing on the right-hand side in the reparametrization above, the SUSY conditions of the lattices **a/bAA** are transformed into the SUSY conditions of the lattices **a/bAB** if simultaneously the complex structure parameter is transformed as $\varrho \to \frac{3}{\varrho(1-b)^2}$. The same transformations take the SUSY conditions of **a/bAB** to those of **a/bBB**. Hence, we encounter here the same symmetry we detected already by analyzing the number of shortest possible cycles in table 4.1.
To determine the action of ϕ on the RR-tadpole cancellation conditions, we need to check the transformation properties of the orientifold planes. The bulk wrapping numbers for the four orientifold planes can be found in table 2.3. For example, the bulk wrapping numbers for the four orientifold planes of the **AA** lattices are indicated in column 4 of table 2.3. These correspond to the barred variables. In order to find the unbarred bulk wrapping numbers in the lattices **AB**, we need to apply the inverse map ϕ^{-1} to the barred variables. By applying ϕ^{-1} on the orientifold planes, we see that they transform in accordance with the transformation laws (4.4) we determined by analyzing the massless closed string spectrum. Thus by applying (4.4) to the exotic charges and ϕ to the bulk wrapping numbers, the RR-tadpole cancellation conditions are correctly mapped from **a/bAA** to **a/bAB** to **a/bBB**.

Exceptional three-cycles

The reparametrization ϕ can be transcribed into the torus wrapping numbers as follows:

$$\phi : \begin{pmatrix} n^1 & m^1 \\ n^2 & m^2 \\ n^3 & m^3 \end{pmatrix} \to \begin{pmatrix} \overline{n}^1 & \overline{m}^1 \\ \overline{n}^2 & \overline{m}^2 \\ \overline{n}^3 & \overline{m}^3 \end{pmatrix} = \begin{pmatrix} \frac{1}{1-b}(m^1+bn^1) & -(1-b)n^1 - \frac{b}{1-b}(m^1+bn^1) \\ -m^2 & n^2+m^2 \\ n^3 & m^3 \end{pmatrix} . \tag{4.6}$$

This correspond to a rotation of the basis cycles by an angle of $-\pi/2$ on the first torus and a rotation by an angle of $\pi/3$ on the second torus, while the third torus is left invariant.
The next step consists in verifying whether this rotation allows to go from the twisted RR-tadpole cancellation conditions of one lattice to those of another lattice. Let us consider the $\mathbb{Z}_2^{(1)}$ twisted sector. From table 2.7, we see that for this first twisted sector, we have $x_\alpha^{(1)} \sim n^1$ and $y_\alpha^{(1)} \sim m^1$, thus the transformation law of the exceptional wrapping numbers $x_\alpha^{(1)}$, $y_\alpha^{(1)}$ is given by:

$$\overline{x}_\alpha^{(1)} = \frac{1}{1-b}(y_{\alpha'}^{(1)} + bx_{\alpha'}^{(1)}) , \tag{4.7}$$

$$\overline{y}_\alpha^{(1)} = -(1-b)x_{\alpha'}^{(1)} - \frac{b}{1-b}(y_{\alpha'}^{(1)} + bx_{\alpha'}^{(1)}) . \tag{4.8}$$

In the next step, we need to determine the transformation law of the index α appearing above and in the twisted RR-tadpole cancellation conditions given in table 2.9, which corresponds to the index of the exceptional three-cycles $\varepsilon_\alpha^{(1)}$ and $\tilde{\varepsilon}_\alpha^{(1)}$. A rotation by $+\pi/3$ on the second torus transforms the index α of the exceptional three-cycles as follows: $\varepsilon_3^{(1)} \to \varepsilon_5^{(1)} \to \varepsilon_4^{(1)} \to \varepsilon_3^{(1)}$, idem for the $\tilde{\varepsilon}_\alpha^{(1)}$. The indices $\alpha = 0, 1, 2$ remain invariant. These transformation laws can be read off from the exceptional basis cycles in expression (2.21) as follows: take for example $(\overline{n}^2, \overline{m}^2)$=(odd,even) in the lattices **AA**, going through fixed points 1 and 4 on the second two-torus. It follows from the right-hand side of (4.6) that (n^2, m^2)=(odd,odd), which corresponds to the fixed points 1 and 6. So 4 goes to 6 on the second torus, whereas the point 1 is left invariant. The fixed point labels on the third torus are left invariant under ϕ, hence we obtain the following transformation law for the indices of the exceptional two-cycles: $e_{4\beta}^{(1)} \overset{\phi}{\to} e_{6\beta}^{(1)}$. Studying the other two possible cases for $(\overline{n}^2, \overline{m}^2)$, i.e. $(\overline{n}^2, \overline{m}^2)$=(odd,odd) and $(\overline{n}^2, \overline{m}^2)$=(even,odd), the transformation laws of all the exceptional two-cycles $e_{\alpha\beta}^{(1)}$, $\alpha, \beta \in \{1, 4, 5, 6\}$, can be determined, from which in turn the transformation laws of the index α of the exceptional basis three-cycles $\varepsilon_\alpha^{(1)}$ and $\tilde{\varepsilon}_\alpha^{(1)}$ can be deduced.
Consequently, the equations in table 2.9 with $\alpha = 0, 1, 2, 3$ of the lattices **AA** should be mapped to the equations with $\alpha = 0, 1, 2, 5$ of the lattices **AB**. Applying the map ϕ to the equations of the lattices **AA** and recalling that under this map $\eta_{(1)} \to -\eta_{(1)}$, we obtain:

$$\begin{cases} \sum_a N_a (1 - \eta_{(1)}) \overline{x}_{\alpha,a}^{(1)} = 0 \\ \sum_a N_a [(1 + \eta_{(1)}) \overline{y}_{\alpha,a}^{(1)} + 2\eta_{(1)} b \overline{x}_{\alpha,a}^{(1)}] = 0 \end{cases} \qquad \alpha = 0, 1, 2, 3 \tag{4.9a}$$

$$\overset{\phi}{\to} \begin{cases} \sum_a N_a (1 + \eta_{(1)}) (y_{\alpha,a}^{(1)} + bx_{\alpha,a}^{(1)}) = 0 \\ \sum_a N_a [(\eta_{(1)} - 1)(1-b) x_{\alpha,a}^{(1)} - (1 + \eta_{(1)}) \frac{b}{1-b} (y_{\alpha,a}^{(1)} + bx_{\alpha,a}^{(1)})] = 0 \end{cases} \qquad \alpha = 0, 1, 2, 5 \tag{4.9b}$$

The equations in the **AB** lattices are given by:

$$\begin{cases} \sum_a N_a[(1+\eta_{(1)})y^{(1)}_{\alpha,a} + 2\eta_{(1)} b x^{(1)}_{\alpha,a}] = 0 \\ \sum_a N_a(1-\eta_{(1)})x^{(1)}_{\alpha,a} = 0 \end{cases} \qquad \alpha = 0,1,2,5\,. \tag{4.10}$$

In order to test whether the equations (4.9b) and (4.10) are equivalent, a case differentiation $\eta_{(1)} = -1$ and $\eta_{(1)} = 1$ should be performed, giving:

$\boxed{\eta_{(1)} = 1}$

Equation (4.9b): $\begin{cases} \sum_a N_a(y^{(1)}_{\alpha,a} + b x^{(1)}_{\alpha,a}) = 0 \\ \sum_a \frac{b}{1-b} N_a(y^{(1)}_{\alpha,a} + b x^{(1)}_{\alpha,a}) = 0 \end{cases}$ Equation (4.10): $\sum_a (N_a y^{(1)}_{\alpha,a} + b x^{(1)}_{\alpha,a}) = 0$.

$\boxed{\eta_{(1)} = -1}$

Equation (4.9b): $\sum_a N_a x^{(1)}_{\alpha,a} = 0$ Equation (4.10): $\begin{cases} \sum_a N_a b x^{(1)}_{\alpha,a} = 0 \\ \sum_a N_a x^{(1)}_{\alpha,a} = 0\,. \end{cases}$

We see from the expressions above that the equations (4.9b) and (4.10) are equivalent for both cases $\eta_{(1)} = 1$ and $\eta_{(1)} = -1$. This can be checked by considering $b = 0$ and $b = 1/2$ explicitly.
It remains to be seen whether the RR-tadpole cancellation conditions in table 2.9 appearing with indices $\alpha = 4,5$ for the lattices **AA** are correctly mapped to the conditions with $\alpha = 3,4$ for the lattices **AB**. A straightforward application of ϕ with $(\alpha = 4) \to (\alpha = 3)$ and $(\alpha = 5) \to (\alpha = 4)$ leads to:

$$\sum_a N_a(\overline{x}^{(1)}_{4,a} - \eta_{(1)}\overline{x}^{(1)}_{5,a}) = 0 \xrightarrow{\phi} \sum_a N_a[y^{(1)}_{3,a} + \eta_{(1)} y^{(1)}_{4,a} + b(x^{(1)}_{3,a} + \eta_{(1)} x^{(1)}_{4,a})] = 0\,, \tag{4.11}$$

$$\sum_a N_a[\overline{y}^{(1)}_{4,a} + \eta_{(1)}\overline{y}^{(1)}_{5,a} + b(\overline{x}^{(1)}_{4,a} + \eta_{(1)}\overline{x}^{(1)}_{5,a})] = 0 \xrightarrow{\phi} \sum_a N_a(x^{(1)}_{3,a} - \eta_{(1)} x^{(1)}_{4,a}) = 0\,. \tag{4.12}$$

This time, the RR-tadpole cancellation conditions are mapped directly to each other, so that a case differentiation is unnecessary.
A similar analysis to the one performed above shows that it is straightforward to check that the equations of **a/bAB** are mapped under ϕ to the equations of **a/bBB**.

Now let us concentrate on the second and third $\mathbb{Z}_2^{(l)}$ (with $l = 2,3$) twisted sectors. Let us start with $l = 2$. As before, the first step consists in determining the transformation law of the index α associated to the exceptional three-cycles $\varepsilon^{(2)}_\alpha$ and $\tilde{\varepsilon}^{(2)}_\alpha$. This is done by analyzing the transformation law of the exceptional two-cycles $e^{(2)}_{\alpha\beta}$ under ϕ.
In the second twisted sector, the second label of the exceptional two-cycles corresponds to the label of the fixed points on the third two-torus, which is invariant under the map ϕ. Consequently, the second label β of the exceptional two-cycles does not transform under ϕ: $e^{(2)}_{\alpha\beta} \to e^{(2)}_{\alpha'\beta}$.
The first label α corresponds to the fixed points on the first two-torus, upon which ϕ acts as a rotation of $-\pi/2$. For the untilted lattice ($b = 0$), the map ϕ leaves invariant the fixed points labels $\alpha = 1$ and $\alpha = 3$, whereas it exchanges the other two labels: $(\alpha = 2) \overset{\phi}{\leftrightarrow} (\alpha = 4)$. For the tilted lattice $b = 1/2$, the labels $\alpha = 1$ and $\alpha = 4$ are invariant, while the other two

labels are exchanged: $(\alpha = 2) \overset{\phi}{\leftrightarrow} (\alpha = 3)$. In the second and third twisted sectors, the label α in the exceptional two-cycles $e^{(2)}_{\alpha\beta}$ is the same α as the one appearing in the exceptional three-cycles $\varepsilon^{(2)}_\alpha$ and $\tilde{\varepsilon}^{(2)}_\alpha$, see (2.22).
The transformation law of the exceptional wrapping numbers $x^{(2)}_\alpha, y^{(2)}_\alpha$ under ϕ are the same as those of n^2, m^2 given in (4.6):

$$\begin{aligned} \overline{x}^{(2)}_\alpha &= -y^{(2)}_{\alpha'} , \\ \overline{y}^{(2)}_\alpha &= x^{(2)}_{\alpha'} + y^{(2)}_{\alpha'} . \end{aligned} \tag{4.13}$$

Now let us consider the third twisted sector. Concerning the transformation law of the index α under ϕ associated to the exceptional three-cycles $\varepsilon^{(3)}_\alpha$ and $\tilde{\varepsilon}^{(3)}_\alpha$, it is the same as the law we determined for the second twisted sector. Indeed, for both the second and third twisted sectors, the index α in the expressions of the exceptional two-cycles $e^{(2)}_{\alpha\beta}$ and $e^{(3)}_{\alpha\beta}$ refers to the fixed points of the first two-torus.
However, the second index β of the exceptional two-cycles $e^{(3)}_{\alpha\beta}$ in table 2.4 now has a non-trivial transformation law under ϕ, as it refers to the fixed points of the second two-torus. We already explained how this transformation law can be found when we discussed the first twisted sector. Indeed, we have e.g. $e^{(3)}_{\alpha 4} \overset{\phi}{\to} e^{(3)}_{\alpha' 6}$.
In table 2.4, we find the following correspondence:

$$\begin{aligned} & e^{(3)}_{\alpha 4}|_{\mathbf{AA}} : \ (\overline{n}^3, \overline{m}^3) \equiv (\overline{x}^{(3)}_\alpha, \overline{y}^{(3)}_\alpha) \\ & \downarrow \ \phi \\ & e^{(3)}_{\alpha' 6}|_{\mathbf{AB}} : \ (-(n^3 + m^3), n^3) \equiv (x^{(3)}_{\alpha'}, y^{(3)}_{\alpha'}) . \end{aligned}$$

However, the map ϕ is supposed to leave the torus wrapping numbers on the third torus invariant, so we have:

$$(\overline{n}^3, \overline{m}^3) = (n^3, m^3) \Leftrightarrow (\overline{x}^{(3)}_\alpha, \overline{y}^{(3)}_\alpha) = (y^{(3)}_{\alpha'}, -(x^{(3)}_{\alpha'} + y^{(3)}_{\alpha'})) . \tag{4.14}$$

Comparing this transformation law to (4.13), we see that except for an overall sign factor, we have the same transformation laws for the exceptional wrapping numbers $x^{(l)}_\alpha, y^{(l)}_\alpha$ in both the second and third twisted sectors ($l = 2$ and $l = 3$). Hence, we can treat these simultaneously. Consider the equations with $\alpha = 1, 2, 3, 4$ of the lattices $\mathbf{a/bAA}$ in table 2.9 for $l = 2, 3$ and $b = 0$. By applying the map and recalling that $\eta_{(2)} \to \eta_{(2)}$ (respectively $\eta_{(3)} \to -\eta_{(3)}$), we find:

$$\begin{cases} \sum_a N_a[(1 - \eta_{(l)})\overline{x}^{(l)}_{\alpha,a} - \eta_{(l)}\overline{y}^{(l)}_{\alpha,a}] = 0 \\ \sum_a N_a(1 + \eta_{(l)})\overline{y}^{(l)}_{\alpha,a} = 0 \end{cases} \qquad \alpha = 1, 2, 3, 4 \tag{4.15a}$$

$$\overset{\phi}{\to} \begin{cases} \sum_a N_a[y^{(l)}_{\alpha,a} + (-1)^l \eta_{(l)} x^{(l)}_{\alpha,a}] = 0 \\ \sum_a N_a(1 + (-1)^l \eta_{(l)})(x^{(l)}_{\alpha,a} + y^{(l)}_{\alpha,a}) = 0 \end{cases} \qquad \alpha = 1, 4, 3, 2 . \tag{4.15b}$$

In the $\mathbf{a/bAB}$ lattices, we have only one associated equation for $b = 0$, as can be seen in table 2.9, given by:

$$\sum_a N_a(x^{(l)}_{\alpha,a} + (-1)^l \eta_{(l)} y^{(l)}_{\alpha,a}) = 0 \quad \alpha = 1, 2, 3, 4 . \tag{4.16}$$

In order to see that equations (4.15b) and (4.16) are equivalent, once more a case differentiation has to be performed:

$\boxed{\eta_{(l)} = 1}$

$$\text{Eq. (4.15b):} \quad \begin{cases} \sum_a N_a(y^{(l)}_{\alpha,a} + (-1)^l x^{(l)}_{\alpha,a}) = 0 \\ \sum_a N_a(1 + (-1)^l)(x^{(l)}_{\alpha,a} + y^{(l)}_{\alpha,a}) = 0 \end{cases} \qquad \text{Eq. (4.16):} \quad \sum_a N_a(x^{(l)}_{\alpha,a} + (-1)^l y^{(l)}_{\alpha,a}) = 0\,.$$

$\boxed{\eta_{(l)} = -1}$

$$\text{Eq. (4.15b):} \quad \begin{cases} \sum_a N_a(y^{(l)}_{\alpha,a} - (-1)^l x^{(l)}_{\alpha,a}) = 0 \\ \sum_a N_a(1 - (-1)^l)(x^{(l)}_{\alpha,a} + y^{(l)}_{\alpha,a}) = 0 \end{cases} \qquad \text{Eq. (4.16):} \quad \sum_a N_a(x^{(l)}_{\alpha,a} - (-1)^l y^{(l)}_{\alpha,a}) = 0\,.$$

We see that for both sectors ($l = 2, 3$) the map works correctly for the untilted lattice ($b = 0$). Indeed, the first equation of (4.15b) is equivalent to (4.16), while the second equation of (4.15b) is either also equivalent to (4.15b) or else is trivial, depending on l.
For the tilted lattice $b = 1/2$, the reasoning above holds true for the equations with $\alpha = 1, 4$. Remember that for $b = 1/2$, the labels $\alpha = 1, 4$ are left invariant under ϕ whereas the labels $\alpha = 2$ and $\alpha = 3$ are interchanged. The equations involving $\alpha = 2, 3$ for $b = 1/2$ are given by:

$$\begin{cases} \sum_a N_a[x^{(l)}_{2,a} - \eta_{(l)} x^{(l)}_{3,a} - \eta_{(l)} y^{(l)}_{3,a}] = 0 \\ \sum_a N_a[x^{(l)}_{3,a} - \eta_{(l)} x^{(l)}_{2,a} - \eta_{(l)} y^{(l)}_{2,a}] = 0 \\ \sum_a N_a[y^{(l)}_{3,a} + \eta_{(l)} y^{(l)}_{2,a}] = 0 \\ \sum_a N_a[y^{(l)}_{2,a} + \eta_{(l)} y^{(l)}_{3,a}] = 0 \end{cases} \tag{4.17a}$$

$$\overset{\phi}{\to} \begin{cases} \sum_a N_a[y^{(l)}_{3,a} + (-1)^l \eta_{(l)} x^{(l)}_{2,a}] = 0 \\ \sum_a N_a[y^{(l)}_{2,a} + (-1)^l \eta_{(l)} x^{(l)}_{3,a}] = 0 \\ \sum_a N_a[x^{(l)}_{2,a} + y^{(l)}_{2,a} + (-1)^l \eta_{(l)}(x^{(l)}_{3,a} + y^{(l)}_{3,a})] = 0 \\ \sum_a N_a[x^{(l)}_{3,a} + y^{(l)}_{3,a} + (-1)^l \eta_{(l)}(x^{(l)}_{2,a} + y^{(l)}_{2,a})] = 0\,. \end{cases} \tag{4.17b}$$

For the **AB** lattices, the equations involving $\alpha = 2, 3$ for $b = 1/2$ are given by:

$$\begin{cases} \sum_a N_a[x^{(l)}_{2,a} + (-1)^l \eta_{(l)} y^{(l)}_{3,a}] = 0 \\ \sum_a N_a[x^{(l)}_{3,a} + (-1)^l \eta_{(l)} y^{(l)}_{2,a}] = 0\,. \end{cases} \tag{4.18}$$

In order to see that the equations (4.17b) and (4.18) are equivalent, it is sufficient to multiply the first two equations of (4.17b) by the factor $(-1)^l \eta_{(l)}$ and taking into account that $(-1)^l \eta_{(l)} (-1)^l \eta_{(l)} = 1$. This leads to the two equations of (4.18). The last two equations of (4.17b) are simply linear combinations of the first two equations of (4.17b).

All in all, we showed that the map ϕ provides a one-to-one relation between the consistency conditions of the lattices **AA** and **AB**, which is valid for the untwisted sector as well as the three $\mathbb{Z}_2^{(k)}$ ($k = 1, 2, 3$) twisted sectors. The same analysis can be redone to pass from the **AB** lattices to the **BB** lattices with the same map ϕ. The map is also compatible with the choice of the shifts in table 2.8, i.e., the map holds in presence of shifts.

Let me point out that the maps (4.5) and (4.6) with $b = 0$ have already been proposed in [66] for the **a**-type lattice of the $T^6/\mathbb{Z}_6'$ orbifold. It turned out that the map also worked for the **a**-type lattice of the $T^6/(\mathbb{Z}_2 \times \mathbb{Z}_6)$ orbifold under consideration. The complete extension of the map to the **b**-type lattices was proposed in our publication [63] for the first time.

The map acts as a rotation on the one-cycles, such that the relative angle between the cycles is preserved. The same holds true for the shift. This leads to the fact that the area defined by three intersecting D6-branes and the bulk part of the intersection numbers between D6-branes is invariant under the map. Due to the permutation of the labels of the exceptional two-cycles, also the Wilson lines and $\mathbb{Z}_2^{(l)}$ eigenvalues are unaffected by the map. This leads to the fact that also the exceptional part of the intersection numbers is preserved under the map.
The area defined by three intersecting D6-branes is related to the Yukawa coupling at tree level, whereas the intersection numbers are linked to the matter spectrum and also the discrete symmetries. Therefore, the relevant physical measurable quantities treated in the present work are invariant under the map, and the lattices **aAA**, **aAB** and **aBB** give rise to the same physical models. The same holds true for the lattices **bAA**, **bAB** and **bBB**. As a conclusion, we are left with two non equivalent types of lattices: the **a**-type lattices and the **b**-type lattices. We choose the lattices **aAA** and **bAA** to perform our search for particle physics models.

4.2 Supersymmetric three-cycles

The first step in model building consists in finding adequate three-cycles that D6-branes can wrap. The first set of consistency conditions corresponds to the SUSY equations (2.46), involving only the bulk part of the fractional three-cycles. Thus, the first aim is to find suitable bulk three-cycles allowing for SUSY models. The bulk cycles are characterized by the six torus wrapping numbers n^i, m^i, $i = 1, 2, 3$. This leads to a lot of combinations to test. For example, letting the torus wrapping numbers vary from -10 to 10, we have a priori $21^6 =$ 85 766 121 combinations. However, as we have seen on page 21, it is sufficient to consider (n^3, m^3)=(odd,odd) and $n^3 > 0$ in order to single out an orbifold representative and avoid orientation flips by an angle of π. Furthermore, $(n^1, \tilde{m}^1) \in \left\{(\frac{1}{1-b}, 0), (0, 1), (n^1 > 0, \tilde{m}^1 > 0)\right\}$ permits to single out an orientifold representative. Also, the torus wrapping numbers (n^i, m^i), $i = 1, 2, 3$ have to be coprime for each i. The remaining possible combinations of torus wrapping numbers n^i, m^i, $i = 1, 2, 3$ are used to calculate the corresponding bulk wrapping numbers P, Q, U, V defined in (2.12), which in turn are tested whether they satisfy the SUSY conditions (2.46).

4.2.1 Upper bounds on the bulk wrapping numbers

A sensible aspect to check is whether upper limits for the bulk wrapping numbers can be found. Such limits can indeed be found by analyzing the SUSY and bulk RR-tadpole cancellation conditions. The SUSY conditions (2.46) imply that the left-hand side of the RR-tadpole cancellation conditions (2.50) have only positive contributions. Indeed, the SUSY conditions (2.46) can be expressed in terms of $(n^1, \tilde{m}^1, X, Y)$ as defined in (2.12). Taking

the two SUSY conditions for the lattice **a/bAA**, we obtain:

$$0 = 3Q + \varrho(2\,\tilde{U} + \tilde{V}) = 3n^1 Y + \varrho\tilde{m}^1(2X + Y)\,, \tag{4.19a}$$
$$0 < 2P + Q + \varrho(-\tilde{V}) = n^1(2X + Y) + \varrho\tilde{m}^1(-Y)\,. \tag{4.19b}$$

The definitions of P, Q, U, V, X, Y in term of the torus wrapping numbers can be found in (2.12). The solution to these SUSY equations can be divided into three types:

1. $\boxed{(n^1, \tilde{m}^1) = (\frac{1}{1-b}, 0)}$ On the first torus, these cycles are parallel to the $\Omega\mathcal{R}$- and $\Omega\mathcal{R}\mathbb{Z}_2^{(1)}$-invariant planes:

$$\begin{aligned} &Y \overset{(4.19a)}{=} 0\,, \qquad X \overset{(4.19b)}{>} 0 \\ &\Rightarrow P > 0 \quad \text{and} \quad Q = \tilde{U} = \tilde{V} = 0\,. \end{aligned} \tag{4.20}$$

2. $\boxed{(n^1, \tilde{m}^1) = (0, 1)}$ On the first torus, these cycles are parallel to the $\Omega\mathcal{R}\mathbb{Z}_2^{(2)}$- and $\Omega\mathcal{R}\mathbb{Z}_2^{(3)}$-invariant planes:

$$\begin{aligned} &-Y \overset{(4.19a)}{=} 2X \overset{(4.19b)}{>} 0 \\ &\Rightarrow P = Q = 0 \quad \text{and} \quad -\tilde{V} = 2\tilde{U} > 0\,. \end{aligned} \tag{4.21}$$

3. $\boxed{n^1 > 0, \tilde{m}^1 > 0}$ This is the most generic case:

$$\begin{aligned} &Y \overset{(4.19a)}{=} -\frac{\varrho}{3}\frac{\tilde{m}^1}{n^1}(2\,X + Y)\,, \qquad \left(n^1 + \frac{\varrho^2}{3}\frac{(\tilde{m}^1)^2}{n^1}\right)(2\,X + Y) \overset{(4.19b)}{>} 0 \\ &\Rightarrow (2\,X + Y) > 0 \Rightarrow -\tilde{V} = \frac{\varrho}{3}\left(\frac{\tilde{m}^1}{n^1}\right)^2 (2\,P + Q) > 0\,. \end{aligned} \tag{4.22}$$

Note that the solutions of type 1 in (4.20) and 2 in (4.21) are solutions for every value of the complex structure parameter ϱ, i.e. they are independent of ϱ.
With the relations given above it is possible to verify that SUSY three-cycles will have only positive contributions to left-hand side of the RR-tadpole cancellation conditions. The bulk RR-tadpole cancellations for the **a/bAA** lattice can be found in (2.50) and are repeated here for convenience:

$$\sum_a N_a\,(2\,P_a + Q_a) = 8\left(\eta_{\Omega\mathcal{R}} + 3\,\eta_{\Omega\mathcal{R}\mathbb{Z}_2^{(1)}}\right)\,, \tag{4.23a}$$
$$\sum_a N_a\,(-\tilde{V}_a) = 8\,(1-b)\left(\eta_{\Omega\mathcal{R}\mathbb{Z}_2^{(2)}} + \eta_{\Omega\mathcal{R}\mathbb{Z}_2^{(3)}}\right)\,. \tag{4.23b}$$

All SUSY bulk three-cycles contribute either zero or positively to the left-hand sides of the equations above, as can be checked case-by-case:

- $\boxed{(n^1, \tilde{m}^1) = (\frac{1}{1-b}, 0)}$
  - positive contribution to the left-hand side of (4.23a),
  - zero contribution to the left-hand side of (4.23b).
- $\boxed{(n^1, \tilde{m}^1) = (0, 1)}$

- zero contribution to the left-hand side of (4.23a),
- positive contribution to the left-hand side of (4.23b).

- $\boxed{n^1 > 0, \tilde{m}^1 > 0}$
  - positive contributions to the left-hand side of both (4.23a) and (4.23b).

Hence, the right-hand side needs to be positive (or zero) in order for the equations to be satisfied. Consequently, the $\Omega\mathcal{R}\mathbb{Z}_2^{(1)}$-invariant O6-plane cannot support an exotic charge, i.e. $\eta_{\Omega\mathcal{R}\mathbb{Z}_2^{(1)}} = -1$ is prohibited. Similarly, any combinations of three exotic charges would also make it impossible for the three-cycles to satisfy both the SUSY conditions and the RR-tadpole cancellation conditions.
The SUSY equations (4.19a) and (4.19b) suggest a separation of the second and third tori from the first torus. Indeed, the solutions (4.20), (4.21) and (4.22) show that the torus wrapping numbers $n^1, \tilde{m}^1$ can be separated from X, Y, which only involve the torus wrapping numbers n^i, m^i for $i = 2, 3$ and are independent of the type of lattice (b=0 or b=1/2) under consideration. Thus, it is sensible to concentrate on X, Y first and only subsequently include $n^1, \tilde{m}^1$.
Since the contributions to the left-hand side of the bulk RR-tadpole cancellation conditions are always positive (or zero), the right hand-side provides an upper limit for $X, Y, n^1, \tilde{m}^1$. Hence, the lower bounds for X, Y are given by the SUSY conditions and the upper bounds by the RR-tadpole cancellation conditions:

$$\begin{cases} 0 \leq X \leq 16 \\ Y = 0 \end{cases} \text{ or } \begin{cases} 0 \leq 2X + Y \leq 16 \\ -16 \leq Y \leq 0 \end{cases}, \tag{4.24}$$

where the left-hand side corresponds to the following choice of the exotic charge:

$$(\eta_{\Omega\mathcal{R}}, \eta_{\Omega\mathcal{R}\mathbb{Z}_2^{(1)}}, \eta_{\Omega\mathcal{R}\mathbb{Z}_2^{(2)}}, \eta_{\Omega\mathcal{R}\mathbb{Z}_2^{(3)}}) = (1, 1, 1, -1) \text{ or } (1, 1, -1, 1),$$

and the right-hand side corresponds to:

$$(\eta_{\Omega\mathcal{R}}, \eta_{\Omega\mathcal{R}\mathbb{Z}_2^{(1)}}, \eta_{\Omega\mathcal{R}\mathbb{Z}_2^{(2)}}, \eta_{\Omega\mathcal{R}\mathbb{Z}_2^{(3)}}) = (-1, 1, 1, 1).$$

The three cases enumerated in (4.20)-(4.22) should be treated separately.

4.2.2 Full classification of bulk three-cycles

In the first case (4.20) and the second case (4.21), we always have $Y \in 2\mathbb{Z}$. Since we also have $Y = n^2m^3 + m^2(n^3 + m^3)$ and (n^3, m^3)=(odd,odd), we see that (n^2, m^2) must be (even,odd). The bulk two-cycles satisfying the conditions on X and Y in (4.20) or (4.21) and compatible with (4.24) are listed in the first two blocks of the left column in table B.2 in appendix B.3. The remaining step consists in adding to X and Y the torus wrapping numbers $(n^1, m^1) \in \left\{\left(\frac{1}{1-b}, \frac{-b}{1-b}\right), (0, 1)\right\}$ of the first two-torus. By taking care of eliminating all orbifold and orientifold images, we have eight bulk cycles which are of type 1 (4.20) and 2 (4.21). Four of these correspond to bulk three-cycles parallel to the O6-planes and the additional four are listed in table 4.2.

These cycles have the property that they are SUSY for arbitrary values of the complex structure parameter ϱ.

ϱ-independent SUSY bulk three-cycles on a/bAA							
$(n^i, m^i)_{i\in\{1,2,3\}}$	ϱ	X	Y	P	Q	U	$\tilde{V}$
$(\frac{1}{1-b}, \frac{-b}{1-b}; 2, 1; 3, -1)$	$\forall\,\varrho$	7	0	$\frac{7}{1-b}$	0	$\frac{-7b}{1-b}$	0
$(\frac{1}{1-b}, \frac{-b}{1-b}; 4, -1; 3, 1)$	$\forall\,\varrho$	13	0	$\frac{13}{1-b}$	0	$\frac{-13b}{1-b}$	0
$(0, 1; 4, -5; 3, -1)$	$\forall\,\varrho$	7	-14	0	0	7	-14
$(0, 1; 2, -3; 5, -1)$	$\forall\,\varrho$	7	-14	0	0	7	-14

Table 4.2: SUSY bulk three-cycles on **a/bAA** of type 1 (4.20) and 2 (4.21), not overshooting the bulk RR-tadpole cancellation conditions (2.50). In addition to the four three-cycles displayed here, there are four more ϱ-independent three-cycles falling into categories (4.20) and (4.21), given by three-cycles parallel to some O6-plane as listed in table 2.3. The characteristic feature of these eight three-cycles is that they are SUSY for all values of the complex structure parameter ϱ.

Now let us consider the most generic case given in (4.22). One of the SUSY conditions relates the complex structure parameter ϱ to the torus wrapping numbers $(n^1, \tilde{m}^1)$:

$$Y = -\frac{\varrho}{3}\frac{\tilde{m}^1}{n^1}(2X + Y)\,, \qquad\qquad 2X + Y > 0\,. \tag{4.25}$$

As previously, we search all (n^i, m^i) $i = 2, 3$ giving X and Y satisfying the lower bound and the upper bound given in (4.24). The results are classified according to the oddness/evenness of (n^2, m^2) and can be found in tables B.2, B.3 and B.4 in appendix B.3.
Once again, the associated three-cycles are found by adding the torus wrapping numbers (n^1, m^1) such that the upper bound given by the bulk RR-tadpole cancellation conditions is respected:

$$0 \leq 2P + Q \leq 16\,, \tag{4.26}$$

$$0 \leq -\frac{\tilde{V}}{1-b} \leq 16\,. \tag{4.27}$$

The complex structure parameter is chosen in accordance with (4.25), such that the SUSY conditions are satisfied:

$$\varrho = \frac{-3Q}{2\tilde{U} + \tilde{V}} \quad \text{with } 2\tilde{U} + \tilde{V} \neq 0\,. \tag{4.28}$$

The parameter b appears in $\tilde{m}^1$, thus we have to distinguish the **a**-type lattices and the **b**-type lattices. The results are as follows:

- For the **a**-type lattice **aAA**, we found 1760 bulk three-cycles of type 3 (4.22) on top of the eight bulk three-cycles which are independent of ϱ (of type 1 and 2, see (4.20) and (4.21)). These 1760 cycles distribute over 409 values of the complex structure parameter ϱ, which ranges $\frac{1}{80} \leq \varrho \leq 720$.

- For the **b**-type lattice **bAA**, we found 917 bulk three-cycles of type 3, see (4.22) on top of the eight bulk three-cycles which are independent of ϱ (of type 1 and 2, see (4.20) and (4.21)). These 917 cycles distribute over 181 values of the complex structure parameter ϱ, which ranges $\frac{2}{75} \leq \varrho \leq 1350$.

There are too many bulk three-cycles to list them explicitly here, so we will just point out some aspects of the results from the computer scan.
A majority of the values for ϱ allows for at most four SUSY bulk three-cycles of type 3 (4.22). The values for ϱ allowing for nine or more SUSY bulk three-cycles of type 3 (4.22) are listed in table 4.3 for both lattices.
Anticipating the results of chapter 5, we already indicated in table 4.3 the values of ϱ allowing for D6-branes free of matter states transforming in the adjoint or symmetric representation, which is particularly appealing for model building purposes.

Complex structure moduli $\varrho_{\mathbf{a/bAA}}$ with $\geq$ 9 additional SUSY 3-cycles		
# of 3-cycles	$\varrho_{\mathbf{aAA}}$	$\varrho_{\mathbf{bAA}}$
16	$2, \frac{15}{2}, \mathbf{15}$	–
15	$\mathbf{\frac{1}{2}}, \mathbf{6}$	–
14	$\mathbf{\frac{3}{5}}, \mathbf{\frac{3}{2}}, \mathbf{3}, 4, \mathbf{18}, \mathbf{30}$	$\mathbf{6}$
13	$\mathbf{\frac{3}{10}}, \frac{21}{2}, \mathbf{21}$	–
12	$\left(\frac{1}{15}\right), \left(\frac{1}{10}\right), \frac{6}{5}, \frac{9}{2}, \mathbf{36}, \mathbf{42}, \mathbf{45}$	$\left(\frac{2}{15}\right), \mathbf{30}, \mathbf{90}$
11	$\mathbf{\frac{1}{5}}, \mathbf{\frac{3}{14}}, \mathbf{\frac{1}{4}}, \mathbf{\frac{3}{7}}, \frac{6}{7}, \frac{5}{3}, \frac{5}{2}, 8, \mathbf{12}, \mathbf{33}$	$\mathbf{\frac{2}{5}}, \frac{10}{3}, \mathbf{66}$
10	$\left(\frac{1}{12}\right), \left(\frac{1}{8}\right), \left(\frac{1}{6}\right), \mathbf{\frac{3}{4}}, \mathbf{1}, \frac{9}{5}, \frac{9}{4}, 5, \mathbf{9}, \mathbf{24}, \mathbf{48}$	$\mathbf{\frac{6}{5}}, \mathbf{2}, \frac{18}{5}, 10, \mathbf{18}$
9	$\mathbf{\frac{3}{16}}, \mathbf{\frac{3}{8}}, \frac{9}{8}, \frac{7}{2}, \frac{18}{5}, 10, \mathbf{39}, (72), (90), (135)$	$1, 4, \mathbf{42}, \mathbf{78}, (270)$

Table 4.3: Values of the complex structure modulus $\varrho_{\mathbf{a/bAA}}$ allowing for at least nine additional SUSY bulk three-cycles, on top of the eight ϱ-independent three-cycles given in tables 2.3 and 4.2. The ϱ-values in brackets only yield SUSY fractional three-cycles which are accompanied by states in the adjoint representation. The ϱ-values in bold are the most appealing values, as they allow for fractional three-cycles potentially devoid of both matter states in the adjoint representation and in the symmetric representation.

Moreover, figure 4.1 provides on the horizontal axis the values of ϱ allowing for SUSY fractional three-cycles potentially free of both matter states in the adjoint representation and matter states in the symmetric representation. The vertical axis indicates the total number of SUSY bulk three-cycles (not including the ϱ-independent ones) for these ϱ-values, independent of the matter states the D6-branes give rise to. We will come back to this point in sections 5.2 and 5.3.

As a final remark, let us point out that the bulk RR-tadpole cancellation conditions (4.26) and (4.27) provide a direct upper bound of 16 for the torus wrapping numbers on the first torus, n^1, m^1.
There is no such bound for the torus wrapping numbers on the second and third torus. However, computer scans showed that the number of obtained solutions already saturated at values around 14 for n^i, m^i $i = 2, 3$. In order to make sure to obtain all appealing solutions we took n^i, m^i $i = 2, 3$ to vary from -32 to +32. To go to such high values for n^i, m^i $i = 2, 3$ is only possible when splitting the second and third tori from the first torus in a first step, as we have done here. Also, since the number of two-cycles is reduced compared to the number of three-cycles, it is possible to give an explicit list of them in appendix B.3.

Note that high values for the torus wrapping numbers render the fulfillment of the twisted RR-tadpole cancellation conditions in table 2.9 difficult, such that global models are hard to construct, see sections 6.2.3 and 7.2.2.

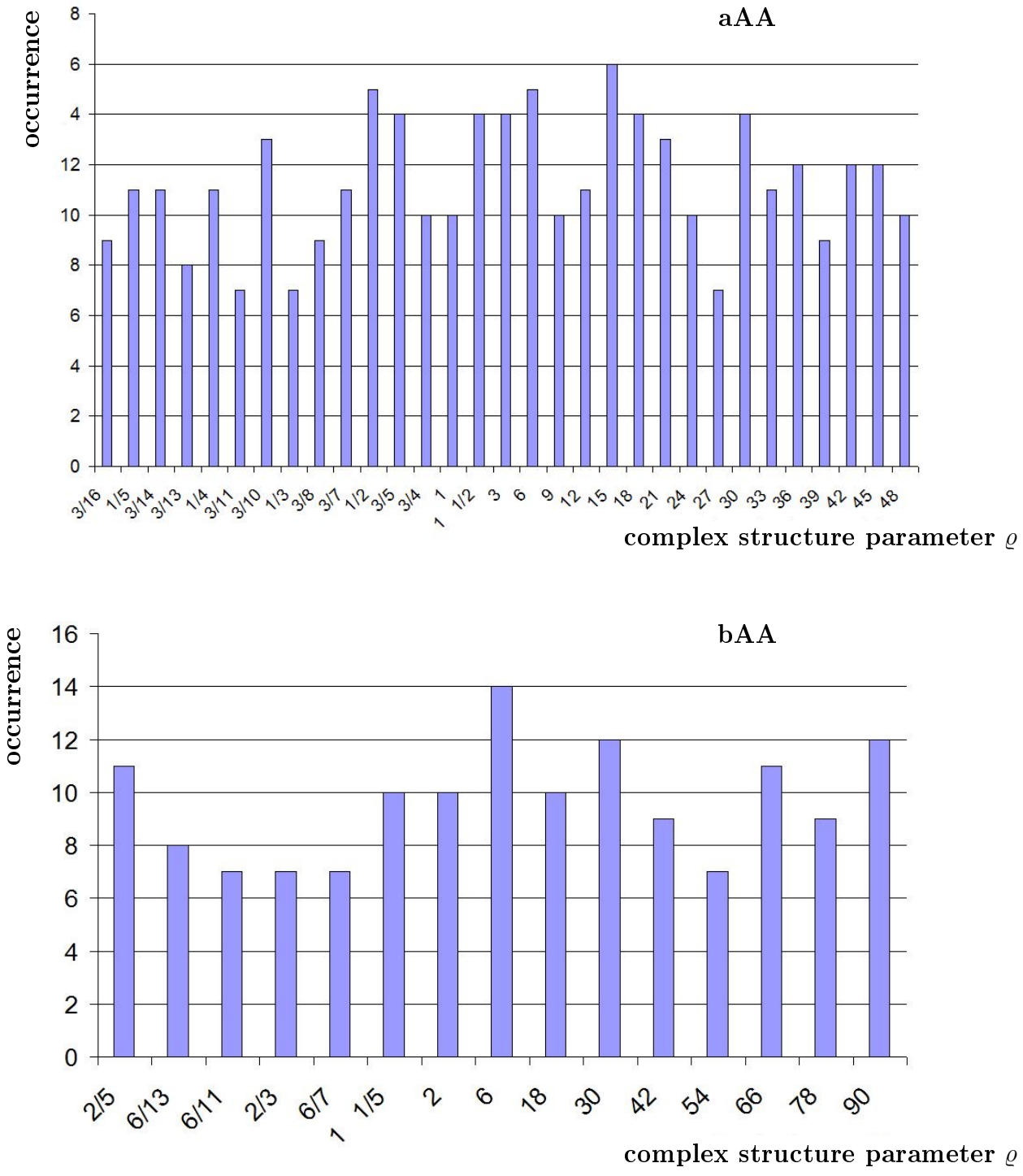

Figure 4.1: Overview of the values of the complex structure parameter ϱ allowing for D6-branes free of matter states in the adjoint and symmetric representations. The vertical axis indicates the total number of bulk three-cycles which are SUSY for the ϱ-values under consideration. The upper figure shows the results for the **aAA** lattice, the lower figure provides the results for the **bAA** lattice.

Chapter 5

Classification of D6-branes

In this chapter, we give results of the classification of D6-branes, closely following our publication [63]. The first step consists in detecting symmetry enhancement of the gauge group in order to determine which type of gauge group the D6-branes give rise to. In the next step, D6-branes are classified according to criteria of rigidity and the presence or absence of matter states transforming in the symmetric and antisymmetric representations. Finally, the last section of this chapter classifies pairs of D6-branes according to the number of generations of particles they generate.

5.1 Gauge symmetry enhancement to USp and SO groups

A first classification criterion of fractional three-cycles is given by the type of gauge group the D6-branes wrapping these three-cycles support, i.e non-Abelian unitary gauge groups $U(N)$, symplectic $USp(2N)$ groups or orthogonal $SO(2N)$ groups. Symmetry enhancement arises when a fractional three-cycle equals its own orientifold image, $\Pi_a = \Pi_{a'}$. In the present orbifold set-up, this is only possible for three-cycles whose bulk part Π_a^{bulk} is parallel to an O6-plane, as these are per definition the fixed loci of the orientifold projection $\Omega\mathcal{R}$. Moreover, the orientifold projection $\Omega\mathcal{R}$ acts on the orientation of the exceptional cycles as indicated in (2.26). The topological conditions on the Wilson lines, shifts and exotic charge in order to have completely $\Omega\mathcal{R}$-invariant fractional three-cycles and thus enhancement are listed in table 5.1. The full classification of enhancement for the **a**-type lattice was derived for the first time in the present work, whereas the classification for the **b**-type lattice is equivalent to the one given in [76, 78] for the $T^6/(\mathbb{Z}_2 \times \mathbb{Z}_6')$ orbifold. The distinction between symmetry enhancement to $USp(2N)$ groups and $SO(2N)$ groups is determined by examining the beta-function coefficients, see for example appendix B of [76] or appendix A.2 of this thesis.

D6-branes supporting symmetry enhancement are interesting for various reasons:

- The symplectic $USp(2)$ group is isomorphic to the special unitary $SU(2)$ group, so $USp(2)$ can be used to account for the $SU(2)_L$ group appearing in the MSSM, left-right symmetric or Pati-Salam models. Similarly, it can also be used to play the rôle of the $SU(2)_R$ group in the left-right symmetric model.

- D6-branes supporting $USp(2)$ groups are used as probe-branes for the K-theory constraints given in (2.51). We will come back to this in chapter 8.

Existence of $\Omega\mathcal{R}$ invariant three-cycles on $T^6/(\mathbb{Z}_2\times\mathbb{Z}_6\times\Omega\mathcal{R})$					
$\uparrow\uparrow$	$(\eta_{(1)},\eta_{(2)},\eta_{(3)})\overset{!}{=}$	$(1,1,-1)$		$(-1,-1,-1)$	
O6		$b=0$	$b=\frac{1}{2}$	$b=0$	$b=\frac{1}{2}$
$\Omega\mathcal{R}$	$\begin{pmatrix}-(-1)^{\sigma^2\tau^2+\sigma^3\tau^3}\\-(-1)^{2b\sigma^1\tau^1+\sigma^3\tau^3}\\-(-1)^{2b\sigma^1\tau^1+\sigma^2\tau^2}\end{pmatrix}$	$\begin{pmatrix}\sigma^1;\tau^1\\ \underline{0;1}\\ 1;1\end{pmatrix}$	$\begin{pmatrix}1;1\\1;1\\ \underline{0;1}\end{pmatrix}$	$\begin{pmatrix}\sigma^1;\tau^1\\ \underline{0;1}\\ \underline{0;1}\end{pmatrix}$	$\begin{pmatrix}1;1\\1;1\\1;1\end{pmatrix}$
		$USp(2N)$	$SO(2N)$	$USp(2N)$	$SO(2N)$
		$+1$ **Anti**	$+1$ **Sym**	$+\emptyset$	$+\emptyset$
$\Omega\mathcal{R}\mathbb{Z}_2^{(1)}$	$\begin{pmatrix}-(-1)^{\sigma^2\tau^2+\sigma^3\tau^3}\\(-1)^{2b\sigma^1\tau^1+\sigma^3\tau^3}\\(-1)^{2b\sigma^1\tau^1+\sigma^2\tau^2}\end{pmatrix}$	$\begin{pmatrix}\sigma^1;\tau^1\\1;1\\ \underline{0;1}\end{pmatrix}$	$\begin{pmatrix}1;1\\ \underline{0;1}\\1;1\end{pmatrix}$	$\begin{pmatrix}\sigma^1;\tau^1\\1;1\\1;1\end{pmatrix}$	$\begin{pmatrix}1;1\\ \underline{0;1}\\ \underline{0;1}\end{pmatrix}$
		$USp(2N)$	$SO(2N)$	$SO(2N)$	$USp(2N)$
		$+5$ **Anti**	$+5$ **Sym**	$+4$ **Anti**	$+4$ **Sym**
$\Omega\mathcal{R}\mathbb{Z}_2^{(2)}$	$\begin{pmatrix}(-1)^{\sigma^2\tau^2+\sigma^3\tau^3}\\-(-1)^{2b\sigma^1\tau^1+\sigma^3\tau^3}\\(-1)^{2b\sigma^1\tau^1+\sigma^2\tau^2}\end{pmatrix}$	$\begin{pmatrix}\sigma^1;\tau^1\\1;1\\1;1\end{pmatrix}$	$\begin{pmatrix}1;1\\ \underline{0;1}\\ \underline{0;1}\end{pmatrix}$	$\begin{pmatrix}\sigma^1;\tau^1\\1;1\\ \underline{0;1}\end{pmatrix}$	$\begin{pmatrix}1;1\\ \underline{0;1}\\1;1\end{pmatrix}$
		$SO(2N)$	$USp(2N)$	$USp(2N)$	$SO(2N)$
		$+1$ **Anti**	$+1$ **Sym**	$+2$ **Anti**	$+2$ **Sym**
$\Omega\mathcal{R}\mathbb{Z}_2^{(3)}$	$\begin{pmatrix}(-1)^{\sigma^2\tau^2+\sigma^3\tau^3}\\(-1)^{2b\sigma^1\tau^1+\sigma^3\tau^3}\\-(-1)^{2b\sigma^1\tau^1+\sigma^2\tau^2}\end{pmatrix}$	$\begin{pmatrix}\sigma^1;\tau^1\\ \underline{0;1}\\ \underline{0;1}\end{pmatrix}$	$\begin{pmatrix}1;1\\1;1\\1;1\end{pmatrix}$	$\begin{pmatrix}\sigma^1;\tau^1\\ \underline{0;1}\\1;1\end{pmatrix}$	$\begin{pmatrix}1;1\\1;1\\ \underline{0;1}\end{pmatrix}$
		$USp(2N)$	$SO(2N)$	$USp(2N)$	$SO(2N)$
		$+1$ **Sym**	$+1$ **Anti**	$+2$ **Anti**	$+2$ **Sym**

Table 5.1: Overview of gauge symmetry enhancement to $USp(2N)$ and $SO(2N)$ gauge groups and matter states in the (anti)symmetric representation on $\Omega\mathcal{R}$-invariant D6-branes. The possibility $\eta_{\Omega\mathcal{R}\mathbb{Z}_2^{(1)}}=-1$ is omitted as it is incompatible with the SUSY conditions (2.46) and bulk RR-tadpole cancellation conditions (2.50). The choice of the exotic charge $\eta_{\Omega\mathcal{R}\mathbb{Z}_2^{(2)}}=-1$ can be obtained from the listed case $\eta_{\Omega\mathcal{R}\mathbb{Z}_2^{(3)}}=-1$ upon exchange of the two-torus labels $2\leftrightarrow 3$. Underlining refers to three choices. For example, the requirement of $\sigma^2\tau^2=0$ leaves open three choices given by $(\sigma^2;\tau^2)\in\{(0;0);(1;0),(0;1)\}$. Underlining of both $(\sigma^2;\tau^2)$ and $(\sigma^3;\tau^3)$ gives nine options, as the choices are independent. For $b=\frac{1}{2}$, we only list the choices for $\sigma^1\tau^1=1$ explicitly, as the choices with $\sigma^1\tau^1=0$ coincide with the choices $\sigma^i\tau^i$ $(i=2,3)$ listed for $b=0$.

- As discussed in [78, 93], three-cycles supporting $USp(2N)$ or $SO(2N)$ groups are needed to derive the sufficiency conditions for the existence of discrete $\mathbb{Z}_n$-symmetries.

- In the case of a $SU(2)$ gauge group factor originating from a symplectic group $USp(2)\simeq SU(2)$, we have a rank $N_a=1$ in the RR-tadpole cancellation conditions in (2.50) and

table 2.9, which is reduced compared to $N_a = 2$ obtained in the case of the $SU(2)$ factor arising from an unitary group $U(2) \simeq SU(2) \times U(1)$. As a consequence, the reduced rank leaves more room for hidden stacks in the RR-tadpole cancellation conditions, which in turn augments the possibilities for model building.

The total number of three-cycles allowing for enhancement can be found by combining the choices of Wilson lines and shifts in table 5.1 with the $2^2 = 4$ independent $\mathbb{Z}_2$-eigenvalues. For the **a**-type lattice, we find 240 combinations of discrete parameters leading to $USp(2N)$ gauge group enhancement and 16 combinations giving $SO(2N)$ enhancement. For the **b**-type lattice, we have 216 combinations for $USp(2N)$ enhancement and 40 combinations with $SO(2N)$ enhancement.
As can be deduced from table 5.1, most three-cycles supporting gauge symmetry enhancement are accompanied by matter states transforming in the symmetric or antisymmetric representation of the gauge group. Matter states transforming in the symmetric representation are not desired on certain stacks from a phenomenological point of view, thus these three-cycles can only scarcely be used in model building. On the other hand, matter states transforming in the antisymmetric representation of a $USp(2)$ or $SO(2)$ (or $U(2)$) gauge group are tolerated in model building, for they correspond to singlet states under the non-Abelian groups.

5.2 Criteria for rigid D6-branes

The number of SUSY bulk three-cycles not overshooting the bulk RR-tadpole cancellation conditions is of order $\mathcal{O}(10^3)$ for both lattice types. Each bulk cycle gives rise to about $\mathcal{O}(10^2)$ fractional cycles. Since most models need to be realized with several stacks each one wrapping a different fractional three-cycle, the total number of configurations to test is tremendous and beyond the scope of a direct computer scan. Therefore, it is expedient to first reduce the number of combinations by imposing certain classification criteria on the three-cycles. The first criterion is the condition on the rigidity of D6-branes, as we mentioned in section 3.1.

5.2.1 Rigidity criteria for MSSM-type models

The criteria of rigidity on the a and b stacks are identical for Pati-Salam models, left-right symmetric models and MSSMs. In this section, we refer to these models as MSSM-type models. The criteria are different for $SU(5)$ models, which we therefore treat separately in the next section 5.2.2.
Due to the absence of a $\mathbb{Z}_6$-action on the first two-torus $T^2_{(1)}$, the angle on the first torus between a cycle a and its orbifold images $(\omega^k a)$, $(k = 1, 2)$ is always vanishing: $\vec{\phi}_{a(\omega^k a)} = \pm\pi(0, -1/3, 1/3)$, $(k = 1, 2)$. Consequently, the correct formula to use in table 3.3 is the second one, and the condition on the absence of matter states in the adjoint representation reads:

$$\varphi^{a(\omega^k a)} \equiv |\chi^{a(\omega^k a)}| = \frac{1}{2}\left(\left|I^{(2\cdot3)}_{a(\omega^k a)}\right| - I^{\mathbb{Z}_2^{(1)},(2\cdot3)}_{a(\omega^k a)}\right) \stackrel{!}{=} 0 \qquad \text{for } k = 1, 2, \tag{5.1}$$

where the toroidal intersection numbers $I^{(2\cdot3)}_{a(\omega^k a)} = I^{(2)}_{a(\omega^k a)} I^{(3)}_{a(\omega^k a)}$ along $T^2_{(2)} \times T^2_{(3)}$ are given by:

$$I^{(l)}_{a(\omega^k a)} = (-)^{k+l}[(n^l_a)^2 + n^l_a m^l_a + (m^l_a)^2] \in \mathbb{Z}_{\text{odd}}\,. \tag{5.2}$$

These can easily be found by using (3.19) and (2.13). The twisted part $I^{\mathbb{Z}_2^{(1)}}_{a(\omega^k a)} = (-1)^{\sigma^2_a\tau^2_a+\sigma^3_a\tau^3_a}$ can be found by proceeding accordingly to the method described in section 3.3.2, which is illustrated on an example in appendix A.2. Remember that each sector, ($k = 1$ and $k = 2$), accounts for half of the degrees of freedom filling up the chiral multiplet transforming in the adjoint representation. This implies $\varphi^{a(\omega a)} = \varphi^{a(\omega^2 a)}$, and the total number of matter states transforming in the adjoint representation is given by:

$$\varphi^{\mathbf{Adj}_a} = \frac{1}{2}\sum_{k=1}^{2} \varphi^{a(\omega^k a)} = \varphi^{a(\omega a)}. \tag{5.3}$$

Since the exceptional part of the intersection number always equals plus or minus one, $I^{\mathbb{Z}_2^{(1)}}_{a(\omega^k a)} = (-1)^{\sigma^2_a\tau^2_a+\sigma^3_a\tau^3_a} = \pm 1$, the only possibility for $\varphi^{\mathbf{Adj}_a}$ to vanish is to have the bulk part of the intersection number equal to one: $\left|I^{(2\cdot3)}_{a(\omega^k a)}\right| = 1$. From (5.2), we see that this condition implies (n^2_a, m^2_a), $(n^3_a, m^3_a) \in \{(\pm1, 0), (0, \pm1), (\pm1, \mp1)\}$. For our choice of the orbifold representative determined on page 21, the only possibilities are $(n^2_a, m^2_a) \in \{(1, 0), (0, 1)\}$, $(n^3_a, m^3_a) = (1, -1)$. This was also confirmed by a computer scan.

For the possibility $(n^2_a, m^2_a) = (0, 1)$, $(n^3_a, m^3_a) = (1, -1)$, the corresponding X_a and Y_a defined in (2.12) satisfy $Y_a = 0$ and $X_a > 0$. The SUSY conditions (4.19a) and (4.19b) then imply the following conditions on the torus wrapping numbers of the first two-torus: $(n^1_a, \tilde{m}^1_a) = (1, 0)$, i.e. $(n^1_a, m^1_a) = (\frac{1}{1-b}, \frac{-b}{1-b})$ ($b = 0, 1/2$), see (4.20). This three-cycle corresponds to an orbifold image of the three-cycle parallel to the $\Omega\mathcal{R}$-invariant plane as appearing in table 2.3. It is of type 1 (see (4.20)) and appears for all values of the complex structure modulus ϱ, as was discussed in section 4.2.
The results for the possibility $(n^2_a, m^2_a) = (1, 0)$, $(n^3_a, m^3_a) = (1, -1)$ differ for the **a**-type lattice and **b**-type lattice:

- For the **a**-type lattice, there are 159 SUSY bulk three-cycles which fulfill $(n^2_a, m^2_a) = (1, 0)$, $(n^3_a, m^3_a) = (1, -1)$, for various values of (n^1_a, m^1_a). These 159 three-cycles distribute over 159 different values of the complex structure modulus ϱ. Therefore, for these values of ϱ there is at most one cycle of the form $(n^2_a, m^2_a) = (1, 0)$, $(n^3_a, m^3_a) = (1, -1)$. The generic form of these cycles is given by $(n^1_a, \tilde{m}^1_a; 1, 0; 1, -1)$ where n^1_a and $\tilde{m}^1_a$ are fixed by the value of ϱ. This orbifold representative has angles $\pi(1/3, 0, -1/3)$ with respect to the $\Omega\mathcal{R}$-invariant direction.

- For the **b**-type lattice, there are 79 SUSY bulk three-cycles adequate to support rigid D6-branes. These 79 three-cycles distribute over 79 different values for ϱ, so once again, there is at most one three-cycle for a fixed value of ϱ fulfilling the criterion of rigidity, apart from the one parallel to the $\Omega\mathcal{R}$-invariant plane.

The condition on the bulk part $\left|I^{(2\cdot3)}_{a(\omega^k a)}\right| = 1$ is a necessary condition but not yet sufficient. Indeed, we also have the exceptional part to take into account:

$$\varphi^{\mathbf{Adj}_a} = \begin{cases} 0 & \sigma^2_a\tau^2_a = \sigma^3_a\tau^3_a \in \{0, 1\} \\ 1 & \sigma^2_a\tau^2_a \neq \sigma^3_a\tau^3_a \in \{0, 1\} \end{cases}. \tag{5.4}$$

Only the upper condition leads to totally rigid D6-branes. The conditions on rigidity are independent of the $\mathbb{Z}_2$-eigenvalues, the choice of the exotic charge and the Wilson lines on the first torus.

There is one big exception to the criteria of rigidity established above, which corresponds to three-cycles supporting gauge group enhancement. Indeed, for these cycles we have $a = a'$, where the prime denotes as usual the orientifold image of the three-cycle. Hence, the intersection sector $a(\omega^k a)$ can be interpreted as $a(\omega^k a)'$, meaning that the representations in which the matter states localized at the intersection points transform can no longer straightforwardly be interpreted as adjoint representations.
Instead, the examination of the beta-function coefficient reveals that the matter states have to transform in the representations listed in table 5.1. The example in appendix A.2 illustrates this statement. For symplectic groups $USp(2N)$, the adjoint representation is equivalent to the symmetric representation, whereas for orthogonal groups $SO(2N)$, it is equivalent to the antisymmetric representation. Hence, in table 5.1, all combinations giving symplectic groups and coming with additional matter states transforming in the antisymmetric representation are allowed to support the $USp(2)$ group showing up in the various particle physics models.
Symmetry enhancement accompanied with matter states transforming in the symmetric representation should be avoided, as such states no longer correspond to gauge singlets under $USp(2N)$.

Summary

Let us briefly summarize the rigidity criteria of MSSM-type models. A D6-brane is completely rigid if it satisfies one of the following rigidity criteria:

- The bulk orbit is of the form $(n_a^1, m_a^1; 1, 0; 1, -1)$ and the discrete parameters satisfy $\sigma_a^2\tau_a^2 = \sigma_a^3\tau_a^3$.
- The bulk orbit is parallel to the $\Omega\mathcal{R}$-invariant plane, with $\sigma_a^2\tau_a^2 = \sigma_a^3\tau_a^3$.
- The bulk orbit is parallel to the $\Omega\mathcal{R}$-invariant plane or some other $\Omega\mathcal{R}\mathbb{Z}_2^{(i)}$-invariant plane ($i = 1, 2, 3$), with σ_a^i, τ_a^i, and $\eta_{\Omega\mathcal{R}}$, $\eta_{\Omega\mathcal{R}\mathbb{Z}_2^{(i)}}$ chosen according to table 5.1 such that enhancement is present and matter states in the symmetric representation are absent.

5.2.2 Non-rigidity criteria for SU(5) models

The criteria of rigidity for $SU(5)$ models differ from those of MSSM-type models. In string theory, the $SU(5)$ model is realized with two stacks. The a stack supports the $SU(5) \subset U(5)$ group, whereas the b stack, supporting a gauge group of rank 1, is necessary to realize the antifundamental representation $\overline{\mathbf{5}}$ housing the matter states $(\overline{\mathbf{3}}, \mathbf{1})$ of the Standard Model gauge group $SU(3)_{QCD} \times SU(2)_L$. This is a stringy construction in the sense that ordinary quantum field theory realizes the $SU(5)$ model with only one gauge factor. In contrast to MSSM-type models, the a stack of the $SU(5)$ model need not be rigid. Indeed, one matter state transforming in the adjoint representation of $U(5)$ can be used as a GUT Higgs, breaking the $U(5)$ GUT group to the gauge group of the Standard Model. Concerning the b stack, there are no constraints on rigidity nor the matter states transforming in the (anti)symmetric

representation of the gauge group supported by b. Symmetry enhancement is tolerated on the b stack, contrarily to the a stack.
Thus, in this section, we are searching for three-cycles having exactly one matter state arising at the intersection between the three-cycle and its orbifold images. The bulk three-cycles susceptible to support one chiral multiplet transforming in the adjoint representation fall into two categories.
The first category corresponds to the bulk three-cycles we used in the previous section, i.e. the fractional three-cycles with bulk orbit parallel to $\Omega\mathcal{R}$ or to an orbit of the form $(n_a^1, m_a^1; 1, 0; 1, -1)$. From formula (5.4) one can deduce immediately that it suffices to take discrete parameters $\sigma_a^2\tau_a^2 \neq \sigma_a^3\tau_a^3$ in order to have one matter state transforming in the adjoint representation.
The other possibility of bulk three-cycles is given by cycles satisfying $\left|I_{a(\omega^k a)}^{(2\cdot 3)}\right| = 3$. For our choice of orbifold representatives given on page 21, one possibility is to take $(n_a^2, m_a^2; n_a^3, m_a^3)$ equal to $(1, -1; 1, 1)$ or equal to $(1, 1; 1, -1)$.
Other possibilities are: $(n_a^2, m_a^2; n_a^3, m_a^3)$ equal to $(2, -1; 1, -1)$ or to $(0, -1; 1, 1)$. The corresponding X_a and Y_a for the latter satisfy $-Y_a = 2X_a > 0$. The SUSY conditions (4.19a) and (4.19b) imply $(n_a^1, m_a^1) = (0, 1)$ (see (4.21)). The last two three-cycles actually correspond to orbifold representatives of the $\Omega\mathcal{R}\mathbb{Z}_2^{(2)}$- and $\Omega\mathcal{R}\mathbb{Z}_2^{(3)}$-invariant planes.
Concerning cycles with $(n_a^2, m_a^2; n_a^3, m_a^3)$ equal to $(1, -1; 1, 1)$ or equal to $(1, 1; 1, -1)$, a computer scan applied to the 1768 and 925 bulk three-cycles found in section 4.2 gave the following results for the **a**-type and **b**-type lattices, respectively:

- For the **a**-type lattice, there are 56 combinations of (n_a^1, m_a^1), giving rise to three-cycles satisfying the SUSY conditions for 56 appropriate values of the complex structure modulus ϱ and not overshooting the RR-tadpole cancellation conditions (2.50), with $(n_a^2, m_a^2; n_a^3, m_a^3)$ equal to $(1, -1; 1, 1)$ or equal to $(1, 1; 1, -1)$.

- For the **b**-type lattice, we have 27 combinations giving rise to three-cycles satisfying the conditions mentioned in the previous bullet point.

Once again, not only the bulk three-cycles need to satisfy certain conditions, but also the discrete Wilson lines and shifts have to be chosen with care:

$$\varphi^{\mathbf{Adj}_a} = \begin{cases} 1 & \sigma_a^2\tau_a^2 = \sigma_a^3\tau_a^3 \in \{0, 1\} \\ 2 & \sigma_a^2\tau_a^2 \neq \sigma_a^3\tau_a^3 \in \{0, 1\} \end{cases}, \tag{5.5}$$

Thus, only the combination $\sigma_a^2\tau_a^2 = \sigma_a^3\tau_a^3 \in \{0, 1\}$ leads to one matter state transforming in the adjoint representation. Once again, the criteria of non-rigidity are independent of $\mathbb{Z}_2$-eigenvalues, the Wilson lines and shifts on the first two-torus, and the choice of the exotic O6-plane.

Summary

The condition of having one chiral multiplet transforming in the adjoint representation of $SU(5)$ is satisfied if a three-cycle satisfies one of the following conditions:

- The three-cycle has its bulk orbit parallel to $(n_a^1, m_a^1; 1, 0; 1, -1)$ with the discrete parameters satisfying $\sigma_a^2\tau_a^2 \neq \sigma_a^3\tau_a^3$.

- The three-cycle has its bulk orbit parallel to the $\Omega\mathcal{R}$-invariant plane with the discrete parameters satisfying $\sigma_a^2\tau_a^2 \neq \sigma_a^3\tau_a^3$.

- The three-cycle has its bulk orbit parallel to $(n_a^1, m_a^1; 1, 1; 1, -1)$ or $(n_a^1, m_a^1; 1, -1; 1, 1)$ with the discrete parameters satisfying $\sigma_a^2\tau_a^2 = \sigma_a^3\tau_a^3$.

- The three-cycle has its bulk orbit parallel to the $\Omega\mathcal{R}\mathbb{Z}_2^{(2)}$- or $\Omega\mathcal{R}\mathbb{Z}_2^{(3)}$-invariant plane and discrete parameters satisfying $\sigma_a^2\tau_a^2 = \sigma_a^3\tau_a^3$.

5.3 Matter states in (anti)symmetric representations

Due to the presence of the orientifold action, matter states transforming in the symmetric or antisymmetric representation of the gauge group can arise at the intersection between a three-cycle and its orientifold image. Matter states transforming in the antisymmetric representation find various applications in the realization of particle physics models, as we showed in section 3.2.1. The various applications can be summarized as follows:

- Charged under the QCD stack supporting $U(3)$, these states can assume the rôle of right-handed quarks.

- Charged under a $U(2)$ or $USp(2)$ group, these states correspond to $SU(2)$ singlets. Thus, they can be associated to right-handed neutrinos.

- Charged under the $U(5)$ group of the $SU(5)$ GUT model, they account for the quarks and leptons transforming in the **10** representation of $U(5)$.

- An antisymmetric representation does not exist for Abelian $U(1)$ groups, although some intersections of D6-branes with their orientifold images can formally give rise to such states.

On the other hand, the phenomenological conditions on matter states transforming in the symmetric representation of a gauge group are much more restrictive. Actually, they are tolerated phenomenologically only if they are charged under the hidden sector or under a mere $U(1)$ gauge factor of the visible sector, when they can account for right-handed leptons, see section 3.2.1. Since the conditions on these states are more restrictive than the ones for the states in the antisymmetric representations, the classification of D6-branes starts with the counting of matter states transforming in the symmetric representation. The next step consists in classifying the found D6-branes further according to restrictions on the number of matter states transforming in the antisymmetric representation, which come on top of the restrictions on the states in the symmetric representation.
Model building in string theory traditionally focuses on the chiral spectrum first, aiming to reproduce the particle content of section 3.2.1. The non-chiral particle content is computed in a second step, but no constraints are put on the non-chiral spectrum, except for the ones we already computed due to the issue of rigidity. Every feature of the non-chiral spectrum which is in agreement with a model from a theoretical point of view is considered as a bonus.

5.3.1 Chiral spectrum

In order to calculate the spectrum of chiral (anti)symmetric states, one can use formula (3.15). However, this formula does not give the contributions from each sector (i.e. for given k in ω^k) separately. When calculating the Yukawa couplings later on, it is necessary to know the matter localization at each sector, though. In order to obtain the sector-per-sector contribution, one can use formula (3.25) instead.
Remember that the criteria of rigidity differ for the MSSM-type models and the $SU(5)$ models, meaning that also the search for (anti)symmetrics should be separated for MSSM-type and $SU(5)$ models.

MSSM-type models

In the MSSM-type models considered in the present work, the stacks which need to be rigid also come with conditions on the symmetric and antisymmetric particle spectrum. The conditions on rigidity for MSSM-type models were given on page 77.
Just as before, the analysis separates into a bulk part and an exceptional part. Running a computer scan on the rigid fractional three-cycles identified on page 77 and imposing the absence of chiral matter states in the symmetric representation $\chi^{\mathbf{Sym}_a} = 0$ leads to the following results:

- For the **aAA** lattice, we have 31 combinations of (n_a^1, m_a^1) leading to bulk three-cycles potentially devoid of matter states transforming in the symmetric representation.

- For the **bAA** lattice, 15 bulk three-cycles can be free of chiral matter states in the symmetric representation for certain combinations of the discrete parameters and the exotic O6-plane charge.

In addition, three-cycles parallel to the four O6-planes are free of chiral matter states in the symmetric and antisymmetric representation, for all choices of the discrete parameters and exotic O6-plane charge. Thus, we have 31 (**aAA** lattice) and 15 (**bAA** lattice) values for the complex structure parameter ϱ where we have, aside from the O6-planes, one additional potentially rigid three-cycle free of chiral matter states in the symmetric representation.
The models considered in this work also come with stacks in the hidden sector or supporting Abelian $U(1)$ gauge groups. There are no constraints of rigidity or on the matter states transforming in the symmetric representation for these stacks. Hence, it is interesting to inquire how many SUSY three-cycles there are in total for each of the 31 respectively 15 values of the complex structure parameter ϱ. This is indicated in table 4.3 and in figure 4.1 in section 4.2.
In table 4.3, we indicated the values of the complex structure parameter ϱ allowing for more than nine ϱ-dependent SUSY bulk three-cycles, the maximum being 16 bulk three-cycles for the **aAA** lattice and 14 for the **bAA** lattice. The restriction on the matter states transforming in the adjoint and symmetric representations reduces the number of appealing ϱ, though we still have one value for ϱ allowing the maximum of SUSY bulk three-cycles, namely $\varrho = 15$ for the **aAA** lattice and $\varrho = 6$ for the **bAA** lattice.
Figure 4.1 shows that all ϱ allowing for three-cycles potentially rigid and free of matter states in the symmetric representation come with at least seven ϱ-dependent SUSY bulk

three-cycles, for both lattices **aAA** lattice and **bAA**.

Just as in the case of the matter states in the adjoint representation, the exceptional part of the intersection numbers leads to certain combinations of the discrete parameters and choices of the exotic O6-plane which guarantee the absence of chiral matter in the symmetric representation. Together with the criteria of rigidity on the discrete parameters given by $\sigma_a^2\tau_a^2 = \sigma_a^3\tau_a^3$, the constraints on the discrete parameters fall into three classes:

(I) The $\Omega\mathcal{R}$-invariant plane is the exotic O6-plane (with $\eta_{\Omega\mathcal{R}} = -1$) and the Wilson lines and shifts satisfy $\sigma_a^2\tau_a^2 = \sigma_a^3\tau_a^3 = 0$.

(II) The $\Omega\mathcal{R}$-invariant plane is the exotic O6-plane (with $\eta_{\Omega\mathcal{R}} = -1$) and the Wilson lines and shifts satisfy $\sigma_a^2\tau_a^2 = \sigma_a^3\tau_a^3 = 1$.

(III) The $\Omega\mathcal{R}\mathbb{Z}_2^{(i)}$-invariant plane ($i = 2, 3$) is the exotic O6-plane (with $\eta_{\Omega\mathcal{R}\mathbb{Z}_2^{(i)}} = -1$) and the Wilson lines and shifts satisfy $\sigma_a^2\tau_a^2 = \sigma_a^3\tau_a^3 = 0$.

These come together with constraints on the torus wrapping numbers of the three-cycles as indicated in table 5.2.
For configurations with the $\Omega\mathcal{R}\mathbb{Z}_2^{(i)}$-invariant plane ($i = 2, 3$) as the exotic O6-plane and $\sigma_a^2\tau_a^2 = \sigma_a^3\tau_a^3 = 1$, all fractional three-cycles support chiral matter states in the symmetric representation.
Note that configuration (III) imposes tight constraints on the second bulk RR-tadpole cancellation condition in (2.50), i.e. $\tilde{V}_a = 0\ \forall a$. The three-cycles in table 5.2 do not satisfy this constraint, so these configurations lead to local models only. Still, we listed them in table 5.2 for reasons of completeness.

Apart from the ϱ-dependent three-cycles listed in table 5.2, we also have the ϱ-independent three-cycles parallel to the O6-planes which can be rigid if fulfilling the criteria on page 77. It turned out that all three-cycles parallel to O6-planes are completely free of chiral matter states in the symmetric and antisymmetric representations, for all combinations of the discrete parameters and choices of the exotic charge, independent of the criteria of rigidity.

Next, we turn our attention to the criteria of antisymmetric representations. These differ for the various MSSM-type models. For example, the MSSM can accommodate up to three states in the antisymmetric representation on its a or QCD stack, whereas the Pati-Salam models should have no antisymmetric representation on their a stack. Hence, it is sensible to search among the three-cycles in table 5.2 for D6-branes supporting at most three chiral matter states in the antisymmetric representation, i.e. $|\chi^{\mathbf{Anti}_a}| \in \{0, 1, 2, 3\}$. Note that in section 3.2.1, we have seen that the antisymmetric representations of the a stack appear in a sum in order to realize the right-handed down-type quarks, namely $|\chi^{ac} + \chi^{ad} - \chi^{\mathbf{Anti}_a}| = 3$. Hence, the conditions $|\chi^{\mathbf{Anti}_a}| \in \{0, 1, 2, 3\}$ may be relaxed as discussed in section 3.2.1. Anticipating the results though, the conditions $|\chi^{\mathbf{Anti}_a}| \in \{0, 1, 2, 3\}$ turned out not to be so stringent as to prevent the realization of three generation particle spectra.
The three-cycles parallel to the O6-planes already fulfill the criterion $|\chi^{\mathbf{Anti}_a}| \in \{0, 1, 2, 3\}$. Furthermore, the following ϱ-dependent three-cycles also fulfill this condition:

- For the **aAA** lattice, only six three-cycles of the form $(1, m_a^1; 1, 0; 1, -1)$ have been found, with $m_a^1 \in \{1, 2, 3, 4, 5, 6\}$.

Classification of bulk orbits $(n_a^1, m_a^1; 1, 0; 1, -1)$ without chiral symmetrics on $T^6/(\mathbb{Z}_2 \times \mathbb{Z}_6 \times \Omega\mathcal{R})$

aAA lattice						**bAA lattice**		
(n_a^1, m_a^1)	ϱ	**Configuration**	(n_a^1, m_a^1)	ϱ	**Configuration**	(n_a^1, m_a^1)	ϱ	**Configuration**
$(1, 16)$	3/16	$(II), (III)$	$(2, 1)$	6	(I)	$(1, 7)$	2/5	$(II), (III)$
$(1, 15)$	1/5	$(II), (III)$	$(3, 1)$	9	(I)	$(1, 6)$	6/13	$(II), (III)$
$(1, 14)$	3/14	$(II), (III)$	$(4, 1)$	12	(I)	$(1, 5)$	6/11	$(II), (III)$
$(1, 13)$	3/13	$(II), (III)$	$(5, 1)$	15	(I)	$(1, 4)$	2/3	$(II), (III)$
$(1, 12)$	1/4	$(II), (III)$	$(6, 1)$	18	(I)	$(1, 3)$	6/7	$(II), (III)$
$(1, 11)$	3/11	$(II), (III)$	$(7, 1)$	21	(I)	$(1, 2)$	6/5	$(II), (III)$
$(1, 10)$	3/10	$(II), (III)$	$(8, 1)$	24	(I)	$(1, 1)$	2	$(II), (III)$
$(1, 9)$	1/3	$(II), (III)$	$(9, 1)$	27	(I)	$(1, 0)$	6	$(I), (II), (III)$
$(1, 8)$	3/8	$(II), (III)$	$(10, 1)$	30	(I)	$(3, -1)$	18	(I)
$(1, 7)$	3/7	$(II), (III)$	$(11, 1)$	33	(I)	$(5, -2)$	30	(I)
$(1, 6)$	1/2	$(II), (III)$	$(12, 1)$	36	(I)	$(7, -3)$	42	(I)
$(1, 5)$	3/5	$(II), (III)$	$(13, 1)$	39	(I)	$(9, -4)$	54	(I)
$(1, 4)$	3/4	$(II), (III)$	$(14, 1)$	42	(I)	$(11, -5)$	66	(I)
$(1, 3)$	1	$(II), (III)$	$(15, 1)$	45	(I)	$(13, -6)$	78	(I)
$(1, 2)$	3/2	$(II), (III)$	$(16, 1)$	48	(I)	$(15, -7)$	90	(I)
$(1, 1)$	3	$(I), (II), (III)$						

Table 5.2: List of torus wrapping numbers $(n_a^1, m_a^1; 1, 0; 1, -1)$ of three-cycles satisfying the criteria of both rigidity and the absence of chiral matter states transforming in the symmetric representation, for the **aAA** lattice (left) and for the **bAA** lattice (right). The third, sixth and ninth columns indicate the choices of the exotic O6-plane and discrete parameters allowing to fulfill the aforementioned criteria. The three distinct configurations $(I), (II)$ and (III) are defined in the main text. The equation $\varrho = 3\frac{n_a^1}{\tilde{m}_a^1}$ arising from the SUSY conditions (2.46) relates the complex structure modulus ϱ to the one-cycle wrapping numbers (n_a^1, m_a^1).

- For the **bAA** lattice, only five three-cycles of the form $(1, m_a^1; 1, 0; 1, -1)$ have been found, with $m_a^1 \in \{0, 1, 2, 3, 4\}$.

For three-cycles of the form $(1, m_a^1; 1, 0; 1, -1)$, we can calculate an explicit sector-per-sector formula for the multiplicity of antisymmetric representations using (3.25). For the **aAA** lattice, we find:

$$\chi_{(\omega^k a)}^{\mathbf{Anti}_a/\mathbf{Sym}_a} = \begin{cases} -\frac{1}{2}\left((-)^{\sigma_a^2\tau_a^2} \pm \eta_{\Omega\mathcal{R}}\right)\left(m_a^1\,\eta_{(1)} - \eta_{(3)}\right) & k = 0, \\ \frac{1}{4}(1 \mp \eta_{\Omega\mathcal{R}})\left(m_a^1(1 - \eta_{(1)}) - \eta_{(2)} - \eta_{(3)}\right) & k = 1, \\ -\frac{1}{2}\left((-)^{\sigma_a^3\tau_a^3} \pm \eta_{\Omega\mathcal{R}}\right)\left(m_a^1\,\eta_{(1)} - \eta_{(2)}\right) & k = 2. \end{cases} \tag{5.6}$$

and for the **bAA** lattice:

$$\chi_{(\omega^k a)}^{\mathbf{Anti}_a/\mathbf{Sym}_a} = \begin{cases} -\frac{1}{4}\left((-)^{\sigma_a^2\tau_a^2} \pm \eta_{\Omega\mathcal{R}}\right)\left(2\tilde{m}_a^1\,\eta_{(1)} - \eta_{(3)}\right) & k = 0, \\ \frac{1}{4}(1 \mp \eta_{\Omega\mathcal{R}})\left(\tilde{m}_a^1(1 - \eta_{(1)}) - \frac{\eta_{(2)}+\eta_{(3)}}{2}\right) & k = 1, \\ -\frac{1}{4}\left((-)^{\sigma_a^3\tau_a^3} \pm \eta_{\Omega\mathcal{R}}\right)\left(2\tilde{m}_a^1\,\eta_{(1)} - \eta_{(2)}\right) & k = 2. \end{cases} \tag{5.7}$$

With these formulas, one can easily find the amount of chiral matter in the antisymmetric representation per sector k, $k \in \{0,1,2\}$. Table 5.3 shows the various results for each class of discrete parameters (I), (II) and (III).

		$\chi^{\mathbf{Anti}_a}$ **for rigid fractional three-cycles with** $\chi^{\mathbf{Sym}_a}=0$ **on** $T^6/(\mathbb{Z}_2\times\mathbb{Z}_6\times\Omega\mathcal{R})$		
		$(\chi_a^{\mathbf{Anti}_a}, \chi_{(\omega a)}^{\mathbf{Anti}_a}, \chi_{(\omega^2 a)}^{\mathbf{Anti}_a})$		
(n_a^1, m_a^1)	ϱ	(I)	(II)	(III)
$(1,1)$	3	$(0,2,0)$	$(0,2,0)$	$(0,0,-2)$ or $(-2,0,0)$
$(1,2)$	3/2	–	$(-1,3,-1)$	$(-1,0,-3)$ or $(-3,0,-1)$
$(1,3)$	1	–	$(-2,4,-2)$	$(-2,0,-4)$ or $(-4,0,-2)$
$(1,4)$	3/4	–	$(-3,5,-3)$	$(-3,0,-5)$ or $(-5,0,-3)$
$(1,5)$	3/5	–	$(-4,6,-4)$	$(-4,0,-6)$ or $(-6,0,-4)$
$(1,6)$	1/2	–	$(-5,7,-5)$	$(-5,0,-7)$ or $(-7,0,-5)$
$(1,0)$	6	$(0,1,0)$	$(0,1,0)$	$(0,0,-1)$ or $(-1,0,0)$
$(1,1)$	2	–	$(-1,2,-1)$	$(-1,0,-2)$ or $(-2,0,-1)$
$(1,2)$	6/5	–	$(-2,3,-2)$	$(-2,0,-3)$ or $(-3,0,-2)$
$(1,3)$	6/7	–	$(-3,4,-3)$	$(-3,0,-4)$ or $(-4,0,-3)$
$(1,4)$	2/3	–	$(-4,5,-4)$	$(-4,0,-5)$ or $(-5,0,-4)$

aAA **bAA**

Table 5.3: List of the net-chiralities $(\chi_a^{\mathbf{Anti}_a}, \chi_{(\omega a)}^{\mathbf{Anti}_a}, \chi_{(\omega^2 a)}^{\mathbf{Anti}_a})$ per sector $(\omega^k a)(\omega^k a)'$ for the rigid fractional three-cycles of table 5.2, with the additional condition $\chi^{\mathbf{Anti}_a} \in \{0, \pm 1, \pm 2, \pm 3\}$. The results are given for the **aAA** and **bAA** lattice, see eqs. (5.6) and (5.7). The first result in the column with configuration (III) corresponds to the choice of the exotic O6-plane charge $\eta_{\Omega\mathcal{R}\mathbb{Z}_2^{(2)}} = -1$, whereas the second result gives the net-chirality with the choice $\eta_{\Omega\mathcal{R}\mathbb{Z}_2^{(3)}} = -1$ for the exotic O6-plane charge.

In table 5.3, we see that although the net-chirality is always $\chi^{\mathbf{Anti}_a} \in \{0, \pm 1, \pm 2, \pm 3\}$, the total amount of matter $\sum_{k=0}^{2} |\chi_{(\omega^k)}^{\mathbf{Anti}_a}|$ can give more then three matter states in the antisymmetric representation. This signifies the presence of non-chiral matter pairs $\mathbf{Anti}_a + \overline{\mathbf{Anti}}_a$. However, not all non-chiral matter states can be detected that way, as non-chiral pairs can arise even within a same sector k.

SU(5) models

The three-cycles satisfying the criteria on the matter states in the adjoint representation for $SU(5)$ models are listed on page 78.

The a-stack supporting $U(5)$ needs to support exactly three chiral matter states transforming in the antisymmetric representation playing the rôle of the three generations of quarks and leptons embedded in the **10** representation of $SU(5)$. There should be no chiral matter states in the symmetric representation of $U(5)$.

For this search, we will not proceed in two steps as before by calculating the symmetric spectrum first and then the antisymmetric spectrum. Instead, we launch the computer

scan by directly imposing both conditions on the symmetric and antisymmetric particle content, i.e. $(\chi^{\mathbf{Anti}_a}, \chi^{\mathbf{Sym}_a}) = (\pm 3, 0)$. The scan reveals that for three-cycles with bulk orbit parallel to $(n_a^1, m_a^1; 1, 0; 1, -1)$ with the discrete parameters satisfying $\sigma_a^2\tau_a^2 \neq \sigma_a^3\tau_a^3$, no combination can be found satisfying $(\chi^{\mathbf{Anti}_a}, \chi^{\mathbf{Sym}_a}) = (\pm 3, 0)$. For three-cycles with orbits parallel to $(n_a^1, m_a^1; 1, 1; 1, -1)$ or $(n_a^1, m_a^1; 1, -1; 1, 1)$ with the discrete parameters satisfying $\sigma_a^2\tau_a^2 = \sigma_a^3\tau_a^3$, the results depend on the choice of sign (3.3) or (3.4), i.e. the choice of the sign in $(\chi^{\mathbf{Anti}_a}, \chi^{\mathbf{Sym}_a}) = (\pm 3, 0)$.
For the plus sign $(\chi^{\mathbf{Anti}_a}, \chi^{\mathbf{Sym}_a}) = (3, 0)$, no three-cycles fulfilling the required conditions can be found on the **aAA** lattice. On the **bAA** lattice, two combinations satisfy $(\chi^{\mathbf{Anti}_a}, \chi^{\mathbf{Sym}_a}) = (3, 0)$: the three-cycles with bulk orbit parallel to $(4, -1; 1, 1; 1, -1)$ or $(4, -1; 1, -1; 1, 1)$. The SUSY conditions require $\varrho = 4$ and the bulk RR-tadpole cancellation conditions imply $\eta_{\Omega\mathcal{R}} = -1$, i.e. the $\Omega\mathcal{R}$-invariant plane is the exotic O6-plane. Using formula (3.25), we can once again provide an explicit formula giving the net-chirality of matter in the (anti)symmetric representation per sector k. For three-cycles with bulk orbit $(4, -1; 1, 1; 1, -1)$, we find:

$$\chi_{(\omega^k a)}^{\mathbf{Anti}_a/\mathbf{Sym}_a} \overset{\eta_{\Omega\mathcal{R}}=-1}{=} \begin{cases} \frac{1}{2}\left((-)^{\sigma_a^1\tau_a^1} - (4 \mp 1)\right) & k = 0, \\ \frac{1}{2}\left(4(-)^{\sigma_a^2\tau_a^2} + (-)^{\sigma_a^1\tau_a^1 + \sigma_a^2\tau_a^2} \pm 3\right) & k = 1, \\ \frac{1}{2}\left(4(-)^{\sigma_a^3\tau_a^3} - 3(-)^{\sigma_a^1\tau_a^1 + \sigma_a^3\tau_a^3} \mp 1\right) & k = 2, \end{cases} \tag{5.8}$$

and for the three-cycles with bulk orbit $(4, -1; 1, -1; 1, 1)$, we obtain:

$$\chi_{(\omega^k a)}^{\mathbf{Anti}_a/\mathbf{Sym}_a} \overset{\eta_{\Omega\mathcal{R}}=-1}{=} \begin{cases} \frac{1}{2}\left((-)^{\sigma_a^1\tau_a^1} - (4 \mp 1)\right) & k = 0, \\ \frac{1}{2}\left(4(-)^{\sigma_a^2\tau_a^2} - 3(-)^{\sigma_a^1\tau_a^1 + \sigma_a^2\tau_a^2} \mp 1\right) & k = 1, \\ \frac{1}{2}\left(4(-)^{\sigma_a^3\tau_a^3} + (-)^{\sigma_a^1\tau_a^1 + \sigma_a^3\tau_a^3} \pm 3\right) & k = 2. \end{cases} \tag{5.9}$$

From these equations, we see that by summing over all sectors $k = 0, 1, 2$, the condition $(\chi^{\mathbf{Anti}_a}, \chi^{\mathbf{Sym}_a}) = (3, 0)$ is satisfied for the combination of discrete parameters $\sigma_a^1\tau_a^1 = \sigma_a^2\tau_a^2 = \sigma_a^3\tau_a^3$. More precisely, the net-chiralities per sector are given by $(\chi_a^{\mathbf{Anti}_a}, \chi_{(\omega a)}^{\mathbf{Anti}_a}, \chi_{(\omega^2 a)}^{\mathbf{Anti}_a}) = (-1, 0, 4)$ and $(\chi_a^{\mathbf{Sym}_a}, \chi_{(\omega a)}^{\mathbf{Sym}_a}, \chi_{(\omega^2 a)}^{\mathbf{Sym}_a}) = (-2, 1, 1)$.

The choice with the minus sign, i.e. imposing the conditions $(\chi^{\mathbf{Anti}_a}, \chi^{\mathbf{Sym}_a}) = (-3, 0)$, leads to different possibilities. In case of this choice, a computer scan yields three-cycles with bulk orbit of the form $(1, m_a^1; 1, 1; 1, -1)$ or $(1, m_a^1; 1, -1; 1, 1)$, with $m_a^1 = 2$ and $\varrho = \frac{1}{2}$ for the **aAA** lattice and $m_a^1 = 1$, $\varrho = \frac{2}{3}$ for the **bAA** lattice. Once again, aiming for global particle physics models imposes the choice $\eta_{\Omega\mathcal{R}} = -1$ for the exotic O6-plane due to the bulk RR-tadpole cancellation conditions. Using formula (3.25), we can once more give explicit expressions for the net-chirality per sector k of matter states in (anti)symmetric representations for three-cycles characterized by the bulk orbit $(1, m_a^1; 1, 1; 1, -1)$:

$$\chi_{(\omega^k a)}^{\mathbf{Anti}_a/\mathbf{Sym}_a} \overset{\eta_{\Omega\mathcal{R}}=-1}{=} \begin{cases} -\frac{1}{2}(1 \pm 1)(\tilde{m}_a^1 - 1 + b) & k = 0, \\ \frac{1}{2}(\tilde{m}_a^1 + 1 - b)\left((-)^{\sigma_a^2\tau_a^2} \pm 1\right) & k = 1, \\ \frac{1}{2}\left[\tilde{m}_a^1\left((-)^{\sigma_a^3\tau_a^3} \mp 3\right) - (1 - b)\left(3(-)^{\sigma_a^3\tau_a^3} \mp 1\right)\right] & k = 2, \end{cases} \tag{5.10}$$

Similarly, the three-cycles with orbit $(1, m_a^1; 1, -1; 1, 1)$ are characterized by the following expressions for the net-chiralities:

$$\chi_{(\omega^k a)}^{\mathbf{Anti}_a/\mathbf{Sym}_a} \overset{\eta_{\Omega\mathcal{R}}=-1}{=} \begin{cases} -\frac{1}{2}(1\pm 1)(\tilde{m}_a^1 - 1 + b) & k=0, \\ \frac{1}{2}\left[\tilde{m}_a^1\left((-)^{\sigma_a^2\tau_a^2}\mp 3\right) - (1-b)\left(3(-)^{\sigma_a^2\tau_a^2}\mp 1\right)\right] & k=1, \\ \frac{1}{2}(\tilde{m}_a^1 + 1 - b)\left((-)^{\sigma_a^3\tau_a^3}\pm 1\right) & k=2. \end{cases} \tag{5.11}$$

The conditions $(\chi^{\mathbf{Anti}_a}, \chi^{\mathbf{Sym}_a}) = (-3, 0)$ are satisfied when the discrete parameters satisfy $\sigma_a^2\tau_a^2 = \sigma_a^3\tau_a^3 = 1$.

As a side-remark, note that in the case of the net-chiralities of bifundamental representations χ^{ab}, the choice of the sign according to (3.3) or (3.4) is not so important, as it can be obtained by a mere exchange of the three-cycles a and b, i.e. $\chi^{ab} = -\chi^{ba}$. This is no longer true in the case of the net-chiralities of (anti)symmetric representations, as these involve only a single three-cycle a and its orientifold image a'. Consequently, the conditions $\chi^{\mathbf{Anti}_a} = 3$ and $\chi^{\mathbf{Anti}_a} = -3$ are not equivalent. For models completely free of matter states in the (anti)symmetric representations, e.g. those considered in chapter 7, the two choices (3.3) and (3.4) give rise to equivalent models.

All in all, one can conclude that there are numerous fractional three-cycles apt to support D6-branes providing the right amount of matter states transforming in the adjoint and chiral (anti)symmetric representations. In the next step, the non-chiral (anti)symmetric spectrum will be calculated from the three-cycles classified previously.

5.3.2 Non-chiral spectrum

In order to clarify the use of table 3.4, we will produce examples to some of the cases appearing in table 3.4.

Three vanishing angles $\vec{\phi}_{(\omega^k a)(\omega^k a)'} = (0, 0, 0)$

This configuration arises when on all three two-tori the angle between a three-cycle $(\omega^k a)$ for some sector k and its orientifold image $(\omega^k a)'$ is zero. This only happens for three-cycles having their bulk orbit parallel to some O6-plane. In appendix A.2, we calculated as an example the contribution to the beta-function coefficient explicitly for a cycle parallel to the $\Omega\mathcal{R}$-plane, in case of the **a**-type lattice. The first sector $k = 0$ gives the following contribution of matter states to the (anti)symmetric representation for both **aAA** and **bAA** lattices:

$$\begin{aligned} b_{aa'}^{\mathcal{A}} + b_{aa'}^{\mathcal{M}} =& N_a\left[\eta_{(1)}(-)^{\sigma_a^2\tau_a^2+\sigma_a^3\tau_a^3} + \eta_{(2)}(-)^{2b\sigma_a^1\tau_a^1+\sigma_a^3\tau_a^3} + \eta_{(3)}(-)^{2b\sigma_a^1\tau_a^1+\sigma_a^2\tau_a^2}\right] \\ & - 2\eta_{\Omega\mathcal{R}}\left[\eta_{(1)}(-)^{2b\sigma_a^1\tau_a^1} + \eta_{(2)}(-)^{\sigma_a^2\tau_a^2} + \eta_{(3)}(-)^{\sigma_a^3\tau_a^3}\right]. \end{aligned} \tag{5.12}$$

The lattice dependence enters via the parameter $b \in \{0, 1/2\}$. In case of gauge symmetry enhancement, the $(\omega^k a)(\omega^k a)'$ sectors cannot be treated independently from the $a(\omega^k a)$ sectors. Avoiding the combinations of discrete parameters giving rise to gauge symmetry enhancement, we can directly read off the number of (anti)symmetric states from the expression

above and distinguish the following cases for the **aAA** lattice:

$$b^{\mathcal{A}}_{aa'}+b^{\mathcal{M}}_{aa'} = \begin{cases} N_a+2 & (\eta_{\Omega\mathcal{R}}=-1,\ \sigma_a^2\tau_a^2=\sigma_a^3\tau_a^3=1), \quad \text{or} \quad (\eta_{\Omega\mathcal{R}\mathbb{Z}_2^{(l)}}=-1,\ \sigma_a^l\tau_a^l=0\neq\sigma_a^k\tau_a^k), \\ N_a-2 & (\eta_{\Omega\mathcal{R}}=-1,\ \sigma_a^2\tau_a^2\neq\sigma_a^3\tau_a^3), \quad \text{or} \quad (\eta_{\Omega\mathcal{R}\mathbb{Z}_2^{(l)}}=-1,\ \sigma_a^2\tau_a^2=\sigma_a^3\tau_a^3), \end{cases} \tag{5.13}$$

with $l,k\in\{2,3\}$ and the parameter combinations $(\sigma_a^k\tau_a^k)$ chosen such that gauge symmetry enhancement is absent. Comparing the expression above to formula (3.26), we see that the first possibility N_a+2 corresponds to a non-chiral pair of symmetric representations $\mathbf{Sym}_a+\overline{\mathbf{Sym}}_a$ of $U(N_a)$ and the second possibility N_a-2 yields a non-chiral pair of antisymmetric representations $\mathbf{Anti}_a+\overline{\mathbf{Anti}}_a$. Note, however, that this is only the contribution from the first sector $k=0$. The total amount of matter states is provided by the sum over all sectors. For the **bAA** lattice, the results are similar to the ones given in section 3.3 of [76].

One vanishing angle: $\vec{\phi}_{(\omega^k a)(\omega^k a)'}=(0_i,\phi_j,-\phi_k)$ on $T^2_{(i)}\times T^2_{(j)}\times T^2_{(k)}$

The angle between a three-cycle $(\omega^k a)$ for some k and its orientifold image $(\omega^k a)'$ on one of the three two-tori can only be zero if this three-cycle is parallel to an O6-plane on the two-torus in question. For example, the eleven cycles discussed in table 5.2 with bulk orbit $(1,m_a^1;1,0;1,-1)$ are such three-cycles. In the first sector $k=0$, they are parallel to the $\Omega\mathcal{R}$-plane and the $\Omega\mathcal{R}\mathbb{Z}_2^{(2)}$-plane on the second torus. A similar situation arises for the third sector $k=2$, where the cycles are parallel to the $\Omega\mathcal{R}$-plane or the $\Omega\mathcal{R}\mathbb{Z}_2^{(3)}$-plane on the third torus. In the second sector $k=1$ though, all three angles are non-vanishing. For the first and third sectors $k=0,2$, the following expressions for the beta-function coefficients can be derived:

$$b^{\mathcal{A}}_{(\omega^k a)(\omega^k a)'}+b^{\mathcal{M}}_{(\omega^k a)(\omega^k a)'} = \begin{cases} \left(\tilde{m}_a^1+(1-b)\eta_{(2)}\right)\left[\frac{N_a}{2}-(-)^{\sigma_a^2\tau_a^2}\eta_{\Omega\mathcal{R}}\right] & k=0, \\ \left(\tilde{m}_a^1+(1-b)\eta_{(3)}\right)\left[\frac{N_a}{2}-(-)^{\sigma_a^3\tau_a^3}\eta_{\Omega\mathcal{R}}\right] & k=2. \end{cases} \tag{5.14}$$

From this expression, one sees that the amount of matter states in the antisymmetric representation matches the net-chiralities in table 5.3. Besides, by looking at table 5.2, we see that for all three cases (I), (II) and (III), the contribution to the non-chiral matter states in the symmetric representation is zero. In other words, the conditions in table 5.2 imposed in order to have vanishing chiral matter states in the symmetric representation imply the vanishing of the non-chiral states in the symmetric representation, at least in sectors $k=0,2$. Actually, the same holds true for the second sector $k=1$, as we will see soon.
Another example is once again given by the second and third sectors ($k=1,2$) of a three-cycle with bulk orbit parallel to $\Omega\mathcal{R}$- or $\Omega\mathcal{R}\mathbb{Z}_2^{(1)}$-plane. In fact, the $\mathbb{Z}_6$-orbifold generator ω does not act on the first two-torus. Using the third formula in table 3.4, the contributions to the matter states in the (anti)symmetric representation is the same for both sectors $k=1,2$:

$$b^{\mathcal{A}}_{(\omega^k a)(\omega^k a)'}+b^{\mathcal{M}}_{(\omega^k a)(\omega^k a)'} = \frac{1}{2}\left(1+\eta_{(1)}\right)\left[\frac{N_a}{2}-(-)^{2b\sigma_a^1\tau_a^1}\eta_{\Omega\mathcal{R}}\right]. \tag{5.15}$$

For the choice $\eta_{(1)}=-1$, we see that this sector gives no contributions. For the choice $\eta_{(1)}=1$, we can have either an antisymmetric non-chiral pair, $\mathbf{Anti}_a+\overline{\mathbf{Anti}}_a$, or a symmetric non-chiral pair, $\mathbf{Sym}_a+\overline{\mathbf{Sym}}_a$, depending on the combination of discrete parameters $2b\sigma_a^1\tau_a^1$.

Three non-vanishing angles $\phi^{(i)}_{(\omega^k a)(\omega^k a)'} \neq 0 \qquad \forall i$

As already mentioned, the sector $(\omega a)(\omega a)'$ of the three-cycles in table 5.2 falls into this category, as none of the three angles between the three-cycle (ωa) and its orientifold image $(\omega a)'$ vanishes. Thus, the last formula in table 3.4 has to be used in order to calculate the beta-function coefficient for both lattices **aAA** and **bAA**:

$$\begin{aligned} b^{\mathcal{A}}_{(\omega a)(\omega a)'} + b^{\mathcal{M}}_{(\omega a)(\omega a)'} &= \left(\frac{N_a}{2} + \eta_{\Omega\mathcal{R}}\right)\left[\frac{\tilde{m}^1_a(1-\eta_{(1)}) - (1-b)(\eta_{(2)}+\eta_{(3)})}{2}\right] \\ &= \begin{cases} \left(\frac{N_a}{2}-1\right)\left[\tilde{m}^1_a + 1 - b\right] & \eta_{\Omega\mathcal{R}} = -1, \\ 0 & \text{else.} \end{cases} \end{aligned} \tag{5.16}$$

Once again, the number of matter states in the antisymmetric representation matches the net-chiralities in table 5.3. It is important to notice that this sector is completely free of matter states in the symmetric representation.
All in all, one can conclude that the three-cycles of table 5.2 are completely devoid of matter states transforming in the symmetric representation.

Summary

We now have at our disposal the three-cycles adequate to support the a and b stacks of the MSSM-type models, as well as the a stack of the $SU(5)$ model. To render the results clear, we give a brief summary of the suitable three-cycles identified in sections 5.2 and 5.3.

For the MSSM-type models, we have the following results:

- The bulk orbit is of the form $(n^1_a, m^1_a; 1, 0; 1, -1)$ with the constraints on n^1_a, m^1_a, on the discrete parameters and on the choice of the exotic charge as listed in table 5.2.
- The bulk orbit is parallel to the $\Omega\mathcal{R}$-plane, with $\sigma^2_a\tau^2_a = \sigma^3_a\tau^3_a$.
- The bulk orbit is parallel to the $\Omega\mathcal{R}$-plane or one of the other $\Omega\mathcal{R}\mathbb{Z}^{(i)}_2$-planes, $i = 1, 2, 3$ with σ^i_a, τ^i_a, and $\eta_{\Omega\mathcal{R}}$, $\eta_{\Omega\mathcal{R}\mathbb{Z}^{(i)}_2}$ $i = 1, 2, 3$ chosen according to table 5.1 such that gauge symmetry enhancement is present and symmetric representations are absent.

For the $SU(5)$ model, we have the following three-cycles able to support the a stack:

- On the **bAA** lattice: three-cycles with bulk orbit parallel to $(4, -1; 1, 1; 1, -1)$ or $(4, -1; 1, -1; 1, 1)$ with $\varrho = 4$, $\eta_{\Omega\mathcal{R}} = -1$ and $\sigma^1_a\tau^1_a = \sigma^2_a\tau^2_a = \sigma^3_a\tau^3_a = 0$.
- On the **bAA** lattice: three-cycles with bulk orbit parallel to $(1, 1; 1, 1; 1, -1)$ or $(1, 1; 1, -1; 1, 1)$ with $\varrho = 2/3$, $\eta_{\Omega\mathcal{R}} = -1$ and $\sigma^2_a\tau^2_a = \sigma^3_a\tau^3_a = 1$.
- On the **aAA** lattice: three-cycles with bulk orbit parallel to $(1, 2; 1, 1; 1, -1)$ or $(1, 2; 1, -1; 1, 1)$ with $\varrho = 1/2$, $\eta_{\Omega\mathcal{R}} = -1$ and $\sigma^2_a\tau^2_a = \sigma^3_a\tau^3_a = 1$.

5.4 Towards a three-generation particle spectrum

So far, we determined suitable three-cycles to support the a and b stacks of the MSSM-type models, as well as the a stack of the $SU(5)$ model. This classification is sufficient to initiate the first step in model building, which consists in computing the first bifundamental representations. For all MSSM-type models, the conditions on the intersection numbers between the a and b stacks are the same, namely $|\chi^{ab} + \chi^{ab'}| = 3$ or $|\chi^{ab}| = 3$ if gauge symmetry enhancement is present on the b stack, see section 3.2. Therefore, instead of launching a direct computer scan over all the stacks appearing in the various models, it is more sensible to start with only the a and b stacks and trying to get three generations of particles with these. In a second step, the a and b stacks can be completed with other stacks to give a full three-generation particle spectrum, which depends on the considered model.

Among the possibilities listed at the end of the previous section, we see that there are three-cycles which are SUSY depending on the value of the complex structure modulus ϱ, whereas other three-cycles parallel to some O6-plane are SUSY for all values of ϱ. From now on, we will refer to the three-cycles parallel to some O6-plane in table 2.3 or parallel to the three-cycles in table 4.2 as ϱ-independent three-cycles. All other three-cycles not belonging to this category are referred to as ϱ-dependent three-cycles. Remember from section 4.2 that we have eight bulk three-cycles of the former and 1760 respectively 917 cycles of the latter, depending on the lattice **aAA** or **bAA**.
An interesting question to answer would be whether it is possible to construct an entire model that is independent of ϱ. Thus, we will separate the analysis into two parts including a search for ϱ-independent models and a search for ϱ-dependent models. Consequently, we will split the models into ϱ-independent and ϱ-dependent models.

5.4.1 ϱ-independent configurations

First of all, let us point out that $SU(5)$ models cannot be ϱ-independent models, since we do not have ϱ-independent three-cycles fulfilling the criteria indicated on page 87. Therefore, the analysis in this section focuses solely on MSSM-type models.

The first step consists in determining exactly which three-cycles of those listed on page 87 may be used for the a stack, and which ones for the b stack. The a stack should support a $U(3)$ gauge group in the case of the MSSM and left-right symmetric models, or a $U(4)$ gauge group in the case of the Pati-Salam model. Neither a $U(3)$ stack nor a $U(4)$ group can be realized through a symplectic or an orthogonal group, as (special) unitary groups are isomorphic to symplectic or orthogonal groups only in particular cases: $USp(2) \simeq SU(2)$ and $SO(2) \simeq U(1)$. It follows that the three-cycle candidate for the a stack cannot support enhancement. However, the ϱ-independent cycles parallel to the O6-planes $\Omega\mathcal{R}\mathbb{Z}_2^{(k)}$, $k = 1, 2, 3$ are rigid only if they present gauge symmetry enhancement, c.f. page 77. Consequently, the a stack cannot be realized by a three-cycle parallel to $\Omega\mathcal{R}\mathbb{Z}_2^{(k)}$, $k = 1, 2, 3$. The only candidate left for the a stack is thus the three-cycle parallel to the $\Omega\mathcal{R}$-plane, with the conditions on rigidity $\sigma_a^2\tau_a^2 = \sigma_a^3\tau_a^3$ and further conditions on the discrete parameters such that gauge group enhancement is absent, see table 5.1.

The next step consists in finding a suitable candidate for the b stack. For this stack, $USp(2)$ gauge group enhancement is allowed since it is intended to support a $SU(2)$ group in all three models considered, which is isomorphic to a symplectic $USp(2)$ group. However, $SU(2)$ is not isomorphic to orthogonal groups, so only $USp(2)$ gauge group enhancement is allowed. Contrarily to D6-branes wrapping the O6-planes $\Omega\mathcal{R}\mathbb{Z}_2^{(k)}$, $k = 1, 2, 3$ which must support a $USp(2)$ gauge group due to the conditions on rigidity, D6-branes wrapping the $\Omega\mathcal{R}$-plane can support either a unitary $U(2)$ or a symplectic $USp(2)$ gauge group. The results yielded by the computer scan for taking the $\Omega\mathcal{R}$-plane as the b stack are given in table 5.4.

$(\chi^{ab}, \chi^{ab'})$ **between D6-brane stacks** a **and** b **for** ϱ**-independent configurations on** $T^6/(\mathbb{Z}_2 \times \mathbb{Z}_6 \times \Omega\mathcal{R})$				
	aAA lattice		**bAA lattice**	
$D6_b$ **stack**	$\eta_{\Omega\mathcal{R}} = -1$	$\eta_{\Omega\mathcal{R}\mathbb{Z}_2^{(2,3)}} = -1$	$\eta_{\Omega\mathcal{R}} = -1$	$\eta_{\Omega\mathcal{R}\mathbb{Z}_2^{(2,3)}} = -1$
$U(2)_b$ without adjoints	$(0,0)$	$(0,0), (\pm 2, 0), (0, \pm 2)$	$(0,0)$	$(0,0), (\pm 2, 0), (0, \pm 2)$
$U(2)_b$ with adjoints	$(0,0), (\pm 1, \pm 1)$	$(0,0), (\pm 1, \mp 1)$	$(0,0), (\pm 1, \pm 1)$	$(0,0), (\pm 1, \mp 1)$
enhanced $USp(2)_b$	$(0), (\pm 2)$	$(0), (\pm 1)$	$(0), (\pm 2)$	$(0), (\pm 1)$

Table 5.4: Overview of the net-chiralities $(\chi^{ab}, \chi^{ab'})$ arising at the intersection of three-cycles with bulk orbit parallel to the $\Omega\mathcal{R}$-plane for the two inequivalent lattice configurations **aAA** and **bAA** and the three choices for the exotic O6-plane charge ($\eta_{\Omega\mathcal{R}} = -1$, $\eta_{\Omega\mathcal{R}\mathbb{Z}_2^{(2)}} = -1$ or $\eta_{\Omega\mathcal{R}\mathbb{Z}_2^{(3)}} = -1$). D6-branes parallel to the $\Omega\mathcal{R}$-plane are SUSY for all values of the complex structure parameter ϱ. The D6-brane stack a is completely rigid (without matter states in the adjoint rep.)in all three cases considered, but the condition of rigidity is relaxed for the b stack in the second case. In the third case with $USp(2)_b$ enhancement, we have $\chi^{ab} \equiv \chi^{ab'}$.

From table 5.4, it is clear that the configuration a parallel ($\uparrow\uparrow$) to b parallel to the $\Omega\mathcal{R}$-plane does not give rise to three generations of particles transforming in the bifundamental representation $(\mathbf{N_a}, \mathbf{2_b})$, i.e. $|\chi^{ab} + \chi^{ab'}| \neq 3$ and also $|\chi^{ab}| = |\chi^{ab'}| \neq 3$. Even by relaxing the condition of rigidity on the b stack, it is not possible to realize three generations.
The other possibility is to take the b stack parallel to one of the remaining O6-planes $\Omega\mathcal{R}\mathbb{Z}_2^{(k)}$, $(k = 1, 2, 3)$ and impose $USp(2)$ gauge group enhancement. The results from the computer scan for this configuration are given in table 5.5.

In table 5.5, some choices for the exotic O6-planes have been excluded right away and not been included in the computer scan. In fact, the $\Omega\mathcal{R}\mathbb{Z}_2^{(k)}$-planes, $k = 2, 3$ are characterized by $\tilde{V}_a \neq 0$. It follows from the second RR-tadpole cancellation condition in (2.50) that the $\Omega\mathcal{R}$-plane must be the exotic O6-plane: $\eta_{\Omega\mathcal{R}} = -1$. Moreover, in table 5.1 we see that in case $\eta_{\Omega\mathcal{R}} = -1$, the $\Omega\mathcal{R}\mathbb{Z}_2^{(1)}$-plane cannot support $USp(2)$ gauge group enhancement on the **aAA** lattice whereas on the **bAA** lattice, the $USp(2)$ gauge group enhancement is accompanied by unwanted matter states in the symmetric representation. Note that the same argument holds for the choices $\eta_{\Omega\mathcal{R}\mathbb{Z}_2^{(2 \text{ or } 3)}} = -1$ and $b \uparrow\uparrow \Omega\mathcal{R}\mathbb{Z}_2^{(2,3)}$, which comes on top of the argument with the RR-tadpole cancellation conditions.
From table 5.5, we immediately see that this time, three generations are indeed possible for $b \uparrow\uparrow \Omega\mathcal{R}\mathbb{Z}_2^{(1)}$ and the choice of the exotic charge $\eta_{\Omega\mathcal{R}\mathbb{Z}_2^{(2 \text{ or } 3)}} = -1$, for both lattices **aAA** and **bAA**. The choice $\eta_{\Omega\mathcal{R}\mathbb{Z}_2^{(2 \text{ or } 3)}} = -1$ in the second bulk RR-tadpole cancellation condition implies that all stacks appearing in the models must have $\tilde{V} = V + bQ = 0$. In total, there are four three-cycles fulfilling this condition: the two cycles parallel to the $\Omega\mathcal{R}$- and $\Omega\mathcal{R}\mathbb{Z}_2^{(1)}$-planes and the three-cycles with bulk orbit parallel to $\left(\frac{1}{1-b}, \frac{-b}{1-b}; 2, 1; 3, -1\right)$ or parallel to

$\chi^{ab} = \chi^{ab'}$ **between D6-brane stacks** a **and** b **for** ϱ**-independent configurations on** $T^6/(\mathbb{Z}_2 \times \mathbb{Z}_6 \times \Omega\mathcal{R})$				
	$D6_a$ **stack** $\uparrow\uparrow \Omega\mathcal{R}$ **on aAA lattice**		$D6_a$ **stack** $\uparrow\uparrow \Omega\mathcal{R}$ **on bAA lattice**	
$D6_b$ **stack**	**exotic O6-plane**	χ^{ab}	**exotic O6-plane**	χ^{ab}
$\uparrow\uparrow \Omega\mathcal{R}\mathbb{Z}_2^{(1)} + 5$ **Anti**	$\eta_{\Omega\mathcal{R}\mathbb{Z}_2^{(2,3)}} = -1$	$0, \pm 1, \pm 3$	$\eta_{\Omega\mathcal{R}\mathbb{Z}_2^{(2,3)}} = -1$	$0, \pm 1, \pm 3$
$\uparrow\uparrow \Omega\mathcal{R}\mathbb{Z}_2^{(2)} + 2$ **Anti**	$\eta_{\Omega\mathcal{R}} = -1$	$\pm 1, \pm 2$	$\eta_{\Omega\mathcal{R}} = -1$	$\pm 2, \pm 4$
$\uparrow\uparrow \Omega\mathcal{R}\mathbb{Z}_2^{(3)} + 2$ **Anti**	$\eta_{\Omega\mathcal{R}} = -1$	$\pm 1, \pm 2$	$\eta_{\Omega\mathcal{R}} = -1$	$\pm 2, \pm 4$

Table 5.5: Summary of the net-chirality $\chi^{ab} = \chi^{ab'}$ between a completely rigid D6-brane stack a (without matter states in the adjoint rep.) and a completely rigid D6-brane stack b. The b stack supports an enhanced $USp(2)$ gauge group and is accompanied by massless states in the antisymmetric representation as indicated in the left column. The a stack has its bulk orbit parallel to the $\Omega\mathcal{R}$-plane, while the bulk orbit of the b stack is parallel to one of the other three O6-planes $\Omega\mathcal{R}\mathbb{Z}_2^{(i=1,2,3)}$. The configuration with the b stack parallel to the $\Omega\mathcal{R}$-plane has already been presented in table 5.4. The second and fourth column give the choice of the exotic O6-plane, while the third and fifth column list the net-chiralities $\chi^{ab} = \chi^{ab'}$ for the considered D6-brane configuration per lattice type.

$\left(\frac{1}{1-b}, \frac{-b}{1-b}; 4, -1; 3, 1\right)$, see table 4.2.
For $a \uparrow\uparrow \Omega\mathcal{R}$ and for $b \uparrow\uparrow \Omega\mathcal{R}\mathbb{Z}_2^{(1)}$ supporting an $USp(2)$ group, with $\eta_{\Omega\mathcal{R}\mathbb{Z}_2^{(2,3)}} = -1$, we can calculate the contribution from these two stacks to the first bulk RR-tadpole cancellation condition in (2.50):

$$\sum_{x \in \{a,b\}} N_x(2P_x + Q_x) = N_a \frac{2}{1-b} + N_b \frac{6}{1-b} = N_a \frac{2}{1-b} + \frac{6}{1-b} \overset{!}{\leq} 32\,. \tag{5.17}$$

For the **bAA** lattice, we have $b = 1/2$, so the condition is $N_a \overset{!}{\leq} 5$. Therefore, even for the Pati-Salam model which comes with the biggest rank $N_a = 4$, the bulk RR-tadpole cancellation conditions are not overshot. In case of the **aAA** lattice with $b = 0$, the condition is $N_a \frac{2}{1-b} \overset{!}{\leq} 13$, so we have even more room left to add the remaining visible stacks and also hidden stacks.

5.4.2 ϱ-dependent configurations

In this section, we will turn our attention to ϱ-dependent models. An important feature of ϱ-dependent models is the fact that they always have $\eta_{\Omega\mathcal{R}} = -1$. All ϱ-dependent bulk three-cycles have $\tilde{V} \neq 0$. The second bulk RR-tadpole cancellation condition thus implies $\eta_{\Omega\mathcal{R}} = -1$, otherwise global models cannot be constructed.
Both MSSM-type and $SU(5)$ models can arise in the case of ϱ-dependent configurations. We will start the analysis with the MSSM-type models.

MSSM-type models

At this stage, a ϱ-dependent model arises when a ϱ-dependent three-cycle sits on the a stack, the b stack, or on both a and b stacks. In the later case, the bulk three-cycle must be the same for the a and the b stack. Indeed, for a ϱ-dependent model we have a fixed value for the complex structure parameter ϱ. Since there is only one rigid ϱ-dependent bulk three-cycle

for a given value of ϱ (see section 5.2.1), both a and b stacks must wrap that same rigid bulk three-cycle. In the following, we will analyze each of the three cases.

a is ϱ-independent and b is ϱ-dependent. Let us start with the case of the a stack harbored by a ϱ-independent three-cycle and the b stack wrapping a ϱ-dependent three-cycle. For the same reasons as those given in the previous section, the a stack must be parallel to the $\Omega\mathcal{R}$-plane and must not support gauge group enhancement. The b stack can wrap any of the three-cycles appearing in table 5.2. Indeed, remember that we have no conditions on the matter states transforming in the antisymmetric representation for the b stack, since the b stack always supports an $U(2)$ or $USp(2)$ group, whose antisymmetric representation is equivalent to a $SU(2)$ singlet. The results of the computer scan for obtaining three generations $|\chi^{ab}+\chi^{ab'}|=3$ of the bifundamental representation $(\mathbf{N_a},\mathbf{2_b})$ are listed in table 5.6. All of the combinations listed in table 5.6 give a net chirality $|\chi^{ab}+\chi^{ab'}|=3$, although

Bulk $D6_b$ orbits for three generations $\chi^{ab}+\chi^{ab'}=\pm3$ with $a\uparrow\uparrow\Omega\mathcal{R}$ on $T^6/(\mathbb{Z}_2\times\mathbb{Z}_6\times\Omega\mathcal{R})$ with $\eta=-1$							
aAA lattice				**bAA lattice**			
$D6_b$ orbit	**ϱ**	**$(\chi^{ab},\chi^{ab'})$**	**Occurrence frequency**	**$D6_b$ orbit**	**ϱ**	**$(\chi^{ab},\chi^{ab'})$**	**Occurrence frequency**
$(1,1;1,0;1,-1)$	3	$(1,2)$	64 out of 16×160 combinations	$(1,0;1,0;1,-1)$	6	$(1,2)$	48 out of 48×160 combinations
		$(-2,-1)$	64 out of 16×160 combinations			$(-2,-1)$	48 out of 48×160 combinations
$(1,3;1,0;1,-1)$	1	$(0,3)$	64 out of 16×16 combinations	$(1,1;1,0;1,-1)$	2	$(0,3)$	48 out of 48×16 combinations
		$(-3,0)$	64 out of 16×16 combinations			$(-3,0)$	48 out of 48×16 combinations
$(1,5;1,0;1,-1)$	3/5	$(-1,4)$	64 out of 16×16 combinations	$(1,2;1,0;1,-1)$	6/5	$(-1,4)$	48 out of 48×16 combinations
		$(-4,1)$	64 out of 16×16 combinations			$(-4,1)$	48 out of 48×16 combinations
$(1,7;1,0;1,-1)$	3/7	$(-2,5)$	64 out of 16×16 combinations	$(1,3;1,0;1,-1)$	6/7	$(-2,5)$	48 out of 48×16 combinations
		$(-5,2)$	64 out of 16×16 combinations			$(-5,2)$	48 out of 48×16 combinations
$(1,9;1,0;1,-1)$	1/3	$(-3,6)$	64 out of 16×16 combinations	$(1,4;1,0;1,-1)$	2/3	$(-3,6)$	48 out of 48×16 combinations
		$(-6,3)$	64 out of 16×16 combinations			$(-6,3)$	48 out of 48×16 combinations
$(1,11;1,0;1,-1)$	3/11	$(-4,7)$	64 out of 16×16 combinations	$(1,5;1,0;1,-1)$	6/11	$(-4,7)$	48 out of 48×16 combinations
		$(-7,4)$	64 out of 16×16 combinations			$(-7,4)$	48 out of 48×16 combinations
$(1,13;1,0;1,-1)$	3/13	$(-5,8)$	64 out of 16×16 combinations	$(1,6;1,0;1,-1)$	6/13	$(-5,8)$	48 out of 48×16 combinations
		$(-8,5)$	64 out of 16×16 combinations			$(-8,5)$	48 out of 48×16 combinations
$(1,15;1,0;1,-1)$	1/5	$(-6,9)$	64 out of 16×16 combinations	$(1,7;1,0;1,-1)$	2/5	$(-6,9)$	48 out of 48×16 combinations
		$(-9,6)$	64 out of 16×16 combinations			$(-9,6)$	48 out of 48×16 combinations

Table 5.6: Complete list of candidate bulk three-cycles for the b stack yielding three generations of states in the bifundamental representation $(\mathbf{N_a},\mathbf{2_b})$ with the a stack having its bulk orbit parallel to the $\Omega\mathcal{R}$-plane and exotic O6-plane charge $\eta_{\Omega\mathcal{R}}=-1$. The discrete parameters are chosen such that both the a stack and the b stack are wrapped by D6-branes fulfilling the criteria on rigidity and on the matter states transforming in the (anti)symmetric representations. The second and sixth column list the values of the complex structure modulus ϱ, which is fixed by the requirement of a SUSY b stack. The third and seventh column give details about the realization of the three generations by the net-chiralities $(\chi^{ab},\chi^{ab'})$, and the fourth and eight column indicate how many combinations of discrete parameters give rise to the net-chiralities under consideration.

not all of them satisfy $|\chi^{ab}|\leq3$ and $|\chi^{ab'}|\leq3$. The non-fulfillment of these last conditions implies the existence of non-chiral pairs of matter states transforming in the bifundamental representation. Only the combinations with $(1,m_b^1)\in\{(1,1),(1,3)\}$ for the **aAA** lattice and $(1,m_b^1)\in\{(1,0),(1,1)\}$ for the **bAA** lattice are a priori free of non-chiral matter states in the bifundamental representation. However, non-chiral states can still arise within a same sector χ^{ab} or $\chi^{ab'}$, which will be verified via the beta-function coefficient at the end of the

analysis.

a is ϱ-dependent and b is ϱ-independent. The next case to consider consists in taking a ϱ-dependent three-cycle for the a stack and a ϱ-independent three-cycle for the b stack. Let us first discuss the possibilities for the b stack. The b stack can a priori be realized by a three-cycle parallel to the $\Omega\mathcal{R}$-plane, with or without gauge group enhancement, or by a three-cycle parallel to some other $\Omega\mathcal{R}\mathbb{Z}_2^{(l)}$-plane $l = 1, 2, 3$ with $USp(2)$ enhancement. One possibility can be excluded right away: ϱ-dependent models always have $\eta_{\Omega\mathcal{R}} = -1$, which excludes the possibility $b \uparrow\uparrow \Omega\mathcal{R}\mathbb{Z}_2^{(1)}$. As argued in the previous section, choosing $\eta_{\Omega\mathcal{R}} = -1$ forces the $\Omega\mathcal{R}\mathbb{Z}_2^{(1)}$-plane to be accompanied by matter states transforming in the symmetric representation in the case of $USp(2)$ enhancement. Therefore, this possibility is excluded right from the beginning.
Now let us discuss the different possibilities of a ϱ-dependent a stack. On the contrary to the b stack, we have constraints on the multiplicity of the antisymmetric representation of the a stack. The weakest constraints come from the MSSM model, where antisymmetric states can account for the right-handed quarks, which imposes $|\chi^{\mathbf{Anti}_a}| \in \{0, 1, 2, 3\}$. Hence, the possible candidates for realizing the a stack can be found in table 5.3.
In order to obtain three generations of the chiral bifundamental representation $(\mathbf{N_a}, \mathbf{2_b})$, the condition $|\chi^{ab} + \chi^{ab'}| = 3$ has to be satisfied in the absence of gauge group enhancement on the b stack, whereas we impose $\chi^{ab} = \chi^{ab'} \stackrel{!}{=} \pm 3$ in presence of gauge group enhancement on the b stack. Another important condition is to preserve compatibility between the chirality of the left-handed and right-handed quarks, which manifests itself as an identical sign between the net-chiralities of particle states in the antisymmetric representation and the bifundamental representation: $\mathrm{sgn}(\chi^{\mathbf{Anti}_a}) = +\mathrm{sgn}(\chi^{ab} + \chi^{ab'})$. In the special case where no states in the antisymmetric representation are present on the a stack, which happens for $a \uparrow\uparrow (1, 3; 1, 0; 1, -1)$ on the **aAA** lattice and $a \uparrow\uparrow (1, 1; 1, 0; 1, -1)$ on the **bAA** lattice (see table 5.3), both sign possibilities for $\chi^{ab} + \chi^{ab'}$ are allowed.

a is ϱ-dependent and b is ϱ-dependent. The last case to consider is having the a stack and the b stack lying on the same ϱ-dependent bulk three-cycle. For the a stack, we have the same conditions on the antisymmetric spectrum as in the previous case, so potential candidates should be taken from table 5.3. Also, the discussion in the previous case about the relative sign between the net-chiralities of particle states in the antisymmetric representation $\chi^{\mathbf{Anti}_a}$ and the bifundamental representation $\chi^{ab} + \chi^{ab'}$ holds true in the present case. Note that in the case of a and b wrapping the same bulk three-cycle, one has to impose that at least one discrete parameter ($\tau^{\mathbb{Z}_2^{(i)}}$, τ^i, σ^i, $i = 1, 2, 3$) of the fractional three-cycles is different, in order to ensure that the three-cycles differ for the a stack and the b stack. Otherwise, only one stack with bigger rank instead of two stacks with smaller ranks would be realized.

The results of the computer scans for the last two cases are listed in table 5.7. A notable absence is given by configurations where the a stack sits on some ϱ-dependent three-cycle and the b stack is parallel to the $\Omega\mathcal{R}\mathbb{Z}_2^{(2)}$- or the $\Omega\mathcal{R}\mathbb{Z}_2^{(3)}$-plane. Indeed, these configurations did not give rise to three generations of chiral states in the bifundamental representation $(\mathbf{N_a}, \mathbf{2_b})$.

	Bulk orbits for three generations $\chi^{ab}+\chi^{ab'}=\pm 3$ on $T^6/(\mathbb{Z}_2\times\mathbb{Z}_6\times\Omega\mathcal{R})$ with $\eta=-1$				
	$D6_a$**-orbit**	$D6_b$**-orbit**	ϱ	$(\chi^{ab},\chi^{ab'})$	**Occurrence Frequency**
aAA	$(1,1;1,0;1,-1)$	$(1,1;1,0;1,-1)$	3	$(0,3)$	864 out of 160×160 combinations
	$(1,3;1,0;1,-1)$	$\uparrow\uparrow\,\Omega\mathcal{R}:(1,0;1,0;1,0)$	1	$(3,0)$	64 out of 16×16 combinations
				$(0,3)$	64 out of 16×16 combinations
	$(1,3;1,0;1,-1)$	$(1,3;1,0;1,-1)$	1	$(0,-3)$	96 out of 16×16 combinations
	$(1,4;1,0;1,-1)$	$\uparrow\uparrow\,\Omega\mathcal{R}:(1,0;1,0;1,0)$	3/4	(-3)	144 out of 16×144 combinations
	$(1,5;1,0;1,-1)$	$\uparrow\uparrow\,\Omega\mathcal{R}:(1,0;1,0;1,0)$	3/5	(-3)	576 out of 16×144 combinations
	$(1,6;1,0;1,-1)$	$\uparrow\uparrow\,\Omega\mathcal{R}:(1,0;1,0;1,0)$	1/2	(-3)	864 out of 16×144 combinations
bAA	$(1,0;1,0;1,-1)$	$(1,0;1,0;1,-1)$	6	$(2,1)$	144 out of 160×160 combinations
	$(1,1;1,0;1,-1)$	$\uparrow\uparrow\,\Omega\mathcal{R}:(2,-1;1,0;1,0)$	2	$(3,0)$	48 out of 16×48 combinations
				$(0,3)$	48 out of 16×48 combinations
				$(-2,-1)$	144 out of 16×48 combinations
				$(-1,-2)$	144 out of 16×48 combinations
	$(1,1;1,0;1,-1)$	$(1,1;1,0;1,-1)$	2	$(0,3)$	128 out of 16×16 combinations
				$(0,-3)$	64 out of 16×16 combinations
	$(1,2;1,0;1,-1)$	$\uparrow\uparrow\,\Omega\mathcal{R}:(2,-1;1,0;1,0)$	6/5	(-3)	432 out of 16×108 combinations
	$(1,3;1,0;1,-1)$	$\uparrow\uparrow\,\Omega\mathcal{R}:(2,-1;1,0;1,0)$	6/7	(-3)	432 out of 16×108 combinations
	$(1,4;1,0;1,-1)$	$(1,4;1,0;1,-1)$	2/3	$(0,-3)$	48 out of 16×48 combinations

Table 5.7: Overview of pairs of bulk orbits of fractional three-cycles allowing for three generations of states in the bifundamental representation $(\mathbf{N_a},\mathbf{2_b})$ with exotic O6-plane charge $\eta_{\Omega\mathcal{R}}=-1$. The discrete parameters are chosen such that both the a stack and the b stack are wrapped by D6-branes fulfilling the criteria on rigidity and on the matter states transforming in the (anti)symmetric representation.The fourth column gives details about the realization of the three generations by the net-chiralities $(\chi^{ab},\chi^{ab'})$, and the fifth column indicates how many combinations of discrete parameters give rise to the net-chiralities under consideration. The net-chirality reads $\chi^{ab}=\chi^{ab'}=-3$ for configurations where the b stack supports a $USp(2)$ gauge group.

This concludes the analysis of the a and b stacks for the MSSM-type models. A summary might be appropriate at this stage to clarify the results found so far. The situation is illustrated in the box diagram of figure 5.1 which should serve as a road map. Next, we will turn our attention to $SU(5)$ GUT models.

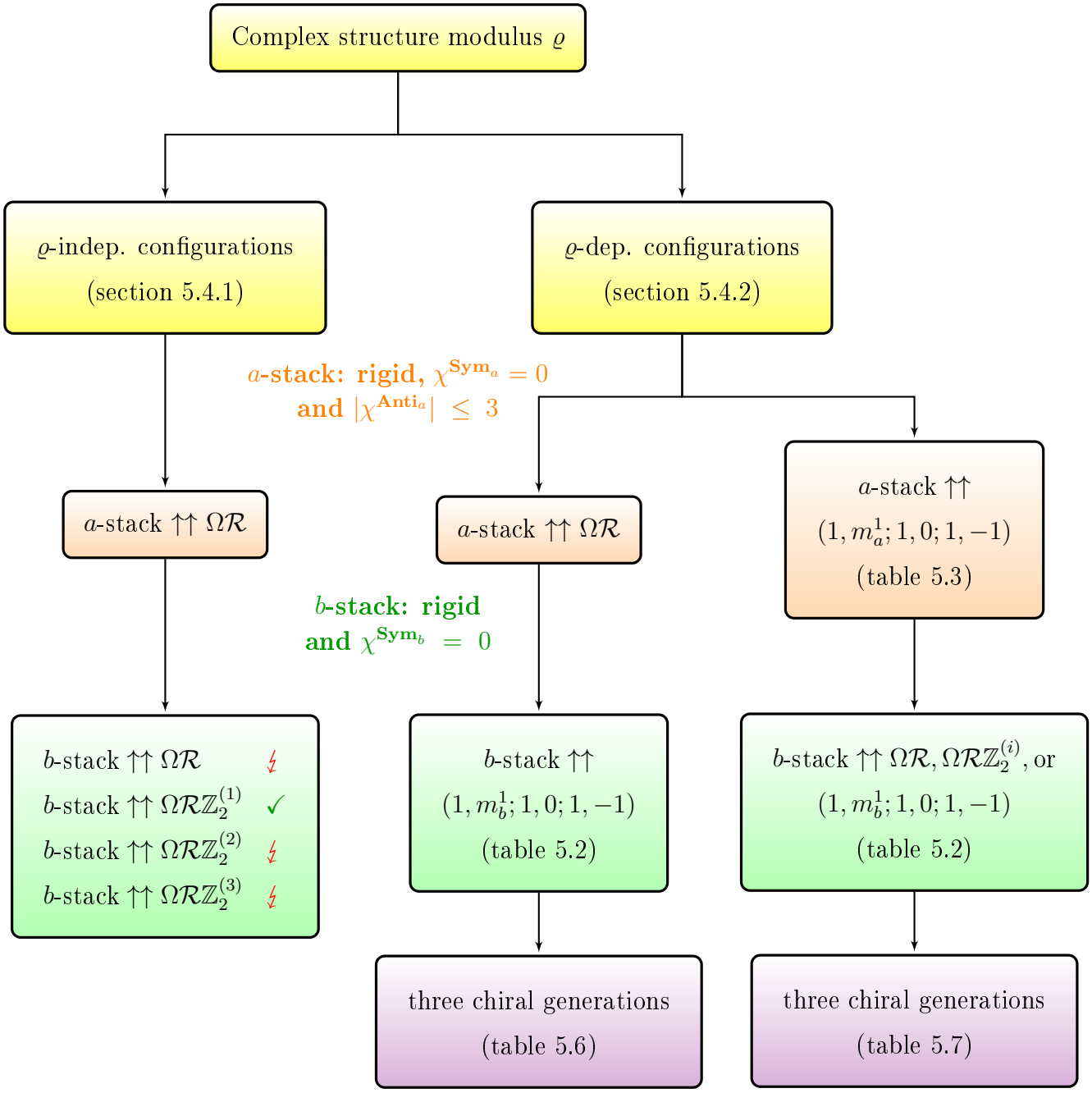

Figure 5.1: Box diagram illustrating the search for MSSM-type models coming with three generations of chiral states in the bifundamental representation $(\mathbf{N_a}, \mathbf{2_b})$, for both lattice types **aAA** and **bAA**, as presented in sections 5.4.1 and 5.4.2. The symbols ✓ and ↯ indicate whether three chiral generations of states in the bifundamental representation $(\mathbf{N_a}, \mathbf{2_b})$ can be realized or not for the respective D6-brane configurations.

$SU(5)$ models

The antisymmetric representation under $SU(5)$ corresponds to the ten-dimensional representation **10**, which encompasses quarks and leptons, see section 3.2.4. Since we have three generations of these, the multiplicity of matter states in the antisymmetric representation is three. On the other hand, part of the quarks and leptons are embedded in the antifundamental five dimensional representation $\overline{\mathbf{5}}$ of $SU(5)$, which should also occur in copies of three. In our string theoretical set-up, this representation can only be realized as a bifundamental representation $(\overline{\mathbf{5}}, \mathbf{1})$ arising at the intersection of the a stack with some b stack. For $SU(5)$ models, the chirality between particles in the ten-dimensional representation **10** and the antifundamental five-dimensional representation $\overline{\mathbf{5}}$ should be reflected in an opposite sign between the net-chiralities, i.e. $\mathrm{sgn}(\chi^{\mathbf{Anti}_a}) = -\mathrm{sgn}(\chi^{ab})$.

The potential candidate three-cycles for housing the a stack supporting the $U(5)$ gauge group have been listed on page 87. The first candidates can be found in the **bAA** lattice and have bulk orbits parallel to $(4,-1;1,-1;1,1)$ or $(4,-1;1,1;1,-1)$, which give positive net-chirality for the matter states in the antisymmetric representation, $\chi^{\mathbf{Anti}_a} = 3$. The net-chirality of matter states in the bifundamental representation should therefore come with a negative sign. The complex structure modulus is fixed to $\varrho = 4$ by these three-cycles. In table 4.3, we see that we have nine ϱ-dependent three-cycles SUSY for $\varrho = 4$. Adding the eight ϱ-independent three-cycles, we have a total of 17 bulk three-cycles apt to house the b stack. A full computer scan over all fractional three-cycles arising from the 17 bulk three-cycles showed that only four bulk orbits used for the b stack satisfy the condition $\chi^{ab} + \chi^{ab'} = -3$ respectively $\chi^{ab} = \chi^{ab'} = -3$ if gauge symmetry enhancement on the b stack is present. The results are listed in table 5.8. The last column gives the number of fractional three-cycles for the a and b stacks giving rise to three generations of matter states transforming in the bifundamental representation $\overline{\mathbf{5}}$ with the correct chirality as indicated in the third column. Note that a priori, each bulk three-cycle could give rise to 256 fractional cycles. However, on the a stack we already have the constraints $\sigma_a^1\tau_a^1 = \sigma_a^2\tau_a^2 = \sigma_a^3\tau_a^3 = 0$ due to the constraint on the multiplicity of matter states in the antisymmetric representation of $SU(5)$, as pointed out on page 87. This leaves $3 \cdot 3 \cdot 3 = 27$ possibilities for the discrete Wilson lines and shifts. We have $2 \cdot 2 = 4$ choices for the two independent $\mathbb{Z}_2$-eigenvalues, which gives in total $4 \cdot 27 = 108$ a priori choices for the fractional three-cycle wrapped by the a stack. For the b stack, we count separately the combinations of discrete parameters giving rise to gauge symmetry enhancement (e.g. 108 combinations for $b \uparrow\uparrow \Omega\mathcal{R}$) or not (e.g. 144 combinations for $b \uparrow\uparrow \Omega\mathcal{R}$). Only a fraction of these combinations lead to three generations of matter states in the bifundamental representation $(\overline{\mathbf{5}}, \mathbf{1})$. Note that the possibility of SO enhancement on the b stack is completely absent, as the computer scan revealed.

The next possibility is given by the choice of negative net-chirality for the matter states in the antisymmetric representation, i.e. $\chi^{\mathbf{Anti}_a} = -3$. Contrarily to the previous case, we now have results for both the **aAA** and **bAA** lattices. In the **aAA** lattice, the three-cycles suitable to support the $U(5)$ group have bulk orbits parallel to $(1,2;1,-1;1,1)$ or parallel to $(1,2;1,1;1,-1)$. These three-cycles are SUSY for $\varrho = 1/2$. There are in total 15 ϱ-dependent bulk three-cycles which are SUSY for this value of the complex structure parameter. Once again, adding the eight ϱ-independent bulk three-cycles gives a total of 23 bulk three-cycles apt to assume the rôle of the b stack. A computer scan on all of these three-cycles leads to

Three generation $U(5)$ GUT models on $T^6/(\mathbb{Z}_2 \times \mathbb{Z}_6 \times \Omega\mathcal{R})$ with $\eta = -1$ (part I)			
$U(5)_a$**-orbit**	$D6_b$**-orbit**	$(\chi^{ab}, \chi^{ab'})$	**Occurrence Frequency**
$(4,-1;1,-1;1,1)$	$\uparrow\uparrow \Omega\mathcal{R} : (2,-1;1,0;1,0)$	$(-2,-1)$	3888 out of 108×144 combinations
		$(-1,-2)$	3888 out of 108×144 combinations
	with USp enhancement	(-3)	1728 out of 108×108 combinations
	$\uparrow\uparrow \Omega\mathcal{R}\mathbb{Z}_2^{(1)} : (2,-1;-1,2;1,-2)$	(-3)	864 out of 108×36 combinations
	with USp enhancement		
	$(4,-1;1,-1;1,1)$	$(0,-3)$	432 out of 108×256 combinations
	$(4,-1;1,1;1,-1)$	$(0,-3)$	432 out of 108×256 combinations
$(4,-1;1,1;1,-1)$	$\uparrow\uparrow \Omega\mathcal{R} : (2,-1;1,0;1,0)$	$(-2,-1)$	3888 out of 108×144 combinations
		$(-1,-2)$	3888 out of 108×144 combinations
	with USp enhancement	(-3)	1728 out of 108×108 combinations
	$\uparrow\uparrow \Omega\mathcal{R}\mathbb{Z}_2^{(1)} : (2,-1;-1,2;1,-2)$	(-3)	864 out of 108×36 combinations
	with USp enhancement		
	$(4,-1;1,-1;1,1)$	$(0,-3)$	432 out of 108×256 combinations
	$(4,-1;1,1;1,-1)$	$(0,-3)$	432 out of 108×256 combinations

Table 5.8: Overview of pairs of bulk orbits of fractional three-cycles allowing for three generations of matter states in the antifundamental representation ($\chi^{ab} + \chi^{ab'} = -\chi^{\mathbf{Anti}_a} = -3$) of $U(5)_a$ on the **bAA** lattice with exotic O6-plane charge $\eta_{\Omega\mathcal{R}} = -1$ and complex structure parameter $\varrho = 4$. The discrete parameters are chosen such that the a stack is wrapped by D6-branes fulfilling the criteria on rigidity and on the matter states transforming in the (anti)symmetric representations. The third column gives details about the realization of the three generations by the net-chiralities $(\chi^{ab}, \chi^{ab'})$, and the fourth column indicates how many combinations of discrete parameters give rise to the net-chiralities under consideration. The net-chirality reads $\chi^{ab} = \chi^{ab'} = -3$ for configurations where the b stack supports a $USp(2)$ gauge group.

the configurations given in table 5.9. The net-chirality of matter states in the bifundamental representation must now be of positive sign, i.e. $\chi^{ab} + \chi^{ab'} = +3$ respectively $\chi^{ab} = \chi^{ab'} = +3$ in case of gauge symmetry enhancement on the b stack.

In the **bAA** lattice, three-cycles adequate to accommodate the a stack have bulk orbits parallel to $(1,1;1,-1;1,1)$ or parallel to $(1,1;1,1;1,-1)$. These three-cycles are SUSY for $\varrho = 2/3$. This value for ϱ comes with seven ϱ-dependent bulk three-cycles, plus the eight ϱ-independent bulk three-cycles, giving a total of 15 bulk three-cycles to test as possible candidates for the b stack. A computer scan on all of these candidates produced the configurations of table 5.10, which lead to a full three-generation particle spectrum for the $SU(5)$ model.

Three generation $U(5)$ GUT models on $T^6/(\mathbb{Z}_2 \times \mathbb{Z}_6 \times \Omega\mathcal{R})$ with $\eta = -1$ (part II)			
$U(5)_a$**-orbit**	$D6_b$**-orbit**	$(\chi^{ab}, \chi^{ab'})$	**Occurrence Frequency**
$(1,2;1,-1;1,1)$	$\uparrow\uparrow\ \Omega\mathcal{R}\mathbb{Z}_2^{(2)} : (0,1;1,0;1,-2)$	$(3,0)$	192 out of 16×208 combinations
		$(0,3)$	192 out of 16×208 combinations
	$\uparrow\uparrow\ \Omega\mathcal{R}\mathbb{Z}_2^{(3)} : (0,1;1,-2;1,0)$	$(3,0)$	256 out of 16×208 combinations
		$(2,1)$	576 out of 16×208 combinations
		$(1,2)$	576 out of 16×208 combinations
		$(0,3)$	256 out of 16×208 combinations
	with USp enhancement	(3)	192 out of 16×48 combinations
	$(1,2;1,-1;1,1)$	$(3,0)$	48 out of 16×256 combinations
		$(4,-1)$	144 out of 16×256 combinations
	$(1,2;1,1;1,-1)$	$(3,0)$	96 out of 16×256 combinations
	$(1,3;2,1;1,-1)$	$(3,0)$	64 out of 16×256 combinations
	$(1,6;1,0;1,-1)$	$(3,0)$	48 out of 16×256 combinations
	$(0,1;4,-5;3,-1)$	$(3,0)$	64 out of 16×256 combinations
	$(0,1;2,-3;5,-1)$	$(-3,6)$	64 out of 16×256 combinations
$(1,2;1,1;1,-1)$	$\uparrow\uparrow\ \Omega\mathcal{R}\mathbb{Z}_2^{(2)} : (0,1;1,0;1,-2)$	$(3,0)$	256 out of 16×208 combinations
		$(2,1)$	576 out of 16×208 combinations
		$(1,2)$	576 out of 16×208 combinations
		$(0,3)$	256 out of 16×208 combinations
	with USp enhancement	(3)	192 out of 16×48 combinations
	$\uparrow\uparrow\ \Omega\mathcal{R}\mathbb{Z}_2^{(3)} : (0,1;1,-2;1,0)$	$(3,0)$	192 out of 16×208 combinations
		$(0,3)$	192 out of 16×208 combinations
	$(1,2;1,1;1,-1)$	$(3,0)$	48 out of 16×256 combinations
		$(4,-1)$	144 out of 16×256 combinations
	$(1,2;1,-1;1,1)$	$(3,0)$	96 out of 16×256 combinations
	$(1,3;0,1;1,-3)$	$(3,0)$	64 out of 16×256 combinations
	$(1,6;1,0;1,-1)$	$(3,0)$	48 out of 16×256 combinations
	$(0,1;4,-5;3,-1)$	$(-3,6)$	64 out of 16×256 combinations
	$(0,1;2,-3;5,-1)$	$(3,0)$	64 out of 16×256 combinations

Table 5.9: Overview of pairs of bulk orbits of fractional three-cycles allowing for three generations of matter states in the antifundamental representation ($\chi^{ab} + \chi^{ab'} = -\chi^{\mathbf{Anti}_a} = +3$) of $U(5)_a$ on the **aAA** lattice with exotic O6-plane charge $\eta_{\Omega\mathcal{R}} = -1$ and complex structure parameter $\varrho = \frac{1}{2}$. The discrete parameters are chosen such that the a stack is wrapped by D6-branes fulfilling the criteria on rigidity and on the matter states transforming in the (anti)symmetric representation. The third column gives details about the realization of the three generations by the net-chiralities $(\chi^{ab}, \chi^{ab'})$, and the fourth column indicates how many combinations of discrete parameters give rise to the net-chiralities under consideration. The net-chirality reads $\chi^{ab} = \chi^{ab'} = -3$ for configurations where the b stack supports a $USp(2)$ gauge group.

Three generation $U(5)$ GUT models on $T^6/(\mathbb{Z}_2 \times \mathbb{Z}_6 \times \Omega\mathcal{R})$ with $\eta = -1$ (part III)							
$U(5)_a$-orbit	$D6_b$-orbit	$(\chi^{ab}, \chi^{ab'})$	Occurrence Frequency	$U(5)_a$-orbit	$D6_b$-orbit	$(\chi^{ab}, \chi^{ab'})$	Occurrence Frequency
$(1,1;1,-1;1,1)$	$\uparrow\uparrow\, \Omega\mathcal{R}\mathbb{Z}_2^{(2)} : (0,1;1,0;1,-2)$	$(3,0)$	160 out of 16×208 combinations	$(1,1;1,1;1,-1)$	$\uparrow\uparrow\, \Omega\mathcal{R}\mathbb{Z}_2^{(2)} : (0,1;1,0;1,-2)$	$(3,0)$	256 out of 16×208 combinations
		$(2,1)$	144 out of 16×208 combinations			$(2,1)$	576 out of 16×208 combinations
		$(1,2)$	144 out of 16×208 combinations			$(1,2)$	576 out of 16×208 combinations
		$(0,3)$	160 out of 16×208 combinations			$(0,3)$	256 out of 16×208 combinations
		$(4,-1)$	48 out of 16×208 combinations		with USp enhancement	(3)	144 out of 16×36 combinations
		$(-1,4)$	48 out of 16×208 combinations		with SO enhancement	(3)	48 out of 16×12 combinations
	with SO enhancement	(3)	48 out of 16×12 combinations				
	$\uparrow\uparrow\, \Omega\mathcal{R}\mathbb{Z}_2^{(3)} : (0,1;1,-2;1,0)$	$(3,0)$	256 out of 16×208 combinations		$\uparrow\uparrow\, \Omega\mathcal{R}\mathbb{Z}_2^{(3)} : (0,1;1,-2;1,0)$	$(3,0)$	160 out of 16×208 combinations
		$(2,1)$	576 out of 16×208 combinations			$(2,1)$	144 out of 16×208 combinations
		$(1,2)$	576 out of 16×208 combinations			$(1,2)$	144 out of 16×208 combinations
		$(0,3)$	256 out of 16×208 combinations			$(0,3)$	160 out of 16×208 combinations
	with USp enhancement	(3)	144 out of 16×36 combinations			$(4,-1)$	48 out of 16×208 combinations
	with SO enhancement	(3)	48 out of 16×12 combinations			$(-1,4)$	48 out of 16×208 combinations
					with SO enhancement	(3)	48 out of 16×12 combinations
	$(1,1;1,1;1,-1)$	$(3,0)$	96 out of 16×256 combinations		$(1,1;1,-1;1,1)$	$(3,0)$	96 out of 16×256 combinations
	$(1,1;1,-1;1,1)$	$(3,0)$	48 out of 16×256 combinations		$(1,1;1,1;1,-1)$	$(3,0)$	48 out of 16×256 combinations
		$(1,2)$	48 out of 16×256 combinations			$(1,2)$	48 out of 16×256 combinations
		$(0,3)$	64 out of 16×256 combinations			$(0,3)$	64 out of 16×256 combinations
		$(4,-1)$	144 out of 16×256 combinations			$(4,-1)$	144 out of 16×256 combinations
	$(1,4;1,0;1,-1)$	$(1,2)$	48 out of 16×256 combinations		$(1,4;1,0;1,-1)$	$(1,2)$	48 out of 16×256 combinations
		$(3,0)$	192 out of 16×256 combinations			$(3,0)$	192 out of 16×256 combinations
	$(0,1;2,-3;5,-1)$	$(-3,6)$	64 out of 16×256 combinations		$(0,1;4,-5;3,-1)$	$(-3,6)$	64 out of 16×256 combinations
	$(0,1;4,-5;3,-1)$	$(3,0)$	48 out of 16×256 combinations		$(0,1;2,-3;5,-1)$	$(3,0)$	48 out of 16×256 combinations
		$(0,3)$	16 out of 16×256 combinations			$(0,3)$	16 out of 16×256 combinations

Table 5.10: Overview of pairs of bulk orbits of fractional three-cycles allowing for three generations of matter states in the antifundamental representation ($\chi^{ab} + \chi^{ab'} = -\chi^{\mathbf{Anti}_a} = +3$) of $U(5)_a$ on the **bAA** lattice with exotic O6-plane charge $\eta_{\Omega\mathcal{R}} = -1$ and complex structure parameter $\varrho = \frac{2}{3}$. The discrete parameters are chosen such that the a stack is wrapped by D6-branes fulfilling the criteria on rigidity and on the matter states transforming in the (anti)symmetric representation. The third and seventh column give details about the realization of the three generations by the net-chiralities $(\chi^{ab}, \chi^{ab'})$, while the fourth and eight column indicate how many combinations of discrete parameters give rise to the net-chiralities under consideration. The net-chirality reads $\chi^{ab} = \chi^{ab'} = -3$ for configurations where the b stack supports a $USp(2)$ or $SO(2)$ gauge group.

Chapter 6

The construction of $SU(5)$ and Pati-Salam models

In Type IIA string theory, the aim of model building consists in finding SUSY versions of famous particle physics models. In the previous chapter, we identified D6-branes apt to house the a and b stacks of MSSM-type models, which included the MSSM itself, left-right symmetric and Pati-Salam models. On the other hand, we procured the D6-branes suited to harbor the a and b stacks of the $SU(5)$ model. However, apart from the $SU(5)$ model, all other particle physics models need more than two stacks to support their gauge group. Thus, the next step is to add additional stacks in order to provide a global completion of the particle physics models under consideration. The aim is to construct models which satisfy all consistency conditions given by the bulk and twisted RR-tadpole cancellation conditions as well as the K-theory constraints.
In order to avoid overloading the subject, we split it into two parts, to improve the readability. This chapter 6 focuses on $SU(5)$ models and Pati-Salam models as we derived them in our publication [63]. In the next chapter 7, we concentrate on left-right symmetric and MSSM-like models as we presented them in our publication [64].

6.1 Construction of local $SU(5)$ models

The $SU(5)$ model provides nice explanations for certain phenomena, such as electric charge quantization [51] for example, which the Standard Model fails to explain. However, previous work on similar toroidal backgrounds revealed that globally consistent $SU(5)$ models are the hardest to construct in the set-up of intersecting D6-branes of Type IIA string theory. To my present knowledge, only locally consistent $SU(5)$ models have been constructed so far [95, 130, 182, 69, 76].
In the previous chapter we identified adequate D6-branes to support the a and b stacks of the $SU(5)$ model. Since the $SU(5)$ model has a gauge group consisting of only one gauge factor, no further visible stacks are needed to complete the model. It remains to check whether the candidates for the a and b stacks given in tables 5.8, 5.9 and 5.10 in the previous chapter satisfy the bulk and twisted RR-tadpole cancellation conditions, possibly with the addition of hidden stacks.

On the **bAA** lattice, the first candidate for the a stack was given by the three-cycle with

bulk orbit parallel to $(4,-1;1,-1;1,1)$ or $(4,-1;1,1;1,-1)$, with $\varrho = 4$ and $\eta_{\Omega\mathcal{R}} = -1$. However, this three-cycle alone is already sufficient to overshoot the first bulk RR-tadpole cancellation condition because:

$$N_a(2P_a + Q_a) = 5 \cdot (2 \cdot 8 - 4) = 60 > 16\,, \tag{6.1}$$

where 16 corresponds to the maximal allowed contribution to the first bulk RR-tadpole cancellation condition for the choice of the exotic charge $\eta_{\Omega\mathcal{R}} = -1$. The value 16 is fixed by the RR-charges of the O6-planes, see (2.50). This excludes already the possibilities listed in table 5.8, i.e. they can only give rise to local models.
The second candidate for the a stack on the **bAA** lattice was given by the three-cycle with bulk orbit parallel to $(1,1;1,-1;1,1)$ or $(1,1;1,1;1,-1)$, with $\varrho = \frac{2}{3}$ and exotic O6-plane $\eta_{\Omega\mathcal{R}} = -1$. The contribution of the a stack to the bulk RR-tadpole cancellation conditions does not overshoot the RR-charges of the O6-planes this time:

$$N_a(2P_a + Q_a) = 5 \cdot (2 \cdot 2 - 1) = 15 < 16\,, \tag{6.2}$$

$$-N_a \frac{V_a + bQ_a}{1-b} = -5 \cdot 2 \cdot \left(-1 + \frac{1}{2}(-1)\right) = 15 < 16\,. \tag{6.3}$$

However, none of the candidate bulk three-cycles for the b stack appearing in table 5.10 has suitable bulk wrapping numbers which could cancel the remaining RR-charges of the O6-planes in the equations above.
As a conclusion, we can assert that all SUSY $SU(5)$ models on the **bAA** lattice of the orientifold $T^6/(\mathbb{Z}_2 \times \mathbb{Z}_6 \times \Omega\mathcal{R})$ with discrete torsion can only be local models.

The remaining step in our analysis consists in searching for global $SU(5)$ models on the **aAA** lattice. In this case, the candidate bulk three-cycles for supporting the a stack have orbits parallel to $(1,2;1,-1;1,1)$ or $(1,2;1,1;1,-1)$, with $\varrho = \frac{1}{2}$ and exotic O6-plane $\eta_{\Omega\mathcal{R}} = -1$. For both bulk orbits, their contributions to the bulk RR-tadpole cancellation conditions are given by:

$$N_a(2P_a + Q_a) = 5 \cdot (2 \cdot 2 - 1) = 15 < 16\,, \tag{6.4}$$

$$-N_a V_a = -5 \cdot (-2) = 10 < 16\,. \tag{6.5}$$

Due to the absence of the factor $\frac{1}{1-b}$ in the second equation, we are left with more freedom to cancel the remaining RR-charges of the O6-planes than in the case of the **bAA** lattice. In order to obtain a full three generation spectrum, the candidate bulk three-cycle for the b stack has to be taken from table 5.9. There is exactly one bulk-three cycle with orbit $(1,6;1,0;1,-1)$ which cancels the remaining RR-charges of the O6-planes when added to the equations above:

$$\sum_{x\in\{a,b\}} N_x(2P_x + Q_x) = 5 \cdot (2 \cdot 2 - 1) + 1 \cdot (2 \cdot 1 - 1) \overset{\checkmark}{=} 16\,, \tag{6.6}$$

$$-\sum_{x\in\{a,b\}} N_x V_x = -(5 \cdot (-2) + 1 \cdot (-6)) \overset{\checkmark}{=} 16\,. \tag{6.7}$$

In table 6.1, an explicit example is given of a model satisfying the bulk RR-tadpole cancellation conditions and giving rise to a full three generation particle spectrum. The complete

D6-brane configuration of a local $SU(5)$ GUT model on the aAA lattice with $\varrho = \frac{1}{2}$						
	wrapping numbers	$\frac{\text{Angle}}{\pi}$	$\mathbb{Z}_2^{(i)}$**-eigenvalues**	$(\vec{\tau})$	$(\vec{\sigma})$	**gauge group**
a	$(1,2;1,-1;1,1)$	$(\frac{1}{6},-\frac{1}{3},\frac{1}{6})$	$(-+-)$	$(0,1,1)$	$(0,1,1)$	$U(5)$
b	$(1,6;1,0;1,-1)$	$(\frac{1}{3},0,-\frac{1}{3})$	$(+++)$	$(0,0,1)$	$(0,0,1)$	$U(1)$

Table 6.1: Data of a local $SU(5)$ GUT model consisting of two stacks of D6-branes with gauge group $SU(5)_a \times U(1)_a \times U(1)_b$ on the **aAA** lattice. The $\Omega\mathcal{R}$-plane is chosen exotic with $\eta_{\Omega\mathcal{R}} = -1$.

Massless spectrum of a local two-stack $SU(5)$ GUT model		
State	Sector	$(SU(5)_a)_{U(1)_a \times U(1)_b}$
$\mathbf{10}$	aa'	$3 \times (\mathbf{10})_{(2_{\mathbf{Anti}},0)}$
$\overline{\mathbf{5}}$	ab	$3 \times (\overline{\mathbf{5}})_{(-1,1)}$
$\Phi_{\mathbf{24}}, \Phi_{\mathbf{1}}$	aa	$(\mathbf{24}_{\mathbf{Adj}})_{(0,0)} + (\mathbf{1})_{(0_{\mathbf{Adj}},0)}$
B	bb	$(\mathbf{1})_{(0,0_{\mathbf{Adj}})}$
$\Sigma_a^{i\in\{1,2,3\}}$, $\tilde{\Sigma}_a^{i\in\{1,2,3\}}$	aa'	$3 \times \left[(\mathbf{15})_{(2_{\mathbf{Sym}},0)} + h.c.\right]$
Σ_b	bb'	$5 \times (\mathbf{1})_{(0,2_{\mathbf{Sym}})}$

Table 6.2: Overview of the chiral and non-chiral massless particle content associated to the $SU(5)$ GUT model with D6-brane configuration given in table 6.1.

spectrum of the chiral particles and the non-chiral pairs of particles corresponding to the model in table 6.1 is given in table 6.2.

By looking at the spectrum displayed in table 6.2, several shortcomings become immediately apparent. Indeed, we have no electroweak Higgs pair H_u and H_d arising in the non-chiral sectors of ab or ab', so the breaking of the electroweak group $SU(2)_L \times U(1)_Y$ to the electromagnetic group $U(1)_{EM}$ needs another mechanism than the traditional one used in the Standard Model. Moreover, we have non-chiral pairs transforming in the symmetric representation $\mathbf{15} + \overline{\mathbf{15}}$ of the $SU(5)$ group supported by the a stack. In order to effectively remove these states from the model, they ought to be very heavy.
However, the crucial drawback for this model is the lack of fulfilling the twisted part of the RR-tadpole cancellation conditions. As a matter of fact, the contribution of the a and b stacks of this $SU(5)$ model to the twisted RR-tadpole cancellation conditions is given by:

$$\sum_{i=1}^{3} \sum_{x\in\{a,b\}} N_x(\Pi_x^{\mathbb{Z}_2^{(i)}} + \Pi_{x'}^{\mathbb{Z}_2^{(i)}}) = \begin{cases} -8\,\varepsilon_3^{(1)} + 4\,\varepsilon_4^{(1)} + 4\,\varepsilon_5^{(1)} + 24\,\tilde{\varepsilon}_4^{(1)} - 24\,\tilde{\varepsilon}_5^{(1)} \\ +18\,\varepsilon_1^{(2)} + 18\,\varepsilon_2^{(2)} \\ -14\varepsilon_1^{(3)} - 14\varepsilon_2^{(3)}. \end{cases} \tag{6.8}$$

Adding additional hidden stacks to the twisted RR-tadpole cancellation conditions above may cancel the contributions of the visible a and b stacks. However, in that case, the bulk RR-tadpole cancellation conditions would be overshot, as the SUSY conditions only allow for positive contributions to the bulk RR-tadpole cancellation conditions, see section 4.2. Hence, the bulk part and the twisted part of the RR-tadpole cancellation conditions cannot be simultaneously fulfilled, and the $SU(5)$ model is again local only.

The present analysis holds true for the other 47 models associated to a=(1,2; 1,-1; 1,1) and b= (1,6; 1,0; 1,-1) as well as for all 48 models with bulk orbits a=(1,2; 1,1; 1,-1) and b= (1,6; 1,0; 1,-1) given in table 5.9. More concisely, all 96 models give rise to the same massless chiral and non-chiral spectrum presented in table 6.2, and all 96 models are characterized by non-vanishing twisted RR-tadpole cancellation conditions similar to (6.8).
The obtainment of identical particle spectra is a hint for equivalences among the models. As a matter of fact, in [76, 64], classes of models have been identified. It was found that models with identical relative $\mathbb{Z}_2$-eigenvalues $\Delta\tau_{ab}^{\mathbb{Z}_2^{(i)}} \equiv \tau_a^{\mathbb{Z}_2^{(i)}} - \tau_b^{\mathbb{Z}_2^{(i)}}$ as well as identical shifts and Wilson lines always give rise to the same particle spectrum, so that they can be considered to be equivalent. These equivalent models always come at the number of four, since the a stack for example has four possibilities of combinations for its $\mathbb{Z}_2$-eigenvalues $\tau_a^{\mathbb{Z}_2^{(i)}}$, $i = 1, 2, 3$, and the $\mathbb{Z}_2$-eigenvalue of the second stack is then automatically fixed for each possibility, as the models must have equal relative $\mathbb{Z}_2$-eigenvalues between their two stacks. We cross-checked explicitly on probe-wise computer scans that the models with identical relative $\mathbb{Z}_2$-eigenvalues, identical Wilson lines and shifts always come at the number of four. Therefore, the number of physically non-equivalent models corresponds to 24 models rather than 96 models.
To conclude, on the present toroidal orbifold $T^6/(\mathbb{Z}_2 \times \mathbb{Z}_6 \times \Omega\mathcal{R})$ with discrete torsion, no global $SU(5)$ GUT models can be constructed.

6.2 Archetypes of local and global Pati-Salam models

In the set-up of Type IIA string theory, where particle physics models are realized by intersections of D6-branes, the Pati-Salam models are the easiest to construct. Previous work on similar toroidal backgrounds revealed this fact, see for example [76, 93]. Hence, it is sensible to start by searching for global Pati-Salam models, as they are most likely to be found.

The gauge group of the Pati-Salam models corresponds to $SU(4) \times SU(2)_L \times SU(2)_R$. Thus, three stacks are needed to support the three gauge factors, which are referred to as the a, b and c stacks. The first step consists in determining precisely which three-cycles from section 5.4 can be used for the a and the b stacks in the case of the Pati-Salam models.
In the Pati-Salam model, the a stack should be rigid and it should support no chiral matter states transforming in the symmetric nor the antisymmetric[1] representation of $SU(4)$. Three-cycles with these properties can be found in table 5.3. Table 5.3 reveals that there are two bulk three-cycles per lattice supporting no chiral matter states transforming in the antisymmetric representation. These correspond to three-cycles parallel to the $\Omega\mathcal{R}$-plane, and to three-cycles with bulk orbit of the form (1,m_a^1; 1,0; 1,-1) with $m_a^1 = 3$ on the **aAA** lattice and $m_a^1 = 1$ on the **bAA** lattice.
Concerning the b stack supporting $SU(2)_L$, it should be rigid and free of matter states transforming in the symmetric representation of $SU(2)_L$. There are no conditions on the number of matter states in the antisymmetric representation, as these correspond to singlets under

[1] In principle, this condition can be relaxed by allowing one matter state in the antisymmetric representation of $SU(4)$, in order to reproduce the models described in [185, 186]. However, we will not consider these models in the present work.

$SU(2)_L$. Thus, other than being parallel to some O6-plane with adequate conditions on rigidity, the three-cycles from which the b stack can be chosen are indicated in table 5.2. Once again, tables 5.4, 5.5, 5.6 and 5.7 yield that not all of these can be paired off with a suitable a stack to give three generations of bifundamentals $(\mathbf{4_a}, \mathbf{2_b})$.

Finally, the only possible combinations left for the a and b stacks are:

- Table 5.5: the first combination,
- Table 5.6: all combinations,
- Table 5.7: combinations two (second line), three (fourth line) for the **aAA** lattice, combinations eight (ninth line) and nine (thirteenth line) for the **bAA** lattice.

In a next step, the a and b stacks have to be completed with a suitable c stack and possibly also with hidden stacks to have global consistency.

6.2.1 Local Pati-Salam models on the bAA lattice

As shown in the box diagram 5.1, the models can be divided into two classes: models which are completely independent of the complex structure parameter ϱ, and the models which are ϱ-dependent, i.e. models which contain at least one stack wrapping a bulk three-cycle which is only SUSY for a given value of ϱ.
We will start the discussion on the **bAA** lattice with ϱ-independent Pati-Salam models.

ϱ-independent Pati-Salam models: The candidate bulk three-cycles for the a and b stacks can be found in table 5.5. Table 5.5 yields that in order to have three generations for the first two stacks of the model, the a stack has to be parallel to the $\Omega\mathcal{R}$-plane, the b stack has to lie along the $\Omega\mathcal{R}\mathbb{Z}_2^{(1)}$-plane, and the $\Omega\mathcal{R}\mathbb{Z}_2^{(2)}$-plane or $\Omega\mathcal{R}\mathbb{Z}_2^{(3)}$-plane has to be chosen to be the exotic O6-plane, i.e. $\eta_{\Omega\mathcal{R}\mathbb{Z}_2^{(2)}} = -1$ or $\eta_{\Omega\mathcal{R}\mathbb{Z}_2^{(3)}} = -1$. The contribution of the a and b stacks to the first bulk RR-tadpole cancellation condition equals $\sum_{x\in\{a,b\}} N_x(2P_x + Q_x) = 28 < 32$, where 32 is the maximal allowed contribution (see (2.50)). Note that $N_b = 1$ and not $N_b = 2$ since we have gauge symmetry enhancement on the b stack supporting a symplectic $USp(2)$ group rather than an unitary $U(2)$ group. The next step consists in finding a suitable candidate for the c stack supporting the $SU(2)_R$ group, which must not contribute more than 4 to the first bulk RR-tadpole cancellation condition. The only ϱ-independent bulk three-cycle fulfilling $2P + Q \leq 4$ and $\tilde{V} = 0$ is the cycle parallel to the $\Omega\mathcal{R}$-plane which satisfies $2P + Q = 4$. However, looking at table 5.4, we see that two three-cycles with bulk orbit parallel to the $\Omega\mathcal{R}$-plane cannot give rise to three generations. Thus, we cannot have three generations in the ac sector, i.e. $\chi^{ac} + \chi^{ac'} \neq \pm 3$ and also $\chi^{ac} = \chi^{ac'} \neq \pm 3$ in case of gauge symmetry enhancement on c. In other words, the right-handed matter states of the Pati-Salam model do not come in three generations, which is rejectable from a phenomenological point of view.
As a conclusion, we can state that ϱ-independent global Pati-Salam models cannot be realized on the **bAA** lattice in the present set-up of $T^6/(\mathbb{Z}_2 \times \mathbb{Z}_6 \times \Omega\mathcal{R})$ with discrete torsion.
It remains to be checked whether ϱ-dependent global Pati-Salam models can be constructed on the **bAA** lattice in this framework.

ϱ-dependent Pati-Salam models: We will start with the first possibility of a and b stacks listed on page 103. Remember that global ϱ-dependent models can only be realized if the $\Omega\mathcal{R}$-plane is chosen to be the exotic O6-plane, i.e. $\eta_{\Omega\mathcal{R}} = -1$. This is due to the fact that ϱ-dependent bulk three-cycles always have $\tilde{V} \neq 0$, so the second bulk RR-tadpole cancellation condition imposes $\eta_{\Omega\mathcal{R}\mathbb{Z}_2^{(2)}} = \eta_{\Omega\mathcal{R}\mathbb{Z}_2^{(3)}} = 1 \Rightarrow \eta_{\Omega\mathcal{R}} = -1$. This condition on the choice of the exotic charge rules out the possibility to construct ϱ-dependent models starting from the a and b stacks corresponding to the first combination in table 5.5.

The second possibility is given by the set of bulk three-cycle candidates for the a and b stack presented in table 5.6. This possibility corresponds to the a stack parallel to the $\Omega\mathcal{R}$-plane and the b stack wrapping some ϱ-dependent bulk three-cycle indicated in table 5.6. However, the a stack parallel to the $\Omega\mathcal{R}$-plane gives a contribution to the first bulk RR-tadpole cancellation condition which already equals the maximal allowed contribution: $N_a(2P_a + Q_a) = 4 \cdot 4 = 16$. In other words, the b stack should give no contribution at all to the first bulk RR-tadpole cancellation condition. However, none of the bulk three-cycles given in table 5.6 gives zero contribution, meaning that once again, the bulk RR-tadpole cancellation conditions cannot be satisfied. Therefore, the second set of candidates for the a and b stacks listed on page 103 cannot give rise to global Pati-Salam models on the **bAA** lattice.

There remains the last possibility listed on page 103 given by combination eight and nine of table 5.7. Combination eight corresponds to $a \uparrow\uparrow (1,1;1,0;1,-1)$ and $b \uparrow\uparrow \Omega\mathcal{R}$ while combination nine corresponds to $a \uparrow\uparrow b \uparrow\uparrow (1,1;1,0;1,-1)$. Both combinations are associated to the value of the complex structure modulus $\varrho = 2$, which is fixed by the bulk three-cycle with bulk orbit (1,1; 1,0; 1,-1). The c stack supporting the $SU(2)_R$ group ought to be rigid, so it should have the same bulk orbit (1,1; 1,0; 1,-1) as the a stack, or it can be parallel to some O6-plane. Concerning that last possibility, only the $\Omega\mathcal{R}$-plane as the c stack gives rise to three generations of right-handed matter states in the ac sector, as can be concluded from table 5.7[2]. The remaining four possibilities are listed in table 6.3, which also indicates the respective contributions to the bulk RR-tadpole cancellation conditions. Remember that for $\eta_{\Omega\mathcal{R}} = -1$, the three visible stacks of the Pati-Salam models should satisfy the upper bounds given by the two independent bulk RR-tadpole cancellation conditions as follows:

$$\begin{aligned} \sum_{x\in\{a,b,c\}} N_x(2P_x + Q_x) &\leq 16, \\ -2 \sum_{x\in\{a,b,c\}} N_x \tilde{V}_x &\leq 16. \end{aligned} \tag{6.9}$$

Comparing these upper bounds with the contributions to the bulk RR-tadpole cancellation conditions given in table 6.3, we see that for all four combinations, one of the two bulk RR-tadpole cancellation conditions is overshot.

As a conclusion, we can state that on the **bAA** lattice of $T^6/(\mathbb{Z}_2 \times \mathbb{Z}_6 \times \Omega\mathcal{R})$ with discrete torsion, no global Pati-Salam models can be constructed.

[2]Note that taking b or c along $\Omega\mathcal{R}\mathbb{Z}_2^{(1)}$ could give rise to three generations, but it would be accompanied by $SO(2)$ gauge enhancement on b or c, which is not desirable from the point of view of model building.

Summary of local Pati-Salam models on the bAA lattice of $T^6/(\mathbb{Z}_2 \times \mathbb{Z}_6 \times \Omega\mathcal{R})$ with $\varrho = 2$ and $\eta = -1 = \eta_{\Omega\mathcal{R}}$				
Bulk orbits for the Pati-Salam gauge groups			**bulk RR tadpoles**	
a-stack	b-stack	c-stack	$\sum_{x\in\{a,b,c\}} N_x(2P_x + Q_x)$	$-2\sum_{x\in\{a,b,c\}} N_x\tilde{V}_x$
$(1,1;1,0;1,-1)$	$\uparrow\uparrow\,\Omega\mathcal{R} : (2,-1;1,0;1,0)$	$(1,1;1,0;1,-1)$	$N_a + 4N_b + N_c = 14$	$3N_a + 3N_c = 18$
$(1,1;1,0;1,-1)$	$\uparrow\uparrow\,\Omega\mathcal{R} : (2,-1;1,0;1,0)$	$\uparrow\uparrow\,\Omega\mathcal{R} : (2,-1;1,0;1,0)$	$N_a + 4N_b + 4N_c = 20$	$3N_a = 12$
$(1,1;1,0;1,-1)$	$(1,1;1,0;1,-1)$	$(1,1;1,0;1,-1)$	$N_a + N_b + N_c = 8$	$3N_a + 3N_b + 3N_c = 24$
$(1,1;1,0;1,-1)$	$(1,1;1,0;1,-1)$	$\uparrow\uparrow\,\Omega\mathcal{R} : (2,-1;1,0;1,0)$	$N_a + N_b + 4N_c = 14$	$3N_a + 3N_b = 18$

Table 6.3: Overview of candidate bulk three-cycles on the **bAA** lattice for the a, b and c stacks satisfying the conditions on rigidity and matter states transforming in the (anti)symmetric representation. The respective contributions of the bulk three-cycles listed in the first three columns to the first and second RR-tadpole cancellation conditions are given in the last two columns.

Nonetheless, in our publication [63], we classified the local Pati-Salam models appearing in table 6.3 into two types of local models. This analysis will be presented in the current thesis also. Two Pati-Salam models are considered to be of the same type or class, referred to as prototype, if they support identical gauge groups and give rise to the same chiral and non-chiral particle spectrum. A specific model for the first combination of bulk orbits in table 6.3 is displayed in table 6.4. The associated chiral and non-chiral particle content is

D6-brane configuration of a local Pati-Salam model on the bAA lattice with $\varrho = 2$: prototype I						
	wrapping numbers	$\frac{\text{Angle}}{\pi}$	$\mathbb{Z}_2^{(i)}$**-eigenvalues**	$(\vec{\tau})$	$(\vec{\sigma})$	**gauge group**
a	$(1,1;1,0;1,-1)$	$(\frac{1}{3},0,-\frac{1}{3})$	$(--+)$	$(0,1,1)$	$(0,1,1)$	$U(4)$
b	$(2,-1;1,0;1,0)$	$(0,0,0)$	$(+--)$	$(1,0,0)$	$(1,0,0)$	$U(2)$
c	$(1,1;1,0;1,-1)$	$(\frac{1}{3},0,-\frac{1}{3})$	$(+++)$	$(0,1,1)$	$(0,1,1)$	$U(2)$

Table 6.4: Data of a local Pati-Salam model consisting of three stacks of D6-branes with gauge group $SU(4)_a \times SU(2)_b \times SU(2)_c \times U(1)_a \times U(1)_b \times U(1)_c$ on the **bAA** lattice. The $\Omega\mathcal{R}$-plane is chosen exotic with $\eta_{\Omega\mathcal{R}} = -1$.

given in table 6.5.

Spectrum of the prototype I local Pati-Salam model on bAA		
State	Sector	$(SU(4)_a \times SU(2)_b \times SU(2)_c)_{U(1)_a \times U(1)_b \times U(1)_c}$
(Q_L, L)	ab	$2 \times (\mathbf{4},\mathbf{2},\mathbf{1})_{(1,-1,0)}$
(Q_L, L)	ab'	$(\mathbf{4},\mathbf{2},\mathbf{1})_{(1,1,0)}$
(Q_R, R)	ac'	$3 \times (\overline{\mathbf{4}},\mathbf{1},\mathbf{2})_{(-1,0,-1)}$
$A, \tilde{A}$	aa'	$2 \times [(\mathbf{6_{Anti}},\mathbf{1},\mathbf{1})_{(2,0,0)} + h.c.]$
$B, \tilde{B}$	bb'	$(\mathbf{1},\mathbf{1_{Anti}},\mathbf{1})_{(0,2,0)} + h.c.$
$C, \tilde{C}$	cc'	$2 \times [(\mathbf{1},\mathbf{1},\mathbf{1_{Anti}})_{(0,0,2)} + h.c.]$
$G_H, \tilde{G}_H$	ac	$2 \times \left[(\mathbf{4},\mathbf{1},\mathbf{2})_{(1,0,-1)} + h.c.\right]$

Table 6.5: Overview of the chiral and non-chiral massless particle content associated to the prototype I local Pati-Salam model with D6-brane configuration given in table 6.4.

A second prototype of local Pati-Salam models on the **bAA** lattice is given by the third

combination of bulk three-cycles in table 6.3. An explicit example of the second class of models is given in table 6.6. The chiral and non-chiral particle spectrum corresponding to

D6-brane configuration of a local Pati-Salam model on the bAA lattice with $\varrho = 2$: prototype II						
	wrapping numbers	$\frac{\text{Angle}}{\pi}$	$\mathbb{Z}_2^{(i)}$**-eigenvalues**	$(\vec{\tau})$	$(\vec{\sigma})$	**gauge group**
a	$(1,1;1,0;1,-1)$	$(\frac{1}{3},0,-\frac{1}{3})$	$(+--)$	$(0,1,1)$	$(0,1,1)$	$U(4)$
b	$(1,1;1,0;1,-1)$	$(\frac{1}{3},0,-\frac{1}{3})$	$(+++)$	$(0,1,1)$	$(0,1,1)$	$U(2)$
c	$(1,1;1,0;1,-1)$	$(\frac{1}{3},0,-\frac{1}{3})$	$(-+-)$	$(0,1,1)$	$(0,1,1)$	$U(2)$

Table 6.6: Data of a local Pati-Salam model consisting of three stacks of D6-branes with gauge group $SU(4)_a \times SU(2)_b \times SU(2)_c \times U(1)_a \times U(1)_b \times U(1)_c$ on the **bAA** lattice. The $\Omega\mathcal{R}$-plane is chosen exotic with $\eta_{\Omega\mathcal{R}} = -1$.

the second class of local Pati-Salam models on the **bAA** lattice is shown in table 6.7.

Spectrum of the prototype II local Pati-Salam model on bAA		
State	Sector	$(SU(4)_a \times SU(2)_b \times SU(2)_c)_{U(1)_a \times U(1)_b \times U(1)_c}$
(Q_L, L)	ab'	$3 \times (\mathbf{4},\mathbf{2},\mathbf{1})_{(1,1,0)}$
(Q_R, R)	ac'	$3 \times (\overline{\mathbf{4}},\mathbf{1},\mathbf{2})_{(-1,0,-1)}$
(H_u, H_d)	bc'	$3 \times (\mathbf{1},\mathbf{2},\mathbf{2})_{(0,-1,-1)}$
	aa'	$2 \times [(\mathbf{6_{Anti}},\mathbf{1},\mathbf{1})_{(2,0,0)} + h.c.]$
	bb'	$2 \times [(\mathbf{1},\mathbf{1_{Anti}},\mathbf{1})_{(0,2,0)} + h.c.]$
	cc'	$2 \times [(\mathbf{1},\mathbf{1},\mathbf{1_{Anti}})_{(0,0,2)} + h.c.]$
	ab	$(\mathbf{4},\mathbf{2},\mathbf{1})_{(1,-1,0)} + h.c.$
	ab'	$(\mathbf{4},\mathbf{2},\mathbf{1})_{(1,1,0)} + h.c.$
$G_H, \tilde{G}_H$	ac	$2 \times [(\mathbf{4},\mathbf{1},\mathbf{2})_{(1,0,-1)} + h.c.]$
(H_u, H_d)	bc	$2 \times [(\mathbf{1},\mathbf{2},\mathbf{2})_{(0,1,-1)} + h.c.]$

Table 6.7: Overview of the chiral and non-chiral massless particle content associated to the prototype II local Pati-Salam model with D6-brane configuration given in table 6.6.

All other models arising from the first and third combinations of table 6.3 can be classified into one of these two classes of local Pati-Salam models. Similarly, the models arising from the second and fourth combinations of table 6.3 can also be classified into these two classes, up to a trivial exchange in the ac sector of the c stack and its orientifold image c': $\chi^{ac} \leftrightarrow \chi^{ac'}$.

To conclude this section, we will briefly discuss the particle content of both classes of local Pati-Salam models. A first observation concerns the realization of the three generations of left-handed matter states. In the first class of models, the three generations are obtained from both sectors ab and ab', as can be checked in table 6.5. In the second class of models, the particle spectrum of which is displayed in table 6.7, the three generations of left-handed matter states arise solely from the ab' sector.
A serious shortcoming of the first prototype of local Pati-Salam models is the absence of the electroweak Higgs, which should arise in the chiral or non-chiral bc and bc' sectors.

Thus, the electroweak group $SU(2)_L \times U(1)_Y$ of the Standard Model must be broken to the electromagnetic group $U(1)_{\rm EM}$ by a different mechanism than the usual Higgs mechanism of the Standard Model. In this regard, the second prototype of local Pati-Salam models is more attractive from a phenomenological point of view, as it provides several electroweak Higgs doublets coming both from the chiral bc' sector and the non-chiral bc sector.
Finally, both classes of models offer the attractive feature of supporting GUT-Higgses G_H and $\tilde{G}_H$ in the non-chiral ac sector. These GUT-Higgses can be used for breaking the GUT group $SU(4) \times SU(2)_R$ down to the gauge group of the Standard Model $SU(3)_{\rm QCD} \times U(1)_Y$, as described for example in [185, 186].
This concludes the analysis of Pati-Salam models on the **bAA** lattice of $T^6/(\mathbb{Z}_2 \times \mathbb{Z}_6 \times \Omega\mathcal{R})$ with discrete torsion. In the next section, we will focus on the construction of Pati-Salam models on the **aAA** lattice, for which the bulk RR-tadpole cancellation conditions are less constraining.

6.2.2 Global ϱ-independent Pati-Salam models on the aAA lattice

Just as for the **bAA** lattice, the models can be separated into ϱ-independent and ϱ-dependent models. Once again, we will start with the former models.
We have seen in the previous section that the bulk RR-tadpole cancellation conditions on the **bAA** lattice are very constraining regarding the construction of ϱ-independent models. The situation is clearly different on the **aAA** lattice. Once again, the candidate bulk three-cycles for the a and b stacks for ϱ-independent models can be found in table 5.5. The contribution of the a and b stacks to the first bulk RR-tadpole cancellation condition sum up to: $\sum_{x\in\{a,b\}} N_x(2P_x + Q_x) = 4 \cdot 2 + 1 \cdot 6 = 14 \leq 32$, where 32 is the maximally allowed contribution for the choice of the exotic charge $\eta_{\Omega\mathcal{R}\mathbb{Z}_2^{(2)}} = -1$ or $\eta_{\Omega\mathcal{R}\mathbb{Z}_2^{(3)}} = -1$. This leaves ample room to complete the model with a c stack and even a suitable hidden sector. This has to be compared to the **bAA** lattice, where the contributions of the first two stacks added up to 28 already, leaving hardly any room for the c stack.
The c stack should be rigid, free of matter states in the symmetric representation, be ϱ-independent, satisfy $V_c = 0$ due to the second bulk RR-tadpole cancellation condition, and provide three generations of chiral matter states in the ac (and/or ac') sector. In addition, it should support a unitary $U(2)$ or symplectic $USp(2)$ group, but not an orthogonal $SO(2)$ group, in order to provide a proper Pati-Salam model with gauge factor $SU(2)_R$. The only candidate bulk three-cycle left satisfying these conditions is the three-cycle with bulk orbit parallel to the $\Omega\mathcal{R}\mathbb{Z}_2^{(1)}$-plane. In order to be rigid, it must present $USp(2)$ enhancement. The three stacks chosen so far give the following total contribution to the first bulk RR-tadpole cancellation condition:

$$\sum_{x\in\{a,b,c\}} N_x(2P_x + Q_x) = 2N_a + 6N_b + 6N_c = 20 \leq 32. \tag{6.10}$$

Note that $N_c = 1$ and not $N_c = 2$ because gauge symmetry enhancement is present on the c stack, just as it is the case for the b stack. It remains to add an adequate hidden sector permitting to completely cancel the RR-charges of the O6-planes. As the second bulk RR-tadpole cancellation condition imposes $V_x = 0$, the only bulk three-cycles left to form the hidden sector have bulk orbits parallel to the $\Omega\mathcal{R}$-plane, or parallel to the $\Omega\mathcal{R}\mathbb{Z}_2^{(1)}$-plane, or bulk orbits given by (1,0; 2,1; 3,-1) or (1,0; 4,-1; 3,1). However, these last two

orbits offer too high a contribution to the first RR-tadpole cancellation condition, as they have bulk wrapping numbers $2P_x + Q_x > 12$. Hence, they cannot be used to construct the hidden sector. Consequently, this leads to two classes of four-stack Pati-Salam models, the gauge groups of which differ in the hidden sector. More precisely, the hidden stack can be taken parallel to the $\Omega\mathcal{R}$-plane with rank $N_h = 6$, or parallel to the $\Omega\mathcal{R}\mathbb{Z}_2^{(1)}$-plane with rank $N_h = 2$. Of course, one could also add several hidden stacks with reduced rank, for example two hidden stacks parallel to the $\Omega\mathcal{R}$-plane with each having a reduced rank $N_{h_i} = 3,\ i = 1, 2$, leading to a five-stack Pati-Salam model. However, the more stacks a model has, the more computational power and processing time is needed in order to analyze the properties of the model. Therefore, in the present work, we will restrict the analysis to Pati-Salam models with at most four stacks.

Thus, we are left with two possibilities for the hidden sector, which both fulfill the bulk RR-tadpole cancellation conditions. It remains to be checked whether the twisted part of the RR-tadpole cancellation conditions can also be fulfilled by taking into account the exceptional part of the fractional three-cycles. A complete computer scan yielded 1 152 global four-stack Pati-Salam models for the first type of models with hidden rank $N_h = 6$, and 10 368 global four-stack Pati-Salam models for the second type of models with hidden rank $N_h = 2$. These models fulfill the bulk and twisted part of all the RR-tadpole cancellation conditions. The computer scan also revealed that the hidden stack of all the models does not exhibit enhancement, i.e. the gauge group of the hidden stack supports unitary groups $U(6)$ and $U(2)$ and not symplectic groups $USp(12)$ and $USp(4)$ or orthogonal groups $SO(12)$ and $SO(4)$, respectively.

Not all of the models are physically independent models. Just as in the case of the $SU(5)$ models, the Pati-Salam models with identical relative $\mathbb{Z}_2$-eigenvalues $\Delta\tau_{ab}^{\mathbb{Z}_2^{(i)}} \equiv \tau_a^{\mathbb{Z}_2^{(i)}} - \tau_b^{\mathbb{Z}_2^{(i)}}$, $\Delta\tau_{ac}^{\mathbb{Z}_2^{(i)}}$ and $\Delta\tau_{ah}^{\mathbb{Z}_2^{(i)}}$ as well as identical shifts and Wilson lines always produce the same particle spectrum, so that they can be considered to be equivalent. Another remark concerns the fact that models with $\eta_{\Omega\mathcal{R}\mathbb{Z}_2^{(2)}} = -1$ are related to models with $\eta_{\Omega\mathcal{R}\mathbb{Z}_2^{(3)}} = -1$ via an exchange of the two-torus labels $i = 2 \leftrightarrow i = 3$ of $T^2_{(i)}$. We checked explicitly that we always obtained an equal amount of models for both choices of the exotic O6-plane charge. Therefore, the numbers of physically non-equivalent models correspond to $1\,152 \div 8 = 144$ and $10\,368 \div 8 = 1\,296$ for the first type and second type of Pati-Salam models, respectively.

An explicit example including the list of discrete parameters for the first type of the global four-stack Pati-Salam models is given in table 6.8.

D6-brane configuration of a global Pati-Salam model on the aAA lattice: prototype I						
	wrapping numbers	$\frac{\text{Angle}}{\pi}$	$\mathbb{Z}_2^{(i)}$**-eigenvalues**	$(\vec{\tau})$	$(\vec{\sigma})$	**gauge group**
a	$(1,0;1,0;1,0)$	$(0,0,0)$	$(--+)$	$(0,1,1)$	$(0,1,1)$	$U(4)$
b	$(1,0;-1,2;1,-2)$	$(0,\frac{1}{2},-\frac{1}{2})$	$(+++)$	$(0,0,1)$	$(0,0,1)$	$USp(2)$
c	$(1,0;-1,2;1,-2)$	$(0,\frac{1}{2},-\frac{1}{2})$	$(--+)$	$(0,0,1)$	$(0,0,1)$	$USp(2)$
h	$(1,0;1,0;1,0)$	$(0,0,0)$	$(+--)$	$(0,1,1)$	$(0,1,1)$	$U(6)$

Table 6.8: Data of a global Pati-Salam model consisting of four stacks with gauge group $SU(4)_a \times USp(2)_b \times USp(2)_c \times SU(6)_h \times U(1)_a \times U(1)_h$ on the **aAA** lattice. The $\Omega\mathcal{R}\mathbb{Z}_2^{(2)}$-plane is chosen exotic with $\eta_{\Omega\mathcal{R}\mathbb{Z}_2^{(2)}} = -1$.

The corresponding spectrum of chiral and non-chiral particles is exhibited in table 6.9.

Spectrum of the prototype I global Pati-Salam model on aAA		
State	Sector	$(SU(4)_a \times USp(2)_b \times USp(2)_c \times SU(6)_h)_{U(1)_a \times U(1)_h}$
(Q_L, L)	$ab = ab'$	$3 \times (\mathbf{4}, \mathbf{2}, \mathbf{1}, \mathbf{1})_{(1,0)}$
(Q_R, R)	$ac = ac'$	$3 \times (\overline{\mathbf{4}}, \mathbf{1}, \mathbf{2}, \mathbf{1})_{(-1,0)}$
(H_u, H_d)	$bc = bc'$	$10 \times (\mathbf{1}, \mathbf{2}, \mathbf{2}, \mathbf{1})_{(0,0)}$
	$bh = bh'$	$3 \times (\mathbf{1}, \mathbf{2}, \mathbf{1}, \mathbf{6})_{(0,1)}$
	$ch = ch'$	$3 \times (\mathbf{1}, \mathbf{1}, \mathbf{2}, \overline{\mathbf{6}})_{(0,-1)}$
	aa'	$2 \times \left[(\mathbf{6_{Anti}}, \mathbf{1}, \mathbf{1}, \mathbf{1})_{(2,0)} + h.c.\right]$
	bb'	$5 \times (\mathbf{1}, \mathbf{1_{Anti}}, \mathbf{1}, \mathbf{1})_{(0,0)}$
	cc'	$5 \times (\mathbf{1}, \mathbf{1}, \mathbf{1_{Anti}}, \mathbf{1})_{(0,0)}$
	hh'	$2 \times [(\mathbf{1}, \mathbf{1}, \mathbf{1}, \mathbf{15_{Anti}}))_{(0,2} + h.c.]$
	ah	$2 \times [(\mathbf{4}, \mathbf{1}, \mathbf{1}, \overline{\mathbf{6}})_{(1,-1)} + h.c.]$
	ah'	$(\mathbf{4}, \mathbf{1}, \mathbf{1}, \mathbf{6})_{(1,1)} + h.c.$

Table 6.9: Overview of the chiral and non-chiral massless particle content associated to the prototype I global Pati-Salam model with D6-brane configuration given in table 6.8.

The example for the second class of global four-stack Pati-Salam models is given in table 6.10, and the corresponding massless particle spectrum can be found in table 6.11.

D6-brane configuration of a global Pati-Salam model on the aAA lattice: prototype II						
	wrapping numbers	$\frac{\text{Angle}}{\pi}$	$\mathbb{Z}_2^{(i)}$**-eigenvalues**	$(\vec{\tau})$	$(\vec{\sigma})$	**gauge group**
a	$(1,0;1,0;1,0)$	$(0,0,0)$	$(--+)$	$(0,1,1)$	$(0,1,1)$	$U(4)$
b	$(1,0;-1,2;1,-2)$	$(0,\frac{1}{2},-\frac{1}{2})$	$(+++)$	$(0,0,1)$	$(0,0,1)$	$USp(2)$
c	$(1,0;-1,2;1,-2)$	$(0,\frac{1}{2},-\frac{1}{2})$	$(--+)$	$(0,0,1)$	$(0,0,1)$	$USp(2)$
h	$(1,0;-1,2;1,-2)$	$(0,\frac{1}{2},-\frac{1}{2})$	$(+++)$	$(0,0,0)$	$(0,0,0)$	$U(2)$

Table 6.10: Data of a global Pati-Salam model consisting of four stacks with gauge group $SU(4)_a \times USp(2)_b \times USp(2)_c \times SU(2)_h \times U(1)_a \times U(1)_h$ on the **aAA** lattice. The $\Omega\mathcal{R}\mathbb{Z}_2^{(2)}$-plane is chosen exotic with $\eta_{\Omega\mathcal{R}\mathbb{Z}_2^{(2)}} = -1$.

Once again, we will finish this section with a discussion of the similarities and differences between the two classes of models. Aside from the different gauge factor on the hidden stack, there are also differences in the non-chiral part of the massless particle spectrum. In the second class of models, we have for example non-chiral matter states in the bh and ch sectors, which are not present in the first class of models. On the other hand, the chiral particle content is realized in both types of models in exactly the same manner. Luckily, there are also ten electroweak Higgses available in both types of models, arising in the bc sector. A disadvantage in both models is the presence of several exotic matter states. Remember from section 3.2.1 that exotic matter states are matter states which are charged under both the three visible stacks forming the gauge group of the Pati-Salam model and the fourth hidden

Spectrum of the prototype II global Pati-Salam model on aAA		
State	Sector	$(SU(4)_a \times USp(2)_b \times USp(2)_c \times SU(2)_h)_{U(1)_a \times U(1)_h}$
(Q_L, L)	$ab = ab'$	$3 \times (\mathbf{4}, \mathbf{2}, \mathbf{1}, \mathbf{1})_{(1,0)}$
(Q_R, R)	$ac = ac'$	$3 \times (\overline{\mathbf{4}}, \mathbf{1}, \mathbf{2}, \mathbf{1})_{(-1,0)}$
(H_u, H_d)	$bc = bc'$	$10 \times (\mathbf{1}, \mathbf{2}, \mathbf{2}, \mathbf{1})_{(0,0)}$
	$bh = bh'$	$3 \times (\mathbf{1}, \mathbf{2}, \mathbf{1}, \mathbf{2})_{(0,1)}$
	$ch = ch'$	$3 \times (\mathbf{1}, \mathbf{1}, \mathbf{2}, \mathbf{2})_{(0,-1)}$
	aa'	$2 \times \left[(\mathbf{6_{Anti}}, \mathbf{1}, \mathbf{1}, \mathbf{1})_{(2,0)} + h.c.\right]$
	bb'	$5 \times (\mathbf{1}, \mathbf{1_{Anti}}, \mathbf{1}, \mathbf{1})_{(0,0)}$
	cc'	$5 \times (\mathbf{1}, \mathbf{1}, \mathbf{1_{Anti}}, \mathbf{1})_{(0,0)}$
	hh'	$6 \times [(\mathbf{1}, \mathbf{1}, \mathbf{1}, \mathbf{1_{Anti}})_{(0,2)} + h.c.]$
	ah	$2 \times [(\mathbf{4}, \mathbf{1}, \mathbf{1}, \mathbf{2})_{(1,-1)} + h.c.]$
	ah'	$(\mathbf{4}, \mathbf{1}, \mathbf{1}, \mathbf{2})_{(1,1)} + h.c.$
	$bh = bh'$	$3 \times [(\mathbf{1}, \mathbf{2}, \mathbf{1}, \mathbf{2})_{(0,-1)} + h.c.]$
	$ch = ch'$	$3 \times [(\mathbf{1}, \mathbf{1}, \mathbf{2}, \mathbf{2})_{(0,-1)} + h.c.]$

Table 6.11: Overview of the chiral and non-chiral massless particle content associated to the prototype II global Pati-Salam model with D6-brane configuration given in table 6.10.

stack. Such particles are not desired from a phenomenological point of view, for they would be detectable by ordinary particle detectors, as they interact by exchange of ordinary visible gauge bosons, on top of the hidden gauge boson carrier of a new fundamental force. Particles charged exclusively under the hidden sector, and not charged under the visible sector, are acceptable, since they would interact solely via the new fundamental force and thus escape notice of ordinary particle detectors.
Another shortcoming of the two classes of models is the absence of GUT-Higgses which should naturally arise from the non-chiral ac and ac' sectors. Thus, another mechanism would need to be devised to break the Pati-Salam GUT group to the gauge group of the Standard Model.

6.2.3 The situation of ϱ-dependent Pati-Salam models on the aAA lattice

This section is meant to give the reader a superficial overview of the situation of ϱ-dependent Pati-Salam models in the case of the **aAA** lattice. The aim is not to provide a complete and thorough search for global Pati-Salam models, as we have already found some in the previous section. Remember that for ϱ-dependent models, the exotic O6-plane charge has to be $\eta_{\Omega\mathcal{R}} = -1$, otherwise the second bulk RR-tadpole cancellation condition is violated by at least one stack.
The first step consists in finding suitable candidates of bulk three-cycles to support the a and b stacks, which can be found in table 5.6 and 5.7. Remember that the a stack should also be free of matter states in the antisymmetric representation, so possible candidate bulk

three-cycles are given by all entries in table 5.6 as well as the second and fourth lines of table 5.7. We will choose only one combination in order to illustrate the situation of ϱ-dependent models. The combination we choose has the a stack parallel to the $\Omega\mathcal{R}$-plane and the b stack has its bulk orbit parallel to the ϱ-dependent orbit (1,1; 1,0; 1,-1). The associated complex structure parameter is $\varrho = 3$. This value for the complex structure parameter allows for 14 bulk three-cycles which are SUSY for $\varrho = 3$, on top of the eight ϱ-independent bulk three-cycles which are SUSY for all values of ϱ. Thus, this leaves a total of 22 bulk three-cycles at our disposal to support the c stack and the hidden stacks. Since the c stack should be rigid, it must either be parallel to some O6-plane with an adequate choice of discrete parameters, or it must be parallel to the same bulk three-cycle as the b stack (1,1; 1,0; 1,-1) with constraints on rigidity. However, tables 5.4 and 5.5 reveal that by taking the c stack parallel to some O6-plane, no three generations of right-handed matter states can be realized in the ac and ac' sectors with $\eta_{\Omega\mathcal{R}} = -1$. Hence, the only candidate for the c stack is the bulk three-cycle with orbit (1,1; 1,0; 1,-1). A full computer scan yielded 256 combinations for the a, b and c stacks giving a full three generation chiral particle content.
The next step is to check the bulk RR-tadpole cancellation conditions, in order to cancel them with a suitable hidden sector. The $\Omega\mathcal{R}$-plane has bulk wrapping numbers $(P, Q, U, V) = (1, 0, 0, 0)$ on the **aAA** lattice, the three-cycle (1,1; 1,0; 1,-1) has bulk wrapping numbers $(P, Q, U, V) = (1, -1, 1, -1)$. Hence, the sum over the first three stacks yields for the bulk RR-tadpole cancellation conditions the following contributions:

$$\begin{aligned} &\textstyle\sum_{x=a,b,c} N_x(2P_x + Q_x) = 2N_a + N_b + N_c = 12 < 16\,, \\ &-\textstyle\sum_{x=a,b,c} N_x V_x = N_b + N_c = 4 < 16\,. \end{aligned} \tag{6.11}$$

The first bulk RR-tadpole cancellation condition leaves room for a maximal contribution of four $(16 - 12 = 4)$ for the hidden sector, the second bulk RR-tadpole cancellation condition leaves room for a maximal hidden contribution of twelve $(16 - 4 = 12)$. A scan over all 22 bulk three-cycles, that preserve SUSY for $\varrho = 3$, reveals a list given in table 6.12 of nine bulk three-cycles which can be added to the bulk RR-tadpole cancellation conditions above without overshooting them. These nine bulk three-cycles can be combined with different ranks N_i in order to fulfill both bulk RR-tadpole cancellation conditions as indicated in table 6.13. In table 6.13, we see that there is no combination which can satisfy both bulk RR-tadpole cancellation conditions with only one hidden stack, which would be the preferred combination. The next best combinations are those coming with two hidden stacks. There are eight of them:

$$\begin{array}{c|c|c|c} N_1 = 1 \text{ and } N_4 = 1 & N_1 = 1 \text{ and } N_5 = 1 & N_2 = 3 \text{ and } N_4 = 1 & N_2 = 3 \text{ and } N_5 = 1 \\ N_2 = 4 \text{ and } N_8 = 4 & N_2 = 4 \text{ and } N_9 = 4 & N_7 = 2 \text{ and } N_9 = 6 & N_7 = 2 \text{ and } N_8 = 6 \end{array}\,. \tag{6.12}$$

A complete scan over all 256 combinations of the visible sector combined with the $256 \cdot 256$ possibilities of the two hidden stacks revealed that none of the eight possibilities above satisfied all of the twisted RR-tadpole cancellation conditions.
Since global five-stack Pati-Salam models cannot be constructed with the current choice of the visible sector, the next step is to check whether global six-stack models with three hidden stacks can be constructed. The scan now runs over a total of $256 \cdot 256 \cdot 256 \cdot 256$

Candidate bulk 3-cycles for the hidden sector				
rank	$(n^1, m^1; n^2, m^2; n^3, m^3)$	(P, Q, U, V)	$2P+Q$	V
N_1	$(1,1;1,-2;1,1)$	$(3,-3,3,-3)$	3	-3
N_2	$(1,1;1,0;1,-1)$	$(1,-1,1,-1)$	1	-1
N_3	$(1,2;4,-1;1,-1)$	$(3,-4,6,-8)$	2	-8
N_4	$(1,3;3,-1;1,-1)$	$(2,-3,6,-9)$	1	-9
N_5	$(1,3;1,-1;3,-1)$	$(2,-3,6,-9)$	1	-9
N_6	$(1,2;0,-1;1,3)$	$(3,-4,6,-8)$	2	-8
N_7	$\Omega\mathcal{R}$	$(1,0,0,0)$	2	0
N_8	$\Omega\mathcal{R}\mathbb{Z}_2^{(2)}$	$(0,0,1,-2)$	0	-2
N_9	$\Omega\mathcal{R}\mathbb{Z}_2^{(3)}$	$(0,0,1,-2)$	0	-2

Table 6.12: List of bulk three-cycles that are SUSY for $\varrho = 3$ and do not overshoot the bulk RR-tadpole cancellation conditions (6.11). The second column gives the torus wrapping numbers, the third one gives the bulk wrapping numbers and the last two columns provide the contributions to the first respectively second bulk RR-tadpole cancellation conditions. To each three-cycle a rank N_i is associated in the first column with values indicated in table 6.13.

combinations, which lengthens the processing time more or less by a factor of 256 compared to the five-stack models. In addition, in table 6.13 we can find a total of 20 combinations with three hidden stacks, as compared to the eight possibilities we had before for the two hidden stacks. A complete computer scan over all 20 combinations revealed once more that none of them would fulfill all the twisted RR-tadpole cancellation conditions.
The remaining 13 out of the initial 41 combinations all come with four hidden stacks. I did not perform a scan over these, as the processing time is augmented once more by a factor 256 compared to the previous scan, due to the addition of one hidden stack. Moreover, it is likely that these combinations too will not fulfill the twisted RR-tadpole cancellation conditions, as all the previous scans running over a total of 86 033 563 648 combinations already have failed. Note also that the combinations indicated in table 6.13 only correspond to combinations where the hidden stacks wrap different bulk three-cycles. The table could be extended by taking hidden stacks wrapped on the same bulk three-cycles with reduced rank, but considering different exceptional cycles so that the hidden stacks wrap different fractional three-cycles. For example, the first combination with two hidden stacks of table 6.13 could be extended to eight hidden stacks, each supporting a gauge factor with rank one $N_i = 1$, $i = 1, \ldots 8$. These options have not been pursued in this thesis, as they involve too much computational power.

To conclude, we can state that the possibilities to construct the hidden sector for the present visible sector are more numerous than in the case of the ϱ-independent models we have analyzed before. Therefore, a complete and thorough analysis exhausting all the possibilities needs a tremendous amount of processing power and time. The computer scans performed in this section already indicate that the results obtained at the end of a full analysis might be meager. Indeed, the torus wrapping numbers of the three-cycles used

Combinations of hidden stacks fulfilling the bulk RR-tad.c.c.																	
N_1	N_2	N_3	N_4	N_5	N_6	N_7	N_8	N_9	N_1	N_2	N_3	N_4	N_5	N_6	N_7	N_8	N_9
0	0	0	0	0	0	2	0	6	0	2	0	0	0	0	1	3	2
0	0	0	0	0	0	2	1	5	0	2	0	0	0	0	1	4	1
0	0	0	0	0	0	2	2	4	0	2	0	0	0	0	1	5	0
0	0	0	0	0	0	2	3	3	0	2	0	0	0	1	0	0	1
0	0	0	0	0	0	2	4	2	0	2	0	0	0	1	0	1	0
0	0	0	0	0	0	2	5	1	0	2	1	0	0	0	0	0	1
0	0	0	0	0	0	2	6	0	0	2	1	0	0	0	0	1	0
0	0	0	0	0	1	1	0	2	0	3	0	0	1	0	0	0	0
0	0	0	0	0	1	1	1	1	0	3	0	1	0	0	0	0	0
0	0	0	0	0	1	1	2	0	0	4	0	0	0	0	0	0	4
0	0	1	0	0	0	1	0	2	0	4	0	0	0	0	0	1	3
0	0	1	0	0	0	1	1	1	0	4	0	0	0	0	0	2	2
0	0	1	0	0	0	1	2	0	0	4	0	0	0	0	0	3	1
0	1	0	0	1	0	1	0	1	0	4	0	0	0	0	0	4	0
0	1	0	0	1	0	1	1	0	1	0	0	0	1	0	0	0	0
0	1	0	1	0	0	1	0	1	1	0	0	1	0	0	0	0	0
0	1	0	1	0	0	1	1	0	1	1	0	0	0	0	0	0	4
0	2	0	0	0	0	1	0	5	1	1	0	0	0	0	0	1	3
0	2	0	0	0	0	1	1	4	1	1	0	0	0	0	0	2	2
0	2	0	0	0	0	1	2	3	1	1	0	0	0	0	0	3	1
									1	1	0	0	0	0	0	4	0

Table 6.13: This table provides in total 41 combinations of the bulk three-cycles given in table 6.12 with various ranks N_i which satisfy both bulk RR-tadpole cancellation conditions (RR-tad.c.c.) in (6.11) exactly when added to the visible sector.

for the visible sector are already chosen to be as small as possible, so that they give the smallest possible contributions to the twisted RR-tadpole cancellation conditions. Still, all 256 combinations of the visible sector give a maximal contribution of ± 24 to at least one of the twisted RR-tadpole cancellation condition. The likelihood of this large contribution to be canceled exactly by a hidden sector is rather small. In comparison, in the case of ϱ-independent Pati-Salam models, the maximal contribution of the visible sector to the twisted RR-tadpole cancellation conditions was no more than ± 8, which can be canceled much more easily by an adequate hidden sector.

As a final remark, note that the issue of physically non-equivalent models was not addressed at all in this section, since the focus lied on detecting global models and not on analyzing local models.

All in all, instead of investing a lot more effort and time in a thorough analysis of all the possibilities of the hidden sector and different visible sectors and risking meager results, I preferred to drop any further search for global ϱ-dependent Pati-Salam models and rather concentrate on the phenomenology of the global models I already found.

Chapter 7

The construction of left-right symmetric and MSSM-like models

7.1 Five-stack and six-stack left-right symmetric models

Left-right symmetric models are closer in construction to the coveted MSSM than Pati-Salam models are. Therefore, they are more appealing from a phenomenological point of view than Pati-Salam models. Unfortunately, global models are also harder to construct as previous work on similar toroidal backgrounds has shown [187, 76].
The gauge group of the left-right symmetric model is given by $SU(3) \times SU(2)_L \times SU(2)_R \times U(1)_{B-L}$. Since we have four gauge factors, we need four stacks in order to construct left-right symmetric models. The conditions on the first two stacks denoted by a and b are similar to the conditions on the first two stacks of the Pati-Salam model. The first two stacks should be rigid, exempt of chiral matter states transforming in the symmetric representation, and the a stack should also be free of chiral matter states in the antisymmetric representation. Hence, the potential candidate three-cycles for the first two stacks are the same than those for the Pati-Salam models.
However, since previous work on similar backgrounds taught us that global left-right symmetric models are harder to realize than global Pati-Salam models, we will loosen the constraints on the c stack, so that the conditions on the third stack supporting $SU(2)_R$ are less stringent than in the case of the Pati-Salam models. Thus, the c stack can come with matter states in the symmetric or adjoint representation. Apart from the condition of giving rise to three generations of particles, no further condition is put on the c stack. The conditions on the b and c stacks are thus slightly asymmetric, despite the name of "left-right symmetric". On the fourth stack labeled by d, there are no constraints on the particle states other than giving rise to three generations of particles, because any irreducible representation under an Abelian $U(1)$ group is a singlet representation.
We have seen in the previous chapter that ϱ-independent models seem to be particularly inclined to give rise to global models. This is due to the fact that the torus wrapping numbers of three-cycles parallel to some O6-plane are quite small and thus the twisted RR-tadpole cancellation conditions are more easily fulfilled than in the ϱ-dependent case. On the other hand, we have seen that ϱ-dependent three-cycles tend to produce larger contributions to the twisted RR-tadpole cancellation conditions, so that global models are less likely to arise. Also, the number of possibilities for the construction of ϱ-dependent models is tremendous,

whereas the number of combinations for ϱ-independent models is rather small, which renders a systematic and complete analysis possible. Therefore, it is sensible to focus the search on ϱ-independent models. We will only give a brief overview of a quick scan for ϱ-dependent models in section 7.2.2.

7.1.1 Search for the visible sector of left-right symmetric models

Remember that for ϱ-independent models, the only suitable candidates of three-cycles for the a and b stacks are given by $a \uparrow\uparrow \Omega\mathcal{R}$ and $b \uparrow\uparrow \Omega\mathcal{R}\mathbb{Z}_2^{(1)}$ and $\eta_{\Omega\mathcal{R}\mathbb{Z}_2^{(2 \text{ or } 3)}} = -1$, as we have seen in the case of the Pati-Salam models in the previous chapter. For this choice of the exotic charge, the two bulk RR-tadpole cancellation conditions are given by:

$$\begin{aligned} &\textstyle\sum_{x\in\{a,b,c,d\}} N_x(2P_x + Q_x) = \frac{12}{1-b} + N_c(2P_c + Q_c) + (2P_d + Q_d) \leq 32\,, \\ &\textstyle\sum_{x\in\{a,b,c,d\}} N_x(V_x + b\,Q_x) = 0 \Rightarrow \tilde{V}_x = 0 \;\forall x\,. \end{aligned} \tag{7.1}$$

where $N_c = 2$ if no gauge symmetry enhancement is present on c and $N_c = 1$ if $USp(2)$ enhancement is present. Just as for the Pati-Salam models, these conditions permit to exclude a number of possible candidate three-cycles for the c and d stacks right from the beginning. Table 7.1 gives a list of all SUSY ϱ-independent bulk-three cycles which satisfy the second bulk RR-tadpole cancellation condition. We can already exclude the last bulk three-cycle in table 7.1, as it overshoots the first bulk RR-tadpole cancellation condition for both lattices **aAA** and **bAA**. This leaves only three candidate bulk three-cycles for the c and d stacks as well as any hidden stack.

Overview of SUSY bulk three-cycles in compliance with $\tilde{V}_x = 0 \;\; \forall\, \varrho$			
aAA lattice		**bAA** lattice	
bulk wrapping numbers	$(2P + Q, V)$	bulk wrapping numbers	$(2P + Q, V + \frac{1}{2}Q)$
$\Omega\mathcal{R} : (1,0;1,0;1,0)$	$(2,0)$	$\Omega\mathcal{R} : (2,-1;1,0;1,0)$	$(4,0)$
$\Omega\mathcal{R}\mathbb{Z}_2^{(1)} : (1,0;-1,2;1,-2)$	$(6,0)$	$\Omega\mathcal{R}\mathbb{Z}_2^{(1)} : (2,-1;-1,2;1,-2)$	$(12,0)$
$(1,0;2,1;3,-1)$	$(14,0)$	$(2,-1;2,1;3,-1)$	$(28,0)$
$(1,0;4,-1;3,1)$	$(26,0)$	$(2,-1;4,-1;3,1)$	$(52,0)$

Table 7.1: Bulk orbits of candidate three-cycles for the c and d stacks satisfying $\tilde{V}_x = 0$, in the context of ϱ-independent left-right symmetric models on the **a**/**bAA** lattices. Except for the last bulk orbit, the bulk three-cycles are consistent with the RR-tadpole cancellation conditions (7.1) and can be used for SUSY model building.

Left-right symmetric models on the bAA lattice

Once again, we will start the discussion with the **bAA** lattice. A look at table 7.1 and the RR-tadpole cancellation conditions (7.1) reveals that the last three bulk three-cycles have to be excluded, as their contributions overshoot the maximally allowed contribution $2P + Q > 8$ of the first bulk RR-tadpole cancellation condition. The only possibility left is

to take both the c and d stacks parallel to the $\Omega\mathcal{R}$-plane. In that case, the first bulk RR-tadpole cancellation is fulfilled, leaving no room for hidden sectors. However, as table 5.4 yields, taking c parallel to the $\Omega\mathcal{R}$-plane renders the realization of three generations of right-handed quarks impossible, i.e. $|\chi^{ac}+\chi^{ac'}|=3$, or $|\chi^{ac}|\equiv|\chi^{ac'}|=3$ with gauge symmetry enhancement on c cannot be satisfied. In conclusion, one can state that ϱ-independent left-right symmetric models can only be local on the **bAA** lattice on $T^6/(\mathbb{Z}_2\times\mathbb{Z}_6\times\Omega\mathcal{R})$ with discrete torsion.
Instead of providing examples of local models on the **bAA** lattice as we did for Pati-Salam models, we will rather continue our search for global models on the **aAA** lattice, since the primary goal is to find global models.

Left-right symmetric models on the aAA lattice

Contrarily to the **bAA** lattice, there are a priori three bulk three-cycles not overshooting the first bulk RR-tadpole cancellation condition on the **aAA** lattice. The second and third columns in table 7.2 provide an overview of all possible combinations for the c and d stacks with the mentioned three bulk three-cycles. The fourth and fifth columns indicate the contribution of these combinations to the first bulk RR-tadpole cancellation condition, on top of the contributions coming from the a and b stacks. The sixth column reveals whether three generations of right-handed quarks can be realized, i.e. whether $|\chi^{ac}+\chi^{ac'}|=3$, or $|\chi^{ac}|\equiv|\chi^{ac'}|=3$ with gauge symmetry enhancement on c can be satisfied. Note also that the correct chirality between the right-handed and left-handed quarks must be reflected in a relative sign, $\chi^{ac}+\chi^{ac'}=-\chi^{ab}$ or $\chi^{ac}=-\chi^{ab}$. The seventh column indicates if three generations of left-handed leptons can be realized, i.e. whether $|\chi^{bd}|=3$ with the correct chirality $\chi^{ab}=+\chi^{bd}$. Finally, the numbers in parentheses show the compatibility between the exigence of having three generations of right-handed quarks and three generations of left-handed leptons, with correct relative sign. The numbers indicate the amount of combinations of discrete parameters found fulfilling the aforementioned conditions. Note, however, the number indicated in table 7.2 counts non-equivalent models.

As already mentioned in the previous chapter in the case of the presented $SU(5)$ model and the global Pati-Salam models, classes of models can be identified. Also in the present case, models with identical relative $\mathbb{Z}_2$-eigenvalues $\Delta\tau_{ab}^{\mathbb{Z}_2^{(i)}}\equiv\tau_a^{\mathbb{Z}_2^{(i)}}-\tau_b^{\mathbb{Z}_2^{(i)}}$, $\Delta\tau_{ac}^{\mathbb{Z}_2^{(i)}}$, and $\Delta\tau_{ad}^{\mathbb{Z}_2^{(i)}}$ as well as identical shifts and Wilson lines always give rise to the same particle spectrum, so that they can be considered to be equivalent. We cross-checked explicitly for certain combinations of table 7.2 that the models with identical relative $\mathbb{Z}_2$-eigenvalues, identical Wilson lines and shifts always come at the number of four. Thus, the number of models given in table 7.2 corresponds to the number of independent models, which is four times less than the total number of models found.
Another remark concerns the fact that models with $\eta_{\Omega\mathcal{R}\mathbb{Z}_2^{(2)}}=-1$ are related to models with $\eta_{\Omega\mathcal{R}\mathbb{Z}_2^{(3)}}=-1$ via an exchange of the two-torus labels $i=2\leftrightarrow i=3$ of $T^2_{(i)}$, just as in the case of the global Pati-Salam models found in the previous chapter. We checked once more explicitly that we always obtained an equal amount of models for both choices of the exotic O6-plane charge. Thus, the overall total number of models has to be divided by eight in order to avoid counting redundant models and to obtain the number of non-equivalent models given in table 7.2.
Finally, it should be noted that in order to find the number of models given in table 7.2, we

Four-stack combinations with gauge group $U(3)_a \times USp(2)_b \times U(2)_c \vert\vert USp(2)_c \times U(1)_d$ on aAA						
	c stack	d stack	RR-tadpoles: $\sum_{x\in\{a,b,c,d\}}(2P_x + Q_x)$	≤ 32	$3\,q_R$	$3\,L$
1	$\Omega\mathcal{R}$	$\Omega\mathcal{R}$	$2N_a + 6N_b + 2N_c + 2N_d = 18$	✓	↯	✓$_{9840}$
2	$\Omega\mathcal{R}$ with $USp(2)_c$	$\Omega\mathcal{R}$	$2N_a + 6N_b + 2N_c + 2N_d = 16$	✓	↯	✓$_{2304}$
3	$\Omega\mathcal{R}$	$\Omega\mathcal{R}\mathbb{Z}_2^{(1)}$	$2N_a + 6N_b + 2N_c + 6N_d = 22$	✓	↯	✓$_{198720}$
4	$\Omega\mathcal{R}$ with $USp(2)_c$	$\Omega\mathcal{R}\mathbb{Z}_2^{(1)}$	$2N_a + 6N_b + 2N_c + 6N_d = 20$	✓	↯	✓$_{46080}$
5	$\Omega\mathcal{R}$	$(1,0;2,1;3,-1)$	$2N_a + 6N_b + 2N_c + 14N_d = 30$	✓	↯	✓$_{9936}$
6	$\Omega\mathcal{R}$ with $USp(2)_c$	$(1,0;2,1;3,-1)$	$2N_a + 6N_b + 2N_c + 14N_d = 28$	✓	↯	✓$_{2304}$
7	$\Omega\mathcal{R}\mathbb{Z}_2^{(1)}$	$\Omega\mathcal{R}$	$2N_a + 6N_b + 6N_c + 2N_d = 26$	✓	↯	✓$_{9984}$
8	$\Omega\mathcal{R}\mathbb{Z}_2^{(1)}$ with $USp(2)_c$	$\Omega\mathcal{R}$	$2N_a + 6N_b + 6N_c + 2N_d = 20$	✓	✓$_{59616}$	✓$_{2304}$(✓$_{288}$)
9	$\Omega\mathcal{R}\mathbb{Z}_2^{(1)}$	$\Omega\mathcal{R}\mathbb{Z}_2^{(1)}$	$2N_a + 6N_b + 6N_c + 6N_d = 30$	✓	↯	✓$_{197760}$
10	$\Omega\mathcal{R}\mathbb{Z}_2^{(1)}$ with $USp(2)_c$	$\Omega\mathcal{R}\mathbb{Z}_2^{(1)}$	$2N_a + 6N_b + 6N_c + 6N_d = 24$	✓	✓$_{59904}$	✓$_{46080}$(✓$_{5760}$)
11	$\Omega\mathcal{R}\mathbb{Z}_2^{(1)}$	$(1,0;2,1;3,-1)$	$2N_a + 6N_b + 6N_c + 14N_d = 38$	↯	↯	✓$_{9984}$
12	$\Omega\mathcal{R}\mathbb{Z}_2^{(1)}$ with $USp(2)_c$	$(1,0;2,1;3,-1)$	$2N_a + 6N_b + 6N_c + 14N_d = 32$	✓	✓$_{73728}$	✓$_{2304}$(✓$_{288}$)
13	$(1,0;2,1;3,-1)$	$\Omega\mathcal{R}$	$2N_a + 6N_b + 14N_c + 2N_d = 42$	↯	↯	✓$_{12288}$
14	$(1,0;2,1;3,-1)$	$\Omega\mathcal{R}\mathbb{Z}_2^{(1)}$	$2N_a + 6N_b + 14N_c + 6N_d = 46$	↯	↯	✓$_{245760}$
15	$(1,0;2,1;3,-1)$	$(1,0;2,1;3,-1)$	$2N_a + 6N_b + 14N_c + 14N_d = 54$	↯	↯	✓$_{12240}$

Table 7.2: Overview of candidate pairs of bulk three-cycles for the c and d stacks of SUSY left-right symmetric models on the **aAA** lattice, with exotic charge $\eta_{\Omega\mathcal{R}\mathbb{Z}_2^{(2\text{ or }3)}} = -1$. The fourth and fifth columns test the respective contributions to the first bulk RR-tadpole cancellation condition in (7.1) of the pairs of three-cycles displayed in the second and third columns, on top of the contributions coming from the a and b stacks. The sixth column verifies whether the condition of three right-handed quark generations is fulfilled, i.e. $|\chi^{ac}| \equiv |\chi^{ac'}| = 3$ for $USp(2)_c$ or $|\chi^{ac} + \chi^{ac'}| = 3$ for $U(2)_c$. The last column does the same for three left-handed lepton generations, i.e. $|\chi^{bd}| \equiv |\chi^{bd'}| = 3$. The symbol in parentheses in the last column tests compatibility between these two conditions. The correct chirality between left- and right-handed particles has been taken into account via sign factors. The subscript indicates the number of combinatorial possibilities of discrete parameters $(\vec{\sigma}_x)$, $(\vec{\tau}_x)$ and $(-1)^{\tau_x^{\mathbb{Z}_2^{(k)}}}$ for $x \in \{a,b,c,d\}$ with the constraints discussed in the main text. The original number was divided by eight in order to count only non-equivalent models as discussed in the main text. Concerning the a and b stacks, remember that we have the following configuration: $a \uparrow\uparrow \Omega\mathcal{R}$ and $b \uparrow\uparrow \Omega\mathcal{R}\mathbb{Z}_2^{(1)}$.

imposed the condition that if three-cycles have identical bulk orbits, they should differ by at least one discrete parameter in order to actually correspond to distinct fractional three-cycles. Also, when we are dealing with three-cycles parallel to O6-planes, the orientifold images of these only differ by the $\mathbb{Z}_2$-eigenvalues from the original three-cycles. The Wilson lines and shifts are not affected by the orientifold projection, while the $\mathbb{Z}_2$-eigenvalues transform as follows:

$$(-1)^{\tau^{\mathbb{Z}_2^{(i)}}} \overset{\Omega\mathcal{R}}{\to} \pm\eta_{(i)}(-1)^{2b^j\sigma^j\tau^j + 2b^k\sigma^k\tau^k}(-1)^{\tau^{\mathbb{Z}_2^{(i)}}}\,, \tag{7.2}$$

where i,j,k are cyclic permutations of 1,2,3, and $b^1 = b$, $b^2 = b^3 = 1/2$. The plus sign is used if the bulk part of the three-cycle is anti-parallel to its orientifold image on the i^{th} two-torus $T^2_{(i)}$. In the other cases, i.e. parallel cycles or cycles neither parallel nor anti-parallel, the minus sign is used. Thus, in case both cycles for the c and d stacks have the same bulk orbit and are parallel to some O6-plane, and have on top of that identical

Wilson lines and shifts, additional conditions have to be imposed on the $\mathbb{Z}_2$-eigenvalues in agreement with formula (7.2), so that the three-cycles are not orientifold images of each other. Without this condition, it is possible that the bifundamental representation produces a negative contribution to the beta-function coefficients, which does not make sense as the beta-function coefficients are supposed to count the total number of particles, irrespective of chirality. This happens because, if two stacks are orientifold images of each other, they do not give rise to the bifundamental representation, but rather to the symmetric or antisymmetric representation. Thus, the correct formulas to use for the beta-function coefficients would be those in table 3.4 and not table 3.3.
With all these conditions, we see that only combinations 8, 10 and 12 in table 7.2 are apt to provide a full three generation spectrum with all RR-tadpole cancellation conditions fulfilled.

7.1.2 Semi-global five-stack left-right symmetric models

In the following, we will analyze each of the three combinations 8, 10 and 12 and test their potential to give rise to global three generation left-right symmetric models. In table 7.2, there is one combination which fully satisfies the bulk RR-tadpole cancellation conditions: combination 12.

Combination 12: It remains to be seen whether combination 12 leads to a full three generation spectrum, that is to say, whether also three generations of right-handed leptons can be produced with $|\chi^{cd}| = 3$ and correct relative sign $\chi^{cd} = -\chi^{ab}$. With this additional condition, the number of models for combination 12 is reduced from 288 to 144. The final step consists in checking the local or global character of these 144 models. A full computer scan over all 144 models of combination 12 yielded that none of them would fulfill all twisted RR-tadpole cancellation conditions.

This leaves combinations 8 and 10. In order to fulfill the bulk RR-tadpole cancellation conditions exactly, hidden stacks have to be added, which should be chosen from table 7.1. Combination 8 leaves room for a contribution of 12 from the hidden sector, while combination 10 has room for a contribution of 8. Let us start with combination 8.

Combination 8: The aim is to have as few stacks as possible in the hidden sector. Hence, the first try consists in finding global five-stack left-right symmetric models with one stack in the hidden sector. Only if no such model can be found, should the hidden sector be extended to include two hidden stacks. There are two possibilities to realize a five-stack model with combination 8 with vanishing bulk RR-tadpole cancellation conditions. The first possibility consists in taking the hidden stack parallel to the $\Omega\mathcal{R}$-plane with rank $N_h = 6$. The second possibility is given by taking the hidden stack parallel to the $\Omega\mathcal{R}\mathbb{Z}_2^{(1)}$-plane, with rank $N_h = 2$. These are the only possibilities, as the other two bulk three-cycles in table 7.1 overshoot the room left in the first bulk RR-tadpole cancellation condition in (7.1). The additional constraint of giving rise to three generations of right-handed electrons does not reduce the number of 288 models in table 7.2 any further. However, a full computer scan over all 288 models revealed that none of them would fulfill all the twisted RR-tadpole cancellation conditions, for both possibilities of the hidden stack. Therefore, combination 8 can

only give rise to local five-stack left-right symmetric models.

Next, we will turn our attention to combination 10.

Combination 10: By adding the condition of having three generations of right-handed electrons, the number of non-equivalent models was reduced from 5 760 to 5 184. The only possibility to fulfill the first bulk RR-tadpole cancellation condition with one hidden stack exactly is to take the hidden stack parallel to the $\Omega\mathcal{R}$-plane with rank $N_h = 4$. A full computer scan over all 5 184 models yielded that 1 296 combinations of these 5 184 models with the hidden stack fulfill all twisted RR-tadpole cancellation conditions. However, contrarily to Pati-Salam models, this is still insufficient to guarantee the global character of the model. In fact, there is one last set of consistency conditions to fulfill, namely the K-theory constraints (2.51). In our Pati-Salam models, the rank of the a stack was four and thus even, and the hidden stack had also an even rank of six or two, depending on the class of model. Thus, these stacks already provide even contributions to the K-theory constraints. The b and c stacks had rank equal to one, but they presented gauge symmetry enhancement, so the intersection between these and the probe-branes also supporting gauge symmetry enhancement is zero. This is due to the fact that the intersection between two $\Omega\mathcal{R}$-even cycles (i.e. cycles invariant under the orientifold projection) is always zero, as we will see in chapter 8. Thus, the presented Pati-Salam models satisfying the RR-tadpole cancellation conditions were global models automatically. In the case of the left-right symmetric models though, the a stack has an odd rank of three, and does not support gauge symmetry enhancement. Hence, the K-theory constraints must be checked explicitly. A scan running over all 1 296 models checking the K-theory constraints in (2.51) yielded that none of the models would satisfy all the K-theory constraints. Consequently, these models are semi-global but not global, i.e. they satisfy the RR-tadpole cancellation conditions but not the K-theory constraints. In the following, we will give a concrete example of such a left-right symmetric model. In the next chapter, we will also derive an explicit analytical expression for the K-theory constraints, and show which of the K-theory constraints are violated for this particular model.
A computer scan over all 1 296 models revealed that the chiral particle content as well as the non-chiral particle spectrum is identical for all these models, up to the trivial exchange of the hidden stack h with its orientifold image h'. Since the naming of a stack and its orientifold image is arbitrary, this exchange has no profound physical meaning and is just an artificial construct. Thus, the spectra of all models are truly equivalent. Also, a complete computer scan over all 1 296 models revealed that there is no gauge symmetry enhancement on the hidden stack, meaning that the gauge group of the hidden stack is a unitary $U(4)$ group and not a symplectic $USp(8)$ or orthogonal $SO(8)$ group.
A prototype of a semi-global five-stack left-right symmetric model is presented in table 7.3.

The associated chiral and non-chiral open string spectrum to the model in table 7.3 is indicated in table 7.4.

As usual, we will discuss certain points of the particle content of table 7.4. In the visible sector, aside from three generations of left-handed and right-handed quarks and leptons, we also have electroweak Higgses in the bc sector. Less desirable from a phenomenological point of view is the abundant presence of non-chiral massless states in the visible sector, arising in the ad, ad', bd and cd sectors. Also, the visible sector is not completely decoupled from the hidden sector, as we have once again exotic states charged under both the visible and hidden

D6-brane configuration of a 5-stack Left-Right Symmetric model on the aAA lattice						
	wrapping numbers	$\frac{\text{Angle}}{\pi}$	$\mathbb{Z}_2^{(i)}$**-eigenvalues**	$(\vec{\tau})$	$(\vec{\sigma})$	**gauge group**
a	$(1,0;1,0;1,0)$	$(0,0,0)$	$(--+)$	$(0,1,1)$	$(0,1,1)$	$U(3)$
b	$(1,0;-1,2;1,-2)$	$(0,\frac{1}{2},-\frac{1}{2})$	$(+++)$	$(0,1,0)$	$(0,1,0)$	$USp(2)$
c	$(1,0;-1,2;1,-2)$	$(0,\frac{1}{2},-\frac{1}{2})$	$(-+-)$	$(0,1,0)$	$(0,1,0)$	$USp(2)$
d	$(1,0;-1,2;1,-2)$	$(0,\frac{1}{2},-\frac{1}{2})$	$(+--)$	$(0,0,0)$	$(0,0,0)$	$U(1)$
h	$(1,0;1,0;1,0)$	$(0,0,0)$	$(+++)$	$(0,1,1)$	$(0,1,1)$	$U(4)$

Table 7.3: Data of a semi-global left-right symmetric model consisting of five stacks of D6-branes with gauge group $SU(3)_a \times USp(2)_b \times USp(2)_c \times U(4)_h \times U(1)_a \times U(1)_d$ on the **aAA** lattice. The $\Omega\mathcal{R}\mathbb{Z}_2^{(3)}$-plane is chosen exotic with $\eta_{\Omega\mathcal{R}\mathbb{Z}_2^{(3)}} = -1$. The RR-tadpole cancellation conditions are satisfied, not so the K-theory constraints.

gauge factors. An intriguing feature is the fact that the model could also be interpreted as a five-stack Pati-Salam model, with the hidden stack h supporting the $SU(4)$ gauge group of the Pati-Salam model, and the a and d stacks corresponding to a $U(3) \times U(1)$ hidden sector. Interesting is the presence of Pati-Salam GUT Higgses $(\mathbf{1},\mathbf{1},\mathbf{2},\overline{\mathbf{4}})_{(0,0,-1)}$ in the ch or ch' sectors, rendering such a Pati-Salam model particularly appealing. Remember that in the previously presented global four-stack Pati-Salam models, GUT-Higgses were missing. On the other hand, the model presented in this section is semi-global only and not global, making it less attractive than the previous Pati-Salam models. A last remark concerns the outermost right columns in table 7.4, which indicate the charges of the particles under the discrete symmetries. We will come back to this point later in the next chapter.
Hitherto, we exhausted all the possibilities of construction of ϱ-independent five-stack left-right symmetric models. The analysis produced only semi-global models that are not global models, which is not so attractive a feature in model building. It is thus clear that in order to find global ϱ-independent left-right symmetric models, the models have to be extended to six-stack models, including two stacks in the hidden sector.

7.1.3 Global six-stack left-right symmetric models

Previously, we identified combinations 8 and 10 in table 7.2 as candidates suited to potentially give rise to global left-right symmetric models. In the current section, the aim is to complete combinations 8 and 10 by two hidden stacks to form global six-stack left-right symmetric models. Once again, we will start with combination 8.

Combination 8

Combination 8 left room for a total contribution of 12 in the hidden sector in order to fulfill the first bulk RR-tadpole cancellation condition. As can be deduced from table 7.1, only the first two bulk three-cycles of table 7.1 can be used, as the other ones already overshoot the maximally allowed contribution in the hidden sector. There are in total three possibilities to achieve a total contribution of 12 with two hidden stacks:

- Both hidden stacks are parallel to the $\Omega\mathcal{R}$-plane, with the following combinations of ranks: $N_{h_1} = N_{h_2} = 3$, $N_{h_1} = 4$ and $N_{h_2} = 2$, or $N_{h_1} = 5$ and $N_{h_2} = 1$. Of course,

Overview of the Spectrum for 5-stack Left-Right Symm. on the aAA lattice				
sector	state	$(SU(3)_a \times USp(2)_b \times USp(2)_c \times SU(4)_h)_{U(1)_a \times U(1)_d \times U(1)_h}$	$\mathbb{Z}_3$	$\mathbb{Z}_4$
$ab \equiv ab'$	Q_L	$3 \times (\mathbf{3}, \mathbf{2}, \mathbf{1}, \mathbf{1})_{(1,0,0)}$	1	0
$ac \equiv ac'$	Q_R	$3 \times (\overline{\mathbf{3}}, \mathbf{1}, \mathbf{2}, \mathbf{1})_{(-1,0,0)}$	2	0
ad		$(\mathbf{3}, \mathbf{1}, \mathbf{1}, \mathbf{1})_{(1,-1,0)} + h.c.$	1	0
ad'		$2 \times \left[(\mathbf{3}, \mathbf{1}, \mathbf{1}, \mathbf{1})_{(1,1,0)} + h.c.\right]$	$1\|\|2$	0
$bc \equiv bc'$	(H_u, H_d)	$10 \times (\mathbf{1}, \mathbf{2}, \mathbf{2}, \mathbf{1})_{(0,0,0)}$	0	0
$bd \equiv b'd$	L	$3 \times (\mathbf{1}, \mathbf{2}, \mathbf{1}, \mathbf{1})_{(0,-1,0)}$	0	0
$bd \equiv b'd$		$3 \times \left[(\mathbf{1}, \mathbf{2}, \mathbf{1}, \mathbf{1})_{(0,-1,0)} + h.c.\right]$	0	0
$cd \equiv c'd$	R	$3 \times (\mathbf{1}, \mathbf{1}, \mathbf{2}, \mathbf{1})_{(0,1,0)}$	0	0
$cd \equiv c'd$		$3 \times \left[(\mathbf{1}, \mathbf{1}, \mathbf{2}, \mathbf{1})_{(0,1,0)} + h.c.\right]$	0	0
ah		$2 \times \left[(\mathbf{3}, \mathbf{1}, \mathbf{1}, \overline{\mathbf{4}})_{(1,0,-1)} + h.c.\right]$	$1\|\|2$	$3\|\|1$
ah'		$(\mathbf{3}, \mathbf{1}, \mathbf{1}, \mathbf{4})_{(1,0,1)} + h.c.$	$1\|\|2$	$1\|\|3$
$bh \equiv b'h$		$3 \times (\mathbf{1}, \mathbf{2}, \mathbf{1}, \mathbf{4})_{(0,0,1)}$	0	1
$ch \equiv c'h$		$3 \times (\mathbf{1}, \mathbf{1}, \mathbf{2}, \overline{\mathbf{4}})_{(0,0,-1)}$	0	3
dh		$2 \times \left[(\mathbf{1}, \mathbf{1}, \mathbf{1}, \overline{\mathbf{4}})_{(0,1,-1)} + h.c.\right]$	0	$3\|\|1$
dh'		$(\mathbf{1}, \mathbf{1}, \mathbf{1}, \mathbf{4})_{(0,1,1)} + h.c.$	0	1
aa'		$2 \times [(\overline{\mathbf{3}}_\mathbf{A}, \mathbf{1}, \mathbf{1}, \mathbf{1})_{(2,0,0)} + h.c.]$	$2\|\|1$	0
$bb' \equiv bb$		$5 \times (\mathbf{1}, \mathbf{1}_\mathbf{A}, \mathbf{1}, \mathbf{1})_{(0,0,0)}$	0	0
$cc' \equiv cc$		$5 \times (\mathbf{1}, \mathbf{1}, \mathbf{1}_\mathbf{A}, \mathbf{1})_{(0,0,0)}$	0	0
dd		$4 \times (\mathbf{1}, \mathbf{1}, \mathbf{1}, \mathbf{1})_{(0,0,0)}$	0	0
hh'		$2 \times [(\mathbf{1}, \mathbf{1}, \mathbf{1}, \mathbf{6}_\mathbf{A})_{(0,0,2)} + h.c.]$	0	2

Table 7.4: Overview of the chiral and non-chiral massless particle content associated to the semi-global left-right symmetric model with D6-brane configuration given in table 7.3. Anticipating the results from chapter 8, the last two columns display the charges of the particles under two discrete $\mathbb{Z}_n$-symmetries for future reference. For non-chiral pairs of particles, we denoted the $\mathbb{Z}_n$-charges by the logic symbol ||.

for the last two combinations the ranks can be switched, but this would only lead to equivalent models as the hidden sector is symmetric in its two stacks.

- Both hidden stacks are parallel to the $\Omega\mathcal{R}\mathbb{Z}_2^{(1)}$-plane, each one coming with a rank of one, $N_{h_1} = N_{h_2} = 1$.

- The first hidden stack is parallel to the $\Omega\mathcal{R}$-plane with rank $N_{h_1} = 3$ and the second stack is parallel to the $\Omega\mathcal{R}\mathbb{Z}_2^{(1)}$-plane with rank $N_{h_2} = 1$. Of course, the two stacks can be switched, but this would only lead to equivalent models.

We will discuss each of these possibilities, starting with the third possibility listed in the bullet points above.

$h_1 \uparrow\uparrow \Omega\mathcal{R}$ and $h_2 \uparrow\uparrow \Omega\mathcal{R}\mathbb{Z}_2^{(1)}$: A complete computer scan over all combinations of the 288 local four-stack models with the two hidden stacks revealed a total of 20 736 six-stack left-right symmetric models satisfying all twisted RR-tadpole cancellation conditions. However, the same scan also revealed that none of these models would satisfy all the K-theory constraints. Thus, these models with an inhomogeneous hidden sector are semi-global models but not global models. Since we have already presented a semi-global five-stack left-right symmetric model in the previous section, we will not analyze these semi-global six-stack models any further. Instead, we will turn our attention to the two possibilities with an homogeneous hidden sector.

$h_1 \uparrow\uparrow \Omega\mathcal{R}$ and $h_2 \uparrow\uparrow \Omega\mathcal{R}$: A full computer scan yielded that the first possibility listed in the bullet points above with $N_{h_1} = 4$, $N_{h_2} = 2$ and $N_{h_1} = 5$, $N_{h_2} = 1$, produces only local models. Actually, a probe-wise computer scan on the semi-global six-stack models found in this section revealed that the contributions from the visible sector and the hidden sector to the twisted RR-tadpole cancellation conditions generally cancel separately. Therefore, introducing an asymmetry in the hidden sector by giving different ranks to the two hidden stacks leads to the fact that the contributions from the two hidden stacks do not cancel each other anymore. Also, the asymmetry in the ranks cannot easily be compensated by an asymmetry in the torus wrapping numbers, as the two hidden stacks are parallel to the same bulk three-cycle.
A complete computer scan yielded that the possibility with ranks in the hidden sector given by $N_{h_1} = N_{h_2} = 3$ allows for a total of 271 296 semi-global models, 105 408 of which are also global models. This number can be divided by two, as the hidden sector is completely symmetric, allowing for a simple switch of the two hidden stacks $h_1 \leftrightarrow h_2$. None of the models present gauge symmetry enhancement in the hidden sector, which was checked explicitly. In general, it is hard to produce a complete analysis of six-stack models, for their number is large compared to five-stack models and thus substantial computational power and processing time is needed. Therefore, the classification of models is done by checking explicitly several examples in order to provide prototypes. A concise example of a global six-stack left-right symmetric model with hidden gauge group $U(3) \times U(3)$, which we will refer to as prototype I, is provided in table 7.5.

D6-brane configuration for a 6-stack LRS model (prototype I) on the aAA lattice						
	wrapping numbers	$\frac{\text{Angle}}{\pi}$	$\mathbb{Z}_2^{(i)}$**-eigenvalues**	$(\vec{\tau})$	$(\vec{\sigma})$	**gauge group**
a	$(1,0;1,0;1,0)$	$(0,0,0)$	$(+++)$	$(0,1,1)$	$(0,1,1)$	$U(3)$
b	$(1,0;-1,2;1,-2)$	$(0,\frac{1}{2},-\frac{1}{2})$	$(+++)$	$(0,1,0)$	$(0,1,0)$	$USp(2)$
c	$(1,0;-1,2;1,-2)$	$(0,\frac{1}{2},-\frac{1}{2})$	$(-+-)$	$(0,1,0)$	$(0,1,0)$	$USp(2)$
d	$(1,0;1,0;1,0)$	$(0,0,0)$	$(+--)$	$(0,1,1)$	$(0,1,1)$	$U(1)$
h_1	$(1,0;1,0;1,0)$	$(0,0,0)$	$(+++)$	$(0,0,0)$	$(0,0,0)$	$U(3)$
h_2	$(1,0;1,0;1,0)$	$(0,0,0)$	$(+--)$	$(0,0,0)$	$(0,0,0)$	$U(3)$

Table 7.5: Data of a global left-right symmetric model consisting of six stacks of D6-branes with gauge group $SU(3)_a \times USp(2)_b \times USp(2)_c \times SU(3)_{h_1} \times SU(3)_{h_2} \times U(1)_a \times U(1)_d \times U(1)_{h_1} \times U(1)_{h_2}$ on the **aAA** lattice. The $\Omega\mathcal{R}\mathbb{Z}_2^{(3)}$-plane is chosen exotic with $\eta_{\Omega\mathcal{R}\mathbb{Z}_2^{(3)}} = -1$.

The corresponding massless chiral and non-chiral open string spectrum is given in table 7.6.

Overview of the Spectrum for prototype I LRS Model on the aAA lattice					
sector	state	$(SU(3)_a \times USp(2)_b \times USp(2)_c \times SU(3)_{h_1} \times SU(3)_{h_2})_{U(1)_a \times U(1)_d \times U(1)_{h_1} \times U(1)_{h_2}}$	$\mathbb{Z}_2$	$\mathbb{Z}_3$	$\mathbb{Z}_6$
$ab \equiv ab'$	Q_L	$3 \times (\mathbf{3},\mathbf{2},\mathbf{1},\mathbf{1},\mathbf{1})_{(1,0,0,0)}$	1	1	1
$ac \equiv ac'$	Q_R	$3 \times (\overline{\mathbf{3}},\mathbf{1},\mathbf{2},\mathbf{1},\mathbf{1})_{(-1,0,0,0)}$	1	2	5
ad		$(\mathbf{3},\mathbf{1},\mathbf{1},\mathbf{1},\mathbf{1})_{(1,-1,0,0)} + h.c.$	0	1||2	4||2
ad'		$2 \times \left[(\mathbf{3},\mathbf{1},\mathbf{1},\mathbf{1},\mathbf{1})_{(1,1,0,0)} + h.c.\right]$	0	1||2	4||2
$bc \equiv bc'$	(H_u, H_d)	$10 \times (\mathbf{1},\mathbf{2},\mathbf{2},\mathbf{1},\mathbf{1})_{(0,0,0,0)}$	0	0	0
$bd \equiv b'd$	L	$3 \times (\mathbf{1},\mathbf{2},\mathbf{1},\mathbf{1},\mathbf{1})_{(0,-1,0,0)}$	1	0	3
$cd \equiv c'd$	R	$3 \times (\mathbf{1},\mathbf{1},\mathbf{2},\mathbf{1},\mathbf{1})_{(0,1,0,0)}$	1	0	3
ah_1		$2 \times (\overline{\mathbf{3}},\mathbf{1},\mathbf{1},\mathbf{3},\mathbf{1})_{(-1,0,1,0)}$	0	0	0
ah_2		$2 \times (\mathbf{3},\mathbf{1},\mathbf{1},\mathbf{1},\overline{\mathbf{3}})_{(1,0,0,-1)}$	0	0	0
$bh_1 \equiv b'h_1$		$(\mathbf{1},\mathbf{2},\mathbf{1},\overline{\mathbf{3}},\mathbf{1})_{(0,0,-1,0)}$	1	2	5
$bh_1 \equiv b'h_1$		$(\mathbf{1},\mathbf{2},\mathbf{1},\overline{\mathbf{3}},\mathbf{1})_{(0,0,-1,0)} + h.c.$	1	2||1	5||1
$bh_2 \equiv b'h_2$		$(\mathbf{1},\mathbf{2},\mathbf{1},\mathbf{1},\mathbf{3})_{(0,0,0,1)}$	1	1	1
$bh_2 \equiv b'h_2$		$(\mathbf{1},\mathbf{2},\mathbf{1},\mathbf{1},\mathbf{3})_{(0,0,0,1)} + h.c.$	1	1||2	1||5
$ch_1 \equiv c'h_1$		$(\mathbf{1},\mathbf{1},\mathbf{2},\overline{\mathbf{3}},\mathbf{1})_{(0,0,-1,0)}$	1	2	5
$ch_1 \equiv c'h_1$		$(\mathbf{1},\mathbf{1},\mathbf{2},\overline{\mathbf{3}},\mathbf{1})_{(0,0,-1,0)} + h.c.$	1	2||1	5||1
$ch_2 \equiv c'h_2$		$(\mathbf{1},\mathbf{1},\mathbf{2},\mathbf{1},\mathbf{3})_{(0,0,0,1)}$	1	1	1
$ch_2 \equiv c'h_2$		$(\mathbf{1},\mathbf{1},\mathbf{2},\mathbf{1},\mathbf{3})_{(0,0,0,1)} + h.c.$	1	1||2	1||5
dh_1		$2 \times (\mathbf{1},\mathbf{1},\mathbf{1},\overline{\mathbf{3}},\mathbf{1})_{(0,1,-1,0)}$	0	2	2
dh_2		$2 \times (\mathbf{1},\mathbf{1},\mathbf{1},\mathbf{1},\mathbf{3})_{(0,-1,0,1)}$	0	1	4
h_1h_2		$(\mathbf{1},\mathbf{1},\mathbf{1},\mathbf{3},\overline{\mathbf{3}})_{(0,0,1,-1)} + h.c.$	0	0	0
h_1h_2'		$2 \times \left[(\mathbf{1},\mathbf{1},\mathbf{1},\mathbf{3},\mathbf{3})_{(0,0,1,1)} + h.c.\right]$	0	2||1	2||4
aa'		$2 \times [(\overline{\mathbf{3}}_\mathbf{A},\mathbf{1},\mathbf{1},\mathbf{1},\mathbf{1})_{(2,0,0,0)} + h.c.]$	0	2||1	2||4
$bb' \equiv bb$		$5 \times (\mathbf{1},\mathbf{1}_\mathbf{A},\mathbf{1},\mathbf{1},\mathbf{1})_{(0,0,0,0)}$	0	0	0
$cc' \equiv cc$		$5 \times (\mathbf{1},\mathbf{1},\mathbf{1}_\mathbf{A},\mathbf{1},\mathbf{1})_{(0,0,0,0)}$	0	0	0
h_1h_1'		$2 \times [(\mathbf{1},\mathbf{1},\mathbf{1},\overline{\mathbf{3}}_\mathbf{A},\mathbf{1})_{(0,0,2,0)} + h.c.]$	0	2||1	2||4
h_2h_2'		$2 \times [(\mathbf{1},\mathbf{1},\mathbf{1},\mathbf{1},\overline{\mathbf{3}}_\mathbf{A})_{(0,0,0,2)} + h.c.]$	0	2||1	2||4

Table 7.6: Overview of the chiral and non-chiral massless particle content associated to the prototype I left-right symmetric model with D6-brane configuration given in table 7.5. Anticipating the results from chapter 8, the last three columns display the charges of the particles under three discrete $\mathbb{Z}_n$-symmetries for future reference. For non-chiral pairs of particles, we denoted the $\mathbb{Z}_n$-charges by the logic symbol ||.

Table 7.6 shows that this time, non-chiral matter states arise in the visible sector only in the ad, ad' sectors. Once again, we have three generations of leptons and quarks as well as several electroweak Higgses. A shortcoming of the model is the coupling of the visible sector to the hidden sector through numerous chiral exotic particles.

There remains one last possibility to be tested for combination number 8, namely the hidden sector supporting gauge groups with rank one.

$h_1 \uparrow\uparrow \Omega\mathcal{R}\mathbb{Z}_2^{(1)}$ and $h_2 \uparrow\uparrow \Omega\mathcal{R}\mathbb{Z}_2^{(1)}$: A complete computer scan revealed 271 872 semi-global models, 105 984 of which are also global models. Once again, the hidden sector is symmetric in its two stacks, so this number can be divided by two. Also, none of the models presented gauge symmetry enhancement in the hidden sector. An explicit example is provided in table 7.7, its associated massless open string spectrum can be found in table 7.8.

D6-brane configuration for a 6-stack LRS model (prototype II) on the aAA lattice						
	wrapping numbers	$\frac{\text{Angle}}{\pi}$	$\mathbb{Z}_2^{(i)}$**-eigenvalues**	$(\vec{\tau})$	$(\vec{\sigma})$	**gauge group**
a	$(1,0;1,0;1,0)$	$(0,0,0)$	$(+++)$	$(0,1,1)$	$(0,1,1)$	$U(3)$
b	$(1,0;-1,2;1,-2)$	$(0,\frac{1}{2},-\frac{1}{2})$	$(+++)$	$(0,1,0)$	$(0,1,0)$	$USp(2)$
c	$(1,0;-1,2;1,-2)$	$(0,\frac{1}{2},-\frac{1}{2})$	$(-+-)$	$(0,1,0)$	$(0,1,0)$	$USp(2)$
d	$(1,0;1,0;1,0)$	$(0,0,0)$	$(+--)$	$(0,1,1)$	$(0,1,1)$	$U(1)$
h_1	$(1,0;-1,2;1,-2)$	$(0,\frac{1}{2},-\frac{1}{2})$	$(+++)$	$(0,0,0)$	$(0,0,0)$	$U(1)$
h_2	$(1,0;-1,2;1,-2)$	$(0,\frac{1}{2},-\frac{1}{2})$	$(+--)$	$(0,0,0)$	$(0,0,0)$	$U(1)$

Table 7.7: Data of a global left-right symmetric model consisting of six stacks of D6-branes with gauge group $SU(3)_a \times USp(2)_b \times USp(2)_c \times U(1)_a \times U(1)_d \times U(1)_{h_1} \times U(1)_{h_2}$ on the **aAA** lattice. The $\Omega\mathcal{R}\mathbb{Z}_2^{(3)}$-plane is chosen exotic with $\eta_{\Omega\mathcal{R}\mathbb{Z}_2^{(3)}} = -1$.

Overview of the spectrum for prototype II LRS model on the aAA lattice				
sector	state	$(SU(3)_a \times USp(2)_b \times USp(2)_c)_{U(1)_a \times U(1)_d \times U(1)_{h_1} \times U(1)_{h_2}}$	$\widetilde{U(1)}_{B-L}$	$\mathbb{Z}_6$
$ab \equiv ab'$	Q_L	$3 \times (\mathbf{3},\mathbf{2},\mathbf{1})_{(1,0,0,0)}$	$1/3$	1
$ac \equiv ac'$	Q_R	$3 \times (\overline{\mathbf{3}},\mathbf{1},\mathbf{2})_{(-1,0,0,0)}$	$-1/3$	5
ad	$X^{ad} + \tilde{X}^{ad}$	$(\mathbf{3},\mathbf{1},\mathbf{1})_{(1,-1,0,0)} + h.c.$	$\pm 4/3$	$4\|\|2$
ad'	$X^{ad'(i)} + \tilde{X}^{ad'(i)}$	$2 \times \left[(\mathbf{3},\mathbf{1},\mathbf{1})_{(1,1,0,0)} + h.c.\right]$	$\mp 2/3$	$4\|\|2$
$bc \equiv bc'$	(H_u, H_d)	$10 \times (\mathbf{1},\mathbf{2},\mathbf{2})_{(0,0,0,0)}$	0	0
$bd \equiv b'd$	L	$3 \times (\mathbf{1},\mathbf{2},\mathbf{1})_{(0,-1,0,0)}$	1	3
$cd \equiv c'd$	R	$3 \times (\mathbf{1},\mathbf{1},\mathbf{2})_{(0,1,0,0)}$	-1	3
ah_1		$2 \times \left[(\mathbf{3},\mathbf{1},\mathbf{1})_{(1,0,-1,0)} + h.c.\right]$	$\pm 4/3$	$4\|\|2$
ah_1'		$(\mathbf{3},\mathbf{1},\mathbf{1})_{(1,0,1,0)} + h.c.$	$\mp 2/3$	$4\|\|2$
ah_2		$2 \times \left[(\mathbf{3},\mathbf{1},\mathbf{1})_{(1,0,0,-1)} + h.c.\right]$	$\mp 2/3$	$4\|\|2$
ah_2'		$(\mathbf{3},\mathbf{1},\mathbf{1})_{(1,0,0,1)} + h.c.$	$\pm 4/3$	$4\|\|2$
$bh_1 \equiv b'h_1$		$3 \times (\mathbf{1},\mathbf{2},\mathbf{1})_{(0,0,1,0)}$	-1	3
$bh_1 \equiv b'h_1$		$3 \times \left[(\mathbf{1},\mathbf{2},\mathbf{1})_{(0,0,-1,0)} + h.c.\right]$	± 1	3
$bh_2 \equiv b'h_2$		$3 \times (\mathbf{1},\mathbf{2},\mathbf{1})_{(0,0,0,-1)}$	-1	3
$bh_2 \equiv b'h_2$		$3 \left[\times(\mathbf{1},\mathbf{2},\mathbf{1})_{(0,0,0,1)} + h.c.\right]$	± 1	3
$ch_1 \equiv c'h_1$		$3 \times (\mathbf{1},\mathbf{1},\mathbf{2})_{(0,0,-1,0)}$	1	3
$ch_1 \equiv c'h_1$		$3 \times \left[(\mathbf{1},\mathbf{1},\mathbf{2})_{(0,0,1,0)} + h.c.\right]$	∓ 1	3
$ch_2 \equiv c'h_2$		$3 \times (\mathbf{1},\mathbf{1},\mathbf{2})_{(0,0,0,1)}$	1	3
$ch_2 \equiv c'h_2$		$3 \left[\times(\mathbf{1},\mathbf{1},\mathbf{2})_{(0,0,0,1)} + h.c.\right]$	± 1	3
dh_1	$X^{dh_1(i)} + \tilde{X}^{dh_1(i)}$	$2 \times \left[(\mathbf{1},\mathbf{1},\mathbf{1})_{(0,1,-1,0)} + h.c.\right]$	0	0
dh_1'	$X^{dh_1'} + \tilde{X}^{dh_1'}$	$(\mathbf{1},\mathbf{1},\mathbf{1})_{(0,1,1,0)} + h.c.$	∓ 2	0
dh_2	$X^{dh_2(i)} + \tilde{X}^{dh_2(i)}$	$2 \times \left[(\mathbf{1},\mathbf{1},\mathbf{1})_{(0,1,0,-1)} + h.c.\right]$	∓ 2	0
dh_2'	$X^{dh_2'} + \tilde{X}^{dh_2'}$	$(\mathbf{1},\mathbf{1},\mathbf{1})_{(0,1,0,1)} + h.c.$	0	0
h_1h_2		$5 \times \left[(\mathbf{1},\mathbf{1},\mathbf{1})_{(0,0,1,-1)} + h.c.\right]$	∓ 2	0
h_1h_2'		$6 \times \left[(\mathbf{1},\mathbf{1},\mathbf{1})_{(0,0,1,1)} + h.c.\right]$	0	0
aa'		$2 \times [(\overline{\mathbf{3}}_{\mathbf{A}},\mathbf{1},\mathbf{1})_{(2,0,0,0)} + h.c.]$	$\pm 2/3$	$2\|\|4$
$bb' \equiv bb$		$5 \times (\mathbf{1},\mathbf{1}_{\mathbf{A}},\mathbf{1})_{(0,0,0,0)}$	0	0
$cc' \equiv cc$		$5 \times (\mathbf{1},\mathbf{1},\mathbf{1}_{\mathbf{A}})_{(0,0,0,0)}$	0	0
h_1h_1		$4 \times (\mathbf{1},\mathbf{1},\mathbf{1})_{(0,0,0,0)}$	0	0
h_2h_2		$4 \times (\mathbf{1},\mathbf{1},\mathbf{1})_{(0,0,0,0)}$	0	0

Table 7.8: Overview of the chiral and non-chiral massless particle content associated to the prototype II left-right symmetric model with D6-brane configuration given in table 7.7. Anticipating the results from chapter 8, the second-to-last column displays the charges of the particles under a gauged generalized baryon-lepton number $U(1)$-symmetry for future reference, while the last column provides the charges under a discrete $\mathbb{Z}_6$-symmetry.

The visible spectrum of both prototypes in tables 7.6 and 7.8 is identical since we chose identical stacks a, b, c and d. The main difference in the spectrum is thus located in the hidden sector. Indeed, for prototype II, the chiral exotic particles are even more abundant than in prototype I. There are other fundamental differences between the properties of the two prototypes, as will be pointed out in the next chapter 8 about discrete symmetries.
Our probe-wise scan over the spectra of the global six-stack left-right symmetric models arising from combination 8 with hidden group $U(1) \times U(1)$ unearthed other prototypes with different particle content in the hidden sector.
We refer to these additional prototypes as prototype IIb and IIc. Prototype IIb is particularly interesting because it comes with a hidden sector completely decoupled from the visible sector. An explicit configuration for a prototype IIb model is given in table 7.9 with its associated massless chiral and non-chiral open string spectrum indicated in table 7.10.

D6-brane configuration for a 6-stack LRS model (prototype IIb) on the aAA lattice						
	wrapping numbers	$\frac{\text{Angle}}{\pi}$	$\mathbb{Z}_2^{(i)}$**-eigenvalues**	$(\vec{\tau})$	$(\vec{\sigma})$	**gauge group**
a	$(1,0;1,0;1,0)$	$(0,0,0)$	$(--+)$	$(0,1,1)$	$(1,1,1)$	$U(3)$
b	$(1,0;-1,2;1,-2)$	$(0,\frac{1}{2},-\frac{1}{2})$	$(+--)$	$(0,1,0)$	$(1,1,0)$	$USp(2)$
c	$(1,0;-1,2;1,-2)$	$(0,\frac{1}{2},-\frac{1}{2})$	$(--+)$	$(0,1,0)$	$(1,1,0)$	$USp(2)$
d	$(1,0;1,0;1,0)$	$(0,0,0)$	$(-+-)$	$(0,1,1)$	$(1,1,1)$	$U(1)$
h_1	$(1,0;-1,2;1,-2)$	$(0,\frac{1}{2},-\frac{1}{2})$	$(-+-)$	$(0,0,0)$	$(0,0,0)$	$U(1)$
h_2	$(1,0;-1,2;1,-2)$	$(0,\frac{1}{2},-\frac{1}{2})$	$(--+)$	$(0,0,0)$	$(0,0,0)$	$U(1)$

Table 7.9: Data of a global left-right symmetric model consisting of six stacks of D6-branes with gauge group $SU(3)_a \times USp(2)_b \times USp(2)_c \times U(1)_a \times U(1)_d \times U(1)_{h_1} \times U(1)_{h_2}$ on the **aAA** lattice. The $\Omega\mathcal{R}\mathbb{Z}_2^{(3)}$-plane is chosen exotic with $\eta_{\Omega\mathcal{R}\mathbb{Z}_2^{(3)}} = -1$.

An explicit model for prototype IIc is given in table 7.11 with its corresponding particle content in table 7.12.

Overview of the Spectrum for prototype IIb LRS Model on the aAA lattice			
sector	state	$(SU(3)_a \times USp(2)_b \times USp(2)_c)_{U(1)_a \times U(1)_d \times U(1)_{h_1} \times U(1)_{h_2}}$	$\widetilde{U(1)}_{B-L}$
$ab \equiv ab'$	Q_L	$3 \times (\mathbf{3}, \mathbf{2}, \mathbf{1})_{(1,0,0,0)}$	$1/3$
$ac \equiv ac'$	Q_R	$3 \times (\overline{\mathbf{3}}, \mathbf{1}, \mathbf{2})_{(-1,0,0,0)}$	$-1/3$
ad		$(\mathbf{3}, \mathbf{1}, \mathbf{1})_{(1,-1,0,0)} + h.c.$	$\pm 4/3$
ad'		$2 \times \left[(\mathbf{3}, \mathbf{1}, \mathbf{1})_{(1,1,0,0)} + h.c.\right]$	$\mp 2/3$
$bc \equiv bc'$	(H_u, H_d)	$10 \times (\mathbf{1}, \mathbf{2}, \mathbf{2})_{(0,0,0,0)}$	0
$bd \equiv b'd$	L	$3 \times (\mathbf{1}, \mathbf{2}, \mathbf{1})_{(0,-1,0,0)}$	1
$cd \equiv c'd$	R	$3 \times (\mathbf{1}, \mathbf{1}, \mathbf{2})_{(0,1,0,0)}$	-1
$h_1 h_2$		$5 \times \left[(\mathbf{1}, \mathbf{1}, \mathbf{1})_{(0,0,1,-1)} + h.c.\right]$	∓ 2
$h_1 h_2'$		$6 \times \left[(\mathbf{1}, \mathbf{1}, \mathbf{1})_{(0,0,1,1)} + h.c.\right]$	0
aa'		$2 \times [(\overline{\mathbf{3}}_{\mathbf{A}}, \mathbf{1}, \mathbf{1})_{(2,0,0,0)} + h.c.]$	$\pm 2/3$
$bb' \equiv bb$		$5 \times (\mathbf{1}, \mathbf{1}_{\mathbf{A}}, \mathbf{1})_{(0,0,0,0)}$	0
$cc' \equiv cc$		$5 \times (\mathbf{1}, \mathbf{1}, \mathbf{1}_{\mathbf{A}})_{(0,0,0,0)}$	0
$h_1 h_1$		$4 \times (\mathbf{1}, \mathbf{1}, \mathbf{1})_{(0,0,0,0)}$	0
$h_2 h_2$		$4 \times (\mathbf{1}, \mathbf{1}, \mathbf{1})_{(0,0,0,0)}$	0

Table 7.10: Overview of the chiral and non-chiral massless particle content associated to the prototype IIb left-right symmetric model with D6-brane configuration given in table 7.9. Anticipating the results from chapter 8, the last column displays the charges of the particles under the global, no longer gauged, generalized baryon-lepton number symmetry for future reference.

D6-brane configuration for a 6-stack LRS model (prototype IIc) on the aAA lattice						
	wrapping numbers	$\frac{\text{Angle}}{\pi}$	$\mathbb{Z}_2^{(i)}$**-eigenvalues**	$(\vec{\tau})$	$(\vec{\sigma})$	**gauge group**
a	$(1,0;1,0;1,0)$	$(0,0,0)$	$(--+)$	$(0,1,1)$	$(0,1,1)$	$U(3)$
b	$(1,0;-1,2;1,-2)$	$(0,\frac{1}{2},-\frac{1}{2})$	$(+--)$	$(0,1,0)$	$(0,1,0)$	$USp(2)$
c	$(1,0;-1,2;1,-2)$	$(0,\frac{1}{2},-\frac{1}{2})$	$(--+)$	$(0,1,0)$	$(0,1,0)$	$USp(2)$
d	$(1,0;1,0;1,0)$	$(0,0,0)$	$(-+-)$	$(0,1,1)$	$(0,1,1)$	$U(1)$
h_1	$(1,0;-1,2;1,-2)$	$(0,\frac{1}{2},-\frac{1}{2})$	$(+++)$	$(0,0,1)$	$(0,0,1)$	$U(1)$
h_2	$(1,0;-1,2;1,-2)$	$(0,\frac{1}{2},-\frac{1}{2})$	$(+++)$	$(0,0,1)$	$(1,1,1)$	$U(1)$

Table 7.11: Data of a global left-right symmetric model consisting of six stacks of D6-branes with gauge group $SU(3)_a \times USp(2)_b \times USp(2)_c \times U(1)_a \times U(1)_d \times U(1)_{h_1} \times U(1)_{h_2}$ on the **aAA** lattice. The $\Omega\mathcal{R}\mathbb{Z}_2^{(3)}$-plane is chosen exotic with $\eta_{\Omega\mathcal{R}\mathbb{Z}_2^{(3)}} = -1$.

Overview of the Spectrum for prototype IIc LRS Model on the aAA lattice			
sector	state	$(SU(3)_a \times USp(2)_b \times USp(2)_c)_{U(1)_a \times U(1)_d \times U(1)_{h_1} \times U(1)_{h_2}}$	$\widetilde{U(1)}_{B-L}$
$ab \equiv ab'$	Q_L	$3 \times (\mathbf{3}, \mathbf{2}, \mathbf{1})_{(1,0,0,0)}$	$1/3$
$ac \equiv ac'$	Q_R	$3 \times (\overline{\mathbf{3}}, \mathbf{1}, \mathbf{2})_{(-1,0,0,0)}$	$-1/3$
ad		$(\mathbf{3}, \mathbf{1}, \mathbf{1})_{(1,-1,0,0)} + h.c.$	$\pm 4/3$
ad'		$2 \times \left[(\mathbf{3}, \mathbf{1}, \mathbf{1})_{(1,1,0,0)} + h.c.\right]$	$\mp 2/3$
$bc \equiv bc'$	(H_u, H_d)	$10 \times (\mathbf{1}, \mathbf{2}, \mathbf{2})_{(0,0,0,0)}$	0
$bd \equiv b'd$	L	$3 \times (\mathbf{1}, \mathbf{2}, \mathbf{1})_{(0,-1,0,0)}$	1
$cd \equiv c'd$	R	$3 \times (\mathbf{1}, \mathbf{1}, \mathbf{2})_{(0,1,0,0)}$	-1
ah_1		$3 \times (\overline{\mathbf{3}}, \mathbf{1}, \mathbf{1})_{(-1,0,1,0)}$	$-4/3$
ah_1'		$3 \times (\mathbf{3}, \mathbf{1}, \mathbf{1})_{(1,0,1,0)}$	$-2/3$
$bh_1 \equiv b'h_1$		$4 \times \left[(\mathbf{1}, \mathbf{2}, \mathbf{1})_{(0,0,-1,0)} + h.c.\right]$	± 1
$ch_1 \equiv c'h_1$		$6 \times (\mathbf{1}, \mathbf{1}, \mathbf{2})_{(0,0,-1,0)}$	1
$ch_1 \equiv c'h_1$		$2 \times \left[(\mathbf{1}, \mathbf{1}, \mathbf{2})_{(0,0,1,0)} + h.c.\right]$	∓ 1
dh_1		$3 \times (\mathbf{1}, \mathbf{1}, \mathbf{1})_{(0,1,-1,0)}$	0
dh_1'		$3 \times (\mathbf{1}, \mathbf{1}, \mathbf{1})_{(0,-1,-1,0)}$	-2
aa'		$2 \times [(\overline{\mathbf{3}}_\mathbf{A}, \mathbf{1}, \mathbf{1})_{(2,0,0,0)} + h.c.]$	$\pm 2/3$
$bb' \equiv bb$		$5 \times (\mathbf{1}, \mathbf{1}_\mathbf{A}, \mathbf{1})_{(0,0,0,0)}$	0
$cc' \equiv cc$		$5 \times (\mathbf{1}, \mathbf{1}, \mathbf{1}_\mathbf{A})_{(0,0,0,0)}$	0
h_1h_1		$4 \times (\mathbf{1}, \mathbf{1}, \mathbf{1})_{(0,0,0,0)}$	0
h_2h_2		$4 \times (\mathbf{1}, \mathbf{1}, \mathbf{1})_{(0,0,0,0)}$	0

Table 7.12: Overview of the chiral and non-chiral massless particle content associated to the prototype IIc left-right symmetric model with D6-brane configuration given in table 7.11. Anticipating the results from chapter 8, the last column displays the charges of the particles under the global, no longer gauged, generalized baryon-lepton number symmetry for future reference.

All three prototypes of left-right symmetric models arising from combination 8 have an identical massless open string spectrum in the visible sector, but different ones in the hidden sector. Prototype IIb has the most attractive particle spectrum, as it does not only have no chiral exotics charged under both the visible and the hidden gauge factors, but it is even free of non-chiral exotics. Thus, its visible sector is completely decoupled from the hidden sector. The non-chiral pair charged solely under the hidden gauge could be a candidate for dark matter, as it can interact with the visible quarks and leptons of the Standard Model only via gravity and no other fundamental force.
As to the issue of the baryon-lepton number symmetry charges indicated in the outermost right column, more details will be given in the next chapter on discrete symmetries.

Combination 10

We now focus on combination 10, which comes with 5 184 candidates apt to be completed into global six-stack left-right symmetric models. These are more numerous than those from combination 8, and in the case of five-stack left-right symmetric models, they also proved to be more fertile since they allowed at least for semi-global models, contrarily to those of combination 8. The maximally allowed contribution from the hidden sector to the first bulk RR-tadpole cancellation condition is reduced to 8, though. Consequently, there are only two possibilities to add two hidden stacks summing up to a total contribution of 8:

- Both hidden stacks are parallel to the $\Omega\mathcal{R}$-plane, each having a rank equal to two, $N_{h_1} = N_{h_2} = 2$, or having ranks equal to $N_{h_1} = 3$ and $N_{h_2} = 1$. Once more, switching the ranks of the latter combination to $N_{h_1} = 1$ and $N_{h_2} = 3$ only leads to equivalent models.

- The first hidden stack is parallel to the $\Omega\mathcal{R}$-plane with rank $N_{h_1} = 1$ and the second hidden stack is parallel to the $\Omega\mathcal{R}\mathbb{Z}_2^{(1)}$-plane with equal rank $N_{h_2} = 1$. Once again, switching the hidden stacks does not lead to new non-equivalent models.

We will initiate the analysis with the first possibility.

$h_1 \uparrow\uparrow \Omega\mathcal{R}$ and $h_2 \uparrow\uparrow \Omega\mathcal{R}$: A full computer scan over the 5 184 candidates combined with the two hidden stacks having ranks $N_{h_1} = 3$ and $N_{h_2} = 1$ only yielded local models. Once again, this can be traced back to the asymmetry in the ranks of hidden stacks being parallel to the same bulk three-cycle.
A complete scan over all combinations of the 5 184 candidates with the two hidden stacks having ranks $N_{h_1} = N_{h_2} = 2$ produced 1 283 040 semi-global models, none of which would fulfill all the K-theory constraints. An interesting aspect of this combination is the fact that gauge symmetry enhancement in the hidden sectors is allowed for the semi-global models, contrarily to the models we have analyzed so far. Still, as we have already dug out a substantial number of global left-right symmetric models, we will not dally with semi-global models. Let us continue with the second possibility.

$h_1 \uparrow\uparrow \Omega\mathcal{R}$ and $h_2 \uparrow\uparrow \Omega\mathcal{R}\mathbb{Z}_2^{(1)}$: The computer scan counted 933 120 semi-global models, 20 736 of which were also global models. As typical, none of the models allowed for gauge symmetry enhancement in the hidden sector. Just as before, we computed the particle content for several examples, but found only one type of spectrum. This spectrum was identical

to the one of prototype II in table 7.8, except for an exchange of the d stack with the first hidden stack h_1, which leads to a large number of non-chiral matter states in the visible sector. The numbers of models found, however, indicate that there is no one-to-one relation between prototype II models arising from combination 8 and the models coming from combination 10. Indeed, the d stack cannot be simply exchanged systematically with the first hidden stack h_1, as we have conditions on d coming from the number of generations of the particle content, but no such conditions on the hidden stacks. Since we found one type of spectrum for combination 10, but three types of spectra from combination 8, we suspect that the models arising from combination 10 constitute a subset of the models arising from combination 8, regarding the particle content. However, since we did not perform a full computer scan over all models, there might be more prototypes lurking around. Note that different prototypes should produce different spectra which are not related through some trivial exchange of stacks or stacks and their orientifold images, such as $b \leftrightarrow c$, $h_1 \leftrightarrow h_2$ or $h_{i=1,2} \leftrightarrow h'_{i=1,2}$. In the chapters 8 and 9 about string phenomenology, we will concentrate on the models arising from combination 8, as they seem to provide more varied prototypes.

Table 7.13 provides an overview in numbers of all six-stack left-right symmetric models treated in the present and previous sections.

Summary of ϱ-independent LRS Models on the aAA lattice			
Combination	**Hidden gauge factor**	**Global**	**Semi-global**
$n°8$	$U(3)_{h_1} \times U(3)_{h_2}$	52 704	135 648
	$U(1)_{h_1} \times U(1)_{h_2}$	52 992	135 936
	$U(3)_{h_1} \times U(1)_{h_2}$	0	20 736
$n°10$	$U(4)_h$	0	1 296
	$U(1)_{h_1} \times U(1)_{h_2}$	20 736	933 120
	$U(2)_{h_1} \times U(2)_{h_2}$	0	1 283 040
	$USp(4)_{h_1} \times U(2)_{h_2}$	0	69 984
	$USp(4)_{h_1} \times USp(4)_{h_2}$	0	5 832

Table 7.13: List of ϱ-independent five- and six-stack left-right symmetric models on the **aAA** lattice with various hidden sectors. The second-to-last column gives the number of models satisfying both the RR-tadpole cancellation conditions and the K-theory constraints. The last column gives the number of models satisfying the RR-tadpole cancellation conditions. The initial number of models found was divided by eight in order to count only non-equivalent models as explained in the main text of section 7.1.1.

7.2 Searching for global MSSM-like D6-brane models

The MSSMs are the particle physics models hardest to construct in the set-up of Type IIA string theory. Previous work on similar toroidal compact spaces yielded few MSSMs as e.g. in [187], and these were always accompanied by unwanted features, such as global inconsistency or the presence of chiral multiplets transforming in the adjoint representation.

To my present knowledge, MSSM-like models with completely rigid D6-branes have not been constructed so far.

7.2.1 Global five-stack ϱ-independent MSSM-like models

As we already argued in the previous section, we will focus on the search for ϱ-independent models, as they seem to be more fertile. The gauge group of the Standard Model in particle physics is given by $SU(3)_{QCD} \times SU(2)_L \times U(1)_Y$. In our stringy set-up, this gauge group can be constructed either with three stacks supporting $U(3)_a \times U(2)_b \times U(1)_c$ (or $U(3)_a \times USp(2)_b \times U(1)_c$) or with four stacks supporting $U(3)_a \times U(2)_b \times U(1)_c \times U(1)_d$ (or $U(3)_a \times USp(2)_b \times U(1)_c \times U(1)_d$), as we presented it in section 3.2.1. The conditions on the a and b stacks are similar to the ones of the left-right symmetric models: the a and b stack must be rigid, support no chiral matter states in the symmetric representation, and a must present at most three chiral matter states in the antisymmetric representation. The three-cycles from the first entry of table 5.5 (corresponding to a parallel to the $\Omega\mathcal{R}$-plane and b parallel to the $\Omega\mathcal{R}\mathbb{Z}_2^{(1)}$-plane), which we have used so far to constitute ϱ-independent a and b stacks, fulfill all these requirements so that we can use them once more for the construction of MSSM models. There are a priori no conditions of rigidity and matter states in the (anti)symmetric representation on the c and d stacks. The numerous Abelian $U(1)$ factors combine into the hypercharge of the MSSM as follows:

$$\text{3-stack: } Q_Y = \frac{1}{6}Q_a + \frac{x_c}{2}Q_c, \qquad \text{4-stack: } Q_Y = \frac{1}{6}Q_a + \frac{x_c}{2}Q_c + \frac{x_d}{2}Q_d, \tag{7.3}$$

where $x_c, x_d \in \{\pm 1\}$. Comparing appendix B.1 to section 3.2.1 we see that a sign change of a $U(1)$-charge, for example $Q_c \leftrightarrow -Q_c$, is equivalent to exchanging the stack with its orientifold image $c \leftrightarrow c'$. The attribution of the name "orientifold image" to a three-cycle is arbitrary, and in order to exhaust all the possibilities of model building, the analysis should be done separately for all four definitions of the hypercharge. However, in our case, we are dealing with three-cycles the bulk parts of which are orientifold invariant. Thus, the three-cycles differ from their orientifold images only through the $\mathbb{Z}_2$-eigenvalues. Since we are always running our computer scans over all values for the discrete parameters, the exchange of the three-cycles with their orientifold images is already included in the analysis automatically. Exchanging the labels explicitly would lead to a redundant counting of models. Thus, in the current work, we will settle on the definition with plus-signs everywhere: $x_c = x_d = +1$. Note that also more exotic choices for the hypercharge like $Q_Y = \frac{1}{6}Q_a + \frac{1}{2}Q_c \pm \frac{3}{2}Q_d$ are excluded. Indeed, this last definition would imply that the right-handed down-quarks d_R must arise solely from the antisymmetric representation of the a stack. However, three-cycles parallel to some O6-plane do not give rise to chiral matter states transforming in the antisymmetric representation, whereupon this definition of the hypercharge must be rejected since the a stack is parallel to the $\Omega\mathcal{R}$-plane.
In the MSSM, the attribution of the chiral matter states to the different intersection sectors is more involved than in the case of the previously studied GUT models. Hence, we reproduce the precise conditions we imposed on the various intersection numbers in table 7.14. Note that in table 7.14, we took into account that we have gauge symmetry enhancement on the b stack, which simplifies the formulas lightly. Note also, that the conditions to impose a priori should be more stringent, including constraints on the signs of each term appearing in the

Overview of topological intersection # for chiral MSSM spectrum				
	$U(3)_a \times USp(2)_b \times U(1)_c$		$U(3)_a \times USp(2)_b \times U(1)_c \times U(1)_d$	
state	sector	chirality	sector	chirality
Q_L	ab	$\chi^{ab} \equiv \chi^{ab'} = \pm 3$	ab	$\chi^{ab} \equiv \chi^{ab'} = \pm 3$
d_R	ac	$\chi^{ac} = \mp 3$	$ac + ad$	$\chi^{ac} + \chi^{ad} = \mp 3$
u_R	ac'	$\chi^{ac'} = \mp 3$	$ac' + ad'$	$\chi^{ac'} + \chi^{ad'} = \mp 3$
L	bc	$\chi^{bc} = \pm 3$	$bc + bd$	$\chi^{bc} + \chi^{bd} = \pm 3$
e_R	cc'	$\chi^{\mathbf{Sym}_c} = \pm 3$	$cc' + dd' + cd'$	$\chi^{\mathbf{Sym}_c} + \chi^{\mathbf{Sym}_d} + \chi^{cd'} = \pm 3$

Table 7.14: Conditions on the intersection numbers of a three generation chiral MSSM-like spectrum with the hypercharge prescription $x_c = x_d = 1$ in eq. (7.3), for both three-stack and four-stack realizations of the MSSM. The four-stack realization was presented in section 3.2.1 in the most general case and is adapted in this table in order to take the particularities of the considered models into account. More precisely, the absence of antisymmetric representations on the a stack, gauge symmetry enhancement on the b stack and the restriction to the weaker conditions, as discussed in the main text, have been included in the conditions displayed in this table. As explained in section 3.2.1, the right-handed neutrinos ν_R can in principle be realized via any singlet states under the MSSM gauge group, provided that Yukawa couplings can be attributed to them.

sums, as can be reviewed in section 3.2.1. The stringent conditions should avoid the presence of too abundant pairs of non-chiral matter states in the visible sector. However, a complete computer scan revealed that no models could be found satisfying the strong constraints, not even local models. Therefore, we had to loosen the constraints from section 3.2.1 to the ones indicated in table 7.14.

As usual, we will start with the **bAA** lattice. Remember from formula (7.1) that the maximal allowed total contribution to the first bulk RR-tadpole cancellation condition after summation over the first two stacks equals $32 - \frac{12}{1-b} = 8$. Once again, table 7.1 tells us that the only candidate three-cycle for constituting the c or d stack must have its bulk orbit parallel to the $\Omega\mathcal{R}$-plane. This already excludes the possibility of a three-stack MSSM. In fact, table 5.4 tells us that three generations cannot be realized in the intersection sector of ac or ac' if both a and c stacks are parallel to the $\Omega\mathcal{R}$-plane. Looking in turn at table 7.14, we deduce that neither right-handed up-quarks nor right-handed down-quarks can come in three generations. Still, for the sake of completeness, we ran a computer scan in order to provide the number of left-handed leptons in table 7.15.

The situation is a bit different concerning the construction of four-stack MSSMs. Indeed, taking the c and d stacks both parallel to the $\Omega\mathcal{R}$-plane satisfies the bulk RR-tadpole cancellation conditions. Also, since the right-handed quarks are now realized as a sum over different intersection sectors, i.e. $ac + ad$ and $ac' + ad'$, we can no longer easily exclude right from the start the possibility of having a full three generation spectrum. However, a full computer scan revealed that no model can be found with three generations of right-handed quarks on the **bAA** lattice, see table 7.15. This can also be checked explicitly by use of the entries in table 5.4. On this account, we conclude once more that global ϱ-independent MSSMs cannot be realized on the **bAA** lattice on $T^6/(\mathbb{Z}_2 \times \mathbb{Z}_6 \times \Omega\mathcal{R})$ with discrete torsion.

3- or 4-stack combinations with gauge group $U(3)_a \times USp(2)_b \times U(1)_c\,(\times U(1)_d)$						
	c stack	d stack	RR-tadpoles: $\sum_{x\in\{a,b,c,d\}}(2P_x + Q_x)$	≤ 32	$3\,q_R$	$3\,L$
$3-$stack	$\Omega\mathcal{R}$		$4N_a + 12N_b + 4N_c = 28$	✓	↯	$\checkmark_{36}$
$4-$stack	$\Omega\mathcal{R}$	$\Omega\mathcal{R}$	$4N_a + 12N_b + 4N_c + 4N_d = 32$	✓	↯	$\checkmark_{19008}$

Table 7.15: Overview of candidate pairs of bulk three-cycles for the c and d stacks of ϱ-independent MSSM-like models on the **bAA** lattice, with exotic charge $\eta_{\Omega\mathcal{R}\mathbb{Z}_2^{(2\text{ or }3)}} = -1$. The fourth and fifth columns test the respective contributions to the first bulk RR-tadpole cancellation condition in (7.1) of the pairs of three-cycles displayed in the second and third columns, on top of the contributions coming from the a and b stacks. The sixth column verifies whether the condition of three right-handed quark generations is fulfilled according to table 7.14, and the last column does the same for three left-handed lepton generations. The subscript indicates the number of combinatorial possibilities of discrete parameters $(\vec{\sigma}_x)$, $(\vec{\tau}_x)$ and $(-1)^{\tau_x^{\mathbb{Z}_2^{(k)}}}$ for $x \in \{a,b,c,d\}$ with the constraints discussed in the main text of section 7.1.1. The original number was divided by eight in order to count only non-equivalent models as discussed in the main text.

Let us turn our attention to the **aAA** lattice. The total allowed contribution of the c and d stacks to the first RR-tadpole cancellation condition is $32 - \frac{12}{1-b} = 20$ for the **aAA** lattice. Thus, the first three bulk three-cycles in table 7.1 are potential candidates for supporting the c and d stacks. In table 7.16, we indicate all possible combinations for the c and d stacks with these three bulk three-cycles, for both three-stack and four-stack realizations of the MSSM. Although the last combination overshoots the first bulk RR-tadpole cancellation condition, we included it in the table for the sake of completeness.

Contrarily to the left-right symmetric models, gauge symmetry enhancement to symplectic groups on the c stack is not allowed, as the c stack of the MSSM should support an Abelian $U(1)$ gauge factor and not a symplectic $USp(2)$ group. Concerning gauge symmetry enhancement to orthogonal groups, table 5.1 yields that with our choice of the exotic charge $\eta_{\Omega\mathcal{R}\mathbb{Z}_2^{(2\text{ or }3)}} = -1$, $SO(2N)$ enhancement does not occur for three-cycles parallel to the $\Omega\mathcal{R}$-plane or the $\Omega\mathcal{R}\mathbb{Z}_2^{(1)}$-plane on the **aAA** lattice.

The numbers indicated in table 7.16 were found in the same way as those of table 7.2 for the left-right symmetric models, meaning we divided the original numbers by eight in order to eliminate equivalent models. Moreover, we imposed once more that the fractional three-cycles wrapping the c and d stacks must be different from each other and must not be orientifold images of each other.

In table 7.16, a symmetry manifests itself by an equal number of models upon the exchange of the c and d stacks. Table 7.14 shows that in the case of the four-stack realization of the MSSM, c and d appear symmetrically in the conditions on the particle spectrum, hence the symmetry upon the exchange $c \leftrightarrow d$. Combinations related by this symmetry are physically identical.

From table 7.16, we see that only combinations 5, 6 and 8 allow for three generations of right-handed quarks and left-handed leptons without overshooting the first bulk RR-tadpole cancellation condition. Combinations 6 and 8 fulfill the bulk RR-tadpole cancellation conditions exactly and leave no room for a hidden sector. However, a complete computer scan over these 144 + 144 models yielded that none of these would fulfill all the twisted RR-tadpole

Three-stack combinations with gauge group $U(3)_a \times USp(2)_b \times U(1)_c$					
	c stack	RR-tadpoles: $\sum_{x\in\{a,b,c\}}(2P_x + Q_x)$	≤ 32	$3\,q_R$	$3\,L$
1	$\Omega\mathcal{R}$	$2N_a + 6N_b + 2N_c + = 14$	✓	↯	✓$_{48}$
2	$\Omega\mathcal{R}\mathbb{Z}_2^{(1)}$	$2N_a + 6N_b + 6N_c = 18$	✓	↯	✓$_{960}$
3	$(1,0;2,1;3,-1)$	$2N_a + 6N_b + 14N_c = 26$	✓	↯	✓$_{48}$

Four-stack combinations with gauge group $U(3)_a \times USp(2)_b \times U(1)_c \times U(1)_d$						
	c stack	d stack	RR-tadpoles: $\sum_{x\in\{a,b,c,d\}}(2P_x + Q_x)$	≤ 32	$3\,q_R$	$3\,L$
1	$\Omega\mathcal{R}$	$\Omega\mathcal{R}$	$2N_a + 6N_b + 2N_c + 2N_d = 16$	✓	↯	✓$_{25344}$
2	$\Omega\mathcal{R}$	$\Omega\mathcal{R}\mathbb{Z}_2^{(1)}$	$2N_a + 6N_b + 2N_c + 6N_d = 20$	✓	↯	✓$_{157824}$
3	$\Omega\mathcal{R}$	$(1,0;2,1;3,-1)$	$2N_a + 6N_b + 2N_c + 14N_d = 28$	✓	↯	✓$_{23760}$
4	$\Omega\mathcal{R}\mathbb{Z}_2^{(1)}$	$\Omega\mathcal{R}$	$2N_a + 6N_b + 6N_c + 2N_d = 20$	✓	↯	✓$_{157824}$
5	$\Omega\mathcal{R}\mathbb{Z}_2^{(1)}$	$\Omega\mathcal{R}\mathbb{Z}_2^{(1)}$	$2N_a + 6N_b + 6N_c + 6N_d = 24$	✓	✓$_{1152}$	✓$_{316800}$(✓$_{576}$)
6	$\Omega\mathcal{R}\mathbb{Z}_2^{(1)}$	$(1,0;2,1;3,-1)$	$2N_a + 6N_b + 6N_c + 14N_d = 32$	✓	✓$_{576}$	✓$_{201024}$(✓$_{144}$)
7	$(1,0;2,1;3,-1)$	$\Omega\mathcal{R}$	$2N_a + 6N_b + 14N_c + 2N_d = 28$	✓	↯	✓$_{23760}$
8	$(1,0;2,1;3,-1)$	$\Omega\mathcal{R}\mathbb{Z}_2^{(1)}$	$2N_a + 6N_b + 14N_c + 6N_d = 32$	✓	✓$_{576}$	✓$_{201024}$(✓$_{144}$)
9	$(1,0;2,1;3,-1)$	$(1,0;2,1;3,-1)$	$2N_a + 6N_b + 14N_c + 14N_d = 40$	↯	↯	✓$_{24768}$

Table 7.16: Overview of candidate pairs of bulk three-cycles for the c and d stacks of ϱ-independent MSSM-like three- or four-stack models on the **aAA** lattice, with exotic charge $\eta_{\Omega\mathcal{R}\mathbb{Z}_2^{(2\text{ or }3)}} = -1$. The fourth and fifth columns test the respective contributions to the first bulk RR-tadpole cancellation condition in (7.1) of the pairs of three-cycles displayed in the second and third columns, on top of the contributions coming from the a and b stacks. The sixth column verifies whether the condition of three right-handed quark generations is fulfilled according to table 7.14, and the last column does the same for three left-handed lepton generations. The symbol in parentheses in the last column tests compatibility between these two conditions. The subscript indicates the number of combinatorial possibilities of discrete parameters $(\vec{\sigma}_x)$, $(\vec{\tau}_x)$ and $(-1)^{\tau_x^{\mathbb{Z}_2^{(k)}}}$ for $x \in \{a,b,c,d\}$ with the constraints discussed in the main text of section 7.1.1. The original number was divided by eight in order to count only non-equivalent models as discussed in the main text.

cancellation conditions.
This leaves only one combination to be completed with a hidden sector, namely combination 5. The additional condition on the right-handed electrons e_R does not reduce the number of 576 models indicated in table 7.16. It turns out that the number of generations of right-handed neutrinos ν_R also equals three for all 576 models, if they are taken from the cd sector. In order to complete these 576 models with a hidden sector, we first need to check what maximal contribution is allowed for the hidden sector by the first bulk RR-tadpole cancellation condition:

$$12 + 2P_c + Q_c + 2P_d + Q_d = 12 + 6 + 6 = 24 < 32\,. \tag{7.4}$$

Thus, the maximal contribution permitted for the hidden sector is eight: $32 - 24 = 8$. As usual, the aim is to add one hidden stack only, to reduce processing time. A look at table 7.1 tells us that the only possibility to add a single hidden stack is to take the hidden stack parallel to the $\Omega\mathcal{R}$-plane with rank $N_h = 4$.
A complete computer scan over all combinations of the 576 models with the hidden stack

provided a total of 288 models which fulfill all the twisted RR-tadpole cancellation conditions. The computer scan also revealed that all 288 semi-global models also satisfy all the K-theory constraints. Thus, we have a total of 288 global five-stack MSSMs. Since the number of models is small, a full computer scan of the particle spectrum can be performed. The scan shows that there is only one type of chiral and non-chiral massless particle spectrum, up to trivial exchanges such as $c \leftrightarrow d$ and $h \leftrightarrow h'$. Taking these exchanges into account, the number of models is reduced to $288 \div 4 = 72$ models. An explicit prototype of a global five-stack MSSM is given in table 7.17, with the corresponding massless open string spectrum indicated in table 7.18.

D6-brane configuration of a global 5-stack MSSM configuration on the aAA lattice						
	wrapping numbers	$\frac{\text{Angle}}{\pi}$	$\mathbb{Z}_2^{(i)}$**-eigenvalues**	$(\vec{\tau})$	$(\vec{\sigma})$	**gauge group**
a	$(1,0;1,0;1,0)$	$(0,0,0)$	$(--+)$	$(0,1,1)$	$(0,1,1)$	$U(3)$
b	$(1,0;-1,2;1,-2)$	$(0,\frac{1}{2},-\frac{1}{2})$	$(+++)$	$(0,1,0)$	$(0,1,0)$	$USp(2)$
c	$(1,0;-1,2;1,-2)$	$(0,\frac{1}{2},-\frac{1}{2})$	$(+--)$	$(0,1,1)$	$(0,1,1)$	$U(1)$
d	$(1,0;-1,2;1,-2)$	$(0,\frac{1}{2},-\frac{1}{2})$	$(-+-)$	$(0,0,1)$	$(0,0,1)$	$U(1)$
h	$(1,0;1,0;1,0)$	$(0,0,0)$	$(+++)$	$(0,1,1)$	$(0,1,1)$	$U(4)$

Table 7.17: Data of a global MSSM-like model consisting of five stacks of D6-branes with gauge group $SU(3)_a \times USp(2)_b \times SU(4)_h \times U(1)_a \times U(1)_c \times U(1)_d \times U(1)_h$ on the **aAA** lattice. The $\Omega\mathcal{R}\mathbb{Z}_2^{(3)}$-plane is chosen exotic with $\eta_{\Omega\mathcal{R}\mathbb{Z}_2^{(3)}} = -1$.

Overview of the massless matter spectrum for global 5-stack MSSM on the aAA lattice						
sector	state	$(SU(3)_a \times USp(2)_b \times SU(4)_h)_{U(1)_a \times U(1)_c \times U(1)_d \times U(1)_h}$	Q_Y	Q_{PQ}	$\mathbb{Z}_3$	$\mathbb{Z}_6$
$ab \equiv ab'$	Q_L	$3 \times (\mathbf{3},\mathbf{2},\mathbf{1})_{(1,0,0,0)}$	$1/6$	0	0	0
ac	d_R	$6 \times (\overline{\mathbf{3}},\mathbf{1},\mathbf{1})_{(-1,1,0,0)}$	$1/3$	1	1	2
ad	$\overline{d_R}$	$3 \times (\mathbf{3},\mathbf{1},\mathbf{1})_{(1,0,-1,0)}$	$-1/3$	1	1	2
ad'	u_R	$3 \times (\overline{\mathbf{3}},\mathbf{1},\mathbf{1})_{(-1,0,-1,0)}$	$-2/3$	1	1	2
$bc \equiv b'c$	H_u	$3 \times (\mathbf{1},\mathbf{2},\mathbf{1})_{(0,1,0,0)}$	$1/2$	1	1	2
$bc \equiv b'c$	$H_u + H_d$	$3 \times \left[(\mathbf{1},\mathbf{2},\mathbf{1})_{(0,1,0,0)} + h.c.\right]$	$\pm 1/2$	± 1	$1\|\|2$	$2\|\|4$
$bd \equiv b'd$	L	$6 \times (\mathbf{1},\mathbf{2},\mathbf{1})_{(0,0,-1,0)}$	$-1/2$	1	1	2
$bd \equiv b'd$	$\tilde{H}_u + \tilde{H}_d$	$2 \times \left[(\mathbf{1},\mathbf{2},\mathbf{1})_{(0,0,1,0)} + h.c.\right]$	$\pm 1/2$	∓ 1	$2\|\|1$	$4\|\|2$
cd	ν_R	$3 \times (\mathbf{1},\mathbf{1},\mathbf{1})_{(0,-1,1,0)}$	0	-2	1	2
cd	$\Sigma^{cd} + \tilde{\Sigma}^{cd}$	$3 \times \left[(\mathbf{1},\mathbf{1},\mathbf{1})_{(0,-1,1,0)} + h.c.\right]$	0	∓ 2	$1\|\|2$	$2\|\|4$
cd'	e_R	$3 \times (\mathbf{1},\mathbf{1},\mathbf{1})_{(0,1,1,0)}$	1	0	0	0
cd'	$X^{cd'} + \tilde{X}^{cd'}$	$3 \times \left[(\mathbf{1},\mathbf{1},\mathbf{1})_{(0,1,1,0)} + h.c.\right]$	± 1	0	0	0
ah	$h_a + \tilde{h}_a$	$2 \times \left[(\mathbf{3},\mathbf{1},\overline{\mathbf{4}})_{(1,0,0,-1)} + h.c.\right]$	$\pm 1/6$	0	$1\|\|2$	$5\|\|1$
ah'	$\underline{h}_a + \tilde{\underline{h}}_a$	$(\mathbf{3},\mathbf{1},\mathbf{4})_{(1,0,0,1)} + h.c.$	$\pm 1/6$	0	$2\|\|1$	$1\|\|5$
$bh \equiv b'h$	$\underline{h}_b$	$3 \times (\mathbf{1},\mathbf{2},\mathbf{4})_{(0,0,0,1)}$	0	0	2	1
ch'	$\underline{h}_c$	$6 \times (\mathbf{1},\mathbf{1},\overline{\mathbf{4}})_{(0,-1,0,-1)}$	$-1/2$	-1	0	3
dh	h_d	$3 \times (\mathbf{1},\mathbf{1},\overline{\mathbf{4}})_{(0,0,1,-1)}$	$1/2$	-1	0	3
dh'	$\underline{h}_d$	$3 \times (\mathbf{1},\mathbf{1},\mathbf{4})_{(0,0,1,1)}$	$1/2$	-1	1	5
aa'		$2 \times [(\overline{\mathbf{3}}_\mathbf{A},\mathbf{1},\mathbf{1})_{(2,0,0,0)} + h.c.]$	$\pm 1/3$	0	0	0
$bb' \equiv bb$	$\mathbf{Anti}_b^{(i)}$	$5 \times (\mathbf{1},\mathbf{1}_\mathbf{A},\mathbf{1})_{(0,0,0,0)}$	0	0	0	0
cc		$4 \times (\mathbf{1},\mathbf{1},\mathbf{1})_{(0,0,0,0)}$	0	0	0	0
dd	$\mathbf{Adj}_d^{(i)}$	$5 \times (\mathbf{1},\mathbf{1},\mathbf{1})_{(0,0,0,0)}$	0	0	0	0
dd'	$\mathbf{Sym}_d + \overline{\mathbf{Sym}}_d$	$(\mathbf{1},\mathbf{1},\mathbf{1})_{(0,0,2,0)} + (\mathbf{1},\mathbf{1},\mathbf{1})_{(0,0,-2,0)}$	± 1	∓ 2	$1\|\|2$	$2\|\|4$
hh'		$2 \times [(\mathbf{1},\mathbf{1},\mathbf{6}_\mathbf{A})_{(0,0,0,2)} + h.c.]$	0	0	1	$2\|\|4$

Table 7.18: Overview of the chiral and non-chiral massless particle content associated to the MSSM-like model with D6-brane configuration given in table 7.17. Anticipating the results from chapter 8, the last four columns display the charges of the particles under the massless hypercharge symmetry, a massive Peccei-Quinn symmetry, and two discrete $\mathbb{Z}_n$-symmetries for future reference. For non-chiral pairs of particles, we denoted the $\mathbb{Z}_n$-charges by the logic symbol ||.

As already mentioned, we were forced to loosen the constraints on the particle spectrum by allowing a considerable amount of non-chiral pairs in the visible sector. Looking at table 7.18 we behold a considerable amount of right-handed down quarks d_R appearing in the ac intersection sector as well as a substantial amount of left-handed leptons arising in the bd intersection sector. In the low-energy regime, the numerous $U(1)$ factors combine into the effective hypercharge $Q_Y = \frac{1}{6}Q_a + \frac{1}{2}Q_c + \frac{1}{2}Q_d$, as explained in section 3.2.1. Under the Standard Model group $SU(3)_{QCD} \times SU(2)_L \times U(1)_Y$, the right-handed down-type quarks d_R from the ac sector are charged as $(\overline{\mathbf{3}}, \mathbf{1})_{\frac{1}{3}}$, whereas the particles $\overline{d_R}$ from the ad sector are charged as $(\mathbf{3}, \mathbf{1})_{-\frac{1}{3}}$. Therefore, in the effective low-energy theory, these particles are hermitian conjugates to each other and can form non-chiral pairs, which are less annoying phenomenologically than chiral matter states, since they can potentially become heavy. By pairing off three of the six right-handed down-type quarks d_R of the ac sector with the three right-handed down-type quarks $\overline{d_R}$ from the ad sector, we are left effectively with three generations of chiral right-handed down-type quarks d_R at low energies. The same can potentially be done with the superfluous left-handed leptons L arising in the bd sector, three of which can be paired off with the three particles H_u appearing in the bc sector. This leaves us potentially with a full three generation particle spectrum in the effective MSSM. We will investigate the feasibility of this scenario in chapter 9. Note also that we will comment on the last three columns in table 7.18 with the symmetries in the next chapter.

7.2.2 Some results for ϱ-dependent models

In this subsection, we will provide examples of computer scans in order to illustrate the generic situation of ϱ-dependent MSSMs. Once again, we will focus on the **aAA** lattice, as its bulk RR-tadpole cancellation conditions are less stringent. The combination we will focus on is the second combination in table 5.7, which corresponds to taking the a stack parallel to the orbit (1,3; 1,0; 1-1) and the b stack parallel to the $\Omega\mathcal{R}$-plane. The ϱ-dependent bulk three-cycle (1,3; 1,0; 1,-1) is associated to $\varrho = 1$. There are in total ten ϱ-dependent bulk three-cycles which are SUSY for $\varrho = 1$, plus the eight ϱ-independent bulk three-cycles which are SUSY for every value of the complex structure parameter ϱ. Table 5.7 indicates that we have a total of 128 combinations for the a and b stacks under consideration giving rise to three generations of left-handed quarks.
The first aim is to find MSSM-like models satisfying the conditions on the particle spectrum presented in section 3.2.1. Using the stringent version of the conditions limiting the amount of non-chiral matter pairs in the visible sector, a full computer scan over all combinations of the 128 pairs a and b with the possible $18 \cdot 18$ combinations for the c and d stacks yielded 12 800 models giving rise to a three-generation particle spectrum, except for the right-handed neutrinos. By imposing also the conditions on the cd sector in order to have three generations of right-handed neutrinos, the number of models is reduced to 4 608 local models. The computer scan yielded the following constellations of bulk three-cycles for the

c and d stacks:

number	c	d
1152	$\Omega\mathcal{R}\mathbb{Z}_2^{(1)}$	$\Omega\mathcal{R}\mathbb{Z}_2^{(3)}$
1152	$\Omega\mathcal{R}\mathbb{Z}_2^{(1)}$	$\Omega\mathcal{R}\mathbb{Z}_2^{(2)}$
1152	$\Omega\mathcal{R}\mathbb{Z}_2^{(3)}$	$\Omega\mathcal{R}\mathbb{Z}_2^{(1)}$
1152	$\Omega\mathcal{R}\mathbb{Z}_2^{(2)}$	$\Omega\mathcal{R}\mathbb{Z}_2^{(1)}$

(7.5)

However, the computer scan also revealed that all 4 608 models present gauge symmetry enhancement on the bulk three-cycle parallel to the $\Omega\mathcal{R}\mathbb{Z}_2^{(1)}$-plane. Gauge symmetry enhancement on the d stack is not wanted for MSSM-like models nor for left-right symmetric models. Thus, only the 2 304 models where the c stack is parallel to the $\Omega\mathcal{R}\mathbb{Z}_2^{(1)}$-plane are usable for model building. In all 2 304 models, the c stack gives rise to an orthogonal $SO(2)$ group. The models thus do not correspond to genuine MSSMs, but still expose similar properties to MSSM-like models.

The next step is to check the bulk RR-tadpole cancellation conditions. The bulk wrapping numbers of three-cycles parallel to the $\Omega\mathcal{R}\mathbb{Z}_2^{(1)}$-plane and the $\Omega\mathcal{R}\mathbb{Z}_2^{(2,3)}$-planes are given by $(P,Q,U,V) = (3,0,0,0)$ and $(P,Q,U,V) = (0,0,1,-2)$, respectively. Hence, the sum over the four stacks yields the following contributions to the two bulk RR-tadpole cancellation conditions, for $\eta_{\Omega\mathcal{R}} = -1$:

$$\sum_{x\in\{a,b,c,d\}} N_x(2P_x + Q_x) = N_a + 2N_b + 6N_c = 3 + 2\cdot 2 + 6\cdot 1 = 13 \leq 16\,, \tag{7.6}$$

$$-\sum_{x\in\{a,b,c,d\}} N_x V_x = 3N_a + 2N_d = 3\cdot 3 + 2\cdot 1 = 11 \leq 16\,. \tag{7.7}$$

Out of the 18 bulk three-cycles SUSY for $\varrho = 1$, the following bulk three-cycles can be added to the bulk RR-tadpole cancellation conditions above without overshooting them:

$(n_1,m_1;n_2,m_2;n_3,m_3)$	(P,Q,U,V)	$2P+Q$	V	rank
$(1,3;1,0;1,-1)$	$(1,-1,3,-3)$	1	-3	N_1
$(1,1;1,-1;1,1)$	$(2,-1,2,-1)$	3	-1	N_2
$(1,1;1,1;1,-1)$	$(2,-1,2,-1)$	3	-1	N_3
$\Omega\mathcal{R}$	$(1,0,0,0)$	2	0	N_4
$\Omega\mathcal{R}\mathbb{Z}_2^{(2)}$	$(0,0,1,-2)$	0	-2	N_5
$\Omega\mathcal{R}\mathbb{Z}_2^{(3)}$	$(0,0,1,-2)$	0	-2	N_6

(7.8)

We see that none of these bulk three-cycles cancels both RR-tadpole cancellation conditions exactly, so that the hidden sector necessarily has to contain more than one stack. A computer scan produced the following eight combinations of the bulk three-cycles above with different

ranks N_i which cancel both bulk RR-tadpole cancellation conditions exactly:

N_1	N_2	N_3	N_4	N_5	N_6
1	0	0	1	1	0
0	1	0	0	2	0
0	0	1	0	2	0
1	0	0	1	0	1
0	1	0	0	1	1
0	0	1	0	1	1
0	1	0	0	0	2
0	0	1	0	0	2

(7.9)

The most interesting combinations are those with two hidden stacks, as the processing time for the analysis is reduced compared to the configurations involving three hidden stacks. We have in total four of these combinations corresponding to:

h_1	h_2	N_{h_1}	N_{h_2}
$\Omega\mathcal{R}\mathbb{Z}_2^{(2)}$	$(1,1;1,-1;1,1)$	2	1
$\Omega\mathcal{R}\mathbb{Z}_2^{(2)}$	$(1,1;1,1;1,-1)$	2	1
$\Omega\mathcal{R}\mathbb{Z}_2^{(3)}$	$(1,1;1,-1;1,1)$	2	1
$\Omega\mathcal{R}\mathbb{Z}_2^{(3)}$	$(1,1;1,1;1,-1)$	2	1

(7.10)

However, a full computer scan over all $4 \cdot 2\,304 \cdot 256 \cdot 256 = 603\,979\,776$ possibilities listed above found that none of these models would fulfill all the twisted RR-tadpole cancellation conditions. The search could be extended to seven-stack MSSM models, though it is very unlikely that global MSSM models can be found with the combination of stacks given above. Indeed, the visible stacks contribute always with ± 36 to at least one of the twisted RR-tadpole cancellations, which is bigger than the contribution we found for the ϱ-dependent Pati-Salam models.

Conclusion

In this summery section, we provide a brief overview of the particle physics models analyzed in the previous chapter and this chapter.
For the **bAA** lattice, we have proven that:

- Global $SU(5)$ models cannot be constructed on **bAA**.
- Global Pati-Salam models cannot be constructed on **bAA**.
- Global ϱ-independent left-right symmetric models cannot be constructed on **bAA**.
- Global ϱ-independent MSSMs cannot be constructed on **bAA**.

It remains to be seen whether global ϱ-dependent left-right symmetric and MSSM-like models can be constructed, but this analysis is not included in the present doctoral work due to time limitations.

For the **aAA** lattice, the results can be summarized as follows:

- Global $SU(5)$ models cannot be constructed on **aAA**.
- Global ϱ-independent Pati-Salam models can be constructed on **aAA**.
- Global ϱ-independent left-right symmetric models can be constructed on **aAA**.
- Global ϱ-independent MSSMs can be constructed on **aAA**.

It remains to be seen whether global ϱ-dependent Pati-Salam models, global ϱ-dependent left-right symmetric and MSSM-like models can be constructed, but this analysis goes beyond the scope of the present doctoral work due to the high processing time and power involved.

Chapter 8

Discrete Symmetries

8.1 Massless $U(1)$ and discrete $\mathbb{Z}_n$-symmetries

The two previous chapters focused on model building in Type IIA string theory. The next two chapters will rather focus on phenomenological features of the constructed models. The present chapter concentrates on the existence of massless, i.e. gauged, $U(1)$ symmetries and discrete $\mathbb{Z}_n$-symmetries, while the next chapter focuses on the Yukawa couplings.

We will start with the conditions for the existence of massless $U(1)$ gauge symmetries. As we explained in section 3.2.1, a so-called massless $U(1)$ symmetry refers to (a combination of) Abelian $U(1)$ symmetries which is not broken spontaneously and whose gauge boson therefore remains massless without acquiring mass through the Stückelberg mechanism. For example, in the Standard Model or the minimal SUSY extension thereof, the MSSM, the hypercharge $U(1)_Y$ is associated to a massless $U(1)$ combination, see section 3.2.1. In left-right symmetric models, a massless $U(1)$ symmetry is usually present as the baryon-lepton number symmetry $U(1)_{B-L}$. The detection of any supplementary massless $U(1)$ combination in a model would imply the existence of an additional massless photon, the dark photon.
The conditions on the existence of such a massless gauged $U(1)$ symmetry are given by the following set of topological constraints, which correspond to the Stückelberg coupling [188–190, 66]:

$$\Pi_i^{\Omega\mathcal{R}\text{-even}} \circ \left(\sum_a q_a N_a \Pi_a^{\text{frac}} \right) = 0 \;\forall\; i \in \{0, \dots h_{21}\} \;, \tag{8.1}$$

with $q_a \in \mathbb{Q}$ and $\Pi_i^{\Omega\mathcal{R}\text{-even}}$ referring to a three-cycle invariant under the orientifold projection $\Omega\mathcal{R}$. Since the right-hand side of the equation above is zero, we can also take $q_a \in \mathbb{Z}$ when checking the equations above. We see that the equations above correspond exactly to the equations for the existence of $\mathbb{Z}_n$-symmetries (8.5) introduced below, except that the right-hand side "$= 0$ mod n" in (8.5) has to be replaced by "$= 0$", in other words the equations (8.5) have to be satisfied for every value of n.

The next issue to address is the existence of discrete $\mathbb{Z}_n$-symmetries. As mentioned in section 3.2.1, discrete $\mathbb{Z}_n$-symmetries can be invoked to suppress unwanted couplings which may lead to undesirable effects such as proton decay, see [157]. The possible discrete symmetries present in the MSSM have been classified in [191] in terms of three generators given by $\mathcal{R}_n = e^{i2\pi\mathcal{R}/n}$, $\mathfrak{L}_n = e^{i2\pi\mathfrak{L}/n}$ and $\mathcal{A}_n = e^{i2\pi\mathcal{A}/n}$. The definition of the generators $\mathcal{R}$, $\mathfrak{L}$

and $\mathcal{A}$ can be found in [191, 100, 78]. The most generic $\mathbb{Z}_n$-symmetry allowing all standard Yukawa couplings is given by [191, 100]:

$$g_n = \mathcal{R}_n^m \cdot \mathcal{A}_n^k \cdot \mathfrak{L}_n^p, \qquad m,k,p = 0,1,\ldots,n-1\,. \tag{8.2}$$

The discrete $\mathbb{Z}_n$-symmetry generator acts on chiral superfields Φ_j with a global phase factor [191]:

$$\Phi_j \to e^{iQ_j 2\pi/n}\Phi_j\,, \tag{8.3}$$

where Q_j are the discrete charges of the states under the $\mathbb{Z}_n$-generator, defined up to *mod* n. The charges of the MSSM particles under the generator g_n are given by [78, 191, 100]:

$$\begin{aligned} &Q_{Q_L} = 0, && Q_{u_R} = -m, && Q_{d_R} = m-k, \\ &Q_L = -k-p, && Q_{e_R} = m+p && Q_{\nu_R} = -m+k+p, \\ &Q_{H_u} = m, && Q_{H_d} = -m+k. \end{aligned} \tag{8.4}$$

This charge assignment allows for $\mathbb{Z}_n$-invariant Yukawa couplings. The charges of the left-handed quarks Q_L are traditionally chosen to be zero. This can be achieved through a base shift, i.e. a shift by a massless $U(1)$ symmetry like for instance the hypercharge. A base shift consists in multiplying the generator of the discrete $\mathbb{Z}_n$-symmetries by a discrete subgroup of a massless $U(1)_x$ generator, $e^{\frac{i2\pi Q_x}{n}}$. Note that any combination of $U(1)$'s leading to a massless gauged $U(1)$ symmetry, i.e. any element satisfying (8.1), can be added to the equations (8.5), since their contribution is zero in that case. This reflects the shift of the discrete $\mathbb{Z}_n$-symmetries by this massless $U(1)$ combination. The procedure will become clearer when we analyze concrete examples.

The $\mathbb{Z}_n$-symmetries are considered to arise from broken continuous gauge $U(1)$ symmetries. Therefore, they should also satisfy anomaly constraints. In [192, 191], it was shown that only three discrete symmetries satisfy all the anomaly constraints of the MSSM, namely matter parity given by the generator $\mathcal{R}_2$, baryon triality given by the generator $\mathcal{B}_3 \equiv \mathcal{R}_3\mathcal{L}_3$ and a combination thereof corresponding to proton hexality given by $\mathcal{P}_6 \equiv \mathcal{R}_6^5\mathcal{L}_6^2$ [193, 78]. Using (8.4), the charges of the MSSM states under matter parity, baryon triality and proton hexality can be computed and are given in table 8.1.

$\mathbb{Z}_n$-**charges of the MSSM-particles,** $n = 2,3,6$									
Name	$\mathbb{Z}_n$	Q_L	u_R	d_R	L	e_R	ν_R	H_u	H_d
R-parity	$\mathbb{Z}_2$	0	1	1	0	1	1	1	1
baryon triality	$\mathbb{Z}_3$	0	2	1	2	2	0	1	2
proton hexality	$\mathbb{Z}_6$	0	1	5	4	1	3	5	1

Table 8.1: Standard charge assignment of the MSSM particles under the discrete $\mathbb{Z}_2$, $\mathbb{Z}_3$ and $\mathbb{Z}_6$-symmetries associated to respectively matter parity, baryon triality and proton hexality.

In [100], it was shown that in our string set-up the existence of a discrete $\mathbb{Z}_n$-symmetry follows from a set of topological conditions:

$$\Pi_i^{\Omega\mathcal{R}\text{-even}} \circ \left(\sum_a k_a N_a \Pi_a^{\text{frac}}\right) = 0 \bmod n \quad \forall\, i \in \{0,\ldots h_{21}\} \qquad \text{with } Q_{\mathbb{Z}_n} = \sum_a k_a Q_a\,. \tag{8.5}$$

The three-cycle Π_a^{frac} corresponds to any fractional three-cycle present in the model and giving rise to a $U(1)_a$ group. In other words, the sum $\sum_a$ goes over those stacks present in the model which support unitary groups $U(N_a) \simeq SU(N_a) \times U(1)_a$. A three-cycle denoted by $\Pi_i^{\Omega\mathcal{R}\text{-even}}$ refers to a three-cycle invariant under the orientifold projection $\Omega\mathcal{R}$. Here $Q_{\mathbb{Z}_n}$, Q_a are the charges of the states under the $\mathbb{Z}_n$-symmetry and the $U(1)_a$ symmetries, respectively. In order to avoid double counting of discrete $\mathbb{Z}_n$-symmetries, the coefficients $k_a \in \mathbb{Z}$ need to lie within the interval $0 \leq k_a < n$ and satisfy the conditions $gcd(n, k_a, k_b, \dots) = 1$.

Further reading about discrete $\mathbb{Z}_n$-symmetries and their incorporation in string theory can be found in [194–201, 167, 168]. In this chapter, we will follow the approach proposed in [78, 93, 102, 64].
In the chapters 6 and 7, we found several prototypes of local, semi-global and global models, including $SU(5)$ and Pati-Salam models, left-right symmetric and MSSM-like models. We will not derive for each of these its phenomenological properties, since we want to avoid boring the reader by repeating a hundred times the same analysis. Instead, we will pick only a few of the global models found and analyze their discrete symmetries in this chapter as well as their Yukawa couplings in the next chapter. The phenomenologically more interesting models are the left-right symmetric and MSSM models, as they are the closest to the Standard Model of particle physics. Hence, we will concentrate the analysis on the global five-stack effective MSSM and the global six-stack left-right symmetric models including prototype I, prototype II, and a quick discussion of prototypes IIb and IIc. Remember that these models all have exotic O6-plane charge $\eta_{\Omega\mathcal{R}\mathbb{Z}_2^{(2 \text{ or } 3)}} = -1$. Since these two choices are related through a simple permutation of the indices of the second and third two-torus $T^2_{(i)}$, we will derive the results for $\eta_{\Omega\mathcal{R}\mathbb{Z}_2^{(3)}} = -1$ only. Similarly, we will derive the results only for the **aAA** lattice, as the **bAA** lattice does not yield global models easily.

8.2 Explicit expression for the conditions on $\mathbb{Z}_n$-symmetries

In this section, we will derive a concrete analytical expression for the conditions on discrete symmetries (8.5), which implies the reduction of the $\Omega\mathcal{R}$-even three-cycles $\Pi^{\Omega\mathcal{R}\text{-even}}$ to linearly independent three-cycles.

There are two types of $\Omega\mathcal{R}$-even three-cycles $\Pi^{\Omega\mathcal{R}\text{-even}}$ which can be inserted in equation (8.5). The first possibility consists in inserting pure bulk three-cycles and pure exceptional three-cycles which are even under the orientifold projection. The pure bulk or exceptional even three-cycles will provide a set of necessary conditions. The non-fulfillment of the necessary conditions implies the non-existence of discrete $\mathbb{Z}_n$-symmetries. However, the fulfillment of the necessary conditions does not imply the existence of discrete $\mathbb{Z}_n$-symmetries.
The second possibility is to insert fractional three-cycles which are even under the orientifold projection in formula (8.5). In our case, the fractional three-cycles which are even under the orientifold projection correspond to the three-cycles parallel to the O6-planes and presenting USp or SO enhancement as indicated in table 5.1. Inserting these in (8.5) provides us with a set of equations giving sufficient conditions for the existence of discrete $\mathbb{Z}_n$-symmetries.
We will see that the analytical expressions of the necessary conditions are less complicated than those of the sufficient conditions. Thus, it is sensible to check via the necessary con-

ditions which discrete $\mathbb{Z}_n$-symmetries may exist at all. In a second step, the $\mathbb{Z}_n$-symmetries detected should be tested via the sufficient conditions.

First of all, the pure bulk and pure exceptional $\Omega\mathcal{R}$-even and $\Omega\mathcal{R}$-odd three-cycles and their intersection numbers should be computed. The results are indicated in tables 8.2 and 8.3.

$\Omega\mathcal{R}$-even and -odd bulk three-cycles on $T^6/(\mathbb{Z}_2 \times \mathbb{Z}_6 \times \Omega\mathcal{R})$		
$\Omega\mathcal{R}$-even	**$\Omega\mathcal{R}$-odd**	**Intersection Numbers**
ρ_1	ρ_3	$\rho_1 \circ \rho_3 = 8$
$\rho_3 - 2\rho_4$	$\rho_1 - 2\rho_2$	$[\rho_3 - 2\rho_4] \circ [\rho_1 - 2\rho_2] = -24$

Table 8.2: List of the $\Omega\mathcal{R}$-even and $\Omega\mathcal{R}$-odd pure bulk three-cycles with the choice of the exotic O6-plane charge $\eta_{\Omega\mathcal{R}\mathbb{Z}_2^{(3)}} = -1$ for the **aAA** lattice. The right column lists all intersections numbers between the bulk three-cycles (vanishing intersection numbers are omitted).

Note that all other intersections of the form $\Pi^{\Omega\mathcal{R}\text{-even}} \circ \Pi^{\Omega\mathcal{R}\text{-odd}}$ in table 8.2, for instance $\rho_1 \circ (\rho_1 - 2\rho_2)$, are zero, as can be deduced from formula (2.10). Clearly, also intersections of the form $\Pi^{\Omega\mathcal{R}\text{-even}} \circ \Pi^{\Omega\mathcal{R}\text{-even}}$ and $\Pi^{\Omega\mathcal{R}\text{-odd}} \circ \Pi^{\Omega\mathcal{R}\text{-odd}}$ are zero, as can be explicitly verified using formula (2.10).

$\Omega\mathcal{R}$-even and -odd exceptional three-cycles on $T^6/(\mathbb{Z}_2 \times \mathbb{Z}_6 \times \Omega\mathcal{R})$			
$\Omega\mathcal{R}$-even	**$\Omega\mathcal{R}$-odd**	α	**Intersection Numbers**
$\tilde{\varepsilon}_\alpha^{(1)}$	$\varepsilon_\alpha^{(1)}$	$0,1,2,3$	$\tilde{\varepsilon}_0^{(1)} \circ \varepsilon_0^{(1)} = 12, \quad \tilde{\varepsilon}_\alpha^{(1)} \circ \varepsilon_\alpha^{(1)} = 4$ for $\alpha = 1,2,3$
$\varepsilon_4^{(1)} - \varepsilon_5^{(1)}$	$\tilde{\varepsilon}_4^{(1)} - \tilde{\varepsilon}_5^{(1)}$		$[\varepsilon_4^{(1)} - \varepsilon_5^{(1)}] \circ [\tilde{\varepsilon}_4^{(1)} - \tilde{\varepsilon}_5^{(1)}] = -8$
$\tilde{\varepsilon}_4^{(1)} + \tilde{\varepsilon}_5^{(1)}$	$\varepsilon_4^{(1)} + \varepsilon_5^{(1)}$		$[\tilde{\varepsilon}_4^{(1)} + \tilde{\varepsilon}_5^{(1)}] \circ [\varepsilon_4^{(1)} + \varepsilon_5^{(1)}] = 8$
$\varepsilon_\alpha^{(2)} - 2\tilde{\varepsilon}_\alpha^{(2)}$	$\varepsilon_\alpha^{(2)}$	$1,2,3,4$	$[\varepsilon_\alpha^{(2)} - 2\tilde{\varepsilon}_\alpha^{(2)}] \circ \varepsilon_\alpha^{(2)} = -8$
$\varepsilon_\alpha^{(3)}$	$\varepsilon_\alpha^{(3)} - 2\tilde{\varepsilon}_\alpha^{(3)}$	$1,2,3,4$	$\varepsilon_\alpha^{(3)} \circ [\varepsilon_\alpha^{(3)} - 2\tilde{\varepsilon}_\alpha^{(3)}] = 8$

Table 8.3: List of the $\Omega\mathcal{R}$-even and $\Omega\mathcal{R}$-odd pure exceptional three-cycles with the choice of the exotic O6-plane charge $\eta_{\Omega\mathcal{R}\mathbb{Z}_2^{(3)}} = -1$ for the **aAA** lattice. The right column lists all intersections numbers between the exceptional three-cycles (vanishing intersection numbers are omitted).

Once again, all other combinations of intersection numbers in table 8.3 are zero, as can be checked explicitly by using formula (2.24). These pure bulk or exceptional $\Omega\mathcal{R}$-even and $\Omega\mathcal{R}$-odd three-cycles form the building blocks of any fractional three-cycle. In other words, any generic fractional three-cycle can be expanded in terms of the $\Omega\mathcal{R}$-even and $\Omega\mathcal{R}$-odd

cycles as follows:

$$\begin{aligned}
\Pi_a^{\text{frac}} =& \frac{1}{4}\Pi_a^{\text{bulk}} + \frac{1}{4}\sum_{i=1}^{3}\Pi_a^{\mathbb{Z}_2^{(i)}} \\
=& \frac{1}{4}\left(P_a\rho_1 + Q_a\rho_2 + U_a\rho_3 + V_a\rho_4\right) + \frac{1}{4}\sum_{\alpha=0}^{5}\left(x_{\alpha,a}^{(1)}\,\varepsilon_\alpha^{(1)} + y_{\alpha,a}^{(1)}\,\tilde{\varepsilon}_\alpha^{(1)}\right) + \frac{1}{4}\sum_{l=2,3}\sum_{\alpha=1}^{4}\left(x_{\alpha,a}^{(l)}\,\varepsilon_\alpha^{(l)} + y_{\alpha,a}^{(l)}\,\tilde{\varepsilon}_\alpha^{(l)}\right), \\
=& \frac{1}{4}\left(\left(P_a + \frac{Q_a}{2}\right)\rho_1 - Q_a\frac{\rho_1 - 2\rho_2}{2} + \left(U_a + \frac{V_a}{2}\right)\rho_3 - V\frac{\rho_3 - 2\rho_4}{2}\right) + \sum_{\alpha=0}^{3}\frac{1}{4}\left(x_{\alpha,a}^{(1)}\,\varepsilon_\alpha^{(1)} + y_{\alpha,a}^{(1)}\,\tilde{\varepsilon}_\alpha^{(1)}\right) \\
&+ \frac{1}{4}\left(\frac{x_{4,a}^{(1)} + x_{5,a}^{(1)}}{2}[\varepsilon_4^{(1)} + \varepsilon_5^{(1)}] + \frac{x_{4,a}^{(1)} - x_{5,a}^{(1)}}{2}[\varepsilon_4^{(1)} - \varepsilon_5^{(1)}]\right) + \frac{1}{4}\left(\frac{y_{4,a}^{(1)} + y_{5,a}^{(1)}}{2}[\tilde{\varepsilon}_4^{(1)} + \tilde{\varepsilon}_5^{(1)}] + \frac{y_{4,a}^{(1)} - y_{5,a}^{(1)}}{2}[\tilde{\varepsilon}_4^{(1)} - \tilde{\varepsilon}_5^{(1)}]\right) \\
&+ \sum_{l=2,3}\sum_{\alpha=1}^{4}\frac{1}{4}\left(\left(x_{\alpha,a}^{(l)} + \frac{y_{\alpha,a}^{(l)}}{2}\right)\varepsilon_\alpha^{(l)} - y_{\alpha,a}^{(l)}\,\frac{\varepsilon_\alpha^{(l)} - 2\tilde{\varepsilon}_\alpha^{(l)}}{2}\right).
\end{aligned} \tag{8.6}$$

Rewritten, this gives:

$$\begin{aligned}
\Pi_a^{\text{frac}} =& \Pi_a^{\text{frac,even}} + \Pi_a^{\text{frac,odd}} \qquad \text{with} \\
\Pi_a^{\text{frac,even}} =& \frac{1}{4}\left(\left(P_a + \frac{Q_a}{2}\right)\rho_1 - V_a\frac{\rho_3 - 2\rho_4}{2}\right) + \sum_{\alpha=0}^{3}\frac{1}{4}\left(y_{\alpha,a}^{(1)}\,\tilde{\varepsilon}_\alpha^{(1)} + \frac{x_{4,a}^{(1)} - x_{5,a}^{(1)}}{2}[\varepsilon_4^{(1)} - \varepsilon_5^{(1)}] + \frac{y_{4,a}^{(1)} + y_{5,a}^{(1)}}{2}[\tilde{\varepsilon}_4^{(1)} + \tilde{\varepsilon}_5^{(1)}]\right) \\
&+ \sum_{\alpha=1}^{4}\frac{1}{4}\left(-y_{\alpha,a}^{(2)}\,\frac{\varepsilon_\alpha^{(2)} - 2\tilde{\varepsilon}_\alpha^{(2)}}{2}\right) + \sum_{\alpha=1}^{4}\frac{1}{4}\left(\left(x_{\alpha,a}^{(3)} + \frac{y_{\alpha,a}^{(3)}}{2}\right)\varepsilon_\alpha^{(3)}\right), \\
\Pi_a^{\text{frac,odd}} =& \frac{1}{4}\left(-Q_a\frac{\rho_1 - 2\rho_2}{2} + \left(U_a + \frac{V_a}{2}\right)\rho_3\right) + \sum_{\alpha=0}^{3}\frac{1}{4}\left(x_{\alpha,a}^{(1)}\,\varepsilon_\alpha^{(1)} + \frac{x_{4,a}^{(1)} + x_{5,a}^{(1)}}{2}[\varepsilon_4^{(1)} + \varepsilon_5^{(1)}] + \frac{y_{4,a}^{(1)} - y_{5,a}^{(1)}}{2}[\tilde{\varepsilon}_4^{(1)} - \tilde{\varepsilon}_5^{(1)}]\right) \\
&+ \sum_{\alpha=1}^{4}\frac{1}{4}\left(\left(x_{\alpha,a}^{(2)} + \frac{y_{\alpha,a}^{(2)}}{2}\right)\varepsilon_\alpha^{(2)}\right) + \sum_{\alpha=1}^{4}\frac{1}{4}\left(-y_{\alpha,a}^{(3)}\,\frac{\varepsilon_\alpha^{(3)} - 2\tilde{\varepsilon}_\alpha^{(3)}}{2}\right).
\end{aligned} \tag{8.7}$$

The intersection number with any $\Omega\mathcal{R}$-even cycle $\Pi^{\Omega\mathcal{R}\text{-even}}$ is then given by:

$$\Pi^{\Omega\mathcal{R}\text{-even}} \circ \Pi_a^{\text{frac}} = \Pi^{\Omega\mathcal{R}\text{-even}} \circ \Pi_a^{\text{frac,odd}}, \tag{8.8}$$

since we always have $\Pi^{\Omega\mathcal{R}\text{-even}} \circ \Pi_a^{\text{frac,even}} = 0$ as we mentioned before.
The expressions above allow us to compute the intersection numbers of pure bulk and exceptional $\Omega\mathcal{R}$-even three-cycles with any fractional three-cycle in terms of the bulk and exceptional wrapping numbers of the latter. Using formula (8.8) above and the expression (8.7), as well as the intersection numbers in tables 8.2 and 8.3, one finds the results given in table 8.4. The right column in table 8.4 will be used to derive the necessary and sufficient $\mathbb{Z}_n$-conditions.

Writing out explicitly the results in table 8.4, we find a set of 16 equations which form the necessary conditions on the existence of $\mathbb{Z}_n$-symmetries from pure bulk and pure exceptional

Intersection numbers with basic $\Omega\mathcal{R}$-even three-cycles	
$\Pi^{\Omega\mathcal{R}\text{-even}}$	$\Pi^{\Omega\mathcal{R}\text{-even}} \circ \sum_a N_a \Pi_a^{\text{frac}}$
ρ_1	$\sum_a N_a (2U_a + V_a)$
$\rho_3 - 2\rho_4$	$\sum_a N_a \, 3Q_a$
$\tilde{\varepsilon}_0^{(1)}$	$\sum_a N_a \, 3x_{0,a}^{(1)}$
$\tilde{\varepsilon}_{\alpha\in\{1,2,3\}}^{(1)}$	$\sum_a N_a x_{\alpha,a}^{(1)}$
$\varepsilon_4^{(1)} - \varepsilon_5^{(1)}$	$-\sum_a N_a (y_{4,a}^{(1)} - y_{5,a}^{(1)})$
$\tilde{\varepsilon}_4^{(1)} + \tilde{\varepsilon}_5^{(1)}$	$\sum_a N_a (x_{4,a}^{(1)} + x_{5,a}^{(1)})$
$\varepsilon_\alpha^{(2)} - 2\tilde{\varepsilon}_\alpha^{(2)}$	$-\sum_a N_a (2\, x_{\alpha,a}^{(2)} + y_{\alpha,a}^{(2)})$
$\varepsilon_\alpha^{(3)}$	$-\sum_a N_a y_{\alpha,a}^{(3)}$

Table 8.4: Ingredients for the computation of the K-theory and $\mathbb{Z}_n$-symmetry constraints. The right column gives the intersection numbers of the $\Omega\mathcal{R}$-even pure bulk or exceptional three-cycles listed in the left column with any fractional three-cycle, in terms of the bulk and exceptional wrapping numbers of the latter.

cycles:

$$\sum_a k_a N_a \begin{pmatrix} 2U_a + V_a \\ 3\,Q_a \\ \hline 3x_{0,a}^{(1)} \\ x_{1,a}^{(1)} \\ x_{2,a}^{(1)} \\ x_{3,a}^{(1)} \\ x_{4,a}^{(1)} + x_{5,a}^{(1)} \\ -(y_{4,a}^{(1)} - y_{5,a}^{(1)}) \\ -(2\, x_{1,a}^{(2)} + y_{1,a}^{(2)}) \\ -(2\, x_{2,a}^{(2)} + y_{2,a}^{(2)}) \\ -(2\, x_{3,a}^{(2)} + y_{3,a}^{(2)}) \\ -(2\, x_{4,a}^{(2)} + y_{4,a}^{(2)}) \\ \hline -y_{1,a}^{(3)} \\ -y_{2,a}^{(3)} \\ -y_{3,a}^{(3)} \\ -y_{4,a}^{(3)} \end{pmatrix} \overset{!}{=} 0 \bmod n\,. \tag{8.9}$$

From the intersection numbers in tables 8.2 and 8.3, we see that the pure bulk and pure exceptional $\Omega\mathcal{R}$-even/odd three-cycles do not form an unimodular lattice. This means that these pure bulk or exceptional three-cycles only span a sublattice. Some information might be lost if one uses only these three-cycles to obtain the conditions on discrete symmetries. In order to capture all $\mathbb{Z}_n$-symmetries correctly, the necessary conditions are complemented

with a set of sufficient conditions derived from fractional three-cycles.

The sufficient conditions are provided by the fractional three-cycles supporting gauge symmetry enhancement as in table 5.1. On the **aAA** lattice, there are in total 240 $\Omega\mathcal{R}$-even fractional three-cycles, supporting either USp or SO enhancement. However, since we only have the $b_3^{\text{bulk}+\mathbb{Z}_2} = h_{21}^{\text{bulk}+\mathbb{Z}_2} + 1 = 16$ independent basis $\Omega\mathcal{R}$-even three-cycles indicated in tables 8.2 and 8.3, only 16 of these 240 fractional three-cycles can be linearly independent. Thus, the sufficient conditions can be reduced from 240 to 16 linearly independent equations. We will start with the fractional three-cycles supporting USp enhancement. Should these provide less than 16 linearly independent equations, then the three-cycles supporting SO enhancement would also need to be taken into account. On the **aAA** lattice, table 5.1 tells us that with $\eta_{\Omega\mathcal{R}\mathbb{Z}_2^{(3)}} = -1$, we can have three types of fractional three-cycles giving rise to USp enhancement, lying either parallel to the $\Omega\mathcal{R}$-plane, the $\Omega\mathcal{R}\mathbb{Z}_2^{(1)}$-plane or the $\Omega\mathcal{R}\mathbb{Z}_2^{(3)}$-plane. These can be expressed as follows:

$$\begin{aligned}
\Pi^{\text{frac}}_{USp(2)_{\uparrow\uparrow\Omega\mathcal{R}}} =& \frac{1}{4}\left(\Pi^{\text{bulk}}_{\Omega\mathcal{R}} + (-1)^{\tau^{\mathbb{Z}_2^{(1)}}}\ \Pi^{\mathbb{Z}_2^{(1)}}_{\text{h},(\sigma_2,1)} + (-1)^{\tau^{\mathbb{Z}_2^{(2)}}}\ \Pi^{\mathbb{Z}_2^{(2)}}_{\text{h},(\sigma_1,1)} + (-1)^{\tau^{\mathbb{Z}_2^{(1)}}+\tau^{\mathbb{Z}_2^{(2)}}}\ \Pi^{\mathbb{Z}_2^{(3)}}_{\text{h},(\sigma_1,\sigma_2)}\right),\\
\Pi^{\text{frac}}_{USp(2)_{\uparrow\uparrow\Omega\mathcal{R}\mathbb{Z}_2^{(1)}}} =& \frac{1}{4}\left(\Pi^{\text{bulk}}_{\Omega\mathcal{R}\mathbb{Z}_2^{(1)}} + (-1)^{\tau^{\mathbb{Z}_2^{(1)}}}\ \Pi^{\mathbb{Z}_2^{(1)}}_{\text{h},(1,\sigma_3)} + (-1)^{\tau^{\mathbb{Z}_2^{(2)}}}\ \Pi^{\mathbb{Z}_2^{(2)}}_{\text{v},(\sigma_1,\sigma_3)} - (-1)^{\tau^{\mathbb{Z}_2^{(1)}}+\tau^{\mathbb{Z}_2^{(2)}}}\ \Pi^{\mathbb{Z}_2^{(3)}}_{\text{v},(\sigma_1,1)}\right),\\
\Pi^{\text{frac}}_{USp(2)_{\uparrow\uparrow\Omega\mathcal{R}\mathbb{Z}_2^{(3)}}} =& \frac{1}{4}\left(\Pi^{\text{bulk}}_{\Omega\mathcal{R}\mathbb{Z}_2^{(3)}} + (-1)^{\tau^{\mathbb{Z}_2^{(1)}}}\ \Pi^{\mathbb{Z}_2^{(1)}}_{\text{v},(\sigma_2,\sigma_3)} - (-1)^{\tau^{\mathbb{Z}_2^{(2)}}}\ \Pi^{\mathbb{Z}_2^{(2)}}_{\text{v},(\sigma_1,\sigma_3)} + (-1)^{\tau^{\mathbb{Z}_2^{(1)}}+\tau^{\mathbb{Z}_2^{(2)}}}\ \Pi^{\mathbb{Z}_2^{(3)}}_{\text{h},(\sigma_1,\sigma_2)}\right),
\end{aligned} \tag{8.10}$$

with $\Pi^{\text{bulk}}_{\Omega\mathcal{R}} = \rho_1$, $\Pi^{\text{bulk}}_{\Omega\mathcal{R}\mathbb{Z}_2^{(1)}} = 3\rho_1$ and $\Pi^{\text{bulk}}_{\Omega\mathcal{R}\mathbb{Z}_2^{(3)}} = \rho_3 - 2\rho_4$. The various expressions for the "horizontal" contributions $\Pi^{\mathbb{Z}_2^{(i)}}_{\text{h},(\cdot,\cdot)}$ and the "vertical" contributions $\Pi^{\mathbb{Z}_2^{(i)}}_{\text{v},(\cdot,\cdot)}$ can be found in [65] and are reproduced in table 8.5 for convenience.

The first step in establishing the sufficient conditions for the discrete $\mathbb{Z}_n$-symmetries consists in reducing the number of linearly dependent fractional three-cycles given above. More precisely, the condition to check in our case whether r fractional three-cycles are linearly dependent is the following:

$$\lambda_1\Pi_1 + \ldots \lambda_r\Pi_r \stackrel{?}{=} 0 \text{ for } \lambda_i \in \{-1, +1\}\ . \tag{8.11}$$

If this equation is fulfilled, the fractional three-cycles are linearly dependent. The reduction can be done by hand, as illustrated on examples in our publication [64]. However, it can also been done numerically, which we will briefly comment here. Using table 8.5, the expressions (8.10) can be defined as functions of the discrete parameters $(\tau^{\mathbb{Z}_2^{(i)}}, \tau^i, \sigma^i)$. Loops over the discrete parameters provide the 240 fractional three-cycles supporting USp enhancement. The next step in the algorithm tests for two-by-two dependencies among the fractional three-cycles. If the following condition is satisfied,

$$\lambda_1\Pi_1 + \lambda_2\Pi_2 = 0 \text{ for } \lambda_i \in \{-1, +1\}\ , \tag{8.12}$$

one of the two three-cycles is deleted, as they are linearly dependent. Once all the two-by-two dependencies are eliminated, the algorithm tests for three-by-three dependencies,

$$\lambda_1\Pi_1 + \lambda_2\Pi_2 + \lambda_3\Pi_3 = 0 \text{ for } \lambda_i \in \{-1, +1\}\,, \tag{8.13}$$

and so on. It turned out that all the fractional three-cycles parallel to the $\Omega\mathcal{R}\mathbb{Z}_2^{(1)}$-plane can be written as linear combinations of the fractional three-cycles parallel to the $\Omega\mathcal{R}$-plane.

Exceptional contributions to $\Omega\mathcal{R}$-invariant 3-cycles for $T^6/(\mathbb{Z}_2\times\mathbb{Z}_6\times\Omega\mathcal{R})$ on aAA	
aAA : $\mathbb{Z}_2^{(1)}$	
$\Pi^{\mathbb{Z}_2^{(1)}}_{\mathrm{h},(0,0)}$	$\varepsilon_0^{(1)}+(-1)^{\tau_2}\,\varepsilon_1^{(1)}+(-1)^{\tau_3}\,\varepsilon_2^{(1)}+(-1)^{\tau_2+\tau_3}\,\varepsilon_3^{(1)}$
$\Pi^{\mathbb{Z}_2^{(1)}}_{\mathrm{h},(1,0)}$	$[1+(-1)^{\tau_2}]\,\varepsilon_1^{(1)}+(-1)^{\tau_3}\,\varepsilon_4^{(1)}+(-1)^{\tau_2+\tau_3}\,\varepsilon_5^{(1)}$
$\Pi^{\mathbb{Z}_2^{(1)}}_{\mathrm{h},(0,1)}$	$[1+(-1)^{\tau_3}]\,\varepsilon_2^{(1)}+(-1)^{\tau_2}\,\varepsilon_4^{(1)}+(-1)^{\tau_2+\tau_3}\,\varepsilon_5^{(1)}$
$\Pi^{\mathbb{Z}_2^{(1)}}_{\mathrm{h},(1,1)}$	$[(-1)^{\tau_2}+(-1)^{\tau_3}]\,\varepsilon_3^{(1)}+(-1)^{\tau_2+\tau_3}\,\varepsilon_4^{(1)}+\varepsilon_5^{(1)}$
$\Pi^{\mathbb{Z}_2^{(1)}}_{\mathrm{v},(0,0)}$	$\tilde{\varepsilon}_0^{(1)}+(-1)^{\tau_2}\tilde{\varepsilon}_1^{(1)}+(-1)^{\tau_3}\tilde{\varepsilon}_2^{(1)}+(-1)^{\tau_2+\tau_3}\tilde{\varepsilon}_3^{(1)}$
$\Pi^{\mathbb{Z}_2^{(1)}}_{\mathrm{v},(1,0)}$	$[1+(-1)^{\tau_2}]\tilde{\varepsilon}_1^{(1)}+(-1)^{\tau_3}\tilde{\varepsilon}_4^{(1)}+(-1)^{\tau_2+\tau_3}\tilde{\varepsilon}_5^{(1)}$
$\Pi^{\mathbb{Z}_2^{(1)}}_{\mathrm{v},(0,1)}$	$[1+(-1)^{\tau_3}]\tilde{\varepsilon}_2^{(1)}+(-1)^{\tau_2}\tilde{\varepsilon}_4^{(1)}+(-1)^{\tau_2+\tau_3}\tilde{\varepsilon}_5^{(1)}$
$\Pi^{\mathbb{Z}_2^{(1)}}_{\mathrm{v},(1,1)}$	$[(-1)^{\tau_2}+(-1)^{\tau_3}]\tilde{\varepsilon}_3^{(1)}+(-1)^{\tau_2+\tau_3}\tilde{\varepsilon}_4^{(1)}+\tilde{\varepsilon}_5^{(1)}$
aAA : $\mathbb{Z}_2^{(i)}$ with $(i,j)\in\{(2,3),(3,2)\}$	
$\Pi^{\mathbb{Z}_2^{(i)}}_{\mathrm{h},(\sigma_1,0)}$	$(-1)^{\tau_j}\left[\varepsilon^{(i)}_{k_1}+(-1)^{\tau_1}\varepsilon^{(i)}_{k_2}\right]$
$\Pi^{\mathbb{Z}_2^{(i)}}_{\mathrm{h},(\sigma_1,1)}$	$-(-1)^{\tau_j}\varepsilon^{(i)}_{k_1}-[1-(-1)^{\tau_j}]\tilde{\varepsilon}^{(i)}_{k_1}-(-1)^{\tau_1}\left[(-1)^{\tau_j}\varepsilon^{(i)}_{k_2}+[1-(-1)^{\tau_j}]\tilde{\varepsilon}^{(i)}_{k_2}\right]$
$\Pi^{\mathbb{Z}_2^{(i)}}_{\mathrm{v},(\sigma_1,0)}$	$(-1)^{\tau_j}\left[-\varepsilon^{(i)}_{k_1}+2\tilde{\varepsilon}^{(i)}_{k_1}+(-1)^{\tau_1}\left(-\varepsilon^{(i)}_{k_2}+2\tilde{\varepsilon}^{(i)}_{k_2}\right)\right]$
$\Pi^{\mathbb{Z}_2^{(i)}}_{\mathrm{v},(\sigma_1,1)}$	$[2-(-1)^{\tau_j}]\varepsilon^{(i)}_{k_1}-[1+(-1)^{\tau_j}]\tilde{\varepsilon}^{(i)}_{k_1}+(-1)^{\tau_1}\left[[2-(-1)^{\tau_j}]\varepsilon^{(i)}_{k_2}-[1+(-1)^{\tau_j}]\tilde{\varepsilon}^{(i)}_{k_2}\right]$

Table 8.5: Contributions of the exceptional three-cycles to the fractional three-cycles supporting USp enhancement as defined in (8.10) on the **aAA** lattice. The subscript of the three-cycles in the left column indicates whether the one-cycle on $T^2_{(i)}$ of the $\mathbb{Z}_2^{(i)}$ exceptional three-cycle is parallel to the $\Omega\mathcal{R}$-plane (h) or perpendicular to it (v). Also, it gives the discrete shifts (σ_j,σ_k) on $T^2_{(j)}\times T^2_{(k)}$ for the three-cycles of the $\mathbb{Z}_2^{(i)}$ twisted sector.

In the end, the algorithm provided a set of 16 linearly independent fractional three-cycles parallel to the $\Omega\mathcal{R}$- and $\Omega\mathcal{R}\mathbb{Z}_2^{(3)}$-planes, which we give in appendix B.2. We see from appendix B.2 that in the present case, the three-cycles supporting USp enhancement already provide the full set of 16 linearly independent equations.
Thus, it is not needed to include the fractional three-cycles supporting SO enhancement, since these are necessarily linear combinations of the 16 fractional three-cycles given in appendix B.2. The 16 fractional three-cycles can be arranged into a nicer form in order to

subsequently derive the 16 sufficient conditions by using table 8.4:

$$\left(\begin{array}{c}
\frac{\rho_1}{4}+\frac{\varepsilon_4^{(1)}-\varepsilon_5^{(1)}}{4}+\frac{\varepsilon_1^{(2)}-2\,\tilde{\varepsilon}_1^{(2)}}{4}+\frac{\varepsilon_2^{(2)}-2\,\tilde{\varepsilon}_2^{(2)}}{4}+\frac{\varepsilon_1^{(3)}+\varepsilon_2^{(3)}}{4}\\
\varepsilon_1^{(3)}\\
\frac{\varepsilon_1^{(2)}-2\,\tilde{\varepsilon}_1^{(2)}}{2}+\frac{\varepsilon_1^{(3)}}{2}\\
\varepsilon_2^{(3)}\\
\frac{\varepsilon_2^{(2)}-2\,\tilde{\varepsilon}_2^{(2)}}{2}+\frac{\varepsilon_2^{(3)}}{2}\\
\frac{\varepsilon_4^{(1)}-\varepsilon_5^{(1)}}{2}+\frac{\varepsilon_1^{(3)}+\varepsilon_2^{(3)}}{2}\\
\hline
\frac{\rho_1}{4}+\frac{\varepsilon_4^{(1)}-\varepsilon_5^{(1)}}{4}+\frac{\varepsilon_3^{(2)}-2\,\tilde{\varepsilon}_3^{(2)}}{4}+\frac{\varepsilon_4^{(2)}-2\,\tilde{\varepsilon}_4^{(2)}}{4}+\frac{\varepsilon_3^{(3)}+\varepsilon_4^{(3)}}{4}\\
\varepsilon_4^{(3)}\\
\frac{\varepsilon_4^{(2)}-2\,\tilde{\varepsilon}_4^{(2)}}{2}+\frac{\varepsilon_4^{(3)}}{2}\\
\frac{\varepsilon_4^{(1)}-\varepsilon_5^{(1)}}{2}+\frac{\varepsilon_3^{(3)}+\varepsilon_4^{(3)}}{2}\\
\hline
\frac{\rho_3-2\rho_4}{4}+\frac{\tilde{\varepsilon}_0^{(1)}+\tilde{\varepsilon}_1^{(1)}+\tilde{\varepsilon}_2^{(1)}+\tilde{\varepsilon}_3^{(1)}}{4}+\frac{(\varepsilon_2^{(2)}-2\tilde{\varepsilon}_2^{(2)})+(\varepsilon_3^{(2)}-2\tilde{\varepsilon}_3^{(2)})}{4}+\frac{\varepsilon_2^{(3)}+\varepsilon_3^{(3)}}{4}\\
\frac{\tilde{\varepsilon}_0^{(1)}+\tilde{\varepsilon}_2^{(1)}}{2}\\
\frac{\tilde{\varepsilon}_1^{(1)}+\tilde{\varepsilon}_2^{(1)}}{2}\\
\tilde{\varepsilon}_3^{(1)}\\
\frac{\tilde{\varepsilon}_1^{(1)}+\tilde{\varepsilon}_3^{(1)}}{2}+\frac{\varepsilon_2^{(3)}+\varepsilon_3^{(3)}}{2}\\
\hline
\frac{\rho_3-2\rho_4}{4}+\frac{2\,\tilde{\varepsilon}_1^{(1)}+\left(\tilde{\varepsilon}_4^{(1)}+\tilde{\varepsilon}_5^{(1)}\right)}{4}+\frac{(\varepsilon_2^{(2)}-2\,\tilde{\varepsilon}_2^{(2)})+(\varepsilon_3^{(2)}-2\,\tilde{\varepsilon}_3^{(2)})}{4}-\frac{\varepsilon_2^{(3)}+\varepsilon_3^{(3)}}{4}
\end{array}\right)\circ\sum_a N_a\,k_a\Pi_a^{\text{frac}}$$

$$=\sum_a N_a\,k_a\left(\begin{array}{c}
\frac{2U_a+V_a-(y_{4,a}^{(1)}-y_{5,a}^{(1)})-(2\,x_{1,a}^{(2)}+y_{1,a}^{(2)})-(2\,x_{2,a}^{(2)}+y_{2,a}^{(2)})-y_{1,a}^{(3)}-y_{2,a}^{(3)}}{4}\\
-y_{1,a}^{(3)}\\
-\frac{(2\,x_{1,a}^{(2)}+y_{1,a}^{(2)})+y_{1,a}^{(3)}}{2}\\
-y_{2,a}^{(3)}\\
-\frac{(2\,x_{2,a}^{(2)}+y_{2,a}^{(2)})+y_{2,a}^{(3)}}{2}\\
-\frac{(y_{4,a}^{(1)}-y_{5,a}^{(1)})+y_{1,a}^{(3)}+y_{2,a}^{(3)}}{2}\\
\hline
\frac{2U_a+V_a-(y_{4,a}^{(1)}-y_{5,a}^{(1)})-(2\,x_{3,a}^{(2)}+y_{3,a}^{(2)})-(2\,x_{4,a}^{(2)}+y_{4,a}^{(2)})-y_{3,a}^{(3)}-y_{4,a}^{(3)}}{4}\\
-y_{4,a}^{(3)}\\
-\frac{(2\,x_{4,a}^{(2)}+y_{4,a}^{(2)})+y_{4,a}^{(3)}}{2}\\
-\frac{(y_{4,a}^{(1)}-y_{5,a}^{(1)})+y_{3,a}^{(3)}+y_{4,a}^{(3)}}{2}\\
\hline
\frac{3Q_a+(3x_{0,a}^{(1)}+x_{1,a}^{(1)}+x_{2,a}^{(1)}+x_{3,a}^{(1)})-(2\,x_{2,a}^{(2)}+y_{2,a}^{(2)})-(2\,x_{3,a}^{(2)}+y_{3,a}^{(2)})-y_{2,a}^{(3)}-y_{3,a}^{(3)}}{4}\\
\frac{3x_{0,a}^{(1)}+x_{2,a}^{(1)}}{2}\\
\frac{x_{1,a}^{(1)}+x_{2,a}^{(1)}}{2}\\
x_{3,a}^{(1)}\\
\frac{x_{1,a}^{(1)}+x_{3,a}^{(1)}-y_{2,a}^{(3)}-y_{3,a}^{(3)}}{2}\\
\frac{3Q_a+2x_{1,a}^{(1)}+(x_{4,a}^{(1)}+x_{5,a}^{(1)})-(2\,x_{2,a}^{(2)}+y_{2,a}^{(2)})-(2\,x_{3,a}^{(2)}+y_{3,a}^{(2)})+y_{2,a}^{(3)}+y_{3,a}^{(3)}}{4}
\end{array}\right)\overset{!}{=}0\bmod n\,. \tag{8.14}$$

The 16 equations above also contain the K-theory constraints, which can be seen by comparing (8.5) and (2.51). Indeed, by taking $k_a = 1\ \forall a$, and $n = 2$ in equation (8.5), we find exactly the K-theory constraints (2.51), as Π_{probe} in (2.51) corresponds to any cycle carrying an USp group. In other words, the fulfilling of the K-theory constraints guarantees a discrete $\mathbb{Z}_2$-symmetry. This is only valid in the particular case where all the $\mathbb{Z}_n$-conditions are derived from three-cycles supporting USp enhancement. Had we been forced to also take into consideration the $\Omega\mathcal{R}$-even three-cycles supporting SO enhancement in order to obtain a full set of 16 linearly independent $\Omega\mathcal{R}$-even fractional three-cycles, the K-theory constraints could not have been derived as easily from the $\mathbb{Z}_n$-conditions (8.14).

In the next sections, we will determine the discrete $\mathbb{Z}_n$-symmetries and massless $U(1)$ symmetries for the global MSSM and left-right symmetric models we have previously unearthed.

8.3 $\mathbb{Z}_n$-symmetries in the global five-stack MSSM

In this section, we will derive the $\mathbb{Z}_n$-conditions for the global effective MSSM-like model we dug out in the previous chapter. For this first model, we will derive the results in some detail in order to show how the computation is done. For the following models in the next sections, we will only indicate the results, and we will avoid giving all the intermediate steps.
The $\mathbb{Z}_n$-symmetries can be used to reinforce the interpretation of the chiral spectrum, as the charges of the particles under these discrete symmetries should be compatible with the results found from the field theoretical side of SUSY models. Also, they provide a solid consistency check with the results derived in the next chapter 9.
To this end, we need the bulk and exceptional wrapping numbers of the various stacks associated to the model indicated in table 7.17. Remember that the bulk wrapping numbers of the five stacks were $(P,Q,U,V) = (1,0,0,0)$ for a,h, and $(P,Q,U,V) = (3,0,0,0)$ for b,c,d, with the ranks: $N_a = 3,\ N_b = N_c = N_d = 1,\ N_h = 4$.
For the first twisted sector, the exceptional wrapping numbers for each stack can be found in table 8.6.

The exceptional wrapping numbers of the five stacks in the second and third twisted sectors

Pairs $(x^{(1)}_{\alpha,z}, y^{(1)}_{\alpha,z}),\ \alpha = 0\ldots5,\ z \in \{a,b,c,d,h\}$ **of the global MSSM**												
Stack	$x^{(1)}_0$	$y^{(1)}_0$	$x^{(1)}_1$	$y^{(1)}_1$	$x^{(1)}_2$	$y^{(1)}_2$	$x^{(1)}_3$	$y^{(1)}_3$	$x^{(1)}_4$	$y^{(1)}_4$	$x^{(1)}_5$	$y^{(1)}_5$
a	0	0	0	0	0	0	2	0	-1	0	-1	0
b	0	0	0	0	0	0	0	0	1	0	-1	0
c	0	0	0	0	0	0	-2	0	1	0	1	0
d	0	0	0	0	0	0	0	0	-1	0	1	0
h	0	0	0	0	0	0	-2	0	1	0	1	0

Table 8.6: Exceptional wrapping numbers of the first $\mathbb{Z}_2$-twisted sector for the five stacks of the global MSSM-like model found on $T^6/(\mathbb{Z}_2 \times \mathbb{Z}_6 \times \Omega\mathcal{R})$ with discrete torsion, $\eta = \eta_{\Omega\mathcal{R}\mathbb{Z}_2^{(3)}} = -1$.

can be found in table 8.7.

With these data, we can derive first the necessary conditions for the existence of discrete

Pairs $(x^{(2,3)}_{\alpha,z}, y^{(2,3)}_{\alpha,z})$, $\alpha = 1\ldots4$, $z \in \{a,b,c,d,h\}$ **of the global MSSM**																
Stack	$x_1^{(2)}$	$y_1^{(2)}$	$x_2^{(2)}$	$y_2^{(2)}$	$x_3^{(2)}$	$y_3^{(2)}$	$x_4^{(2)}$	$y_4^{(2)}$	$x_1^{(3)}$	$y_1^{(3)}$	$x_2^{(3)}$	$y_2^{(3)}$	$x_3^{(3)}$	$y_3^{(3)}$	$x_4^{(3)}$	$y_4^{(3)}$
a	-1	2	-1	2	0	0	0	0	1	-2	1	-2	0	0	0	0
b	-1	2	-1	2	0	0	0	0	-3	0	-3	0	0	0	0	0
c	-3	0	-3	0	0	0	0	0	3	0	3	0	0	0	0	0
d	3	0	3	0	0	0	0	0	-1	2	-1	2	0	0	0	0
h	1	-2	1	-2	0	0	0	0	1	-2	1	-2	0	0	0	0

Table 8.7: Exceptional wrapping numbers of the second and third $\mathbb{Z}_2$-twisted sectors for the five stacks of the global MSSM-like model found on $T^6/(\mathbb{Z}_2 \times \mathbb{Z}_6 \times \Omega\mathcal{R})$ with discrete torsion, $\eta = \eta_{\Omega\mathcal{R}\mathbb{Z}_2^{(3)}} = -1$.

symmetries from (8.9):

$$k_a \begin{pmatrix} 0 \\ 0 \\ \hline 0 \\ 0 \\ 0 \\ 6 \\ -6 \\ 0 \\ 0 \\ 0 \\ 0 \\ 0 \\ \hline 6 \\ 6 \\ 0 \\ 0 \end{pmatrix} + k_c \begin{pmatrix} 0 \\ 0 \\ \hline 0 \\ 0 \\ 0 \\ -2 \\ 2 \\ 0 \\ 6 \\ 6 \\ 0 \\ 0 \\ \hline 0 \\ 0 \\ 0 \\ 0 \end{pmatrix} + k_d \begin{pmatrix} 0 \\ 0 \\ \hline 0 \\ 0 \\ 0 \\ 0 \\ 0 \\ 0 \\ -6 \\ -6 \\ 0 \\ 0 \\ \hline -2 \\ -2 \\ 0 \\ 0 \end{pmatrix} + k_h \begin{pmatrix} 0 \\ 0 \\ \hline 0 \\ 0 \\ 0 \\ -8 \\ 8 \\ 0 \\ 0 \\ 0 \\ 0 \\ 0 \\ \hline 8 \\ 8 \\ 0 \\ 0 \end{pmatrix} \stackrel{!}{=} 0 \bmod n\,. \tag{8.15}$$

We see that we have no contributions from the b stack, since the associated entries are all zero. Thus, k_b is arbitrary, which is due to the fact that the b stack supports a symplectic $USp(2)$ group and not an unitary $U(2) = SU(2) \times U(1)$ group, and so the b stack does not give rise to a $U(1)_b$ factor.

A look at the equations immediately reveals that ten out of the 16 equations are trivially satisfied, as they have zero entries. Also, there are redundancies among the remaining six equations. In fact, we are left with three equations which are not trivial and which are not

multiples of each other:

$$\begin{aligned} -6k_a + 2k_c + 8k_h &\stackrel{!}{=} 0 \bmod n, \\ 6k_c - 6k_d &\stackrel{!}{=} 0 \bmod n, \\ 6k_a - 2k_d + 8k_h &\stackrel{!}{=} 0 \bmod n. \end{aligned} \tag{8.16}$$

These equations give a first hint for the existence of discrete $\mathbb{Z}_n$-symmetries. The massless $U(1)$ combinations can be obtained by setting the right-hand side equal to zero:

$$\begin{aligned} &(1) \qquad -6k_a + 2k_c + 8k_h = 0\,, \\ &(2) \qquad 6k_c - 6k_d = 0\,, \\ &(3) \qquad 6k_a - 2k_d + 8k_h = 0\,. \end{aligned}$$

For a massless $U(1)$, the second equation immediately implies $k_c = k_d$. Taking this into account and adding the first and third equation gives us:

$$\begin{aligned} &(1) \qquad -6k_a + 2k_c + 8k_h = 0\,, \\ &(2), (1)+(3) \qquad 16k_h = 0\,. \end{aligned}$$

Thus, the solutions are of the form $(k_a, 3k_a, 3k_a, 0)$. Non-equivalent solutions satisfy $gcd(k_a, 3k_a, 3k_a, 0) = 1$, so the only solution left is $(k_a, k_c, k_d, k_h) = (1, 3, 3, 0)$. This solution corresponds in fact up to normalization to the $U(1)_Y$ hypercharge defined as:

$$Q_y = \frac{1}{6}Q_a + \frac{1}{2}Q_c + \frac{1}{2}Q_d\,. \tag{8.17}$$

Hence, this is the only massless $U(1)$ combination we have. The standard definition we chose in the previous chapter for the hypercharge is thus consistent with our results in the present section, and the hypercharge acts as an unbroken gauge symmetry $U(1)_Y$, and not as a global $U(1)$ symmetry. Since it is the only solution to the equations above, we can already conclude that the global effective five-stack MSSM-like model does not present dark photons. Anticipating a bit, let us also point out that this definition for the hypercharge also satisfies the sufficient conditions given by the equations derived below. Thus, the hypercharge can be used to induce a base shift of the discrete symmetries in order to put the $\mathbb{Z}_n$-charges of the left-handed quarks equal to zero.
In a second step, we have to insert the bulk and exceptional wrapping numbers given above

into the equations (8.14) in order to derive the sufficient conditions:

$$k_a \begin{pmatrix} 3 \\ 6 \\ 3 \\ 6 \\ 3 \\ 6 \\ \hline 0 \\ 0 \\ 0 \\ 0 \\ \hline 3 \\ 0 \\ 0 \\ 6 \\ 6 \\ -3 \end{pmatrix} + k_c \begin{pmatrix} 3 \\ 0 \\ 3 \\ 0 \\ 3 \\ 0 \\ \hline 0 \\ 0 \\ 0 \\ 0 \\ \hline 1 \\ 0 \\ 0 \\ -2 \\ -1 \\ 2 \end{pmatrix} + k_d \begin{pmatrix} -4 \\ -2 \\ -4 \\ -2 \\ -4 \\ -2 \\ \hline 0 \\ 0 \\ 0 \\ 0 \\ \hline -2 \\ 0 \\ 0 \\ 0 \\ -1 \\ -1 \end{pmatrix} + k_h \begin{pmatrix} 4 \\ 8 \\ 4 \\ 8 \\ 4 \\ 8 \\ \hline 0 \\ 0 \\ 0 \\ 0 \\ \hline 0 \\ 0 \\ 0 \\ -8 \\ 0 \\ 0 \end{pmatrix} \stackrel{!}{=} 0 \bmod n\,. \tag{8.18}$$

This time, six equations out of the 16 equations are trivial, as they have zero entries. The set of different non-trivial equations is given by:

$$\begin{aligned} 3k_a + 3k_c - 4k_d + 4k_h &\stackrel{!}{=} 0 \bmod n, \\ 6k_a - 2k_d + 8k_h &\stackrel{!}{=} 0 \bmod n, \\ 3k_a + k_c - 2k_d &\stackrel{!}{=} 0 \bmod n, \\ 6k_a - 2k_c - 8k_h &\stackrel{!}{=} 0 \bmod n, \\ 6k_a - k_c - k_d &\stackrel{!}{=} 0 \bmod n, \\ -3k_a + 2k_c - k_d &\stackrel{!}{=} 0 \bmod n. \end{aligned} \tag{8.19}$$

However, since we have only four stacks yielding a $U(1)$ factor with already a massless $U(1)_Y$ present, we expect at most three linearly independent equations by taking both the necessary and sufficient conditions together. For example, the first, the third and the fifth equation of the sufficient conditions above are linearly independent. In order to get an idea of the possible discrete symmetries showing up, a computer scan is helpful, which can be found in appendix B.2.2.

However, not all the discrete symmetries found in appendix B.2.2 correspond to non-equivalent $\mathbb{Z}_n$-symmetries. Indeed, the five stacks of this particular model provide a total of four $U(1)$'s. Thus, we can have at most three independent discrete $\mathbb{Z}_n$-symmetries, giving together with the continuous $U(1)_Y$ hypercharge we already found, a total of four independent $U(1)$ combinations. In order to detect equivalent $\mathbb{Z}_n$-symmetries, the $\mathbb{Z}_n$-charges of the particle spectrum have to be calculated. Since a $\mathbb{Z}_n$-symmetry with high values of n

often can be decomposed into $\mathbb{Z}_n$-symmetries with low values for n, it is unlikely to find independent $\mathbb{Z}_n$-symmetries with high values for n. We will illustrate this on some examples of $\mathbb{Z}_n$-symmetries taken from the table given in appendix B.2.2.
Let us consider the examples of $\mathbb{Z}_n$-symmetries given in table 8.8.

Sample of discrete $\mathbb{Z}_n$-symmetries									
k_a	k_c	k_d	k_h	n	k_a	k_c	k_d	k_h	n
1	1	1	1	2	3	2	2	0	7
0	1	2	2	3	3	1	1	0	8
1	0	0	0	3	1	0	6	3	9
0	0	0	1	4	4	2	2	5	10
2	1	1	0	5	4	1	1	0	11
0	2	4	1	6	0	4	8	5	12

Table 8.8: Sample of discrete $\mathbb{Z}_n$-symmetries taken from appendix B.2.2. In order to detect independent $\mathbb{Z}_n$-symmetries, the charges of the matter states of the global MSSM under these discrete $\mathbb{Z}_n$-symmetries have to be analyzed.

The charges are calculated in the same way as the hypercharge by writing $Q_{\mathbb{Z}_n} = k_a Q_a + k_c Q_c + k_d Q_d + k_h Q_h$. Table 8.9 shows the charges of the matter states under the symmetries displayed in table 8.8. Note that the upper label of $\mathbb{Z}_3^i$ in table 8.9 just numerates the discrete symmetries in the same order as they appear in table 8.8. For example, $\mathbb{Z}_3^1$ corresponds to the first $\mathbb{Z}_3$-symmetry appearing in table 8.8, namely the one given by $(k_a, k_c, k_d, k_h) = (0, 1, 2, 2)$.

Note that in the case of non-chiral pairs of matter states, only the charge of one member of the pair is indicated in table 8.9.
In a second step, each $\mathbb{Z}_n$-charge is shifted by a certain factor times the hypercharge so that the $\mathbb{Z}_n$-charges of the left-handed quarks arising in the $ab = ab'$ sector become zero, as indicated in table 8.10.

Now we can compare the different $\mathbb{Z}_n$-symmetries and see whether they are truly independent. We see that the most exotic discrete symmetries such as $\mathbb{Z}_5, \mathbb{Z}_7, \mathbb{Z}_8$ and $\mathbb{Z}_{11}$ all act trivially on the particle spectrum after a shift by the hypercharge, so these do not give rise to any new charge selection rules on the couplings and have no influence whatsoever in the model. Thus, these symmetries just correspond to discrete subgroups of the continuous hypercharge.
The $\mathbb{Z}_{10}$ is clearly homomorphic to the $\mathbb{Z}_2$ symmetry as a look at the charges in table 8.10 yields. Similarly, $\mathbb{Z}_9$ is equivalent to $\mathbb{Z}_3^1$. Moreover, the charges of $\mathbb{Z}_6$ and those of $\mathbb{Z}_{12}$ can for both symmetries be mapped to the charges of $\mathbb{Z}_3^1$. The mapping can be done as follows:

$\mathbb{Z}_6$-charges	$\longrightarrow$	$\mathbb{Z}_3^1$-charges	$\mathbb{Z}_{12}$-charges	$\longrightarrow$	$\mathbb{Z}_3^1$-charges
$0, 3$	$\longrightarrow$	0	$0, 3, 6, 9$	$\longrightarrow$	0
$2, 5$	$\longrightarrow$	1	$1, 4, 7, 10$	$\longrightarrow$	1
$1, 4$	$\longrightarrow$	2	$2, 5, 8, 11$	$\longrightarrow$	2

(8.20)

These examples illustrate that indeed, all discrete $\mathbb{Z}_n$-symmetries with higher values of n can be mapped to $\mathbb{Z}_n$-symmetries with lower values for n. Thus, it makes sense to restrict

Examples of discrete $\mathbb{Z}_n$-symmetries and charges for the global MSSM-like model														
sector		$(6\cdot)Q_Y$	$\mathbb{Z}_2$	$\mathbb{Z}_3^1$	$\mathbb{Z}_3^2$	$\mathbb{Z}_4$	$\mathbb{Z}_5$	$\mathbb{Z}_6$	$\mathbb{Z}_7$	$\mathbb{Z}_8$	$\mathbb{Z}_9$	$\mathbb{Z}_{10}$	$\mathbb{Z}_{11}$	$\mathbb{Z}_{12}$
$ab = ab'$	$3 \times (\mathbf{3},\mathbf{2},\mathbf{1})_{(1,0,0,0)}$	1	1	0	1	0	2	0	3	3	1	4	4	0
ac	$6 \times (\overline{\mathbf{3}},\mathbf{1},\mathbf{1})_{(-1,1,0,0)}$	2	0	1	2	0	4	2	6	6	8	8	8	4
ad	$3 \times (\mathbf{3},\mathbf{1},\mathbf{1})_{(1,0,-1,0)}$	-2	0	1	1	0	1	2	1	2	4	2	3	4
ad'	$3 \times (\overline{\mathbf{3}},\mathbf{1},\mathbf{1})_{(-1,0,-1,0)}$	-4	0	1	2	0	2	2	2	4	2	4	6	4
$bc = b'c$	$3 \times (\mathbf{1},\mathbf{2},\mathbf{1})_{(0,1,0,0)}$	3	1	1	0	0	1	2	2	1	0	2	1	4
$bc = b'c$	$3 \times \left[(\mathbf{1},\mathbf{2},\mathbf{1})_{(0,1,0,0)} + h.c.\right]$	3	1	1	0	0	1	2	2	1	0	2	1	4
$bd = b'd$	$6 \times (\mathbf{1},\mathbf{2},\mathbf{1})_{(0,0,-1,0)}$	-3	1	1	0	0	4	2	5	7	3	8	10	4
$bd = b'd$	$2 \times \left[(\mathbf{1},\mathbf{2},\mathbf{1})_{(0,0,-1,0)} + h.c.\right]$	-3	1	1	0	0	4	2	5	7	3	8	10	4
cd	$3 \times (\mathbf{1},\mathbf{1},\mathbf{1})_{(0,-1,1,0)}$	0	0	1	0	0	0	2	0	0	6	0	0	4
cd	$3 \times \left[(\mathbf{1},\mathbf{1},\mathbf{1})_{(0,-1,1,0)} + h.c.\right]$	0	0	1	0	0	0	2	0	0	6	0	0	4
cd'	$3 \times (\mathbf{1},\mathbf{1},\mathbf{1})_{(0,1,1,0)}$	6	0	0	0	0	2	0	4	2	6	4	2	0
cd'	$3 \times \left[(\mathbf{1},\mathbf{1},\mathbf{1})_{(0,1,1,0)} + h.c.\right]$	6	0	0	0	0	2	0	4	2	6	4	2	0
ah	$2 \times \left[(\mathbf{3},\mathbf{1},\overline{\mathbf{4}})_{(1,0,0,-1)} + h.c.\right]$	1	0	1	1	3	2	5	3	3	7	9	4	7
ah'	$(\mathbf{3},\mathbf{1},\mathbf{4})_{(1,0,0,1)} + h.c.$	1	0	2	1	1	2	1	3	3	4	9	4	5
$bh = b'h$	$3 \times (\mathbf{1},\mathbf{2},\mathbf{4})_{(0,0,0,1)}$	0	1	2	0	1	0	1	0	0	3	5	0	5
ch'	$6 \times (\mathbf{1},\mathbf{1},\overline{\mathbf{4}})_{(0,-1,0,-1)}$	-3	0	0	0	3	4	3	5	7	6	3	10	3
dh	$3 \times (\mathbf{1},\mathbf{1},\overline{\mathbf{4}})_{(0,0,1,-1)}$	3	0	0	0	3	1	3	2	1	3	7	1	3
dh'	$3 \times (\mathbf{1},\mathbf{1},\mathbf{4})_{(0,0,1,1)}$	3	0	1	0	1	1	5	2	1	0	7	1	1
aa'	$2 \times [(\mathbf{3_A},\mathbf{1},\mathbf{1})_{(2,0,0,0)} + h.c.]$	2	0	0	2	0	4	0	6	6	2	8	8	0
$bb' \equiv bb$	$5 \times (\mathbf{1},\mathbf{1_A},\mathbf{1})_{(0,0,0,0)}$	0	0	0	0	0	0	0	0	0	0	0	0	0
cc	$4 \times (\mathbf{1},\mathbf{1},\mathbf{1})_{(0,0,0,0)}$	0	0	0	0	0	0	0	0	0	0	0	0	0
dd	$5 \times (\mathbf{1},\mathbf{1},\mathbf{1})_{(0,0,0,0)}$	0	0	0	0	0	0	0	0	0	0	0	0	0
hh'	$2 \times [(\mathbf{1},\mathbf{1},\mathbf{6_A})_{(0,0,0,2)} + h.c.]$	0	0	1	0	2	0	2	0	0	6	0	0	10

Table 8.9: Discrete $\mathbb{Z}_n$-charges of the massless open string spectrum of the global MSSM-like model. For non-chiral pairs of particles, only the charges of the first state are indicated. The representations of the particles correspond to the gauge group $(SU(3)_a \times USp(2)_b \times SU(4)_h)_{U(1)_a \times U(1)_c \times U(1)_d \times U(1)_h}$.

the analysis to values of n less than e.g. six: $n = 2, 3, 4, 5, 6$.
Note that we also always obtain a set of discrete symmetries arising from the centers of the non-Abelian $U(N)$ gauge factors. Indeed, the actual gauge group of a stack without gauge group enhancement is given by $U(N) = \frac{SU(N)\times U(1)}{\mathbb{Z}_N}$. The commuting group element $\mathrm{diag}(\alpha \dots \alpha)$ with $\alpha = e^{2i\pi/N}$ can be considered to belong either to $SU(N)$ or $U(1)$. Taking the quotient by $\mathbb{Z}_N$ expresses that the two viewpoints are equivalent. However, the charges of the states under this $\mathbb{Z}_N$-symmetry are the same as those under $SU(N)$, so these discrete symmetries arising as centers of gauge groups provide no selection rules distinct from the $SU(N)$ gauge invariance itself [100]. Hence, such discrete symmetries are not really relevant in phenomenology. In our case, the $\mathbb{Z}_3^2$ and $\mathbb{Z}_4$ are such symmetries.

The results can be summarized as follows:

Examples of shifted discrete $\mathbb{Z}_n$-symmetries and charges for the global MSSM-like model														
sector		$(6\cdot)Q_Y$	$\mathbb{Z}_2$	$\mathbb{Z}_3^1$	$\mathbb{Z}_3^2$	$\mathbb{Z}_4$	$\mathbb{Z}_5$	$\mathbb{Z}_6$	$\mathbb{Z}_7$	$\mathbb{Z}_8$	$\mathbb{Z}_9$	$\mathbb{Z}_{10}$	$\mathbb{Z}_{11}$	$\mathbb{Z}_{12}$
$ab = ab'$	$3 \times (\mathbf{3},\mathbf{2},\mathbf{1})_{(1,0,0,0)}$	1	0	0	0	0	0	0	0	0	0	0	0	0
ac	$6 \times (\overline{\mathbf{3}},\mathbf{1},\mathbf{1})_{(-1,1,0,0)}$	2	0	1	0	0	0	2	0	0	6	0	0	4
ad	$3 \times (\mathbf{3},\mathbf{1},\mathbf{1})_{(1,0,-1,0)}$	-2	0	1	0	0	0	2	0	0	6	0	0	4
ad'	$3 \times (\overline{\mathbf{3}},\mathbf{1},\mathbf{1})_{(-1,0,-1,0)}$	-4	0	1	0	0	0	2	0	0	6	0	0	4
$bc = b'c$	$3 \times (\mathbf{1},\mathbf{2},\mathbf{1})_{(0,1,0,0)}$	3	0	1	0	0	0	2	0	0	6	0	0	4
$bc = b'c$	$3 \times \left[(\mathbf{1},\mathbf{2},\mathbf{1})_{(0,1,0,0)} + h.c.\right]$	3	0	1	0	0	0	2	0	0	6	0	0	4
$bd = b'd$	$6 \times (\mathbf{1},\mathbf{2},\mathbf{1})_{(0,0,-1,0)}$	-3	0	1	0	0	0	2	0	0	6	0	0	4
$bd = b'd$	$2 \times \left[(\mathbf{1},\mathbf{2},\mathbf{1})_{(0,0,-1,0)} + h.c.\right]$	-3	0	1	0	0	0	2	0	0	6	0	0	4
cd	$3 \times (\mathbf{1},\mathbf{1},\mathbf{1})_{(0,-1,1,0)}$	0	0	1	0	0	0	2	0	0	6	0	0	4
cd	$3 \times \left[(\mathbf{1},\mathbf{1},\mathbf{1})_{(0,-1,1,0)} + h.c.\right]$	0	0	1	0	0	0	2	0	0	6	0	0	4
cd'	$3 \times (\mathbf{1},\mathbf{1},\mathbf{1})_{(0,1,1,0)}$	6	0	0	0	0	0	0	0	0	0	0	0	0
cd'	$3 \times \left[(\mathbf{1},\mathbf{1},\mathbf{1})_{(0,1,1,0)} + h.c.\right]$	6	0	0	0	0	0	0	0	0	0	0	0	0
ah	$2 \times \left[(\mathbf{3},\mathbf{1},\overline{\mathbf{4}})_{(1,0,0,-1)} + h.c.\right]$	1	1	1	0	3	0	5	0	0	6	5	0	7
ah'	$(\mathbf{3},\mathbf{1},\mathbf{4})_{(1,0,0,1)} + h.c.$	1	1	2	0	1	0	1	0	0	3	5	0	5
$bh = b'h$	$3 \times (\mathbf{1},\mathbf{2},\mathbf{4})_{(0,0,0,1)}$	0	1	2	0	1	0	1	0	0	3	5	0	5
ch'	$6 \times (\mathbf{1},\mathbf{1},\overline{\mathbf{4}})_{(0,-1,0,-1)}$	-3	1	0	0	3	0	3	0	0	0	5	0	3
dh	$3 \times (\mathbf{1},\mathbf{1},\overline{\mathbf{4}})_{(0,0,1,-1)}$	3	1	0	0	3	0	3	0	0	0	5	0	3
dh'	$3 \times (\mathbf{1},\mathbf{1},\mathbf{4})_{(0,0,1,1)}$	3	1	1	0	1	0	5	0	0	6	5	0	1
aa'	$2 \times [(\mathbf{3_A},\mathbf{1},\mathbf{1})_{(2,0,0,0)} + h.c.]$	2	0	0	0	0	0	0	0	0	0	0	0	0
$bb' \equiv bb$	$5 \times (\mathbf{1},\mathbf{1_A},\mathbf{1})_{(0,0,0,0)}$	0	0	0	0	0	0	0	0	0	0	0	0	0
cc	$4 \times (\mathbf{1},\mathbf{1},\mathbf{1})_{(0,0,0,0)}$	0	0	0	0	0	0	0	0	0	0	0	0	0
dd	$5 \times (\mathbf{1},\mathbf{1},\mathbf{1})_{(0,0,0,0)}$	0	0	0	0	0	0	0	0	0	0	0	0	0
hh'	$2 \times [(\mathbf{1},\mathbf{1},\mathbf{6_A})_{(0,0,0,2)} + h.c.]$	0	0	1	0	2	0	2	0	0	6	0	0	10

Table 8.10: Discrete $\mathbb{Z}_n$-charges of the massless open string spectrum of the global MSSM-like model after a shift by the massless hypercharge. The shift is performed in such a way that the charges of the left-handed quarks Q_L are zero. The representations of the particles correspond to the gauge group $(SU(3)_a \times USp(2)_b \times SU(4)_h)_{U(1)_a \times U(1)_c \times U(1)_d \times U(1)_h}$.

1. The combination $(k_a, k_c, k_d, k_h) = (1, 0, 0, 0)$ associated to $\mathbb{Z}_3^2$ gives rise to a $\mathbb{Z}_3$-symmetry inherited from the $SU(3)_a$ group of the a stack. This symmetry is homomorphic to the center of the gauge group $SU(3)_a$, acting as a baryon-number-like discrete symmetry. Upon a basis shift by the massless hypercharge, this symmetry acts trivially on both the visible and the hidden sector.

2. The combination $(k_a, k_c, k_d, k_h) = (0, 0, 0, 1)$ gives rise to a $\mathbb{Z}_4$-symmetry inherited from the $SU(4)_h$ group of the hidden stack, homomorphic to the center of the gauge group $SU(4)_h$. It acts trivially on the visible sector, but non-trivially on exotic matter states. As mentioned before, it provides no new coupling selection rule beyond $SU(4)$ gauge invariance.

3. The combination $(k_a, k_c, k_d, k_h) = (1, 1, 1, 1)$ gives rise to the $\mathbb{Z}_2$-symmetry inherited from the K-theory constraints. It acts trivially on the visible spectrum, but non-trivially on the exotic matter states arising in the hidden sector. However, this $\mathbb{Z}_2$-symmetry corresponds to a linear combination of the $\mathbb{Z}_2$-symmetry hidden inside the massless hypercharge and the $\mathbb{Z}_2$-symmetry hidden as a sub-symmetry of the $\mathbb{Z}_4$-symmetry of the previous bullet point. This can be seen via the charges: after a shift by the massless hypercharge, the charges of the $\mathbb{Z}_4$-symmetry can be mapped to those of the $\mathbb{Z}_2$-symmetry by identifying the charge 0 of $\mathbb{Z}_2$ with the charges 0 and 2 of the $\mathbb{Z}_4$-symmetry, and the charge 1 of $\mathbb{Z}_2$ is mapped to the charges 1 and 3 of $\mathbb{Z}_4$. Thus, this $\mathbb{Z}_2$-symmetry should not be considered as an independent symmetry.

4. Finally, the combination $(k_a, k_c, k_d, k_h) = (0, 2, 4, 1)$ gives rise to a $\mathbb{Z}_6$-symmetry. However, in the low-energy effective field theory, it can be reduced to an effective $\mathbb{Z}_3$-symmetry, namely $\mathbb{Z}_3^1$ associated to $(k_a, k_c, k_d, k_h) = (0, 1, 2, 2)$, as we have shown above in (8.20).

The $\mathbb{Z}_6$ or effective $\mathbb{Z}_3$-symmetry merits a closer inspection, as it is the only one not arising from the center of some non-Abelian gauge factor or the K-theory constraints. Thus, it is the only one containing additional information compared to the information already contained in the gauge factors.
In table 7.18, we indicate the charges of the particle spectrum under the $\mathbb{Z}_6$-symmetry in the last column, and the charges under the effective $\mathbb{Z}_3$-symmetry are given in the second-to-last column. Comparing the charges of this discrete $\mathbb{Z}_3$-symmetry with the charges given in table 8.1 for baryon triality, we see that they do not match. Thus, the $\mathbb{Z}_3$ present in the global effective five-stack MSSM analyzed here corresponds to a new stringy discrete symmetry, which is not present in the field theory of the MSSM.
However, a closer look at the charges given in table 7.18 also reveals that the generator of this new stringy discrete symmetry seems a priori unsuited to be decomposed as has been done in (8.2). Indeed, the charges of the Higgses and the right-handed up quarks given in (8.4) are incompatible with table 7.18:

$$\begin{aligned} H_u: &\quad m = 1 \mod 3\,, \\ u_R: &\quad -m = 1 \mod 3\,. \end{aligned} \tag{8.21}$$

This is linked to the fact that we have an effective MSSM with an extended right-handed down quark sector, an extended left-handed lepton sector and an extended Higgs sector. Indeed, in the next chapter about Yukawa couplings, we will see that $\tilde{H}_u$ arising from the $bd = b'd$ sector couples to the right-handed up quarks as $Q_L \cdot \tilde{H}_u u_R$, whereas H_d arising from the $bc = b'c$ sector couples to the right-handed down quarks as $Q_L \cdot H_d d_R$. Consequently, if we replace H_u by $\tilde{H}_u$, which has a different $\mathbb{Z}_3$-charge, as shown in table 7.18, the constraints on the charges become:

$$\begin{aligned} \tilde{H}_u: &\quad m = 2 \mod 3\,, \\ u_R: &\quad -m = 1 \mod 3\,. \end{aligned} \tag{8.22}$$

This is perfectly compatible. Similarly, our stringy $\mathbb{Z}_3$-symmetry forbids by charge selection rules the three-point coupling of $\tilde{H}_d$ to the right-handed down quarks d_R, which is consistent

with our results in the next chapter. Such a coupling would have been problematic as we have:

$$\begin{aligned} \tilde{H}_d: &\quad -m+k=1 \mod 3\,, \\ d_R: &\quad m-k=1 \mod 3\,. \end{aligned} \tag{8.23}$$

Since only H_d appears in our Yukawa couplings though, the decomposition works out:

$$\begin{aligned} H_d: &\quad -m+k=2 \mod 3\,, \\ d_R: &\quad m-k=1 \mod 3\,. \end{aligned} \tag{8.24}$$

This is compatible. In fact, we can take for the generator of our stringy $\mathbb{Z}_3$-symmetry the product $\mathcal{R}_3^2\mathcal{A}_3\mathcal{L}_3$, i.e. $m=2, k=1, p=1$. Inserting these values into (8.4) gives us almost the charges indicated in table 7.18.
An exception is given by the right-handed neutrinos. More precisely, table 7.18 tells us that the $\mathbb{Z}_3$-charge of the right-handed neutrinos arising in the *cd* sector equals one. However, the formulas (8.4) imply that the charges of the right-handed neutrinos should be zero: $-m+k+p = -2+1+1 = 0$. Since this is not the case, the right-handed neutrinos cannot be paired off with the Higgs field $\tilde{H}_u$ to provide invariant Yukawa terms. Instead, they couple to H_u to produce Yukawa couplings, which is confirmed by our results in the next chapter. Hence, the singlet states arising in the *cd* sector may not correspond to the right-handed neutrinos of the MSSM, just as H_u and $\tilde{H}_d$ should not be interpreted as the traditional Higgs fields of the MSSM. The issue can be solved by identifying the right-handed neutrino states with the singlet states arising in the *cc* or *dd* sectors, instead of the singlet states coming from the *cd* sector as is traditionally done. With this new interpretation, the right-handed neutrinos can be given mass with a cubic coupling involving $\tilde{H}_u$, as we will see in the next chapter. Also, they would then present the correct $\mathbb{Z}_3$-charge under the decomposition $\mathcal{R}_3^2\mathcal{A}_3\mathcal{L}_3$. A disadvantage is the fact that with the latter identification, the right-handed neutrinos no longer come in three generations.

Finally, in table 7.18, we indicated the charges of the particles under a Peccei-Quinn symmetry defined by $Q_{PQ} = Q_c - Q_d$. In the present MSSM-like model though, we have already seen that we only have one gauged massless $U(1)$ symmetry, which corresponds to the hypercharge. The absence of further massless $U(1)$ symmetries prohibits the interpretation of the Peccei-Quinn symmetry as a massless gauged symmetry. Instead, the Peccei-Quinn symmetry acts as a global $U(1)$ symmetry at low energies which is non-perturbatively broken. An interesting observation is given by the fact that in the visible sector, the charges of the particles under the stringy $\mathbb{Z}_3$-symmetry can be mapped to the charges of the Peccei-Quinn symmetry, as can be seen in table 7.18. Thus, any coupling in the visible sector allowed by the discrete $\mathbb{Z}_3$-symmetry will also be automatically invariant under the Peccei-Quinn symmetry.

In summary, we can say that the gauge group of the present MSSM-like model containing the total information about the charge selection rules is given by the gauge group $SU(3)_a \times USp(2)_b \times U(1)_Y \times SU(4)_h \times \mathbb{Z}_3$ at low energies.

8.4 $\mathbb{Z}_n$-symmetries in the global six-stack left-right symmetric models

In this section, we will briefly discuss the discrete symmetries for prototype I and prototype II left-right symmetric models. As already mentioned, we will refrain from giving all the details of the computation and focus on the main results instead. The massless $U(1)$ symmetry desired in the left-right symmetric models corresponds to the baryon-lepton number symmetry. The traditional definition of the baryon-lepton number symmetry in the left-right symmetric models is given by $Q_{B-L} = \frac{1}{3}Q_a + Q_d$ within D-brane models. If this symmetry is present as a massless gauged symmetry in our models, it should come as a combination $(k_a, k_d, k_{h_1}, k_{h_2}) = (1, 3, 0, 0)$. Note that in all our left-right symmetric models, the b and the c stack support a $USp(2)$ group, which does not give rise to a $U(1)$ factor. Thus, we have no contributions from the b nor the c stacks.

8.4.1 Prototype I left-right symmetric model

Remember that the prototype I left-right symmetric model is characterized by the following gauge group: $U(3)_a \times USp(2)_b \times USp(2)_c \times U(1)_d \times U(3)_{h_1} \times U(3)_{h_2}$. The data for this model can be found in table 7.5. We will directly write down the set of necessary and sufficient $\mathbb{Z}_n$-conditions without indicating the exceptional wrapping numbers. The set of necessary conditions is given by:

$$k_a \begin{pmatrix} 0 \\ 0 \\ \hline 0 \\ 0 \\ 0 \\ -6 \\ 6 \\ 0 \\ 0 \\ 0 \\ 0 \\ 0 \\ \hline 6 \\ 6 \\ 0 \\ 0 \end{pmatrix} + k_d \begin{pmatrix} 0 \\ 0 \\ \hline 0 \\ 0 \\ 0 \\ -2 \\ 2 \\ 0 \\ 0 \\ 0 \\ 0 \\ 0 \\ \hline -2 \\ -2 \\ 0 \\ 0 \end{pmatrix} + k_{h_1} \begin{pmatrix} 0 \\ 0 \\ \hline 9 \\ 3 \\ 3 \\ 3 \\ 3 \\ 0 \\ 0 \\ -6 \\ -6 \\ 0 \\ 0 \\ \hline 0 \\ 0 \\ 0 \\ 0 \end{pmatrix} + k_{h_2} \begin{pmatrix} 0 \\ 0 \\ \hline 9 \\ 3 \\ 3 \\ 3 \\ 3 \\ 0 \\ 0 \\ 6 \\ 6 \\ 0 \\ 0 \\ \hline 0 \\ 0 \\ 0 \\ 0 \end{pmatrix} \stackrel{!}{=} 0 \bmod n\,. \tag{8.25}$$

Once more, several conditions have zero entries and are thus trivial, while others are only multiples of each other. We are left with a set of five non-trivial equations:

$$\begin{aligned} 3k_{h_1} + 3k_{h_2} &\stackrel{!}{=} 0 \bmod n, \\ -6k_a - 2k_d + 3k_{h_1} + 3k_{h_2} &\stackrel{!}{=} 0 \bmod n, \\ 6k_a + 2k_d &\stackrel{!}{=} 0 \bmod n, \\ -6k_{h_1} + 6k_{h_2} &\stackrel{!}{=} 0 \bmod n, \\ 6k_a - 2k_d &\stackrel{!}{=} 0 \bmod n. \end{aligned} \tag{8.26}$$

This set of equations has to be completed by the set of sufficient conditions, given by:

$$k_a \begin{pmatrix} 3 \\ 6 \\ 3 \\ 6 \\ 3 \\ 6 \\ \hline 0 \\ 0 \\ 0 \\ 0 \\ \hline 0 \\ 0 \\ 0 \\ -6 \\ 0 \\ 0 \end{pmatrix} + k_d \begin{pmatrix} -1 \\ -2 \\ -1 \\ -2 \\ -1 \\ -2 \\ \hline 0 \\ 0 \\ 0 \\ 0 \\ \hline -1 \\ 0 \\ 0 \\ -2 \\ -2 \\ 1 \end{pmatrix} + k_{h_1} \begin{pmatrix} -3 \\ 0 \\ -3 \\ 0 \\ -3 \\ 0 \\ \hline 0 \\ 0 \\ 0 \\ 0 \\ \hline 3 \\ 6 \\ 3 \\ 3 \\ 3 \\ 0 \end{pmatrix} + k_{h_2} \begin{pmatrix} 3 \\ 0 \\ 3 \\ 0 \\ 3 \\ 0 \\ \hline 0 \\ 0 \\ 0 \\ 0 \\ \hline 6 \\ 6 \\ 3 \\ 3 \\ 3 \\ 3 \end{pmatrix} \stackrel{!}{=} 0 \bmod n. \tag{8.27}$$

The first block gives only two different equations, with the second equation already contained in the necessary conditions. The second block is trivial, and the third block produces five equations which are not multiples of each other. However, two of the latter appeared already before in the necessary conditions. Note also that the last two and the first equations of the third block are not linearly independent. Thus, we obtain three supplementary constraints:

$$\begin{aligned} 3k_a - k_d - 3k_{h_1} + 3k_{h_2} &\stackrel{!}{=} 0 \bmod n, \\ -k_d + 3k_{h_1} + 6k_{h_2} &\stackrel{!}{=} 0 \bmod n, \\ -2k_d + 3k_{h_1} + 3k_{h_2} &\stackrel{!}{=} 0 \bmod n. \end{aligned} \tag{8.28}$$

Once again, both necessary and sufficient conditions together can provide at most four linearly independent equations, as the six stacks give rise to four $U(1)$ symmetries only. For example, the three sufficient equations together with the first necessary condition form four linearly independent equations.

First, we will start by looking for massless $U(1)$ combinations, i.e. for combinations of coefficients k_i which satisfy the necessary and sufficient conditions for every value of n. By putting the right-hand side of the necessary conditions to zero, we already deduce from the necessary conditions that the only solution is the trivial one: $k_a = k_c = k_{h_1} = k_{h_2} = 0$. Thus, the prototype I left-right symmetric model does not provide any massless $U(1)$ symmetry. In particular, the absence of a massless $U(1)$ symmetry implies that the baryon-lepton number symmetry $U(1)_{B-L}$ acts as a global symmetry.

Next, we turn our attention to the discrete $\mathbb{Z}_n$-symmetries. A similar code to the one used for the MSSM in appendix B.2.2 yielded 46 combinations of k_i's giving various $\mathbb{Z}_2$, $\mathbb{Z}_3$ and $\mathbb{Z}_6$ symmetries. No other values for n were found, at least not for values of $k_i \leq 16$, which is in stark contrast to the MSSM where all values for n up to 45 have been found. We will not give the combinations explicitly. Comparing once again the $\mathbb{Z}_n$-charges of the particles in order to detect equivalent symmetries, we obtain the following results:

- Since we are in presence of a global model, the K-theory constraints are satisfied and provide the $\mathbb{Z}_2$-symmetry associated to the combination $(k_a, k_c, k_{h_1}, k_{h_2}) = (1, 1, 1, 1)$. By looking at the third-to-last column of table 7.6, we see that the $\mathbb{Z}_2$-charges of the particles in the visible sector are identical to the ones of the massive baryon-lepton number symmetry associated to $Q_{B-L} = Q_a + 3Q_d$. Therefore, one might be tempted to consider the $\mathbb{Z}_2$-symmetry arising from the K-theory constraints as the remnant of the broken baryon-lepton number symmetry. However, the exotic particles of the hidden sector are also charged under the $\mathbb{Z}_2$-symmetry, which raises the suspicion that the $\mathbb{Z}_2$-symmetry in question might be the remnant of some generalized baryon-lepton number symmetry under which the hidden sector is also charged.
  Furthermore, table 7.6 also reveals that only states transforming in the fundamental representation **2** of either $USp(2)_b$ or $USp(2)_c$ are charged under the $\mathbb{Z}_2$-symmetry. Hence, the charge selection rules coming from the $\mathbb{Z}_2$-symmetry are identical to the ones coming from $USp(2)_b$ or $USp(2)_c$ and contain no additional information.

- As expected, we also have the three $\mathbb{Z}_3$-symmetries homomorphic to the centers of the three $SU(3)$ groups supported by the a stack and the two hidden stacks. These correspond to the combinations $(k_a, k_c, k_{h_1}, k_{h_2}) = (1, 0, 0, 0), (0, 0, 1, 0), (0, 0, 0, 1)$. Hence, these discrete symmetries also do not provide any additional selection rules to the ones given by the associated non-Abelian $SU(3)$ gauge groups.

- A $\mathbb{Z}_6$-symmetry is for example given by the combination $(k_a, k_c, k_{h_1}, k_{h_2}) = (1, 3, 1, 1)$. The charges of the particles under this symmetry are listed in the last column of table 7.6. By comparing these charges to the charges of the $\mathbb{Z}_2$-symmetry, we see that the charge 0 of $\mathbb{Z}_2$ is associated to an even charge number of $\mathbb{Z}_6$, while the charge 1 of $\mathbb{Z}_2$ is associated to an odd charge number of $\mathbb{Z}_6$. This indicates that the $\mathbb{Z}_2$-symmetry is a sub-symmetry of $\mathbb{Z}_6$, so that the latter also gives rise to an effective $\mathbb{Z}_3$-symmetry. Indeed, the charges of $\mathbb{Z}_6$ can be mapped to the charges of the $\mathbb{Z}_3$-symmetry associated to the combination $(k_a, k_c, k_{h_1}, k_{h_2}) = (1, 0, 1, 1)$. We can use the same mapping as the one defined in (8.20), except that the rôle of the 1 and 2 charges of $\mathbb{Z}_3$ have to be inverted. However, the latter $\mathbb{Z}_3$-symmetry corresponds to a linear combination of the

three $\mathbb{Z}_3$-symmetries discussed in the previous point. Thus, this symmetry is not an independent symmetry and provides no new charge selection rules.

Consequently, in this prototype I left-right symmetric model we do not obtain any $\mathbb{Z}_n$-symmetry providing additional charge selection rules beyond the ones given by gauge invariance.

8.4.2 Prototype II left-right symmetric model

In this section, we will analyze the symmetries of the prototype II left-right symmetric model the data of which can be found in table 7.7. Using these data, the necessary $\mathbb{Z}_n$-conditions can be computed:

$$k_a \begin{pmatrix} 0 \\ 0 \\ \hline 0 \\ 0 \\ 0 \\ -6 \\ 6 \\ 0 \\ 0 \\ 0 \\ 0 \\ 0 \\ \hline 6 \\ 6 \\ 0 \\ 0 \end{pmatrix} + k_d \begin{pmatrix} 0 \\ 0 \\ \hline 0 \\ 0 \\ 0 \\ -2 \\ 2 \\ 0 \\ 0 \\ 0 \\ 0 \\ 0 \\ \hline -2 \\ -2 \\ 0 \\ 0 \end{pmatrix} + k_{h_1} \begin{pmatrix} 0 \\ 0 \\ \hline 3 \\ 1 \\ 1 \\ 1 \\ 0 \\ 0 \\ 0 \\ 0 \\ 0 \\ 0 \\ \hline 2 \\ 2 \\ 0 \\ 0 \end{pmatrix} + k_{h_2} \begin{pmatrix} 0 \\ 0 \\ \hline 3 \\ 1 \\ 1 \\ 1 \\ 0 \\ 0 \\ 0 \\ 0 \\ 0 \\ 0 \\ \hline -2 \\ -2 \\ 0 \\ 0 \end{pmatrix} \stackrel{!}{=} 0 \bmod n\,. \tag{8.29}$$

Four non-trivial equations, not multiples of each other, can be deduced:

$$\begin{aligned} k_{h_1} + k_{h_2} &\stackrel{!}{=} 0 \bmod n, \\ -6k_a - 2k_d + k_{h_1} + k_{h_2} &\stackrel{!}{=} 0 \bmod n, \\ 6k_a + 2k_d &\stackrel{!}{=} 0 \bmod n, \\ 6k_a - 2k_d + 2k_{h_1} - 2k_{h_2} &\stackrel{!}{=} 0 \bmod n. \end{aligned} \tag{8.30}$$

Just as in the case of the two previous models, these equations have to be supplemented with the set of sufficient conditions:

$$k_a \begin{pmatrix} 3 \\ 6 \\ 3 \\ 6 \\ 3 \\ 6 \\ \hline 0 \\ 0 \\ 0 \\ 0 \\ \hline 0 \\ 0 \\ 0 \\ -6 \\ 0 \\ 0 \end{pmatrix} + k_d \begin{pmatrix} -1 \\ -2 \\ -1 \\ -2 \\ -1 \\ -2 \\ \hline 0 \\ 0 \\ 0 \\ 0 \\ \hline -1 \\ 0 \\ 0 \\ -2 \\ -2 \\ 1 \end{pmatrix} + k_{h_1} \begin{pmatrix} 1 \\ 2 \\ 1 \\ 2 \\ 1 \\ 2 \\ \hline 0 \\ 0 \\ 0 \\ 0 \\ \hline 2 \\ 2 \\ 1 \\ 1 \\ 2 \\ 0 \end{pmatrix} + k_{h_2} \begin{pmatrix} -1 \\ -2 \\ -1 \\ -2 \\ -1 \\ -2 \\ \hline 0 \\ 0 \\ 0 \\ 0 \\ \hline 1 \\ 2 \\ 1 \\ 1 \\ 0 \\ 1 \end{pmatrix} \stackrel{!}{=} 0 \text{ mod } n. \tag{8.31}$$

The first block provides one equation, whereas the third block offers three additional equations to the necessary conditions, giving a total of four sufficient conditions:

$$\begin{aligned} 3k_a - k_d + k_{h_1} - k_{h_2} &\stackrel{!}{=} 0 \text{ mod } n, \\ -k_d + 2k_{h_1} + k_{h_2} &\stackrel{!}{=} 0 \text{ mod } n, \\ -2k_d + 2k_{h_1} &\stackrel{!}{=} 0 \text{ mod } n, \\ k_d + k_{h_2} &\stackrel{!}{=} 0 \text{ mod } n. \end{aligned} \tag{8.32}$$

However, only three out of the eight non-trivial necessary and sufficient conditions are truly independent. A set of three linearly independent equations is for example given by the first three sufficient conditions. This is in accordance with the fact that, although the six stacks give rise to four $U(1)$ factors, only three independent $\mathbb{Z}_n$-symmetries arise since we have a massless $U(1)$ symmetry in this model. Indeed, setting the right-hand side of the necessary conditions (8.30) equal to zero without the "mod n", the first two equations yield $k_{h_1} = -k_{h_2}$ and $k_d = -3k_a$. Putting these into the third equation yields $k_{h_1} = -3k_a$. Thus, the solution of the necessary condition is of the form $(k_a, -3k_a, -3k_a, 3k_a)$. By putting $k_a = 1$ in order to have $gcd\,(k_a, \ldots, k_{h_2}) = 1$, and by inserting this solution into the sufficient conditions (8.32), we see that the latter are satisfied as well by this combination of k_i's for every value of n. Thus, contrarily to the previous prototype I left-right symmetric model, this time we have a massless $U(1)$ which can be associated to a generalized baryon-lepton number symmetry:

$$\widetilde{U(1)}_{B-L} = \frac{1}{3}U(1)_a - U(1)_d - U(1)_{h_1} + U(1)_{h_2}. \tag{8.33}$$

Under this generalized baryon-lepton number symmetry, not only the visible sector but also the hidden sector is charged. The charges of the particles of the prototype II left-right symmetric model under the generalized baryon-lepton number symmetry are indicated in table 7.8. A stark contrast between prototype I and prototype II models is the fact that in the former, the generalized baryon-lepton number symmetry acts as a global symmetry whereas it acts as a gauged massless symmetry in the latter.
Next, we will turn our attention to the existence of discrete $\mathbb{Z}_n$-symmetries. Following once more the same reasoning as the one performed in the case of the MSSM-like model, the results can be summarized as follows:

- As usual, we have the $\mathbb{Z}_2$-symmetry arsing from the K-theory constraints and corresponding to the combination $(k_a, k_d, k_{h_1}, k_{h_2}) = (1, 1, 1, 1)$. The $\mathbb{Z}_2$-symmetry in the prototype I model was associated to the remnants of a broken massive generalized baryon-lepton number symmetry, while the $\mathbb{Z}_2$-symmetry in the present case can be interpreted as a sub-symmetry of the massless generalized $\widetilde{U(1)}_{B-L}$ symmetry. Indeed, after a shift of the $\mathbb{Z}_2$-charges by the massless $\widetilde{U(1)}_{B-L}$ symmetry, these are all set to zero. Thus, this symmetry does not contain any new information.

- The non-Abelian gauge factor $SU(3)_a$ gives rise to a discrete $\mathbb{Z}_3$-symmetry, associated to the combination $(k_a, k_d, k_{h_1}, k_{h_2}) = (1, 0, 0, 0)$ and homomorphic to the center of $SU(3)_a$. Once again, a shift of the $\mathbb{Z}_3$-charges by the massless $\widetilde{U(1)}_{B-L}$ symmetry puts all the charges equal to zero. Hence, this symmetry also acts only trivially on the low-energy particle spectrum, and does not give rise to any new charge selection rules.

- Finally, we have once more a $\mathbb{Z}_6$-symmetry corresponding to the linear combination $(k_a, k_d, k_{h_1}, k_{h_2}) = (1, 3, 3, 3)$. However, all the charges of the particles under this $\mathbb{Z}_6$-symmetry are also put to zero upon a shift by the massless $\widetilde{U(1)}_{B-L}$ symmetry, indicating that the $\mathbb{Z}_6$-symmetry corresponds to a discrete sub-symmetry of the generalized baryon-lepton number symmetry. Moreover, the $\mathbb{Z}_6$-symmetry can be decomposed into the $\mathbb{Z}_2$-symmetry arising from the K-theory constraints and the $\mathbb{Z}_3$-symmetry arising from the center of $SU(3)_a$, which both act trivially after a $\widetilde{U(1)}_{B-L}$-shift, as pointed out in the previous bullet points. Thus, this $\mathbb{Z}_6$-symmetry is not a new independent symmetry and does not yield any new charge selection rules.

All in all, we can conclude that the full gauge group of the prototype II left-right symmetric model at low energies is given by: $SU(3)_a \times USp(2)_b \times USp(2)_c \times \widetilde{U(1)}_{B-L}$.

8.4.3 Brief overview of the results for the other prototypes

In this section, we will briefly discuss the results for the other left-right symmetric models including the semi-global five-stack left-right symmetric model and the global six-stack prototype IIb and IIc left-right symmetric models. We will explicitly show how the RR-tadpole cancellation conditions are fulfilled, but not the K-theory constraints for the five-stack left-right symmetric model. Subsequently, we will discuss potential massless $U(1)$ combinations and discrete symmetries. In the case of the prototype IIb and prototype IIc left-right symmetric models, we will restrain the analysis to the existence of massless $U(1)$ combinations, since the results for the $\mathbb{Z}_n$-symmetries are very similar to the ones obtained for the prototype II left-right symmetric model, as can be reviewed in our publication [64].

Five-stack semi-global left-right symmetric model

In this section, we will pin down exactly which sector is responsible for the incompatibility between the fulfillment of the RR-tadpole cancellation conditions and the fulfillment of the K-theory constraints. This can be done only after having derived the explicit analytical expression for the K-theory constraints, as we have done in the present chapter. That explains why we postponed the analysis to this chapter instead of performing it already in chapter 7.
We will start by checking explicitly the RR-tadpole cancellation conditions and the K-theory constraints. The data for the five-stack semi-global left-right symmetric model was given in table 7.3. The associated exceptional wrapping numbers are indicated in tables 8.11 and 8.12. In tables 8.11 and 8.12, the second-to-last line checks the RR-tadpole cancellation conditions, which can be found in (2.50) and table 2.9. Remember that our choice for the exotic charge is given by $\eta_{\Omega\mathcal{R}\mathbb{Z}_2^{(3)}} = -1$, implying that $\eta_{(1)} = \eta_{(2)} = 1$ and $\eta_{(3)} = -1$. For this choice of the exotic O6-plane charge, the only non-trivial twisted RR-tadpole cancellations conditions in the first $\mathbb{Z}_2$-twisted sector are given by:

$$\sum_{z\in\{a,b,c,d,h\}} N_z y^{(1)}_{\alpha,z} = 0, \qquad \alpha = 0,1,2,3\,, \tag{8.34}$$

$$\sum_{z\in\{a,b,c,d,h\}} N_z (x^{(1)}_{4,z} - x^{(1)}_{5,z}) = 0\,, \tag{8.35}$$

$$\sum_{z\in\{a,b,c,d,h\}} N_z (y^{(1)}_{4,z} + y^{(1)}_{5,z}) = 0\,. \tag{8.36}$$

A look at the entries of the second-to-last line of table 8.11 yields that these are all fulfilled. The last line in tables 8.11 and 8.12 checks whether the K-theory constraints arising from the pure bulk and exceptional three-cycles, which we call the "pure K-theory" constraints, are satisfied. These can be found in (8.9), by putting $k_i = 1\ \forall\ i$ and $n = 2$. They can be summarized as follows:

$$\sum_{z\in\{a,b,c,d,h\}} N_z 3x^{(1)}_{0,z} = 0 \bmod 2\,, \tag{8.37}$$

$$\sum_{z\in\{a,b,c,d,h\}} N_z x^{(1)}_{\alpha,z} = 0 \bmod 2 \qquad \alpha = 1,2,3\,, \tag{8.38}$$

$$\sum_{z\in\{a,b,c,d,h\}} N_z (x^{(1)}_{4,z} + x^{(1)}_{5,z}) = 0 \bmod 2\,, \tag{8.39}$$

$$-\sum_{z\in\{a,b,c,d,h\}} N_z (y^{(1)}_{4,z} - y^{(1)}_{5,z}) = 0 \bmod 2\,. \tag{8.40}$$

Inserting the exceptional wrapping numbers of the first twisted sector indicated in the third-to-last line of table 8.11 into the formulas above, the last line in table 8.11 shows that the exceptional wrapping numbers $x^{(1)}_{\alpha,z}$, $\alpha = 0,1,2,3$ do not satisfy the pure K-theory constraints.
A look at the third-to-last line in table 8.12 tells us that the sum over the stacks of the exceptional wrapping numbers of the second twisted sector are zero. Thus, the RR-tadpole cancellation conditions and the pure K-theory constraints in the second sector are trivially satisfied. In the third twisted sector, the only non-trivial twisted RR-tadpole cancellation

conditions for our choice of the exotic charge are given by:

$$\sum_{z\in\{a,b,c,d,h\}} N_z(2x^{(3)}_{\alpha,z} + y^{(3)}_{\alpha,z}) = 0 \qquad \alpha = 1,2,3,4\,. \tag{8.41}$$

The exceptional wrapping numbers given in table 8.12 fulfill these conditions, as indicated in the second-to-last line in table 8.12. The exceptional wrapping numbers of the third twisted sector also satisfy the pure K-theory constraints, which can be summarized as follows:

$$-\sum_{z\in\{a,b,c,d,h\}} N_z y^{(3)}_{\alpha,z} = 0 \bmod 2 \qquad \alpha = 1,2,3,4\,. \tag{8.42}$$

Verification of the RR-t.c.c. and pure K-theory constraints, part I													
z	N	(P,Q,U,V)	$x_0^{(1)}$	$y_0^{(1)}$	$x_1^{(1)}$	$y_1^{(1)}$	$x_2^{(1)}$	$y_2^{(1)}$	$x_3^{(1)}$	$y_3^{(1)}$	$x_4^{(1)}$	$y_4^{(1)}$	$x_5^{(1)}$	$y_5^{(1)}$
a	3	$(1,0,0,0)$	0	0	0	0	0	0	2	0	-1	0	-1	0
b	1	$(3,0,0,0)$	0	0	0	0	0	0	0	0	1	0	-1	0
c	1	$(3,0,0,0)$	0	0	0	0	0	0	0	0	-1	0	1	0
d	1	$(3,0,0,0)$	1	0	1	0	1	0	1	0	0	0	0	0
h	4	$(1,0,0,0)$	0	0	0	0	0	0	-2	0	1	0	1	0
$\sum_z N_z z$		$(16,0,0,0)$	1	0	1	0	1	0	-1	0	1	0	1	0
RR-t.c.c.?		✓		✓		✓		✓		✓		✓		✓
K-pure?		✓		all violated								✓		✓

Table 8.11: Bulk and exceptional wrapping numbers and verification of the fulfillment of the RR-tadpole cancellation conditions (RR-t.c.c.) and pure K-theory constraints (K-pure) in the bulk and the first $\mathbb{Z}_2$-twisted sectors of the semi-global five-stack left-right symmetric model (LRS).

Verification of the RR-t.c.c. and pure K-theory constraints, part II																
z	N	$x_1^{(2)}$	$y_1^{(2)}$	$x_2^{(2)}$	$y_2^{(2)}$	$x_3^{(2)}$	$y_3^{(2)}$	$x_4^{(2)}$	$y_4^{(2)}$	$x_1^{(3)}$	$y_1^{(3)}$	$x_2^{(3)}$	$y_2^{(3)}$	$x_3^{(3)}$	$y_3^{(3)}$	$x_4^{(3)}$	$y_4^{(3)}$
a	3	-1	2	-1	2	0	0	0	0	1	-2	1	-2	0	0	0	0
b	1	-1	2	-1	2	0	0	0	0	-3	0	-3	0	0	0	0	0
c	1	-1	2	-1	2	0	0	0	0	3	0	3	0	0	0	0	0
d	1	1	-2	1	-2	0	0	0	0	-1	2	-1	2	0	0	0	0
h	4	1	-2	1	-2	0	0	0	0	1	-2	1	-2	0	0	0	0
$\sum_z N_z z$		0	0	0	0	0	0	0	0	6	-12	6	-12	0	0	0	0
RR-t.c.c.?		✓		✓		✓		✓		✓		✓		✓		✓	
K-pure?		✓		✓		✓		✓		✓		✓		✓		✓	

Table 8.12: Exceptional wrapping numbers and verification of the fulfillment of the RR-tadpole cancellation conditions (RR-t.c.c.) and pure K-theory constraints (K-pure) in the second and third $\mathbb{Z}_2$-twisted sectors of the semi-global five-stack left-right symmetric (LRS) model.

This concludes the proof that the five-stack left-right symmetric model is a semi-global model but not a global model, i.e. it fulfills all the RR-tadpole cancellation conditions but not the K-theory constraints.

Next, we will turn our attention to the existence of massless $U(1)$ and discrete $\mathbb{Z}_n$-symmetries. For this model, we have a set of four non-trivial necessary conditions given by:

$$\begin{aligned} k_d &\stackrel{!}{=} 0 \bmod n, \\ 6k_a + k_d - 8k_h &\stackrel{!}{=} 0 \bmod n, \\ -6k_a + 8k_h &\stackrel{!}{=} 0 \bmod n, \\ 6k_a - 2k_d + 8k_h &\stackrel{!}{=} 0 \bmod n. \end{aligned} \tag{8.43}$$

Since we have gauge group enhancement on the b and c stacks, these do not appear in the conditions above as they do not yield a $U(1)$ symmetry. The detection of a massless $U(1)$ can be done by putting the right-hand side of the equations above equal to zero without the mod n. Clearly, there is no solution apart from the trivial one $k_i = 0 \; \forall \; i$. Thus, we do not have any massless $U(1)$ symmetry in this specific model. In particular, we have once again no massless gauged baryon-lepton number symmetry. As usual, the necessary conditions have to be completed by a set of sufficient conditions which yield four additional non-trivial equations:

$$\begin{aligned} 3k_a - k_d + 4k_h &\stackrel{!}{=} 0 \bmod n, \\ 3k_a + k_d &\stackrel{!}{=} 0 \bmod n, \\ 6k_a &\stackrel{!}{=} 0 \bmod n, \\ 3k_a - k_d &\stackrel{!}{=} 0 \bmod n. \end{aligned} \tag{8.44}$$

The presence of only three $U(1)$ gauge factors implies that only three conditions can be linearly independent. The first three sufficient conditions for example are linearly independent. Consequently, in the absence of a massless $U(1)$ symmetry, we can have up to three independent discrete $\mathbb{Z}_n$-symmetries. For k_i varying between 0 and 16, only seven combinations of the k_i's show up, associated to values of n equal to $3, 4, 6, 12$. The results can be summarized as follows:

- Exactly one $\mathbb{Z}_3$-symmetry shows up, associated to the combination $(k_a, k_d, k_h) = (1, 0, 0)$ and homomorphic to the center of the non-Abelian gauge factor $SU(3)_a$. The charges of the particles under this discrete symmetry are given in the second-to-last column of table 7.4. We see that only quark-like particles, i.e. particles attached to the a stack, are charged under this discrete $\mathbb{Z}_3$-symmetry, which is obvious as it arises from the center of $SU(3)_a$. Thus, this symmetry acts as usual as a baryon-number-like symmetry. Also, it does not yield any additional charge selection rules to the ones already imposed by the non-Abelian $SU(3)_a$.

- There is only one $\mathbb{Z}_4$-symmetry, associated to the combination $(k_a, k_d, k_h) = (0, 0, 1)$ and homomorphic to the center of the non-Abelian hidden gauge factor $SU(4)_h$. The charges of the particles under this discrete symmetry are given in the last column of table 7.4. As the $\mathbb{Z}_4$-symmetry arises from the hidden stack, only exotic particles are charged under it. As usual, it does not yield any additional charge selection rules to the ones already imposed by the non-Abelian $SU(4)_h$.

- We have one $\mathbb{Z}_6$-symmetry associated to the combination $(k_a, k_d, k_h) = (2, 0, 3)$. However, this is clearly a combination of the $\mathbb{Z}_3$ and $\mathbb{Z}_4$ symmetries discussed in the previous bullet points. Also, the four remaining combinations giving rise to $\mathbb{Z}_{12}$-symmetries are characterized by $k_d = 0$ and thus correspond to linear combinations of the $\mathbb{Z}_3$ and $\mathbb{Z}_4$ symmetries.

- Let us explicitly point out the absence of the $\mathbb{Z}_2$-symmetry associated to the K-theory constraints $(k_a, k_d, k_h) = (1, 1, 1)$. It is clear that the latter combination does not satisfy the necessary and sufficient K-theory constraints. This is to be expected from a model that is semi-global but not global.

All in all, we can conclude that the five-stack semi-global left-right symmetric model is free of non-trivial discrete symmetries and massless $U(1)$'s.

Prototype IIb and Prototype IIc left-right symmetric models

Since the crucial difference between prototype I and prototype II left-right symmetric models seemed to be the existence of a massless $U(1)$ symmetry, we will focus on this aspect rather than the discrete $\mathbb{Z}_n$-symmetries.
The data of the prototype IIb left-right symmetric model can be found in table 7.9. The necessary conditions can be reduced to four non-trivial equations reading:

$$\begin{aligned} -k_{h_1} - k_{h_2} &\stackrel{!}{=} 0 \bmod n\,, \\ 6k_a + 2k_d - k_{h_1} - k_{h_2} &\stackrel{!}{=} 0 \bmod n\,, \\ -6k_a - 2k_d &\stackrel{!}{=} 0 \bmod n\,, \\ 6k_a - 2k_d &\stackrel{!}{=} 0 \bmod n\,. \end{aligned} \tag{8.45}$$

Note that the third equation above is a linear combination of the first two equations. Concentrating on the existence of massless $U(1)$ symmetries, we put the right-hand side of the equations above equal to zero without the "mod n" and find the following solution: $(k_a, k_d, k_{h_1}, k_{h_2}) = (0, 0, 1, -1)$. The next step consists in checking whether this solution is compatible with the sufficient conditions. However, the first sufficient condition already reads:

$$-k_{h_1} + k_{h_2} = 0 \bmod n, \tag{8.46}$$

which is in conflict with the unique solution found from the necessary conditions, when putting the right-hand side equal to zero without the "mod n". Thus, prototype IIb does not present any massless $U(1)$ symmetry. In particular, the generalized gauged baryon-lepton number symmetry found for the prototype II model only acts as a global $U(1)$ symmetry in the present prototype IIb model. The charges of the particles under this global $U(1)$ symmetry are indicated in the last column of table 7.10.

Next, let us turn our attention to the prototype IIc left-right symmetry model. The data associated to this model can be found in table 7.11. The necessary conditions for this model

boil down to four non-trivial conditions reading:

$$\begin{aligned} -2k_{h_1} &\overset{!}{=} 0 \bmod n\,, \\ -2k_{h_2} &\overset{!}{=} 0 \bmod n\,, \\ 6k_a + 2k_d &\overset{!}{=} 0 \bmod n\,, \\ 6k_a - 2k_d + 2k_{h_1} &\overset{!}{=} 0 \bmod n\,. \end{aligned} \tag{8.47}$$

Putting the right-hand side to zero without mod n, we see that the only solution is the trivial one $(k_a, k_d, k_{h_1}, k_{h_2}) = (0, 0, 0, 0)$. Thus, we do not even need to write down the sufficient conditions as the necessary conditions already prohibit the existence of a massless $U(1)$ symmetry. Once again, the generalized baryon-lepton number symmetry found for prototype II acts only as a global $U(1)$ symmetry in the prototype IIc model. The charges of the particles under this global symmetry can be found in the last column of table 7.12.
In our publication [64], we also briefly analyzed the discrete $\mathbb{Z}_n$-symmetries for both prototype IIb and IIc left-right symmetric models, but did not detect any new non-trivial discrete symmetry.

All in all, we can conclude that of all the left-right symmetric models found, only the prototype II model allows for the existence of a massless $U(1)$ symmetry, which on top acts similarly to the coveted baryon-lepton number symmetry. This aspect renders the prototype II left-right symmetric model more attractive from a phenomenological point of view than its fellow prototype left-right symmetric models.

Chapter 9

Three- and four-point couplings at leading order

9.1 Yukawa and other cubic couplings

In Type IIA string model building, the second step after constructing suitable particle physics spectra consists in reproducing the correct low-energy field theory. Whereas the first part of model building focuses on reproducing the correct particle content, the second part concentrating on field theory considerations includes additional features, such as discrete symmetries or the correct three-point couplings. Hitherto, our particles associated to open string excitations localized at D6-brane intersections are massless. To obtain a useful particle physics model, the particles need to acquire masses corresponding to the masses measured at particle detectors. In the Standard Model of particle physics, the particles obtain mass through the Yukawa couplings, which correspond to cubic couplings, i.e. interaction terms involving three different fields, see section 3.2.1. Usually, one of the fields is the Higgs field, which acquires a vacuum expectation value (VEV) and thus yields mass terms for the other fields. In Type IIA string theory, the procedure of giving mass to the particles is identical, albeit the constraints on the coupling terms are more stringent than from the mere field theoretical point of view. Moreover, a realistic stringy particle physics model should also allow for a mass hierarchy between the different particle generations in agreement with experimental data.
Finally, in string theory cubic couplings also provide a useful tool to identify correctly the open string spectrum with the particle content. Indeed, we already pointed out in the previous chapter that it occurs that two different sectors can give rise to particle states having the same SM quantum numbers. A striking example is given by the right-handed neutrinos ν_R, which are gauge group singlets and could thus be associated to any sector giving rise to singlet states. Yukawa couplings and other cubic couplings potentially provide the means for a correct identification of the different particle states.

Just as in field theory, not all cubic couplings are allowed. In string theory, there are two rules to respect. The first rule is given by the "charge selection rule", which states that any term in the perturbative part of the superpotential $\mathcal{W}$ must be a gauge singlet. More precisely, it means that the fields transforming in various representations of the gauge group must combine into interaction terms in such a way that they form gauge singlets under all

gauge group factors, including $U(1)$-factors and $\mathbb{Z}_n$-symmetries. In general, a cubic coupling in the perturbative part of the superpotential has the following form:

$$\mathcal{W}_{\text{per}} \ni W_{xyz}\phi^x_{ab}\phi^y_{bc}\phi^z_{ca}, \tag{9.1}$$

where W_{xyz} is the coupling constant and the ϕ^k_{ij} are superfields associated to open string states localized at the intersection points of the D6-branes i and j with $i, j \in \{a, b, c\}$. The subscripts a, b and c refer to the fractional three-cycles Π^{frac}_a, Π^{frac}_b and Π^{frac}_c which the three D6-branes wrap, while the superscripts x, y and z are related to the multiplicities or generations of the respective states. A mass term arises when the scalar component of one of the three superfields acquires a VEV. In that case, the mass is given by a combination of the VEV and the coupling constant W_{xyz}.
The second rule is a purely stringy selection rule and has no equivalent in the field theoretical language. The "stringy selection rule" states that the torus three-cycles Π^{torus}_a, Π^{torus}_b and Π^{torus}_c supporting the intersecting D6-branes have to form a closed triangular sequence denoted by $[a, b, c] = [a, b][b, c][c, a]$ on each two-torus $T^2_{(i)}$. The three states ϕ^x_{ab}, ϕ^y_{bc} and ϕ^z_{ca} are then localized at the three apexes of the triangle, corresponding to pairwise intersection points of the D6-branes. The physical interpretation in case of the six-torus is that the defined triangular surface on each two-torus is spanned by a worldsheet instanton, as can be shown with techniques of scattering amplitudes. We will not delve deeper into this aspect in this work, but instead refer the interested reader to [202–207].
The coupling constant W_{xyz} is related to the sum of the triangular areas in the following way [202–207]:

$$W_{xyz} \simeq e^{-\sum_{i=1}^{3}\mathcal{A}^{(i)}_{xyz}/(2\pi\alpha')}, \tag{9.2}$$

where $\mathcal{A}^{(i)}_{xyz}$ is the area of the closed triangle $[a, b, c]$ with apexes occupied by the three states ϕ^x_{ab}, ϕ^y_{bc} and ϕ^z_{ca} on the two-torus $T^2_{(i)}$, which is in general given as a fraction of the total area of the two-torus. The parameter α' is called Regge slope and is related to the tension of the string. In case the three-cycles a, b and c intersect in a single point on a two-torus, the corresponding contribution to the coupling constant is of order $\mathcal{O}(1)$. If the three-cycles do not form a closed sequence on some two-torus, the coupling W_{xyz} is zero.
In the present work, we focus on the couplings at leading order to estimate the strength of the couplings, i.e. in equation (9.2), we restrict the analysis to the smallest possible triangles. Due to the periodicity of the underlying six-torus, an infinite number of triangles for a same set of apexes can be obtained, each one coming with an increased area. However, these correspond to higher order correction terms in the superpotential [202–207]. Furthermore, the equation (9.2) is a classical expression and neglects the quantum contribution. In this work, we will restrict the analysis to the classical part. For details on the quantum correction, see [202, 207–210]. Note also that in (9.2) additional constraints arise which are related to the $\mathbb{Z}_2$-eigenvalues, Wilson lines and shifts of the D6-branes. These give the exact localization of particle states at the intersection points and were derived in appendix A of [64]. Finally, let us point out that the cubic couplings or three-point couplings can be generalized to m-point couplings. In that case, the couplings are realized by generic m-polygons.

The precise computation of the coupling constant W_{xyz} in Type IIA string theory is a large benefit of string theory compared to field theory. Actually, in the Standard Model of particle physics, the Yukawa coupling constants cannot be derived from first principles. Instead, they

correspond to free parameters of the theory, which have to be fitted by hand to the experimental data. Subsequently, also the hierarchy is produced by hand in the Standard Model. In contrast, Type IIA string theory provides the tools to associate geometrical meaning to the mass couplings, making them natural and computable. For concrete computations of m-point couplings on similar backgrounds to the one used here, see for example [75, 74, 76]. These references also include discussions about the correct hierarchy reproduction.

As a final remark, note that in all our global models the bulk three-cycles are parallel to the $\Omega\mathcal{R}$- or $\Omega\mathcal{R}\mathbb{Z}_2^{(1)}$-plane. In particular, on the first two-torus $T^2_{(1)}$ the one-cycles always have wrapping numbers $(n^1, m^1) = (1, 0)$, as both the orbifold and orientifold actions act trivially on the $\Omega\mathcal{R}$ and $\Omega\mathcal{R}\mathbb{Z}_2^{(1)}$-planes on the first two-torus. Thus, the contribution from the first two-torus $T^2_{(1)}$ to the total area is always zero. Consequently, in the present work, we will focus on the couplings coming from the second and third two-torus $T^2_{(2)} \times T^2_{(3)}$.
In order to avoid confusions, we will fix the labels of the intersection points right from the start. The following figure exposes all possible combinations of bulk orbits arising in our models and their intersection points, and the figure also puts a label to each intersection point:

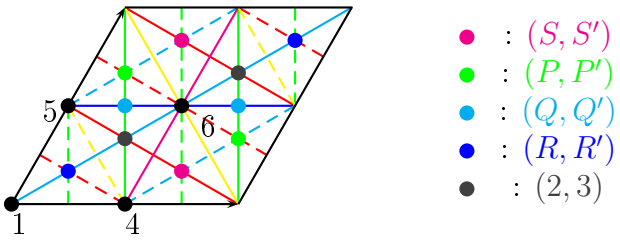

The solid lines indicate various possibilities of bulk orbits which appear in our models without shifts. The dashed lines correspond to the bulk orbits in presence of shifts. The black points correspond to $\mathbb{Z}_2$-fixed points. All the other points form $\mathbb{Z}_2$-invariant pairs of points of the form (X, X'). The points in gray labeled by 2 and 3 are $\mathbb{Z}_3$-fixed points (see figure 2.4), and together form a $\mathbb{Z}_2$-invariant pair of points. The points (X, X') will be denoted in the following by a further index $i = 2, 3$ as (X_i, X_i') in order to refer to the two-torus under consideration, i.e. the second $T^2_{(2)}$ or third two-torus $T^2_{(3)}$.

9.2 Cubic couplings in the global MSSM-like model

As we already pointed out in the previous chapter about discrete symmetries, we will not derive the field theoretical properties for all the models we found, but restrict the analysis to the global MSSM-like model and the left-right symmetric models. In this section, we will concentrate on the cubic couplings arising in the five-stack MSSM-like model. Once again, we will derive the results in some detail for the MSSM, but only provide the final results for the left-right symmetric models.

Generic discussion of the superpotential

Remember some of the features of the global MSSM model at hand: we have an extended Higgs sector, extended left-handed lepton and right-handed quark sectors, as well as a non-

trivial $\mathbb{Z}_3$-symmetry. In addition, we have a global Peccei-Quinn symmetry $U(1)_{PQ} \equiv U(1)_c - U(1)_d$, which is reflected in the charges of the particle spectrum under this symmetry, see table 7.18 [101, 102]. This is confirmed by the form of our perturbative superpotential. Anticipating the results, the superpotential can schematically be written in terms of five different contributions we are interested in:

$$\mathcal{W}_{\text{per}} \supset \mathcal{W}_{\text{MSSM}} + \mathcal{W}_{\text{extra}} + \mathcal{W}_{\text{DFSZ}} + \mathcal{W}_{\nu} + \mathcal{W}_{\text{hidden}} \,, \tag{9.3}$$

where the five contributions read (schematically) as follows:

$$\mathcal{W}_{\text{MSSM}} = y_u \, Q_L \cdot \tilde{H}_u u_R + y_d \, Q_L \cdot H_d d_R + y_e \, L \cdot H_d e_R + y_\nu \, L \cdot H_u \nu_R, \tag{9.4a}$$

$$\mathcal{W}_{\text{extra}} = \kappa \, \bar{d}_R \Sigma^{cd} d_R + \tilde{\kappa} \, L \cdot H_u \Sigma^{cd}, \tag{9.4b}$$

$$\mathcal{W}_{\text{DFSZ}} = \mu \, H_u \cdot \tilde{H}_d \Sigma^{cd} + \tilde{\mu} \, \tilde{H}_u \cdot H_d \tilde{\Sigma}^{cd}, \tag{9.4c}$$

$$\mathcal{W}_{\nu} = \mathfrak{B} L \cdot \tilde{H}_u \mathbf{Anti}_b + \mathfrak{U} L \cdot \tilde{H}_u \mathbf{Adj}_d, \tag{9.4d}$$

$$\mathcal{W}_{\text{hidden}} = \mathfrak{h}_u \, \underline{h}_b \cdot H_u \underline{h}_c + \mathfrak{h}_d \, \underline{h}_b \cdot \tilde{H}_d h_d. \tag{9.4e}$$

An remarkable absence is given by certain Yukawa couplings involving H_u or $\tilde{H}_d$, such as e.g. $y_u \; Q_L \cdot H_u u_R$, which do neither satisfy the stringy selection rules nor the charge selection rules. This has been checked explicitly case-by-case; albeit in this work, we will only go through some choice examples explicitly.

The first part of the superpotential (9.4a) constitutes the usual superpotential of the MSSM, containing the Yukawa couplings indicated in section 3.2.1. However, there is a significant difference due to the fact that in the present couplings, two sorts of Higgses appear, the ones with a tilde and the ones without tilde. More precisely, we have only one sort of down-type Higgses H_d appearing, but two sorts of Higgs fields H_u and $\tilde{H}_u$ for the up-type Higgses. In the previous chapter 8, we have seen that by interpreting the right-handed neutrinos in the usual way as matter states arising in the cd sector, as we do in (9.4a), the charges of the right-handed neutrinos ν_R under the $\mathbb{Z}_3$-symmetry in table 7.17 are in conflict with those deduced from formulas (8.4). This issue can be solved by identifying the right-handed neutrinos with the singlet states arising in the antisymmetric sector of b or the adjoint sector of d. The drawback of this interpretation is that the right-handed neutrinos no longer come in three generations. In this chapter, we will analyze mass terms for all three possible interpretations of the right-handed neutrinos ν_R.

The second contribution to the superpotential (9.4b) involves cubic couplings for the numerous right-handed quarks and left-handed leptons. The scalars in the superfields Σ^{cd} and $\tilde{\Sigma}^{cd}$, which we will call axions, can develop a VEV, producing a supersymmetric mass term for the right-handed quarks and left-handed leptons. If the coupling constant is high enough, the superfluous generations of non-chiral right-handed quarks and left-handed leptons could be lifted to high energies. Consequently, we would be left effectively with three generations of right-handed quarks and left-handed leptons at low energies. Hence, it is important to determine these cubic couplings and compare them with the traditional Yukawa couplings of the MSSM.

The third component of the superpotential (9.4c) is the SUSY version of the DFSZ model, see e.g. [101, 211]. Basically, the DFSZ model forms an extension of the Standard Model

by the Peccei-Quinn symmetry and an extra singlet field. Its aim is to solve the strong CP-problem [212, 213]. The original proposition of Peccei and Quinn [162, 163] associated the breaking scale of the $U(1)_{PQ}$ symmetry to the electroweak scale. However, this leads to phenomenologically undesired effects so that the original Peccei-Quinn model has been ruled out, see [214–216]. The breaking scale of the $U(1)_{PQ}$ symmetry can be decoupled from the electroweak scale by associating the former to the VEV of a new scalar field, which is a singlet under the MSSM gauge group, but charged under $U(1)_{PQ}$. This is the scenario used in the DFSZ model. In our case, the Σ^{cd} axion arising in the non-chiral cd sector could assume the rôle of this scalar field, as it is a singlet under the MSSM gauge group but charged under $U(1)_{PQ}$. Also, the Higgs fields possess the correct Peccei-Quinn charges to form together with Σ^{cd} a $U(1)_{PQ}$ singlet term.

The fourth contribution to the superpotential (9.4d) consists in cubic couplings for the right-handed neutrinos in the case they are associated to the states arising in the antisymmetric sector of b or the adjoint sector of d.

The final contribution to the perturbative superpotential (9.4e) is dedicated to cubic couplings involving chiral exotic particle states from the hidden sector. The sates $\underline{h}_b$ play the rôle of exotic left-handed leptons in the hidden sector, since they constitute an electroweak doublet. The exotic states $\underline{h}_c$ and h_d can be interpreted as exotic right-handed leptons, corresponding to neutrino-like exotics and electron-like exotics respectively. They can be coupled to the Higgs doublets arising in the visible sector, in a similar way to their leptonic counterparts in the visible sector. Should the coupling constants $\mathfrak{h}_u$ and $\mathfrak{h}_d$ reveal themselves to be of order one, then the chiral exotic particles are lifted to energies high above current detectors' reach and are no longer observable.

Localization of matter states

The determination of cubic couplings needs the information in which sectors $x(\omega^k y)_{k=0,1,2}$ the matter states arise precisely. Tables 9.1 and 9.2 contain the matter localization per sector, according to the data given in table 7.17. This data is not yet sufficient to determine the exact localization of matter states at precise $\mathbb{Z}_2$-fixed points or $\mathbb{Z}_2$-invariant pairs of points. In fact, the chiral states can be localized precisely, since in our case the number of intersection points of torus three-cycles agrees with the number of states determined by the intersection numbers, as we will see in the following sections. The rule is that chiral states are located at a $\mathbb{Z}_2$-fixed point on at least one of the two two-tori $T^2_{(2)} \times T^2_{(3)}$. The non-chiral states are in general located on $\mathbb{Z}_2$-invariant pairs of points on both two-tori. However, in the present context, we will also encounter non-chiral states including a $\mathbb{Z}_2$-fixed point in their location. In that case, we have to determine precisely the location of each member of the non-chiral pair, as in general only one member of the non-chiral pair is used in cubic couplings. The precise localization can be performed by using the Chan-Paton labels. This method is also an alternative to computing the intersection numbers sector-per-sector. The method is quite technical, so we will not go into detail here. The technique is presented in appendix A of our publication [64], where discrete Wilson lines and shifts have been included in the computation for the first time. I will only use the results to illustrate the computation of cubic couplings and refer the reader to [64] for more detailed information.

Total amount of matter per sector for a 5-stack MSSM model on the aAA lattice					
$(\chi^{xy}, \chi^{x(\omega y)}, \chi^{x(\omega^2 y)})$	$y=a$	$y=b$	$y=c$	$y=d$	$y=h$
$x=a$	$(0,0,0)$	$(2,1,0)$	$(-4,-1,-1)$	$(2,1,0)$	$(\|2\|,1,-1)$
$x=b$		$(0,\frac{3+\|2\|}{2},\frac{-3+\|2\|}{2})$	$(0,-3+\|2\|,\|4\|)$	$(0,3+\|2\|,3+\|2\|)$	$(-2,-1,0)$
$x=c$			$(0,\frac{\|4\|}{2},\frac{\|4\|}{2})$	$(0,\|4\|,-3+\|2\|)$	$(0,0,0)$
$x=d$				$(0,\frac{-3+\|2\|}{2},\frac{3+\|2\|}{2})$	$(2,1,0)$
$x=h$					$(0,0,0)$

Table 9.1: Complete list of the multiplicities of the chiral and non-chiral states per sector $x(\omega^k y)$ in the case of the global five-stack MSSM-like model of table 7.17. Non-chiral states arise in sectors $x(\omega^k y)$ characterized by net-chirality $|\chi^{x(\omega^k y)}| < \varphi^{x(\omega^k y)}$, in which case the multiplicity of the non-chiral states is given by $n_{NC}^{x(\omega^k y)} \equiv \varphi^{x(\omega^k y)} - |\chi^{x(\omega^k y)}|$. Such non-chiral pairs of particles are referred to as $|n_{NC}^{x(\omega^k y)}|$. For example, $|n_{NC}^{a(\omega^0 h)}| = |2|$ corresponds to one non-chiral pair of states transforming in the bifundamental representation in the sector $a(\omega^0 h)$. The diagonal entries of the table given by $\varphi^{x(\omega x)} = \varphi^{x(\omega^2 x)} = \frac{\varphi^{\mathbf{Adj}_x}}{2}$ count the number of states transforming in the adjoint representation of the x-stack, except for the stack b presenting gauge group enhancement, in which case they correspond to states in the antisymmetric representation. For example, the expression $(0,\frac{-3+|2|}{2},\frac{3+|2|}{2})$ for the d-stack refers to five multiplets in the adjoint representation with half of the degrees of freedom localized in the $d(\omega d)$ sector and the other half localized in the $d(\omega^2 d)$ sector.

Total amount of matter per sector for a 5-stack MSSM model				
$(\chi^{xy'}, \chi^{x(\omega y)'}, \chi^{x(\omega^2 y)'})$	$y=a$	$y=c$	$y=d$	$y=h$
$x=a$	$\binom{(\|2\|,-1,1)}{(0,0,0)}$	$(0,0,0)$	$(-2,0,-1)$	$(\|2\|,0,0)$
$x=c$		$\binom{(\|2\|,3+\|2\|,-3+\|2\|)}{(0,0,0)}$	$(0,3+\|2\|,\|4\|)$	$(-4,-1,-1)$
$x=d$			$\binom{(0,3+\|2\|,-3+\|2\|)}{(\|2\|,0,0)}$	$(2,1,0)$
$x=h$				$\binom{(\|2\|,-1,1)}{(0,0,0)}$

Table 9.2: Complete list of the multiplicities of the chiral and non-chiral states per sector $x(\omega^k y)'$ in the case of the global five-stack MSSM-like model of table 7.17. The notation used for counting bifundamental states is the same as the one used in table 9.1. The diagonal entries of the table associated to the sectors $x(\omega x)'$ count the number of states transforming in the (anti)symmetric representation of the x-stack, with the upper entries counting the numbers of antisymmetric representations and the lower entries the symmetric ones. The invariance of the b stack under the orientifold projection $\Omega\mathcal{R}$ implies $b(\omega^k x)' = b(\omega^k x)$, which can be found in table 9.1. Since the D6-brane stacks c and d support $U(1)$ gauge groups, the states in the antisymmetric representation do not exist. Still, we include their formal counting for reasons of completeness.

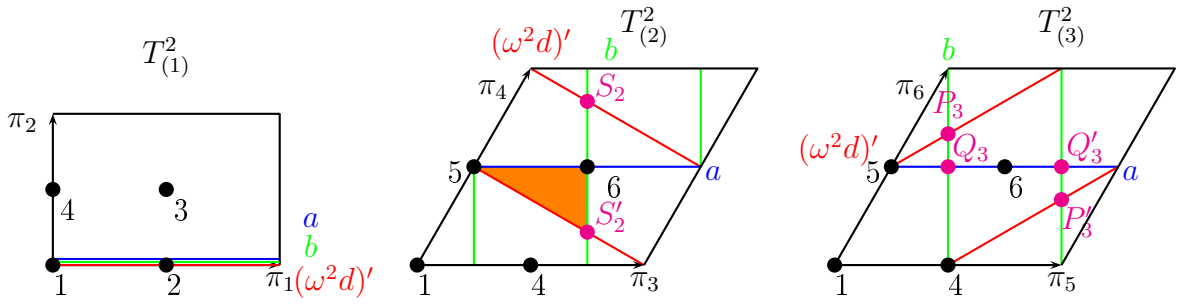

Figure 9.1: The three-cycle denoted by a is depicted in blue, the three-cycle labeled by b is indicated in green, and the three-cycle $(\omega^2 d)'$ is given in red. These three-cycles give rise to a quarkonic Yukawa coupling of the form $y_u Q_L \cdot \tilde{H}_u u_R$. On the second two-torus $T^2_{(2)}$, an example of a triangle formed by a, b and $(\omega^2 d)'$ is depicted in orange.

9.2.1 Quarkonic cubic couplings

In this section, we will focus on cubic couplings involving quarks, which we refer to as "quarkonic" couplings. We will go through the calculation of one of the Yukawa couplings involving quarks explicitly, and only give the final results for all the other quarkonic cubic couplings. The example we will examine explicitly shall be the Yukawa coupling $y_u Q_L \cdot \tilde{H}_u u_R$ of the MSSM part of the superpotential, which gives mass to the up-type quarks after EWSB.

Example of calculation: The Yukawa coupling $y_u Q_L \cdot \tilde{H}_u u_R$

In table 9.1 we see that the three generations of left-handed quarks Q_L arising in the sectors $a(\omega^k b)$ (see table 7.18) are spread over two different sectors $k = 0, 1$.
The same holds true for the right-handed up-type quarks arising in the sectors $a(\omega^k d)'$ (see tables 7.18 and 9.2) with $k = 0, 2$. Consequently, different orbifold images of the cycles b and d' have to be used to provide mass terms for all three generations of up-type quarks.
We will start with the sequence $[a, b, (\omega^2 d)']$.

Triangles formed by the sequence $[a, b, (\omega^2 d)']$: The situation is illustrated in figure 9.1. We see in figure 9.1 that these three torus three-cycles fulfill the stringy selection rule, as they form a closed sequence. In addition, the Yukawa coupling $y_u Q_L \cdot \tilde{H}_u u_R$ consists of representations which form a singlet under the gauge group of the MSSM. Besides, the $U(1)$-charges also cancel: $(Q_a, Q_c, Q_d, Q_h) = (1, 0, 0, 0) + (0, 0, 1, 0) + (-1, 0, -1, 0)$. Remember that the various charges of the particle content for this MSSM model can be found in table 7.18. Therefore, the cubic coupling under consideration also satisfies the charge selection rule.
On the first two-torus $T^2_{(1)}$, all the one-cycles are coincident, as all three-cycles have $(n^1, m^1) = (1, 0)$ and the orbifold generators as well as the orientifold projection act trivially on this one-cycle on the first two-torus. Note that also none of the three-cycles present in this MSSM model comes with a shift on the first two-torus, as can be checked from table 7.17. As we already pointed out at the beginning of this chapter, we will focus on the second and third two-torus $T^2_{(2)} \times T^2_{(3)}$.
On the second two-torus $T^2_{(2)}$, we see that all three one-cycles intersect in one single point, the $\mathbb{Z}_2$-fixed point labeled by 5. Other intersection points are given by the $\mathbb{Z}_2$-fixed point labeled by 6, and the $\mathbb{Z}_2$-invariant pair of intersection points (S_2, S'_2) depicted in magenta. In the fundamental domain of $T^2_{(2)}$, already two closed triangles can be seen, given by the

intersection points $5, 6, S_2$ and $5, 6, S_2'$, which are $\mathbb{Z}_2$-images of each other. However, other triangles with other apexes exist which only close after identification of the boundaries of the fundamental domain. They can be detected by drawing several lattice cells.
On the third two-torus $T^2_{(3)}$, we have two $\mathbb{Z}_2$-fixed points labeled by 4 and 5 as intersection points. There are four more intersection points. Already by drawing only one lattice cell, we can detect two small triangles given by the intersection points $5, P_3, Q_3$ and their $\mathbb{Z}_2$-image, and two bigger triangles formed by the intersection points $4, 5, Q_3$ and their $\mathbb{Z}_2$-images. Further triangles can be found by drawing several lattice cells.
In summary, we have the following intersection points and localization of matter states:

state	xy	χ^{xy}	$T^2_{(2)}$	$T^2_{(3)}$
$Q_L^{(1,2)}$	ab	2	$5, 6$	(Q_3, Q_3')
$u_R^{(1)}$	$a(\omega^2 d)'$	-1	5	5
$\tilde{H}_u^{(2)}$ $(+\tilde{H}_d^{(2)},\ L^{(1,2,3)})$	$b(\omega^2 d)'$	$\lvert 2\rvert$ (-3)	$5, (S_2, S_2')$	$4, (P_3, P_3')$

(9.5)

The first column gives the particles appearing in the Yukawa coupling under consideration, and the second column gives the intersection sector xy in which the states arise. The third column yields the multiplicity (and chirality in case of chiral states) of the states given in the first column. The fourth and fifth columns provide the labels of the intersection points of the one-cycles x and y on the second respectively third two-torus.
We see that in the ab sector, we have two chiral states labeled $Q_L^{(1,2)}$, which matches the number of intersection points. Indeed, one chiral left-handed quark state, let it be denoted by $Q_L^{(1)}$, is localized at the $\mathbb{Z}_2$-invariant pair of intersection points $(6, (Q_3, Q_3'))$, whereas the second left-handed quark state $Q_L^{(2)}$ is situated at $(5, (Q_3, Q_3'))$ on $T^2_{(2)} \times T^2_{(3)}$. Note that a state sitting at a $\mathbb{Z}_2$-invariant pair of points is shared between the two points. Thus, the area of a triangle and its $\mathbb{Z}_2$-image is only counted once.
Also the multiplicity of the chiral right-handed up-type quark matches the number of intersection points, i.e. one state localized at the intersection point $(5, 5)$ on $T^2_{(2)} \times T^2_{(3)}$.
However, in the $b(\omega^2 d)'$ sector, we see that we have four $\mathbb{Z}_2$-invariant pairs of intersection points $(5, 4)$, $(5, (P_3, P_3'))$, $((S_2, S_2'), 4)$ and $((S_2, S_2'), (P_3, P_3'))$, but only one non-chiral state denoted by $\tilde{H}_u^{(2)} + \tilde{H}_d^{(2)}$ which we are interested in. A look at table 9.2 reveals that this sector also comes with three chiral states $L^{(1,2,3)}$, but we are not interested in these, since they have different $U(1)$-charges (see table 7.18) than the up-type Higgs $\tilde{H}_u^{(2)}$ and thus do not satisfy the charge selection rule. In order to calculate the correct Yukawa coupling, the exact position of the non-chiral pair has to be determined. Since we only have one non-chiral pair in the considered sector, it is clear that it will be localized at the $\mathbb{Z}_2$-invariant pair of intersection points $((S_2, S_2'), (P_3, P_3'))$, while the three chiral leptonic states $L^{(1,2,3)}$ will place themselves at the intersection points involving some $\mathbb{Z}_2$-fixed points, i.e. $(5, (P_3, P_3'))$, $((S_2, S_2'), 4)$ and $(5, 4)$.
Note that the feature of having both chiral and non-chiral matter states arising in the same sector is rather unusual, and has not been encountered in previous studies of Yukawa couplings with intersecting D6-branes.

Next, we draw all possible triangles and compute the corresponding areas:

triangles on $T^2_{(2)}$	$\frac{\text{Area}}{v_2}$	triangles on $T^2_{(3)}$	$\frac{\text{Area}}{v_3}$
$[5]_2$	0	$[(Q_3, Q_3'), 5, 4]_3$	$\frac{3}{16}$
$[5, 6, 5]_2$	$\frac{3}{4}$	$[(P_3, P_3'), (Q_3, Q_3'), 5]_3$	$\frac{1}{48}$
$[5, (S_2, S_2'), 5]_2$	$\frac{1}{3}$		
$[(S_2, S_2'), 5, 6]_2$	$\frac{1}{12}$		

(9.6)

The quantity v_i denotes the total area of the fundamental domain of the two-torus $T^2_{(i)}$ in units of α'. A priori, we have $4 \cdot 2 = 8$ possible combinations of triangles $[\ ]_2$ and $[\ ]_3$. However, not all of these can be used since we have only one non-chiral Higgs pair sitting at the point $((S_2, S_2'), (P_3, P_3'))$. Hence, the triangles $[5]_2$ and $[5, 6, 5]_2$ of the second two-torus and the triangle $[(Q_3, Q_3'), 5, 4]_3$ on the third two-torus cannot be used. In the end, we have two possible combinations left to provide mass terms for the two left-handed quarks $Q_L^{(1,2)}$ and the right-handed up-type quark $u_R^{(1)}$. The results can be summarized as follows:

Coupling	Triangles on $T^2_{(2)} \times T^2_{(3)}$	Parameter
$Q_L^{(2)} \cdot \tilde{H}_u^{(2)} u_R^{(1)}$	$\{[5, (S_2, S_2'), 5], [(Q_3, Q_3'), (P_3, P_3'), 5]\}$	$y_u^{(221)} \sim \mathcal{O}\left(e^{-\frac{16v_2+v_3}{48}}\right)$
$Q_L^{(1)} \cdot \tilde{H}_u^{(2)} u_R^{(1)}$	$\{[6, (S_2, S_2'), 5], [(Q_3, Q_3'), (P_3, P_3'), 5]\}$	$y_u^{(121)} \sim \mathcal{O}\left(e^{-\frac{4v_2+v_3}{48}}\right)$

The parameters $y_u^{(ijk)}$, $i, j, k \in \{1, 2\}$ are the up-type Yukawa coupling constants with the superscript referring to the particle generation involved in the coupling. The exponent of the coupling gives the area enclosed by the sequence. We denoted the Higgs particle arising in this sector $b(\omega^2 d)'$ by $\tilde{H}_u^{(2)}$. There is one generation-mixing mass term given by the Yukawa coupling $y_u^{(221)}$, and one diagonal mass term $y_u^{(121)}$ without generation mixing. The generation-mixing terms should be suppressed compared to the diagonal terms in order to produce a realistic structure of the Yukawa couplings. This agrees with our choice of the label (i) in $Q_L^{(i=1,2)}$ insofar that the non-diagonal Yukawa coupling $y_u^{(221)}$ is suppressed compared to the diagonal one $y_u^{(121)}$, i.e $y_u^{(221)} < y_u^{(121)}$.
So far, only one generation of up-type quarks has acquired mass. To produce mass terms for the remaining up-type quarks, we have to analyze another sequence, involving for example the three-cycles $a, (\omega b), d'$.

Triangles formed by the sequence $[a, (\omega b), d']$**:** The three torus three-cycles lie on the six-torus as indicated in figure 9.2. On the second two-torus $T^2_{(2)}$ in figure 9.2, we see that we have no intersection point where all three one-cycles meet. Instead, we have two pairs of $\mathbb{Z}_2$-invariant intersection points in which two one-cycles meet. Thus, already on the fundamental domain of the two-torus, a triangle is apparent, formed by the three points $P_2, Q_2, 6$. The third two-torus $T^2_{(3)}$ comes with the obvious triangle the apexes of which are $6, 5, R_3$, as well as its usual $\mathbb{Z}_2$-image. Furthermore, the $\mathbb{Z}_2$-fixed point denoted by 6 is an intersection point of all three one-cycles. Once again, drawing further lattice cells reveals other triangles with other apexes.

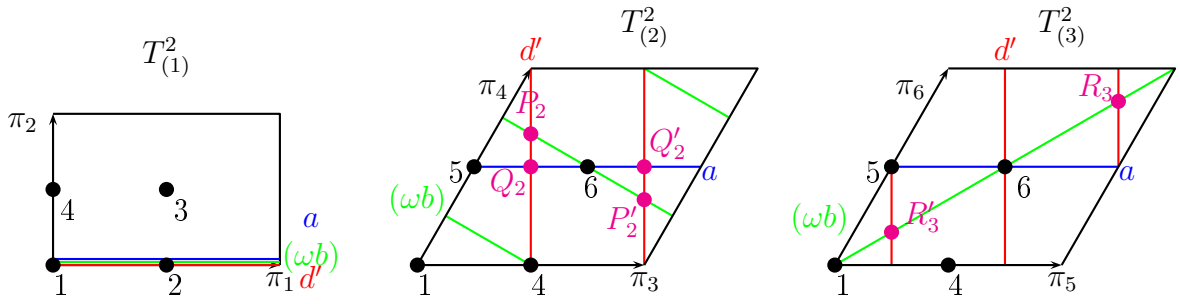

Figure 9.2: The three-cycle denoted by a is depicted in blue, the three-cycle labeled by (ωb) is indicated in green, and the three-cycle d' is given in red. These three-cycles give rise to a quarkonic Yukawa coupling of the form $y_u Q_L \cdot \tilde{H}_u u_R$.

All in all, we have the following intersection points and localizations of matter states:

state	xy	χ^{xy}	$T^2_{(2)}$	$T^2_{(3)}$
$Q_L^{(3)}$	$a(\omega b)$	1	6	6
$u_R^{(2,3)}$	ad'	-2	(Q_2, Q'_2)	$5, 6$
$\tilde{H}_u^{(1)}$ $(+\tilde{H}_d^{(1)},\ L^{(4,5,6)})$	$(\omega b)d'$	$\lvert 2\rvert$ (-3)	$4, (P_2, P'_2)$	$6, (R_3, R'_3)$

(9.7)

Once again, the multiplicity of the chiral states matches with the intersection points of one-cycles. In the non-chiral sector, we have once more one relevant non-chiral state and three non-relevant chiral states. [1] As usual, the non-chiral state $\tilde{H}_u^{(1)} + \tilde{H}_d^{(1)}$ sits on the $\mathbb{Z}_2$-invariant pair of points $((P_2, P'_2), (R_3, R'_3))$ on $T^2_{(2)} \times T^2_{(3)}$.
The triangles are given by:

triangle on $T^2_{(2)}$	$\frac{\text{Area}}{v_2}$	triangle on $T^2_{(3)}$	$\frac{\text{Area}}{v_3}$
$[(Q_2, Q'_2), (P_2, P'_2), 6]_2$	$\frac{1}{48}$	$[(R_3, R'_3), 5, 6]_3$	$\frac{1}{12}$
$[(Q_2, Q'_2), 4, 6]_2$	$\frac{3}{16}$	$[6, (R_3, R'_3), 6]_3$	$\frac{1}{3}$
		$[6]_3$	0
		$[6, 5, 6]_3$	$\frac{3}{4}$

(9.8)

We have again eight possibilities to choose combinations of triangles on the second and third torus, albeit not all can be realized as we have only one non-chiral Higgs pair. In conclusion, the possible Yukawa couplings are uniquely determined and can be summarized as follows:

Coupling	Triangles on $T^2_{(2)} \times T^2_{(3)}$	Parameter
$Q_L^{(3)} \cdot \tilde{H}_u^{(1)} u_R^{(2)}$	$\{[6, (P_2, P'_2), (Q_2, Q'_2)], [6, (R_3, R'_3), 6]\}$	$y_u^{(312)} \sim \mathcal{O}\left(e^{-\frac{v_2+16v_3}{48}}\right)$
$Q_L^{(3)} \cdot \tilde{H}_u^{(1)} u_R^{(3)}$	$\{[6, (P_2, P'_2), (Q_2, Q'_2)], [6, (R_3, R'_3), 5]\}$	$y_u^{(313)} \sim \mathcal{O}\left(e^{-\frac{v_2+4v_3}{48}}\right)$

We have a diagonal mass term associated to the coupling $y^{(313)}$, corresponding to the third generation of up-type quarks. There is no diagonal term for the second generation of up-type

[1] Note that we have the following relation between intersection numbers or sectors: $(\omega b)d' = b(\omega^2 d') = b(\omega d)'$. In general, we have $(\omega^k x)(\omega^l y) = x(\omega^{l-k} y)$, and switching the orientifold projection with the orbifold action boils down to switching the second and third sectors $\omega^1 \leftrightarrow \omega^2$, or more generic, replacing the exponent of the ω-action by minus the exponent. This can be checked explicitly by using (2.13) and (2.18).

quarks involving $Q_L^{(2)}$ and $u_R^{(2)}$, though the latter appears in the generation-mixing coupling associated to $y^{(312)}$. Once again, the off-diagonal term is suppressed compared to the diagonal term. Also, having a look at the diagonal Yukawa couplings $y^{(121)}$ and $y^{(313)}$, we see that we can create a mass hierarchy between the generations of particles by choosing $v_2 > v_3$ or $v_2 < v_3$. Hence, this stringy set-up allows to explain mass hierarchy in a natural way. However, note that the parameters v_i are still free parameters, but they can be related to geometrical quantities.

Other cubic couplings involving quarks

In this section, we will briefly summarize and comment on the results concerning the other cubic couplings involving quarks in (9.3). The results for the down-type quarks can be derived similarly to the ones for the up-type quarks and are given in tables 9.3 and 9.4.

Quarkonic Yukawa couplings in (9.4a): The results in table 9.3 can be summarized as follows: contrarily to the up-type quarks, we have diagonal Yukawa couplings for all three generations of down-type quarks, given by $y_d^{(1,i,1)}$, $i = 2, 3$, $y_d^{(2,1,2)}$, and $y_d^{(3,i,3)}$, $i = 2, 3$. We see that in the $b(\omega^2 c)$ sector, we have two non-chiral Higgs pairs labeled by $i = 2, 3$. The labeling i is chosen as follows: $i = 3$ corresponds to the Higgs pair $H_u^{(3)} + H_d^{(3)}$ located at the usual intersection points involving two pairs of $\mathbb{Z}_2$-invariant points, for example $((S_2, S_2'), (P_3, P_3'))$. The localization of the second Higgs pair $H_u^{(2)} + H_d^{(2)}$ labeled by $i = 2$ is more complicated. Indeed, the computation via Chan-Paton labels revealed that the up-type Higgs doublet $H_u^{(2)}$ is located at intersection points of the form $((Y, Y'), X)$ on $T^2_{(2)} \times T^2_{(3)}$, while the down-type Higgs doublet $H_d^{(2)}$ is situated at intersection points of the form $(X, (Y, Y'))$ on $T^2_{(2)} \times T^2_{(3)}$, where (Y, Y') denotes a $\mathbb{Z}_2$-invariant pair of points and X a $\mathbb{Z}_2$-fixed point. This has been taken into account in the Yukawa couplings of table 9.3. The presence of two non-chiral Higgs pairs clearly enriches the Yukawa structure, as can be seen by comparing the couplings of the up-type quarks with those of the down-type quarks. This is related to the fact that more closed triangles with occupied apexes can be used when one of the Higgs doublets sits on a $\mathbb{Z}_2$-fixed point on one of the two tori $T^2_{(2)}$ or $T^2_{(3)}$.

A look at table 9.3 reveals a suppression of the off-diagonal terms $y_d^{(112)}$, $y_d^{(231)}$, and $y_d^{(33i\in\{4,5,6\})}$ with respect to the diagonal couplings $y_d^{(212)}$, $y_d^{(131)}$ and $y_d^{(333)}$ respectively. However, this holds not true for the Yukawa couplings involving the Higgs doublet labeled by $H_d^{(2)}$, as $y_d^{(221)}$ for instance is larger than $y_d^{(121)}$.

As a side-remark, note that the ordering of the apexes of the triangles in the third column of table 9.3 (and the following tables as well) reflects the localization of the matter states in the same order as the states appear in the Yukawa couplings of the first column.

Cubic couplings for the superpotential (9.3) of a global 5-stack MSSM (part I)				
Coupling	**Sequence**	**Triangles on $T^2_{(2)} \times T^2_{(3)}$**	**Enclosed Area**	**Parameter**
$Q_L^{(2)} \cdot \tilde{H}_u^{(2)} u_R^{(1)}$	$[a, b, (\omega^2 d)']$	$\{[5, (S_2, S_2'), 5], [(Q_3, Q_3'), (P_3, P_3'), 5]\}$	$\frac{v_2}{3} + \frac{v_3}{48}$	$y_u^{(221)} \sim \mathcal{O}\left(e^{-\frac{16v_2+v_3}{48}}\right)$
$Q_L^{(1)} \cdot \tilde{H}_u^{(2)} u_R^{(1)}$		$\{[6, (S_2, S_2'), 5], [(Q_3, Q_3'), (P_3, P_3'), 5]\}$	$\frac{v_2}{12} + \frac{v_3}{48}$	$y_u^{(121)} \sim \mathcal{O}\left(e^{-\frac{4v_2+v_3}{48}}\right)$
$Q_L^{(3)} \cdot \tilde{H}_u^{(1)} u_R^{(2)}$	$[a, (\omega b), d']$	$\{[6, (P_2, P_2'), (Q_2, Q_2')], [6, (R_3, R_3'), 6]\}$	$\frac{v_2}{48} + \frac{v_3}{3}$	$y_u^{(312)} \sim \mathcal{O}\left(e^{-\frac{v_2+16v_3}{48}}\right)$
$Q_L^{(3)} \cdot \tilde{H}_u^{(1)} u_R^{(3)}$		$\{[6, (P_2, P_2'), (Q_2, Q_2')], [6, (R_3, R_3'), 5]\}$	$\frac{v_2}{48} + \frac{v_3}{12}$	$y_u^{(313)} \sim \mathcal{O}\left(e^{-\frac{v_2+4v_3}{48}}\right)$
$Q_L^{(2)} \cdot H_d^{(1)} d_R^{(2)}$	$[a, b, (\omega c)]$	$\{[5, (R_2, R_2'), 6], [(Q_3, Q_3'), (P_3, P_3'), 5]\}$	$\frac{v_2}{12} + \frac{v_3}{48}$	$y_d^{(212)} \sim \mathcal{O}\left(e^{-\frac{4v_2+v_3}{48}}\right)$
$Q_L^{(1)} \cdot H_d^{(1)} d_R^{(2)}$		$\{[6, (R_2, R_2'), 6], [(Q_3, Q_3'), (P_3, P_3'), 5]\}$	$\frac{v_2}{3} + \frac{v_3}{48}$	$y_d^{(112)} \sim \mathcal{O}\left(e^{-\frac{16v_2+v_3}{48}}\right)$
$Q_L^{(2)} \cdot H_d^{(2)} d_R^{(1)}$	$[a, b, (\omega^2 c)]$	$\{[5], [(Q_3, Q_3'), (P_3, P_3'), 6]\}$	$\frac{v_3}{48}$	$y_d^{(221)} \sim \mathcal{O}\left(e^{-\frac{v_3}{48}}\right)$
$Q_L^{(2)} \cdot H_d^{(3)} d_R^{(1)}$		$\{[5, (S_2, S_2'), 5], [(Q_3, Q_3'), (P_3, P_3'), 6]\}$	$\frac{v_2}{3} + \frac{v_3}{48}$	$y_d^{(231)} \sim \mathcal{O}\left(e^{-\frac{16v_2+v_3}{48}}\right)$
$Q_L^{(1)} \cdot H_d^{(2)} d_R^{(1)}$		$\{[6, 5, 5], [(Q_3, Q_3'), (P_3, P_3'), 6]\}$	$\frac{3v_2}{4} + \frac{v_3}{48}$	$y_d^{(121)} \sim \mathcal{O}\left(e^{-\frac{36v_2+v_3}{48}}\right)$
$Q_L^{(1)} \cdot H_d^{(3)} d_R^{(1)}$		$\{[6, (S_2, S_2'), 5], [(Q_3, Q_3'), (P_3, P_3'), 6]\}$	$\frac{v_2}{12} + \frac{v_3}{48}$	$y_d^{(131)} \sim \mathcal{O}\left(e^{-\frac{4v_2+v_3}{48}}\right)$
$Q_L^{(3)} \cdot H_d^{(2)} d_R^{(3)}$	$[a, (\omega b), c]$	$\{[6, 6, 5], [6, (R_3, R_3'), 5]\}$	$\frac{3v_2}{4} + \frac{v_3}{12}$	$y_d^{(323)} \sim \mathcal{O}\left(e^{-\frac{9v_2+v_3}{12}}\right)$
$Q_L^{(3)} \cdot H_d^{(3)} d_R^{(3)}$		$\{[6, (R_2, R_2'), 5], [6, (R_3, R_3'), 5]\}$	$\frac{v_2}{12} + \frac{v_3}{12}$	$y_d^{(333)} \sim \mathcal{O}\left(e^{-\frac{v_2+v_3}{12}}\right)$
$Q_L^{(3)} \cdot H_d^{(2)} d_R^{(4)}$		$\{[6, 6, 5], [6, (R_3, R_3'), 6]\}$	$\frac{3v_2}{4} + \frac{v_3}{3}$	$y_d^{(324)} \sim \mathcal{O}\left(e^{-\frac{9v_2+4v_3}{12}}\right)$
$Q_L^{(3)} \cdot H_d^{(3)} d_R^{(4)}$		$\{[6, (R_2, R_2'), 5], [6, (R_3, R_3'), 6]\}$	$\frac{v_2}{12} + \frac{v_3}{3}$	$y_d^{(334)} \sim \mathcal{O}\left(e^{-\frac{v_2+4v_3}{12}}\right)$
$Q_L^{(3)} \cdot H_d^{(2)} d_R^{(5)}$		$\{[6], [6, (R_3, R_3'), 5]\}$	$\frac{v_3}{12}$	$y_d^{(325)} \sim \mathcal{O}\left(e^{-\frac{v_3}{12}}\right)$
$Q_L^{(3)} \cdot H_d^{(3)} d_R^{(5)}$		$\{[6, (R_2, R_2'), 6], [6, (R_3, R_3'), 5]\}$	$\frac{v_2}{3} + \frac{v_3}{12}$	$y_d^{(335)} \sim \mathcal{O}\left(e^{-\frac{4v_2+v_3}{12}}\right)$
$Q_L^{(3)} \cdot H_d^{(2)} d_R^{(6)}$		$\{[6], [6, (R_3, R_3'), 6]\}$	$\frac{v_3}{3}$	$y_d^{(326)} \sim \mathcal{O}\left(e^{-\frac{v_3}{3}}\right)$
$Q_L^{(3)} \cdot H_d^{(3)} d_R^{(6)}$		$\{[6, (R_2, R_2'), 6], [6, (R_3, R_3'), 6]\}$	$\frac{v_2}{3} + \frac{v_3}{3}$	$y_d^{(336)} \sim \mathcal{O}\left(e^{-\frac{v_2+v_3}{3}}\right)$

Table 9.3: Complete list of the quarkonic Yukawa couplings in (9.4a) of the global five-stack MSSM-like model of table 7.17 involving the left-handed and right-handed quarks. The second column indicates the D6-brane stacks used to form the triangles given in the third column by $[x]$ or $[x, y, z]$ with apexes (intersection points) x, y, z on $T^2_{(i=2,3)}$ according to the cubic couplings given in the first column. The fourth column provides the area for the respective triangles in terms of the areas v_i of the two-tori $T^2_{(i=2,3)}$, while the last column presents the resulting coupling constants.

Quarkonic couplings in (9.4b): Table 9.4 provides cubic couplings for the redundant right-handed down-type quarks $\overline{d_R}^{(1,2,3)}$ and $d_R^{(4,5,6)}$ with the axions $\Sigma^{cd(1,2,3)}$. The hope was that some of the couplings with $\Sigma^{cd(1,2,3)}$ would come with large coupling constants so that superfluous effective non-chiral pairs $\overline{d_R} + d_R$ acquire a mass big enough to put them out of today's detector ranges. Unfortunately, we see that none of the couplings κ is of order $\mathcal{O}(1)$. Instead, they are all exponentially suppressed. Obviously, another mechanism has to be derived in order to explain why only three generations of right-handed down-quarks $d_R^{(1,2,3)}$ appear at low energies. However, the derivation of such a mechanism is not a topic included in this thesis, and has to be performed in future work.
Note that also here we have two non-chiral pairs of axions $\Sigma^{cd(1,2)}$ arising in the $c(\omega d)$ sector, labeled by $i = 1, 2$. Once again, this feature enriches considerably the Yukawa structure.

Cubic couplings for the superpotential (9.3) of a global 5-stack MSSM (part II)				
Coupling	**Sequence**	**Triangles on $T^2_{(2)} \times T^2_{(3)}$**	**Enclosed Area**	**Parameter**
$\overline{d_R}^{(3)}\Sigma^{cd(1)}d_R^{(3)}$	$[a, c, (\omega d)]$	$\{[5], [5, (S_3, S_3'), 5]\}$	$\frac{v_3}{3}$	$\kappa^{(313)} \sim \mathcal{O}\left(e^{-\frac{v_3}{3}}\right)$
$\overline{d_R}^{(3)}\Sigma^{cd(2)}d_R^{(3)}$		$\{[5, (S_2, S_2'), 5], [5, (S_3, S_3'), 5]\}$	$\frac{v_2}{3} + \frac{v_3}{3}$	$\kappa^{(323)} \sim \mathcal{O}\left(e^{-\frac{v_2+v_3}{3}}\right)$
$\overline{d_R}^{(3)}\Sigma^{cd(1)}d_R^{(4)}$		$\{[5], [6, (S_3, S_3'), 5]\}$	$\frac{v_3}{12}$	$\kappa^{(314)} \sim \mathcal{O}\left(e^{-\frac{v_3}{12}}\right)$
$\overline{d_R}^{(3)}\Sigma^{cd(2)}d_R^{(4)}$		$\{[5, (S_2, S_2'), 5], [6, (S_3, S_3'), 5]\}$	$\frac{v_2}{3} + \frac{v_3}{12}$	$\kappa^{(324)} \sim \mathcal{O}\left(e^{-\frac{4v_2+v_3}{12}}\right)$
$\overline{d_R}^{(3)}\Sigma^{cd(1)}d_R^{(5)}$		$\{[6, 5, 5], [5, (S_3, S_3'), 5]\}$	$\frac{3v_2}{4} + \frac{v_3}{3}$	$\kappa^{(315)} \sim \mathcal{O}\left(e^{-\frac{9v_2+4v_3}{12}}\right)$
$\overline{d_R}^{(3)}\Sigma^{cd(2)}d_R^{(5)}$		$\{[6, (S_2, S_2'), 5], [5, (S_3, S_3'), 5]\}$	$\frac{v_2}{12} + \frac{v_3}{3}$	$\kappa^{(325)} \sim \mathcal{O}\left(e^{-\frac{v_2+4v_3}{12}}\right)$
$\overline{d_R}^{(3)}\Sigma^{cd(1)}d_R^{(6)}$		$\{[6, 5, 5], [6, (S_3, S_3'), 5]\}$	$\frac{3v_2}{4} + \frac{v_3}{12}$	$\kappa^{(316)} \sim \mathcal{O}\left(e^{-\frac{9v_2+v_3}{12}}\right)$
$\overline{d_R}^{(3)}\Sigma^{cd(2)}d_R^{(6)}$		$\{[6, (S_2, S_2'), 5], [6, (S_3, S_3'), 5]\}$	$\frac{v_2}{12} + \frac{v_3}{12}$	$\kappa^{(326)} \sim \mathcal{O}\left(e^{-\frac{v_2+v_3}{12}}\right)$
$\overline{d_R}^{(1)}\Sigma^{cd(3)}d_R^{(1)}$	$[a, (\omega^2 c), (\omega d)]$	$\{[5, (S_2, S_2'), 5], [6, (P_3, P_3'), 5]\}$	$\frac{v_2}{6} + \frac{v_3}{24}$	$\kappa^{(131)} \sim \mathcal{O}\left(e^{-\frac{4v_2+v_3}{24}}\right)$
$\overline{d_R}^{(2)}\Sigma^{cd(3)}d_R^{(2)}$	$[a, (\omega c), d]$	$\{[6, (P_2, P_2'), (Q_2, Q_2')], [5, (S_3, S_3'), 5]\}$	$\frac{v_2}{48} + \frac{v_3}{3}$	$\kappa^{(232)} \sim \mathcal{O}\left(e^{-\frac{v_2+16v_3}{48}}\right)$
$\overline{d_R}^{(1)}\Sigma^{cd(3)}d_R^{(2)}$		$\{[6, (P_2, P_2'), (Q_2, Q_2')], [5, (S_3, S_3'), 6]\}$	$\frac{v_2}{48} + \frac{v_3}{12}$	$\kappa^{(132)} \sim \mathcal{O}\left(e^{-\frac{v_2+4v_3}{48}}\right)$
$\overline{d_R}^{(2)}\Sigma^{cd(1)}d_R^{(1)}$	$[a, (\omega^2 c), d]$	$\{[5, 4, (Q_2, Q_2')], [6, (R_3, R_3'), 5]\}$	$\frac{3v_2}{16} + \frac{v_3}{12}$	$\kappa^{(211)} \sim \mathcal{O}\left(e^{-\frac{12v_2+4v_3}{48}}\right)$
$\overline{d_R}^{(2)}\Sigma^{cd(2)}d_R^{(1)}$		$\{[5, (P_2, P_2'), (Q_2, Q_2')], [6, (R_3, R_3'), 5]\}$	$\frac{v_2}{48} + \frac{v_3}{12}$	$\kappa^{(221)} \sim \mathcal{O}\left(e^{-\frac{v_2+4v_3}{48}}\right)$
$\overline{d_R}^{(1)}\Sigma^{cd(1)}d_R^{(1)}$		$\{[5, 4, (Q_2, Q_2')], [6, (R_3, R_3'), 6]\}$	$\frac{3v_2}{16} + \frac{v_3}{3}$	$\kappa^{(111)} \sim \mathcal{O}\left(e^{-\frac{9v_2+16v_3}{48}}\right)$
$\overline{d_R}^{(1)}\Sigma^{cd(2)}d_R^{(1)}$		$\{[5, (P_2, P_2'), (Q_2, Q_2')], [6, (R_3, R_3'), 6]\}$	$\frac{v_2}{48} + \frac{v_3}{3}$	$\kappa^{(121)} \sim \mathcal{O}\left(e^{-\frac{v_2+16v_3}{48}}\right)$

Table 9.4: Complete list of the quarkonic cubic couplings $\overline{d_R}\Sigma^{cd}d_R$ in (9.4b) of the global five-stack MSSM-like model of table 7.17 involving the right-handed down-type quarks. The second column indicates the D6-brane stacks used to form the triangles given in the third column by $[x]$ or $[x, y, z]$ with apexes (intersection points) x, y, z on $T^2_{(i=2,3)}$ according to the cubic couplings given in the first column. The fourth column provides the area for the respective triangles in terms of the areas v_i of the two-tori $T^2_{(i=2,3)}$, while the last column presents the resulting coupling constants.

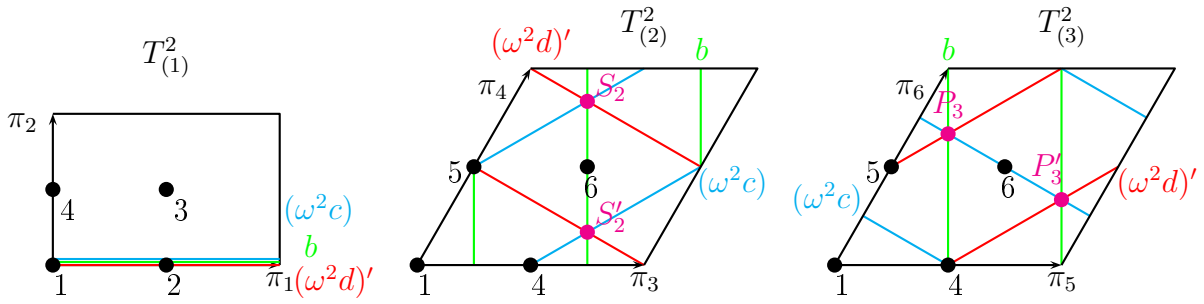

Figure 9.3: The three-cycle denoted by $(\omega^2 c)$ is depicted in cyan, the three-cycle labeled by b is indicated in green, and the three-cycle $(\omega^2 d)'$ is given in red. These three-cycles give rise to a leptonic Yukawa coupling of the form $y_e L \cdot H_d e_R$.

9.2.2 Leptonic cubic couplings

In this section, we will focus on the states that are uncharged under the strong interactions, i.e. leptonic states. These include the leptons per se, but also the Higgs doublets which have similar quantum numbers to the left-handed leptons. We choose to present in some detail the Yukawa couplings $y_e L \cdot H_d e_R$ of the electron-like leptons.

Example of calculation: The Yukawa coupling $y_e L \cdot H_d e_R$

In table 7.18, we see that the left-handed leptons L of the low-energy MSSM arise in the bd sector, the right-handed electrons in the cd' sector and the Higgs doublet H_d from the non-chiral bc sector. A look at table 9.2 reveals that the three generations of right-handed electrons e_R are localized in a single sector $c(\omega^k d)'$ with $k = 1$. Consequently, we need only one sequence of orbifold and orientifold images of the cycles b, c, d to give mass to all three generations, unlike the situation for the up-type quarks where the three generations of quarks spread over two sectors.

Triangles formed by the sequence $[b, (\omega^2 c), (\omega^2 d)']$: The position of the three torus three-cycles on the three two-tori is given in figure 9.3. The situation is a bit different compared to the one of the up-type quarks. Indeed, we now have on both two-tori two intersection points where all three one-cycles meet, namely a $\mathbb{Z}_2$-fixed point (5 on $T^2_{(2)}$ and 4 on $T^2_{(3)}$) and a pair of $\mathbb{Z}_2$-invariant points ((S_2, S'_2) on $T^2_{(2)}$ and (P_3, P'_3) on $T^2_{(3)}$). Contrarily to the case of the up-type quarks, the apexes of the triangles include both members of the $\mathbb{Z}_2$-invariant pair of points. The precise matter localization per sector is given by:

state	xy	χ^{xy}	$T^2_{(2)}$	$T^2_{(3)}$
$L^{(1,2,3)}$ $(+\tilde{H}_u^{(2)} + \tilde{H}_d^{(2)})$	$b(\omega^2 d)'$	-3 $(+\lvert 2\rvert)$	$5, (S_2, S'_2)$	$4, (P_3, P'_3)$
$H_d^{(2,3)}$ $(+H_u^{(2,3)})$	$b(\omega^2 c)$	$\lvert 4\rvert$	$5, (S_2, S'_2)$	$4, (P_3, P'_3)$
$e_R^{(1,2,3)}$ $(+X^{cd(1)} + \tilde{X}^{cd(1)})$	$(\omega^2 c)(\omega^2 d)'$	3 $(+\lvert 2\rvert)$	$5, (S_2, S'_2)$	$4, (P_3, P'_3)$

(9.9)

In the $b(\omega^2 d)'$ sector, we have on top of the three chiral states $L^{(1,2,3)}$ also a non-chiral Higgs pair $\tilde{H}_u^{(2)} + \tilde{H}_d^{(2)}$. Once again, the non-chiral pair is placed on some combination of states involving the $\mathbb{Z}_2$-invariant pairs of points $((S_2, S'_2), (P_3, P'_3))$. The three chiral states sit on the three combinations left involving at least one $\mathbb{Z}_2$-fixed point. The same holds true for

the $(\omega^2 c)(\omega^2 d)'$ sector[2]. The $b(\omega^2 c)$ sector comes with two non-chiral pairs of Higgs doublets $H_u^{(2,3)} + H_d^{(2,3)}$. The labeling and positioning of the two Higgs doublets is of course the same as before in the case of the Yukawa couplings involving down-type quarks, which was discussed at the end of the previous section.

The triangles visible in the fundamental domain are the only possible ones. Drawing several lattice cells does not yield any new triangles except for higher order copies. The triangles of the form $[4,(P_3,P_3'),(P_3,P_3')]$ and $[(S_2,S_2'),(S_2,S_2'),5]$ have an area equal to $\frac{v_i}{6}$. Together with the intersection points where all three one-cycles meet, we have a total of nine combinations to pair off closed sequences of both two-tori.
However, not all combinations can be used to produce Yukawa couplings as not all intersection points support all states. For example, both Higgs doublets $H_d^{(2)}$ and $H_d^{(3)}$ involve the $\mathbb{Z}_2$-invariant pair of points (P_3,P_3') on the third two-torus $T^2_{(3)}$. Thus, we cannot use the triangle given by a single intersection point $[4]_3$ on the third two-torus. This has been taken into account in table 9.5. The first block of table 9.5 summarizes the results for the electron-like leptons. The labels of the leptons i have been chosen in such a way that a realistic mass hierarchy pattern is reproduced. Indeed, the off-diagonal couplings involving the first and third generations $L^{(1,3)}$ and $e_R^{(1,3)}$ are more suppressed than the couplings involving the second and third generations $L^{(2,3)}$ and $e_R^{(2,3)}$, i.e. $y_e^{(322)} \approx y_e^{(223)} > y_e^{(133)} \approx y_e^{(331)}$. Hence, the Yukawa couplings for the second generation of electron-like leptons are larger than the ones for the first generation. Contrarily to the first and second generations, the third generation comes with a diagonal term $y_e^{(323)}$, which is of order one.

As a side-remark, note that we could also have written down three-point couplings for other states (e.g. $X^{cd(1)} + \tilde{X}^{cd(1)}$) appearing in the intersection sectors under consideration. However, these states have very similar couplings to the ones given in table 9.5, and are related to them by a simple relabeling of the states. We omitted writing them down explicitly in order to avoid overloading the tables.

[2]Once more, we have the following relation between intersection numbers: $(\omega^2 c)(\omega^2 d)' = (\omega^2 c)(\omega d') = c(\omega^{-1} d') = c(\omega^2 d') = c(\omega d)'$.

Other leptonic cubic couplings

The cubic couplings for the other leptons can be derived in much the same way, as we always have the D6-branes b, c, d and their orbifold and orientifold images involved.

Yukawa couplings for the neutrinos in (9.4a): The results for the neutrinos are given in the second block of table 9.5. All three generations of right-handed neutrinos can be given mass with the same mass hierarchy we had for the electrons, i.e. $y_\nu^{(622)} \approx y_\nu^{(523)} > y_\nu^{(433)} \approx y_\nu^{(631)}$. However, the left-handed leptons $L^{(4,5,6)}$ appearing in the cubic coupling of the neutrinos are not the same as those left-handed leptons $L^{(1,2,3)}$ appearing in the coupling of the electrons, since different $b(\omega^k d)$ sectors are involved. This is a bit annoying, since we wanted to give three generations of leptons L out of the six generations of leptons masses large enough so that the MSSM at low energies has only effectively three generations of leptons. This aim is in contradiction to the fact that all six generations are needed to provide mass terms for both electrons and neutrinos at low energies. However, this is only a problem if we identify the right-handed neutrinos ν_R with the singlet states arising in the $c(\omega^k d)$ sectors. As mentioned already several times, an alternative identification can be done using the antisymmetric sector of b or the adjoint sector of d, which we will analyze in section 9.2.3.

Cubic couplings for the superpotential (9.3) of a global 5-stack MSSM (part III)				
Coupling	**Sequence**	**Triangles on $T^2_{(2)} \times T^2_{(3)}$**	**Enclosed Area**	**Parameter**
$L^{(3)} \cdot H_d^{(2)} e_R^{(2)}$	$[b, (\omega^2 c), (\omega^2 d)']$	$\{[5], [(P_3, P_3'), (P_3, P_3'), 4]\}$	$\frac{v_3}{6}$	$y_e^{(322)} \sim \mathcal{O}\left(e^{-\frac{v_3}{6}}\right)$
$L^{(2)} \cdot H_d^{(2)} e_R^{(3)}$		$\{[5], [4, (P_3, P_3'), (P_3, P_3')]\}$	$\frac{v_3}{6}$	$y_e^{(223)} \sim \mathcal{O}\left(e^{-\frac{v_3}{6}}\right)$
$L^{(3)} \cdot H_d^{(2)} e_R^{(3)}$		$\{[5], [(P_3, P_3')]\}$	0	$y_e^{(323)} \sim \mathcal{O}(1)$
$L^{(1)} \cdot H_d^{(3)} e_R^{(3)}$		$\{[(S_2, S_2'), (S_2, S_2'), 5], [4, (P_3, P_3'), (P_3, P_3')]\}$	$\frac{v_2+v_3}{6}$	$y_e^{(133)} \sim \mathcal{O}(e^{-\frac{v_2+v_3}{6}})$
$L^{(3)} \cdot H_d^{(3)} e_R^{(1)}$		$\{[5, (S_2, S_2'), (S_2, S_2')], [(P_3, P_3'), (P_3, P_3'), 4]\}$	$\frac{v_2+v_3}{6}$	$y_e^{(331)} \sim \mathcal{O}(e^{-\frac{v_2+v_3}{6}})$
$L^{(6)} \cdot H_u^{(2)} \nu_R^{(2)}$	$[b, (\omega^2 c), (\omega d)]$	$\{[(S_2, S_2'), (S_2, S_2'), 5], [4]\}$	$\frac{v_2}{6}$	$y_\nu^{(622)} \sim \mathcal{O}(e^{-\frac{v_2}{6}})$
$L^{(6)} \cdot H_u^{(3)} \nu_R^{(1)}$		$\{[(S_2, S_2'), (S_2, S_2'), 5], [4, (P_3, P_3'), (P_3, P_3')]\}$	$\frac{v_2+v_3}{6}$	$y_\nu^{(631)} \sim \mathcal{O}(e^{-\frac{v_2+v_3}{6}})$
$L^{(5)} \cdot H_u^{(2)} \nu_R^{(3)}$		$\{[5, (S_2, S_2'), (S_2, S_2')], [4]\}$	$\frac{v_2}{6}$	$y_\nu^{(523)} \sim \mathcal{O}(e^{-\frac{v_2}{6}})$
$L^{(4)} \cdot H_u^{(3)} \nu_R^{(3)}$		$\{[5, (S_2, S_2'), (S_2, S_2')], [(P_3, P_3'), (P_3, P_3'), 4]\}$	$\frac{v_2+v_3}{6}$	$y_\nu^{(433)} \sim \mathcal{O}(e^{-\frac{v_2+v_3}{6}})$
$L^{(6)} \cdot H_u^{(2)} \nu_R^{(3)}$		$\{[(S_2, S_2')], [4]\}$	0	$y_\nu^{(623)} \sim \mathcal{O}(1)$

Table 9.5: Complete list of the leptonic Yukawa couplings of (9.4a) of the global five-stack MSSM-like model of table 7.17 involving the left-handed and right-handed leptons. The second column indicates the D6-brane stacks used to form the triangles given in the third column by $[x]$ or $[x, y, z]$ with apexes (intersection points) x, y, z on $T^2_{(i=2,3)}$ according to the cubic couplings given in the first column. The fourth column provides the area for the respective triangles in terms of the areas v_i of the two-tori $T^2_{(i=2,3)}$, while the last column presents the resulting coupling constants.

Leptonic couplings in (9.4b): Now let us consider table 9.6. This table includes cubic coupling terms for the numerous left-handed leptons with the axions $\Sigma^{cd(1,2,3)}$, which develop a VEV in order to provide additional mass terms. Both sets of leptons $L^{(1,2,3)}$ and $L^{(4,5,6)}$ couple to the axions $\Sigma^{cd(1,2)}$ and $\Sigma^{cd(3)}$, respectively, with different sets of Yukawa couplings. Thus, one set of leptons could possibly be rendered heavier than the other. In fact, a possibility to decouple $L^{(1,2,3)}$ from $L^{(4,5,6)}$ would be by increasing the VEV of $\Sigma^{cd(3)}$ compared to the VEV of $\Sigma^{cd(1,2)}$, which would render the leptons $L^{(4,5,6)}$ heavier than the leptons $L^{(1,2,3)}$. However, the field $\Sigma^{cd(3)}$ also appears in the couplings $\kappa^{(131)}$, $\kappa^{(232)}$ and $\kappa^{(132)}$ of table 9.4. A large VEV for $\Sigma^{cd(3)}$ would imply a large mass for the right handed down-type quarks $d_R^{(1)}$ and $d_R^{(2)}$, which is phenomenologically undesirable as these down-type quarks are needed to provide three generations of right-handed down-type quarks at low energies. The same holds true when lifting the VEV of $\Sigma^{cd(1,2)}$ in order to render $L^{(1,2,3)}$ heavy. Thus, just as in the case of the redundant right-handed quarks, another mechanism needs to be found in order to explain why this MSSM model appears as an effective three-generation model at low energies.

Note that we have a total of six up-type Higgses $H_u^{(1\ldots6)}$ appearing in table 9.6. The label $i = 2, 3$ refers to the Higgs doublets we have already encountered before. These Higgses arise in the non-chiral sector of $b(\omega^2 c)$, with $H_u^{(3)}$ being situated at an $\mathbb{Z}_2$-invariant pair of points of the form $((Y, Y'), (X, X'))$ on $T^2_{(2)} \times T^2_{(3)}$ and $H_u^{(2)}$ localized at intersection points of the form $((Y, Y'), X)$ on $T^2_{(2)} \times T^2_{(3)}$. The Higgs doublet arising in the non-chiral sector of $b(\omega c)$ is denoted by $H_u^{(1)}$.

Apart from the non-chiral Higgses we also have three additional chiral Higgses $H_u^{(4,5,6)}$ arising in the chiral sector of $b(\omega c)$. They are referred to as up-type Higgses because they present the same quantum numbers as the electroweak up-type Higgs doublets arising from the non-chiral sectors. The Higgses $H_u^{(4,5,6)}$ play a similar rôle to the extra down-type quarks $\overline{d_R}$ we have encountered in the previous section, insofar that they form hermitian conjugates with three out of the six redundant leptons $L^{(1\ldots6)}$. They can thus effectively pair off with the latter to form non-chiral pairs of states.

Finally, we will briefly comment on the labeling of the axions $\Sigma^{cd(1,2)}$. In the non-chiral sector of $c(\omega d)$, we have two pairs of axions labeled by $\Sigma^{cd(1,2)} + \tilde{\Sigma}^{cd(1,2)}$. We labeled by $\Sigma^{cd(2)}$ $(+\tilde{\Sigma}^{cd(2)})$ the pair of axions localized at an intersection point of the form $((Y, Y'), (X, X'))$ on $T^2_{(2)} \times T^2_{(3)}$, and the axion labeled by $\Sigma^{cd(1)}$ sits at an intersection point of the form $(Y, (X, X'))$ on $T^2_{(2)} \times T^2_{(3)}$. Let us already point out, for later reference, that the second member of the first non-chiral pair denoted by $\tilde{\Sigma}^{cd(1)}$ lives at an intersection point of the form $((Y, Y'), X)$ on $T^2_{(2)} \times T^2_{(3)}$. This has been explicitly computed in our publication [64] via the method involving Chan-Paton factors.

Cubic couplings for the superpotential (9.3) of a global 5-stack MSSM (part IV)				
Coupling	**Sequence**	**Triangles on $T^2_{(2)} \times T^2_{(3)}$**	**Enclosed Area**	**Parameter**
$L^{(5)} \cdot H_u^{(3)} \Sigma^{cd(3)}$	$[b, (\omega^2 c), (\omega d)]$	$\{[5, (S_2, S_2'), (S_2, S_2')], [4, (P_3, P_3'), (P_3, P_3')]\}$	$\frac{v_2+v_3}{6}$	$\tilde{\kappa}^{(533)} \sim \mathcal{O}(e^{-\frac{v_2+v_3}{6}})$
$L^{(4)} \cdot H_u^{(2)} \Sigma^{cd(3)}$		$\{[5, (S_2, S_2'), (S_2, S_2')], [(P_3, P_3'), 4, (P_3, P_3')]\}$	$\frac{v_2+v_3}{6}$	$\tilde{\kappa}^{(423)} \sim \mathcal{O}(e^{-\frac{v_2+v_3}{6}})$
$L^{(4)} \cdot H_u^{(3)} \Sigma^{cd(3)}$		$\{[5, (S_2, S_2'), (S_2, S_2')], [(P_3, P_3')]\}$	$\frac{v_2}{6}$	$\tilde{\kappa}^{(433)} \sim \mathcal{O}(e^{-\frac{v_2}{6}})$
$L^{(6)} \cdot H_u^{(3)} \Sigma^{cd(3)}$		$\{[(S_2, S_2')], [4, (P_3, P_3'), (P_3, P_3')]\}$	$\frac{v_3}{6}$	$\tilde{\kappa}^{(633)} \sim \mathcal{O}(e^{-\frac{v_3}{6}})$
$L^{(3)} \cdot H_u^{(4)} \Sigma^{cd(1)}$	$[b, (\omega c), (\omega^2 d)]$	$\{[6], [(P_3, P_3'), 4, (P_3, P_3')]\}$	$\frac{v_3}{6}$	$\tilde{\kappa}^{(341)} \sim \mathcal{O}(e^{-\frac{v_3}{6}})$
$L^{(2)} \cdot H_u^{(5)} \Sigma^{cd(1)}$		$\{[6], [4, (P_3, P_3'), (P_3, P_3')]\}$	$\frac{v_3}{6}$	$\tilde{\kappa}^{(251)} \sim \mathcal{O}(e^{-\frac{v_3}{6}})$
$L^{(3)} \cdot H_u^{(5)} \Sigma^{cd(1)}$		$\{[6], [(P_3, P_3')]\}$	0	$\tilde{\kappa}^{(351)} \sim \mathcal{O}(1)$
$L^{(1)} \cdot H_u^{(5)} \Sigma^{cd(2)}$		$\{[(R_2, R_2'), 6, (R_2, R_2')], [4, (P_3, P_3'), (P_3, P_3')]\}$	$\frac{v_2+v_3}{6}$	$\tilde{\kappa}^{(152)} \sim \mathcal{O}(e^{-\frac{v_2+v_3}{6}})$
$L^{(3)} \cdot H_u^{(6)} \Sigma^{cd(2)}$		$\{[6, (R_2, R_2'), (R_2, R_2')], [(P_3, P_3'), 4, (P_3, P_3')]\}$	$\frac{v_2+v_3}{6}$	$\tilde{\kappa}^{(362)} \sim \mathcal{O}(e^{-\frac{v_2+v_3}{6}})$
$L^{(2)} \cdot H_u^{(1)} \Sigma^{cd(2)}$		$\{[6, (R_2, R_2'), (R_2, R_2')], [4, (P_3, P_3'), (P_3, P_3')]\}$	$\frac{v_2+v_3}{6}$	$\tilde{\kappa}^{(212)} \sim \mathcal{O}(e^{-\frac{v_2+v_3}{6}})$
$L^{(3)} \cdot H_u^{(1)} \Sigma^{cd(2)}$		$\{[6, (R_2, R_2'), (R_2, R_2')], [(P_3, P_3')]\}$	$\frac{v_2}{6}$	$\tilde{\kappa}^{(312)} \sim \mathcal{O}(e^{-\frac{v_2}{6}})$
$L^{(1)} \cdot H_u^{(1)} \Sigma^{cd(1)}$		$\{[(R_2, R_2'), (R_2, R_2'), 6], [4, (P_3, P_3'), (P_3, P_3')]\}$	$\frac{v_2+v_3}{6}$	$\tilde{\kappa}^{(111)} \sim \mathcal{O}(e^{-\frac{v_2+v_3}{6}})$
$L^{(1)} \cdot H_u^{(1)} \Sigma^{cd(2)}$		$\{[(R_2, R_2')], [4, (P_3, P_3'), (P_3, P_3')]\}$	$\frac{v_3}{6}$	$\tilde{\kappa}^{(112)} \sim \mathcal{O}(e^{-\frac{v_3}{6}})$

Table 9.6: Complete list of the leptonic cubic couplings $L \cdot H_u \Sigma^{cd}$ in (9.4b) of the global five-stack MSSM-like model of table 7.17. The second column indicates the D6-brane stacks used to form the triangles given in the third column by $[x]$ or $[x, y, z]$ with apexes (intersection points) x, y, z on $T^2_{(i=2,3)}$ according to the cubic couplings given in the first column. The fourth column provides the area for the respective triangles in terms of the areas v_i of the two-tori $T^2_{(i=2,3)}$, while the last column presents the resulting coupling constants.

Couplings in (9.4c): There is one last sort of couplings involving leptonic states, given in table 9.7. The couplings $H_u \cdot \tilde{H}_d \tilde{\Sigma}^{cd}$ and $\tilde{H}_u \cdot H_d \tilde{\Sigma}^{cd}$ are part of the SUSY formulation of the DFSZ axion model as explained beforehand. The electroweak Higgs doublets denoted with tilde arise from the non-chiral sectors of $b(\omega d)$ and $b(\omega^2 d)$.
Once again, both sets of untilded Higgses from the chiral sector $H_u^{(4,5,6)}$ and the non-chiral sectors $H_u^{(1,2,3)}$ can be used in the couplings, since they have the same quantum numbers. Note that table 9.7 is the only table containing the tilded members of the non-chiral axions, i.e. for instance $\tilde{\Sigma}^{cd(1)}$, which we already mentioned in the previous paragraph.
In table 9.7, we also see some couplings with the symbol of infinity ∞ appearing. Indeed, for some couplings it occurs that the intersection points occupied with particle states do not form closed triangles. The same phenomena appears for other couplings such as those involving the neutrinos, but we only wrote down two examples explicitly in table 9.7 since such couplings do not exist.
As a final remark, note that we could have interpreted the leptons $L^{(1,\dots,6)}$ as down-type Higgses $\tilde{H}_d$, since they have the same quantum numbers. In that sense, tables 9.6 and 9.7 belong to the same discussion.

Cubic couplings for the superpotential (9.3) of a global 5-stack MSSM (part V)				
Coupling	**Sequence**	**Triangles on $T^2_{(2)} \times T^2_{(3)}$**	**Enclosed Area**	**Parameter**
$H_u^{(4)} \cdot \tilde{H}_d^{(2)} \Sigma^{cd(1)}$	$[b,(\omega c),(\omega^2 d)]$	$\{[6,(R_2,R_2'),6],[4,(P_3,P_3'),(P_3,P_3')]\}$	$\infty + \frac{v_3}{6}$	$\mu^{(421)} \sim \mathcal{O}(0)$
$H_u^{(4)} \cdot \tilde{H}_d^{(2)} \Sigma^{cd(2)}$		$\{[6,(R_2,R_2'),(R_2,R_2')],[4,(P_3,P_3'),(P_3,P_3')]\}$	$\frac{v_2}{6} + \frac{v_3}{6}$	$\mu^{(422)} \sim \mathcal{O}\left(e^{-\frac{v_2+v_3}{6}}\right)$
$H_u^{(5)} \cdot \tilde{H}_d^{(2)} \Sigma^{cd(1)}$		$\{[6,(R_2,R_2'),6],[(P_3,P_3')]\}$	∞	$\mu^{(521)} \sim \mathcal{O}(0)$
$H_u^{(5)} \cdot \tilde{H}_d^{(2)} \Sigma^{cd(2)}$		$\{[6,(R_2,R_2'),(R_2,R_2')],[(P_3,P_3')]\}$	$\frac{v_2}{6}$	$\mu^{(522)} \sim \mathcal{O}\left(e^{-\frac{v_2}{6}}\right)$
$H_u^{(6)} \cdot \tilde{H}_d^{(2)} \Sigma^{cd(1)}$		$\{[(R_2,R_2'),(R_2,R_2'),6],[4,(P_3,P_3'),(P_3,P_3')]\}$	$\frac{v_2}{6} + \frac{v_3}{6}$	$\mu^{(621)} \sim \mathcal{O}\left(e^{-\frac{v_2+v_3}{6}}\right)$
$H_u^{(6)} \cdot \tilde{H}_d^{(2)} \Sigma^{cd(2)}$		$\{[(R_2,R_2')],[4,(P_3,P_3'),(P_3,P_3')]\}$	$\frac{v_3}{6}$	$\mu^{(622)} \sim \mathcal{O}\left(e^{-\frac{v_3}{6}}\right)$
$H_u^{(1)} \cdot \tilde{H}_d^{(2)} \Sigma^{cd(1)}$		$\{[(R_2,R_2'),(R_2,R_2'),6],[(P_3,P_3')]\}$	$\frac{v_2}{6}$	$\mu^{(121)} \sim \mathcal{O}\left(e^{-\frac{v_2}{6}}\right)$
$H_u^{(1)} \cdot \tilde{H}_d^{(2)} \Sigma^{cd(2)}$		$\{[(R_2,R_2')],[(P_3,P_3')]\}$	0	$\mu^{(122)} \sim \mathcal{O}(1)$
$\tilde{H}_u^{(2)} \cdot H_d^{(1)} \tilde{\Sigma}^{cd(1)}$		$\{[(R_2,R_2')],[(P_3,P_3'),(P_3,P_3'),4]\}$	$\frac{v_3}{6}$	$\tilde{\mu}^{(211)} \sim \mathcal{O}\left(e^{-\frac{v_3}{6}}\right)$
$\tilde{H}_u^{(2)} \cdot H_d^{(1)} \tilde{\Sigma}^{cd(2)}$		$\{[(R_2,R_2')],[(P_3,P_3')]\}$	0	$\tilde{\mu}^{(212)} \sim \mathcal{O}(1)$
$H_u^{(2)} \cdot \tilde{H}_d^{(1)} \Sigma^{cd(3)}$	$[b,(\omega^2 c),(\omega d)]$	$\{[(S_2,S_2')],[4,(P_3,P_3'),(P_3,P_3')]\}$	$\frac{v_3}{6}$	$\mu^{(213)} \sim \mathcal{O}\left(e^{-\frac{v_3}{6}}\right)$
$H_u^{(3)} \cdot \tilde{H}_d^{(1)} \Sigma^{cd(3)}$		$\{[(S_2,S_2')],[(P_3,P_3')]\}$	0	$\mu^{(313)} \sim \mathcal{O}(1)$
$\tilde{H}_u^{(1)} \cdot H_d^{(2)} \tilde{\Sigma}^{cd(3)}$		$\{[(S_2,S_2'),5,(S_2,S_2')],[(P_3,P_3')]\}$	$\frac{v_2}{6}$	$\tilde{\mu}^{(123)} \sim \mathcal{O}\left(e^{-\frac{v_2}{6}}\right)$
$\tilde{H}_u^{(1)} \cdot H_d^{(3)} \tilde{\Sigma}^{cd(3)}$		$\{[(S_2,S_2')],[(P_3,P_3')]\}$	0	$\tilde{\mu}^{(133)} \sim \mathcal{O}(1)$

Table 9.7: Complete list of the Higgs-axion couplings in (9.4c) of the global five-stack MSSM-like model of table 7.17. The second column indicates the D6-brane stacks used to form the triangles given in the third column by $[x]$ or $[x,y,z]$ with apexes (intersection points) x,y,z on $T^2_{(i=2,3)}$ according to the cubic couplings given in the first column. The fourth column provides the area for the respective triangles in terms of the areas v_i of the two-tori $T^2_{(i=2,3)}$, while the last column presents the resulting coupling constants. The symbol ∞ refers to stacks not forming a closed sequence and giving rise to zero coupling constants.

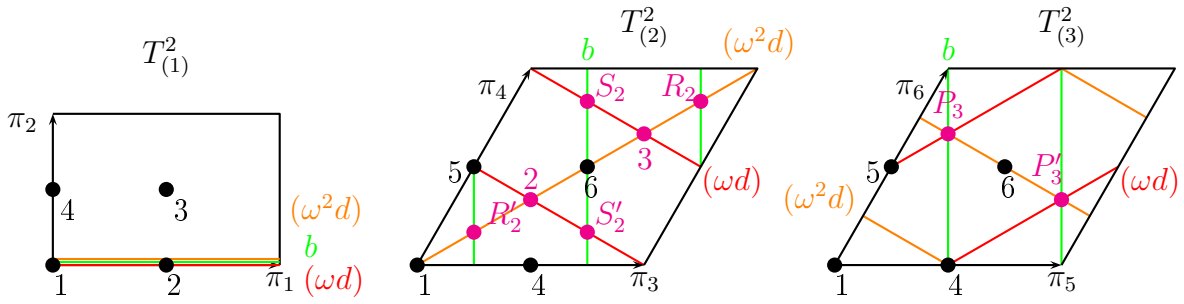

Figure 9.4: The three-cycle denoted by $(\omega^2 d)$ is depicted in orange, the three-cycle labeled by b is indicated in green, and the three-cycle (ωd) is given in red. These three-cycles give rise to a coupling of the form $L \cdot \tilde{H}_u \mathbf{Adj}_d$.

9.2.3 Alternative couplings for the neutrinos

We have seen that by identifying the right-handed neutrino states with the singlet states arising in the $c(\omega^2 d)$ sector, troubles arise concerning the charge of the right-handed neutrinos ν_R under the non-trivial $\mathbb{Z}_3$-symmetry. Alternative singlet states can be used to play the rôle of the right-handed neutrinos, such as the five singlet states from the $b(\omega^{k=1,2}b)'$ sectors $\mathbf{Anti}_b = (\mathbf{1}, \mathbf{1_A}, \mathbf{1})_{(0,0,0,0)}$ corresponding to the antisymmetric representation of $USp(2)_b$, or the four and five singlet states arising in the $c(\omega^{k=1,2})c$ respectively $d(\omega^{k=1,2})d$ sectors corresponding to the adjoint representation of $U(1)_c$ respectively $U(1)_d$.
The Yukawa couplings associated to these singlet states are then of the form $L \cdot \tilde{H}_u \mathbf{Adj}$ respectively $L \cdot \tilde{H}_u \mathbf{Anti}$. It is not possible to provide a coupling of the form $L \cdot \tilde{H}_u \mathbf{Adj}$ with the states $\mathbf{Adj}$ arising in the $c(\omega^{k=1,2}c)$ sectors and satisfying the stringy selection rule. The other two possibilities involving the antisymmetric states from the $b(\omega^{k=1,2}b)'$ sectors and the states in the adjoint representation coming from the $d(\omega^{k=1,2})d$ sectors on the other hand allow for couplings fulfilling the stringy selection rule. Once more, we will derive one coupling explicitly, and provide the final results of the remaining couplings.

Example of calculation: The coupling $L \cdot \tilde{H}_u \mathbf{Adj}_d$

The Yukawa coupling $L \cdot \tilde{H}_u \mathbf{Adj}_d$ involves the stacks $b, (\omega d)$ and $(\omega^2 d)$. Remember that the leptons arising from the chiral sector of $b(\omega d)$ are labeled $L^{(4,5,6)}$, those arising from $b(\omega^2 d)$ are labeled $L^{(1,2,3)}$. The up-type Higgs $\tilde{H}_u^{(2)}$ arises from the non-chiral sector of $b(\omega^2 d)$ while the up-type Higgs $\tilde{H}_u^{(1)}$ arises from the non-chiral sector of $b(\omega d)$. All six Yukawa couplings for the six generations of left-handed leptons can be realized with the same sequence $[b, (\omega d), (\omega^2 d)]$. These three-cycles lie on the three two-tori as indicated in figure 9.4. On the second two-torus $T^2_{(2)}$, there is no intersection point where all three one-cycles meet. Pairwise intersection points are given by the points labeled 1, 5, 6, (R_2, R'_2), $(2, 3)$ and (S_2, S'_2). On the fundamental domain, we can already detect two triangles and their $\mathbb{Z}_2$-images $[5, (2, 3), (R_2, R'_2)]$ and $[6, (2, 3), (S_2, S'_2)]$. Other triangles become apparent when drawing several lattice cells. On the third two-torus $T^2_{(3)}$, all three one-cycles intersect in the $\mathbb{Z}_2$-fixed point 4 and in the $\mathbb{Z}_2$-invariant pair of points (P_3, P'_3). An obvious triangle and its $\mathbb{Z}_2$-image is given by the apexes $[4, (P_3, P'_3), (P_3, P'_3)]$.
There are two possibilities to interpret the matter localization in the different sectors, ac-

cording to which set of leptons one is considering. The first possibility is given by:

state	xy	χ^{xy}	$T^2_{(2)}$	$T^2_{(3)}$
$L^{(1,2,3)}$ $(+\tilde{H}_u^{(2)} + \tilde{H}_d^{(2)})$	$b(\omega^2 d)$	3 $(+\lvert 2\rvert)$	$6, (R_2, R_2')$	$4, (P_3, P_3')$
$\tilde{H}_u^{(1)}$ $(+\tilde{H}_d^{(1)},\ L^{(4,5,6)})$	$b(\omega d)$	$\lvert 2\rvert$ $(+3)$	$5, (S_2, S_2')$	$4, (P_3, P_3')$
$\mathbf{Adj}_d^{(1,2,3,4,5)}$	$(\omega d)(\omega^2 d) + (\omega^2 d)(\omega d)$	$\lvert 5\rvert$	$1, (2, 3)$	$4, (P_3, P_3')$

(9.10)

Once again, the three chiral leptons $L^{(1,2,3)}$ sit on the points involving some $\mathbb{Z}_2$-fixed points, i.e. $(6, (P_3, P_3'))$, $(6, 4)$ and $((R_2, R_2'), 4)$ on $T^2_{(2)} \times T^2_{(3)}$. The non-chiral Higgs $\tilde{H}_u^{(1)} + \tilde{H}_d^{(1)}$ sits at the points $((S_2, S_2'), (P_3, P_3'))$. We have a pair of states in the adjoint representation denoted by $\mathbf{Adj}_d^{(4)} + \mathbf{Adj}_d^{(5)}$ living on $((2, 3), (P_3, P_3'))$. The state in the adjoint representation denoted by $\mathbf{Adj}_d^{(2)}$ is taken to live on $((2, 3), 4)$, the state in the adjoint representation denoted by $\mathbf{Adj}_d^{(3)}$ is associated to $(1, (P_3, P_3'))$. The state labeled by $\mathbf{Adj}_d^{(1)}$ sits on the point $(1, 4)$. However, it cannot be involved in Yukawa couplings because its presence implies that one of the apexes of a triangle is left unoccupied. The possible triangles on $T^2_{(2)} \times T^2_{(3)}$ which can be formed with all apexes occupied by some state are given in the first block of table 9.8.
The other set of leptons can gain mass by the following interpretation of matter localization:

state	xy	χ^{xy}	$T^2_{(2)}$	$T^2_{(3)}$
$L^{(4,5,6)}$ $(+\tilde{H}_u^{(1)} + \tilde{H}_d^{(1)})$	$b(\omega d)$	3 $(+\lvert 2\rvert)$	$5, (S_2, S_2')$	$4, (P_3, P_3')$
$\tilde{H}_u^{(2)}$ $(+\tilde{H}_d^{(2)},\ L^{(1,2,3)})$	$b(\omega^2 d)$	$\lvert 2\rvert$ $(+3)$	$6, (R_2, R_2')$	$4, (P_3, P_3')$
$\mathbf{Adj}_d^{(1,2,3,4,5)}$	$(\omega d)(\omega^2 d) + (\omega^2 d)(\omega d)$	$\lvert 5\rvert$	$1, (2, 3)$	$4, (P_3, P_3')$

(9.11)

Thus, the localization of matter states at intersection points is now slightly different. It can be derived from the previous interpretation by exchanging the labels $6 \leftrightarrow 5$ and $(R_2, R_2') \leftrightarrow (S_2, S_2')$. The results are indicated in the second block of table 9.8.

In the second block of table 9.8 we see that we can provide mass terms for four out of the five singlet states $\mathbf{Adj}_d^{(1,2,3,4,5)}$. Both set of leptons $L^{(1,2,3)}$ and $L^{(4,5,6)}$ can be coupled off. Unfortunately, none of the couplings is of order one, which could have removed some of the redundant leptons. However, the set of leptons $L^{(1,2,3)}$ and $L^{(4,5,6)}$ involve couplings to different Higgses $\tilde{H}_u^{(1)}$ respectively $\tilde{H}_u^{(2)}$. Thus, by cranking up the VEV of the field $\tilde{H}_u^{(2)}$, some of the leptons could be effectively removed from the low-energy model. This is not viable from a phenomenological point of view though, as the field $\tilde{H}_u^{(2)}$ also appears in the Yukawa couplings of the up-type quarks, see table 9.3. Lifting the VEV of $\tilde{H}_u^{(2)}$ would render some of the up-type quarks too heavy. The same reasoning holds true for the couplings involving $\tilde{H}_u^{(1)}$ and $L^{(1,2,3)}$. Therefore, this scenario does not allow either to provide an argument for a three-generation effective low-energy MSSM. In the next section, we will comment on the results for the remaining alternative interpretation of the singlet states, albeit without giving the explicit derivation.

Cubic couplings for the superpotential (9.3) of a global 5-stack MSSM (part VI)				
Coupling	**Sequence**	**Triangles on $T^2_{(2)} \times T^2_{(3)}$**	**Enclosed Area**	**Parameter**
$L^{(5)} \cdot \tilde{H}_u^{(2)} \mathbf{Adj}_d^{(4)}$	$[b, (\omega d), (\omega^2 d)]$	$\{[5, (R_2, R_2'), (2,3)], [4, (P_3, P_3'), (P_3, P_3')]\}$	$\frac{v_2}{24} + \frac{v_3}{6}$	$\mathfrak{A}^{(524)} \sim \mathcal{O}\left(e^{-\frac{v_2+4v_3}{24}}\right)$
$L^{(5)} \cdot \tilde{H}_u^{(2)} \mathbf{Adj}_d^{(5)}$		$\{[5, (R_2, R_2'), (2,3)], [4, (P_3, P_3'), (P_3, P_3')]\}$	$\frac{v_2}{24} + \frac{v_3}{6}$	$\mathfrak{A}^{(525)} \sim \mathcal{O}\left(e^{-\frac{v_2+4v_3}{24}}\right)$
$L^{(4)} \cdot \tilde{H}_u^{(2)} \mathbf{Adj}_d^{(2)}$		$\{[5, (R_2, R_2'), (2,3)], [(P_3, P_3'), (P_3, P_3'), 4]\}$	$\frac{v_2}{24} + \frac{v_3}{6}$	$\mathfrak{A}^{(422)} \sim \mathcal{O}\left(e^{-\frac{v_2+4v_3}{24}}\right)$
$L^{(4)} \cdot \tilde{H}_u^{(2)} \mathbf{Adj}_d^{(4)}$		$\{[5, (R_2, R_2'), (2,3)], [(P_3, P_3')]\}$	$\frac{v_2}{24}$	$\mathfrak{A}^{(424)} \sim \mathcal{O}\left(e^{-\frac{v_2}{24}}\right)$
$L^{(4)} \cdot \tilde{H}_u^{(2)} \mathbf{Adj}_d^{(5)}$		$\{[5, (R_2, R_2'), (2,3)], [(P_3, P_3')]\}$	$\frac{v_2}{24}$	$\mathfrak{A}^{(425)} \sim \mathcal{O}\left(e^{-\frac{v_2}{24}}\right)$
$L^{(6)} \cdot \tilde{H}_u^{(2)} \mathbf{Adj}_d^{(3)}$		$\{[(S_2, S_2'), (R_2, R_2'), 1], [4, (P_3, P_3'), (P_3, P_3')]\}$	$\frac{v_2}{24} + \frac{v_3}{6}$	$\mathfrak{A}^{(623)} \sim \mathcal{O}\left(e^{-\frac{v_2+4v_3}{24}}\right)$
$L^{(6)} \cdot \tilde{H}_u^{(2)} \mathbf{Adj}_d^{(4)}$		$\{[(S_2, S_2'), (R_2, R_2'), (2,3)], [4, (P_3, P_3'), (P_3, P_3')]\}$	$\frac{3v_2}{8} + \frac{v_3}{6}$	$\mathfrak{A}^{(624)} \sim \mathcal{O}\left(e^{-\frac{9v_2+4v_3}{24}}\right)$
$L^{(6)} \cdot \tilde{H}_u^{(2)} \mathbf{Adj}_d^{(5)}$		$\{[(S_2, S_2'), (R_2, R_2'), (2,3)], [4, (P_3, P_3'), (P_3, P_3')]\}$	$\frac{3v_2}{8} + \frac{v_3}{6}$	$\mathfrak{A}^{(625)} \sim \mathcal{O}\left(e^{-\frac{9v_2+4v_3}{24}}\right)$
$L^{(2)} \cdot \tilde{H}_u^{(1)} \mathbf{Adj}_d^{(4)}$	$[b, (\omega^2 d), (\omega d)]$	$\{[6, (S_2, S_2'), (2,3)], [4, (P_3, P_3'), (P_3, P_3')]\}$	$\frac{v_2}{24} + \frac{v_3}{6}$	$\mathfrak{A}^{(214)} \sim \mathcal{O}\left(e^{-\frac{v_2+4v_3}{24}}\right)$
$L^{(2)} \cdot \tilde{H}_u^{(1)} \mathbf{Adj}_d^{(5)}$		$\{[6, (S_2, S_2'), (2,3)], [4, (P_3, P_3'), (P_3, P_3')]\}$	$\frac{v_2}{24} + \frac{v_3}{6}$	$\mathfrak{A}^{(215)} \sim \mathcal{O}\left(e^{-\frac{v_2+4v_3}{24}}\right)$
$L^{(3)} \cdot \tilde{H}_u^{(1)} \mathbf{Adj}_d^{(2)}$		$\{[6, (S_2, S_2'), (2,3)], [(P_3, P_3'), (P_3, P_3'), 4]\}$	$\frac{v_2}{24} + \frac{v_3}{6}$	$\mathfrak{A}^{(312)} \sim \mathcal{O}\left(e^{-\frac{v_2+4v_3}{24}}\right)$
$L^{(3)} \cdot \tilde{H}_u^{(1)} \mathbf{Adj}_d^{(4)}$		$\{[6, (S_2, S_2'), (2,3)], [(P_3, P_3')]\}$	$\frac{v_2}{24}$	$\mathfrak{A}^{(314)} \sim \mathcal{O}\left(e^{-\frac{v_2}{24}}\right)$
$L^{(3)} \cdot \tilde{H}_u^{(1)} \mathbf{Adj}_d^{(5)}$		$\{[6, (S_2, S_2'), (2,3)], [(P_3, P_3')]\}$	$\frac{v_2}{24}$	$\mathfrak{A}^{(315)} \sim \mathcal{O}\left(e^{-\frac{v_2}{24}}\right)$
$L^{(1)} \cdot \tilde{H}_u^{(1)} \mathbf{Adj}_d^{(3)}$		$\{[(S_2, S_2'), (R_2, R_2'), 1], [4, (P_3, P_3'), (P_3, P_3')]\}$	$\frac{v_2}{24} + \frac{v_3}{6}$	$\mathfrak{A}^{(113)} \sim \mathcal{O}\left(e^{-\frac{v_2+4v_3}{24}}\right)$
$L^{(1)} \cdot \tilde{H}_u^{(1)} \mathbf{Adj}_d^{(4)}$		$\{[(S_2, S_2'), (R_2, R_2'), (2,3)], [4, (P_3, P_3'), (P_3, P_3')]\}$	$\frac{3v_2}{8} + \frac{v_3}{6}$	$\mathfrak{A}^{(114)} \sim \mathcal{O}\left(e^{-\frac{9v_2+4v_3}{24}}\right)$
$L^{(1)} \cdot \tilde{H}_u^{(1)} \mathbf{Adj}_d^{(5)}$		$\{[(S_2, S_2'), (R_2, R_2'), (2,3)], [4, (P_3, P_3'), (P_3, P_3')]\}$	$\frac{3v_2}{8} + \frac{v_3}{6}$	$\mathfrak{A}^{(115)} \sim \mathcal{O}\left(e^{-\frac{9v_2+4v_3}{24}}\right)$

Table 9.8: Complete list of the cubic couplings (9.4d) of the global five-stack MSSM-like model of table 7.17 involving the alternative candidates for the right-handed neutrinos. The second column indicates the D6-brane stacks used to form the triangles given in the third column by $[x]$ or $[x, y, z]$ with apexes (intersection points) x, y, z on $T^2_{(i=2,3)}$ according to the cubic couplings given in the first column. The fourth column provides the area for the respective triangles in terms of the areas v_i of the two-tori $T^2_{(i=2,3)}$, while the last column presents the resulting coupling constants.

Other couplings involving right-handed neutrinos

The other possible interpretation of the right-handed neutrino states is given by the five singlet states arising in the antisymmetric sector of $b(\omega^{k=1,2}b)'$. The corresponding Yukawa coupling is of the form $L \cdot \tilde{H}_u \mathbf{Anti}_b$. Just as in the previous computation, four out of the five singlet states can be paired off to the six generations of leptons with the sequences $[b,(\omega^2 d)(\omega^2 b)']$ and $[b,(\omega d)(\omega b)']$. The results are given in the first and second block of table 9.9. The situation is very similar to the one of the previous interpretation of right-handed neutrinos. Indeed, none of the couplings is of order one, meaning that all six generations of left-handed leptons remain present at low energies.

All in all, we can conclude that two out of the three alternative identifications of the right-handed neutrinos give rise to Yukawa couplings. Hence, we can extend the perturbative superpotential by adding the following terms:

$$\begin{aligned} \mathcal{W}_{per} \supset \; & \mathfrak{B}^{(i1k)} L^{(i)} \cdot \tilde{H}_u^{(1)} \mathbf{Anti}_b^{(k)} + \tilde{\mathfrak{B}}^{(j1k)} L^{(j)} \cdot \tilde{H}_u^{(2)} \mathbf{Anti}_b^{(k)} \\ & + \mathfrak{A}^{(i1k)} L^{(i)} \cdot \tilde{H}_u^{(1)} \mathbf{Adj}_d^{(k)} + \tilde{\mathfrak{A}}^{(j1k)} L^{(j)} \cdot \tilde{H}_u^{(2)} \mathbf{Adj}_d^{(k)}, \end{aligned} \tag{9.12}$$

with $i \in \{1,2,3\}$, $j \in \{4,5,6\}$ and $k \in \{2,3,4,5\}$. The precise form of the associated sequences and Yukawa couplings is given in table 9.9. Note that for the two possible identifications of the right-handed neutrinos presented in this section, we have a total of ten generations of right-handed neutrinos, as we have five states in the antisymmetric sector of $b(\omega^{k=1,2}b)'$ and five states in the adjoint sector of $d(\omega^{k=1,2}d)$. This is phenomenologically acceptable, as many theoretical models include so-called sterile neutrinos. These are right-handed neutrinos which are used e.g. as candidates for dark matter states. For a review on sterile neutrinos, see for instance [217].

Cubic couplings for the superpotential (9.3) of a global 5-stack MSSM (part VII)				
Coupling	**Sequence**	**Triangles on $T^2_{(2)} \times T^2_{(3)}$**	**Enclosed Area**	**Parameter**
$L^{(2)} \cdot \tilde{H}_u^{(1)} \mathbf{Anti}_b^{(4)}$	$[b, (\omega^2 d), (\omega^2 b)']$	$\{[6, (R_2, R_2'), (R_2, R_2')], [4, (R_3, R_3'), (2, 3)]\}$	$\frac{v_2}{6} + \frac{v_3}{24}$	$\mathfrak{B}^{(214)} \sim \mathcal{O}(e^{-\frac{4v_2+v_3}{24}})$
$L^{(2)} \cdot \tilde{H}_u^{(1)} \mathbf{Anti}_b^{(5)}$		$\{[6, (R_2, R_2'), (R_2, R_2')], [4, (R_3, R_3'), (2, 3)]\}$	$\frac{v_2}{6} + \frac{v_3}{24}$	$\mathfrak{B}^{(215)} \sim \mathcal{O}(e^{-\frac{4v_2+v_3}{24}})$
$L^{(3)} \cdot \tilde{H}_u^{(1)} \mathbf{Anti}_b^{(2)}$		$\{[6, (R_2, R_2'), (R_2, R_2')], [(P_3, P_3'), (R_3, R_3'), 1)]\}$	$\frac{v_2}{6} + \frac{v_3}{24}$	$\mathfrak{B}^{(312)} \sim \mathcal{O}(e^{-\frac{4v_2+v_3}{24}})$
$L^{(3)} \cdot \tilde{H}_u^{(1)} \mathbf{Anti}_b^{(4)}$		$\{[6, (R_2, R_2'), (R_2, R_2')], [(P_3, P_3'), (R_3, R_3'), (2, 3)]\}$	$\frac{v_2}{6} + \frac{3v_3}{8}$	$\mathfrak{B}^{(314)} \sim \mathcal{O}(e^{-\frac{4v_2+9v_3}{24}})$
$L^{(3)} \cdot \tilde{H}_u^{(1)} \mathbf{Anti}_b^{(5)}$		$\{[6, (R_2, R_2'), (R_2, R_2')], [(P_3, P_3'), (R_3, R_3'), (2, 3)]\}$	$\frac{v_2}{6} + \frac{3v_3}{8}$	$\mathfrak{B}^{(315)} \sim \mathcal{O}(e^{-\frac{4v_2+9v_3}{24}})$
$L^{(1)} \cdot \tilde{H}_u^{(1)} \mathbf{Anti}_b^{(3)}$		$\{[(R_2, R_2'), (R_2, R_2'), 6], [4, (R_3, R_3'), (2, 3)]\}$	$\frac{v_2}{6} + \frac{v_3}{24}$	$\mathfrak{B}^{(113)} \sim \mathcal{O}(e^{-\frac{4v_2+v_3}{24}})$
$L^{(1)} \cdot \tilde{H}_u^{(1)} \mathbf{Anti}_b^{(4)}$		$\{[(R_2, R_2'), [4, (R_3, R_3'), (2, 3)]\}$	$\frac{v_3}{24}$	$\mathfrak{B}^{(114)} \sim \mathcal{O}(e^{-\frac{v_3}{24}})$
$L^{(1)} \cdot \tilde{H}_u^{(1)} \mathbf{Anti}_b^{(5)}$		$\{[(R_2, R_2')], [4, (R_3, R_3'), (2, 3)]\}$	$\frac{v_3}{24}$	$\mathfrak{B}^{(115)} \sim \mathcal{O}(e^{-\frac{v_3}{24}})$
$L^{(5)} \cdot \tilde{H}_u^{(2)} \mathbf{Anti}_b^{(4)}$	$[b, (\omega d), (\omega b)']$	$\{[5, (S_2, S_2'), (S_2, S_2')], [4, (S_3, S_3'), (2, 3)]\}$	$\frac{v_2}{6} + \frac{v_3}{24}$	$\mathfrak{B}^{(524)} \sim \mathcal{O}(e^{-\frac{4v_2+v_3}{24}})$
$L^{(5)} \cdot \tilde{H}_u^{(2)} \mathbf{Anti}_b^{(5)}$		$\{[5, (S_2, S_2'), (S_2, S_2')], [4, (S_3, S_3'), (2, 3)]\}$	$\frac{v_2}{6} + \frac{v_3}{24}$	$\mathfrak{B}^{(525)} \sim \mathcal{O}(e^{-\frac{4v_2+v_3}{24}})$
$L^{(4)} \cdot \tilde{H}_u^{(2)} \mathbf{Anti}_b^{(2)}$		$\{[5, (S_2, S_2'), (S_2, S_2')], [(P_3, P_3'), (S_3, S_3'), 1)]\}$	$\frac{v_2}{6} + \frac{v_3}{24}$	$\mathfrak{B}^{(422)} \sim \mathcal{O}(e^{-\frac{4v_2+v_3}{24}})$
$L^{(4)} \cdot \tilde{H}_u^{(2)} \mathbf{Anti}_b^{(4)}$		$\{[5, (S_2, S_2'), (S_2, S_2')], [(P_3, P_3'), (S_3, S_3'), (2, 3)]\}$	$\frac{v_2}{6} + \frac{3v_3}{8}$	$\mathfrak{B}^{(424)} \sim \mathcal{O}(e^{-\frac{4v_2+9v_3}{24}})$
$L^{(4)} \cdot \tilde{H}_u^{(2)} \mathbf{Anti}_b^{(5)}$		$\{[5, (S_2, S_2'), (S_2, S_2')], [(P_3, P_3'), (S_3, S_3'), (2, 3)]\}$	$\frac{v_2}{6} + \frac{3v_3}{8}$	$\mathfrak{B}^{(425)} \sim \mathcal{O}(e^{-\frac{4v_2+9v_3}{24}})$
$L^{(6)} \cdot \tilde{H}_u^{(2)} \mathbf{Anti}_b^{(3)}$		$\{[(S_2, S_2'), (S_2, S_2'), 5], [4, (S_3, S_3'), (2, 3)]\}$	$\frac{v_2}{6} + \frac{v_3}{24}$	$\mathfrak{B}^{(623)} \sim \mathcal{O}(e^{-\frac{4v_2+v_3}{24}})$
$L^{(6)} \cdot \tilde{H}_u^{(2)} \mathbf{Anti}_b^{(4)}$		$\{[(S_2, S_2'), [4, (S_3, S_3'), (2, 3)]\}$	$\frac{v_3}{24}$	$\mathfrak{B}^{(624)} \sim \mathcal{O}(e^{-\frac{v_3}{24}})$
$L^{(6)} \cdot \tilde{H}_u^{(2)} \mathbf{Anti}_b^{(5)}$		$\{[(S_2, S_2')], [4, (S_3, S_3'), (2, 3)]\}$	$\frac{v_3}{24}$	$\mathfrak{B}^{(625)} \sim \mathcal{O}(e^{-\frac{v_3}{24}})$

Table 9.9: Complete list of the cubic couplings (9.4d) of the global five-stack MSSM-like model of table 7.17 involving the alternative candidates for the right-handed neutrinos. The second column indicates the D6-brane stacks used to form the triangles given in the third column by $[x]$ or $[x, y, z]$ with apexes (intersection points) x, y, z on $T^2_{(i=2,3)}$ according to the cubic couplings given in the first column. The fourth column provides the area for the respective triangles in terms of the areas v_i of the two-tori $T^2_{(i=2,3)}$, while the last column presents the resulting coupling constants.

9.2.4 Hidden sector cubic couplings

This section is the final step in our search for cubic couplings and involves the exotic states of the hidden sector. Since exotic particles are unappealing from a phenomenological point of view, the hope is that they become substantially heavy. The exotic states can in principle be given mass by coupling them to the various Higgs doublets arising in the visible sector.
As a first observation, let us consider the exotic states arising in the non-chiral sectors of ah and ah' as shown in tables 9.1 and 9.2. This involves the D6-branes a, h, h'. In the case of a non-chiral pair of states, the most convenient way to provide mass terms with cubic couplings would be to pair off both members of the non-chiral pair simultaneously to some singlet state. However, this is not possible, as the singlet states involve either the D6-branes c or d. Thus, more than three cycles would be needed, which would lead to quartic couplings instead of cubic couplings. Since we want to limit the analysis to cubic couplings, we will not consider the exotic particles from the ah and ah' sectors here and rather focus on the exotic particles arising in the sectors of $bh = bh'$, ch', dh and dh'. Note that the two non-chiral pairs in the antisymmetric sector of hh' are completely decoupled from the visible sector and are thus not bothersome from the phenomenological point of view. Hence, we will not try to give them masses.
To simplify the notation, we will label the states arising from the sectors xh and xh' by h_x respectively $\underline{h}_x$, $x = b, c, d$. As usual, we will compute one cubic coupling in some detail, and only give the final results for the others. We choose to present the coupling $\underline{h}_b \cdot H_u \underline{h}_c$ in some detail.

Example of calculation: The Yukawa coupling $\underline{h}_b \cdot H_u \underline{h}_c$

In the ch' sector, we have six generations of particles arising. Thus, our first aim is to pair off as many of these as possible. We can couple them to the chiral states coming from the bh' sector, together with the non-chiral Higgs from the bc sector, giving the following cubic coupling: $\underline{h}_b \cdot H_u \underline{h}_c$. This coupling satisfies the charge selection rules: $(Q_a, Q_c, Q_d, Q_h) = (0,0,0,1) + (0,1,0,0) + (0,-1,0,-1)$. Let us label the matter states per sector as follows:
$(\chi^{bc}, \chi^{b(\omega c)}, \chi^{b(\omega^2 c)}) = (0, |2|\ (-3), |4|) : \Big(0, H_u^{(1)}\ (+H_d^{(1)}, H_u^{(4,5,6)}), H_u^{(2,3)}\ (+H_d^{(2,3)})\Big)$,
$(\chi^{bh'}, \chi^{b(\omega h)'}, \chi^{b(\omega^2 h)'}) = (2,1,0) : (\underline{h}_b^{(1,2)}, \underline{h}_b^{(3)}, 0)$,
$(\chi^{ch'}, \chi^{c(\omega h)'}, \chi^{c(\omega^2 h)'}) = (-4,-1,-1) : (\underline{h}_c^{(3,4,5,6)}, \underline{h}_c^{(1)}, \underline{h}_c^{(2)})$.
To give the first generation of exotic particles $\underline{h}_c$ a mass, we can take the sequence $[b, (\omega c), h']$.

Triangles formed by the sequence $[b, (\omega c), h']$: The three-cycles $b, (\omega c), h'$ lie on the three two-tori as indicated in figure 9.5. Looking at the fundamental domain of the second two-torus $T^2_{(2)}$, it seems a priori that no closed sequence can be found, apart from $\mathbb{Z}_2$-fixed point 6, where all three one-cycles meet. However, the triangles close only after identification of the borders of the fundamental domain. This can be seen by drawing several lattice cells. On the third two-torus $T^2_{(3)}$, already two triangles and their $\mathbb{Z}_2$-images are apparent on the fundamental domain. We see that the coupling under consideration satisfies the stringy selection rule as it allows for closed sequences.

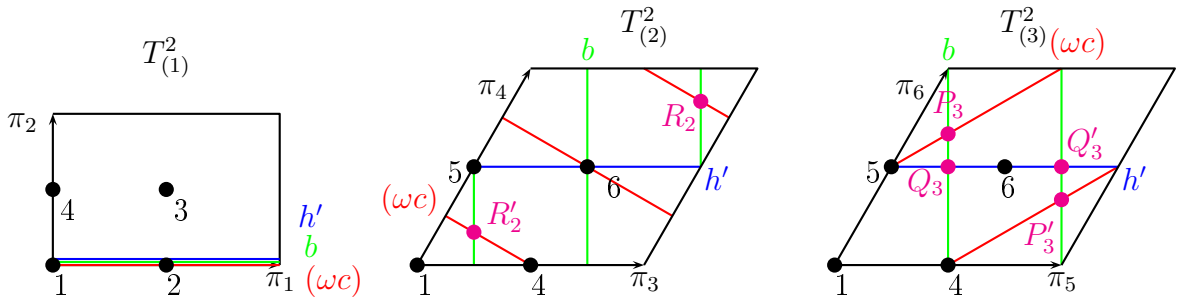

Figure 9.5: The three-cycle denoted by h' is depicted in blue, the three-cycle labeled by b is indicated in green, and the three-cycle (ωc) is given in red. These three-cycles give rise to a Yukawa coupling of the form $\underline{h}_b \cdot H_u \underline{h}_c$.

The localization of matter states per sector is:

state	xy	χ^{xy}	$T^2_{(2)}$	$T^2_{(3)}$
$\underline{h}_b^{(1,2)}$	bh'	2	$5, 6$	(Q_3, Q'_3)
$H_u^{(1)}$ $(+H_d^{(1)}, H_u^{(4,5,6)})$	$b(\omega c)$	$\lvert 2\rvert$ (-3)	$6, (R_2, R'_2)$	$4, (P_3, P'_3)$
$\underline{h}_c^{(1)}$	$(\omega c)h'$	-1	6	5

(9.13)

Once again, the non-chiral Higgs pair $H_u^{(1)} + H_d^{(1)}$ sits on the $\mathbb{Z}_2$-invariant pair of points $((R_2, R'_2), (P_3, P'_3))$, while the three chiral states $H_u^{(4)}$, $H_u^{(5)}$ and $H_u^{(6)}$ sit on the points $(6, 4)$, $(6, (P_3, P'_3))$ and $((R_2, R'_2), 4)$ respectively. The following closed sequences are present:

triangle on $T^2_{(2)}$	$\frac{\text{Area}}{v_2}$	triangle on $T^2_{(3)}$	$\frac{\text{Area}}{v_3}$
$[6, 5, 6]_2$	$\frac{3}{4}$	$[(Q_3, Q'_3), 4, 5]_3$	$\frac{3}{16}$
$[6, (R_2, R'_2), 6]_2$	$\frac{1}{3}$	$[(Q_3, Q'_3), (P_3, P'_3), 5]_3$	$\frac{1}{48}$
$[5, (R_2, R'_2), 6]_2$	$\frac{1}{12}$		
$[6]_2$	0		

(9.14)

We will restrict ourselves to the couplings involving the non-chiral Higgs pair $H_u^{(1)} + H_d^{(1)}$, and omit the couplings involving the chiral states $H_u^{(4,5,6)}$ in order to avoid overloading the tables. The allowed Yukawa couplings involving the non-chiral Higgs $H_u^{(1)}$ are listed in the first block of table 9.10. As usual, we have chosen in table 9.10 the labels i in $\underline{h}_b^{(i)}$ in a way aiming to suppress the non-diagonal terms with respect to the diagonal terms, so that generation mixing is disfavored. In other words, we have chosen $\underline{h}_b^{(2)}$ to sit at the point $(6, (Q_3, Q'_3))$ and $\underline{h}_b^{(1)}$ to sit at the point $(5, (Q_3, Q'_3))$ on $T^2_{(2)} \times T^2_{(3)}$.

The second generation of particles $\underline{h}_c^{(2)}$ is situated in another sector of ch', so we have to take another sequence to provide it with a mass term. An appropriate sequence is given by $[b, (\omega^2 c), h']$.

Triangles formed by the sequence $[b, (\omega^2 c), h']$: The three-cycles $b, (\omega^2 c), h'$ lie on the three two-tori as depicted in figure 9.6. Once again, several closed triangles are apparent already on the fundamental domains of $T^2_{(2)} \times T^2_{(3)}$. The localization of matter states per

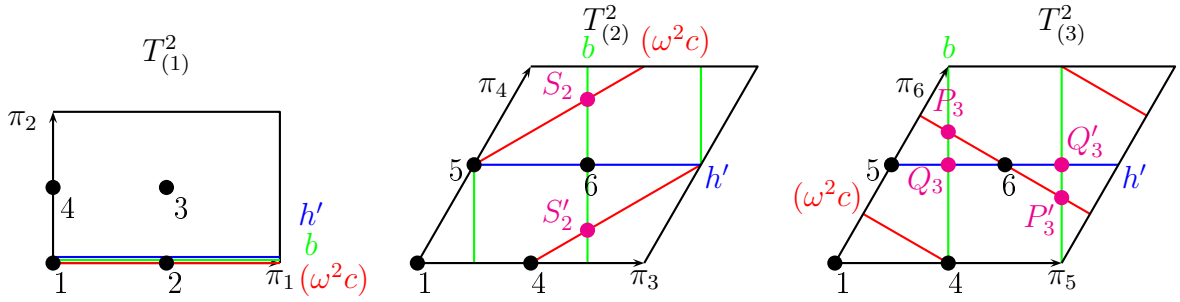

Figure 9.6: The three-cycle denoted by h' is depicted in blue, the three-cycle labeled by b is indicated in green, and the three-cycle $(\omega^2 c)$ is given in red. These three-cycles give rise to a Yukawa coupling of the form $\underline{h}_b \cdot H_u \underline{h}_c$.

sector is as follows:

state	xy	χ^{xy}	$T^2_{(2)}$	$T^2_{(3)}$
$\underline{h}_b^{(1,2)}$	bh'	2	$5,6$	(Q_3, Q_3')
$H_u^{(2,3)}$ $(+H_d^{(2,3)})$	$b(\omega^2 c)$	$\lvert 4\rvert$	$5,(S_2,S_2')$	$4,(P_3,P_3')$
$\underline{h}_c^{(2)}$	$(\omega^2 c)h'$	-1	5	6

(9.15)

Once again, we have two non-chiral Higgs pairs $H_u^{(2,3)}+H_d^{(2,3)}$ in the $b(\omega^2 c)$ sector. As before, $H_u^{(3)}$ sits on the $\mathbb{Z}_2$-invariant pair of points $((S_2,S_2'),(P_3,P_3'))$, whereas the Higgs $H_u^{(2)}$ sits on some combination of a $\mathbb{Z}_2$-fixed point and a $\mathbb{Z}_2$-invariant pair of points, namely $((S_2,S_2'),4)$. The presence of two Higgses once more enhances the possible Yukawa structures. The various closed triangles are as follows:

triangle on $T^2_{(2)}$	$\frac{\text{Area}}{v_2}$	triangle on $T^2_{(3)}$	$\frac{\text{Area}}{v_3}$
$[5,(S_2,S_2'),5]_2$	$\frac{1}{3}$	$[(Q_3,Q_3'),4,6]_3$	$\frac{3}{16}$
$[5,6,5]_2$	$\frac{3}{4}$	$[(Q_3,Q_3'),(P_3,P_3'),6]_3$	$\frac{1}{48}$
$[5,(S_2,S_2'),6]_2$	$\frac{1}{12}$		
$[5]_2$	0		

(9.16)

There are eight possible combinations of triangles on both two-tori. Once again, not all possible combinations can be taken to provide Yukawa couplings since some apexes are unoccupied by the states under consideration. The possible Yukawa couplings are listed in the second block of table 9.10. Once again, the choice of labels i in $\underline{h}_b^{(i)}$ we have made for the previous sequence allows also for this sequence to suppress the non-diagonal terms with respect to the diagonal terms.

Finally, we have one remaining generation of the exotic particles $\underline{h}_b$ and four remaining generations for the exotic $\underline{h}_c$ particles. These can be paired off by taking for example the sequence $[b,(\omega^2 c),(\omega h)']$.

Triangles formed by the sequence $[b,(\omega^2 c),(\omega h)']$**:** The three cycles $b,(\omega^2 c),(\omega h)'$ lie on the three two-tori as given in figure 9.7. Once again, on the second two-torus closed triangles

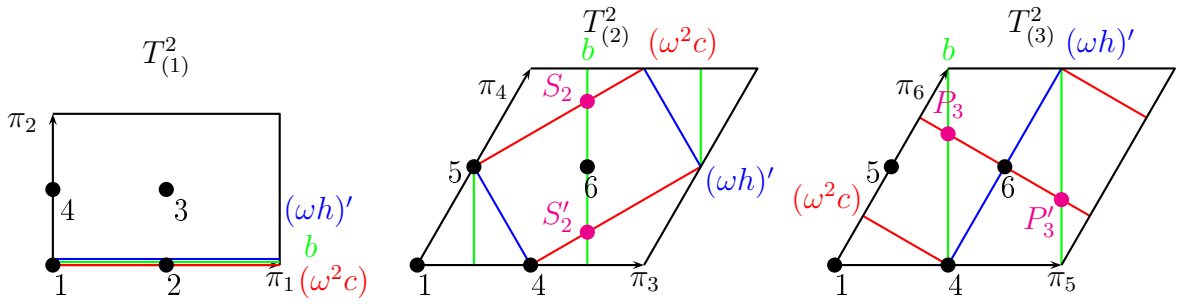

Figure 9.7: The three-cycle denoted by $(\omega h)'$ is depicted in blue, the three-cycle labeled by b is indicated in green, and the three-cycle $(\omega^2 c)$ is given in red. These three-cycles give rise to a Yukawa coupling of the form $\underline{h}_b \cdot H_u \underline{h}_c$.

only become apparent after identification of the borders of the fundamental domain. The matter localization per sector is given by:

state	xy	χ^{xy}	$T^2_{(2)}$	$T^2_{(3)}$
$\underline{h}_b^{(3)}$	$b(\omega h)'$	1	5	4
$H_u^{(2,3)}$ $(+H_d^{(2,3)})$	$b(\omega^2 c)$	$\lvert 4\rvert$	$5, (S_2, S_2')$	$4, (P_3, P_3')$
$\underline{h}_c^{(3,4,5,6)}$	$(\omega^2 c)(\omega h)'$	-4	$4, 5$	$4, 6$

(9.17)

Once more, we have two non-chiral Higgs pairs, which enriches the Yukawa structure. The various closed triangles are as follows:

triangle on $T^2_{(2)}$	$\frac{\text{Area}}{v_2}$	triangle on $T^2_{(3)}$	$\frac{\text{Area}}{v_3}$
$[5, (S_2, S_2'), 5]_2$	$\frac{1}{3}$	$[(P_3, P_3'), 4, 4]_3$	$\frac{1}{3}$
$[5, 4, 5]_2$	$\frac{3}{4}$	$[4, 6, 4]_3$	$\frac{3}{4}$
$[5, (S_2, S_2'), 4]_2$	$\frac{1}{12}$	$[4, (P_3, P_3'), 6]_3$	$\frac{1}{12}$
$[5]_2$	0	$[4]_3$	0

(9.18)

We have a total of 16 possible combinations. The combinations which can be taken to provide Yukawa couplings are listed in the third block of table 9.10. Once again, we chose the labels i in $\underline{h}_c^{(i)}$ such that the off-diagonal terms are suppressed with respect to the diagonal mass term, at least for the couplings involving $H_u^{(3)}$. The pattern is no longer valid for couplings involving the field $H_u^{(2)}$.

Remaining hidden sector cubic couplings

There are two particles which remain to be decoupled, namely the state h_d arising in the dh sector and the exotic state $\underline{h}_d$ coming from the sector dh'. The latter cannot be coupled to a Higgs particle in a cubic coupling satisfying simultaneously the charge selection rule and the stringy selection rule. Indeed, $\underline{h}_d$ has $Q_h = +1$, so it cannot be paired with the chiral exotic $\underline{h}_b$, because that would violate the charge selection rule. It cannot be paired either with a Higgs particle together with $\underline{h}_c$ or h_d, since that would not satisfy the stringy selection rules. The remaining state h_d can instead be coupled to the tilded Higgses arising in the bd sector and the exotic states $\underline{h}_b$ which we already used in the previous coupling. The sequences giving the corresponding Yukawa couplings are shown in blocks four and five

of table 9.10. Once more, the off-diagonal terms are suppressed with respect to the diagonal terms. As a final remark, note once again that the tilded down-type Higgses $\tilde{H}_d^{(1,2)}$ could have been replaced with the leptons $L^{(1,\dots,6)}$, giving rise to other couplings. However, we focused on the Yukawa couplings with the traditional interpretation of the Higgses arising from the non-chiral sector in order to avoid overloading the tables.

This concludes the analysis of the Yukawa couplings of the MSSM, which we investigated in some detail. On the one hand, the analysis turned out to be quite interesting as the global five-stack MSSM model allows to include Yukawa couplings such as (9.4c) and (9.4b), hinting at extensions of the usual MSSM in the field theoretical context. Also, an inherent mass hierarchy was apparent, and generally the off-diagonal couplings were suppressed compared to the diagonal ones, as it ought to be in a realistic model. On the other hand, we saw that there is no clear way to decouple the candidate SM sector from redundant matter states, which makes it difficult to introduce a separation of mass scales based solely on the superpotential couplings.

In the next section, we will concentrate on the global six-stack left-right symmetric models.

Cubic couplings for the superpotential (9.3) of a global 5-stack MSSM (part VIII)				
Coupling	**Sequence**	**Triangles on $T^2_{(2)} \times T^2_{(3)}$**	**Enclosed Area**	**Parameter**
$\underline{h}_b^{(2)} \cdot H_u^{(1)} \underline{h}_c^{(1)}$	$[b, \omega c, h']$	$\{[6,(R_2,R_2'),6],[(Q_3,Q_3'),(P_3,P_3'),5]\}$	$\frac{v_2}{3}+\frac{v_3}{48}$	$\mathfrak{h}_u^{(211)} \sim \mathcal{O}\left(e^{-\frac{16v_2+v_3}{48}}\right)$
$\underline{h}_b^{(1)} \cdot H_u^{(1)} \underline{h}_c^{(1)}$		$\{[5,(R_2,R_2'),6],[(Q_3,Q_3'),(P_3,P_3'),5]\}$	$\frac{v_2}{12}+\frac{v_3}{48}$	$\mathfrak{h}_u^{(111)} \sim \mathcal{O}\left(e^{-\frac{4v_2+v_3}{48}}\right)$
$\underline{h}_b^{(1)} \cdot H_u^{(3)} \underline{h}_c^{(2)}$	$[b, \omega^2 c, h']$	$\{[5,(S_2,S_2'),5],[(Q_3,Q_3'),(P_3,P_3'),6]\}$	$\frac{v_2}{3}+\frac{v_3}{48}$	$\mathfrak{h}_u^{(132)} \sim \mathcal{O}\left(e^{-\frac{16v_2+v_3}{48}}\right)$
$\underline{h}_b^{(2)} \cdot H_u^{(3)} \underline{h}_c^{(2)}$		$\{[6,(S_2,S_2'),5],[(Q_3,Q_3'),(P_3,P_3'),6]\}$	$\frac{v_2}{12}+\frac{v_3}{48}$	$\mathfrak{h}_u^{(232)} \sim \mathcal{O}\left(e^{-\frac{4v_2+v_3}{48}}\right)$
$\underline{h}_b^{(1)} \cdot H_u^{(2)} \underline{h}_c^{(2)}$		$\{[5,(S_2,S_2'),5],[(Q_3,Q_3'),4,6]\}$	$\frac{v_2}{3}+\frac{3v_3}{16}$	$\mathfrak{h}_u^{(122)} \sim \mathcal{O}\left(e^{-\frac{16v_2+9v_3}{48}}\right)$
$\underline{h}_b^{(2)} \cdot H_u^{(2)} \underline{h}_c^{(2)}$		$\{[6,(S_2,S_2'),5],[(Q_3,Q_3'),4,6]\}$	$\frac{v_2}{12}+\frac{3v_3}{16}$	$\mathfrak{h}_u^{(222)} \sim \mathcal{O}\left(e^{-\frac{4v_2+9v_3}{48}}\right)$
$\underline{h}_b^{(3)} \cdot H_u^{(3)} \underline{h}_c^{(6)}$	$[b, \omega^2 c, (\omega h)']$	$\{[5,(S_2,S_2'),5],[4,(P_3,P_3'),4]\}$	$\frac{v_2}{3}+\frac{v_3}{3}$	$\mathfrak{h}_u^{(336)} \sim \mathcal{O}\left(e^{-\frac{v_2+v_3}{3}}\right)$
$\underline{h}_b^{(3)} \cdot H_u^{(3)} \underline{h}_c^{(5)}$		$\{[5,(S_2,S_2'),5],[4,(P_3,P_3'),6]\}$	$\frac{v_2}{3}+\frac{v_3}{12}$	$\mathfrak{h}_u^{(335)} \sim \mathcal{O}\left(e^{-\frac{4v_2+v_3}{12}}\right)$
$\underline{h}_b^{(3)} \cdot H_u^{(3)} \underline{h}_c^{(4)}$		$\{[5,(S_2,S_2'),4],[4,(P_3,P_3'),4]\}$	$\frac{v_2}{12}+\frac{v_3}{3}$	$\mathfrak{h}_u^{(334)} \sim \mathcal{O}\left(e^{-\frac{v_2+4v_3}{12}}\right)$
$\underline{h}_b^{(3)} \cdot H_u^{(3)} \underline{h}_c^{(3)}$		$\{[5,(S_2,S_2'),4],[4,(P_3,P_3'),6]\}$	$\frac{v_2}{12}+\frac{v_3}{12}$	$\mathfrak{h}_u^{(333)} \sim \mathcal{O}\left(e^{-\frac{v_2+v_3}{12}}\right)$
$\underline{h}_b^{(3)} \cdot H_u^{(2)} \underline{h}_c^{(6)}$		$\{[5,(S_2,S_2'),5],[4]\}$	$\frac{v_2}{3}$	$\mathfrak{h}_u^{(326)} \sim \mathcal{O}\left(e^{-\frac{v_2}{3}}\right)$
$\underline{h}_b^{(3)} \cdot H_u^{(2)} \underline{h}_c^{(5)}$		$\{[5,(S_2,S_2'),5],[4,4,6]\}$	$\frac{v_2}{3}+\frac{3v_3}{4}$	$\mathfrak{h}_u^{(325)} \sim \mathcal{O}\left(e^{-\frac{4v_2+9v_3}{12}}\right)$
$\underline{h}_b^{(3)} \cdot H_u^{(2)} \underline{h}_c^{(4)}$		$\{[5,(S_2,S_2'),4],[4]\}$	$\frac{v_2}{12}$	$\mathfrak{h}_u^{(324)} \sim \mathcal{O}\left(e^{-\frac{v_2}{12}}\right)$
$\underline{h}_b^{(3)} \cdot H_u^{(2)} \underline{h}_c^{(3)}$		$\{[5,(S_2,S_2'),4],[4,4,6]\}$	$\frac{v_2}{12}+\frac{3v_3}{4}$	$\mathfrak{h}_u^{(323)} \sim \mathcal{O}\left(e^{-\frac{v_2+9v_3}{12}}\right)$
$\underline{h}_b^{(1)} \cdot \tilde{H}_d^{(2)} h_d^{(1)}$	$[b, (\omega^2 d), h]$	$\{[5,(R_2,R_2'),6],[(Q_3,Q_3'),(P_3,P_3'),6]\}$	$\frac{v_2}{12}+\frac{v_3}{48}$	$\mathfrak{h}_d^{(121)} \sim \mathcal{O}\left(e^{-\frac{4v_2+v_3}{48}}\right)$
$\underline{h}_b^{(2)} \cdot \tilde{H}_d^{(2)} h_d^{(1)}$		$\{[6,(R_2,R_2'),6],[(Q_3,Q_3'),(P_3,P_3'),6]\}$	$\frac{v_2}{3}+\frac{v_3}{48}$	$\mathfrak{h}_d^{(221)} \sim \mathcal{O}\left(e^{-\frac{16v_2+v_3}{48}}\right)$
$\underline{h}_b^{(3)} \cdot \tilde{H}_d^{(1)} h_d^{(3)}$	$[\omega^2 b, d, h]$	$\{[5,(Q_2,Q_2'),(P_2,P_2')],[5,(S_3,S_3'),6]\}$	$\frac{v_2}{48}+\frac{v_3}{12}$	$\mathfrak{h}_d^{(313)} \sim \mathcal{O}\left(e^{-\frac{v_2+4v_3}{48}}\right)$
$\underline{h}_b^{(3)} \cdot \tilde{H}_d^{(1)} h_d^{(2)}$		$\{[5,(Q_2,Q_2'),(P_2,P_2')],[5,(S_3,S_3'),5]\}$	$\frac{v_2}{48}+\frac{v_3}{3}$	$\mathfrak{h}_d^{(312)} \sim \mathcal{O}\left(e^{-\frac{v_2+16v_3}{48}}\right)$

Table 9.10: Complete list of the cubic couplings (9.4e) of the global five-stack MSSM-like model of table 7.17 involving the exotic states of the hidden sector. The second column indicates the D6-brane stacks used to form the triangles given in the third column by $[x]$ or $[x, y, z]$ with apexes (intersection points) x, y, z on $T^2_{(i=2,3)}$ according to the cubic couplings given in the first column. The fourth column provides the area for the respective triangles in terms of the areas v_i of the two-tori $T^2_{(i=2,3)}$, while the last column presents the resulting coupling constants.

9.3 Yukawa couplings for the global left-right symmetric models

In left-right symmetric models in general, the right-handed particles join up in $SU(2)_R$ doublets, which reduces the spectrum. Therefore, the possible cubic couplings are also reduced in left-right symmetric models compared to the MSSM-like models. This fact renders the analysis less interesting from a phenomenological point of view due to the restricted possibilities in model building, so we will present the analysis only superficially by giving some final results without deriving them in detail. Moreover, we add a section including quartic couplings in order to augment the possibilities for discussions and analysis.
A first remark about the four prototypes I, II, IIb and IIc of the six-stack global left-right symmetric models concerns the visible sector of particles. Indeed, a look at tables 7.6, 7.8, 7.12 and 7.10 reveals that all prototypes have the same content of visible particles, i.e. particles charged under the visible gauge group $U(3)_a \times USp(2)_b \times USp(2)_c \times U(1)_d$. Thus, by reducing the analysis to the visible sector, all four prototypes can be discussed simultaneously. There is, however, a subtlety to consider. Actually, a look at tables 7.5, 7.7, 7.11 and 7.9 yields that the prototype I and II models have exactly the same visible stacks a, b, c, d, i.e. same bulk orbits, same $\mathbb{Z}_2$-eigenvalues, same Wilson lines and identical shifts. These differ, however, from those used for the prototype IIb and IIc models. As a consequence, the matter localization per sector may differ for these prototypes. Still, the discrete Wilson lines $\tau^i,\ i = 2, 3$ and shifts $\sigma^i,\ i = 2, 3$ agree on the second and third two-torus $T^2_{(2,3)}$ for all prototype models, so that they come with a similar Yukawa structure, as we focus on the second and third two-torus only. We will restrict our analysis to the prototype II model.

9.3.1 Cubic couplings

The cubic Yukawa couplings of a left-right symmetric model have the following structure:

$$\mathcal{W}_{\text{Yuk}} = y_Q Q_L(H_u, H_d)Q_R + y_L L(H_u, H_d)R. \tag{9.19}$$

As anticipated, the structure is simpler than the one of the Yukawa couplings for the MSSM, see (9.4a). Also, we have no apparent extension of the left-right symmetric model as we had in (9.3) for the global five-stack MSSM. An advantage of the six-stack left-right symmetric models compared to the five-stack MSSM-like model is the fact that we do not have redundant generations of right-handed quarks and left-handed leptons. This permits to avoid the terms in (9.4b) we had for the five-stack MSSM-like model. Since we limit the analysis to the visible sector, a term similar to (9.4e) is not computed here. The Yukawa couplings (9.19) satisfy the charge selection rules. It remains to be seen whether adequate sequences can be found to fulfill the stringy selection rules.
The first ingredient for finding suitable sequences is to determine the matter states' localization per sector. This information is given for the prototype II model in tables 9.11 and 9.12.

Total amount of matter per sector for a 6-stack Left-Right Symmetric model on the aAA lattice						
$(\chi^{xy}, \chi^{x(\omega y)}, \chi^{x(\omega^2 y)})$	$y=a$	$y=b$	$y=c$	$y=d$	$y=h_1$	$y=h_2$
$x=a$	$(0,0,0)$	$(2,0,1)$	$(-2,-1,0)$	$(\lvert 2\rvert,0,0)$	$(\lvert 2\rvert,-1,1)$	$(\lvert 2\rvert,1,-1)$
$x=b$		$(0,\frac{3+\lvert 2\rvert}{2},\frac{-3+\lvert 2\rvert}{2})$	$(\lvert 2\rvert,\lvert 4\rvert,\lvert 4\rvert)$	$(2,1,0)$	$(0,\lvert 4\rvert,-3+\lvert 2\rvert)$	$(0,\lvert 4\rvert,3+\lvert 2\rvert)$
$x=c$			$(0,\frac{3+\lvert 2\rvert}{2},\frac{-3+\lvert 2\rvert}{2})$	$(-2,0,-1)$	$(0,3+\lvert 2\rvert,\lvert 4\rvert)$	$(0,-3+\lvert 2\rvert,\lvert 4\rvert)$
$x=d$				$(0,0,0)$	$(\lvert 2\rvert,1,-1)$	$(\lvert 2\rvert,-1,1)$
$x=h_1$					$(0,\frac{\lvert 4\rvert}{2},\frac{\lvert 4\rvert}{2})$	$(\lvert 2\rvert,\lvert 4\rvert,\lvert 4\rvert)$
$x=h_2$						$(0,\frac{\lvert 4\rvert}{2},\frac{\lvert 4\rvert}{2})$

Table 9.11: Complete list of the multiplicities of the chiral and non-chiral states per sector $x(\omega^k y)$ in the case of the global six-stack prototype II LRS model of table 7.7. Non-chiral states arise in sectors $x(\omega^k y)$ characterized by a net-chirality $|\chi^{x(\omega^k y)}| < \varphi^{x(\omega^k y)}$, in which case the multiplicity of the non-chiral states is given by $n_{NC}^{x(\omega^k y)} \equiv \varphi^{x(\omega^k y)} - |\chi^{x(\omega^k y)}|$. Such non-chiral pairs of particles are referred to as $|n_{NC}^{x(\omega^k y)}|$. The diagonal entries of the table given by $\varphi^{x(\omega x)} = \varphi^{x(\omega^2 x)} = \frac{\varphi^{\mathbf{Adj}_x}}{2}$ count the number of states transforming in the adjoint representation of the x-stack, except for the stacks b and c presenting enhancement, in which case they correspond to states in the antisymmetric representation.

Total amount of matter per sector for a 6-stack Left-Right Symmetric model				
$(\chi^{xy'}, \chi^{x(\omega y)'}, \chi^{x(\omega^2 y)'})$	$y=a$	$y=d$	$y=h_1$	$y=h_2$
$x=a$	$\binom{(\lvert 2\rvert,-1,1)}{(0,0,0)}$	$(\lvert 2\rvert,-1,1)$	$(\lvert 2\rvert,0,0)$	$(\lvert 2\rvert,0,0)$
$x=d$		$\binom{(\lvert 2\rvert,-1,1)}{(0,0,0)}$	$(\lvert 2\rvert,0,0)$	$(\lvert 2\rvert,0,0)$
$x=h_1$			$\binom{(\lvert 2\rvert,3+\lvert 2\rvert,-3+\lvert 2\rvert)}{(0,0,0)}$	$(\lvert 2\rvert,3+\lvert 2\rvert,-3+\lvert 2\rvert)$
$x=h_2$				$\binom{(\lvert 2\rvert,3+\lvert 2\rvert,-3+\lvert 2\rvert)}{(0,0,0)}$

Table 9.12: Complete list of the multiplicities of the chiral and non-chiral states per sector $x(\omega^k y)'$ in the case of the global six-stack prototype II LRS model of table 7.7. The notation used for counting bifundamental states is the same as the one used in table 9.11. The diagonal entries of the table associated to the sectors $x(\omega x)'$ count the number of states transforming in the (anti)symmetric representation of the x-stack, with the upper entries counting the numbers of antisymmetric representations and the lower entries the symmetric ones. The invariance of the b and the c-stack under the orientifold projection $\Omega\mathcal{R}$ implies $b(\omega^k x)' = b(\omega^k x)$ and $c(\omega^k x)' = c(\omega^k x)$ respectively, which can be found in table 9.11. Since the D6-brane stacks d, h_1 and h_2 support $U(1)$ gauge groups, the states in the antisymmetric representation do not exist. Still, we include their formal counting for reasons of completeness.

Once again, the information in tables 9.11 and 9.12 has to be completed by the data of matter states' localizations at the various intersection points. The results are the same as for the MSSM-like model in the previous section: Chiral matter states are localized at intersection points involving at least one $\mathbb{Z}_2$-fixed point. Non-chiral pairs of matter states spread over pairs of $\mathbb{Z}_2$-invariant points, except when more than one non-chiral pair is present in a same sector, in which case the non-chiral pairs of matter states also sit on intersection points involving $\mathbb{Z}_2$-fixed points.
The results for the Yukawa couplings in (9.19) are given in tables 9.13 and 9.14. By comparing both tables, we can see that there is a symmetry between quarks and leptons; By exchanging left-handed quarks with left-handed leptons $Q_L^{(i)} \leftrightarrow L^{(i)}$ and right-handed quarks with right-handed leptons $Q_R^{(i)} \leftrightarrow R^{(i)}$, we obtain the same order of magnitude for the Yukawa couplings. Subsequently, we will restrict the discussion to the quarks, since the same observations are also valid for the leptons.
In the case of left-right symmetric models, the Higgses arising from the non-chiral sectors already come in doublets. More precisely, in the MSSM-like model, the amount of non-chiral matter $n_{NC} = |2|$ denoted one non-chiral Higgs pair $H_u + H_d$. In case of left-right symmetric models, the amount of $n_{NC} = |2|$ corresponds to two non-chiral Higgs doublets of the form $(H_u, H_d)^{(1)}$ and $(H_u, H_d)^{(2)}$. Thus, the numbering of Higgses $(H_u, H_d)^{(i)}$ emerging from the $b(\omega^k c)_{k=0,1,2}$ sectors follow the natural ordering with $i \in \{1, 2\}$ for $k = 0$, $i \in \{3, 4, 5, 6\}$ for $k = 1$ and $i \in \{7, 8, 9, 10\}$ for $k = 2$.
Table 9.13 yields that we have four diagonal Yukawa couplings for both the second and third generation of quarks. These couplings involve the Higgs doublets $(H_u, H_d)^{(3,4,5,6)}$ and give rise to identical Yukawa couplings for fixed i in $(H_u, H_d)^{(i)}$. There is no diagonal mass term for the first generation of quarks $Q_L^{(1)}$ and $Q_R^{(1)}$, although both states appear in generation-mixing terms with the third respectively the second generation of quarks. Moreover, the Yukawa couplings including $(H_u, H_d)^{(3)}$ present suppression of the off-diagonal terms compared to the diagonal terms. Unluckily, the Yukawa couplings involving the Higgses $(H_u, H_d)^{(4,5,6)}$ present the opposite pattern, which makes a microscopical explanation of the structure of the CKM matrix not straightforward.
The Higgses $(H_u, H_d)^{(1,2)}$ arising in the bc sector constitute a noticeable absence in table 9.13. Indeed, they cannot be localized precisely at $\mathbb{Z}_2 \times \mathbb{Z}_2$ invariant intersection points via the method of Chan-Paton labels. Without going into details, this aspect is related to the fact that the orbits of the b and c stacks are fully parallel on all three two-tori $T^2_{(i)}$. A deeper investigation on this phenomenon goes beyond the scope of this doctoral work though, so that we will not treat the cubic couplings involving $(H_u, H_d)^{(1,2)}$ in this work.

9.3.2 Quartic couplings

Hitherto, we have only provided mass terms for the chiral states of the visible sector. However, there are also non-chiral pairs of matter states present in the visible sector, as can be deduced from table 7.8. These arise in the ad and ad' sectors. The most suitable way to provide these states with mass terms would be to couple them to some singlet states arising in the dd or dd' sectors. However, in the prototypes presented in this work, no such singlet states are present, see e.g. table 7.8. Consequently, only quartic couplings may allow to produce mass terms for the non-chiral states in the visible sector. Since the number of cubic couplings is reduced, we will extend the analysis to include a very brief discussion of quartic

couplings for the prototype II model. The prototype II left-right symmetric model comes with abundant non-chiral pairs of matter states in the hidden sector, which provides us with ample possibilities to pair off the non-chiral states arising in the visible sector. We can write down the following quartic couplings satisfying the charge selection rules:

$$\begin{aligned}\mathcal{W}_{\text{extra}} \;=\; & \frac{\mu_{h_1}^{ij}}{M_{\text{string}}} X^{ad}\tilde{X}^{ad'(i)}X^{dh_1(j)}X^{dh_1'} + \frac{\mu_{h_2}^{ij}}{M_{\text{string}}} X^{ad}\tilde{X}^{ad'(i)}X^{dh_2(j)}X^{dh_2'} \\ & + \frac{\tilde{\mu}_{h_1}^{ij}}{M_{\text{string}}} \tilde{X}^{ad}X^{ad'(i)}\tilde{X}^{dh_1(j)}\tilde{X}^{dh_1'} + \frac{\tilde{\mu}_{h2}^{ij}}{M_{\text{string}}} \tilde{X}^{ad}X^{ad'(i)}\tilde{X}^{dh_2(j)}\tilde{X}^{dh_2'},\end{aligned} \tag{9.20}$$

with $i,j \in \{1,2\}$ and M_{string} the string mass scale. Obviously, these couplings can only be written down for the prototype II and IIc left-right symmetric models, since the prototype IIb lacks exotic particles, i.e. particles charged under both the visible and hidden sectors such as those arising in the dh_1, dh_1', dh_2 and dh_2' sectors. The next step would consist in the exact localization of the particle states at the intersection points, with the same method mentioned before, i.e. via the Chan-Paton labels. Also, the stringy selection rule should be satisfied, implying the existence of closed quadrilateral shapes with all corners occupied by particle states. However, a closer look reveals that the non-chiral pair of states $X^{ad} + \tilde{X}^{ad}$ arises solely in the first ad sector, i.e. $a(\omega^{k=0})d$. Since the orbits of a and d are parallel on all three two-tori $T^2_{(i)}$, we run into the same issue encountered before with the Higgses $(H_u, H_d)^{(1,2)}$ in the cubic couplings, namely that the localization of $X^{ad} + \tilde{X}^{ad}$ at intersection points is not possible, as these states live on the full toroidal cycle shared by a and d. Therefore, we will not write down explicit sequences and couplings strengths for the quartic left-right symmetric couplings in this work, as a better understanding of conformal field theory methods for m-point couplings on toroidal orbifolds with $\mathbb{Z}_2$-factors is needed.

Yukawa couplings (9.19) for prototype II Left-Right Symmetric Model (part I)				
Coupling	**Sequence**	**Triangles on $T^2_{(2)} \times T^2_{(3)}$**	**Enclosed Area**	**Parameter**
$Q_L^{(1)}(H_u,H_d)^{(3)}Q_R^{(3)}$	$[a,b,(\omega c)]$	$\{[5,6,6],[(Q_3,Q_3'),(2,3),6]\}$	$\frac{3v_2}{4}+\frac{v_3}{48}$	$y_Q^{(113)} \sim \mathcal{O}(e^{-\frac{36v_2+v_3}{48}})$
$Q_L^{(1)}(H_u,H_d)^{(4)}Q_R^{(3)}$		$\{[5,(R_2,R_2'),6],[(Q_3,Q_3'),1,6]\}$	$\frac{v_2}{12}+\frac{3v_3}{16}$	$y_Q^{(143)} \sim \mathcal{O}\left(e^{-\frac{4v_2+9v_3}{48}}\right)$
$Q_L^{(1)}(H_u,H_d)^{(i=5,6)}Q_R^{(3)}$		$\{[5,(R_2,R_2'),6],[(Q_3,Q_3'),(2,3),6]\}$	$\frac{v_2}{12}+\frac{v_3}{48}$	$y_Q^{(1i3)} \sim \mathcal{O}(e^{-\frac{4v_2+v_3}{48}})$
$Q_L^{(3)}(H_u,H_d)^{(3)}Q_R^{(3)}$		$\{[6],[(Q_3,Q_3'),(2,3),6]\}$	$\frac{v_3}{48}$	$y_Q^{(333)} \sim \mathcal{O}(e^{-\frac{v_3}{48}})$
$Q_L^{(3)}(H_u,H_d)^{(4)}Q_R^{(3)}$		$\{[6,(R_2,R_2'),6],[(Q_3,Q_3'),1,6]\}$	$\frac{v_2}{3}+\frac{3v_3}{16}$	$y_Q^{(343)} \sim \mathcal{O}\left(e^{-\frac{16v_2+9v_3}{48}}\right)$
$Q_L^{(3)}(H_u,H_d)^{(i=5,6)}Q_R^{(3)}$		$\{[6,(R_2,R_2'),6],[(Q_3,Q_3'),(2,3),6]\}$	$\frac{v_2}{3}+\frac{v_3}{48}$	$y_Q^{(3i3)} \sim \mathcal{O}(e^{-\frac{16v_2+v_3}{48}})$
$Q_L^{(2)}(H_u,H_d)^{(7)}Q_R^{(3)}$	$[a,(\omega^2 b),(\omega c)]$	$\{[5,4,6],[5,(2,3),6]\}$	$\frac{3v_2}{8}+\frac{v_3}{24}$	$y_Q^{(273)} \sim \mathcal{O}\left(e^{-\frac{9v_2+v_3}{24}}\right)$
$Q_L^{(2)}(H_u,H_d)^{(8)}Q_R^{(3)}$		$\{[5,(P_2,P_2'),6],[5,1,6]\}$	$\frac{v_2}{24}+\frac{3v_3}{8}$	$y_Q^{(283)} \sim \mathcal{O}\left(e^{-\frac{v_2+9v_3}{24}}\right)$
$Q_L^{(2)}(H_u,H_d)^{(i=9,10)}Q_R^{(3)}$		$\{[5,(P_2,P_2'),6],[5,(2,3),6]\}$	$\frac{v_2+v_3}{24}$	$y_Q^{(2i3)} \sim \mathcal{O}\left(e^{-\frac{v_2+v_3}{24}}\right)$
$Q_L^{(2)}(H_u,H_d)^{(3)}Q_R^{(2)}$	$[a,(\omega^2 b),c]$	$\{[5],[5,(2,3),(Q_3,Q_3')]\}$	$\frac{v_3}{48}$	$y_Q^{(232)} \sim \mathcal{O}\left(e^{-\frac{v_3}{48}}\right)$
$Q_L^{(2)}(H_u,H_d)^{(4)}Q_R^{(2)}$		$\{[5,(S_2,S_2'),5],[5,1,(Q_3,Q_3')]\}$	$\frac{v_2}{3}+\frac{3v_3}{16}$	$y_Q^{(242)} \sim \mathcal{O}\left(e^{-\frac{16v_2+9v_3}{48}}\right)$
$Q_L^{(2)}(H_u,H_d)^{(i=5,6)}Q_R^{(2)}$		$\{[5,(S_2,S_2'),5],[5,(2,3),(Q_3,Q_3')]\}$	$\frac{v_2}{3}+\frac{v_3}{48}$	$y_Q^{(2i2)} \sim \mathcal{O}\left(e^{-\frac{16v_2+v_3}{48}}\right)$
$Q_L^{(2)}(H_u,H_d)^{(3)}Q_R^{(1)}$		$\{[5,5,6],[5,(2,3),(Q_3,Q_3')]\}$	$\frac{3v_2}{4}+\frac{v_3}{48}$	$y_Q^{(231)} \sim \mathcal{O}\left(e^{-\frac{36v_2+v_3}{48}}\right)$
$Q_L^{(2)}(H_u,H_d)^{(4)}Q_R^{(1)}$		$\{[5,(S_2,S_2'),6],[5,1,(Q_3,Q_3')]\}$	$\frac{v_2}{12}+\frac{3v_3}{16}$	$y_Q^{(241)} \sim \mathcal{O}\left(e^{-\frac{4v_2+9v_3}{48}}\right)$
$Q_L^{(2)}(H_u,H_d)^{(i=5,6)}Q_R^{(1)}$		$\{[5,(S_2,S_2'),6],[5,(2,3),(Q_3,Q_3')]\}$	$\frac{v_2}{12}+\frac{v_3}{48}$	$y_Q^{(2i1)} \sim \mathcal{O}\left(e^{-\frac{4v_2+v_3}{48}}\right)$

Table 9.13: List of the quarkonic Yukawa couplings of (9.19) of the global six-stack left-right symmetric model of prototype II of table 7.7. The second column indicates the D6-brane stacks used to form the triangles given in the third column by $[x]$ or $[x,y,z]$ with apexes (intersection points) x,y,z on $T^2_{(i=2,3)}$ according to the cubic couplings given in the first column. The fourth column provides the area for the respective triangles in terms of the areas v_i of the two-tori $T^2_{(i=2,3)}$, while the last column presents the resulting coupling constants.

Yukawa couplings (9.19) for prototype II Left-Right Symmetric Model (part II)				
Coupling	**Sequence**	**Triangles on $T^2_{(2)} \times T^2_{(3)}$**	**Enclosed Area**	**Parameter**
$L^{(1)}(H_u,H_d)^{(3)}R^{(3)}$	$[b,(\omega c),d]$	$\{[5,6,6],[(Q_3,Q_3'),(2,3),6]\}$	$\frac{3v_2}{4}+\frac{v_3}{48}$	$y_L^{(133)} \sim \mathcal{O}(e^{-\frac{36v_2+v_3}{48}})$
$L^{(1)}(H_u,H_d)^{(4)}R^{(3)}$		$\{[5,(R_2,R_2'),6],[(Q_3,Q_3'),1,6]\}$	$\frac{v_2}{12}+\frac{3v_3}{16}$	$y_L^{(143)} \sim \mathcal{O}\left(e^{-\frac{4v_2+9v_3}{48}}\right)$
$L^{(1)}(H_u,H_d)^{(i=5,6)}R^{(3)}$		$\{[5,(R_2,R_2'),6],[(Q_3,Q_3'),(2,3),6]\}$	$\frac{v_2}{12}+\frac{v_3}{48}$	$y_L^{(1i3)} \sim \mathcal{O}(e^{-\frac{4v_2+v_3}{48}})$
$L^{(3)}(H_u,H_d)^{(3)}R^{(3)}$		$\{[6],[(Q_3,Q_3'),(2,3),6]\}$	$\frac{v_3}{48}$	$y_L^{(333)} \sim \mathcal{O}(e^{-\frac{v_3}{48}})$
$L^{(3)}(H_u,H_d)^{(4)}R^{(3)}$		$\{[6,(R_2,R_2'),6],[(Q_3,Q_3'),1,6]\}$	$\frac{v_2}{3}+\frac{3v_3}{16}$	$y_L^{(343)} \sim \mathcal{O}\left(e^{-\frac{16v_2+9v_3}{48}}\right)$
$L^{(3)}(H_u,H_d)^{(i=5,6)}R^{(3)}$		$\{[6,(R_2,R_2'),6],[(Q_3,Q_3'),(2,3),6]\}$	$\frac{v_2}{3}+\frac{v_3}{48}$	$y_L^{(3i3)} \sim \mathcal{O}(e^{-\frac{16v_2+v_3}{48}})$
$L^{(2)}(H_u,H_d)^{(7)}R^{(3)}$	$[b,(\omega^2 c),(\omega d)]$	$\{[6,5,4],[4,(2,3),5]\}$	$\frac{3v_2}{8}+\frac{v_3}{24}$	$y_L^{(273)} \sim \mathcal{O}\left(e^{-\frac{9v_2+v_3}{24}}\right)$
$L^{(2)}(H_u,H_d)^{(8)}R^{(3)}$		$\{[6,(S_2,S_2'),4],[4,1,5]\}$	$\frac{v_2}{24}+\frac{3v_3}{8}$	$y_L^{(283)} \sim \mathcal{O}\left(e^{-\frac{v_2+9v_3}{24}}\right)$
$L^{(2)}(H_u,H_d)^{(i=9,10)}R^{(3)}$		$\{[6,(S_2,S_2'),4],[4,(2,3),5]\}$	$\frac{v_2+v_3}{24}$	$y_L^{(2i3)} \sim \mathcal{O}\left(e^{-\frac{v_2+v_3}{24}}\right)$
$L^{(2)}(H_u,H_d)^{(3)}R^{(2)}$	$[b,(\omega c),(\omega d)]$	$\{[6],[4,(2,3),(R_3,R_3')]\}$	$\frac{v_3}{48}$	$y_L^{(232)} \sim \mathcal{O}\left(e^{-\frac{v_3}{48}}\right)$
$L^{(2)}(H_u,H_d)^{(4)}R^{(2)}$		$\{[6,(R_2,R_2'),6],[4,1,(R_3,R_3')]\}$	$\frac{v_2}{3}+\frac{3v_3}{16}$	$y_L^{(242)} \sim \mathcal{O}\left(e^{-\frac{16v_2+9v_3}{48}}\right)$
$L^{(2)}(H_u,H_d)^{(i=5,6)}R^{(2)}$		$\{[6,(R_2,R_2'),6],[4,(2,3),(R_3,R_3')]\}$	$\frac{v_2}{3}+\frac{v_3}{48}$	$y_L^{(2i2)} \sim \mathcal{O}\left(e^{-\frac{16v_2+v_3}{48}}\right)$
$L^{(2)}(H_u,H_d)^{(3)}R^{(1)}$		$\{[6,6,4],[4,(2,3),(R_3,R_3')]\}$	$\frac{3v_2}{4}+\frac{v_3}{48}$	$y_L^{(231)} \sim \mathcal{O}\left(e^{-\frac{36v_2+v_3}{48}}\right)$
$L^{(2)}(H_u,H_d)^{(4)}R^{(1)}$		$\{[6,(R_2,R_2'),4],[4,1,(R_3,R_3')]\}$	$\frac{v_2}{12}+\frac{3v_3}{16}$	$y_L^{(241)} \sim \mathcal{O}\left(e^{-\frac{4v_2+9v_3}{48}}\right)$
$L^{(2)}(H_u,H_d)^{(i=5,6)}R^{(1)}$		$\{[6,(R_2,R_2'),4],[4,(2,3),(R_3,R_3')]\}$	$\frac{v_2}{12}+\frac{v_3}{48}$	$y_L^{(2i1)} \sim \mathcal{O}\left(e^{-\frac{4v_2+v_3}{48}}\right)$

Table 9.14: List of the leptonic Yukawa couplings of (9.19) of the global six-stack left-right symmetric model of prototype II of table 7.7. The second column indicates the D6-brane stacks used to form the triangles given in the third column by $[x]$ or $[x,y,z]$ with apexes (intersection points) x,y,z on $T^2_{(i=2,3)}$ according to the cubic couplings given in the first column. The fourth column provides the area for the respective triangles in terms of the areas v_i of the two-tori $T^2_{(i=2,3)}$, while the last column presents the resulting coupling constants.

Chapter 10

Conclusion

10.1 Summary and discussion

This doctoral work discusses model building and string phenomenology in Type IIA string theory on the geometrical background $T^6/(\mathbb{Z}_2 \times \mathbb{Z}_6 \times \Omega\mathcal{R})$ with discrete torsion.

The first three chapters mainly form the introduction. The first chapter provides a basic insight into string theory and Type IIA string theory in particular. The second chapter focuses in a first step on the geometry of the orbifold used for dimensional reduction. In a second step, Type IIA string theory is introduced on this particular background, by incorporating closed and open strings as well as D6-branes. Finally, the third and last introductory chapter presents string model building and phenomenology. In a first step, the particle physics models considered in this work are presented, including the MSSM, left-right symmetric and Pati-Salam models, as well as $SU(5)$ models. In a second step, the realization of these particle physics models in the context of intersecting D6-brane models is explained.

In the first part of the fourth chapter, we brought to light existing symmetries between different torus lattices. The original six lattice configurations have been reduced to only two independent ones, which simplifies the analysis drastically. The first hint for symmetries has been detected by counting the number of shortest possible three-cycles for different lattice configurations. The analysis of the closed string spectrum of different lattices yielded a map between the exotic O6-plane charges of different lattice configurations, consolidating the existence of relations between lattices. The final evidence was given by providing a map allowing to pass from the set of consistency conditions of one lattice configuration to the set of consistency conditions of another one. The discussion was completed by evaluating the invariance of physical quantities computed in this work under the considered map, which resulted in the reduction of the analysis to two independent lattice configurations.
In the second part of the fourth chapter, we launched a systematic search to determine all bulk three-cycles suitable to support D6-branes satisfying the SUSY conditions. The first step consisted in deriving upper and lower bounds for the bulk wrapping numbers. In a second step, the possible solutions of the SUSY equations have been classified into three types of solutions according to whether the one-cycle on the first two-torus $T^2_{(1)}$ was parallel or orthogonal to the first O6-plane $\Omega\mathcal{R}$, or neither of these. The first two types of SUSY solutions correspond to bulk three-cycles which satisfy the SUSY conditions for every value

of the complex structure parameter ϱ. The third type of SUSY solutions is given by three-cycles which are SUSY only for fixed values of ϱ. A computer scan revealed four bulk-three cycles of the first type of solutions and again four bulk-three cycles for the second type of solutions, this for both considered lattice configurations **aAA** and **bAA**. The scan yielded further 1760 bulk three-cycles of the third type for the **aAA** lattice and 917 ϱ-dependent bulk three-cycles for the **bAA** lattice.

The fifth chapter starts with the classification of D6-branes according to the gauge group they support. Using the beta-function coefficient, the configurations of discrete parameters and exotic O6-plane charges giving rise to gauge symmetry enhancement to symplectic or orthogonal groups were determined. This analysis was performed analytically.
In the second part of the chapter, candidates of D6-branes suitable for string model building were identified. The criteria differ for MSSM-type models including the MSSM, left-right symmetric and Pati-Salam models, and for the $SU(5)$ models. The first criterion analyzed was the criterion of rigidity of the D6-branes, which is given by the absence or presence of matter states transforming in the adjoint representation. The analysis, performed partly by hand, partly numerically, yielded about $\mathcal{O}(10^2)$ SUSY bulk three-cycles satisfying the rigidity criteria in case of the MSSM-type models and about $\mathcal{O}(10)$ in case of the $SU(5)$ model, for each of the two lattice configurations.
The second criterion for model building is given by the absence of matter states transforming in the symmetric representation, and a limited number of matter states transforming in the antisymmetric representation. The analysis produced about $\mathcal{O}(10)$ SUSY and rigid bulk three-cycles satisfying the criteria on (anti)symmetric matter states in case of MSSM-type models, for each of the two torus lattices. In case of the $SU(5)$ models, only four bulk three-cycles satisfying the rigidity criteria and the criteria of matter states in the (anti)symmetric representations were found for the **bAA** lattice, and only two bulk three-cycles for the **aAA** lattice.
The third and final part of the chapter concentrates on the first steps in string model building. It consists in detecting pairs of D6-branes giving rise to three generations of chiral matter states transforming in the bifundamental representation $(\mathbf{N_a}, \mathbf{2_b})$. The analysis, which can only be performed with computer scans, can be separated into ϱ-independent D6-brane configurations and ϱ-dependent configurations in case of the MSSM-type models. For the former, we found about $\mathcal{O}(10^2)$ suitable D6-brane configurations and for the latter, about $\mathcal{O}(10^3)$ adequate pairs of D6-branes were detected. In case of the $SU(5)$ models, only ϱ-dependent configurations are realizable, coming with a number of about $\mathcal{O}(10^4)$. These numbers already indicated that the total number of D6-brane configurations to test would need substantial processing power and time, especially in the case of ϱ-dependent models.

The sixth and seventh chapters are dedicated to the search for concrete globally consistent particle physics models. The sixth chapter concentrates on the search for Pati-Salam and $SU(5)$ models, while the seventh chapter focuses on left-right symmetric and MSSM-like models. In chapter six, we showed that no global $SU(5)$ models can be constructed, which agrees with the results obtained on all other orbifolds to date, see [95, 130, 182, 69, 76]. However, locally consistent three particle generation $SU(5)$ models can be realized, an explicit example of which was provided. The same results hold true for Pati-Salam models on the **bAA** lattice configuration. In case of Pati-Salam models though, the situation is different

for the **aAA** lattice configuration. The less stringent RR-tadpole cancellation conditions of the **aAA** lattice permitted the construction of three-generation globally consistent four-stack Pati-Salam models, which on top were independent of the complex structure modulus ϱ. The models numbered about $\mathcal{O}(10^3)$ and could be divided into two classes according to their hidden sector and particle spectrum. One explicit example per class was provided. Concerning the construction of ϱ-dependent Pati-Salam models, it turned out that local three-generation models can be realized in tremendous numbers. However, numerous computer scans showed that global ϱ-dependent Pati-Salam models are extremely scarce in comparison, if they exist at all. The difficulties encountered during the search for global ϱ-dependent Pati-Salam models have been illustrated. In the end, we preferred to abandon this fruitless search and concentrate instead on the construction of ϱ-independent global models.

Chapter seven focuses on the meticulous search for ϱ-independent global left-right symmetric and MSSM-like models. We showed once again that for the **bAA** lattice, only local left-right symmetric and MSSM-like ϱ-independent models can be constructed. We refrained from giving explicit examples, as we already did so for the Pati-Salam and $SU(5)$ models in chapter six. In the case of the **aAA** lattice, we showed that left-right symmetric models can be globally consistent only if they contain at least six stacks of D6-branes. The total number of global six-stack left-right symmetric models found was about $\mathcal{O}(10^5)$. We provided four different explicit examples of global six-stack left-right symmetric models. Moreover, we found five-stack left-right symmetric models which satisfy the consistency conditions only partially, namely they fulfilled the RR-tadpole cancellation conditions but not the K-theory constraints. We referred to the models satisfying the former but not necessarily the latter as semi-global models. The climax of the research was given by the discovery of full three-generation global ϱ-independent effective five-stack MSSM-like models. They come with an extended left-handed lepton and right-handed quark sector, which has the potential to effectively be reduced to a three-generation particle content at low energies. We found about $\mathcal{O}(10^2)$ such models. We also showed that globally consistent MSSM-like models can only be constructed with at least five stacks of D6-branes, and we noted that three-generation MSSM-like models with only three stacks cannot be constructed at all, regardless of their local or global character.

The eighth chapter concentrates on phenomenological aspects of the global models found, namely the detection of massless Abelian $U(1)$ symmetries and discrete $\mathbb{Z}_n$-symmetries. We started the chapter by deriving explicit expressions for the conditions of existence of these symmetries and for the K-theory constraints, which in our case provided automatically a $\mathbb{Z}_2$-symmetry if fulfilled.
In order to avoid repeating the same analysis several times, we restricted the detection of these symmetries to the global MSSM-like and left-right symmetric models. The MSSM-like model under consideration yielded exactly one massless $U(1)$ combination, which corresponded to the standard definition of the hypercharge. Also, it came with a non-trivial $\mathbb{Z}_3$-symmetry which provided a first hint that an alternative identification of the right-handed neutrinos may be necessary. The existence of these symmetries consolidates the phenomenological appeal of this global five-stack MSSM-like model, as explained in section 3.2.1.
We presented the analysis for the MSSM-like model in some detail, but only provided the final results for the left-right symmetric models. We explicitly pointed out the absence of the

$\mathbb{Z}_2$-symmetry associated to the violation of the K-theory constraint in case of the semi-global five-stack left-right symmetric model. Moreover, we showed that only one of the four examined global six-stack left-right symmetric models yielded a massless $U(1)$ combination, which has been associated to a generalization of the baryon-lepton number symmetry. However, none of the examined left-right symmetric models yielded any $\mathbb{Z}_n$-symmetry not arising from the center of some gauge group or from the K-theory constraints.

The final ninth chapter focuses on field theoretical aspects of the global MSSM-like and left-right symmetric models, namely the Yukawa couplings and other cubic couplings at tree level. Due to the extended left-handed lepton and Higgs sector as well as the extended right-handed quark sector, the global MSSM-like model in particular exhibited a rich cubic coupling structure. All the usual Yukawa couplings of the MSSM have been derived, and some inherent mass hierarchy was manifest as well. Also, the cubic couplings allowed for the inclusion of Higgs-axion couplings as they appear in extensions of the MSSM, such as Peccei-Quinn models or DFSZ models. We were also able to provide mass terms for the redundant left-handed leptons and right-handed quarks, though these turned out to be of the same order of magnitude as the usual Yukawa couplings of the MSSM. Furthermore, the exotic chiral particles of the hidden sector have been paired off with the Higgs doublets, providing hidden Yukawa couplings. However, none of the couplings was of order one, which would have effectively removed these undesired particles from the model at low energies. Finally, we showed that cubic couplings can be provided for alternative candidates of the right-handed neutrinos. The advantage of the alternative identifications of the right-handed neutrinos is that the charges under the non-trivial $\mathbb{Z}_3$-symmetry come out correctly. The drawback is the fact that with the alternative identifications, the right-handed neutrinos come no longer in three generations.
In the case of the left-right symmetric models, we reduced the analysis to the visible sector in order to discuss all four examples of left-right symmetric models simultaneously. We showed that the usual Yukawa couplings can be constructed for left-handed and right-handed leptons and quarks. At the end of the chapter, we also briefly discussed four-point couplings of the left-right symmetric models.

10.2 Outlook

As expected from previous work on similar backgrounds, the orbifold $T^6/(\mathbb{Z}_2 \times \mathbb{Z}_6 \times \Omega\mathcal{R})$ turned out to be particularly fertile for string model building purposes. Actually, it turned out to be almost too fertile, as it produces tremendous numbers of local three-generation models, which renders the detection of global models very hard. Future work could certainly focus on the extension of the search for global MSSM-type models, which include left-right symmetric, Pati-Salam and MSSM-like models, to the ϱ-dependent models. A substantial amount of processing power is certainly needed to complete the search for global ϱ-dependent models.

Also in the case of ϱ-independent models, explicit examples of local MSSM-like and left-right symmetric models can be given for the **bAA** lattice, as we did for the Pati-Salam and $SU(5)$ models. Moreover, due to the substantial number of global left-right symmetric

models found, we used only a probe-wise scan to classify the left-right symmetric models into four types of models. A complete computer scan may reveal further classes of left-right symmetric models.

In addition to model building, the analysis of the global models on the orbifold $T^6/(\mathbb{Z}_2 \times \mathbb{Z}_6 \times \Omega\mathcal{R})$ could be extended in many different ways. For example, the detection of discrete $\mathbb{Z}_n$-symmetries [100, 167, 168, 78, 93, 64] could also be performed in the context of the global Pati-Salam models found. The same holds true for the computation of Yukawa couplings. Also, the presence of DFSZ couplings in the global MSSM-like model suggests a further exploitation of axion models and the investigation of related cosmological aspects in general. The analysis could thus be extended along the lines of [57, 218] or [219, 220, 101] for instance. Note that in our case, the axion arises from the open string sector, so that a scenario as described in [220, 101] should be considered, in contrast to those described in [221, 219, 222, 223], where the axion arises from the closed string sector.

Moreover, we have seen that the redundant left-handed lepton sector and right-handed quark sector could not be completely decoupled from the model using Yukawa couplings alone. Another mechanism should be devised in order to explain why the global MSSM-like model appears as an effective three-generation particle physics model at low energies. Similarly, we have seen that three out of the four classes of global left-right symmetric models do not come with any massless $U(1)$ combination. The impact of this aspect should also be investigated, for example by analyzing the breaking of the left-right symmetric GUT gauge group to the gauge group of the SM.

An aspect we did not consider in the present work is the gauge couplings [224, 72, 73, 225, 67, 226, 227]. At tree level, these are related to the volumes of the D6-branes, which we computed when counting the number of shortest possible three-cycles in the context of lattice symmetries. Higher order terms are given by the massive string excitations, i.e. the threshold corrections expressed in terms of the gauge kinetic function. This analysis could be performed for each of the global particle physics models found. In this context, it would be interesting to know how our global models fare in the analysis of low string scale scenarios at the LHC, see for instance [228–235, 218, 236, 76].

Furthermore, we limited the analysis in this doctoral work to perturbative effects. The superpotential could also be extended to involve non-perturbative effects such as D6-brane instantons [237].

Another interesting feature to examine would be different patterns of SUSY breaking. In the present work, we derived SUSY versions of well-known particle physics models. In order to retrieve the non-SUSY particle physics models, SUSY should be broken at some energy scale. This could for example be achieved by the formation of a gaugino condensate [238, 239] in the hidden sector. Another possibility to break SUSY could be achieved by deformations of the $\mathbb{Z}_2$-fixed points, as has been suggested e.g. in [110, 109].

Acknowledgments

This work is partially supported by the Cluster of Excellence "Precision Physics, Fundamental Interactions and Structure of Matter" (PRISMA) DGF no. EXC 1098 and the DFG Research Training Group "Symmetry Breaking in Fundamental Interactions" GRK 1581.

Appendix A

Explicit examples of constructions and computations

The tools used to do calculations on the toroidal orbifold $T^6/(\mathbb{Z}_2 \times \mathbb{Z}_6 \times \Omega\mathcal{R})$ with discrete torsion are rather technical, and maybe also a little more complicated than those necessary to do computations on other toroidal orbifolds, such as $T^6/(\mathbb{Z}_2 \times \mathbb{Z}_6' \times \Omega\mathcal{R})$ for instance. In order to render more transparent the techniques used in this work and described in the main text, we will provide in this appendix explicit examples of constructions and computations. More precisely, we will first illustrate how the exceptional wrapping numbers can be derived. These are necessary both to calculate intersection numbers with the orbifold invariant method and to check the twisted RR-tadpole cancellation conditions.
In the second section of this appendix, we will explicitly derive the beta-function coefficients for three-cycles with bulk orbits parallel to the $\Omega\mathcal{R}$-invariant plane. The derivation is based on computing intersection numbers with the sector-per-sector method. Only with this method the beta-function coefficients can be derived, and only with this method the full matter localization per sector can be determined, the latter being unavoidable to correctly compute the Yukawa couplings.

A.1 Explicit construction of a fractional cycle

In a first step, we provide table A.1 allowing to determine the exceptional wrapping numbers $(x_\alpha^{(k)}, y_\alpha^{(k)})$ in function of torus wrapping numbers (n^k, m^k), $\mathbb{Z}_2$-eigenvalues $(-1)^{\tau^{\mathbb{Z}_2^{(i)}}}$ $(i = 1, 2, 3)$, displacements $(\vec{\sigma})$ and Wilson lines $(\vec{\tau})$.

$(n^2,m^2;n^3,m^3)$	$\mathbb{Z}_2^{(1)}$ **Exceptional wrapping numbers** $(x_\alpha^{(1)},y_\alpha^{(1)})$ **in dependence of torus wrapping numbers** (n^1,m^1), $\mathbb{Z}_2$**-eigenvalues** $(-1)^{\tau_2^{(1)}}$, **displacements** $(\vec{\sigma})$ **and Wilson lines** $(\vec{\tau})$			
	$(\sigma^2;\sigma^3)=(0;0)$	$(1;0)$	$(0;1)$	$(1;1)$
(odd,odd;odd,odd)	$(z_\alpha^{(1)}n^1,\ z_\alpha^{(1)}m^1)_{\alpha=0,1,2,4}$	$(\hat{z}_\alpha^{(1)}n^1,\ \hat{z}_\alpha^{(1)}m^1)_{\alpha=1}$ $(z_\alpha^{(1)}n^1,\ z_\alpha^{(1)}m^1)_{\alpha=5,3}$	$(\hat{z}_\alpha^{(1)}n^1,\ \hat{z}_\alpha^{(1)}m^1)_{\alpha=2}$ $(z_\alpha^{(1)}n^1,\ z_\alpha^{(1)}m^1)_{\alpha=5,3}$	$(\hat{z}_\alpha^{(1)}n^1,\ \hat{z}_\alpha^{(1)}m^1)_{\alpha=4}$ $(z_\alpha^{(1)}n^1,\ z_\alpha^{(1)}m^1)_{\alpha=3,5}$
(odd,even;odd,odd)	$(z_\alpha^{(1)}n^1,\ z_\alpha^{(1)}m^1)_{\alpha=0,1,2,5}$	$(\hat{z}_\alpha^{(1)}n^1,\ \hat{z}_\alpha^{(1)}m^1)_{\alpha=1}$ $(z_\alpha^{(1)}n^1,\ z_\alpha^{(1)}m^1)_{\alpha=3,4}$	$(\hat{z}_\alpha^{(1)}n^1,\ \hat{z}_\alpha^{(1)}m^1)_{\alpha=2}$ $(z_\alpha^{(1)}n^1,\ z_\alpha^{(1)}m^1)_{\alpha=3,4}$	$(\hat{z}_\alpha^{(1)}n^1,\ \hat{z}_\alpha^{(1)}m^1)_{\alpha=5}$ $(z_\alpha^{(1)}n^1,\ z_\alpha^{(1)}m^1)_{\alpha=4,3}$
(even,odd;odd,odd)	$(z_\alpha^{(1)}n^1,\ z_\alpha^{(1)}m^1)_{\alpha=0,1,2,3}$	$(\hat{z}_\alpha^{(1)}n^1,\ \hat{z}_\alpha^{(1)}m^1)_{\alpha=1}$ $(z_\alpha^{(1)}n^1,\ z_\alpha^{(1)}m^1)_{\alpha=4,5}$	$(\hat{z}_\alpha^{(1)}n^1,\ \hat{z}_\alpha^{(1)}m^1)_{\alpha=2}$ $(z_\alpha^{(1)}n^1,\ z_\alpha^{(1)}m^1)_{\alpha=4,5}$	$(\hat{z}_\alpha^{(1)}n^1,\ \hat{z}_\alpha^{(1)}m^1)_{\alpha=3}$ $(z_\alpha^{(1)}n^1,\ z_\alpha^{(1)}m^1)_{\alpha=5,4}$
	$z_\alpha^{(1)}=(-)^{\tau_2^{(1)}}\begin{cases}1 & \alpha=0\to0\to0\\ (-)^{\tau^2} & \alpha=1\to1\to1\\ (-)^{\tau^3} & \alpha=2\to2\to2\\ (-)^{\tau^2+\tau^3} & \alpha=4\to5\to3\end{cases}$	$\hat{z}_\alpha^{(1)}=(-)^{\tau_2^{(1)}}(1+(-)^{\tau^2})\quad \alpha=1\to1\to1$ $z_\alpha^{(1)}=(-)^{\tau_2^{(1)}+\tau^3}\quad \alpha=5\to3\to4$ $z_\alpha^{(1)}=(-)^{\tau_2^{(1)}+\tau^2+\tau^3}\quad \alpha=3\to4\to5$	$\hat{z}_\alpha^{(1)}=(-)^{\tau_2^{(1)}}(1+(-)^{\tau^3})\quad \alpha=2\to2\to2$ $z_\alpha^{(1)}=(-)^{\tau_2^{(1)}+\tau^2}\quad \alpha=5\to3\to4$ $z_\alpha^{(1)}=(-)^{\tau_2^{(1)}+\tau^2+\tau^3}\quad \alpha=3\to4\to5$	$\hat{z}_\alpha^{(1)}=(-)^{\tau_2^{(1)}}((-)^{\tau^2}+(-)^{\tau^3})\quad \alpha=4\to5\to3$ $z_\alpha^{(1)}=(-)^{\tau_2^{(1)}}\quad \alpha=3\to4\to5$ $z_\alpha^{(1)}=(-)^{\tau_2^{(1)}+\tau^2+\tau^3}\quad \alpha=5\to3\to4$
(n^3,m^3)	$\mathbb{Z}_2^{(2)}$ **Exceptional wrapping numbers** $(x_\alpha^{(2)},y_\alpha^{(2)})$ **in dependence of torus wrapping numbers** (n^2,m^2), $\mathbb{Z}_2$**-eigenvalues** $(-1)^{\tau_2^{(2)}}$, **displacements** $(\vec{\sigma})$ **and Wilson lines** $(\vec{\tau})$			
	$(\sigma^1,\sigma^3)=(0,0)$	$(1,0)$	$(0,1)$	$(1,1)$
(odd,odd)	$(-\zeta_\alpha^{(2)}(n^2+m^2),\zeta_\alpha^{(2)}n^2)_{\alpha=1}$ $(-\zeta_\alpha^{(2)}(n^2+m^2),\zeta_\alpha^{(2)}n^2)_{\alpha\in\{3,2,4\}}$	$(-\zeta_\alpha^{(2)}(n^2+m^2),\zeta_\alpha^{(2)}n^2)_{\alpha\in\{2,3\}}$ $(-\zeta_\alpha^{(2)}(n^2+m^2),\zeta_\alpha^{(2)}n^2)_{\alpha\in\{3,4\}}$	$\left(\hat{\zeta}_\alpha^{(2)}\,n^2+\zeta_\alpha^{(2)}\,m^2\ ,\ -\zeta_\alpha^{(2)}\,n^2+(\hat{\zeta}_\alpha^{(2)}-\zeta_\alpha^{(2)})\,m_a^2\right)_{\alpha=1}$ $\left(\hat{\zeta}_\alpha^{(2)}\,n^2+\zeta_\alpha^{(2)}\,m^2\ ,\ -\zeta_\alpha^{(2)}\,n^2+(\hat{\zeta}_\alpha^{(2)}-\zeta_\alpha^{(2)})\,m^2\right)_{\alpha\in\{3,2,4\}}$	$\left(\hat{\zeta}_\alpha^{(2)}\,n^2+\zeta_\alpha^{(2)}\,m^2\ ,\ -\zeta_\alpha^{(2)}\,n^2+(\hat{\zeta}_\alpha^{(2)}-\zeta_\alpha^{(2)})\,m^l\right)_{\alpha\in\{2,3\}}$ $\left(\hat{\zeta}_\alpha^{(2)}\,n^2+\zeta_\alpha^{(2)}\,m^2\ ,\ -\zeta_\alpha^{(2)}\,n^2+(\hat{\zeta}_\alpha^{(2)}-\zeta_\alpha^{(2)})\,m^2\right)_{\alpha\in\{3,4\}}$
	$\zeta_\alpha^{(2)}=\begin{cases}(-)^{\tau_2^{(2)}+\tau^3} & \alpha=1\to1\to1\\ (-)^{\tau_2^{(2)}+\tau^1+\tau^3} & \alpha=3\to2\to4\end{cases}$	$\zeta_\alpha^{(2)}=\begin{cases}(-)^{\tau_2^{(2)}+\tau^3} & \alpha=2\to3\to2\\ (-)^{\tau_2^{(2)}+\tau^1+\tau^3} & \alpha=4\to4\to3\end{cases}$	$\zeta_\alpha^{(2)}=\hat{\zeta}_\alpha^{(2)}(-)^{\tau^3},\quad \hat{\zeta}_\alpha^{(2)}=\begin{cases}(-)^{\tau_2^{(2)}} & \alpha=1\to1\to1\\ (-)^{\tau_2^{(2)}+\tau^1} & \alpha=3\to2\to4\end{cases}$	$\zeta_\alpha^{(2)}=\hat{\zeta}_\alpha^{(2)}(-)^{\tau^3},\quad \hat{\zeta}_\alpha^{(2)}=\begin{cases}(-)^{\tau_2^{(2)}} & \alpha=2\to3\to2\\ (-)^{\tau_2^{(2)}+\tau^1} & \alpha=4\to4\to3\end{cases}$
(n^2,m^2)	$\mathbb{Z}_2^{(3)}$ **Exceptional wrapping numbers** $(x_\alpha^{(3)},y_\alpha^{(3)})$ **in dependence of torus wrapping numbers** (n^3,m^3), $\mathbb{Z}_2$**-eigenvalues** $(-1)^{\tau_2^{(3)}}$, **displacements** $(\vec{\sigma})$ **and Wilson lines** $(\vec{\tau})$			
	$(\sigma^1,\sigma^2)=(0,0)$	$(1,0)$	$(0,1)$	$(1,1)$
(odd,odd)	$(-\zeta_\alpha^{(3)}(n^3+m^3),\zeta_\alpha^{(3)}n^3)_{\alpha=1}$ $(-\zeta_\alpha^{(3)}(n^3+m^3),\zeta_\alpha^{(3)}n^3)_{\alpha\in\{3,2,4\}}$	$(-\zeta_\alpha^{(3)}(n^3+m^3),\zeta_\alpha^{(3)}n^3)_{\alpha\in\{2,3\}}$ $(-\zeta_\alpha^{(3)}(n^3+m^3),\zeta_\alpha^{(3)}n^3)_{\alpha\in\{3,4\}}$	$\left(\hat{\zeta}_\alpha^{(3)}\,n^3+\zeta_\alpha^{(3)}\,m^3\ ,\ -\zeta_\alpha^{(3)}\,n^3+(\hat{\zeta}_\alpha^{(3)}-\zeta_\alpha^{(3)})\,m_a^3\right)_{\alpha=1}$ $\left(\hat{\zeta}_\alpha^{(3)}\,n^3+\zeta_\alpha^{(3)}\,m^3\ ,\ -\zeta_\alpha^{(3)}\,n^3+(\hat{\zeta}_\alpha^{(3)}-\zeta_\alpha^{(3)})\,m^3\right)_{\alpha\in\{3,2,4\}}$	$\left(\hat{\zeta}_\alpha^{(3)}\,n^3+\zeta_\alpha^{(3)}\,m^3\ ,\ -\zeta_\alpha^{(3)}\,n^3+(\hat{\zeta}_\alpha^{(3)}-\zeta_\alpha^{(3)})\,m^3\right)_{\alpha\in\{2,3\}}$ $\left(\hat{\zeta}_\alpha^{(3)}\,n^3+\zeta_\alpha^{(3)}\,m^3\ ,\ -\zeta_\alpha^{(3)}\,n^3+(\hat{\zeta}_\alpha^{(3)}-\zeta_\alpha^{(3)})\,m^3\right)_{\alpha\in\{3,4\}}$
(odd, even)	$(\zeta_\alpha^{(3)}m^3,-\zeta_\alpha^{(3)}(n^3+m^3))_{\alpha=1}$ $(\zeta_\alpha^{(3)}m^3,-\zeta_\alpha^{(3)}(n^3+m^3))_{\alpha\in\{3,2,4\}}$	$(\zeta_\alpha^{(3)}m^3,-\zeta_\alpha^{(3)}(n^3+m^3))_{\alpha\in\{2,3\}}$ $(\zeta_\alpha^{(3)}m^3,-\zeta_\alpha^{(3)}(n^3+m^3))_{\alpha\in\{3,4\}}$	$(-\zeta_\alpha^{(3)}n^3+(\hat{\zeta}_\alpha^{(3)}-\zeta_\alpha^{(3)})m^3,(\zeta_\alpha^{(3)}-\hat{\zeta}_\alpha^{(3)})n^3-\hat{\zeta}_\alpha^{(3)}m^3)_{\alpha=1}$ $(-\zeta_\alpha^{(3)}n^3+(\hat{\zeta}_\alpha^{(3)}-\zeta_\alpha^{(3)})m^3,(\zeta_\alpha^{(3)}-\hat{\zeta}_\alpha^{(3)})n^3-\hat{\zeta}_\alpha^{(3)}m^3)_{\alpha\in\{2,3,4\}}$	$(-\zeta_\alpha^{(3)}n^3+(\hat{\zeta}_\alpha^{(3)}-\zeta_\alpha^{(3)})m^3,(\zeta_\alpha^{(3)}-\hat{\zeta}_\alpha^{(3)})n^3-\hat{\zeta}_\alpha^{(3)}m^3)_{\alpha\in\{2,3\}}$ $(-\zeta_\alpha^{(3)}n^3+(\hat{\zeta}_\alpha^{(3)}-\zeta_\alpha^{(3)})m^3,(\zeta_\alpha^{(3)}-\hat{\zeta}_\alpha^{(3)})n^3-\hat{\zeta}_\alpha^{(3)}m^3)_{\alpha\in\{3,4\}}$
(even,odd)	$(\zeta_\alpha^{(3)}n^3,\zeta_\alpha^{(3)}m^3)_{\alpha=1}$ $(\zeta_\alpha^{(3)}n^3,\zeta_\alpha^{(3)}m^3)_{\alpha\in\{3,2,4\}}$	$(\zeta_\alpha^{(3)}n^3,\zeta_\alpha^{(3)}m^3)_{\alpha\in\{2,3\}}$ $(\zeta_\alpha^{(3)}n^3,\zeta_\alpha^{(3)}m^3)_{\alpha\in\{3,4\}}$	$((\zeta_\alpha^{(3)}-\hat{\zeta}_\alpha^{(3)})n^3-\hat{\zeta}_\alpha^{(3)}m^3,\hat{\zeta}_\alpha^{(3)}n^3+\zeta_\alpha^{(3)}m^3)_{\alpha=1}$ $((\zeta_\alpha^{(3)}-\hat{\zeta}_\alpha^{(3)})n^3-\hat{\zeta}_\alpha^{(3)}m^3,\hat{\zeta}_\alpha^{(3)}n^3+\zeta_\alpha^{(3)}m^3)_{\alpha\in\{2,3,4\}}$	$((\zeta_\alpha^{(3)}-\hat{\zeta}_\alpha^{(3)})n^3-\hat{\zeta}_\alpha^{(3)}m^3,\hat{\zeta}_\alpha^{(3)}n^3+\zeta_\alpha^{(3)}m^3)_{\alpha\in\{2,3\}}$ $((\zeta_\alpha^{(3)}-\hat{\zeta}_\alpha^{(3)})n^3-\hat{\zeta}_\alpha^{(3)}m^3,\hat{\zeta}_\alpha^{(3)}n^3+\zeta_\alpha^{(3)}m^3)_{\alpha\in\{3,4\}}$
	$\zeta_\alpha^{(3)}=\begin{cases}(-)^{\tau_2^{(3)}+\tau^2} & \alpha=1\to1\to1\\ (-)^{\tau_2^{(3)}+\tau^1+\tau^2} & \alpha=3\to2\to4\end{cases}$	$\zeta_\alpha^{(3)}=\begin{cases}(-)^{\tau_2^{(3)}+\tau^2} & \alpha=2\to3\to2\\ (-)^{\tau_2^{(3)}+\tau^1+\tau^2} & \alpha=4\to4\to3\end{cases}$	$\zeta_\alpha^{(3)}=\hat{\zeta}_\alpha^{(3)}(-)^{\tau^2},\quad \hat{\zeta}_\alpha^{(3)}=\begin{cases}(-)^{\tau_2^{(3)}} & \alpha=1\to1\to1\\ (-)^{\tau_2^{(3)}+\tau^1} & \alpha=3\to2\to4\end{cases}$	$\zeta_\alpha^{(3)}=\hat{\zeta}_\alpha^{(3)}(-)^{\tau^2},\quad \hat{\zeta}_\alpha^{(3)}=\begin{cases}(-)^{\tau_2^{(3)}} & \alpha=2\to3\to2\\ (-)^{\tau_2^{(3)}+\tau^1} & \alpha=4\to4\to3\end{cases}$

Table A.1: Exceptional wrapping numbers $(x_\alpha^{(i)},y_\alpha^{(i)})_{i=1,2,3}$ in dependence of the discrete parameters, as schematically displayed in table 2.7. The torus wrapping numbers (n^3,m^3) are chosen to be (odd,odd) in order to select an orbifold representative as explained on page 21. The subscript α refers to exceptional wrapping numbers with non-zero entries. A chain of indices α, for example $\alpha=3\to2\to4$ means the following: for (n^1,m^1) =(odd,odd) the factor $\zeta_\alpha^{(l=2,3)}$ (or $\hat{\zeta}_\alpha^{(l=2,3)}$) with subscript $\alpha=3$ takes the indicated expression, for (n^1,m^1) =(odd, even) the factor with $\alpha=2$ takes the expression in question and for (n^1,m^1) =(even,odd) the factor with $\alpha=4$ takes on the considered expression. The same holds true for the non-zero factors $z_\alpha^{(1)}$ and $\hat{z}_\alpha^{(1)}$ given in the fourth row of the table, for (n^2,m^2) =(odd,odd), (odd,even), or (even,odd) respectively.

In a second step, we illustrate by some examples how the entries of table A.1 can be computed.
A fractional three-cycle is given as a sum of a bulk three-cycle and three exceptional three-cycles:

$$\Pi^{\text{frac}} = \frac{1}{4}\left(\Pi^{\text{bulk}} + \Pi^{\mathbb{Z}_2^{(1)}} + \Pi^{\mathbb{Z}_2^{(2)}} + \Pi^{\mathbb{Z}_2^{(3)}}\right) . \tag{A.1}$$

Only those exceptional three-cycles are added whose associated $\mathbb{Z}_2$-fixed points are traversed by the bulk three-cycle. In this section, we will illustrate by an example how the entries of table A.1 can be derived.
Let us consider the three-cycle characterized by the torus wrapping numbers of the form $(n^1,m^1;\, n^2,m^2;\, n^3,m^3)$=(odd,odd; odd,even; odd,odd).
We will start the discussion with the first $\mathbb{Z}_2$-twisted sector $\mathbb{Z}_2^{(1)}$. In a first step, we assume that we have no shift on the second and third two-torus, i.e. $\sigma^2 = \sigma^3 = 0$. On the second torus, the three-cycle thus passes through the fixed points 1 and 4, since we have (n^2,m^2)=(odd,even). On the third torus, it passes through points 1 and 6 as we have (n^3,m^3)=(odd,odd). These four fixed points give us a total of four combinations of exceptional two-cycles $e^{(1)}_{\kappa\lambda}$ with $\kappa \in \{1,4\}$ and $\lambda \in \{1,6\}$. Each of the four exceptional two-cycles is tensored with the one-cycle $n^1\pi_1 + m^1\pi_2$, giving an exceptional three-cycle. The last step consists in taking all orbifold images of the exceptional three-cycles. The orbifold orbits of these four exceptional three-cycles can directly be read off from table 2.4:

$$\begin{aligned} &T_{(2)} \times T_{(3)} \\ &\quad 11 \to n^1\varepsilon^{(1)}_0 + m^1\tilde{\varepsilon}^{(1)}_0 \\ &\quad 16 \to (n^1\varepsilon^{(1)}_2 + m^1\tilde{\varepsilon}^{(1)}_2)(-1)^{\tau^3} \\ &\quad 41 \to (n^1\varepsilon^{(1)}_1 + m^1\tilde{\varepsilon}^{(1)}_1)(-1)^{\tau^2} \\ &\quad 46 \to (n^1\varepsilon^{(1)}_5 + m^1\tilde{\varepsilon}^{(1)}_5)(-1)^{\tau^2+\tau^3} \end{aligned}$$

The τ^i describe the Wilson lines, which give rise to a different sign according to the relative orientation of the exceptional two-cycles located at different fixed points. For example, passing from the first to the second line above gives a Wilson line $(-1)^{\tau^3}$, since on the third torus we pass from the reference fixed point 1 to the fixed point 6. In the end, the entire exceptional three-cycle has to be multiplied by a factor $(-1)^{\tau^{\mathbb{Z}_2^{(1)}}}$, corresponding to the absolute orientation of the involved exceptional two-cycles. The exceptional wrapping numbers thus depend on the oddness/evenness and the numerical value of the torus wrapping numbers, the $\mathbb{Z}_2^{(1)}$-eigenvalues, the Wilson lines and the shifts. Shortly, we will see how they depend on the shift. All in all, the exceptional three-cycle of the first $\mathbb{Z}_2$-twisted sector associated to the bulk wrapping numbers and discrete parameters under consideration can be written as follows:

$$\begin{aligned} \Pi^{\mathbb{Z}_2^{(1)}} = (-1)^{\tau^{\mathbb{Z}_2^{(1)}}} \Big(&n^1\varepsilon^{(1)}_0 + m^1\tilde{\varepsilon}^{(1)}_0 + (n^1\varepsilon^{(1)}_2 + m^1\tilde{\varepsilon}^{(1)}_2)(-1)^{\tau^3} \\ &+ (n^1\varepsilon^{(1)}_1 + m^1\tilde{\varepsilon}^{(1)}_1)(-1)^{\tau^2} + (n^1\varepsilon^{(1)}_5 + m^1\tilde{\varepsilon}^{(1)}_5)(-1)^{\tau^2+\tau^3}\Big) . \end{aligned}$$

From the expression above, we can read off the exceptional wrapping numbers of the first

$\mathbb{Z}_2$-twisted sector:

$$\begin{array}{l|l|l|l} x_0^{(1)} = (-1)^{\tau^{\mathbb{Z}_2^{(1)}}} n^1 & x_2^{(1)} = (-1)^{\tau^{\mathbb{Z}_2^{(1)}}+\tau^3} n^1 & x_1^{(1)} = (-1)^{\tau^{\mathbb{Z}_2^{(1)}}+\tau^2} n^1 & x_5^{(1)} = (-1)^{\tau^{\mathbb{Z}_2^{(1)}}+\tau^2+\tau^3} n^1 , \\ y_0^{(1)} = (-1)^{\tau^{\mathbb{Z}_2^{(1)}}} m^1 & y_2^{(1)} = (-1)^{\tau^{\mathbb{Z}_2^{(1)}}+\tau^3} m^1 & y_1^{(1)} = (-1)^{\tau^{\mathbb{Z}_2^{(1)}}+\tau^2} m^1 & y_5^{(1)} = (-1)^{\tau^{\mathbb{Z}_2^{(1)}}+\tau^2+\tau^3} m^1 . \end{array} \tag{A.2}$$

The remaining four exceptional wrapping numbers are zero: $(x_\alpha^{(1)}, y_\alpha^{(1)}) = (0,0)$, for $\alpha = 3,4$. Note that in this case, each exceptional three-cycle $\varepsilon_\alpha^{(1)}$, $\tilde{\varepsilon}_\alpha^{(1)}$ and thus the corresponding exceptional wrapping numbers receives a contribution from only one exceptional two-cycle $e_{\kappa\lambda}^{(1)}$. In the main text (c.f. table 2.7) we referred to these as type I exceptional wrapping numbers. The coefficients $z_\alpha^{(1)}$ associated to the pairs $(x_\alpha^{(1)}, y_\alpha^{(1)})$ appearing in tables 2.7 and A.1 are thus given by $z_0^{(1)} = (-1)^{\tau^{\mathbb{Z}_2^{(1)}}}$, $z_2^{(1)} = (-1)^{\tau^{\mathbb{Z}_2^{(1)}}+\tau^3}$, $z_1^{(1)} = (-1)^{\tau^{\mathbb{Z}_2^{(1)}}+\tau^2}$ and $z_5^{(1)} = (-1)^{\tau^{\mathbb{Z}_2^{(1)}}+\tau^2+\tau^3}$.

Before moving on to the second $\mathbb{Z}_2$-twisted sector, let us briefly consider how the presence of shifts effects the results. Consider for example a shift on the second torus: $\sigma^2 = 1$. Then the points $(1,4)$ on the second torus are shifted to the points $(5,6)$, accordingly to table 2.8. Some orbits now contribute twice:

$$\begin{aligned} &T_{(2)} \times T_{(3)} \\ &\quad 51 \to n^1 \varepsilon_1^{(1)} + m^1 \tilde{\varepsilon}_1^{(1)} \\ &\quad 56 \to (n^1 \varepsilon_3^{(1)} + m^1 \tilde{\varepsilon}_3^{(1)})(-1)^{\tau^3} \\ &\quad 61 \to (n^1 \varepsilon_1^{(1)} + m^1 \tilde{\varepsilon}_1^{(1)})(-1)^{\tau^2} \\ &\quad 66 \to (n^1 \varepsilon_4^{(1)} + m^1 \tilde{\varepsilon}_4^{(1)})(-1)^{\tau^2+\tau^3} \end{aligned}$$

We see that the exceptional three-cycles $\varepsilon_1^{(1)}$ and $\tilde{\varepsilon}_1^{(1)}$ now have two contributions from the exceptional two-cycles $e_{51}^{(1)}$ and $e_{61}^{(1)}$, giving:

$$\underbrace{(-1)^{\tau^{\mathbb{Z}_2^{(1)}}} n^1 (1+(-1)^{\tau^2})}_{x_1^{(1)}} \varepsilon_1^{(1)} + \underbrace{(-1)^{\tau^{\mathbb{Z}_2^{(1)}}} m^1 (1+(-1)^{\tau^2})}_{y_1^{(1)}} \tilde{\varepsilon}_1^{(1)} . \tag{A.3}$$

Thus, in this particular example, the exceptional wrapping numbers $x_1^{(1)}$ and $y_1^{(1)}$ are said to be of type II. The coefficient $\hat{z}$ appearing in table 2.7 associated to $x_1^{(1)}$ and $y_1^{(1)}$ is thus $\hat{z}_1^{(1)} = (-1)^{\tau^{\mathbb{Z}_2^{(1)}}} (1+(-1)^{\tau^2})$.

Now let us concentrate on the second $\mathbb{Z}_2$-twisted sector. Remember that the bulk three-cycle under consideration is characterized by torus wrapping numbers of the form $(n^1, m^1; n^3, m^3)$=(odd,odd odd,odd). Let us come back to the situations where there are no shifts, i.e. $\sigma^1 = \sigma^3 = 0$. On the first torus, the bulk cycle passes through the points $(1,3)$, on the third torus it passes through $(1,6)$. The possible combinations of fixed points are:

$$\begin{aligned} &T_{(1)} \times T_{(3)} \\ &\quad 11 \to \text{ no contribution} \\ &\quad 16 \to (-(n^2+m^2)\varepsilon_1^{(2)} + n^2 \tilde{\varepsilon}_1^{(2)})(-1)^{\tau^3} \\ &\quad 31 \to \text{ no contribution} \end{aligned}$$

$$36 \to (-(n^2+m^2)\varepsilon_3^{(2)} + n^2\tilde{\varepsilon}_3^{(2)})(-1)^{\tau^1+\tau^3}$$

The orbifold invariant exceptional three-cycles corresponding to these fixed points can once again be read off from table 2.4.
We find that exceptional two-cycles of the type $e_{\kappa 1}^{(2)}$ give no contributions in table 2.4. This is due to the fact that fixed points labeled by 1 situated at the origins of the three two-tori are invariant under the orbifold action, so the sum over the orbits is zero:

$$\begin{aligned}(1+\omega+\omega^2)(n^2 e_{\kappa 1}^{(2)} \otimes \pi_3 + m^2 e_{\kappa 1}^{(2)} \otimes \pi_4) =& n^2 e_{\kappa 1}^{(2)} \otimes \pi_3 + n^2 e_{\kappa 1}^{(2)} \otimes \pi_{-4} + n^2 e_{\kappa 1}^{(2)} \otimes \pi_{4-3} \\ &+ m^2 e_{\kappa 1}^{(2)} \otimes \pi_4 + m^2 e_{\kappa 1}^{(2)} \otimes \pi_{3-4} + m^2 e_{\kappa 1}^{(2)} \otimes \pi_{-3} \\ =& 0\,.\end{aligned}$$

Hence, written out, the exceptional three-cycle in the $\mathbb{Z}_2^{(2)}$ sector is:

$$\Pi^{\mathbb{Z}_2^{(2)}} = (-1)^{\tau^{\mathbb{Z}_2^{(2)}}} \left(-(n^2+m^2)\varepsilon_1^{(2)} + n^2\tilde{\varepsilon}_1^{(2)} + (-1)^{\tau^1}(-(n^2+m^2)\varepsilon_3^{(2)} + n^2\tilde{\varepsilon}_3^{(2)})\right)(-1)^{\tau^3}\,. \tag{A.4}$$

Thus, we can again read off the exceptional wrapping numbers:

$$\begin{array}{l|l} x_1^{(2)} = -(n^2+m^2)(-1)^{\tau^{\mathbb{Z}_2^{(2)}}+\tau^3} & x_3^{(2)} = -(n^2+m^2)(-1)^{\tau^{\mathbb{Z}_2^{(2)}}+\tau^3+\tau^1}, \\ y_1^{(2)} = n^2(-1)^{\tau^{\mathbb{Z}_2^{(2)}}+\tau^3} & y_3^{(2)} = n^2(-1)^{\tau^{\mathbb{Z}_2^{(2)}}+\tau^3+\tau^1}. \end{array} \tag{A.5}$$

The exceptional wrapping numbers $(x_\alpha^{(2)}, y_\alpha^{(2)})$, $\alpha = 1,3$ are of type I, since each pair receives only one contribution from an exceptional two-cycle $e_{\kappa\lambda}^{(2)}$. The remaining eight wrapping numbers have zero entries, $(x_\alpha^{(2)}, y_\alpha^{(2)}) = (0,0)$, $\alpha = 2,4$. The coefficients $\zeta_\alpha^{(2)}$ appearing in tables 2.7 and A.1 are in this example given by $\zeta_1^{(2)} = (-1)^{\tau^{\mathbb{Z}_2^{(2)}}+\tau^3}$ and $\zeta_3^{(2)} = (-1)^{\tau^{\mathbb{Z}_2^{(2)}}+\tau^1+\tau^3}$. The third $\mathbb{Z}_2$-twisted sector can be treated similarly.

All in all, the fractional three-cycles can be written as indicated in (A.1), where each exceptional contribution $\Pi^{\mathbb{Z}_2^{(i)}}$ $i = 1,2,3$ can be computed as illustrated above.

Table A.1 contains, in a compact form, the complete information to derive the exceptional wrapping numbers as we illustrated above. It provides the exceptional wrapping numbers for each possible combination of oddness/evenness of the torus wrapping numbers and shifts. The computer code I wrote to calculate the exceptional wrapping numbers is based on table A.1. Note that a preliminary version of table A.1 was given in [65]. However, the table in [65] did not yet take into account the fact that the new reference points introduced upon shifts have to be chosen in accordance with the orbifold action as we did in table 2.8. Table A.1 in the present work, which is consistent with table 2.8, was introduced for the first time in our publication [63].

A.2 Example of the calculation of beta-function coefficients

A.2.1 Preliminary considerations

In general, the running of the gauge couplings $g_a(\mu)$ in terms of the energy scale μ is given by (see e.g.[240, 66, 67]):

$$\frac{8\pi^2}{g_a(\mu)^2} = \frac{8\pi^2}{g_{a,\text{string}}^2} + \frac{b_a}{2}\ln\left(\frac{M_{\text{string}}}{\mu}\right)^2 + \text{gauge threshold corrections}\,, \tag{A.6}$$

where the reference scale M_{string} is a constant and $g_{a,\text{string}}^2$ is the tree-level gauge coupling, which is related to the volume of the D6-branes in string theory, see e.g. [241].
The coefficient b_a appearing in the second term of (A.6) is called the one-loop beta-function coefficient or simply the beta-function coefficient. It contains information of the particle content charged under the gauge group in question, see e.g. [177, 156, 242]. In string theory, the beta-function coefficient corresponds to the contribution from massless strings running in a loop. The massive string excitations contribute to the gauge threshold corrections, which have to be computed with CFT methods. This has already been well-studied in the past, see for example [243–246] or [247–251] and also [67, 72]. The beta-function coefficient is sufficient for our purpose, since it allows us to detect gauge symmetry enhancement and compute the complete massless open string sector, both chiral and non-chiral.
In the following, we will briefly comment on the various contributions of the particle content to the beta-function coefficients. We define the quadratic Casimir C_2 and the index C of a representation $\mathbf{R}$ as follows:

$$\text{Tr}(T_a^{\mathbf{R}} T_b^{\mathbf{R}}) = C(\mathbf{R})\delta_{ab}, \tag{A.7}$$

$$\sum_{a=1}^{\text{dim Group}} T_a^{\mathbf{R}} T_a^{\mathbf{R}} = C_2(\mathbf{R})\mathbf{1}_{\text{dim }\mathbf{R}}. \tag{A.8}$$

where $T_a^{\mathbf{R}}$ are the infinitesimal generators expressed in the representation $\mathbf{R}$ of the Lie group, and δ_{ab} is the Killing form defined by $\delta_{ab} = \text{Tr}(T_a^{\mathbf{Adj}} T_b^{\mathbf{Adj}})$. The index C of the various representations for the groups considered in this work is given by:

SU(N):	Sp(2N):	SO(2N):
$C(\mathbf{N}) = \frac{1}{2}$	$C(\mathbf{2N}) = \frac{1}{2}$	$C(\mathbf{2N}) = \frac{1}{2}$
$C(\mathbf{Adj}) = N$	$C(\mathbf{Adj}) = N+1$	$C(\mathbf{Adj}) = N-1$
$C(\mathbf{Sym}) = \frac{N+2}{2}$	$C(\mathbf{Sym}) = N+1$	$C(\mathbf{Sym}) = N+1$
$C(\mathbf{Anti}) = \frac{N-2}{2}$	$C(\mathbf{Anti}) = N-1$	$C(\mathbf{Anti}) = N-1$

(A.9)

We have the following relation between C and C_2:

$$C(\mathbf{R})\text{dim(Group)} = C_2(\mathbf{R})\text{dim}(\mathbf{R})\,. \tag{A.10}$$

For the adjoint representation we have dim(Group) = dim(**R**), which implies $C(\mathbf{Adj}) = C_2(\mathbf{Adj})$. The contributions to the beta-function coefficients differ for vector multiplets

(i.e. gauge bosons and their superpartners) and chiral multiplets (i.e. fermions and their superpartners), as the former have different degrees of freedom from the latter. The contributions to the beta-function coefficient from a single vector multiplet ($1V$) and a single chiral multiplet ($1C$) are given by:

$$b(1V) = -3C_2(\mathbf{Adj}), \tag{A.11}$$

$$b(1C) = C(\mathbf{R}). \tag{A.12}$$

In order to find the contributions from all the particles present in the theory, the contributions above have to be multiplied by the multiplicities φ^{xy} of the particles. For an unitary group, the beta-function coefficients can be found e.g. in [66] and are of the form:

$$b_{SU(N_a)} = N_a(-3 + \varphi^{\mathbf{Adj}_a}) + \frac{N_a+2}{2}\varphi^{\mathbf{Sym}_a} + \frac{N_a-2}{2}\varphi^{\mathbf{Anti}_a} + \sum_{b\neq a}\frac{N_b}{2}(\varphi^{ab} + \varphi^{ab'})\,. \tag{A.13}$$

For symplectic gauge factors, the beta-function coefficient is:

$$b_{USp(2N_a)} = (N_a+1)(-3 + \varphi^{\mathbf{Sym}_a}) + (N_a-1)\varphi^{\mathbf{Anti}_a} + \sum_{b\neq a}\frac{N_b}{2}\varphi^{ab}\,. \tag{A.14}$$

We see that for $USp(2)_a \simeq SU(2)$ formula (A.13) with $N_a = 2$ matches with formula (A.14) with $N_a = 1$, as required. The beta-function coefficient for orthogonal gauge groups is:

$$b_{SO(2N_a)} = (N_a-1)(-3 + \varphi^{\mathbf{Anti}_a}) + (N_a+1)\varphi^{\mathbf{Sym}_a} + \sum_{b\neq a}\frac{N_b}{2}\varphi^{ab}\,. \tag{A.15}$$

In our set-up, we can compute the beta-function coefficients with the formulas involving intersection numbers indicated in section 3.3, as we will illustrate on an example in the next section. Comparing the results to (A.13), (A.14) and (A.15), gauge symmetry enhancement can be detected, and the multiplicities φ^{xy} of the various representations can be read off.

A.2.2 Example of computation

Let us consider the three-cycle with bulk orbit parallel to the $\Omega\mathcal{R}$-invariant plane with bulk orbit (1,0;1,0;1,0) on the **aAA** lattice. We have:

$$\begin{aligned}
&a = (1,0;1,0;1,0) && a' = (1,0;1,0;1,0),\\
&(\omega a) = (1,0;0,-1;-1,1) && (\omega a)' = (1,0;-1,1;0,-1),\\
&(\omega^2 a) = (1,0;-1,1;0,-1) && (\omega^2 a)' = (1,0;0,-1;-1,1).
\end{aligned} \tag{A.16}$$

Remember from section 3.3.2 that the bulk and exceptional intersection numbers are given by:

$$\prod_{i=1}^{3}(n_a^i m_b^i - n_b^i m_a^i) \equiv I_{ab}^{(1)} I_{ab}^{(2)} I_{ab}^{(3)}, \tag{A.17}$$

$$I_{ab}^{\mathbb{Z}_2^{(i)}} = (-1)^{\tau_a^{\mathbb{Z}_2^{(i)}} + \tau_b^{\mathbb{Z}_2^{(i)}}} I_{ab}^{\mathbb{Z}_2^{(i)},(j)} I_{ab}^{\mathbb{Z}_2^{(i)},(k)} I_{ab}^{(i)}\,, \tag{A.18}$$

$$= I_{ab}^{\mathbb{Z}_2^{(i)},(j\cdot k)} I_{ab}^{(i)}\,, \tag{A.19}$$

where i,j,k are cyclic permutations of $1,2,3$. We will start by determining the contributions to beta-function coefficients related to the adjoint representation.

The adjoint representation

For the sector aa, the first formula in table 3.3 has to be used. This sector gives a contribution of $b_{aa} = -3N_a$, which corresponds to the vector multiplet containing the gauge boson. Because we are working with fractional three-cycles passing through $\mathbb{Z}_2$-fixed points, no contributions from chiral multiplets arise, which would have corresponded to displacement moduli.
Next, we concentrate on the contributions $b_{a(\omega a)}$ and $b_{a(\omega^2 a)}$. The bulk intersection numbers of these two sectors per two-torus $T^2_{(i)}$, $(i = 2, 3)$ are given by:

$$\begin{aligned}(I^{(1)}_{a(\omega a)}, I^{(2)}_{a(\omega a)}, I^{(3)}_{a(\omega a)}) &= (0_{\uparrow\uparrow}, -1, 1),\\ (I^{(1)}_{a(\omega^2 a)}, I^{(2)}_{a(\omega^2 a)}, I^{(3)}_{a(\omega^2 a)}) &= (0_{\uparrow\uparrow}, 1, -1),\end{aligned} \tag{A.20}$$

where the up arrows $\uparrow\uparrow$ indicate parallel one-cycles. Between the brane a under consideration and its first orbifold image (ωa) is an angle of $(0, \phi, -\phi)$, thus we have to use the second entry of table 3.3 to compute the multiplicity of the second sector $b_{a(\omega a)}$:

$$b_{a(\omega a)} = \frac{1}{4} \underbrace{\delta_{\sigma^1_{a(\omega a)},0}\delta_{\tau^1_{a(\omega a)},0}}_{=1} \left(\underbrace{|I^{(2\cdot 3)}_{a(\omega a)}|}_{=1} - I^{\mathbb{Z}_2^{(1)},(2\cdot 3)}_{a(\omega a)} \right) . \tag{A.21}$$

The orbifold action does not change the discrete Wilson lines nor the shifts or $\mathbb{Z}_2$-eigenvalues, hence we have no relative shifts or Wilson lines $\delta_{\sigma^1_{a(\omega a)},0} = \delta_{\tau^1_{a(\omega a)},0} = 1$. As can be read off from (A.19) and (A.18), the twisted part of the intersection numbers is given by:

$$I^{\mathbb{Z}_2^{(1)},(2\cdot 3)}_{a(\omega a)} = (-1)^{\tau_a^{\mathbb{Z}_2^{(1)}} + \tau^{\mathbb{Z}_2^{(1)}}_{(\omega a)}} I^{\mathbb{Z}_2^{(1)},(2)}_{a(\omega a)} I^{\mathbb{Z}_2^{(1)},(3)}_{a(\omega a)} . \tag{A.22}$$

Note that in the case under consideration, we do not need the bulk part of the intersection numbers on the first two-torus given by $I^{(1)}_{a(\omega a)}$ for the computation of the adjoint representation in (A.21). This is due to the fact that the $\mathbb{Z}_6$-orbifold action does not act on the first two-torus, such that a brane a and its orbifold images $(\omega^k a)$ are always parallel on the first two-torus $T^2_{(1)}$, hence $I^{(1)}_{a(\omega a)} = 0$. Also, we have $\tau_a^{\mathbb{Z}_2^{(i)}} = \tau^{\mathbb{Z}_2^{(i)}}_{(\omega a)}$, implying that: $(-1)^{\tau_a^{\mathbb{Z}_2^{(1)}} + \tau^{\mathbb{Z}_2^{(1)}}_{(\omega a)}} = 1$.
The twisted parts $I^{\mathbb{Z}_2^{(1)},(2)}_{a(\omega a)}$ and $I^{\mathbb{Z}_2^{(1)},(3)}_{a(\omega a)}$ have to be calculated separately for the second and the third two-torus. In order to keep the computation generic, we will derive the results in presence of shifts and without shifts.
To indicate that a bulk cycle passes through the $\mathbb{Z}_2$-fixed points labeled by α and β on a two-torus, we use the notation $\begin{pmatrix}\alpha\\ \beta\end{pmatrix}$ if α is the reference point and $\begin{pmatrix}\beta\\ \alpha\end{pmatrix}$ if β is the reference point. On the second torus $T^2_{(2)}$, the bulk three-cycle passes through the following $\mathbb{Z}_2$-fixed points:

$$(n^2_a, m^2_a) = (1, 0) \Rightarrow \begin{pmatrix}1\\ 4\end{pmatrix} \overset{\text{shift}}{\to} \begin{pmatrix}5\\ 6\end{pmatrix} , \tag{A.23}$$

$$(n^2_{(\omega a)}, m^2_{(\omega a)}) = (0, -1) \Rightarrow \begin{pmatrix}1\\ 5\end{pmatrix} \overset{\text{shift}}{\to} \begin{pmatrix}6\\ 4\end{pmatrix} , \tag{A.24}$$

where we place the label of the reference $\mathbb{Z}_2$-fixed point in the upper entry as aforementioned. According to (3.23), equal upper indices give a factor $+1$, whereas equal lower indices give a factor $(-1)^{(\tau_a^2+\tau_{(\omega a)}^2)}$. Equal indices with one of them in an upper, the second in a lower position give a factor $(-1)^{\tau_a^2 \text{ or } \tau_{(\omega a)}^2}$, see (3.23):

$$\text{no shift:} \quad \begin{pmatrix} 1 \\ 4 \end{pmatrix} \cdot \begin{pmatrix} 1 \\ 5 \end{pmatrix} = 1 = I_{a(\omega a)}^{\mathbb{Z}_2^{(1)},(2)} , \tag{A.25}$$

$$\text{with shift:} \quad \begin{pmatrix} 5 \\ 6 \end{pmatrix} \cdot \begin{pmatrix} 6 \\ 4 \end{pmatrix} = (-1)^{\tau_a^2} = I_{a(\omega a)}^{\mathbb{Z}_2^{(1)},(2)} . \tag{A.26}$$

The result can be written as $I_{a(\omega a)}^{\mathbb{Z}_2^{(1)},(2)} = (-1)^{\tau_a^2\sigma_a^2}$. In fact, with this scripture, both cases for the shift can be accounted for simultaneously. Similarly, on the third two-torus $T^2_{(3)}$ the bulk-three cycles pass through the following $\mathbb{Z}_2$-fixed points:

$$(n_a^3, m_a^3) = (1,0) \Rightarrow \begin{pmatrix} 1 \\ 4 \end{pmatrix} \overset{\text{shift}}{\to} \begin{pmatrix} 5 \\ 6 \end{pmatrix} , \tag{A.27}$$

$$(n_{(\omega a)}^3, m_{(\omega a)}^3) = (-1,1) \Rightarrow \begin{pmatrix} 1 \\ 6 \end{pmatrix} \overset{\text{shift}}{\to} \begin{pmatrix} 4 \\ 5 \end{pmatrix} , \tag{A.28}$$

which give the following contributions to the twisted part of the intersection numbers:

$$\text{no shift:} \quad \begin{pmatrix} 1 \\ 4 \end{pmatrix} \cdot \begin{pmatrix} 1 \\ 6 \end{pmatrix} = 1 = I_{a(\omega a)}^{\mathbb{Z}_2^{(1)},(3)} , \tag{A.29}$$

$$\text{with shift:} \quad \begin{pmatrix} 5 \\ 6 \end{pmatrix} \cdot \begin{pmatrix} 4 \\ 5 \end{pmatrix} = (-1)^{\tau_{(\omega a)}^3} = I_{a(\omega a)}^{\mathbb{Z}_2^{(1)},(3)} . \tag{A.30}$$

Once again, the result can be written as $I_{a(\omega a)}^{\mathbb{Z}_2^{(1)},(3)} = (-1)^{\tau_{(\omega a)}^3\sigma_{(\omega a)}^3}$. As usual, we have $\tau_a^i = \tau_{(\omega a)}^i$ and $\sigma_a^i = \sigma_{(\omega a)}^i$ because the orbifold action does not change the Wilson lines, nor the shifts. Thus, putting all the pieces together in (A.21), the multiplicity of the adjoint representation in the $a(\omega a)$ sector is given by:

$$b_{a(\omega a)} = \frac{1}{4}\left(1 - (-1)^{\sigma_a^2\tau_a^2+\sigma_a^3\tau_a^3}\right) . \tag{A.31}$$

The same results can be derived analogously for the second sector $b_{a(\omega^2 a)}$. The complete contribution to the beta-function coefficient of the adjoint representation is given by the sum of $b_{a(\omega a)}$, $b_{a(\omega^2 a)}$ and b_{aa}. In fact, as already mentioned in section 3.3, $b_{a(\omega a)}$ and $b_{a(\omega^2 a)}$ each provide half of the degrees of freedom of a chiral multiplet. Both together form a chiral $\mathcal{N} = 1$ SUSY multiplet transforming in the adjoint representation, so the multiplicity of the latter is given by $\frac{\varphi^{a(\omega a)}+\varphi^{a(\omega^2 a)}}{2}$.

The contribution to the beta-function coefficient of bifundamental representations can be computed analogously to the calculation illustrated above for the adjoint representation. Therefore, we will not provide an example, but continue with the contributions to the beta-function coefficient of the symmetric and antisymmetric representations.

The symmetric and antisymmetric representations

We consider again the three-cycle with bulk orbit parallel to the first orientifold plane $\Omega\mathcal{R}$. Once again, we have three sectors contributing to the beta-function coefficient, given by $b_{aa'}$, $b_{(\omega a)(\omega a)'}$ and $b_{(\omega^2 a)(\omega^2 a)'}$. We will start with the first one.

The first sector $b_{aa'}$: The torus three-cycle a given by (1,0;1,0;1,0) is invariant under the orientifold projection, so a and a' are parallel on all three two-tori and we have to use the first entry of table 3.4, reading:

$$b_{aa'} = -\frac{N_a}{4}\sum_{i=1}^{3} I_{aa'}^{\mathbb{Z}_2^{(i)},(j\cdot k)} - \frac{1}{2}\sum_{i=1}^{3}\eta_{\Omega\mathcal{R}\mathbb{Z}_2^{(i)}}(-1)^{2b^i\sigma_a^i\tau_a^i}|\tilde{I}_a^{\Omega\mathcal{R}\mathbb{Z}_2^{(i)},(j\cdot k)}|\,, \tag{A.32}$$

where in our background $(b^1,b^2,b^3) = (b,1/2,1/2)$, and $\tilde{I}_a^{\Omega\mathcal{R}\mathbb{Z}_2^{(i)},(j\cdot k)} = N_{O6} I_a^{\Omega\mathcal{R}\mathbb{Z}_2^{(i)},(j\cdot k)}$, with $N_{O6} = 2(1-b),\ b = 0,1/2$.
In our computation, we will also need the torus wrapping numbers of the other three O6-planes, given by:

$$\begin{aligned}
\Omega\mathcal{R}\mathbb{Z}_2^{(1)} &: (1,0;-1,2;1,-2),\\
\Omega\mathcal{R}\mathbb{Z}_2^{(2)} &: (0,1;1,0;1,-2),\\
\Omega\mathcal{R}\mathbb{Z}_2^{(3)} &: (0,1;1,-2;1,0).
\end{aligned}$$

The bulk intersection numbers can subsequently be computed and are given in table A.2.

Bulk intersection numbers needed to compute $b_{aa'}$, $b_{a(\omega a)'}$ and $b_{a(\omega^2 a)'}$, for a parallel to the $\Omega\mathcal{R}$-plane					
y	$\left(I_{yy'}^{(1)}, I_{yy'}^{(2)}, I_{yy'}^{(3)}\right)$	$\left(I_y^{\Omega\mathcal{R},(1)}, I_y^{\Omega\mathcal{R},(2)}, I_y^{\Omega\mathcal{R},(3)}\right)$	$\left(I_y^{\Omega\mathcal{R}\mathbb{Z}_2^{(1)},(1)}, I_y^{\Omega\mathcal{R}\mathbb{Z}_2^{(1)},(2)}, I_y^{\Omega\mathcal{R}\mathbb{Z}_2^{(1)},(3)}\right)$	$\left(I_y^{\Omega\mathcal{R}\mathbb{Z}_2^{(2)},(1)}, I_y^{\Omega\mathcal{R}\mathbb{Z}_2^{(2)},(2)}, I_y^{\Omega\mathcal{R}\mathbb{Z}_2^{(2)},(3)}\right)$	$\left(I_y^{\Omega\mathcal{R}\mathbb{Z}_2^{(3)},(1)}, I_y^{\Omega\mathcal{R}\mathbb{Z}_2^{(3)},(2)}, I_y^{\Omega\mathcal{R}\mathbb{Z}_2^{(3)},(3)}\right)$
a	$(0_{\uparrow\uparrow}, 0_{\uparrow\uparrow}, 0_{\uparrow\uparrow})$	$(0_{\uparrow\uparrow}, 0_{\uparrow\uparrow}, 0_{\uparrow\uparrow})$	$(0_{\uparrow\uparrow}, 2, -2)$	$(1, 0_{\uparrow\uparrow}, -2)$	$(1, -2, 0_{\uparrow\uparrow})$
(ωa)	$(0_{\uparrow\uparrow}, -1, 1)$	$(0_{\uparrow\uparrow}, 1, -1)$	$(0_{\uparrow\uparrow}, -1, 1)$	$(1, 1, 1)$	$(1, 1, -1)$
$(\omega^2 a)$	$(0_{\uparrow\uparrow}, 1, -1)$	$(0_{\uparrow\uparrow}, -1, 1)$	$(0_{\uparrow\uparrow}, -1, 1)$	$(1, -1, 1)$	$(1, 1, 1)$

Table A.2: Bulk intersection numbers of the three-cycles under consideration with their orientifold images or some O6-plane on each of the three two-tori $T^2_{(i)}$, $i = 1,2,3$. Two up arrows indicate one-cycles that are parallel. These intersection numbers are necessary ingredients for the determination of the multiplicity of the symmetric and antisymmetric representations.

The bulk intersection numbers in table A.2 can be used to compute the second sum in (A.32). Only bulk intersection numbers are needed since the O6-planes do not wrap exceptional cycles.

In order to compute the first sum in (A.32), the exceptional intersection numbers are needed. The exceptional intersection numbers are given by:

$$I_{aa'}^{\mathbb{Z}_2^{(i)},(j\cdot k)} = (-1)^{\tau_a^{\mathbb{Z}_2^{(i)}}+\tau_{a'}^{\mathbb{Z}_2^{(i)}}} I_{aa'}^{\mathbb{Z}_2^{(i)},(j)} I_{aa'}^{\mathbb{Z}_2^{(i)},(k)}\,. \tag{A.33}$$

We have to calculate the contributions from each $\mathbb{Z}_2^{(i)}$-twisted sector $i = 1,2,3$ separately.
For the first twisted sector with $i = 1$, the contribution to compute is $I_{aa'}^{\mathbb{Z}_2^{(1)},(2\cdot 3)}$. On the second two-torus, the bulk three-cycles a and a' pass through the following $\mathbb{Z}_2$-fixed points:

$$(n_a^2, m_a^2) = (1,0) \Rightarrow \begin{pmatrix} 1 \\ 4 \end{pmatrix} \overset{\text{shift}}{\to} \begin{pmatrix} 5 \\ 6 \end{pmatrix}\,, \tag{A.34}$$

$$(n^2_{a'}, m^2_{a'}) = (1,0) \Rightarrow \begin{pmatrix} 1 \\ 4 \end{pmatrix} \overset{\text{shift}}{\to} \begin{pmatrix} 5 \\ 6 \end{pmatrix}, \tag{A.35}$$

leading to the following contributions to the exceptional intersection numbers:

$$\text{no shift: } \begin{pmatrix} 1 \\ 4 \end{pmatrix} \cdot \begin{pmatrix} 1 \\ 4 \end{pmatrix} = 1 + (-1)^{\tau^a + \tau^{a'}} = 1 + (-1)^{2\tau^a} = 2 = I^{\mathbb{Z}_2^{(1)},(2)}_{aa'}, \tag{A.36}$$

$$\text{with shift: } \begin{pmatrix} 5 \\ 6 \end{pmatrix} \cdot \begin{pmatrix} 5 \\ 6 \end{pmatrix} = 1 + (-1)^{\tau^a + \tau^{a'}} = 2 = I^{\mathbb{Z}_2^{(1)},(2)}_{aa'}. \tag{A.37}$$

This time, we obtain the same results independently of whether a shift is present or not. The reasoning is the same for the third two-torus. The orientifold projection does not influence the Wilson lines nor the shifts. However, it has an influence on the $\mathbb{Z}_2$-eigenvalues as we will see below, since it acts as a reflexion with respect to the real axis.

In the next step, we have to consider the transformation rule under the orientifold projection of the $\mathbb{Z}_2^{(1)}$-eigenvalue of the cycle a in order to determine the quantity $(-1)^{\tau_a^{\mathbb{Z}_2^{(1)}} + \tau_{a'}^{\mathbb{Z}_2^{(1)}}}$. This can be done by applying subsequently the orientifold projection on the basis cycles and the torus wrapping numbers, and by comparing both. The cycle a passes through the $\mathbb{Z}_2$-fixed points 1 and 4 on both the second and third two-torus, without shift.The exceptional cycle obtained is given by:

$$\Pi_a^{\mathbb{Z}_2^{(1)}} = (\varepsilon_0^{(1)} + \varepsilon_2^{(1)}(-1)^{\tau_a^3} + \varepsilon_1^{(1)}(-1)^{\tau_a^2} + \varepsilon_3^{(1)}(-1)^{\tau_a^2+\tau_a^3})(-1)^{\tau_a^{\mathbb{Z}_2^{(1)}}}. \tag{A.38}$$

By applying the orientifold projection on the basis exceptional cycles as in (2.26), we find:

$$\Omega\mathcal{R}(\Pi_a^{\mathbb{Z}_2^{(1)}}) = -\eta_{(1)}\Pi_a^{\mathbb{Z}_2^{(1)}}. \tag{A.39}$$

On the other hand, we can apply the orientifold projection on the torus wrapping numbers as in (2.18), giving:

$$\Pi_{a'}^{\mathbb{Z}_2^{(1)}} = (\varepsilon_0^{(1)} + \varepsilon_2^{(1)}(-1)^{\tau_a^3} + \varepsilon_1^{(1)}(-1)^{\tau_a^2} + \varepsilon_3^{(1)}(-1)^{\tau_a^2+\tau_a^3})(-1)^{\tau_{a'}^{\mathbb{Z}_2^{(1)}}}. \tag{A.40}$$

By comparing the two expressions, we find that:

$$(-1)^{\tau_{a'}^{\mathbb{Z}_2^{(1)}}} = -\eta_{(1)}(-1)^{\tau_a^{\mathbb{Z}_2^{(1)}}}. \tag{A.41}$$

A correction needs to be added in presence of shifts, giving:

$$(-1)^{\tau_{a'}^{\mathbb{Z}_2^{(1)}}} = -\eta_{(1)}(-1)^{\tau_a^{\mathbb{Z}_2^{(1)}}}(-1)^{2b^2\sigma_a^2\tau_a^2 + 2b^3\sigma_a^3\tau_a^3}, \tag{A.42}$$

with $(b^2, b^3) = (1/2, 1/2)$ in our background. When dealing with three-cycles parallel to some O6-plane, as in the present case, extra care has to be taken. For the three O6-planes $\Omega\mathcal{R}\mathbb{Z}_2^{(i=1,2,3)}$ that are orthogonal to the real axis on two of the three two-tori, a and a' are antiparallel on these two-tori, implying that a and a' differ by a sign factor. However, these three-cycles can give rise to gauge symmetry enhancement, which imposes a to be exactly

equal to a'. Consequently, extra signs have to be introduced if a and a' are antiparallel on some two-tori. This forces us to modify the definition of $\tau_{a'^2}^{\mathbb{Z}_2^{(i)}}$ $(i = 1, 2, 3)$ slightly by turning the overall minus signs into a plus sign if a three-cycle is antiparallel to its orientifold image on the two-torus $T^2_{(i)}$.
Putting all the results together in (A.33), we find the intersection numbers of the first twisted sector:

$$I_{aa'}^{\mathbb{Z}_2^{(1)},(2\cdot3)} = -4\eta_{(1)}(-1)^{\sigma_a^2\tau_a^2+\sigma_a^3\tau_a^3}\,. \tag{A.43}$$

A similar analysis has to be done with the intersection numbers in the second and third twisted sectors $I_{aa'}^{\mathbb{Z}_2^{(2)},(1\cdot3)}$ and $I_{aa'}^{\mathbb{Z}_2^{(3)},(1\cdot2)}$.
With these ingredients, the first sum in formula (A.32) can be computed. The second sum only involves the bulk intersection numbers given in (A.2).
All in all, we obtain for the first sector $b_{aa'}$ the following contribution to the beta-function coefficient, see formula (A.32):

$$\begin{aligned} b_{aa'} = \;& N_a(\eta_{(1)}(-1)^{\sigma_a^2\tau_a^2+\sigma_a^3\tau_a^3} + \eta_{(2)}(-1)^{\sigma_a^3\tau_a^3} + \eta_{(3)}(-1)^{\sigma_a^2\tau_a^2}) \\ & -2(\eta_{\Omega\mathcal{R}\mathbb{Z}_2^{(1)}} + \eta_{\Omega\mathcal{R}\mathbb{Z}_2^{(2)}}(-1)^{\sigma_a^2\tau_a^2} + \eta_{\Omega\mathcal{R}\mathbb{Z}_2^{(3)}}(-1)^{\sigma_a^3\tau_a^3}). \end{aligned} \tag{A.44}$$

The second and third sectors $b_{(\omega a)(\omega a)'}$ and $b_{(\omega^2 a)(\omega^2 a)'}$: Consider now the second sector $b_{(\omega a)(\omega a)'}$. The first orbifold image (ωa) of the cycle a is parallel to $\Omega\mathcal{R}$ or $\Omega\mathcal{R}\mathbb{Z}_2^{(1)}$ on the first two-torus $T^2_{(1)}$. Hence, this situation corresponds to the third entry in table 3.4 with $i = 1$. Given that $b^1 = 0$ since we are working on the **aAA** lattice, the beta-function coefficient is given by:

$$\begin{aligned} b_{(\omega a)(\omega a)'} &= \tfrac{N_a}{4}\left(|I^{(2\cdot3)}_{(\omega a)(\omega a)'}| - |I^{\mathbb{Z}_2^{(1)}(2\cdot3)}_{(\omega a)(\omega a)'}|\right) - \tfrac{1}{2}\left(\eta_{\Omega\mathcal{R}}|\tilde{I}^{\Omega\mathcal{R}(2\cdot3)}_{(\omega a)}| + \eta_{\Omega\mathcal{R}\mathbb{Z}_2^{(1)}}|\tilde{I}^{\Omega\mathcal{R}\mathbb{Z}_2^{(1)}(2\cdot3)}_{(\omega a)}|\right) \\ &= \tfrac{N_a}{4}(1+\eta_{(1)}) - \tfrac{1}{2}\left(\eta_{\Omega\mathcal{R}} + \eta_{\Omega\mathcal{R}\mathbb{Z}_2^{(1)}}\right), \end{aligned} \tag{A.45}$$

where we used similar computations to the ones performed above to pass from the first to the second line. The same can be done for the second orbifold image $(\omega^2 a)$, i.e. the second sector $b_{(\omega^2 a)(\omega^2 a)'}$, leading exactly to the same result.

Concrete examples for the beta-function coefficient

As a first concrete example, let us consider all shifts being zero, $\sigma^i = 0,\ i = 1, 2, 3$. Formula (A.21) gives us $b_{a(\omega a)} = b_{a(\omega^2 a)} = 0$. Furthermore, let the $\Omega\mathcal{R}$-plane be the exotic one, i.e. $\eta_{\Omega\mathcal{R}} = -1 \Rightarrow \eta_{(1)} = -1$. This implies $b_{(\omega a)(\omega a)'} = b_{(\omega^2 a)(\omega^2 a)'} = 0$, as a look at formula (A.45) reveals. The first sector of the contribution from the (anti)symmetric representation gives $b_{aa'} = -3N_a - 6$, see formula (A.44). The beta-function coefficient is given by summing over all sectors $k = 0, 1, 2$ and representations, leading to:

$$\begin{aligned} b_{USp(2N_a)} &= b_{aa} + b_{a(\omega a)} + b_{a(\omega^2 a)} + b_{aa'} + b_{(\omega a)(\omega a)'} + b_{(\omega^2 a)(\omega^2 a)'} + \sum_{b\neq a}\frac{N_b}{2}\varphi^{ab} \\ &= -3N_a - 6 - 3N_a + \sum_{b\neq a}\frac{N_b}{2}\varphi^{ab} \end{aligned}$$

$$= -6(N_a + 1) + \sum_{b \neq a} \frac{N_b}{2} \varphi^{ab},$$

where one $-3N_a$ comes from the symmetric/antisymmetric sector $b_{aa'}$ and the other from the adjoint sector b_{aa}. The explicit expression of the contribution from the bifundamental representations depend on the number of stacks present in the model. We will limit the examples to the adjoint and (anti)symmetric representations.
Since we are considering a three-cycle with bulk orbit parallel to the $\Omega\mathcal{R}$-plane, we have gauge symmetry enhancement with the chosen configuration of discrete parameters and exotic charge ($\sigma^i = 0$ and $\eta_{\Omega\mathcal{R}} = -1$), see table 5.1. The sum in the last line was performed in order to make apparent one of the indices C given in (A.9). In the absence of enhancement, the sectors $b_{a(\omega^k a)}$ and $b_{(\omega^k a)(\omega^k a)'}$ can be interpreted separately. In case of enhancement, they have to be taken together in order to make sense of the spectrum.
As we have enhancement, the three-cycle a is equivalent to its orientifold image a' with $a = a'$, implying that the sectors $b_{a(\omega^k a)}$ and $b_{(\omega^k a)(\omega^k a)'}$ contain redundant information. To avoid double-counting of the multilpicities, the result is divided by 2, giving $b_{USp(2N_a)} = -3(N_a+1)$. The factor -3 is typical for the presence of a vector multiplet, transforming in the adjoint representation. From the formulas (A.9) we see that only for symplectic groups $USp(2N)$ we have $C(\mathbf{Adj}) = N + 1$. Thus, here we are in presence of $USp(2N)$-enhancement of the gauge group.

As a second example, consider the following shifts and Wilson lines: $\sigma_a^2\tau_a^2 = \sigma_a^3\tau_a^3 = 1$ and the exotic charge $\eta_{\Omega\mathcal{R}} = -1$. This is a situation without enhancement, see table 5.1. Summing again over the sectors $k = 0, 1, 2$ and the various representations, we obtain:

$$\begin{aligned} b_{SU(N_a)} &= b_{aa} + b_{a(\omega a)} + b_{a(\omega^2 a)} + b_{aa'} + b_{(\omega a)(\omega a)'} + b_{(\omega^2 a)(\omega^2 a)'} + \sum_{b \neq a} \frac{N_b}{2} \varphi^{ab} \\ &= -3N_a + 0 + 0 + (N_a + 2) + 0 + 0 + \sum_{b \neq a} \frac{N_b}{2} \varphi^{ab} \\ &= -3N_a + \frac{2(N_a + 2)}{2} + \sum_{b \neq a} \frac{N_b}{2} \varphi^{ab}\,. \end{aligned}$$

The term $-3N_a$ is again the contribution b_{aa} from the vector multiplet associated to the gauge bosons, transforming in the adjoint representation of $SU(N_a)$. By further comparing the result above to the list (A.9), we see that the second term corresponds to a contribution from two multiplets transforming in the symmetric representation of $SU(N_a)$, given by $b_{aa'}$.

Finally, consider the case: $\sigma_a^2\tau_a^2 = 0$, $\sigma_a^3\tau_a^3 = 1$ and again $\eta_{\Omega\mathcal{R}} = -1$, so that no enhancement is present. The result for the beta-function coefficient is:

$$\begin{aligned} b_{SU(N_a)} &= b_{aa} + b_{a(\omega a)} + b_{a(\omega^2 a)} + b_{aa'} + b_{(\omega a)(\omega a)'} + b_{(\omega^2 a)(\omega^2 a)'} + \sum_{b \neq a} \frac{N_b}{2} \varphi^{ab} \\ &= -3N_a + \frac{N_a}{2} + \frac{N_a}{2} + (N_a - 2) + 0 + 0 + \sum_{b \neq a} \frac{N_b}{2} \varphi^{ab} \\ &= -3N_a + \frac{N_a}{2} + \frac{N_a}{2} + \frac{2(N_a - 2)}{2} + \sum_{b \neq a} \frac{N_b}{2} \varphi^{ab}\,. \end{aligned}$$

The first term has already been discussed. The second and third terms arising from $b_{a(\omega^{k=1,2}a)}$ provide together a chiral multiplet transforming in the adjoint representation of $SU(N_a)$. These are unwanted for non-Abelian groups from a phenomenological point of view, so that this combination of exotic charge, shifts and Wilson lines should be avoided. Indeed, the chiral multiplets coming from $b_{a(\omega^{k=1,2}a)}$ correspond to deformation moduli of the D6-branes, rendering them non-rigid. The last term coming from $b_{aa'}$ corresponds to two multiplets transforming in the antisymmetric representation of $SU(N_a)$, as can be deduced from (A.9).

Once the beta-function coefficients are computed, the multiplicities φ^{xy} can be directly determined by comparing the expression found with formula (A.13), respectively (A.14) and (A.15) in case of enhancement.

Appendix B

Additional information

B.1 Other definitions of the hypercharge

We will present only one example explicitly, as the conditions on the intersection numbers for the other definitions of the hypercharge can be derived similarly.

Consider, for example, the following definition of the hypercharge:

$$Q_Y = \frac{1}{6}Q_a - \frac{1}{2}Q_c + \frac{1}{2}Q_d\,. \tag{B.1}$$

The conditions on the left-handed quarks remain unaffected by the change of signs. The other constraints, though, change. Indeed, the conditions for the right-handed up-type and down-type quarks become:

Intersection	Chirality/ Multiplicity	Representation under $(SU(3), SU(2))_{(Q_a,Q_b,Q_c,Q_d)}$	Q_Y
χ^{ac}	≤ 0	$(\overline{\mathbf{3}}, \mathbf{1})_{(-1,0,1,0)}$	$-2/3$
$\chi^{ac'}$	≤ 0	$(\overline{\mathbf{3}}, \mathbf{1})_{(-1,0,-1,0)}$	$1/3$
χ^{ad}	≤ 0	$(\overline{\mathbf{3}}, \mathbf{1})_{(-1,0,0,1)}$	$1/3$
$\chi^{ad'}$	≤ 0	$(\overline{\mathbf{3}}, \mathbf{1})_{(-1,0,0,-1)}$	$-2/3$
$\chi^{\mathbf{Anti}_a}$	≥ 0	$(\overline{\mathbf{3}}, \mathbf{1})_{(2,0,0,0)}$	$1/3$
$\chi^{ac'} + \chi^{ad} - \chi^{\mathbf{Anti}_a}$	-3	d_R	$1/3$
$\chi^{ac} + \chi^{ad'}$	-3	u_R	$-2/3$

(B.2)

The particles arising in the ac and ac' sectors now lead to different values of the hypercharge and consequently, they need to be paired off in the sum differently from before in section 3.2.1. A similar phenomenon arises for the left-handed leptons, the conditions for which

become:

Intersection	Chirality/ Multiplicity	Representation under $(SU(3), SU(2))_{(Q_a,Q_b,Q_c,Q_d)}$	Q_Y
χ^{bc}	≤ 0	$(\mathbf{1}, \overline{\mathbf{2}})_{(0,-1,1,0)}$	$-1/2$
$\chi^{bc'}$	≥ 0	$(\mathbf{1}, \mathbf{2})_{(0,1,1,0)}$	$-1/2$
χ^{bd}	≥ 0	$(\mathbf{1}, \mathbf{2})_{(0,1,0,-1)}$	$-1/2$
$\chi^{bd'}$	≤ 0	$(\mathbf{1}, \overline{\mathbf{2}})_{(0,-1,0,-1)}$	$-1/2$
$-\chi^{bc} + \chi^{bd} + \chi^{bc'} - \chi^{bd'}$	3	L	$-1/2$

(B.3)

Finally, for the right-handed electrons, the conditions are:

Intersection	Chirality/ Multiplicity	Representation under $(SU(3), SU(2))_{(Q_a,Q_b,Q_c,Q_d)}$	Q_Y
χ^{cd}	≤ 0	$(\mathbf{1}, \mathbf{1})_{(0,0,-1,1)}$	1
$\chi^{\mathbf{Sym}_c}$	≤ 0	$(\mathbf{1}, \mathbf{1})_{(0,0,-2,0)}$	1
$\chi^{\mathbf{Sym}_d}$	≥ 0	$(\mathbf{1}, \mathbf{1})_{(0,0,0,2)}$	1
$-\chi^{cd} - \chi^{\mathbf{Sym}_c} + \chi^{\mathbf{Sym}_d}$	3	e_R	1

(B.4)

Note that the right-handed electrons now involve the cd sector instead of the cd' sector. Indeed, the cd' sector now gives the right-handed neutrinos:

Intersection	Chirality/ Multiplicity	Representation under $(SU(3), SU(2))_{(Q_a,Q_b,Q_c,Q_d)}$	Q_Y
$\chi^{cd'}$	± 3	$\nu_R:\ (\mathbf{1}, \mathbf{1})_{(0,0,\pm 1,\pm 1)}$	0
$\chi^{\mathbf{Anti}_b}$	≥ 0 or ≤ 0	$(\mathbf{1}, \mathbf{1})_{(0,\pm 2,0,0)}$	0
$\chi^{\mathbf{Adj}_c}$	≥ 0 or ≤ 0	$(\mathbf{1}, \mathbf{1})_{(0,0,0,0)}$	0
$\chi^{\mathbf{Adj}_d}$	≥ 0 or ≤ 0	$(\mathbf{1}, \mathbf{1})_{(0,0,0,0)}$	0

(B.5)

By comparing the conditions derived for this definition of the hypercharge to those derived previously for the standard definition of the hypercharge in section 3.2.1, we see that they coincide after a simple exchange of the c stack with its orienifold image c'.

The conclusion is the same for the two remaining definitions of the hypercharge, $Q_y = \frac{Q_a}{6} + \frac{Q_c}{2} - \frac{Q_d}{2}$ and $Q_y = \frac{Q_a}{6} - \frac{Q_c}{2} - \frac{Q_d}{2}$, where the first corresponds to an exchange $d \leftrightarrow d'$ and the second to a simultaneous exchange $c \leftrightarrow c'$ and $d \leftrightarrow d'$.

B.2 Addendum to chapter 8

In this section, we provide some complementary information to the results discussed in chapter 8.

B.2.1 Linearly independent fractional three-cycles

A set of 16 linearly independent fractional three-cycles is given by:

$$
\begin{aligned}
&\frac{1}{4}\left((\varepsilon_1^{(2)}-2\tilde{\varepsilon}_1^{(2)})+\varepsilon_1^{(3)}+(\varepsilon_2^{(2)}-2\tilde{\varepsilon}_2^{(2)})+\varepsilon_2^{(3)}+(\varepsilon_4^{(1)}-\varepsilon_5^{(1)})+\rho_1\right),\\
&\frac{1}{4}\left((\varepsilon_1^{(2)}-2\tilde{\varepsilon}_1^{(2)})-\varepsilon_1^{(3)}+(\varepsilon_2^{(2)}-2\tilde{\varepsilon}_2^{(2)})-\varepsilon_2^{(3)}-(\varepsilon_4^{(1)}-\varepsilon_5^{(1)})+\rho_1\right),\\
&\frac{1}{4}\left(-(\varepsilon_1^{(2)}-2\tilde{\varepsilon}_1^{(2)})-\varepsilon_1^{(3)}-(\varepsilon_2^{(2)}-2\tilde{\varepsilon}_2^{(2)})-\varepsilon_2^{(3)}+(\varepsilon_4^{(1)}-\varepsilon_5^{(1)})+\rho_1\right),\\
&\frac{1}{4}\left(-(\varepsilon_1^{(2)}-2\tilde{\varepsilon}_1^{(2)})+\varepsilon_1^{(3)}-(\varepsilon_2^{(2)}-2\tilde{\varepsilon}_2^{(2)})+\varepsilon_2^{(3)}-(\varepsilon_4^{(1)}-\varepsilon_5^{(1)})+\rho_1\right),\\
&\frac{1}{4}\left((\varepsilon_4^{(1)}-\varepsilon_5^{(1)})+(\varepsilon_3^{(2)}-2\tilde{\varepsilon}_3^{(2)})+\varepsilon_3^{(3)}+(\varepsilon_4^{(2)}-2\tilde{\varepsilon}_4^{(2)})+\varepsilon_4^{(3)}+\rho_1\right),\\
&\frac{1}{4}\left(-(\varepsilon_4^{(1)}-\varepsilon_5^{(1)})+(\varepsilon_3^{(2)}-2\tilde{\varepsilon}_3^{(2)})-\varepsilon_3^{(3)}+(\varepsilon_4^{(2)}-2\tilde{\varepsilon}_4^{(2)})-\varepsilon_4^{(3)}+\rho_1\right),\\
&\frac{1}{4}\left((\varepsilon_4^{(1)}-\varepsilon_5^{(1)})+(\varepsilon_3^{(2)}-2\tilde{\varepsilon}_3^{(2)})+\varepsilon_3^{(3)}-(\varepsilon_4^{(2)}-2\tilde{\varepsilon}_4^{(2)})-\varepsilon_4^{(3)}+\rho_1\right),\\
&\frac{1}{4}\left(-(\varepsilon_4^{(1)}-\varepsilon_5^{(1)})+(\varepsilon_3^{(2)}-2\tilde{\varepsilon}_3^{(2)})-\varepsilon_3^{(3)}-(\varepsilon_4^{(2)}-2\tilde{\varepsilon}_4^{(2)})+\varepsilon_4^{(3)}+\rho_1\right),\\
&\frac{1}{4}\left((\varepsilon_2^{(2)}-2\tilde{\varepsilon}_2^{(2)})+\varepsilon_2^{(3)}+(\varepsilon_3^{(2)}-2\tilde{\varepsilon}_3^{(2)})+\varepsilon_3^{(3)}+\tilde{\varepsilon}_0^{(1)}+\tilde{\varepsilon}_1^{(1)}+\tilde{\varepsilon}_2^{(1)}+\tilde{\varepsilon}_3^{(1)}+\rho_3-2\rho_4\right),\\
&\frac{1}{4}\left(-(\varepsilon_2^{(2)}-2\tilde{\varepsilon}_2^{(2)})+\varepsilon_2^{(3)}-(\varepsilon_3^{(2)}-2\tilde{\varepsilon}_3^{(2)})+\varepsilon_3^{(3)}+\tilde{\varepsilon}_0^{(1)}+\tilde{\varepsilon}_1^{(1)}-\tilde{\varepsilon}_2^{(1)}-\tilde{\varepsilon}_3^{(1)}+\rho_3-2\rho_4\right),\\
&\frac{1}{4}\left((\varepsilon_2^{(2)}-2\tilde{\varepsilon}_2^{(2)})-\varepsilon_2^{(3)}+(\varepsilon_3^{(2)}-2\tilde{\varepsilon}_3^{(2)})-\varepsilon_3^{(3)}+\tilde{\varepsilon}_0^{(1)}-\tilde{\varepsilon}_1^{(1)}+\tilde{\varepsilon}_2^{(1)}-\tilde{\varepsilon}_3^{(1)}+\rho_3-2\rho_4\right),\\
&\frac{1}{4}\left(-(\varepsilon_2^{(2)}-2\tilde{\varepsilon}_2^{(2)})-\varepsilon_2^{(3)}-(\varepsilon_3^{(2)}-2\tilde{\varepsilon}_3^{(2)})-\varepsilon_3^{(3)}+\tilde{\varepsilon}_0^{(1)}-\tilde{\varepsilon}_1^{(1)}-\tilde{\varepsilon}_2^{(1)}+\tilde{\varepsilon}_3^{(1)}+\rho_3-2\rho_4\right),\\
&\frac{1}{4}\left((\varepsilon_2^{(2)}-2\tilde{\varepsilon}_2^{(2)})-\varepsilon_2^{(3)}+(\varepsilon_3^{(2)}-2\tilde{\varepsilon}_3^{(2)})-\varepsilon_3^{(3)}-\tilde{\varepsilon}_0^{(1)}-\tilde{\varepsilon}_1^{(1)}-\tilde{\varepsilon}_2^{(1)}-\tilde{\varepsilon}_3^{(1)}+\rho_3-2\rho_4\right),\\
&\frac{1}{4}\left(-(\varepsilon_2^{(2)}-2\tilde{\varepsilon}_2^{(2)})+\varepsilon_2^{(3)}-(\varepsilon_3^{(2)}-2\tilde{\varepsilon}_3^{(2)})+\varepsilon_3^{(3)}+2\tilde{\varepsilon}_2^{(1)}+(\tilde{\varepsilon}_4^{(1)}+\tilde{\varepsilon}_5^{(1)})+\rho_3-2\rho_4\right),\\
&\frac{1}{4}\left(-(\varepsilon_2^{(2)}-2\tilde{\varepsilon}_2^{(2)})-\varepsilon_2^{(3)}-(\varepsilon_3^{(2)}-2\tilde{\varepsilon}_3^{(2)})-\varepsilon_3^{(3)}+2\tilde{\varepsilon}_2^{(1)}-(\tilde{\varepsilon}_4^{(1)}+\tilde{\varepsilon}_5^{(1)})+\rho_3-2\rho_4\right),\\
&\frac{1}{4}\left((\varepsilon_2^{(2)}-2\tilde{\varepsilon}_2^{(2)})-\varepsilon_2^{(3)}+(\varepsilon_3^{(2)}-2\tilde{\varepsilon}_3^{(2)})-\varepsilon_3^{(3)}+2\tilde{\varepsilon}_1^{(1)}+(\tilde{\varepsilon}_4^{(1)}+\tilde{\varepsilon}_5^{(1)})+\rho_3-2\rho_4\right).
\end{aligned}
$$

Their independence can be checked by calculating the rank of the associated coefficient matrix.

The corresponding coefficient matrix is the following:

$$\mathrm{Rk}\,\frac{1}{4}\begin{pmatrix}
0&0&0&0&0&0&0&0&1&1&1&1&-1&0&0&0\\
0&0&0&0&0&0&0&0&1&1&-1&-1&-1&0&0&2\\
0&0&0&0&0&0&0&0&1&-1&1&-1&-1&2&2&0\\
0&0&0&0&0&0&0&0&1&-1&-1&1&-1&0&0&0\\
1&-1&1&-1&1&-1&1&-1&0&0&0&0&0&0&0&0\\
0&0&0&0&0&0&0&0&0&0&0&0&0&1&-1&1\\
1&1&-1&-1&0&0&0&0&0&0&0&0&0&0&0&0\\
1&1&-1&-1&0&0&0&0&1&-1&1&-1&1&-1&-1&1\\
0&0&0&0&1&1&1&1&1&-1&1&-1&1&-1&-1&1\\
0&0&0&0&1&1&-1&-1&0&0&0&0&0&0&0&0\\
1&-1&-1&1&0&0&0&0&0&0&0&0&0&0&0&0\\
1&-1&-1&1&0&0&0&0&1&1&-1&-1&-1&1&-1&-1\\
0&0&0&0&1&-1&1&-1&1&1&-1&-1&-1&1&-1&-1\\
0&0&0&0&1&-1&-1&1&0&0&0&0&0&0&0&0\\
1&1&1&1&1&1&1&1&0&0&0&0&0&0&0&0\\
0&0&0&0&0&0&0&0&1&1&1&1&1&1&1&1
\end{pmatrix} = 16, \tag{B.6}$$

where the columns correspond to the coefficients of the cycles. The basis cycles are taken in the same order as in table 8.3. (From top row to bottom row: $\tilde{\varepsilon}_\alpha^{(1)}$,$\varepsilon_4^{(1)} - \varepsilon_5^{(1)}$, $\tilde{\varepsilon}_4^{(1)} + \tilde{\varepsilon}_5^{(1)}$,$\varepsilon_\alpha^{(2)} - 2\tilde{\varepsilon}_\alpha^{(2)}$,$\varepsilon_\alpha^{(3)}$, $\rho_1, \rho_3 - 2\rho_4$.)

B.2.2 Details about the $\mathbb{Z}_n$-symmetries for the global MSSM

The following code illustrates how the necessary and sufficient conditions for the existence of $\mathbb{Z}_n$-symmetries of the MSSM given in table 7.17 should be interpreted:

```
Do[
n1 = ka*3 + kc*3 + kd*(-4) + kh*4;
n2 = ka*3 + kc*1 + kd*(-2) + kh*0;
n3 = ka*(6) + kc*(-1) + kd*(-1) + kh*0;
n = GCD[n1, n2, n3];
If[And[ka < n, kc < n, kd < n, kh < n, GCD[ka, kc, kd, kh, n] == 1, n != 1],
Print[ka, ",", kc, ",", kd, ",", kh, " :  ", n]
]
, {ka, 0, 16},{kc, 0, 16},{kd, 0, 16},{kh, 0, 16}]
```

Thus, for the k_i's varying from zero to 16, the code takes the greatest common divisor n of the contributions n_i from three linearly independent equations of (8.19). Thus n corresponds to the discrete symmetry $\mathbb{Z}_n$.
The code produced a total of 442 different combinations giving discrete symmetries for all

n up to $n = 45$. From $n = 45$ on, some values were missing, but that is probably just due to the fact that we limited the k_i's to 16. In the following table, we only reproduce, as a sample, the symmetries up to $n = 12$ for the D6-brane configuration in table 7.17:

k_a	k_c	k_d	k_h	n	k_a	k_c	k_d	k_h	n	k_a	k_c	k_d	k_h	n	k_a	k_c	k_d	k_h	n
1	1	1	0	2	3	1	1	6	8	2	2	10	1	12	7	1	5	11	12
1	1	1	1	2	5	7	7	0	8	2	2	10	7	12	7	5	1	1	12
0	1	2	2	3	5	7	7	2	8	2	6	6	3	12	7	5	1	4	12
0	2	1	1	3	5	7	7	4	8	2	10	2	5	12	7	5	1	7	12
1	0	0	0	3	5	7	7	6	8	2	10	2	11	12	7	5	1	10	12
1	1	2	2	3	7	5	5	2	8	3	1	5	2	12	7	9	9	0	12
1	2	1	1	3	7	5	5	6	8	3	1	5	5	12	7	9	9	3	12
2	1	2	2	3	1	0	6	3	9	3	1	5	8	12	7	9	9	6	12
2	2	1	1	3	1	6	0	6	9	3	1	5	11	12	7	9	9	9	12
0	0	0	1	4	2	0	3	6	9	3	5	1	1	12	8	0	0	3	12
1	3	3	1	4	2	3	0	3	9	3	5	1	4	12	8	0	0	9	12
2	2	2	1	4	4	3	3	0	9	3	5	1	7	12	8	4	8	5	12
2	2	2	3	4	5	0	3	6	9	3	5	1	10	12	8	4	8	11	12
3	1	1	1	4	5	3	0	3	9	4	0	0	3	12	8	8	4	1	12
3	1	1	3	4	5	6	6	0	9	4	0	0	9	12	8	8	4	7	12
2	1	1	0	5	7	0	6	3	9	4	4	8	5	12	9	7	11	2	12
3	4	4	0	5	7	6	0	6	9	4	4	8	11	12	9	7	11	5	12
0	2	4	1	6	8	0	3	6	9	4	8	4	1	12	9	7	11	8	12
0	4	2	5	6	8	3	0	3	9	4	8	4	7	12	9	7	11	11	12
1	1	5	2	6	4	2	2	5	10	5	3	3	0	12	9	11	7	1	12
1	1	5	5	6	6	8	8	5	10	5	3	3	3	12	9	11	7	4	12
1	5	1	1	6	4	1	1	0	11	5	3	3	6	12	9	11	7	7	12
1	5	1	4	6	5	4	4	0	11	5	3	3	9	12	9	11	7	10	12
2	0	0	3	6	6	7	7	0	11	5	7	11	2	12	10	2	10	1	12
2	2	4	1	6	7	10	10	0	11	5	7	11	5	12	10	2	10	7	12
2	4	2	5	6	0	4	8	5	12	5	7	11	8	12	10	6	6	3	12
4	2	4	1	6	0	4	8	11	12	5	7	11	11	12	10	6	6	9	12
4	4	2	5	6	0	8	4	1	12	5	11	7	1	12	10	10	2	5	12
5	1	5	2	6	0	8	4	7	12	5	11	7	4	12	10	10	2	11	12
5	1	5	5	6	1	3	3	3	12	5	11	7	7	12	11	1	5	2	12
5	5	1	1	6	1	7	11	2	12	5	11	7	10	12	11	1	5	5	12

5	5	1	4	6	1	7	11	5	12	6	2	10	1	12	11	1	5	8	12
3	2	2	0	7	1	7	11	8	12	6	2	10	7	12	11	1	5	11	12
4	5	5	0	7	1	7	11	11	12	6	10	2	5	12	11	5	1	1	12
1	3	3	2	8	1	11	7	1	12	6	10	2	11	12	11	5	1	4	12
3	1	1	0	8	1	11	7	4	12	7	1	5	2	12	11	5	1	7	12
3	1	1	2	8	1	11	7	7	12	7	1	5	5	12	11	5	1	10	12
3	1	1	4	8	1	11	7	10	12	7	1	5	8	12	11	9	9	3	12
															11	9	9	9	12

Only a few of these correspond to actual new independent $\mathbb{Z}_n$-symmetries. Redundancies between the discrete symmetries can be detected by analyzing the charges of the particles under the discrete $\mathbb{Z}_n$-symmetries, as is explained in the main text of chapter 8.

B.3 Classification of SUSY two-cycles on $T^2_{(2)} \times T^2_{(3)}$ with lattice AA

Systematic classification of bulk 2-cycles on $T^2_{(2)} \times T^2_{(3)}$ with lattice AA (part I)

$(n_a^2, m_a^2; n_a^3, m_a^3)$	X_a	Y_a	$2X_a + Y_a$
$(0,1;1,-1)$	1	0	2
$(2,-1;1,1)$	3	0	6
$(2,1;3,-1)$	7	0	14
$(-2,3;1,-3)$	7	0	14
$(4,-1;3,1)$	13	0	26
$(4,-3;1,3)$	13	0	26
$(2,-1;1,-1)$	1	-2	0
$(0,-1;1,1)$	1	-2	0
$(4,-5;3,-1)$	7	-14	0
$(4,1;1,-3)$	7	-14	0
$(2,-3;5,-1)$	7	-14	0
$(2,1;1,-5)$	7	-14	0
$(0,1;1,-3)$	3	-2	4
$(2,1;1,-1)$	3	-2	4
$(0,1;3,-5)$	5	-2	8
$(2,3;1,-1)$	5	-2	8
$(2,-1;3,1)$	7	-2	12
$(0,1;5,-7)$	7	-2	12
$(4,-3;1,1)$	7	-2	12
$(2,5;1,-1)$	7	-2	12
$(0,1;7,-9)$	9	-2	16
$(2,7;1,-1)$	9	-2	16
$(0,-1;1,3)$	3	-4	2
$(4,-1;1,-1)$	3	-4	2
$(2,-1;3,-1)$	5	-4	6
$(0,1;1,-5)$	5	-4	6
$(2,-3;1,1)$	5	-4	6
$(4,1;1,-1)$	5	-4	6
$(0,1;3,-7)$	7	-4	10
$(4,3;1,-1)$	7	-4	10
$(4,5;1,-1)$	9	-4	14
$(0,1;5,-9)$	9	-4	14
$(6,-1;1,-1)$	5	-6	4
$(0,-1;1,5)$	5	-6	4
$(0,1;1,-7)$	7	-6	8
$(6,1;1,-1)$	7	-6	8
$(4,-5;1,1)$	9	-6	12
$(2,-1;5,-1)$	9	-6	12
$(2,-3;1,3)$	11	-6	16
$(0,1;5,-11)$	11	-6	16
$(6,5;1,-1)$	11	-6	16
$(4,-1;3,-1)$	11	-6	16
$(0,-1;3,5)$	5	-8	2
$(8,-3;1,-1)$	5	-8	2
$(2,1;1,-3)$	5	-8	2
$(0,-1;1,7)$	7	-8	6
$(8,-1;1,-1)$	7	-8	6
$(2,-1;5,-3)$	7	-8	6
$(2,-5;1,1)$	7	-8	6
$(8,1;1,-1)$	9	-8	10
$(0,1;1,-9)$	9	-8	10
$(0,1;3,-11)$	11	-8	14
$(8,3;1,-1)$	11	-8	14
$(0,-1;3,7)$	7	-10	4
$(10,-3;1,-1)$	7	-10	4
$(2,-3;3,1)$	9	-10	8
$(10,-1;1,-1)$	9	-10	8
$(0,-1;1,9)$	9	-10	8
$(4,-3;3,-1)$	9	-10	8
$(4,-7;1,1)$	11	-10	12
$(2,-1;7,-3)$	11	-10	12
$(0,1;1,-11)$	11	-10	12
$(10,1;1,-1)$	11	-10	12
$(0,1;3,-13)$	13	-10	16
$(10,3;1,-1)$	13	-10	16
$(0,-1;5,7)$	7	-12	2
$(12,-5;1,-1)$	7	-12	2
$(2,-7;1,1)$	9	-12	6
$(2,-1;7,-5)$	9	-12	6
$(2,3;1,-3)$	11	-12	10
$(12,-1;1,-1)$	11	-12	10
$(0,-1;1,11)$	11	-12	10
$(2,1;3,-5)$	11	-12	10
$(0,1;1,-13)$	13	-12	14
$(12,1;1,-1)$	13	-12	14
$(0,-1;5,9)$	9	-14	4
$(14,-5;1,-1)$	9	-14	4
$(0,-1;3,11)$	11	-14	8
$(14,-3;1,-1)$	11	-14	8
$(0,-1;1,13)$	13	-14	12
$(2,-1;9,-5)$	13	-14	12
$(4,-9;1,1)$	13	-14	12
$(14,-1;1,-1)$	13	-14	12
$(0,1;1,-15)$	15	-14	16
$(14,1;1,-1)$	15	-14	16
$(0,-1;7,9)$	9	-16	2
$(16,-7;1,-1)$	9	-16	2
$(0,-1;5,11)$	11	-16	6
$(2,-1;9,-7)$	11	-16	6
$(16,-5;1,-1)$	11	-16	6
$(2,-9;1,1)$	11	-16	6
$(16,-3;1,-1)$	13	-16	10
$(6,-5;3,-1)$	13	-16	10
$(2,-3;5,1)$	13	-16	10
$(0,-1;3,13)$	13	-16	10
$(0,-1;1,15)$	15	-16	14
$(16,-1;1,-1)$	15	-16	14

Table B.2: Complete list of the torus wrapping numbers satisfying (n_a^2, m_a^2) =**(even, odd)**, (n_a^3, m_a^3) =(odd, odd) and $n_a^3 > 0$ on $T^2_{(2)} \times T^2_{(3)}$, as well as their corresponding bulk wrapping numbers (X_a, Y_a) fulfilling the SUSY constraints (4.20), (4.21) or (4.22) and compatible with the bulk RR-tadpole conditions (4.24) on the **AA** lattice.

Systematic classification of bulk 2-cycles on $T^2_{(2)} \times T^2_{(3)}$ with lattice AA (part II)

$(n^2_a, m^2_a; n^3_a, m^3_a)$	X_a	Y_a	$2X_a + Y_a$	$(n^2_a, m^2_a; n^3_a, m^3_a)$	X_a	Y_a	$2X_a + Y_a$	$(n^2_a, m^2_a; n^3_a, m^3_a)$	X_a	Y_a	$2X_a + Y_a$
$(1,-1;1,1)$	2	-1	3	$(1,-1;7,-3)$	4	-7	1	$(3,-7;1,1)$	10	-11	9
$(1,1;1,-1)$	2	-1	3	$(7,-3;1,-1)$	4	-7	1	$(1,1;3,-7)$	10	-11	9
$(1,-1;1,3)$	4	-1	7	$(7,-1;1,-1)$	6	-7	5	$(11,-1;1,-1)$	10	-11	9
$(1,3;1,-1)$	4	-1	7	$(1,-1;7,-1)$	6	-7	5	$(1,-1;11,-1)$	10	-11	9
$(1,-1;1,5)$	6	-1	11	$(1,-1;7,1)$	8	-7	9	$(1,-1;11,1)$	12	-11	13
$(1,5;1,-1)$	6	-1	11	$(7,1;1,-1)$	8	-7	9	$(3,-1;5,-3)$	12	-11	13
$(1,1;5,-3)$	8	-1	15	$(1,1;3,-5)$	8	-7	9	$(5,-3;3,-1)$	12	-11	13
$(1,-1;1,7)$	8	-1	15	$(3,-5;1,1)$	8	-7	9	$(11,1;1,-1)$	12	-11	13
$(5,-3;1,1)$	8	-1	15	$(7,3;1,-1)$	10	-7	13	$(1,-1;13,-5)$	8	-13	3
$(1,7;1,-1)$	8	-1	15	$(1,-1;7,3)$	10	-7	13	$(1,1;1,-7)$	8	-13	3
$(3,-1;1,-1)$	2	-3	1	$(1,-5;1,1)$	6	-9	3	$(1,-7;1,1)$	8	-13	3
$(1,-1;3,-1)$	2	-3	1	$(1,1;1,-5)$	6	-9	3	$(13,-5;1,-1)$	8	-13	3
$(3,1;1,-1)$	4	-3	5	$(9,-1;1,-1)$	8	-9	7	$(1,-1;13,-3)$	10	-13	7
$(1,-1;3,1)$	4	-3	5	$(1,-1;9,-1)$	8	-9	7	$(13,-3;1,-1)$	10	-13	7
$(-1,3;1,-3)$	8	-3	13	$(1,-1;9,1)$	10	-9	11	$(1,-1;13,-1)$	12	-13	11
$(3,5;1,-1)$	8	-3	13	$(1,-3;1,3)$	10	-9	11	$(13,-1;1,-1)$	12	-13	11
$(1,-1;3,5)$	8	-3	13	$(1,3;1,-3)$	10	-9	11	$(5,-9;1,1)$	14	-13	15
$(1,1;1,-3)$	4	-5	3	$(9,1;1,-1)$	10	-9	11	$(1,-1;13,1)$	14	-13	15
$(1,-1;5,-1)$	4	-5	3	$(5,-7;1,1)$	12	-9	15	$(1,1;5,-9)$	14	-13	15
$(5,-1;1,-1)$	4	-5	3	$(1,1;5,-7)$	12	-9	15	$(13,1;1,-1)$	14	-13	15
$(1,-3;1,1)$	4	-5	3	$(3,1;1,-3)$	6	-11	1	$(-1,-3;1,3)$	8	-15	1
$(5,1;1,-1)$	6	-5	7	$(1,-3;3,1)$	6	-11	1	$(15,-7;1,-1)$	8	-15	1
$(1,-1;5,1)$	6	-5	7	$(1,-1;11,-5)$	6	-11	1	$(1,-1;15,-7)$	8	-15	1
$(1,-1;5,3)$	8	-5	11	$(11,-5;1,-1)$	6	-11	1	$(1,-1;15,-1)$	14	-15	13
$(3,-1;3,-1)$	8	-5	11	$(11,-3;1,-1)$	8	-11	5	$(15,-1;1,-1)$	14	-15	13
$(5,3;1,-1)$	8	-5	11	$(1,-1;11,-3)$	8	-11	5				

Table B.3: Complete list of the torus wrapping numbers satisfying (n^2_a, m^2_a) =**(odd, odd)**, (n^3_a, m^3_a) =(odd, odd) and $n^3_a > 0$ on $T^2_{(2)} \times T^2_{(3)}$, as well as their corresponding bulk wrapping numbers (X_a, Y_a) fulfilling the SUSY constraints (4.20), (4.21) or (4.22) and compatible with the bulk RR-tadpole conditions (4.24) on the **AA** lattice.

Systematic classification of bulk 2-cycles on $T^2_{(2)} \times T^2_{(3)}$ with lattice AA (part III)

$(n_a^2, m_a^2; n_a^3, m_a^3)$	X_a	Y_a	$2X_a + Y_a$	$(n_a^2, m_a^2; n_a^3, m_a^3)$	X_a	Y_a	$2X_a + Y_a$	$(n_a^2, m_a^2; n_a^3, m_a^3)$	X_a	Y_a	$2X_a + Y_a$
$(1,0;1,-1)$	1	-1	1	$(1,-4;1,1)$	5	-7	3	$(1,-2;3,5)$	13	-11	15
$(1,0;3,-1)$	3	-1	5	$(7,-2;1,-1)$	5	-7	3	$(3,-2;5,-1)$	13	-11	15
$(1,2;1,-1)$	3	-1	5	$(1,-2;3,1)$	5	-7	3	$(1,0;13,-11)$	13	-11	15
$(1,0;5,-1)$	5	-1	9	$(3,-2;3,-1)$	7	-7	7	$(11,2;1,-1)$	13	-11	15
$(-1,2;1,-3)$	5	-1	9	$(1,2;1,-3)$	7	-7	7	$(13,-6;1,-1)$	7	-13	1
$(3,-2;1,1)$	5	-1	9	$(1,0;9,-7)$	9	-7	11	$(1,0;7,-13)$	7	-13	1
$(1,4;1,-1)$	5	-1	9	$(7,2;1,-1)$	9	-7	11	$(1,0;9,-13)$	9	-13	5
$(1,0;7,-1)$	7	-1	13	$(1,0;11,-7)$	11	-7	15	$(3,2;1,-3)$	9	-13	5
$(1,6;1,-1)$	7	-1	13	$(1,-2;1,5)$	11	-7	15	$(3,-2;5,-3)$	9	-13	5
$(1,-2;1,1)$	3	-3	3	$(7,4;1,-1)$	11	-7	15	$(13,-4;1,-1)$	9	-13	5
$(1,0;5,-3)$	5	-3	7	$(5,-6;1,1)$	11	-7	15	$(1,0;11,-13)$	11	-13	9
$(3,2;1,-1)$	5	-3	7	$(1,0;5,-9)$	5	-9	1	$(3,-8;1,1)$	11	-13	9
$(3,4;1,-1)$	7	-3	11	$(9,-4;1,-1)$	5	-9	1	$(5,-4;3,-1)$	11	-13	9
$(1,0;7,-3)$	7	-3	11	$(9,-2;1,-1)$	7	-9	5	$(1,-2;5,3)$	11	-13	9
$(-1,2;1,-5)$	9	-3	15	$(1,0;7,-9)$	7	-9	5	$(13,-2;1,-1)$	11	-13	9
$(5,-4;1,1)$	9	-3	15	$(9,2;1,-1)$	11	-9	13	$(1,2;1,-5)$	11	-13	9
$(5,-2;1,-1)$	3	-5	1	$(1,0;11,-9)$	11	-9	13	$(3,-4;3,1)$	13	-13	13
$(1,0;3,-5)$	3	-5	1	$(1,0;7,-11)$	7	-11	3	$(1,-4;1,3)$	13	-13	13
$(5,2;1,-1)$	7	-5	9	$(1,-6;1,1)$	7	-11	3	$(1,-2;7,1)$	9	-15	3
$(1,0;7,-5)$	7	-5	9	$(1,-2;5,1)$	7	-11	3	$(1,-8;1,1)$	9	-15	3
$(3,-4;1,1)$	7	-5	9	$(11,-4;1,-1)$	7	-11	3	$(1,0;11,-15)$	11	-15	7
$(1,-2;1,3)$	7	-5	9	$(11,-2;1,-1)$	9	-11	7	$(15,-4;1,-1)$	11	-15	7
$(5,4;1,-1)$	9	-5	13	$(1,0;9,-11)$	9	-11	7	$(1,0;13,-15)$	13	-15	11
$(1,0;9,-5)$	9	-5	13	$(5,-8;1,1)$	13	-11	15	$(15,-2;1,-1)$	13	-15	11
$(1,0;5,-7)$	5	-7	3	$(1,4;1,-3)$	13	-11	15				

Table B.4: Complete list of the torus wrapping numbers satisfying (n_a^2, m_a^2) =**(odd, even)**, (n_a^3, m_a^3) = (odd, odd) and $n_a^3 > 0$ on $T^2_{(2)} \times T^2_{(3)}$, as well as their corresponding bulk wrapping numbers (X_a, Y_a) fulfilling the SUSY constraints (4.20), (4.21) or (4.22) and compatible with the bulk RR-tadpole conditions (4.24) on the **AA** lattice.

Bibliography

[1] S. Monteil, *Electroweak Precision Tests*, in *Trans-European School of High Energy Physics 2010*, (Izvorani, Romania), July, 2010.

[2] F. Zwicky, *Die Rotverschiebung von extragalaktischen Nebeln*, *Helv. Phys. Acta* **6** (1933) 110–127.

[3] V. C. Rubin and W. K. Ford, Jr., *Rotation of the Andromeda Nebula from a Spectroscopic Survey of Emission Regions*, *Astrophys. J.* **159** (1970) 379–403.

[4] G. Bertone, D. Hooper, and J. Silk, *Particle dark matter: Evidence, candidates and constraints*, *Phys. Rept.* **405** (2005) 279–390, [hep-ph/0404175].

[5] E. Cremmer, B. Julia, and J. Scherk, *Supergravity Theory in Eleven-Dimensions*, *Phys. Lett.* **B76** (1978) 409–412.

[6] C. Rovelli and L. Smolin, *Knot Theory and Quantum Gravity*, *Phys. Rev. Lett.* **61** (1988) 1155.

[7] C. Rovelli and L. Smolin, *Loop Space Representation of Quantum General Relativity*, *Nucl. Phys.* **B331** (1990) 80–152.

[8] H. Nicolai, K. Peeters, and M. Zamaklar, *Loop quantum gravity: An Outside view*, *Class. Quant. Grav.* **22** (2005) R193, [hep-th/0501114].

[9] H. Nicolai and K. Peeters, *Loop and spin foam quantum gravity: A Brief guide for beginners*, *Lect. Notes Phys.* **721** (2007) 151–184, [hep-th/0601129].

[10] G. 't Hooft and M. J. G. Veltman, *One loop divergencies in the theory of gravitation*, *Annales Poincare Phys. Theor.* **A20** (1974) 69–94.

[11] M. H. Goroff and A. Sagnotti, *The Ultraviolet Behavior of Einstein Gravity*, *Nucl. Phys.* **B266** (1986) 709.

[12] J. C. Pati and A. Salam, *Unified Lepton-Hadron Symmetry and a Gauge Theory of the Basic Interactions*, *Phys. Rev.* **D8** (1973) 1240–1251.

[13] J. C. Pati and A. Salam, *Lepton Number as the Fourth Color*, *Phys. Rev.* **D10** (1974) 275–289. [Erratum: Phys. Rev.D11,703(1975)].

[14] H. Fritzsch and P. Minkowski, *Unified Interactions of Leptons and Hadrons*, *Annals Phys.* **93** (1975) 193–266.

[15] H. Georgi and S. L. Glashow, *Unity of All Elementary Particle Forces*, *Phys. Rev. Lett.* **32** (1974) 438–441.

[16] H. Georgi and D. V. Nanopoulos, *T Quark Mass in a Superunified Theory*, *Phys. Lett.* **B82** (1979) 392.

[17] H. Georgi and D. V. Nanopoulos, *Ordinary Predictions from Grand Principles: T Quark Mass in O(10)*, *Nucl. Phys.* **B155** (1979) 52.

[18] H. Georgi and D. V. Nanopoulos, *Masses and Mixing in Unified Theories*, *Nucl. Phys.* **B159** (1979) 16.

[19] J. C. Baez and J. Huerta, *The Algebra of Grand Unified Theories*, *Bull. Am. Math. Soc.* **47** (2010) 483–552, [arXiv:0904.1556].

[20] G. Veneziano, *Scale factor duality for classical and quantum strings*, *Phys. Lett.* **B265** (1991) 287–294.

[21] R. Easther, K.-i. Maeda, and D. Wands, *Tree level string cosmology*, *Phys. Rev.* **D53** (1996) 4247–4256, [hep-th/9509074].

[22] J. M. Maldacena, *The Large N limit of superconformal field theories and supergravity*, *Int. J. Theor. Phys.* **38** (1999) 1113–1133, [hep-th/9711200]. [Adv. Theor. Math. Phys.2,231(1998)].

[23] S. S. Gubser, I. R. Klebanov, and A. M. Polyakov, *Gauge theory correlators from noncritical string theory*, *Phys. Lett.* **B428** (1998) 105–114, [hep-th/9802109].

[24] E. Witten, *Anti-de Sitter space and holography*, *Adv. Theor. Math. Phys.* **2** (1998) 253–291, [hep-th/9802150].

[25] J. H. Conway and S. P. Norton, *Monstrous Moonshine*, *Bull. London Math. Soc.* **11** (1979), no. 3 308–339.

[26] R. E. Borcherds, *Monstrous moonshine and monstrous lie superalgebras*, *INVENT. MATH* **109** (1992).

[27] W. Lerche, C. Vafa, and N. P. Warner, *Chiral Rings in N=2 Superconformal Theories*, *Nucl. Phys.* **B324** (1989) 427.

[28] L. J. Dixon, *SOME WORLD SHEET PROPERTIES OF SUPERSTRING COMPACTIFICATIONS, ON ORBIFOLDS AND OTHERWISE*, in *Summer Workshop in High-energy Physics and Cosmology Trieste, Italy, June 29-August 7, 1987*, 1987.

[29] P. Candelas, X. C. De La Ossa, P. S. Green, and L. Parkes, *A Pair of Calabi-Yau manifolds as an exactly soluble superconformal theory*, *Nucl. Phys.* **B359** (1991) 21–74.

[30] P. Ramond, *Dual Theory for Free Fermions*, *Phys. Rev.* **D3** (1971) 2415–2418.

[31] B. Zwiebach, *A First Course in String Theory*. Cambridge University Press, 2009.

[32] J. Polchinski, *String Theory: Volume 1, An Introduction to the Bosonic String.* Cambridge Monographs on Mathematical Physics. Cambridge University Press, 1998.

[33] J. Polchinski, *String Theory: Volume 2, Superstring Theory and Beyond.* Cambridge Monographs on Mathematical Physics. Cambridge University Press, 1998.

[34] M. Green, J. Schwarz, and E. Witten, *Superstring Theory: Volume 1, Introduction.* Cambridge Monographs on Mathematical Physics. Cambridge University Press, 1988.

[35] M. Green, J. Schwarz, and E. Witten, *Superstring Theory: Volume 2, Loop Amplitudes, Anomalies and Phenomenology.* Cambridge Monographs on Mathematical Physics. Cambridge University Press, 1987.

[36] K. Becker, M. Becker, and J. Schwarz, *String Theory and M-Theory: A Modern Introduction.* Cambridge University Press, 2006.

[37] R. Blumenhagen, D. Lüst, and S. Theisen, *Basic concepts of string theory*, *Springer-Verlag* (2013).

[38] P. West, *Introduction to strings and branes.* Cambridge University Press, 2012.

[39] S. P. Martin, *A Supersymmetry primer*, `hep-ph/9709356`. [Adv. Ser. Direct. High Energy Phys.18,1(1998)].

[40] E. Witten, *New Issues in Manifolds of SU(3) Holonomy*, *Nucl. Phys.* **B268** (1986) 79.

[41] M. Graña, *Flux compactifications in string theory: A Comprehensive review*, *Phys. Rept.* **423** (2006) 91–158, [`hep-th/0509003`].

[42] S. Reffert, *The Geometer's Toolkit to String Compactifications*, in *Conference on String and M Theory Approaches to Particle Physics and Cosmology Florence, Italy, June 13-15, 2007*, 2007. `arXiv:0706.1310`.

[43] B. R. Greene, *String theory on Calabi-Yau manifolds*, in *Fields, strings and duality. Proceedings, Summer School, Theoretical Advanced Study Institute in Elementary Particle Physics, TASI'96, Boulder, USA, June 2-28, 1996*, pp. 543–726, 1996. `hep-th/9702155`.

[44] T. Hubsch, *Calabi-Yau manifolds: A Bestiary for physicists.* World Scientific, Singapore, 1994.

[45] A. Sagnotti, *Open Strings and their Symmetry Groups*, in *NATO Advanced Summer Institute on Nonperturbative Quantum Field Theory (Cargese Summer Institute) Cargese, France, July 16-30, 1987*, 1987. `hep-th/0208020`.

[46] G. Pradisi and A. Sagnotti, *Open String Orbifolds*, *Phys. Lett.* **B216** (1989) 59.

[47] M. Bianchi and A. Sagnotti, *On the systematics of open string theories*, *Phys.Lett.* **B247** (1990) 517–524.

[48] M. Bianchi, G. Pradisi, and A. Sagnotti, *Toroidal compactification and symmetry breaking in open string theories*, *Nucl.Phys.* **B376** (1992) 365–386.

[49] D. Fioravanti, G. Pradisi, and A. Sagnotti, *Sewing constraints and nonorientable open strings*, *Phys. Lett.* **B321** (1994) 349–354, [hep-th/9311183].

[50] J. Polchinski, *Dirichlet Branes and Ramond-Ramond charges*, *Phys. Rev. Lett.* **75** (1995) 4724–4727, [hep-th/9510017].

[51] L. E. Ibáñez and A. M. Uranga, *String theory and particle physics: An introduction to string phenomenology*, *Cambridge University Press* (2012).

[52] R. Blumenhagen, M. Cvetič, P. Langacker, and G. Shiu, *Toward realistic intersecting D-brane models*, *Ann.Rev.Nucl.Part.Sci.* **55** (2005) 71–139, [hep-th/0502005].

[53] R. Blumenhagen, B. Körs, D. Lüst, and S. Stieberger, *Four-dimensional String Compactifications with D-Branes, Orientifolds and Fluxes*, *Phys.Rept.* **445** (2007) 1–193, [hep-th/0610327].

[54] A. M. Uranga, *Chiral four-dimensional string compactifications with intersecting D-branes*, *Class.Quant.Grav.* **20** (2003) S373–S394, [hep-th/0301032].

[55] F. G. Marchesano Buznego, *Intersecting D-brane models*, *hep-th/0307252* (2003) [hep-th/0307252].

[56] T. Ott, *Aspects of stability and phenomenology in type IIA orientifolds with intersecting D6-branes*, *Fortsch. Phys.* **52** (2004) 28–137, [hep-th/0309107].

[57] E. Kiritsis, *D-branes in standard model building, gravity and cosmology*, *Phys.Rept.* **421** (2005) 105–190, [hep-th/0310001].

[58] L. Görlich, *$N = 1$ and nonsupersymmetric open string theories in six and four space-time dimensions*. PhD thesis, Tata Inst., 2003. hep-th/0401040.

[59] D. Lüst, *Intersecting brane worlds: A Path to the standard model?*, *Class. Quant. Grav.* **21** (2004) S1399–1424, [hep-th/0401156].

[60] R. Blumenhagen, *Recent progress in intersecting D-brane models*, *Fortsch. Phys.* **53** (2005) 426–435, [hep-th/0412025].

[61] M. Nakahara, *Geometry, topology, and physics*. Graduate student series in physics. Institute of Physics Publishing, Bristol, Philadelphia, 2003.

[62] P. Griffiths and J. Harris, *Principles of Algebraic Geometry*. Wiley Classics Library. Wiley, 2011.

[63] J. Ecker, G. Honecker, and W. Staessens, *Rigour and rigidity: Systematics on particle physics D6-brane models on $\mathbb{Z}_2 \times \mathbb{Z}_6$*, *Fortsch.Phys.* **62** (2014) 981–1040, [arXiv:1409.1236].

[64] J. Ecker, G. Honecker, and W. Staessens, *D6-brane model building on $\mathbb{Z}_2 \times \mathbb{Z}_6$: MSSM-like and left-right symmetric models*, *Nucl. Phys.* **B901** (2015) 139–215, [arXiv:1509.0004].

[65] S. Förste and G. Honecker, *Rigid D6-branes on $T^6/(\mathbb{Z}_2 \times \mathbb{Z}_{2M} \times \Omega\mathcal{R})$ with discrete torsion*, *JHEP* **1101** (2011) 091, [arXiv:1010.6070].

[66] F. Gmeiner and G. Honecker, *Millions of Standard Models on $\mathbb{Z}_6'$?*, *JHEP* **0807** (2008) 052, [arXiv:0806.3039].

[67] F. Gmeiner and G. Honecker, *Complete Gauge Threshold Corrections for Intersecting Fractional D6-Branes: The $\mathbb{Z}_6$ and $\mathbb{Z}_6'$ Standard Models*, *Nucl.Phys.* **B829** (2010) 225–297, [arXiv:0910.0843].

[68] D. Bailin and A. Love, *Towards the supersymmetric standard model from intersecting D6-branes on the Z-prime(6) orientifold*, *Nucl.Phys.* **B755** (2006) 79–111, [hep-th/0603172].

[69] F. Gmeiner and G. Honecker, *Mapping an Island in the Landscape*, *JHEP* **0709** (2007) 128, [arXiv:0708.2285].

[70] D. Bailin and A. Love, *Almost the supersymmetric standard model from intersecting D6-branes on the Z(6)-prime orientifold*, *Phys.Lett.* **B651** (2007) 324–328, [arXiv:0705.0646].

[71] D. Bailin and A. Love, *Constructing the supersymmetric Standard Model from intersecting D6-branes on the Z(6)-prime orientifold*, *Nucl.Phys.* **B809** (2009) 64–109, [arXiv:0801.3385].

[72] G. Honecker, *Kähler metrics and gauge kinetic functions for intersecting D6-branes on toroidal orbifolds - The complete perturbative story*, *Fortsch.Phys.* **60** (2012) 243–326, [arXiv:1109.3192].

[73] G. Honecker, *Towards exact field theory results for the Standard Model on fractional D6-branes*, *PoS* **EPS-HEP2011** (2011) 129, [arXiv:1109.6533].

[74] G. Honecker and J. Vanhoof, *Yukawa couplings and masses of non-chiral states for the Standard Model on D6-branes on $T^6/\mathbb{Z}_6'$*, *JHEP* **1204** (2012) 085, [arXiv:1201.3604].

[75] G. Honecker and J. Vanhoof, *Towards the field theory of the Standard Model on fractional D6-branes on $T^6/\mathbb{Z}_6'$: Yukawa couplings and masses*, *Fortsch.Phys.* **60** (2012) 1050–1056, [arXiv:1201.5872].

[76] G. Honecker, M. Ripka, and W. Staessens, *The Importance of Being Rigid: D6-Brane Model Building on $T^6/\mathbb{Z}_2 \times \mathbb{Z}_6'$ with Discrete Torsion*, *Nucl.Phys.* **B868** (2013) 156–222, [arXiv:1209.3010].

[77] R. Blumenhagen, V. Braun, B. Körs, and D. Lüst, *Orientifolds of K3 and Calabi-Yau manifolds with intersecting D-branes*, *JHEP* **0207** (2002) 026, [hep-th/0206038].

[78] G. Honecker and W. Staessens, *To Tilt or Not To Tilt: Discrete Gauge Symmetries in Global Intersecting D-Brane Models*, *JHEP* **1310** (2013) 146, [arXiv:1303.4415].

[79] L. J. Dixon, J. A. Harvey, C. Vafa, and E. Witten, *Strings on Orbifolds*, *Nucl. Phys.* **B261** (1985) 678–686.

[80] L. J. Dixon, J. A. Harvey, C. Vafa, and E. Witten, *Strings on Orbifolds. 2.*, *Nucl. Phys.* **B274** (1986) 285–314.

[81] L. J. Dixon, D. Friedan, E. J. Martinec, and S. H. Shenker, *The Conformal Field Theory of Orbifolds*, *Nucl. Phys.* **B282** (1987) 13–73.

[82] D. Bailin and A. Love, *Orbifold compactifications of string theory*, *Phys. Rept.* **315** (1999) 285–408.

[83] A. N. Schellekens, *Introduction to conformal field theory*, *Fortsch. Phys.* **44** (1996) 605–705.

[84] M. R. Gaberdiel, *An Introduction to conformal field theory*, *Rept. Prog. Phys.* **63** (2000) 607–667, [hep-th/9910156].

[85] P. Di Francesco, P. Mathieu, and D. Senechal, *Conformal Field Theory*. Graduate Texts in Contemporary Physics. Springer-Verlag, New York, 1997.

[86] Z. Kakushadze and G. Shiu, *A Chiral N=1 type I vacuum in four-dimensions and its heterotic dual*, *Phys. Rev.* **D56** (1997) 3686–3697, [hep-th/9705163].

[87] G. Aldazabal, A. Font, L. E. Ibanez, and G. Violero, *D = 4, N=1, type IIB orientifolds*, *Nucl. Phys.* **B536** (1998) 29–68, [hep-th/9804026].

[88] R. Blumenhagen, J. P. Conlon, and K. Suruliz, *Type IIA orientifolds on general supersymmetric Z(N) orbifolds*, *JHEP* **07** (2004) 022, [hep-th/0404254].

[89] A. Seifert and G. Honecker, *Model building on the non-factorisable type IIA* $\mathbf{T^6}/(\mathbb{Z}_\mathbf{4} \times \boldsymbol{\Omega\mathcal{R}})$ *orientifold*, 2015. arXiv:1511.0307.

[90] L. Nilse, *Classification of 1-D and 2-D orbifolds*, *AIP Conf. Proc.* **903** (2007) 411–414. [,411(2007)].

[91] S. Reffert, *Toroidal Orbifolds: Resolutions, Orientifolds and Applications in String Phenomenology*. PhD thesis, Munich U., 2006. hep-th/0609040.

[92] R. Blumenhagen, M. Cvetič, F. Marchesano, and G. Shiu, *Chiral D-brane models with frozen open string moduli*, *JHEP* **0503** (2005) 050, [hep-th/0502095].

[93] G. Honecker and W. Staessens, *D6-Brane Model Building and Discrete Symmetries on* $T^6/(\mathbb{Z}_2 \times \mathbb{Z}_6 \times \Omega\mathcal{R})$ *with Discrete Torsion*, *PoS* **Corfu2012** (2013) 107, [arXiv:1303.6845].

[94] G. Honecker and T. Ott, *Getting just the supersymmetric standard model at intersecting branes on the Z(6) orientifold*, *Phys.Rev.* **D70** (2004) 126010, [hep-th/0404055].

[95] G. Honecker, *Chiral N=1 4-D orientifolds with D-branes at angles*, *Mod.Phys.Lett.* **A19** (2004) 1863–1879, [hep-th/0407181].

[96] F. Gmeiner, D. Lüst, and M. Stein, *Statistics of intersecting D-brane models on* $T^6/\mathbb{Z}_6$, *JHEP* **0705** (2007) 018, [hep-th/0703011].

[97] R. Blumenhagen, L. Görlich, and T. Ott, *Supersymmetric intersecting branes on the type 2A T6 / Z(4) orientifold*, *JHEP* **0301** (2003) 021, [hep-th/0211059].

[98] G. Honecker, *Chiral supersymmetric models on an orientifold of Z(4) x Z(2) with intersecting D6-branes*, *Nucl.Phys.* **B666** (2003) 175–196, [hep-th/0303015].

[99] G. Honecker, *Supersymmetric intersecting D6-branes and chiral models on the $T^6/(\mathbb{Z}_4 \times \mathbb{Z}_2)$ orbifold*, in *String phenomenology. Proceedings, 2nd International Conference, Durham, UK, July 29-August 4, 2003*, pp. 191–198, 2003. hep-th/0309158.

[100] M. Berasaluce-González, L. E. Ibáñez, P. Soler, and A. M. Uranga, *Discrete gauge symmetries in D-brane models*, *JHEP* **1112** (2011) 113, [arXiv:1106.4169].

[101] G. Honecker and W. Staessens, *On axionic dark matter in Type IIA string theory*, *Fortsch. Phys.* **62** (2014) 115–151, [arXiv:1312.4517].

[102] G. Honecker and W. Staessens, *Discrete Abelian gauge symmetries and axions*, *J. Phys. Conf. Ser.* **631** (2015), no. 1 012080, [arXiv:1502.0098].

[103] G. Honecker, *From Stringy Particle Physics to Moduli Stabilisation and Cosmology*, in *21st European String Workshop: The String Theory Universe Leuven, Belgium, September 7-11, 2015*, 2015. arXiv:1510.0844.

[104] J. Erler and A. Klemm, *Comment on the generation number in orbifold compactifications*, *Commun. Math. Phys.* **153** (1993) 579–604, [hep-th/9207111].

[105] C. Vafa and E. Witten, *On orbifolds with discrete torsion*, *J.Geom.Phys.* **15** (1995) 189–214, [hep-th/9409188].

[106] C. Vafa, *Modular Invariance and Discrete Torsion on Orbifolds*, *Nucl.Phys.* **B273** (1986) 592.

[107] A. Font, L. E. Ibáñez, and F. Quevedo, *Z(N) x Z(M) ORBIFOLDS AND DISCRETE TORSION*, *Phys.Lett.* **B217** (1989) 272.

[108] T. W. Grimm and J. Louis, *The Effective action of type IIA Calabi-Yau orientifolds*, *Nucl.Phys.* **B718** (2005) 153–202, [hep-th/0412277].

[109] M. Blaszczyk, G. Honecker, and I. Koltermann, *Deformations on Tilted Tori and Moduli Stabilisation at the Orbifold Point*, *JHEP* **11** (2015) 019, [arXiv:1507.0756].

[110] M. Blaszczyk, G. Honecker, and I. Koltermann, *Circling the Square: Deforming fractional D-branes in Type II/$\Omega\mathcal{R}$ orientifolds*, *JHEP* **1407** (2014) 124, [arXiv:1403.2394].

[111] I. Koltermann, M. Blaszczyk, and G. Honecker, *Deforming D-brane models on $T^6/(\mathbb{Z}_2 \times \mathbb{Z}_{2M})$ orbifolds*, in *21st European String Workshop: The String Theory Universe Leuven, Belgium, September 7-11, 2015*, 2015. arXiv:1511.0354.

[112] R. Blumenhagen, L. Görlich, and B. Körs, *Supersymmetric orientifolds in 6-D with D-branes at angles*, *Nucl.Phys.* **B569** (2000) 209–228, [hep-th/9908130].

[113] R. Blumenhagen, L. Görlich, and B. Körs, *Supersymmetric 4-D orientifolds of type IIA with D6-branes at angles*, *JHEP* **0001** (2000) 040, [hep-th/9912204].

[114] S. Förste, G. Honecker, and R. Schreyer, *Supersymmetric Z(N) x Z(M) orientifolds in 4-D with D branes at angles*, *Nucl.Phys.* **B593** (2001) 127–154, [hep-th/0008250].

[115] C. Angelantonj and A. Sagnotti, *Open strings*, *Phys. Rept.* **371** (2002) 1–150, [hep-th/0204089]. [Erratum: Phys. Rept.376,no.6,407(2003)].

[116] D. Joyce, *Lectures on Calabi-Yau and special Lagrangian geometry*, math/0108088.

[117] D. Joyce, *Lectures on special Lagrangian geometry*, *ArXiv Mathematics e-prints* (Nov., 2001) [math/0111111].

[118] E. G. Gimon and J. Polchinski, *Consistency conditions for orientifolds and d manifolds*, *Phys.Rev.* **D54** (1996) 1667–1676, [hep-th/9601038].

[119] G. Zwart, *Four-dimensional N=1 Z(N) x Z(M) orientifolds*, *Nucl. Phys.* **B526** (1998) 378–392, [hep-th/9708040].

[120] R. Blumenhagen, V. Braun, B. Kors, and D. Lust, *The standard model on the quintic*, in *Theory of elementary particles. Proceedings, 35th International Ahrenshoop Symposium, Berlin, Germany, August 26-30, 2002*, 2002. hep-th/0210083.

[121] F. Marchesano, *Progress in D-brane model building*, *Fortsch.Phys.* **55** (2007) 491–518, [hep-th/0702094].

[122] M. B. Green and J. H. Schwarz, *Anomaly cancellations in supersymmetric D = 10 gauge theory and superstring theory*, *Physics Letters B* **149** (Dec., 1984) 117–122.

[123] G. Aldazabal, S. Franco, L. E. Ibáñez, R. Rabadan, and A. M. Uranga, *D = 4 chiral string compactifications from intersecting branes*, *J. Math. Phys.* **42** (2001) 3103–3126, [hep-th/0011073].

[124] M. Karoubi, *K-theory. An elementary introduction*, *ArXiv Mathematics e-prints* (Feb., 2006) [math/0602082].

[125] E. Witten, *D-branes and K theory*, *JHEP* **9812** (1998) 019, [hep-th/9810188].

[126] R. Minasian and G. W. Moore, *K theory and Ramond-Ramond charge*, *JHEP* **11** (1997) 002, [hep-th/9710230].

[127] A. M. Uranga, *D-brane probes, RR tadpole cancellation and K theory charge*, *Nucl.Phys.* **B598** (2001) 225–246, [hep-th/0011048].

[128] E. Witten, *An SU(2) Anomaly*, *Phys.Lett.* **B117** (1982) 324–328.

[129] R. C. McLean, *Deformations Of Calibrated Submanifolds*, *Commun. Analy. Geom* **6** (1998) 705–747.

[130] F. Gmeiner and M. Stein, *Statistics of SU(5) D-brane models on a type II orientifold*, *Phys.Rev.* **D73** (2006) 126008, [hep-th/0603019].

[131] S. Förste and I. Zavala, *Oddness from Rigidness*, *JHEP* **0807** (2008) 086, [arXiv:0806.2328].

[132] D. Bailin and A. Love, *Stabilising the supersymmetric Standard Model on the Z_6' orientifold*, *Nucl.Phys.* **B854** (2012) 700–737, [arXiv:1104.3522].

[133] D. Bailin and A. Love, *Intersecting D6-branes on the $\mathbb{Z}_{12}$-II orientifold*, *JHEP* **1401** (2014) 009, [arXiv:1310.8215].

[134] M. Kerstan and T. Weigand, *The Effective action of D6-branes in N=1 type IIA orientifolds*, *JHEP* **1106** (2011) 105, [arXiv:1104.2329].

[135] C. Angelantonj, C. Condeescu, E. Dudas, and M. Lennek, *Stringy Instanton Effects in Models with Rigid Magnetised D-branes*, *Nucl.Phys.* **B818** (2009) 52–94, [arXiv:0902.1694].

[136] C. Angelantonj, C. Condeescu, E. Dudas, and G. Pradisi, *Non-perturbative transitions among intersecting-brane vacua*, *JHEP* **1107** (2011) 123, [arXiv:1105.3465].

[137] C. Angelantonj, I. Antoniadis, E. Dudas, and A. Sagnotti, *Type I strings on magnetized orbifolds and brane transmutation*, *Phys.Lett.* **B489** (2000) 223–232, [hep-th/0007090].

[138] C. Angelantonj and E. Dudas, *Metastable string vacua*, *Phys.Lett.* **B651** (2007) 239–245, [arXiv:0704.2553].

[139] R. Blumenhagen, B. Kors, D. Lust, and T. Ott, *The standard model from stable intersecting brane world orbifolds*, *Nucl. Phys.* **B616** (2001) 3–33, [hep-th/0107138].

[140] P. Fayet and S. Ferrara, *Supersymmetry*, *Phys. Rept.* **32** (1977) 249–334.

[141] P. Fayet, *Spontaneously Broken Supersymmetric Theories of Weak, Electromagnetic and Strong Interactions*, *Phys. Lett.* **B69** (1977) 489.

[142] G. R. Farrar and P. Fayet, *Phenomenology of the Production, Decay, and Detection of New Hadronic States Associated with Supersymmetry*, *Phys. Lett.* **B76** (1978) 575–579.

[143] P. Fayet, *Scattering Cross-Sections of the Photino and the Goldstino (Gravitino) on Matter*, *Phys. Lett.* **B86** (1979) 272.

[144] G. R. Farrar and P. Fayet, *Searching for the Spin 0 Leptons of Supersymmetry*, *Phys. Lett.* **B89** (1980) 191.

[145] S. Dimopoulos and S. Raby, *Supercolor*, *Nucl. Phys.* **B192** (1981) 353.

[146] M. Dine, W. Fischler, and M. Srednicki, *Supersymmetric Technicolor*, *Nucl. Phys.* **B189** (1981) 575–593.

[147] M. Dine and W. Fischler, *A Phenomenological Model of Particle Physics Based on Supersymmetry*, *Phys. Lett.* **B110** (1982) 227.

[148] J. Goldstone, A. Salam, and S. Weinberg, *Broken Symmetries*, *Phys. Rev.* **127** (1962) 965–970.

[149] P. W. Anderson, *Plasmons, Gauge Invariance, and Mass*, *Phys. Rev.* **130** (1963) 439–442.

[150] G. S. Guralnik, C. R. Hagen, and T. W. B. Kibble, *Global Conservation Laws and Massless Particles*, *Phys. Rev. Lett.* **13** (1964) 585–587.

[151] G. J. Gounaris, R. Kogerler, and H. Neufeld, *Relationship Between Longitudinally Polarized Vector Bosons and their Unphysical Scalar Partners*, *Phys. Rev.* **D34** (1986) 3257.

[152] P. W. Higgs, *Broken symmetries, massless particles and gauge fields*, *Phys. Lett.* **12** (1964) 132–133.

[153] P. W. Higgs, *Broken Symmetries and the Masses of Gauge Bosons*, *Phys. Rev. Lett.* **13** (1964) 508–509.

[154] P. W. Higgs, *Spontaneous Symmetry Breakdown without Massless Bosons*, *Phys. Rev.* **145** (1966) 1156–1163.

[155] F. Englert and R. Brout, *Broken Symmetry and the Mass of Gauge Vector Mesons*, *Phys. Rev. Lett.* **13** (1964) 321–323.

[156] M. Peskin and D. Schroeder, *An Introduction to Quantum Field Theory*. Advanced book classics. Addison-Wesley Publishing Company, 1995.

[157] L. E. Ibanez and G. G. Ross, *Electroweak breaking in supersymmetric models*, `hep-ph/9204201`.

[158] M. Kobayashi and T. Maskawa, *CP Violation in the Renormalizable Theory of Weak Interaction*, *Prog. Theor. Phys.* **49** (1973) 652–657.

[159] R. J. Crewther, P. Di Vecchia, G. Veneziano, and E. Witten, *Chiral Estimate of the Electric Dipole Moment of the Neutron in Quantum Chromodynamics*, *Phys. Lett.* **B88** (1979) 123. [Erratum: Phys. Lett.B91,487(1980)].

[160] V. Baluni, *CP Violating Effects in QCD*, *Phys. Rev.* **D19** (1979) 2227–2230.

[161] C. A. Baker et al., *An Improved experimental limit on the electric dipole moment of the neutron*, *Phys. Rev. Lett.* **97** (2006) 131801, [`hep-ex/0602020`].

[162] R. Peccei and H. R. Quinn, *Constraints Imposed by CP Conservation in the Presence of Instantons*, *Phys.Rev.* **D16** (1977) 1791–1797.

[163] R. Peccei and H. R. Quinn, *CP Conservation in the Presence of Instantons*, *Phys.Rev.Lett.* **38** (1977) 1440–1443.

[164] S. Weinberg, *A New Light Boson?*, *Phys.Rev.Lett.* **40** (1978) 223–226.

[165] F. Wilczek, *Problem of Strong p and t Invariance in the Presence of Instantons*, *Phys.Rev.Lett.* **40** (1978) 279–282.

[166] B. Kors and P. Nath, *Aspects of the Stueckelberg extension*, *JHEP* **07** (2005) 069, [hep-ph/0503208].

[167] L. Ibáñez, A. Schellekens, and A. Uranga, *Discrete Gauge Symmetries in Discrete MSSM-like Orientifolds*, *Nucl.Phys.* **B865** (2012) 509–540, [arXiv:1205.5364].

[168] P. Anastasopoulos, M. Cvetič, R. Richter, and P. K. Vaudrevange, *String Constraints on Discrete Symmetries in MSSM Type II Quivers*, *JHEP* **1303** (2013) 011, [arXiv:1211.1017].

[169] L. Ackerman, M. R. Buckley, S. M. Carroll, and M. Kamionkowski, *Dark Matter and Dark Radiation*, *Phys. Rev.* **D79** (2009) 023519, [arXiv:0810.5126]. [,277(2008)].

[170] **Muon g-2** Collaboration, G. W. Bennett et al., *Final Report of the Muon E821 Anomalous Magnetic Moment Measurement at BNL*, *Phys. Rev.* **D73** (2006) 072003, [hep-ex/0602035].

[171] K. Hagiwara, R. Liao, A. D. Martin, D. Nomura, and T. Teubner, $(g-2)_\mu$ *and* $\alpha(M_Z^2)$ *re-evaluated using new precise data*, *J. Phys.* **G38** (2011) 085003, [arXiv:1105.3149].

[172] M. Davier, A. Hoecker, B. Malaescu, and Z. Zhang, *Reevaluation of the Hadronic Contributions to the Muon g-2 and to alpha(MZ)*, *Eur. Phys. J.* **C71** (2011) 1515, [arXiv:1010.4180]. [Erratum: Eur. Phys. J.C72,1874(2012)].

[173] H. Georgi, H. R. Quinn, and S. Weinberg, *Hierarchy of Interactions in Unified Gauge Theories*, *Phys. Rev. Lett.* **33** (1974) 451–454.

[174] A. J. Buras, J. R. Ellis, M. K. Gaillard, and D. V. Nanopoulos, *Aspects of the Grand Unification of Strong, Weak and Electromagnetic Interactions*, *Nucl. Phys.* **B135** (1978) 66–92.

[175] R. N. Mohapatra and J. C. Pati, *Left-Right Gauge Symmetry and an Isoconjugate Model of CP Violation*, *Phys. Rev.* **D11** (1975) 566–571.

[176] R. N. Mohapatra and J. C. Pati, *A Natural Left-Right Symmetry*, *Phys. Rev.* **D11** (1975) 2558.

[177] P. Langacker, *The Standard Model and Beyond*. Series in High Energy Physics, Cosmology and Gravitation. CRC Press, 2009.

[178] A. M. Uranga, *The standard model in string theory from D-branes*, *Nucl. Phys. Proc. Suppl.* **171** (2007) 119–138.

[179] F. G. Marchesano Buznego, *Intersecting D-brane models*. PhD thesis, Madrid, Autonoma U., 2003. hep-th/0307252.

[180] A. M. Uranga, *Intersecting brane worlds*, *Class. Quant. Grav.* **22** (2005) S41–S76.

[181] M. Berkooz, M. R. Douglas, and R. G. Leigh, *Branes intersecting at angles*, *Nucl. Phys.* **B480** (1996) 265–278, [hep-th/9606139].

[182] M. Cvetič and P. Langacker, *New Grand Unified Models with Intersecting D6-branes, Neutrino Masses, and Flipped SU(5)*, *Nucl.Phys.* **B776** (2007) 118–137, [hep-th/0607238].

[183] M. Cvetič, J. Halverson, and P. Langacker, *Implications of String Constraints for Exotic Matter and Z' s Beyond the Standard Model*, *JHEP* **1111** (2011) 058, [arXiv:1108.5187].

[184] M. Cvetič, P. Langacker, and G. Shiu, *A Three family standard - like orientifold model: Yukawa couplings and hierarchy*, *Nucl. Phys.* **B642** (2002) 139–156, [hep-th/0206115].

[185] I. Antoniadis and G. Leontaris, *A supersymmetric $SU(4) \times O(4)$ model*, *Phys.Lett.* **B216** (1989) 333.

[186] S. King and Q. Shafi, *Minimal supersymmetric $SU(4) \times SU(2)_L \times SU(2)_R$*, *Phys.Lett.* **B422** (1998) 135–140, [hep-ph/9711288].

[187] F. Gmeiner, R. Blumenhagen, G. Honecker, D. Lüst, and T. Weigand, *One in a billion: MSSM-like D-brane statistics*, *JHEP* **0601** (2006) 004, [hep-th/0510170].

[188] L. E. Ibáñez, F. Marchesano, and R. Rabadan, *Getting just the standard model at intersecting branes*, *JHEP* **0111** (2001) 002, [hep-th/0105155].

[189] D. Cremades, L. E. Ibanez, and F. Marchesano, *Intersecting brane models of particle physics and the Higgs mechanism*, *JHEP* **07** (2002) 022, [hep-th/0203160].

[190] D. Ghilencea, L. Ibáñez, N. Irges, and F. Quevedo, *TeV scale Z-prime bosons from D-branes*, *JHEP* **0208** (2002) 016, [hep-ph/0205083].

[191] L. E. Ibáñez and G. G. Ross, *Discrete gauge symmetries and the origin of baryon and lepton number conservation in supersymmetric versions of the standard model*, *Nucl.Phys.* **B368** (1992) 3–37.

[192] L. Ibez and G. Ross, *Discrete gauge symmetry anomalies*, *Physics Letters B* **260** (1991), no. 3 291 – 295.

[193] H. K. Dreiner, C. Luhn, and M. Thormeier, *What is the discrete gauge symmetry of the MSSM?*, *Phys.Rev.* **D73** (2006) 075007, [hep-ph/0512163].

[194] T. Banks and M. Dine, *Note on discrete gauge anomalies*, *Phys.Rev.* **D45** (1992) 1424–1427, [hep-th/9109045].

[195] L. E. Ibanez, *More about discrete gauge anomalies*, *Nucl. Phys.* **B398** (1993) 301–318, [hep-ph/9210211].

[196] S. P. Martin, *Some simple criteria for gauged R-parity*, *Phys. Rev.* **D46** (1992) 2769–2772, [hep-ph/9207218].

[197] K. Kurosawa, N. Maru, and T. Yanagida, *Nonanomalous R symmetry in supersymmetric unified theories of quarks and leptons*, *Phys. Lett.* **B512** (2001) 203–210, [hep-ph/0105136].

[198] R. N. Mohapatra and M. Ratz, *Gauged Discrete Symmetries and Proton Stability*, *Phys. Rev.* **D76** (2007) 095003, [arXiv:0707.4070].

[199] T. Araki, T. Kobayashi, J. Kubo, S. Ramos-Sanchez, M. Ratz, et al., *(Non-)Abelian discrete anomalies*, *Nucl.Phys.* **B805** (2008) 124–147, [arXiv:0805.0207].

[200] H. M. Lee, S. Raby, M. Ratz, G. G. Ross, R. Schieren, K. Schmidt-Hoberg, and P. K. S. Vaudrevange, *A unique $\mathbb{Z}_4^R$ symmetry for the MSSM*, *Phys. Lett.* **B694** (2014) 491–495, [arXiv:1009.0905].

[201] R. Kappl, B. Petersen, S. Raby, M. Ratz, R. Schieren, and P. K. S. Vaudrevange, *String-Derived MSSM Vacua with Residual R Symmetries*, *Nucl. Phys.* **B847** (2011) 325–349, [arXiv:1012.4574].

[202] M. Cvetič and I. Papadimitriou, *Conformal field theory couplings for intersecting D-branes on orientifolds*, *Phys.Rev.* **D68** (2003) 046001, [hep-th/0303083].

[203] S. Abel and A. Owen, *Interactions in intersecting brane models*, *Nucl.Phys.* **B663** (2003) 197–214, [hep-th/0303124].

[204] S. Kachru, S. H. Katz, A. E. Lawrence, and J. McGreevy, *Open string instantons and superpotentials*, *Phys.Rev.* **D62** (2000) 026001, [hep-th/9912151].

[205] D. Cremades, L. Ibáñez, and F. Marchesano, *Yukawa couplings in intersecting D-brane models*, *JHEP* **0307** (2003) 038, [hep-th/0302105].

[206] D. Cremades, L. Ibáñez, and F. Marchesano, *Computing Yukawa couplings from magnetized extra dimensions*, *JHEP* **0405** (2004) 079, [hep-th/0404229].

[207] S. Abel and A. Owen, *N point amplitudes in intersecting brane models*, *Nucl.Phys.* **B682** (2004) 183–216, [hep-th/0310257].

[208] D. Lüst, P. Mayr, R. Richter, and S. Stieberger, *Scattering of gauge, matter, and moduli fields from intersecting branes*, *Nucl.Phys.* **B696** (2004) 205–250, [hep-th/0404134].

[209] E. Cremmer, S. Ferrara, L. Girardello, and A. Van Proeyen, *Yang-Mills Theories with Local Supersymmetry: Lagrangian, Transformation Laws and SuperHiggs Effect*, *Nucl.Phys.* **B212** (1983) 413.

[210] L. J. Dixon, V. Kaplunovsky, and J. Louis, *On Effective Field Theories Describing (2,2) Vacua of the Heterotic String*, *Nucl.Phys.* **B329** (1990) 27–82.

[211] K. Rajagopal, M. S. Turner, and F. Wilczek, *Cosmological implications of axinos*, *Nucl.Phys.* **B358** (1991) 447–470.

[212] A. Zhitnitsky, *On Possible Suppression of the Axion Hadron Interactions. (In Russian)*, *Sov.J.Nucl.Phys.* **31** (1980) 260.

[213] M. Dine, W. Fischler, and M. Srednicki, *A Simple Solution to the Strong CP Problem with a Harmless Axion*, *Phys.Lett.* **B104** (1981) 199.

[214] **PVLAS Collaboration** Collaboration, E. Zavattini et al., *Experimental observation of optical rotation generated in vacuum by a magnetic field*, *Phys.Rev.Lett.* **96** (2006) 110406, [hep-ex/0507107].

[215] K. Ehret, M. Frede, S. Ghazaryan, M. Hildebrandt, E.-A. Knabbe, et al., *New ALPS Results on Hidden-Sector Lightweights*, *Phys.Lett.* **B689** (2010) 149–155, [arXiv:1004.1313].

[216] K. Barth et al., *CAST constraints on the axion-electron coupling*, *JCAP* **1305** (2013) 010, [arXiv:1302.6283].

[217] M. Drewes, *The Phenomenology of Right Handed Neutrinos*, *Int. J. Mod. Phys.* **E22** (2013) 1330019, [arXiv:1303.6912].

[218] L. A. Anchordoqui, I. Antoniadis, H. Goldberg, X. Huang, D. Lüst, et al., *LHC Phenomenology and Cosmology of String-Inspired Intersecting D-Brane Models*, *Phys.Rev.* **D86** (2012) 066004, [arXiv:1206.2537].

[219] P. Svrcek and E. Witten, *Axions In String Theory*, *JHEP* **0606** (2006) 051, [hep-th/0605206].

[220] D. Berenstein and E. Perkins, *Open string axions and the flavor problem*, *Phys.Rev.* **D86** (2012) 026005, [arXiv:1202.2073].

[221] J. P. Conlon, *The QCD axion and moduli stabilisation*, *JHEP* **0605** (2006) 078, [hep-th/0602233].

[222] M. Cicoli, M. Goodsell, and A. Ringwald, *The type IIB string axiverse and its low-energy phenomenology*, *JHEP* **1210** (2012) 146, [arXiv:1206.0819].

[223] A. Belhaj, S. E. Ennadifi, and M. P. G. del Moral, *Axion from Quivers in Type II Superstrings*, arXiv:1508.0719.

[224] R. Blumenhagen and M. Schmidt-Sommerfeld, *Gauge Thresholds and Kähler Metrics for Rigid Intersecting D-brane Models*, *JHEP* **0712** (2007) 072, [arXiv:0711.0866].

[225] D. Lüst and S. Stieberger, *Gauge threshold corrections in intersecting brane world models*, *Fortsch.Phys.* **55** (2007) 427–465, [hep-th/0302221].

[226] M. Berg, M. Haack, and J. U. Kang, *One-Loop Kähler Metric of D-Branes at Angles*, *JHEP* **1211** (2012) 091, [arXiv:1112.5156].

[227] M. Berg, M. Haack, J. U. Kang, and S. Sjörs, *Towards the one-loop Kähler metric of Calabi-Yau orientifolds*, *JHEP* **12** (2014) 077, [arXiv:1407.0027].

[228] E. Accomando, I. Antoniadis, and K. Benakli, *Looking for TeV scale strings and extra dimensions*, *Nucl. Phys.* **B579** (2000) 3–16, [hep-ph/9912287].

[229] S. Cullen, M. Perelstein, and M. E. Peskin, *TeV strings and collider probes of large extra dimensions*, *Phys. Rev.* **D62** (2000) 055012, [hep-ph/0001166].

[230] P. Burikham, T. Figy, and T. Han, *TeV-scale string resonances at hadron colliders*, *Phys. Rev.* **D71** (2005) 016005, [hep-ph/0411094]. [Erratum: Phys. Rev.D71,019905(2005)].

[231] D. Lüst, S. Stieberger, and T. R. Taylor, *The LHC String Hunter's Companion*, *Nucl.Phys.* **B808** (2009) 1–52, [arXiv:0807.3333].

[232] M. Chemtob, *Contact interactions in low scale string models with intersecting D6-branes*, *Phys. Rev.* **D78** (2008) 125020, [arXiv:0808.1242].

[233] L. A. Anchordoqui, H. Goldberg, D. Lüst, S. Nawata, S. Stieberger, and T. R. Taylor, *LHC Phenomenology for String Hunters*, *Nucl. Phys.* **B821** (2009) 181–196, [arXiv:0904.3547].

[234] N. Kitazawa, *A Closer look at string resonances in dijet events at the LHC*, *JHEP* **10** (2010) 051, [arXiv:1008.4989].

[235] L. A. Anchordoqui, I. Antoniadis, H. Goldberg, X. Huang, D. Lüst, et al., *Z'-gauge Bosons as Harbingers of Low Mass Strings*, *Phys.Rev.* **D85** (2012) 086003, [arXiv:1107.4309].

[236] D. Berenstein, *TeV-Scale strings*, *Ann. Rev. Nucl. Part. Sci.* **64** (2014) 197–219, [arXiv:1401.4491].

[237] R. Blumenhagen, M. Cvetič, S. Kachru, and T. Weigand, *D-Brane Instantons in Type II Orientifolds*, *Ann.Rev.Nucl.Part.Sci.* **59** (2009) 269–296, [arXiv:0902.3251].

[238] J. P. Derendinger, L. E. Ibanez, and H. P. Nilles, *On the Low-Energy d = 4, N=1 Supergravity Theory Extracted from the d = 10, N=1 Superstring*, *Phys. Lett.* **B155** (1985) 65.

[239] M. Dine, R. Rohm, N. Seiberg, and E. Witten, *Gluino Condensation in Superstring Models*, *Phys. Lett.* **B156** (1985) 55.

[240] R. Blumenhagen, D. Lüst, and S. Stieberger, *Gauge unification in supersymmetric intersecting brane worlds*, *JHEP* **07** (2003) 036, [hep-th/0305146].

[241] I. R. Klebanov and E. Witten, *Proton decay in intersecting D-brane models*, *Nucl.Phys.* **B664** (2003) 3–20, [hep-th/0304079].

[242] D. Bailin and A. Love, *Introduction to Gauge Field Theory Revised Edition*. Graduate Student Series in Physics. Taylor & Francis, 1993.

[243] L. J. Dixon, V. Kaplunovsky, and J. Louis, *Moduli dependence of string loop corrections to gauge coupling constants*, *Nucl. Phys.* **B355** (1991) 649–688.

[244] P. Mayr and S. Stieberger, *Threshold corrections to gauge couplings in orbifold compactifications*, *Nucl. Phys.* **B407** (1993) 725–748, [hep-th/9303017].

[245] D. Bailin, A. Love, W. A. Sabra, and S. Thomas, *Anisotropic solutions for orbifold moduli from duality invariant gaugino condensates*, *Mod. Phys. Lett.* **A9** (1994) 2543–2555, [hep-th/9405031].

[246] D. Bailin, A. Love, W. A. Sabra, and S. Thomas, *Modular symmetries, threshold corrections and moduli for Z(2) x Z(2) orbifolds*, *Mod. Phys. Lett.* **A10** (1995) 337–346, [hep-th/9407049].

[247] P. Mayr and S. Stieberger, *Moduli dependence of one loop gauge couplings in (0,2) compactifications*, *Phys. Lett.* **B355** (1995) 107–116, [hep-th/9504129].

[248] H. P. Nilles and S. Stieberger, *How to reach the correct* $\sin^2\theta_W$ *and* α_s *in string theory*, *Phys. Lett.* **B367** (1996) 126–133, [hep-th/9510009].

[249] P. Mayr, H. P. Nilles, and S. Stieberger, *String unification and threshold corrections*, *Phys. Lett.* **B317** (1993) 53–59, [hep-th/9307171].

[250] J. A. Harvey and G. W. Moore, *Algebras, BPS states, and strings*, *Nucl. Phys.* **B463** (1996) 315–368, [hep-th/9510182].

[251] H. P. Nilles and S. Stieberger, *String unification, universal one loop corrections and strongly coupled heterotic string theory*, *Nucl. Phys.* **B499** (1997) 3–28, [hep-th/9702110].